ASPECTS OF RATIONAL STRUCTURAL DESIGN OF SWATH SHIPS

by

Constantinos Tolikas, M.Sc.

Thesis submitted for the Degree of Doctor of Philosophy

Department of Naval Architecture and Ocean Engineering
University of Glasgow

July, 1995

ProQuest LLC.
789 East Eisenhower Parkway
P.O. Box 1346
Ann Arbor, MI 48106 – 1346

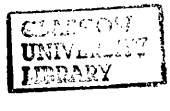

DECLARATION

Except where reference is made to the work of others,
this thesis is believed to be original

ΙΘΑΚΗ

Σὰ βγεῖς στὸν πηγαιμὸ γιὰ τὴν 'Ιθάκη,
νὰ εὔχεσαι νἄναι μακρὺς ὁ δρόμος,
γεμάτος περιπέτειες, γεμάτος γνώσεις.
Τοὺς Λαιστρυγόνας καὶ τοὺς Κύκλωπας,
τὸν θυμωμένο Ποσειδῶνα μὴ φοβᾶσαι,
τέτοια στὸν δρόμο σου ποτέ σου δὲν θὰ βρεῖς,
ἂν μέν' ἡ σκέψις σου ὑψηλή, ἂν ἐκλεκτὴ
συγκίνησις τὸ πνεῦμα καὶ τὸ σῶμα σου ἀγγίζει.
Τοὺς Λαιστρυγόνας καὶ τοὺς Κύκλωπας,
τὸν ἄγριο Ποσειδῶνα δὲν θὰ συναντήσεις,
ἂν δὲν τοὺς κουβανεῖς μὲς στὴν ψυχή σου,
ἂν ἡ ψυχή σου δὲν τοὺς στήνει ἐμπρός σου.

Νὰ εὔχεσαι νἄναι μακρὺς ὁ δρόμος.
Πολλὰ τὰ καλοκαιρινὰ πρωῒὰ νὰ εἶναι
ποὺ μὲ τί εὐχαρίστησι, μὲ τί χαρὰ
θὰ μπαίνεις σὲ λιμένας πρωτοειδωμένους·
νὰ σταματήσεις σ' ἐμπορεῖα Φοινικικά,
καὶ τὲς καλὲς πραγμάτειες ν' ἀποκτήσεις,
σεντέφια καὶ κοράλλια, κεχριμπάρια κ' ἔβενους,
καὶ ἡδονικὰ μυρωδικὰ κάθε λογῆς,
ὅσο μπορεῖς πιὸ ἄφθονα ἡδονικὰ μυρωδικά·
σὲ πόλεις Αἰγυπτιακὲς πολλὲς νὰ πᾶς.
νὰ μάθεις καὶ νὰ μάθεις ἀπ' τοὺς σπουδασμένους.

Πάντα στὸν νοῦ σου νἄχεις τὴν 'Ιθάκη.
Τὸ φθάσιμον ἐκεῖ εἶν' ὁ προορισμός σου.
'Αλλὰ μὴ βιάζεις τὸ ταξεῖδι διόλου.
Καλλίτερα χρόνια πολλὰ νὰ διαρκέσει·
καὶ γέρος πιὰ ν' ἀράξεις στὸ νησί,
πλούσιος μὲ ὅσα κέρδισες στὸν δρόμο,
μὴ προσδοκῶντας πλούτη νὰ σὲ δώσει ἡ 'Ιθάκη.

'Η 'Ιθάκη σ' ἔδωσε τ' ὡραῖο ταξεῖδι.
Χωρὶς αὐτὴν δὲν θἄβγαινες στὸν δρόμο.
"Αλλα δὲν ἔχει νὰ σὲ δώσει πιά.

Κι ἂν πτωχικὴ τὴν βρεῖς, ἡ 'Ιθάκη δὲν σὲ γέλασε.
"Ετσι σοφὸς ποὺ ἔγινες, μὲ τόση πεῖρα,
ἤδη θὰ τὸ κατάλαβες ἡ 'Ιθάκες τί σημαίνουν.

ITHAKA

As you set out for Ithaka
hope your road is a long one.
full of adventure, full of discovery.
Laistrygonians, Cyclops,
angry Poseidon—don't be afraid of them:
you'll never find things like that on your way
as long as you keep your thoughts raised high.
as long as a rare excitement
stirs your spirit and your body.
Laistrygonians, Cyclops.
wild Poseidon—you won't encounter them
unless you bring them along inside your soul.
unless your soul sets them up in front of you.

Hope your road is a long one.
May there be many summer mornings when.
with what pleasure, what joy,
you enter harbors you're seeing for the first time:
may you stop at Phoenician trading stations
to buy fine things.
mother of pearl and coral, amber and ebony.
sensual perfume of every kind—
as many sensual perfumes as you can:
and may you visit many Egyptian cities
to learn and go on learning from their scholars.

Keep Ithaka always in your mind.
Arriving there is what you're destined for.
But don't hurry the journey at all.
Better if it lasts for years.
so you're old by the time you reach the island.
wealthy with all you've gained on the way.
not expecting Ithaka to make you rich.

Ithaka gave you the marvelous journey.
Without her you wouldn't have set out.
She has nothing left to give you now.

And if you find her poor, Ithaka won't have fooled you.
Wise as you will have become, so full of experience.
you'll have understood by then what these Ithakas mean.

Reference

Savidis, G. (Ed.), 'C.P. Cavafy: Collected Poems', The Hogarth Press, London, 1975

Abstract

The aim of the work described herein is to provide the background, underlying assumptions and considerations, as well as describe the tools necessary for the development of reliability-based strength criteria for the design of the structural components of fast, multi-hulled ships (Chapters 1-4) in general, and SWATH ships in particular.

An overall view of the current state and future prospects of the fast marine transportation market, highlighting the limitations and advantages of the application of such advanced marine concepts is provided in Chapter 1. The challenges, both strategic and technological, that would have to be overcome before these concepts enjoy a more widespread acceptance from the passengers, operators, and governments, are identified and form the background within which the work described herein develops. It has been inevitable that a large number of topics had to be covered in order to provide the reader with the overall picture of the structural design problems expected and their solutions in this novel form of transportation. As a result, no claim for completeness is made herein, but instead an 'in width' study of the topic was felt as most appropriate for establishing the degree of interrelation and interaction of the various aspects of structural design, and has therefore been actively pursued.

The problem of estimation of both primary and secondary loads on SWATH ships is tackled in Chapter 2, by reviewing the options and methods available to the designer. Of the secondary loads, the question of slamming load prediction on the underdeck of SWATH ships has been given some attention, via two sets of drop tests (one by the author) carried out at the Department of Naval Architecture and Ocean Engineering, University of Glasgow and the main results described herein. Current approaches for the determination of fatigue damage loading are also described.

Chapter 3 concentrates on the strength modelling aspects and the associated uncertainty as applicable to the fatigue design of both monohull and multi-hull vessels. A brief description of the sources of fatigue strength reduction in welded structures and the possible repair measures, the background to the major steel and aluminium fatigue design codes is presented, coupled

with a comparison of the major aluminium fatigue design codes. The probabilistic derivation of partial safety factors for fatigue strength expressions is also presented but not demonstrated.

In Chapter 4, the work has concentrated mainly in the area of strength modelling for the various structural components of the SWATH ship under all possible load combinations they might be expected to withstand. Although it stops just short of deriving appropriate partial safety factors for the various structural components and failure modes in a multi-hull structure, detailed guidance on how to do so is provided. The reliability-based design procedure to the structural optimisation, with respect to cost, weight and safety, of an example SWATH ship, the M.V. Patria is applied and described instead in Chapter 5. The conclusions of the research, recommendations on the most appropriate strength formulations and the areas which may benefit from further research are all finally identified in Chapter 6.

Note: Description of the various parameters used in individual Chapters is adequately covered in the Notation Section, unless otherwise presented in the text.

Acknowledgements

The author is greatly indebted to his supervisor, Professor D. Faulkner, for his continuous and expert support and guidance throughout this work, as well as for providing the excellent opportunity to meet people from, and see, the world of structures from a different and most exciting viewpoint.

Sincere thanks are also due to Drs. P.K. Das, P.C. Chatterjee and Mr. Y. Pu for their useful discussions at various stages of this research and to Mrs. I.P. Faulkner for the most useful editorial comments and her encouragement for a fast completion of this work, especially in its last stages. Mrs. M. McGrady's and Mr. D. Percival's continuous assistance is greatly appreciated.

Special thanks are due to Professor H. R. Evans and Dr. A. Davies, School of Engineering, University of Wales, Dr. R. Narayanan, Steel Research Institute, Professor G. Sedlacek, RWTH Aachen, Germany, for their valuable discussions and advice on the subject of ultimate strength of plate girders and the provision of experimental data. The author is also indebted to Mr. J. Dwight and Professor P. Bulson, in addition to Messrs. J. McCrickerd, R. Cogden and M. Bayley, of ALCAN U.K. for their brief but very effective introduction to the world of aluminium. Messrs. N. Warren and R.J. Tombleson of FBM Marine Ltd, Isle of Wight, are to be thanked for their demonstration of aspects dominating aluminium shipbuilding.

The co-operation and assistance of the ISSC Committee V.1 (Applied Design-Strength Limit State Formulations', 12th ISSC, Canada) members, Prof. T. Moan, Prof. V. Zanic, Dr. P. Frieze, Dr. G. Permantier and Dr. P. Rigo, is gratefully acknowledged. Professor V. Zanic is to be thanked for implementing and permitting the use of his optimisation software in this work.

My colleagues, Drs. A.C. Morandi and L. Zhu, are due the most special thanks for their continuous support, technical and non-technical discussions and especially most honest friendship throughout these studies.

But most indebted of all, I am to my parents, Stephanos and Carmen, and my sister Mary, without whose understanding, moral support and encouragement, this work would have never been completed.

Contents

List of Tables

List of Figures

Chapter 2

Chapter 3

Chapter 5

A. Notation Used in Chapter 3

a	is the crack depth for a surface flaw or half width for a penetration flaw
a_i	instantaneous crack length
a_{crit}	$(=K_C^2/\pi\sigma_y^2)$ is the crack length for unstable crack propagation
$a_{threshold}$	crack length at which stable crack propagation commences
β	$\overline{Z}/\sigma_Z$, safety index
γ_R	partial safety factor reflecting the uncertainty in the fatigue strength
γ_Q	partial safety factor reflecting the uncertainty in load values
c	crack width
ΔK	$(= Y(a)\,\Delta S\sqrt{\pi a})$ applied stress intensity factor range
ΔS	applied stress range
ΔS_{eq}	$\left(\sum_{i=1}^{k}\Delta S_i^m\, n_i/N\right)^{1/m}$, equivalent stress range
da/dN	the crack growth rate
E	modulus of elasticity of the material
K_C	critical value of the stress intensity factor at which unstable crack propagation commences
K_{max}	maximum stress intensity
$K_{threshold}$	stress intensity factor at which stable crack propagation begins
m	inverse of the slope of the S-N curves and exponent in the Paris-Erdogan rule, as well as in the fatigue strength equation
M_s	correction factor in the crack geometry function depending on the crack shape (a/2c)
M_k	correction factor in the crack geometry function dependent on the weld toe stress concentration, on the weld angle and a/B
M_t	correction factor in the crack geometry function dependent upon the crack length to extreme boundary in the direction of propagation (a/B) and shape (a/2c).
N	$\sum n_i$, total number of cycles in the fatigue life of a detail
N_B	number of 'blocks' to failure in the 'Area Rule'
N_C	constant amplitude life at the greatest stress range in the spectrum for applications of the 'Area Rule'
N_{E_i}	number of exceedances, per loading block, of stress S_i used in the application of the 'Area Rule'
n_i	number of cycles at a given stress range at any given instance

p_i	$S_i = p_i\, S_{max}$, as used in the 'Area Rule'
$\overline{Q}$	mean value of the load distribution
$\overline{R}$	mean value of the resistance distribution
σ	direct in plane axial stress
σ_Q	standard deviation of the load distribution
σ_R	standard deviation of the resistance distribution
σ_Z	standard deviation of the safety margin distribution
S_i	specific stress range (block) in a stress range spectrum
S_{max}	maximum stress range value in a stress range spectrum
τ	shear stress
Y(a)	crack geometry function dependent on crack geometry and size
$\overline{\Phi}_c$	elliptic integral in the crack geometry function dependent on the crack shape (a/2c)
$\overline{Z}$	$\overline{Z} = \overline{R} - \overline{Q}$, mean value of the safety margin distribution

B. Notation for the Design of Flat Plates Under Various Loading Conditions

α	(=a/b) plate aspect ratio
A_{HAZ}	area of HAZ, equal to the plate thickness times the width of the softened area. When used in the residual stress estimation A_{HAZ} should be estimated according to Table 4.1
A_s	stiffener cross-sectional area
A_w	cross sectional area of the weld deposit
a	long side of rectangular plating
a_e	effective width of rectangular plating under transverse compression loading
B_{imp}	reduction factor accounting for the effects of initial imperfections on the ultimate strength of aluminium, unwelded flat plates
b	plate width
b_e	effective width of plating
b_e'	reduced effective width of plating, as conceived by faulkner, to account for the continuous loss of plate stiffness in compression in the post-buckling range
β	$(=(b/t)\sqrt{\sigma_y / E})$ plate slenderness parameter
γ	curve fitting to data constant as used by Valsgard in his expression for biaxial loading (taken as equal to 1)
$\Delta\sigma_m$	reduction in compressive ultimate strength of steel plates due to inelastic plate behaviour
ε	strain under compressive loading, for plates in compression
η	curve fitting to data constant as used by Valsgard in his expression for biaxial loading (taken equal to 0.25)
C	correction factor to predicted strength values by the proposed aluminium model accounting for the effects of initial imperfections in the plates
C_1	reduction factor to the ultimate compressive strength of aluminium plates, accounting for the effects of positioning the welds elsewhere but at the toe of the stiffeners
D	$(=E t^3/12(1-\upsilon^2))$, plate rigidity
HAZ	heat affected zone
E	Young's modulus
E_t	tangent modulus to account for non-linear compressive behaviour of welded structures

k_z	HAZ reduction of strength of parent material of aluminium alloys as calculated in BS8118
λ	column slenderness parameter
L_e	effective length of a column in compression as implied by the boundary conditions assumed
l, L	stiffener length, plate length
M_p	$(=0.25\,t^2\,\sigma_y/\sqrt{1-\upsilon+\upsilon^2})$, plastic moment capacity of plate strip of unit width and thickness t
n	material exponent in Ramberg-Osgood strain-stress relation
$P_{cr,el}$	critical buckling load of plates (or plate elements) in compression
q, p	uniform lateral pressure load (in N/mm^2)
R_x	$(=\sigma_x/\sigma_{xu})$ non-dimensional longitudinal stress ratio
R_y	$(=\sigma_y/\sigma_{yu})$ non-dimensional transverse stress ratio
r	radius of gyration of the cross section of a column
$\sigma_{0.1}$	compressive proof stress of the parent aluminium alloy at 0.1% strain
$\sigma_{0.2}$	compressive proof stress of the parent aluminium alloy at 0.2% strain
$\sigma^*_{0.2}$	$(=w\sigma_{0.2})$ reduced strength of parent material due to HAZ softening in heat-treated aluminium alloys
σ_{max}	maximum stress in a flat plate under lateral pressure loading, when analysed by elastic small deflection analysis
σ_e	edges stress in an effective width approach
σ_p	$(=\sigma_y-\sigma_{rc})$ proportional limit stress in a welded cross section
σ_{rc}	locked-in residual compressive stress in a welded section
σ_y, σ_o	compressive yield/proof stress of the parent material
σ_{xu}	ultimate strength of a plate under in plane axial compression/ bending acting in the x direction ('long' direction)
σ_{yu}	ultimate strength of a plate under in plane axial compression/ bending acting in the y direction ('wide' direction)
τ	shear stress load in N/mm^2
τ_y	$(=\sigma_y/\sqrt{3})$ yield stress of the material in shear
t	plate thickness
t_w	thickness of stiffener web
υ	Poisson's ratio
w	plate deflection, used in the design of flat plates under lateral pressure loading

w	percentage of strength reduction of heat-treated aluminium material due to HAZ softening
w_{max}	maximum *elastic* deflection of flat plates under lateral pressure loading, when analysed by elastic small deflection analysis
w_o	initial plate deflection
w_{pt}	final maximum allowable plate deflection
$w_{stiffener}$	stiffener initial permaset deflection
x	denotes the distance (orthogonal to the line of application of the load) of the plate welds from the loaded edges of the plates. It does not correspond to the length of the weld.
$2z_o$	extent of HAZ softened strength area due to welding in aluminium alloys, prior to reduction for end effects and raised temperature effects
$2z$	$(=2\alpha\eta z_o)$ extent of HAZ softened strength area due to welding in aluminium alloys, after reduction for end effects and raised temperature effects
$2z_w$	extent of HAZ softened strength area due to welding in aluminium alloys, *for stiffener web in the stiffened plate structural arrangement*

C. Notation for the Design of Stiffeners

α	web panel aspect ratio
A_f	cross sectional area of stiffener flange
A_s	cross sectional area of stiffener/ring frame
b	stiffener spacing used in tripping analysis
b, b_w	transverse stiffener spacing in deep plate girders (or length of web plate in aspect ratio estimation)-not for tripping
b_s	depth of transverse stiffener (usually flat bar) of deep plate girder
b_f	flange breadth of stiffener
Γ	longitudinal warping constant of stiffener
γ^*	optimum relative rigidity of stiffener (relative to the plate)
γ	$(=E I_s/D\,d)$ actual relative stiffener flexural rigidity (relative to the plate)
C_s	$(=E t^3/3(1-\upsilon^2)b)$ stable rotational shell stiffness for flat plate stiffeners
C_{on}	$(=\left[E t^3/3\,L(1-\upsilon^2)\right]\left[1+(n\,L/\pi\,R)^2\right]^2)$ stable rotational shell stiffness for the nth mode for ring frames
δ	$(=A_s/d\,t)$ relative (to the plating) cross-sectional area of the stiffener
d, d_w	plate width, web depth, in stiffener rigidity analysis and deep plate girder stiffener design
d	web depth of stiffener/ring frames (in tripping analysis only)
d_c	depth of stiffener to mid-thickness of flange
d_1	distance of outer shell fibre from the neutral axis of the frame section containing an effective width of shell)
d_c	$(\approx d_w + t_f/2)$ distance of shear centre from the shell plating
D	$(=E t^3/12(1-\upsilon^2))$, flexural rigidity of plating
E	material Young's modulus
E_{ts}, E_t	structural tangent modulus
G	shear modulus of material
h	distance of neutral axis of plate stiffener combination from mid-thickness of plating
I	vertical moment of inertia of the stiffener and its associated effective width of plating about the strong neutral axis of the section
I_{zf}	moment of inertia of the stiffener flange about the web plane

I_o polar moment of inertia about the toe of the stiffener/ring frame

I_s moment of inertia of stiffener flange about its own neutral axis parallel to the attached plate

I_z moment of inertia about the web plane of the stiffener/ring frame

J St Venant torsion constant $(=\left(d_{w,stif}\ t_{w,stif}^3 + b_{f,stif}\ t_{f,stif}^3\right)/3$ for Tees)

k empirical coefficient by Faulkner catering for the stabilising and destabilising effects of the plating on the stiffener at tripping

l effective stiffener length as used in tripping strength estimation

m number of buckling half waves along the length of shell

m_p mode number for critical buckling of plate in compression (number of half waves along the length of the stiffener)

m_T mode number for critical tripping of the stiffener in compression (number of half waves along the length of the stiffener)

m_t, m_l amplification factors for the critical rigidity requirement of stiffeners to account for the post-buckling behaviour of the associated plating

n number of complete buckling waves around the circumference

ξ $(=\sigma_T/p_T=\left(\sigma_{fy}/p_{fy}\right)\left(R_f/R_s\right))$, tripping stress/tripping pressure ratio

o-o-c out-of-circularity

p_{c5} $(=\left(\sigma_y\ t/R\right)/\left(1+\gamma\ G\right))$ pressure at which the applied circumferential stress at mid-bay and mid-thickness reaches the shell yield stress

p_e $(=\left(2/\sqrt{3\left(1-\upsilon^2\right)}\right)E\left(t/R\right)^2)$ elastic buckling pressure for spheres

p_d design pressure

p_n Bryant's expression for the overall buckling pressure of ring stiffened cylinders

p_{nf} elastic collapse pressure for the shell and frame combination by Bresse

p_{ns} shell buckling pressure of ring stiffened cylinders in overall collapse mode of failure (by von Mises)

p_{sy} pressure to cause yielding in the centroid of the ring frame

p_m $(=\left(0.919\,E\left(t/R\right)^2\right)/\left(\left(L/\sqrt{\left(R\,t\right)}\right)-0.636\right))$ lowest elastic buckling pressure for the unsupported shell between ring-frames

$$=\left(Et/R\right)\left[n^2-1+k\,\lambda^2\right]^{-1}\left\{\left[n^2\lambda^{-2}+1\right]^{-2}+\left[t^2/12R^2\left(1-\upsilon^2\right)\right]\left[n^2-1+\lambda^2\right]^2\right\}$$

where k=0.5 for hydrostatic pressure and k=0 for radial pressure (original von Mises expression after Kendrick's alterations)

p_y $(=p_{c5})$

p_{fy}	$(=(\sigma_y\, t\, R_f/R^2)/(1-0.5\,\upsilon-\gamma))$ pressure at which the outer fibre of the flange of a ring frame yields
p_{Te}	external pressure to cause elastic tripping in ring frames
p_{Tin}	external pressure to cause inelastic tripping in ring frames
p_{ys}	$(=2\,\sigma_y\, t/R)$ membrane yield pressure for a spherical shell
q_{cre}	lateral (pressure) load per unit length to cause elastic tripping on a pinned stiffener
R	mean shell radius
r	$=\sigma_{rc}/\sigma_y$ ratio of residual compressive stress to material yield stress
σ_{cr}	critical buckling strength of flat plate panel in compression
σ_e	axial stress in the stiffener (usually edge stress based on an effective width approach)
σ^*_{cr}	critical buckling stress of the weakest (depending on the load condition) subpanel associated with the stiffener whose rigidity is considered
σ_E	Euler column buckling stress of stiffener/effective width column (in tripping analysis)
σ_f	stress in the centroid of the flange of the ring frame
σ_T	elastic tripping stress of stiffener
σ_{Ti}	inelastic tripping stress of stiffener
σ_{ps}	$(=p_r\,\sigma_y)$ structural proportional limit for steel structures
σ_y	material yield stress (or 0.2% proof stress for aluminium alloys)
σ_{yf}	yield stress of the flange material
τ_{cr}	critical buckling stress of a web panel/plate in pure shear
t	plate/shell thickness
t_s	thickness of transverse stiffener (usually a flat bar) in plate girders
t_w	web thickness of stiffener/ring frames
υ	Poisson's ratio
V	average value of the ultimate shear force arising in a web panel on either side of the vertical stiffener
V_{cr}	critical buckling shear load for web panels in deep plate girders
$\bar{z}$	distance of centroid of ring frame cross section toe of stiffener

D. Notation for the Design of Unperforated and Perforated Girders

α	web plate aspect ratio
A, A_w	web plate sectional area
A_c	area of web perforation
A_f	sectional areas of the girder flange
b	web plate length
b_e	equivalent effective width of the tension band assuming to act with a circular cutout reinforcement
b_f	width of girder flange
b_o, h_o	length and depth of a rectangular perforation
c	position of plastic hinges on the flanges from the corner of web plate
c_c, c_t	the positions of the plastic hinges on the compressive and tensile flanges respectively
c_r	position of plastic hinge on the reinforcement of rectangular cutouts
δ	extent of width reduction in the tension field due to the presence of rectangular cutout
D	$(= E t^3 / 12(1 - \upsilon^2))$, web plate rigidity
E	modulus of elasticity of the web plate
E_f	modulus of elasticity for the girder flanges
G	$(= E/2(1 + \upsilon))$ modulus of shear rigidity
d	diameter of circular perforation
h	web plate depth
h_{av}	individual sub-panel depth on either side of the longitudinal stiffener in question
θ	angle of inclination of the tension field in the web plate
θ_d	angle of inclination of the diagonal of the girder web plate
I_s	moment of inertia of the effective stiffener section (including effective width of web plating) about an axis parallel to the girder web plate
I	moment of inertia of the cross section about the neutral axis
I_f	second moment of area for the girder flanges
k_1	reduced critical buckling coefficient accounting for the detrimental effect of web perforations
k_o	critical buckling coefficient for an unperforated web plate in shear

k_o $= \begin{cases} 8.98+5.6\,(h/b)^2 & \text{for} \quad \alpha > 1 \\ 5.6+8.98\,(h/b)^2 & \text{for} \quad \alpha < 1 \end{cases}$ (clamped boundary conditions)

l anchoring length of reinforcement for rectangular cutouts

L_r $(= b_o + 2l)$ length of opening reinforcement on the web plate

M_p $(= \left(b_f\, t_f^2\, \sigma_{yf}/4\right)\left(1 - P/P_o\right)^2)$ of the compression and/or tension flanges when these are of equal dimensions, and including any reduction due to axial/bending loads acting in their cross-section

M_p^* $(= M_{pf}/h^2\, t\, \sigma_y)$, non-dimensional flange rigidity parameter

M_{pc}, M_{pt} plastic moment capacities of the compression and tension flanges respectively

M_{pr} plastic moment resistance of the reinforcement of the cutout

M_{pw} $(= 0.25\, t\, h^2\, \sigma_y)$ plastic moment capacity of the web

M_y bending moment required to produce yield in the extreme fibre of the compression flange assuming a fully effective web

n Ramberg-Osgood's exponent accounting for material heat-treatment and hence for various aluminium alloys

P applied compressive force on girder flange

P_o $(= b_f\, t_f\, \sigma_{yf})$ squash resistance of girder flanges

P_1 concentrated load acting on a bearing stiffener

r, r_{max} distance and maximum distance (when at the corner) of the centroid of the opening (whether circular or rectangular) from the centroid of the web panel

$\sigma_{0.2}$ proof stress of web material, used in the expression in place of yield stress in the strength expressions, if the parent material is an aluminium alloy

σ_t^y level of tension field action to cause yielding in the web plate

σ_y yield stress of web plate material

σ_{yf} material yield stress for the girder flanges

σ_{yr} yield stress of reinforcement material

τ_{cr} critical buckling stress in shear

$\tau_{cr,mod}$ reduced shear critical buckling stress of a web plate due to the presence of a web perforation

τ_y $(= \sigma_y/\sqrt{3})$ shear yield stress

t web plate thickness

t_f thickness of girder flange

w	percentage of strength reduction of heat-treated aluminium material due to HAZ softening, relative to parent, unaffected material strength
w_r, t_r	width and thickness of the cutout reinforcement
V	average value of the shear force acting on the web panels and assumed uniformly distributed
V_u	ultimate strength of unperforated web plate in shear
V_y	$(=(\sigma_y/\sqrt{3})\, d\, t)$ shear force causing yield in the girder web
V_v	Vierendeel shear load
V^e_{ult}	ultimate strength of a web plate in shear in the presence of an eccentric (to the tension diagonal) cutout

E. Notation for the Design of Cylindrical Sections

Figure 4.61 may be consulted for additional information on the notation of the geometry of ring framed cylinders. This section also accounts for terms relating to stringers, cones and dome ends.

A	$= A_s \left(R/R_s\right)^2$, equivalent frame area at shell
A_s	cross sectional area of ring frame, or, cross sectional area of stringer stiffener, in design of orthogonally stiffened cylindrical sections
αL	$1.285\, L/\sqrt{R\, t}$
γ	$(= A\,(1-0.5\,\upsilon)/(A + t_w\, t + 2\,N\, t/\alpha))$
C_n	out-of-circularity in the nth mode
δ_p	mean amplitude of interframe initial shell distortion of the plating radially towards the stiffener, $(\delta_p/t \approx 0.1)$
d	overall depth of ring frames
E	material Young' modulus.
G	$(2\,[\sinh 0.5\alpha L \cos 0.5\alpha L + \cosh 0.5\alpha L \sin 0.5\alpha L]/(\sinh \alpha L + \sin \alpha L))$ transcendental function of αL (Fig. 4.62)
η	weld tension block parameter depending on weld conditions
θ	semi-angle of conical transition joint
I_c	second moment of area of combined stiffener plus effective length of shell about the neutral axis parallel to the shell
I_{ec}	second moment of area of stringer plus reduced effective width of shell, s_e
I_z	second moment of area of ring frame alone about its weak neutral axis
λ	$(= \pi\, R/L)$
λ_c	$(= \pi\, R/L_c)$
L	$(= L_s - t_w)$ unsupported shell length between ring frames
L_c	compartment length for general instability
L_e	effective length of shell $= 0.75\, L_s$ or $= 1.56\sqrt{R\, t}$ or $= 1.556\sqrt{R\, t}\, N \Big/ \sqrt{\sqrt{1 + \frac{n^4}{2}\left(\frac{t}{R}\right)^2} + \frac{n^2}{\sqrt{3}}\left(\frac{t}{R}\right)}$ Bijlaard's expression
L_s	ring frame spacing
N	$(=(\cosh \alpha L - \cos \alpha L)/(\sinh \alpha L + \sin \alpha L))$ function of αL (Fig. 4.62)

m	number of half waves between ring frames
n	number of complete buckling waves around the circumference
o-o-c	out-of-circularity
p_b	$(=\sigma_y\, t/R)$ external radial pressure to an infinitely long, unstiffened, perfect cylinder which results in the hoop stress reaching the material yield stress level (boiler pressure)
p_{c5}	$(=p_b/(1-\gamma G))$ pressure at which the applied hoop stress at mid-bay and mid-thickness reaches the shell yield stress
p_{cl}	$\left(=\left(2/\sqrt{3\left(1-\upsilon^2\right)}\right)E\left(t/R\right)^2\right)$ elastic buckling pressure for spherical shell, by van der Neut
p_d	design pressure
p_n	Bryant's expression for general instability of ring stiffened cylinders
p_{nf}	elastic collapse pressure for the shell and frame combination by Bresse
p_{ns}	shell buckling pressure of ring stiffened cylinders in overall collapse mode of failure
p_{sy}	pressure to cause yielding in the centroid of the ring frame
p_m	elastic buckling pressure for the unsupported shell between ring-frames $=(Et/R)\left[n^2-1+k\,\lambda^2\right]^{-1}\left\{\left[n^2\lambda^{-2}+1\right]^{-2}+\left[t^2/12R^2\left(1-\upsilon^2\right)\right]\left[n^2-1+\lambda^2\right]^2\right\}$ original von Mises expression after Kendrick's alterations, where k=0.5 for hydrostatic pressure and k=0 for radial pressure $\left(=\left(0.919\,E\left(t/R\right)^2\right)/\left(\left(L/\sqrt{(R\,t)}\right)-0.636\right)\right)$ least value by Windenburg
p_{yf}	$(=(p_b\, R_f/R)/(1-0.5\,\upsilon-\gamma))$ pressure at which the hoop stress in the flange of a ring frame reaches yield level
p_{ys}	$(=2\,\sigma_y\, t/R)$ membrane yield pressure for a spherical shell
p_{ym}	hydrostatic pressure at which the von Mises equivalent stress (of axial and hoop stress) at mid-bay and mid-thickness of the shell reaches the material yield stress
ρ_h	$\left(=0.134\left(\sqrt{LR}/t\right)^{0.407}\right)$ knockdown factor as used by Cho/Frieze for hydrostatic pressure
R	mean shell radius
R_f	radius to the centroid of the flange of the ring frame
R_m	mean radius of shell in the conical transition joints
R_s	radius to the centroid of ring frame
R_x, R_θ	ratio of applied axial and hoop stresses to yield stress

r	$=\sigma_{rc}/\sigma_y$ ratio of residual compressive stress to material yield stress
σ_{rc}	residual compressive hoop stress induced in the shell due to across and along the weld shrinkage
σ_{rc1}	compressive hoop stresses in the shell induced by the along the weld shrinkage
σ_{rc2}	compressive hoop stresses in the shell induced by the welding distortion of the plating radially towards the stiffener occurring due to across the weld shrinkage
σ_T	elastic tripping stress of ring frame
σ_y	material yield stress (or 0.2% proof stress for aluminium alloys)
σ_{yf}	yield stress of the ring frame flange material (or 0.2% proof stress for aluminium alloys)
σ_{ys}	yield stress of the shell material (or 0.2% proof stress for aluminium alloys)
s	stringer spacing
s_e	effective stringer spacing in the post-buckling range
t	shell thickness
taper	$R_2 - R_1/R_2$ where $R_2 > R_1$ for a conical section
t_w	web thickness of ring frames
υ	Poisson's ratio
ϕ_x	ratio of ultimate axial compression stress to yield stress
ϕ_θ	ratio of ultimate hoop stress (corresponding to interframe shell collapse pressure) to yield stress
$\bar{x}$	distance of stiffener flange from the effective neutral axis
Z, Z_L	$(=\left(L^2/Rt\right)\sqrt{1-\upsilon^2})$ Batdorf parameter
Z_s	$(=\left(s^2/Rt\right)\sqrt{1-\upsilon^2})$ Batdorf shell width parameter

CHAPTER 1

1.0 Introduction

The best indication of the level of development of a country is the infrastructure and efficiency of the domestic transport system and the quality of links with the international physical distribution network. A high quality transportation system, encourages human travel, the exchange of ideas and experiences, supports better understanding between nations and geographical regions and provides a major boost to trade and industrial development. Indeed, worldwide economic growth has been and will be accompanied by an increase in the manufacturing of high-value-added products and international expansion of production bases, resulting in, and based upon, increased cargo movement. To cope with these changes, new means offering high-speed, high volume cargo transportation capabilities are needed. Conventional air and marine cargo carriers are not satisfactory as they both lie on either end of the speed-capacity range of requirements. Fast marine transportation can provide a middle of the road solution by blending to the extent required, high carrying capacity with increased speeds.

Therefore, the modal shift from land to marine transportation becomes increasingly attractive especially as land networks are experiencing tremendous congestion problems worldwide. Trailer transportation 'bottlenecks' highways and when coupled to the dramatic increase in the number of cars on the roads results in traffic congestion and environmental pollution. In addition, the railway system in Europe and around the industrially developed countries, is overloaded, and considering that there is a limit to what can be carried by air, fast marine transportation seems to be the solution.

1.1 The Case for Fast Sea Transportation and Prerequisites for Success

The success of a fast marine transportation service depends on the balanced satisfaction of the client requirements, the shipowner's/operator's technical and financial constraints and the governmental or inter-governmental policies. These individual demands are described next.

1.1.1 The Passenger's Viewpoint

From the passenger's point of view, fast marine transportation can only

compete with the other means of transportation on the basis of

- speed
- economy
- availability and frequency of service
- comfort.

One cannot identify a specific level of passenger acceptance for each of these elements, and the optimum solution, although very dependent on personal preferences, should be a balanced compromise of the above. This is obvious as the *time* of travel is more important for a passenger over short routes while over longer routes the issue of travel *comfort* and seasickness dominates preferences more. The passenger requirements are also expected to vary if the passengers are frequent or occasional travellers and are walkers, drivers or bus users. For example, for *frequent* travellers, whose travel distance is normally 1-25 nautical miles, fast marine transportation has no serious benefit as the routes and hence travel duration is anyway small and is perhaps more dominated by the incompressible time spent in port. The lower limit on travel duration really depends on maneuvering times which tend to cancel out the beneficial effects of extra speed on crossings that require less than one hour of actual navigation time. On longer routes an increased service speed can have greater impact.

On the other hand, *occasional* travellers, which are mostly found in longer routes, have different requirements. If on foot, the passenger has the option of fast trains on land or air transport, and hence time is of essence. 'City centre to city centre' connections become more important for distances up to 100 nautical miles while for larger distances where air transport becomes competitive, the ability of efficient links with the rail, road or indeed the air transport systems are of paramount importance. The fare as well as the relative waiting time prior to departure and after arrival will also play an important role in choosing sea transportation rather than air over long distances. Car drivers however, are more certain customers as neither rail and certainly air transport offer fare efficient transportation of the car. What they are mostly interested in is the time of their travel, although they might opt for the longer overnight conventional ferry crossings which provide more comfort and a large variety of on board entertainment. The fast craft, 'airline style' transportation is not necessarily attractive as it will restrict the passengers to their seats for safety reasons, the feeling of boredom increasing

with the duration of travel. Airline style entertainment can help in alleviating this problem but not as effectively as on the overnight ferries.

More specifically, current trends in traditional and fast *ferry* transportation indicate that the longer the crossing the more passengers tend to choose a fast ferry [1]. Indeed, a market research study on a conventional ferry on a crossing between Italy and Greece [2] showed that 96% of the passengers would travel with a fast ferry if the time of travel was halved at the same fare. This percentage would drop to 85% if the travel were to be undertaken by the passengers indoors (due to high speed) and hence confinement problems would be of greater importance. Small crossings will not be faced with this problem. In terms of fare costs, a large percentage of passengers would be prepared to pay 10% extra for a faster service while only 30% would be prepared to pay 25% extra!. It is worth noting that currently fares charged by ferry operators for fast craft services are about 10-20% more than those charged for passages by conventional ship [3]. Comfort and availability of service were assumed to be as found on current conventional ferries.

It therefore looks likely that fast sea transportation will face competition in the longer routes (150/200 nautical miles) where the overnight ferry provides the opportunity to transform the crossing to an overnight mini-cruise. The shorter routes (50/150 nautical miles) are expected to be dominated by fast marine concepts. Such routes are indicated in Table 1.1 from where the potential for use of advanced marine concepts in Europe is obvious. The northern European routes are more attractive than the southern mainly because of the relative density of the population and the difference in economic development. The routes in the south have the disadvantage of being longer but are less frequent which, when coupled with the influx of tourists from the north to the south, provides a considerable potential for development in this geographical area as well.

1.1.2 The Operator's Viewpoint

Shipowners are slow to embrace fast marine transport, mainly because the technology is largely untried and its financial and technical reliability is not well established yet. Despite this understandable view, some financial advantages on both the initial cost as well as the operational costs are possible. The higher *initial costs* arise primarily from the requirement for a

larger and more powerful power plant, or indeed duplication of power plants (in the case of multi-hull vessels) may well be balanced, if not cancelled out, by the more standard and simplified accommodation arrangement observed in fast craft. After all the avoidance of overnight services (a direct result of high speed and proper management), eliminates the need for passenger and crew cabins, hence reducing the initial investment in hotel and catering service equipment. According to Dobler [4] the initial cost may be 3-4 times lower than for a conventional ship with the same daily carrying capacity. Of course, the consideration of faster speed and the investment into a more powerful and expensive power plant, will also be affected by the operational window of the vessel, as well as on the ability to maximise the ability of extra speed by adding extra trips a day to the ship's schedule. Machinery reliability then becomes important.

When considering *operating costs*, fuel expenses which are closely associated with engine fuel consumption and bunker prices will certainly discourage the choice of a more demanding high speed vessel. Technical considerations affecting the final choice are described in paragraph 1.3. Such considerations have to be properly balanced by the possibility of crew reduction and the associated cost saving that a high speed vessel has to offer. For example, a 450 passenger fast craft vessel can be safely operated by 15-20 crew, while a conventional vessel for the same number of passengers would employ 90-120 staff depending on the importance of the catering services on the vessel's operation [4]. Additional fare earning space will result as well.

Apart from these purely economical considerations, the choice of an advanced marine vehicle in place of the traditional monohull, will also depend on more *practical* and *operational* factors.

Although the ships must be designed to match the sea conditions in the geographical area(s) of interest, their motion response should lie within the passenger's acceptance levels of comfort (usually 0.1g acceleration level). Frequent travellers are more tolerant but it must be remembered that experience from the transportation of military personnel is not necessarily indicative of the behaviour of civilian passengers. Apart from ship design factors, psychological aspects will also contribute to the passenger's feeling of comfort or discomfort. Passenger dissatisfaction will be precipitated by confined spaces, which when coupled with the long-term exposure to

seasickness may drive passengers away from a particular ship type and indeed service. The absence of on board entertainment (in the form of food, drinks, shops, i.e. 'aircraft type' entertainment) will accentuate the problem. In other words, one might be tempted to conclude that the operator's contribution would be to 'tame' the interrelated effects that the various technical, economical, and 'human' parameters in a way that will guarantee the attractiveness of the service. Hence, whether a distance is considered long or short for the application of advanced marine vehicles, will depend on the actual speed, bunker capacity, passenger facilities, and passenger habits all of which will determine the time the passengers are willing to remain on board. The catalytic effect that space and variety of on-board activities available to the passengers have on the aforementioned decisions and considerations should not in any case be underestimated.

Operational considerations require the selection of suitable sealanes for the vessel's operation, a selection closely linked with the selection of the port and terminal location and vice versa. The final choice will depend on the ship's size, the maneuvering characteristics, the traffic density and pattern as well as the regulations controlling the specific sealane. Obviously, it will be inefficient to select a port that will restrict the vessel to operate within sealanes of high traffic density and/or of considerable speed limit restrictions. Smooth connection of ports and terminals to the remaining transportation infrastructure is essential for guarantees on the fast and efficient transit of passengers and cargo to be made. This is only achievable by proper organisation and upgrading of facilities at the terminals. The considerable financial capital investment required for the construction of new infrastructure for the land transportation systems, could be drawn either locally or introduced through a wider governmental or inter-governmental policy on transportation.

1.1.3 The Governmental Viewpoint

Government policies on fast marine transportation, at least in Europe, are directly affected by the new status introduced through the 'European Union'. The removal of national barriers within Europe is revolutionising the transport market which now has to meet the changing patterns of trade and customer requirements. The free and efficient movement of goods, people and services is one of the three (together with energy and telecommunication) policies expected to lead to European integration and

encouraged by the *Trans-European Networks Programme*. Indeed, approximately ECU 220 bn has been allocated for transport infrastructure projects over the next few years [5]. The purpose of this programme is to interconnect the national networks and link island, remote and peripheral areas with the more central areas of the Union. However, the new transportation networks have to be balanced, efficient and environmentally friendlier, in order to avoid rerouting traffic to areas where congestion and pollution is already a problem. This will also encourage the positioning of industrial complexes away from densely populated areas. Unfortunately though, the phenomenon of modal shift form land to sea transportation observed in Japanese government policy (e.g. Techno-superliner project), is far from applicable to Europe, especially as it is against the 'free competition' spirit. Active national government/Commission intervention which would require a transportation modal shift is discouraged as it may eventually prove discriminatory over other transportation modes. Even if environmental considerations demand such a shift, the problem exists of deriving a formula by which fast craft shipping is promoted but not against other means of transportation, whether sea. land or air. Free competition between the various modes of transportation is expected to remain the rule of the game for Europe.

1.2 Economic Considerations and Future Prospects

Having established the 'rules and limitations' under which advanced marine vehicles will have to operate, it is perhaps worth concentrating on the available prospects for their widespread application. Over the last few years the market for different types of high speed vehicles for both passenger and passenger/car transportation is witnessing a considerable growth reaching nearly $ 500 million in 1993 [6, 7]. This general growth trend which commenced in the early seventies is demonstrated in Figure 1.1 while the number of each of the types of high speed marine vehicles delivered in the period of greatest growth (1988-93) is summarised in Table 1.2. Recent increasing orders for large high speed ferries, e.g. HSS catamarans from Finnyards for Stena, Incat wavepiercers for Condor and Stena etc. (Table 1.3), indicate that this growth will continue. But the rate at which this will occur is greatly dependent on the ability of the industry to guarantee reduced economic and technical risk and enable concept comparison by the definition and standardisation of appropriate performance parameters. This is currently not the case as demonstrated in paragraph 1.3.

In general, the fare level is of primary importance to the success of a fast marine service and proper market research should ensure that it remains competitive with that of other transport systems. Figure 1.2 demonstrates the considerable difference in fares among air, sea and land transportation (in japanese yen). Although the lowest fare level (irrespective of travel medium) tends to increase with service speed, fast sea transportation is clearly unable to compete in fares with any other means of transport. The fares are third only to those of the helicopter and the Concorde. Furthermore, despite the reduction in the level of unit fare (L, price per unit travel distance) observed in all modes of transportation for increasing distance travelled (Fig. 1.3), fast craft are still expensive but more attractive than ultra-fast trains and airplanes. A comparison of the normalised operational cost of the individual transport systems with the unit fare (Fig. 1.4) is even more discouraging. In terms of operational costs, the most competitive means of transportation is the ultra-fast rail link for the complete range of distances travelled while other land transport systems are equally attractive for distances approximately up to 200 km, above which air travel takes over. Fast craft are however seen to be operationally cost efficient than the traditional ferry services. It must be remembered that the aforementioned figures and comments can be affected by national government policies on transportation and should therefore be treated only as indicative of the time the study [8] was undertaken (1992-1993). What one may conclude though is that fast marine transportation remains an expensive and costly service and its success will have to be based on routes where the vessels will not be expected to compete with conventional transport systems. Island or inter-island sea routes thus become attractive.

If set more simply, economic success depends on the ability of the service to generate a high return in relation to their mass. Humans are an ideal dense cargo as they load and stow themselves, take up low amount of space and even increase revenue by buying goods on board. Cars on the other hand, are not as attractive as they weigh approximately 15 times more then a passenger, take up more space than a human, do not buy duty-free goods and are not expected to contribute proportionately to the fares paid. Hence, the service of car transportation is there to satisfy the customer requirements rather than to provide additional revenue for the operator. The transportation of freight in standard containers is even a greater problem with regards to its weight and handling costs.

Not surprisingly, as the payload capacity decreases with increasing speed (Fig. 1.5), the current trend is towards small, passenger carrying, fast craft. It is therefore obvious that for fast cargo vessels with increased payload demand and intended for longer routes, new, *large displacement solutions* must be considered. The more weight sensitive and hence complex design concepts are closely associated with high speed and payload limitations but for *large ship sizes* the simpler concepts are likely to be preferred [9]. For fast, large displacement (e.g 12,000 tonnes), cargo carrying craft, catamarans are seriously being considered in addition to SESs which are also attractive due to their operational efficiency. However, the complexities and design limitations of the systems supporting the air-bubble means that their maximum payload would be rather restricted relative to the catamaran option. For displacements up to 6,000 tonnes [9] they remain an attractive option and have been tried for payloads of 1,000 tonnes via the TSL project in Japan. For smaller sizes of vessels, where cargo payload capabilities are not usually a requirement, advanced technological concepts like hovercraft, foil-catamarans, SESs and WIG aircraft will be of much better value for the passenger transportation market. The question of passenger safety will have to be addressed very carefully though.

In terms of transport efficiency, SES and hovercraft achieve the highest values (Table 1.3), despite their higher initial cost and the difficulties in the development of lifting systems for larger size craft (higher than 120m, 3000t full displacement). Catamarans are generally viewed as having the greater potential for size increase, especially as they are able to reach transport efficiencies close to those of hovercraft. Recent orders (the Stena HSS) underline this prospect. Although the transport efficiency for SWATH ships does not seem to deviate from that of the monohulls [3], their speed is restricted to about 35 knots, since the resistance of such types increases more rapidly above this value. Fast monohulls were found [3] (Table 1.3) to possess slightly lower transport efficiencies than those achieved by catamarans and provide equally great potential for size increase as catamarans do. After all their construction is a lot easier and cheaper than that of multi-hull vessels.

Fast sea transportation is not just a question of sailing at high speed. It is also a question of upgrading or establishing new transport *systems* where ships, shore facilities and management services are all geared up and appropriately tuned for the speediest and more efficient operation. As costs

at the port interface have been identified as normally lying between 50-80% of the sea freight [5], the efficiency of *port operations* are of tantamount importance. By reducing the time of cargo/passenger handling in port, the time spent at sea can be increased (if operational strategies permit), the resulting lower speed requirement having 'knock-on' effects on propulsion machinery, fuel costs and eventually payload capabilities. The possibility of speed reduction will reduce freight rates (or increase profit margin). If however, speed reduction in transit is not a strategic aim, freight rates can still be reduced from the increased frequency of departures and the increased cargo quantities per day thus carried.

Reduction of time in port would require an investment in cargo/ passenger handling facilities which should also be properly and smoothly linked to road, rail or even air services. Terminal installations will therefore have to be especially designed to accommodate the geometrical characteristics of the vessel and its operational pattern, allowing the fast and safe berthing and unloading of passengers, cars and cargo. Cargo handling on board the vessel should be reduced to the minimum necessary and completed in the port area while intermodal transportation between the manufacturer and the customer using the same cargo unit all the way is becoming more and more important. Extensive application of electronics and image recognition systems for faster handling of documentation and customs clearance will speed the process considerably. On-land reception facilities should be characterised by the constant availability of services, their reliability, punctuality and adaptability to customer needs, simultaneously maintaining high safety standards. Airport traffic management may well prove a helpful guide towards any necessary changes and adaptations.

1.3 The Comparison of Advanced Marine Transportation Concepts

The classification of these advanced marine vehicles is based on the means by which both buoyancy and speed are generated and is described in greater detail in Appendix 1.1. Figure 1.6 demonstrates the relation between the various forms of lift, the sizes roughly indicating the numbers of vessels of the individual concepts existing worldwide. The current trend is more towards hybrid solutions combining two or all three of the lift forces, the most popular being the surface effect ships.

In trying to identify what is meant by 'small' and 'high speed' no widely

accepted agreement is available. Instead the view of the Committee V.8 of the 1994 ISSC [10] may be used as indicative, which incidentally is based on an earlier proposal by Blyth [11]. It is recommended that an upper limit to the displacement factor $(\text{tonnes}/(L\times B)^{1.5})$ of approximately 0.04 will identify a 'small' vessel while a minimum limit on the volumetric Froude number $(V/(g\times\nabla^{1/3})^{0.5})$ of approximately 1.0 (Fig. 1.7) will imply a 'fast' one. Apart from identification and categorisation difficulties, the evaluation of relative performance is hindered by the lack of worldwide standardisation in the description of parameters which would allow the owners, operators and even the banks to evaluate the performance and economics of the various design concepts.

It is difficult to establish a methodology for effectively evaluating and comparing the performance of advanced marine vehicles, due to the large variety of criteria (35 in number presented in [12] and some in [7]) and concepts available. Any combination of criteria can be inadequate or misleading unless a particular service requirement and/or operational characteristics are identified for which the optimum design for each type of craft will then be obtained. This difficulty is best demonstrated if one compares a SWATH ship with a monohull. If the criterion is set to be the payload (or displacement), assuming the same speed and endurance, the SWATH ship will be larger and more costly (appro. 20% [13, 14]) than a monohull. This cost difference is not necessarily due to the more complex construction methods but mainly due to the larger weight fraction of the SWATH that would require a larger structure for the same payload capability. On the other hand, if the criterion is seakeeping performance a monohull having equivalent seakeeping performance to a SWATH would be 29% bigger and cost 27% more [14]. As it is obvious that preferences will change if the criterion is changed, Betts [13] recommends the comparison to be made on an 'equivalent mission' basis. This implies considerations, appropriately weighted to relative importance, of payload, speed, operability, production cost, manning, operating costs, overall availability, and turn around times.

Lang and Slogett chose to compare the various fast marine transportation concepts by their calm water performance and the effect of waves on the performance, transport efficiency, motions and operational capabilities. Figure 1.8 compares the non-dimensionalised drag coefficient C_d/E

$(=2\,D/(\Delta^{2/3}\,\rho^{1/3}\,V^2))$ with the Froude number for a variety of marine craft in calm water. D is the drag force, E is the propulsive efficiency, V is the vehicle speed, ρ is the fluid density and C_d is the drag coefficient. The figure indicates that the SWATH concept is superior to the other vessels for Froude numbers within 1.2-1.5 and superior to monohulls and catamarans in the range 1.5-2.2. Although the propulsive efficiencies of SWATH vessels are higher than those of monohulls, the higher wetted surface in the former results in drag coefficients at the lower Froude number range which are 70%-75% greater than that of monohulls. However, SWATH vessels have much less wavemaking drag than monohulls so their values for C_d/E tend to be lower than those of monohulls in the transition region between the displacement and planing operational modes. In rough water the performance curves of the SWATH vessels and hydrofoils would not change appreciably but those of the other vessels would rise considerably especially in the higher seastates. Figure 1.9 demonstrates the advantage in powering requirements that SESs have over the other types of vessels and especially over SWATH vessels which seem to be the most demanding type in this respect.

In rough weather, it is the reduction in speed in waves as well as the level of vertical acceleration that can characterise the performance of a vessel. Figure 1.10 shows the wave effect on reducing the speed of various vessel types. The SWATH and hydrofoil remain nearly unaffected by waves and are expected to operate at much higher seastates while monohulls, SES and hovercraft suffer considerably. The air-bubble loss occurring at high sea states is to blame for the considerable reduction in speed observed in hovercraft and SESs. All other types of vessels suffer a less dramatic drop in speeds. Generally, SWATH and hydrofoils exhibit much less acceleration (limit of comfort 0.1g) in waves than hovercraft and SES. (monohull acceleration limits would be expected to lie between the two sets of craft but closer to the monohulls and the SES [15]. Table 1.4 presents data for existing hovercraft, SES, hydrofoils and SWATH vessels showing that waves significantly reduce the transport efficiency (this time expressed in terms of passengers) of the hovercraft and the SES craft but not those of the hydrofoil and the SWATH vessels. In the smaller waves the hovercraft and the SES are the most efficient of the four concepts but for the larger waves the SWATHs and the hydrofoils take over. When the vertical acceleration of the vessels midships is considered (Fig. 1.11), the superior seakeeping characteristics of the SWATH concept become apparent, with a considerably

low acceleration relative to all other fast craft types. The deep-V monohull is the second best type in this respect with the monohull providing the worst comfort on board.

In general, it is the ability of a concept to carry out a pre-specified operation and the criterion of performance for that task that will be the ultimate and most accurate indication on which the final selection should be based.

1.4 The Technical and Strategic Challenges

In the years to come, high speed marine transportation will be of increasing commercial importance for both passenger and cargo transportation and is therefore expected to become part of everyday life. However, the combination of the revolutionary developments in basic technologies required and the considerable involvement of larger industrial groups is expected to change the fast maritime industry from boat-building to a highly international in basic technology and operation, 'aviation-type' industry. The resulting challenge to technical and operational expertise will require close co-operation in many areas, both nationally and internationally.

The main hurdles to be overcome for the widespread application of advanced marine vehicles are generally of research and development, operational and industrial nature. *Industrially,* the technology has to overcome the obvious disadvantage of the high initial investment cost and the great risk involved in it. The obvious cost of prototype construction and the uncertainty in the market volume that would otherwise guarantee the investment are adding considerably to the problem. In the *operational field,* the large liability of the human factor to marine accidents needs to be effectively controlled, especially as the speeds are now much greater leaving no room, or time, for corrective actions or mistakes. Hence, improvements and international standardisation on training and crew communication procedures, standardisation of operating compartments and development of effective navigation and coastal traffic systems, are essential to guarantee the small numbers of accidents enjoyed by the aircraft industry. Even the level of competency as well as evaluation of the crew should perhaps approach those requested by the aviation authorities. *Research and development* efforts are currently concentrating on the load, response prediction and motion control for individual designs, as very well demonstrated in [loc. cit. 8, 1993]. The driving force behind this research is the need for the

development of computational fluid dynamic-based tools that will substitute time consuming and relatively more expensive model test data. The latter are of course essential for the validation and calibration of the computer codes currently actively pursued worldwide (Japan, Korea, Germany, United Kingdom, Norway) for a variety of fast craft types. More details on these projects are available in Appendix 1.2. Structural design of these vessels should be supported by a fresh look into current codes and procedures. The uncertainties in loading and construction, coupled with the lack of experience and the need for light-weight structures, encourages a shift from the deterministic, allowable stress approaches to a reliability-based, limit state representation of structural capacity. The specific research and development needs are very well outlined by Faulkner and the reader is referred to [16, 17, 18] for further information.

Apart from 'structural' aspects, the efficiency of propulsion and machinery systems requires considerable research and development input [19], especially as they will have to abide to stricter regulations on emissions and a variety of operational requirements. The large number of machinery failures observed in DNV classed vessels (Fig. 1.12), suggests that machinery reliability at highly competitive environments is still a problem.

Although a recent visit to Japan and Korea of a number of UK experts on fast marine transportation [9, 20, 21] confirmed that the West can compete at the technical level with the Far Eastern builders in this emerging field, it also concluded that there are still lessons to be learnt on the organisation or re-establishment of the R&D rules of competition between national industries to enable them to effectively compete at the international stage. *A long-term* strategy based on partnerships, rather than short-term collaboration that would result in bitter competition in one or two years time, seems to be the policy of the Far East and looks the only way forward. Government fiscal policies characterised by co-operation rather that protectionism, coupled with a sound transportation policy aiming in the years ahead will greatly encourage inter-firm collaboration. In Japan, such a 'nationalistic' approach to industry is possible and is strongly encouraged by a strong governmental commitment to a modal shift to sea transportation and the presence of a local market for the new technology. As already described earlier (para. 1.1.3) under European Union laws this is not possible, following a more 'European' policy, with its disadvantages in

terms of organisation and effectiveness. After all the Far Eastern yards seem to be quite happy in dictating the future trends rather than following suit developments imposed on them by their international competitors.

However, irrespective of any actions at the political and strategic levels, success is also greatly dependent on the existing organisation and industrial culture. The belief in continuous improvement, teamwork, and workforce commitment to long-term company objectives, have proved to be extremely successful in all industrial sectors in the Far East for so many years, and is believed will be the factors that will decide on who will eventually control the market of Fast Marine Transport Vehicles.

1.5 Aspects of Structural Design of Advanced Marine Vehicles

The number of repairs carried out worldwide, on the existing fleet of fast craft can provide an indication of the designer's experience on matters of structural material selection, the adequacy of available load estimation procedures as well as being informative of the degree of shipyard qualification in carrying out the complex construction tasks required, the adequacy of classification rules and, nonetheless, the operational habits of the owners. According to Wiklund [19], those damages that have to be repaired back to the original standard, are not due to poor design, but due to structural overloading. When however the structure has to be improved or rewelded, it is poor design or workmanship by the yard that are to blame. Reinforcement of the structure will almost certainly imply inadequacy of classification regulations. Based on these comments and with reference to Figure 1.13, one may conclude that most failures are due to load prediction methods and that the available technology is still under development. It is unfortunate that a 'learning from damages' approach is difficult to achieve by the present classification and operation system. A lot of in-service experience, and significant information on structural damages is either 'swept under the carpet' for reasons of maintaining the image of service reliability, or simply because a significant number of vessels are deleted from the class after one or two class periods and their repair records are either incomplete or lost.

As a first step in improving the reliability of the fast marine structures one needs to have a fresh look at the design practices currently used. Two methods for structural design are generally available, *design by rules and*

design from first principles. The advantages of *rule-based design* of ease of application and the very near lack of expertise required to apply them, is overshadowed by the general nature of their application to the variety of fast marine concepts, without the support of any extensive in-service experience and data. Although the guidelines draw from the extensive experience on the more traditional means of sea transportation, the specific needs of fast marine vehicles are obviously not sufficiently addressed and hence any design recommendations and load estimations for these cases will not be much different than educated guesses! Perhaps not surprisingly, these empirical methods of load estimation and scantling derivation should also not be expected to act in the interest of construction or indeed weight saving. Any individual seaway load and response estimations, no matter how detailed and accurate they are, they will have eventually to stand up to the test of the regulator's empirical but conservative predictions, a test at which the most conservative predictions usually prevail. The risk of overdesign or indeed under-design is always present.

As Faulkner [16] points out, the design rules for small fast *monohulls* have *evolved* slowly through the experience of the world's navies although this is not the case for multi-hull forms. For these concepts, the regulations have not *evolved* but simply have *'mushroomed'* within brief times, primarily in response to market needs, and thus following developments instead of dictating them. The lack of design and operational experience for these craft has added to the problem which resulted in regulations [22-27] that demonstrate inconsistencies in their load estimation procedures [28], account for the structural slenderness in a conservative manner rather than using ultimate limit state criteria, and introduce non-uniform levels of safety in the structural components. DNV are considered to be the most comprehensive, having spent more time and investment than any other classification society in researching the loads and structural response of these craft types. But usually such efforts are carried out in support of a wider national research collaboration. A brief review of the major national research and development efforts worldwide are presented in Appendix 1.2 and form considerable input to the current review of the IMO regulations concerning these craft. The previous Code of Safety for Dynamically Supported Craft adopted in 1977 is being substituted by the Code of Safety for High Speed Craft with a renewed safety philosophy which is based more on a risk analysis approach coupled with the traditional philosophy of passive protection in the event of an accident. Human factor engineering, active

safety systems, quality management risk assessment all now become important aspects. The weight sensitivity of the fast marine structures has been recognised and permission is granted for the use of non-conventional lightweight materials on the basis of maintainance of the same safety standard as required from the traditional ships. Stringent navigational and operational requirements are also imposed in view of minimising the risks of collision at high speeds. More details and the outline of the new IMO Code may be obtained from [29].

From the above discussion, it becomes obvious, that a *first principles approach* to design would be more suited to the random requirements and operating profiles of individual fast craft designs and routes. This approach also suffers from the lack of relative service experience of similar sizes and types of vessel, the lack of detailed information on the use of more exotic materials, and the presence of unknown loads and structural responses. The complexities encountered in 'first-principle' design are:

- proper material selection to address the structural requirements of the specific application
- accurate estimation of primary and secondary loads
- limit state strength modelling should be used to account for the post-buckling behaviour of structural elements especially as the slenderness and complexity of structural arrangements and failures by buckling and/or fatigue are increasingly probable
- rational review of the safety factors used in design is essential, to accommodate the larger uncertainties in fast craft structural design. A probabilistic approach to their derivation is more appropriate (para. 1.5.3)
- cost, weight and construction requirements tend to impose conflicting requirements
- the need for expensive, full scale structural testing for novel design concepts, is essential to establish the level of stress loads in the structural components.

Such considerations may only be addressed by a reliability-based, limit state structural design approach, consisting of four stages; (a) development of accurate load prediction tools, (b) limit state modelling, (c) probabilistic modelling and (d) reliability evaluation. These are briefly presented in the following paragraphs.

The main *advantages of a probabilistic approach* to structural design is that, via the introduction of appropriate partial safety factors, it provides consistent levels of reliability over a range of different design situations (loads and structural elements) and hence the large differences in implicit safety levels for different failure modes in a structure are eliminated. The provision of a framework for sensitivity measurements and the implied use of partial safety factors allows the more rational and explicit consideration and evaluation of uncertainties associated with the individual design variables (e.g. loads, material properties and strength modelling). This is particularly useful for novel designs for which the ability for comparison of alternative designs is missing. The generation of designs that are efficient in terms of structural weight and safety is thus possible. In addition, the acceptable risks of failure can be adjusted to the consequences of failure. The determination of efficient and more economical inspection and repair strategies (e.g. determination of frequency of inspection/repair, warranty clauses, spare parts requirements etc.) is also possible [30, 31]. Hence, new design concepts can be created with relative confidence and without prior need for large scale experimental tests which are expensive and time consuming. On the other hand, the main disadvantages are 'user' orientated as statistical concepts are alien to engineers. The designer is required to 'see' and treat the variables as random and not as of fixed, deterministic nature. Such a change in fundamental thinking requires training and time.

1.5.1 The Evaluation of Applicable Load Actions

Loads for high speed vessels are both local and global in nature and their values are a function of the of the vessels' geometry, operational envelope (speed, sea-state, heading), and displacement. Loads used in current design procedures are based on empirical formulations recommended by classification societies and other regulatory bodies. As these expressions have been derived from the known performance of monohull structures already in service, it is questionable whether they would produce the most appropriate answer and correctly model the physical phenomena for new ship concepts and designs.

In the attempt to identify the significant load actions on the vessel, all severe environmental events which are likely to occur during the intended lifetime of the ship should be considered (e.g. dead loads, live loads, accidental loads) requiring proper definition of the intended operational

profile of the vessel. It is also essential to account for the effects of wave energy spreading on the response and load levels. For non-linear sea-ship systems and large amplitude motions the load evaluation should be carried out in the time-domain, a time consuming and computationally intense procedure. If the system is linear, or may be modelled as linear, the simpler analysis in the frequency domain is available, permitting both a short-term or long-term structural response estimation. Systematic studies are essential in order to determine empirical formulations for both primary and secondary loading estimation addressing the possibility of load interactions. In secondary loading, slamming is the attracting most of the research effort both at the theoretical and experimental levels. Proper accountability of the angle of impact, forward speed effects, hydro-elastic and cushioning effects in empirical formulations that would properly consider the panel area is essential and is currently addressed by current research work.

A *detailed fatigue analysis* should be carried out for all components/joints at which fatigue damage may lead to structural collapse. On the contrary, for secondary members, where fatigue failure will only lead to load shedding, a simplified fatigue analysis is sufficient. In the former case a complete and rather detailed description of the applied stress ranges is necessary based on environmental considerations for all operational modes over the vessel's lifetime. After all fatigue damage is a cumulative phenomenon and should be treated as such over the ship's lifetime. In the latter case, a simplified description of the long-term stress range history is more than sufficient.

1.5.2 Limit State Modelling

Strength modelling requires the definition of all possible failure modes in the structure at both the local as well as global structural levels and the description of the component strength for each of these modes by means of an expression of deterministic nature. The extent, level and type of the load fields applicable to the individual structural components should be derived based initially on a 3-D linear finite element modelling of the structural response to externally applied loading of the complete structure, followed by a more detailed analysis of the primary and secondary structural elements. Such an analysis and decisions on the structural areas to be modelled will vary from design to design, and are dependent on the designer's experience. The strength expressions can be placed under two main headings depending on their purpose:

- ultimate limit states (resistance to failure)
- serviceability limit states (stiffness and strength criteria).

Ultimate Limit States account for the maximum load carrying capacity of a member at failure and its ability to withstand the most damaging combinations of extreme lifetime forces. Failure may be in either of three forms:

- local or global instability
- fatigue damage
- material plasticity or excessive yielding.

On the other hand, the *Serviceability Limit States* are associated with constraints on structural members to guarantee that their functional requirements are met and that a sufficient level of load carrying capability before reaching ultimate strength is achieved. These include

- limits on acceptable deformations and deflections
- local instability on stiffeners
- material yield
- vibration.

It is therefore essential to identify first the primary and secondary structural elements of the structure in question and both serviceability and ultimate limit state criteria should thus be derived for each mode of failure of the components, not all of which have the same degree of seriousness.

Stability considerations dominate the provision of ultimate limit states for the main structural elements and provide the main thrust of the work described herein (para. 1.6). These should preferably be addressed by the provision of closed form solutions (wherever possible) describing their behaviour under prescribed stress fields and stress field interactions. The accuracy in their predictions is generally checked against experimental and/or numerical data, this calibration leading eventually to their stochastic description in terms of a bias and standard deviation. The sources of uncertainties in the description of strength and guidelines for good modelling, are briefly described in paragraph 1.5.3.

From the serviceability point of view, the acceptable elastic or plastic deformations should not adversely affect the normal operating conditions and/or appearance. It is essential that the final limits imposed on their values are carefully considered and balanced against the possibility of accepting future repairs depending on their extent and cost extent and cost. Fatigue strength limit states, are associated directly with the damaging effect of repeated loading on welded structural components and joints, which may lead to the loss of a specific function or to structural collapse although the latter is less likely.

It is worth noting that system strength is not considered herein, but is treated instead by Pu in [32]. A component failure approach to design, adds an inherent level of conservatism to the final recommendations as it neglects completely any level of redundancy and alternative load paths that a specific structural arrangement may provide.

1.5.3 Probabilistic Modelling

The second step in a reliability-based structural design procedure is that of *probabilistic modelling* which accounts for the uncertainties involved in the modelling of loads, structural strength and in the values the various design variables can attain in reality. Of these uncertainties, the *objective* ones are beyond the control of the designer and cannot be altered (e.g. environmental loading). On the other hand *subjective uncertainties* can in principle be reduced but their estimation requires a considerable amount of judgement and testing.

Of the subjective uncertainties, *statistical uncertainties* arise because of a limited number of observations available, but is rarely evaluated by engineers. It is incorporated in reliability analyses by letting the statistical parameters which describe the probability distributions (such as mean, variance, etc.) be random variables themselves. The second subgroup of subjective uncertainties are the *modelling uncertainties* which really arise from omissions, simplifications in the theoretical modelling of both strength and load effects. They are determined by the comparison of the theoretical predictions with experimental/numerical data and identified by the bias (equal to the ratio of the actual response over the predicted response) and a COV value. The modelling uncertainty is usually assumed to demonstrate a normal distribution and is the largest and most influential

uncertainty (as Faulkner points out [33]). Typical modelling uncertainties are shown in Table 1.5 (as presented by Faulkner [33]). These values should be treated as indicative only, as the actual uncertainties will be dependent on the individual component and failure mode considered. Specific values are presented in Chapter 4. According to Faulkner in [34] a good strength model, must demonstrate the following qualities:

- should preferably provide mean value predictions over the complete design variable range, the mean bias lying within 0.95 and 1.05
- the modelling uncertainty should be as low as possible and preferably below 15%
- sample sizes on which modelling uncertainties are based should be as high as possible (at least 30). Shooman [35] developed the following expression for estimating the sampling error in the estimated probability of failure:

$$\varepsilon\% = 200\sqrt{\frac{1-p_f}{N\,p_f}} \quad \Leftrightarrow \quad N = \left(\frac{200}{\varepsilon}\right)^2 \frac{1-p_f}{p_f}$$

where N is the total number of simulations (sample size) and p_f is the probability of failure. The aforementioned expression assumes that there is a 95% confidence level that the actual error in the estimated p_f is less than ε. Techniques exist which may reduce the error without increasing the sample size. These techniques are known as variance reduction techniques (Bayesian statistics) and are described in more detail in [36, 37]. Faulkner has used the approximation of setting the error ε equal to $1-p_f$, the probability of non-failure which leads to (by neglecting the expression of the error ε in terms of percentages)

$$N = \frac{2^2}{(1-p_f)\,p_f}$$

Hence for ε=0.1 and p_f=0.9, then N=44 while for ε=0.15 and p_f=0.85, N drops to 31.

- the modelling parameter X_m should show low correlation with any basic design variables. If this is not the case then it should be evaluated (together with the associated COV value) in ranges of the design variable or groupings of design variables

- models should be as simple as possible without sacrificing weight efficiency and prediction accuracy due to over-simplifications. It is important, that formulations should reflect the mechanics of the failure as far as possible. Curve fitting to experimental data should be kept to a minimum
- local failure modes (e.g. local buckling of stiffener elements) should be properly designed out.

The last category of errors in strength estimations that reliability analysis indirectly accounts for, is that of *human uncertainties* which are considered to be the primary cause of major structural collapses and accidental damages. Estimates of the frequency of such errors vary between 50% and 90% and 85% has been quoted as a typical value for marine structures. Faulkner in [33] presents a very good and extensive presentation of these errors and indeed of all the modelling uncertainties and should be consulted for further details.

1.5.3.1 The Uncertainties of the Random Design Variables

The identification of the variability in the design parameters should be undertaken in advance of any design application. These parameters are the design variables constituting the strength expressions (geometrical and material variables) as well as the load effects on each of the structural elements (e.g. bending moments, axial or shear forces, etc.). The randomness of the variables is prescribed in the form of probability density functions usually identified by their corresponding mean and standard deviation values and usually obtained via a series of extensive experimental tests, which are usually time and money consuming.

The uncertainties involved with the 'load' side of the failure equation are characteristic of the individual loading cases and cannot be generalised. They are mostly dependent on the geographical location and operational profile of the individual vessel. Generally, loads which are fixed throughout the weight of the structure, are assumed to possess a normal distribution to their values. On the other hand, for time-varying loads, it is the distribution of maximum load values throughout the operational lifetime of the structure that is of interest, if the target reliability is expressed over the lifetime of the structure. Chapter 2 provides detailed guidance on the final

choice and application of various distributions for the estimation of both primary and fatigue loading.

The uncertainties involved with the 'strength' side of the failure expression are associated with *material parameters* (yield strength and Young's modulus), and *geometrical parameters* (overall structural dimensions and thicknesses).

The *strengths of most ductile materials* are well represented by log-normal distributions [38] which satisfy the practical requirement that the frequency of negative values should be zero. For materials failing in a brittle manner the same reference recommends a Weibull distribution. When the data sample size is small for a particular material property (i.e. less than 50 tests), Bayesian statistics [37, 39, 40] can be used to enhance the variance. This method recognises that the parameter statistical values are themselves random and therefore statistical uncertainty is associated with confidence limits. The actual characteristic values of material strength are usually defined as the 5% fractile of the strength distribution. More detailed information is available on the subject in [41]. Relatively high COV values should be used on yield stress if it is the compressive value that is used in the validation procedure. The compressive value exceeds the tensile value of steel by between 4% and 15% [42].

Furthermore, most *dimensional variables* can be adequately modelled by normal or log-normal distributions. In case of variables which are physically bound a truncated normal distribution is appropriate [38] while the coefficients of variation of structural dimensions are generally found to be less than 5% [38]. Deviations in *plate thickness* values result from the variety of manufacturing treatments but mostly from rolling as well as surface treatment. ISSC [41] proposes a COV for steel plate thickness of approximately 4%. In support come Baker's measurements [43] which resulted in values of 3.6% and 0.7% for 6 mm and 50 mm plates respectively. No measurements on aluminium plates have been reported so these may be assumed as similar to steel.

Faulkner [33] presents the following uncertainties as being generally applicable:

Item	Distribution type	COV %	Bias ζ_i %
Yield Stress	LN	6-9	10 to 15
Young's Modulus	LN	1-3	-2 to 2
Plate Thickness	N	1-4	-2 to 2
Cross Section of Scantlings	N	2-4	-2 to 2
Welding Stresses	LN**	10-15	
Plate Distortions	N*	30-50	
Stiffener Distortions	N*	10-15	

N=Normal Distribution, LN=Log-Normal Distribution
(*) the same type of distribution as for cross sectional dimensions assumed
(**) the same type of distribution as for yield stress assumed

A detailed discussion on the selection of appropriate distributions and the level of their uncertainty for a number of design variables can be found in [41, 44, 45].

1.5.4 Structural Reliability Evaluation

The final stage in a reliability-based structural design procedure is that of *reliability evaluation*. This stage requires the identification of the *failure function*, g(X) (or safety margin Z) which connects the load with the component strength (Fig. 1.14)

$$Z = g(X) = R - Q = 0 \quad \text{at} \quad \text{failure}$$

X being the set of random variables both for the strength and the load components of the expression above, R and Q are the resistance (strength), and the external load on the component. The probability of failure, P_f, of the structural component is then defined as

$$P_f = \int_{g(X)\leq 0} g(x)\, dx$$

where g(X) is the joint probability density function for X. The measure of safety most widely used, is that of reliability index β defined as

$$P_f = \Phi(-\beta) = P(Z \leq 0)$$

where Φ is the standard normal distribution function. The failure probability should not exceed the pre-specified value set via the safety index, $\beta = \overline{Z}/\sigma_Z$ (Fig. 1.14b). Methods for obtaining the probability of failure and the reliability level of the structure or of anyone of its components are presented and described briefly next.

1.5.4.1 Methods of Checking Structural Safety and Selection of Safety Factors

Current methods for checking the resistance capability of structures and their components, fall within one of three categories, namely Levels 1, 2, 3.

Level 1 methods are the traditional deterministic approaches to the description of the failure criterion, in which both capacity, R, and demand, Q, are treated as deterministic quantities. Safety is therefore introduced and guaranteed by means of an empirical factor, which allows for the uncertainties in the design process in the following manner:

$$R \geq SF \times Q$$

It has been common practice to use nominal (characteristic) values for the basic variables of the load and resistance factors, and *deterministic* partial safety factors are ensuring that this is the case.

Level 2 methods account for the randomness of both resistance and load, by modelling them as random variables. Their randomness is fully described by their second moment statistical properties of mean ($\overline{R}$, $\overline{Q}$) and standard deviation (σ_R, σ_Q) rather than their complete distributions as required by Level 3 methods. Not surprisingly, these methods are also called First-Order Second Moment methods because they require a linearisation of the failure criteria in terms of the design variables (first order) and they also use second moments of the random variables. Non-linear structural problems are linearised and the safety check is then carried out only at a selected point on the failure boundary rather than as a continuous process (e.g. Level 3). Reliability levels are defined by the concept of the safety index (or failure probability $P_f = \Phi(-\beta)$). Two main classes of level 2 methods, depending on

the choice of the linearisation point exist, requiring:

- *linearisation about the mean value point.* The point on the failure surface identified by the mean values of the random variables is chosen and the surface linearised about this point using Taylor's expansion:

$$\beta = \frac{\overline{R} - \overline{Q}}{\sqrt{\sigma_R^2 + \sigma_Q^2}} = \frac{\overline{Z}}{\sigma_Z} = \frac{1}{v_Z} \qquad \text{where} \qquad \sigma_Z^2 = \sum_{x_i} \left[\left. \frac{\partial Z}{\partial x_i} \right|_{\overline{x}_i} \sigma_i \right]^2$$

  The major drawback of this method, is its lack of invariance to mechanically equivalent re-statements of the failure function. At such an instance, β can only be used as a relative measure of reliability for cases where the failure function is predefined and fixed. This approach does not provide partial safety factors but can be used to make comparisons between alternatives at the initial stage on the basis that its is much simpler to use than the advanced method. This method was first applied to ships in 1974 [46].
- *linearisation using advanced first order second moment methods* (Hasofer and Lind). In this case linearisation of the safety margin expression using Taylor's expansion does not occur about the mean design point but about some other point for which the reliability index is minimum. Hence the safety index is determined by

$$\beta = \frac{\sum_1^n (\mu_i - x_i^*)\, g_i'(x^*)}{\sum_1^n \alpha_i\, g_i'(x^*)\, \sigma_i} \quad \text{and hence} \quad x_i^* = \mu_i - \alpha_i\, \beta\, \sigma_i \quad \text{where}$$

$$\alpha_i = \frac{g_i'(x^*)\, \sigma_i}{\sqrt{\sum_1^n \left(g_i'(x^*)\, \sigma_i\right)^2}} \quad \text{and} \quad g_i'(x^*) = \left. \frac{\partial g_i}{\partial x_i} \right|_{x_i^*}$$

  where μ_i, x_i^* are the mean and 'design' values of the random variable i respectively, σ_i is the standard deviation and $g_i'(\cdot)$ is the value of the failure function for the design point. An iterative procedure is required to solve the above expressions, the first iteration of which will be with the mean value as input. The advantage of this method is that it can be as accurate as Level 3 methods, enables the calculation of partial safety factors which can be used directly in design and enables the calculation of sensitivity factors that can be used to indicate which variables have

the greatest influence on strength and pinpoint where the maximum effort should be concentrated from the quality control point of view.

Major contributions to the development of Level II methods have been made by Cornell [47] who first introduced the concept of the safety index, Ditlevsen [48], Hasofer and Lind [49], Paloheimo and Hannus [50] and Veneziano [51] and Rackwitz/Fiessler [65]. Very good reviews of these methods are available in [38, 52]. These methods have been extended to system reliability [53-56].

Level 3 methods determine the *exact* probability of failure of the structure or a structural component. They require the expression of all design variables in terms of their full probability distribution functions rather than just the mean and standard deviation values. The probabilities of failure are then evaluated by the computation of convolution integrals (Fig. 1.15).

$$P_f = p(R - Q \leq 0) \qquad \text{and} \qquad P_f = \int_0^\infty F_R(x)\, f_Q(x)\, dx$$

The cumulative distribution $F_R(x)$ represents the probability that the strength R of the structural component will be less or equal to some value x, while $f_Q(q)$ and $f_R(r)$ are the probability density functions of the strength and load respectively (Fig. 1.14). $f_Q(x)$ represents the probability that the load effect Q acting on the structural component has a value between x and x+dx as dx tends to 0. R and Q are assumed uncorrelated and time invariant random variables. The integral above can only be solved numerically, but as the number of variables increases so does the computational time. Monte Carlo simulation techniques [57-59] offer an alternative procedure by random generation of the basic variables and the estimation of the failure probability by the ratio between the number of failures over the number of non-failures. Therefore Level 3 methods can mainly be used as a check of accuracy of the simplified Level 2 and Level 1 methods. Application to everyday design practice is prohibited by the complicated nature of the solution and therefore Level 2 methods should be preferred instead. Level 3 methods were first introduced by Freudenthal et al [60] and first applied to ships in 1972 [61, 62]. The background to the method and its development and applications is briefly presented and adequately referenced in [63, 64].

Advanced First-Order Second Moment methods (AFOSM) are most suitable

for design and code development for reasons stated earlier. The need however exists for the transformation of non-normal variables to normally distributed ones, so that they can be represented by their two statistical moments only. This is achieved by the Rackwitz-Fiessler transformation [65]. This transformation is chosen in such a way that the values of the original density functions f_{X_i} and the original distribution function F_{X_i} for the random variables X_i are equal to the corresponding values of the density function and the distribution function for a normally distributed variable at the design point. The only disadvantage of transformations is that they complicate the limit state functions by making them usually more non-linear [33]. The more accurate option exists of substituting the failure function at the design point by a quadratic surface instead of linearising it (SORM methods) [52]. The computational complications that will however arise are not worth the resulting accuracies in the final result and are seldom justified.

1.5.4.2 The Choice of Target Reliability

The rational choice of a target reliability to which a safety equation is calibrated is important as it controls and determines the values of the PSFs which in turn are strongly linked to structural weight. An increase in the required level of safety, almost certainly leads to an increase in structural weight. Whether this increase will have any effect on the actual structural safety will largely depend on the level of the original level of safety in the structure. Increases in notional levels of reliability originally in the low band ($\beta \approx 2-2.5$) will also almost certainly guarantee improvement in the actual level of safety [17].

Figure 1.16 and Table 1.6 (from [33, 66]), presents approximate values of reliability levels as implied by structural design codes worldwide for a variety of structural systems and components. The high safety level implied in current designs of merchant ships and British bridges is noteworthy while German bridges are more structurally and materially efficient than their equivalent British designs. Merchant ships are generally found to have a wide spread in reliability which is even more pronounced between transversely and longitudinally framed ships. They are still though 2-3 orders of magnitude safer than naval vessels [17].

In a reliability-based design procedure, lower target reliabilities can be accepted if a high standard construction may be achieved and design is carried out based on relatively accurate load and strength models. Structural redundancy should also affect the value of assumed target reliability in the structure and according to Frieze et al [42] a value of β=3 is appropriate for structures with reasonable redundancy. Even conservative assumptions in the load distributions, expressed through log-normally distributed dynamic loads, can justify the use of a lower reliability index.

Such reductions are perhaps, not applicable to the design of fast marine vehicles mainly due to the variety of novelties and complexities associated with their operation, response prediction and construction. What has generally been the trend, is that for cases where designs are derived from first principles (e.g. TLP structures) a β value in the range 3 to 4 is seen to be preferred. The RCC selected β=3.72 ($p_f = 10^{-4}$) as the TLP target reliability. Hence, a target reliability of 4 can be considered as acceptable for fast craft marine applications, until more operation experience on the reliability of design is collected.

1.5.4.3 The Formats of Safety Check Expressions

The choice of an appropriate code format for the safety check expressions, requires choices to be made in the:

- number of PSFs
- positions of the PSFs in the design equations.

Of the large number of options that are thus formed, some may be uneconomical in the use of materials and some may introduce levels of safety for components which are not acceptable when compared to a uniform reliability for the complete structure. Simple formats should be preferred if the consequent cost of the conservatism introduced is within acceptable limits. But the positioning of the PSFs in the strength expression remains of paramount importance in ensuring that *minimum deviations from the predetermined target reliability levels* are attained. A number of combinations should therefore be tried before the final choice is made.

The basic and simplest partial safety factor combination that a code format may take is [67]:

$$\gamma_Q \gamma_f Q \leq \phi_R R \qquad \text{or} \qquad \gamma_{Q,k} \gamma_{f,k} Q_k \leq \phi_{R,k} R_k$$

where γ_Q is the *mean* PSF related to applied load uncertainties, ϕ_R relates to strength uncertainties (e.g. material and fabrication factors) and γ_f relates to the degree of redundancy present in the structure and any economic and loss of life consequences of failure. R and Q are mean values for resistance and load respectively. Subscript k accounts for the preference of characteristic values. This expression requires the resistance and load functions to be uncoupled and the random variables to be statistically independent. The assumption that both ϕ_R and γ_Q are less and greater than 1 respectively is implied. This method was first applied to ships in 1978 [63].

A brief description of other safety expression formats as found in civil engineering [68-75] and marine codes [36, 71, 76, 77, 79], is available by Frieze et al [42] (Table 1.7). As a general comment it may be said that the use of PSFs in civil engineering codes follows the general principles described in the ISO 2394. The various civil engineering formats differ in the ways they account for different load sources in buildings (e.g. dead, live, wind, snow and earthquake loads). Differences are also apparent in the way that the various responses to external loads are grouped together. This of course affects the values of PSFs finally used. Frieze et al [42] may be consulted for a fuller discussion on the subject.

1.5.4.4 The Rational Selection of Partial Safety Factors

Partial safety factors represent the ratio of the value of each random variable *at the failure point* to either (Fig. 1.14) its *mean value*, or a lower probability *characteristic value*. In the first instance, these partial safety factors are non-dimensionalised by the mean value of the variable:

$$\gamma_i, \phi_i = \frac{x_i^*}{x_{im}} = 1 - \beta \alpha_i v_i$$

α_i is the direction cosine at the failure point and is a measure of the sensitivity of β to changes in the design variables (para. 1.5.4.1). It is negative for loading variables and PSFs, γ_i, and positive for resistance variables and PSFs, ϕ_i. The influence of the required level of safety is introduced via β. v_i is the coefficient of variation corresponding to the ith variable.

Some design design codes use characteristic strength values in the safety check equation:

$$\gamma_i , \phi_i = \frac{x_i^*}{x_{ik}} = \frac{1 - \beta \alpha_i v_i}{1 \pm k_i v_i}$$

The positive sign in the denominator applies to loading variables and PSFs, γ_i, and the negative sign to resistance variables and PSFs, ϕ_i. If for example the 5% lower fractile of the variable is required then $0.05=\Phi(-k_R)$. Structural dimensions are usually represented by their mean values while geometrical imperfection and material properties are usually used in their 5% or 1% fractiles. Dynamic loads are also generally used in their pth fractile of their extreme value distributions corresponding to a reference time period (usually the ship's life), p being the probability that the extreme load value will not be exceeded within the same time period. Reference [80] provides a more detailed information on typical values of load and resistance PSFs as implied by various organisations.

The selection of a set of appropriate partial safety factors to match a given target reliability level is an optimisation problem. The solution involves the systematic (trial and error) generation of sets of partial safety factors which would lead to a failure probability level very near (and preferably equal) to the target probability of failure chosen, for a very large randomly generated number of designs. It is indeed a minimisation problem of the difference of the resulting failure probabilities for each design and the target failure probability:

$$S = \left(\beta_i(\bar{\gamma}) - \beta_t\right)^2$$

S is the attribute functions that needs to be minimised, β_t is the required target safety index and $\beta_i(\bar{\gamma})$ is the safety index as calculated for each of the designs for a given set of partial safety factors $\bar{\gamma}$ tried in the *failure function under consideration*. This approach calibrates the code component by component. This approach is also recommended by CIRIA 63 [38] and is presented in Appendix 1.3. References [36, 42, 45, 63, 67, 76-78, 81-91] provide only a few examples of both civil engineering and marine applications of this procedure. The positive effects of redundancy are omitted. Such an omission may give as high as a two to three fold global factor of safety against system failure beyond first component failure [92].

The alternative approach exists by which a global failure probability is chosen to which *the complete set of failure expressions* are calibrated to. The difference with the previous approach lies in that in this case it is the total target reliability of the *system* that has to match the required failure probability. Understandably, it is a more difficult and time consuming method, as a very large number of partial safety factors has to be treated simultaneously by the optimisation routine, and it will be very difficult to find a set of $\bar{\gamma}$ that would satisfy the minimum difference requirement [93]:

$$S = \sum_{i=1}^{m} w_i \left(\beta_i(\bar{\gamma}) - \beta_t\right)^2$$

where w_i is a set of weighting factors indicating the relative importance that the failure of an individual component under a specific failure mode will have on the structural integrity. The advantage however, of such an approach is that it pays due considerations to those structural components and failure modes that will mostly influence the final level of safety, without penalising those components that have the least contribution. Figure 1.17 demonstrates graphically the procedure.

A limit should be introduced on the number of partial safety factors, which should be kept as low as possible and certainly below the number of basic random variables. However, too little variables may result in loss of accuracy and potential increase in structural weight and in lack of invariance of the resulting level of safety to the type of failure function used. At times, *grouped PSFs* are preferred in an attempt to keep the overall number of PSFs down to numbers that are easy to handle. Therefore, groupings of no more than five PSFs, especially for those design variables whose sensitivity factor is small, are not uncommon (e.g. DNV, BS5400). The decision to allocate a partial safety factor to a variable or group it with other factors, will be solely based on the dependence of the strength formulations on each of the design variables. This dependence is identified by checking the variation of the modelling uncertainty (bias) of the strength expression against variations of each of the design variables separately. Alternatively, a high value of the sensitivity factor, α_i^2, for the variable should serve as a strong indication of dependence. If such a dependency of the strength bias to specific design variables is observed, additional partial safety factors, should be introduced to the strength expression, in order to maintain a consistent level of reliability. These partial safety factors should be functions of the dominating design variables.

1.6 Aims and Scope of Current Work

The earlier paragraphs of this Chapter have introduced the aspects that affect the design and operational characteristics of fast marine vehicles in addition to the challenges that face designers and operators if this new technology is to continue growing. Of these challenges (para. 1.4) it is those pertinent to the structural design aspects of fast marine vehicles that have been the centre of this study. As has already been mentioned, the uncertainties in loading and construction, coupled with the lack of operational experience and the need for light-weight structures, encourages a shift from the deterministic, allowable stress approaches to a reliability-based, limit state representation of structural capacity. The main stages in such a rational design procedure also adequately reflect the areas that require particular attention and re-evaluation. These stages are:

- the selection of the structural material, which for the case of weight sensitive structures takes a distinct place in the design spiral

- the accurate estimation of primary and secondary loads by definition of the operational profile (heading, speed, geographical location) of the vessel and associated sea statistics, using appropriately derived RAOs. The estimation of the loads on the structural components, carried out via elastic FE analyses of varying degrees of accuracy is essential

- the estimation of the fatigue loading on the vessel during its lifetime

- the identification of the best ultimate limit state strength models and serviceability requirements for all structural components and failure modes

- the identification of the level of safety to be inherited in the structure, via the selection of a suitable target reliability according to which...

- the values of the partial safety factors in the strength expressions should be probabilistically calibrated well prior to the checks of the integrity of the structural components

- the optimisation of the structure with respect to cost, weight and safety is the last stage in the procedure. These three attributes often tend to introduce conflicting requirements and hence a multi-attribute optimisation routine would be very helpful at this stage.

The aim of the work described herein is to provide, for each of the above areas, the background, underlying assumptions and considerations as well as describe the tools necessary for the development of reliability-based strength criteria for the design of the structural components of fast, multi-hulled ships (Chapters 1-4) in general, and SWATH ships in particular. The work has concentrated mainly in the area of strength modelling for the various structural components of the SWATH ship under all possible load combinations they might be expected to withstand. Although it stops just short of deriving appropriate partial safety factors for the various structural components and failure modes in a multi-hull structure, detailed guidance on how to do so is provided. The reliability-based design procedure to the structural optimisation, with respect to cost, weight and safety, of an example SWATH ship, the M.V. Patria [124, 125] (Chapter 5) is applied instead. The conclusions of the research, recommendations on the most appropriate strength formulations and the areas which may benefit from further research are all finally identified in Chapter 6. It is worth noting that system strength is not considered herein, but is treated instead by Pu in [32].

This Chapter has so far dwelled upon the merits and peculiarities of fast marine transportation and has presented the structural reliability tools and considerations necessary for the derivation of more rational safety checks. Detailed reference and description has also been provided of the method for deriving the partial safety factors in any strength check expression based on a pre-specified level of target reliability. The remaining of this Chapter is devoted to helping the designer make the right choice of material by presenting him with the available options and a brief comparison of the advantages and disadvantages of the choices available to him. Special attention is paid to aluminium and its two marine alloys, mainly because of its increasing use in primary structural elements of middle sized vessels and because it is the structural material of the example ship used herein. The Chapter concludes with a presentation of advantages and disadvantages of the SWATH concept as identified mainly by research in the U.K. and the U.S.A. The results of detailed parametric studies on the main dimensions of

existing SWATH vessels undertaken in the U.S.A. are also presented in view of providing the reader with a first way of establishing primary dimensions at the concept design level. The implications on structural design of the arrangement particular to SWATH ships are finally discussed.

The problem of estimation of both primary and secondary loads on SWATH ships is tackled in Chapter 2, by reviewing the options available to the designer. Empirical formulations on the estimation of primary and secondary load effects on this type of vessels are presented and reviewed although the international effort in theoretical prediction of the load and response of SWATH ships is also briefly described but sufficiently referenced. Of the secondary loads dominating the structural weight of the wet decks and side plating, it is in slamming loads that the work described herein has concentrated. Current approaches for the determination of fatigue damage loading are also described with reference to their applicability to design procedures for the US and Royal Navies.

In order to review and identify the most appropriate ultimate and serviceability limit states applicable to the ultimate strength design of SWATH ships, it is essential to identify first the *primary* structural elements of the structure in question, namely (Fig. 1.18) the cross-deck, the 'knee-joint' (connection of the cross-deck with haunch), the haunch, the strut and the underwater cylindrical hulls. These can, in turn, be 'broken down' to their *secondary* components, the (a) cross-deck deep web plate girder, (b) transversely, longitudinally stiffened flat plating, (c) ring and stringer stiffened shells, (d) stiffeners, and (e) deep plate web of 'knee-joints'. In general both serviceability and ultimate limit state criteria should be defined for each mode of failure of the above components. Ultimate limit state criteria have been defined in detail in Chapters 3 and 4, but the presentation of serviceability criteria is somewhat incomplete. Serviceability limit states associated with the vibration and material yield are not considered herein except those associated with the deformations of plating under lateral pressure and the local buckling criteria of stiffener components (paras. 4.2.7 and 4.3.5, Chapter 4). Ultimate limit states associated with accidental loads such as collisions, fire explosion etc. have been neglected. Material yielding was not tackled directly as a serviceability criterion. Although a necessary addition to any structural design recommendations, it has been neglected on the assumption that the use of stocky sections of plating and stiffening systems should be discouraged by

the need for weight efficiency, and the shift to post-buckling strength design. It is however indirectly accounted for, if it is involved in the final collapse mechanism of the component and its effects are introduced in the design through the strength model (e.g. tension field model for deep plate girder design).

Fatigue strength limit states, are associated directly with the damaging effect of repeated loading on welded structural components and joints, which may lead to the loss of a specific function or to structural collapse although the latter is less likely. Chapter 3 concentrates on the strength modelling aspects and the associated uncertainty as applicable to the fatigue design of both monohull and multi-hull vessels. A brief description of the sources of fatigue strength reduction in welded structures and the possible repair measures, the background to the major steel and aluminium fatigue design codes is presented, coupled with a comparison of the major aluminium fatigue design codes.

Stability considerations dominate the provision of ultimate limit states for the main structural elements and provide the main thrust of the work described in Chapter 4. Closed form solutions describing their behaviour under prescribed stress fields and stress field interactions are reviewed and recommended while their accuracy is presented in terms of the bias and standard deviation relative to experimental and/or numerical data. Ultimate strength modelling of the behaviour of the cross-deck deep web plate girder, the stiffened flat plating under every possible in-plane load combination, inclusive of interframe plate induced collapse and stiffener tripping is reviewed and the best models proposed. The effect of lateral pressure loading has been considered and appropriate elasto-plastic strength criteria suggested. Particular attention has been paid to the behaviour of aluminium plating and the effects of welding on its behaviour, which resulted in the proposal of a model describing the ultimate strength under in-plane buckling loads of aluminium welded and unwelded plates. The model has not been extended to stiffened aluminium plates but indications are provided on how this may be achieved based on the extensive experimental and numerical research effort undertaken in the field of buckling collapse of aluminium columns.

Stiffeners for the cross deck girder are designed against a stiffness and a

column criterion. for flat stiffened plating, stiffener strength should be checked against tripping and buckling and the appropriate models are therefore reviewed and the best recommended. Serviceability requirements on the stiffener dimensions are also proposed.

The stability of ring and stringer stiffened shells against pressure loads is also addressed (para. 4.7) by reviewing the available design methods for ring framed shells, conical transitions and spherical dome ends under external hydrostatic pressure.

Furthermore, the web plate in line of the cross-deck/haunch intersection is viewed as a 'knee-joint', like those encountered in civil engineering practice. Hence research published in the open literature on steel portal frames has been reviewed and extended for application to SWATH vessels. The possible extension to aluminium construction of the model has also been attempted. The proposals recommended herein, however, remain mere suggestions until appropriate experimental data become available.

Finally, the thesis concludes, by applying these models to a global reliability-based optimisation procedure of all the main structural elements of a section of FBM Marine's SWATH ship, MV PATRIA, thus demonstrating that it is possible to consider safety, cost and weight aspects straight from the preliminary design level.

1.7 Aspects of Structural Material Selection

The materials used in weight sensitive applications are generally compared on the basis of *specific strength* (strength per unit weight) and *specific stiffness* [94]. Figure 1.19a shows that on this basis, and although composites offer specific strength advantages over metals, it is only the high performance composites (also the most expensive) which can outperform the metals in terms of specific stiffness. It is therefore not surprising that fibre reinforced plastics are used more in smaller vessels where stiffnesses play a relatively smaller role. In terms of cost, none of the composites is found to be competitive with steel or aluminium in stiffness sensitive applications and only glass-based composites can compete but only in strength-critical areas (Fig. 1.19b).

Material cost is a very important consideration as well (Table 1.8) but the relative cost advantages can be obtained only in terms of *construction cost*, and only on the basis of the same structural configuration. Loscombe has provided such a comparison of structural weight and production cost as functions of displacement for small SWATH ships of different materials [95] (Fig. 1.20). Considerable *cost benefits* are possible in using steel in a homogeneous construction or aluminium/FRP/steel in a hybrid construction. On the other hand, the largest *weight benefits* are observed by using aluminium throughout the structure, while in the case of hybrid construction the largest weight benefits are obtained from an FRP hull/alloy box/alloy superstructure construction arrangement.

Current marine applications use high strength steel for ships of 10,000 tonne displacement and above, while for ships of less than 1,000 tonne displacement aluminium competes with fibre reinforced plastics (Table 1.9). Intermediate size vessels have generally been constructed of mild steel as the weight advantages of using high strength steel in this displacement range are eventually cancelled by thickness margins against corrosion. It is also very difficult to construct lightweight ships of 1,000 tonne and above from FRP because of the high stiffness requirement that these materials cannot guarantee [10]. For high speed marine applications, Faulkner [96], based on Loscombe, suggests the following speed and displacement zones for efficient use of the various material options:

- GRP for $\Delta < 50$ tonne and V<44 knots
- aluminium for all displacements and V>30 knots
- steel for $\Delta > 120$ tonne and V>20-30 knots and increasingly replacing aluminium at higher speeds and displacements
- high strength steel for designs above 1000 tonne and 46 knots.

The shift to vessels greater than 75 m length, will necessarily lead to the re-evaluation of the materials used in fast marine construction as issues of stiffness and impact strength dominate the design thinking. Steel is likely to be used increasingly to provide that extra strength and stiffness required and is expected to be the norm for vessels greater than 120 m in length. The application of high strength steels will also have to address the problem of increased fatigue damages. Lightweight materials could also be used in secondary structure in the form of cladding, requiring good knowledge of detail design, joining methods and relative structural stiffness [97].

The attraction of *steel* lies in its cost, manufacture, fatigue life and fire resistance and the familiarity of all yards with its handling and welding. Its main drawbacks however are those of corrosion and weight and its use is hence restricted to larger and less weight sensitive applications. *FRP* on the other hand, have the advantage of being easily adaptable to local stress requirements, being water resistant and having a high thermal insulation. The low stiffness levels and even lower fire resistance restricts, however, their application to secondary structural and superstructure components. Furthermore, the construction costs associated with these materials are similar to those for aluminium for sandwich structures but increase considerably for single-skin construction [98].

Aluminium is the material most favoured in the construction of medium sized, high speed marine vehicles mainly due to its low density, corrosion resistance and light weight. The alloying elements are generally used to enhance the corrosive protection of the material and magnesium is the most appropriate for this purpose. Copper alloys (e.g. 2000 and 7000 series) are therefore avoided in marine applications in favour of the 5000 and 6000 series whose manganese and magnesium based corrosive resistance is the highest possible. The 5000 series alloys are used for plating while the latter for stiffening systems and extrusions. The characteristic strain-hardening behaviour of aluminium is more notable in the work-hardened 5000 series alloys (low Ramberg-Osgood coefficient, in the range 5-20) than the 6000 series heat-treated alloys whose behaviour tends more towards that of mild steel. Aluminium's relatively small modulus of elasticity results in a structure which is particularly prone to buckling, and HAZ softening of the material strength weakens the structure and results in notch effects that may considerably reduce the fatigue life of welded structural details. According to Chalmers [99], in order to achieve acceptable fatigue life, the stresses in the joint have to be kept so low that almost counterbalance the aluminium's advantageous strength to weight ratio. Although no strength loss is observed at low temperatures, the material has a low melting point (650°C) and will burn at temperatures much higher than those expected on shipborne areas [99]. The relatively high values for both thermal expansion and conductivity (10 times higher than steel) create considerable weld distortion problems.

Apart from the structural weight benefits of aluminium, improvements in

the handling of large structural components are also possible which in turn encourages the more cost and quality efficient modular, undercover construction methods. The resulting cost benefits may help in balancing the increased construction costs associated with inert gas welding (MIG and TIG). Details on aspects of welding aluminium may be obtained from [100]. Furthermore, the potential of the use of extruded sections provided by aluminium allows reduction in the construction costs and reduces the weld content and edge preparation in the structure considerably. A review of the use of large aluminium extrusions and considerations leading to the correct choice and their design in marine applications is available in [101-104]. References [105-108] may be consulted for very detailed information on the properties, applications and background literature and codes governing the use of aluminium alloys.

A very good review of the properties of marine structural materials, their advantages and limitations as well as of the areas of their applicability is provided by Chalmers in [99], paying particular attention to FRP materials. The role of composite materials in marine applications has also been examined in detail by Marchant and Pinzelli [109].

1.8 The SWATH Ship

Although the concept of multi-hulled vessels has been well known for over 200 years since it first originated in Polynesia [110], the first SWATH type vessel was patented by Frederick Creed in 1943. The patented design was a SWATH like aircraft carrier intended to improve performance in the seaway, but never materialised. The actual development of the SWATH concept however, commenced in 1973 when the first SWATH ship, *Kaimalino*, was launched in San Diego. Since then a number (appr. 30) of such ships have been constructed worldwide [110-112] ranging from 1 to 12,000 tonnes and numerous designs exist awaiting interested parties. The biggest SWATH ships built to date are the 3,500 t Japanese vessel Kaiyo constructed in 1984 as an underwater support vessel and the ocean surveillance vessel T-Agos-19 built in 1992 for the US Navy. The most recent and impressive design constructed to date is the cruise liner Radisson Diamond of (11,740 t, 67 m long, 11 knots) [113, 114]. However, since the end of the 'cold war', interest in the SWATH concept has declined because of the obvious lack of need of stable weapon supporting, and seagoing platforms, and due to the increasing interest in concepts which have greater

operational and money earning capability (e.g. catamarans and SES craft). It is not the intention of this Chapter to provide a detailed historical review of the developments in the concept, which is anyway available in [110,-112, 114]. The main advantages, disadvantages and design trends dominating current SWATH design and construction thinking are considered more essential to this work and will be briefly presented next. The twin hull configuration, the main structural elements and the terminology associated with the SWATH concept are presented in Figure 1.18.

1.8.1 The Viability of the SWATH Concept

The *small waterplane area* of SWATH ships is responsible for their most important characteristics, namely excellent seakeeping performance and reduced deck motions and accelerations allowing them to operate in 1-2 seastates higher than monohulls of the same displacement do. Indeed, the removal of most of the buoyancy from the free surface results in longer natural periods of motion (can even be twice as long as the natural periods of comparable monohulls) which do not coincide with the shorter periods of developing seas. Typical SWATH/monohull heave and pitch stiffness ratios are reported [101] to be 20-25% and 10-20% respectively for the same displacement while the heel stiffness of the SWATH is generally higher by a non-identified amount [101]. Natural periods of large SWATH ships (3,000 tonnes) generally lie within 11-13 secs in heave, 14-17 secs in pitch and 18-20 secs in roll [13]. Smaller SWATH ships will have appropriately reduced natural periods. Appropriate design of the underwater hulls coupled with the use of motion control surfaces determines these values. Furthermore, the reduced wave making and wave added resistance relative to a monohull of the same displacement (introduced by the small waterplane area) allows the sustainment of speed at higher sea states (Fig. 1.10). In addition, the excellent directional stability of SWATHs at high speeds causes problems in manoeuvrability at these speeds as higher power demands are made on the steering system for any course changes.

Increasing the cross deck clearance due to the *larger depth and smaller draught* minimises the risk of deck wetness and underdeck slamming at the expense of higher bending moments acting on the cross-deck structure. Further, improved propeller cavitation performance (compared to catamarans etc.) is observed but the presence of long, surface piercing struts

reduces the propulsive efficiency by introducing a non-uniform wake distribution to the propellers.

An additional advantage of the SWATH concept is the *large beam* which increases the working deck area and improves stability. The latter is further enhanced by the presence of a large buoyant deck, which increases the restoring moment once immersed at large heeling angles. This beamy characteristic of the structure also improves manoeuvrability at low speeds and does away with the need for bow thrusters as is usually necessary for monohulls. The turning radius of a SWATH ship may be as small as one ship length at zero forward speed [115].

Although SWATHs have been in the market and researched considerably for approximately 25 years now, the concept has not witnessed the popularity that the other buoyant, twin- hull concept, the catamaran, has enjoyed for years. Despite, the aforementioned advantages, a number of aspects will probably need to be addressed before any widespread use of the SWATH concept is observed.

The *small waterplane area* is to blame for the weight sensitivity of the structure and eventual constraints on the payload. Generally the SWATH structure is expected to consume approximately 40-50% of the design displacement. Smaller (20%-40%) tons per centimetre immersion values than for monohulls [14], are observed, resulting in a twofold to fivefold increase in a SWATH's draught for a given payload. A similar sensitivity (10-20% lower than monohulls) is observed [14] with respect to the moment to change trim 1 centimetre, resulting to large increases in trim values for small shifts of payload along the longitudinal direction of the vessel. The moment to change heel by 1 degree is slightly larger than that for monohulls [14] as the large beam compensates for the small waterplane area and guarantees no great heel angles for loads positioned eccentrically to the centreline. This difficulty counterbalances the positive effect of a very large deck and makes the SWATH concept inappropriate for applications that require the transportation of large, variable and highly mobile loads (e.g. cars, trucks crane weights, etc.).

Stabilising fins are essential to balance the pitch instability (*Munk Moment*) observed at certain speeds due to the longitudinal asymmetry of

the pressure distribution on the underwater hulls coupled with the small pitch restoring moment. Difficulties also arise as the slender nature of the struts, and small hull diameter (especially for ships less than 500 t) interferes with the efficient use of space and volume and inhibits access. Positioning of machinery and system installations on other areas such as the deck or the haunch areas is an attractive but space consuming alternative. In addition, port facilities, canal sealanes, and drydocks have to cater for the large beam and draught which may introduce problems to the inspection and unloading of these vessels from existing terminals.

The multihull nature introduces the need for duplication of propulsive systems thus increasing the initial cost and weight. Higher capital costs (20%-50% according to Louie and Lang [116]) relative to a monohull are also involved in construction when compared on the basis of payload. A reduction in capital costs could result from careful control of the structural weight, simplifications in the fabrication and assembly procedures and the balanced choice of the machinery system in view of the operational and maintenance costs. Unfortunately, maintenance of both structural and mechanical systems, will probably be relatively high due to the structural complexity and the possible difficulty to access machinery spaces.

Furthermore, in SWATH ships the calm water frictional resistance is greater than that of an equivalent monohull, as the same volume is split into two separate hulls. Figure 1.21, developed by McGregor et al [117] from the specific resistance plot of Gabrielli and von Karman [118], demonstrates the high power requirement in calm water of these ships relative to other means of sea transportation. Design of SWATH ships for low speed operation should aim in reducing the dominating frictional resistance while for high speed vehicles, reduction of the wave resistance (wave making and wave added) is more essential. In the former case, minimisation of the wetted surface area is achieved through shorter and lower hull and strut lengths but longer and lower hulls and struts would minimise the wave resistance. The current SWATH design practices of low to medium speed ships, favour short struts over the longer ones used in earlier designs.

Since vehicles which do not approach the levels of generally acceptable economic efficiency should possess special qualities to justify the cost, so SWATH ships have to establish themselves and justify the extra cost

through their seakeeping capabilities. Applications like, pleasure craft, cruise liners, oceanographic survey ships, naval applications, offshore industry put this capability in full use.

1.8.2 Guidelines to the Proportioning of the Main Structural Elements of SWATH Ships

Comparisons of the main dimensions between SWATH ships and monohulls of *the same displacement* have yielded [115] that SWATH ships

(a) are 30-40% shorter in length
(b) are 60-70% wider, to account for the loss of stability due to the smaller waterline
(c) have 60-70% greater draught. The maximum acceptable draught will be determined from port and drydock considerations
(d) have 60% more wetted surface area. The resistance penalty associated with this increase results typically in 1-3 knot top speed advantage for monohulls in calm water for a given installed power [14]
(e) have 75% more depth (50% for large ships)
(f) have 25% greater freeboard.

In proportioning the underwater hulls, one may assume the percentage of displaced volume contained in them to be 65-90% (80% most frequent), their length to diameter in the range of 14-22 (15-17 most common) and the hull prismatic coefficient in the range of 0.45-0.93 (0.70-0.90 most common) [115]. Furthermore, according to Kennell [14] the enclosed volume contained within the struts and hulls is approximately 30%- 50% of the total enclosed volume. Strut volume alone is found to account for 15%-20% of the total volume while the remaining is attributable to the cross deck box structure and the deckhouse, where most of the ship functions are located.

In proportioning the cross-decks, their length to beam ratio can be taken within 3.0-5.0 for large ships (15,000 tonnes) and 2.0-3.0 for smaller vessels as observed by Gore [115]. No direct recommendation can be given as to the choice of a single or tandem strut arrangement. Single struts provide greater static and directional stability, better access to lower hulls, greater space utilisation in struts and improved structural arrangements apart from being simpler to construct, eliminating wave interference between twin struts and

improving survivability and residual strength after damage. On the other hand, the tandem struts provide lower motions and side loads at rest, shorter turning radii [15, 119] and a smaller waterplane area (for a given strut width) leading to longer heave and roll periods. The accessibility to the lower hulls as well as the space provided by the two structural arrangements individually will greatly affect the final choice. Most of the current designs carry a single strut arrangement [119].

Strut and hull separation is dictated from layout and stability considerations. Transverse stability is very good, especially at large angles of heel but difficulty exists in meeting stability criteria for initial heel angles unless the box clearance is kept relatively low. A balance therefore has to be struck between this requirement and the need for a large wet-deck clearance. The tendency seems to be to make the box clearance equal to approximately the design significant wave height [13].

The proportioning of the struts traditionally aimed at large strut heights to keep the box well above the water surface, increases the amount of the marginally useful strut volume and aggravate the bending moment in the box. The submergence depth of the hulls is currently limited by propeller ventilation considerations while the distance of the wet-deck from the water surface is determined by the definition of an acceptable level of slamming within the operational wave height range. The strut volume in current designs is found to be 15-20% of overall, while the ratio of the strut width to the horizontal hull diameter lies between 0.3 and 0.6. Current strut designs demonstrate a length to thickness ratio of 5-15 for tandem struts and 20-40 for single struts. The waterplane coefficient has been found to be between 0.7 and 0.8 [115].

The distribution of the volume and the shape of the underwater hulls is of primary importance to the hydrodynamic and the hydrostatic performance of the hull form. Oval sections (apart from circular) with less height than width have been used in shaping the underwater hulls. This advantages of this shape are that it introduces larger volumes in the hulls, improves the motions in the higher sea states by increasing the damping forces. A reduction in draught and thus in primary bending moment at the expense of a small increase in drag [14] is also observed.

1.8.3 Structural Design Considerations in SWATH Ships

In attempting to design the structure of a SWATH one should bear in mind, three main points, the:

- considerable shear lag effects arising form the box-type nature of the cross deck, and affecting the buckling efficiency of the plating

- presence of high stress concentrations on the transverse bulkheads at four locations, namely, the main deck intersection with the longitudinal bulkhead, the wet deck/haunch/long. bulkhead intersection, the haunch/inboard strut/first platform intersection and the intersection of the outboard strut and first platform

- considerable shear stresses present in the cross-deck girder.

The shear lag effects and local stress concentrations preclude the use of classical beam theory approaches for deck and side plating design. The stress distribution in the structure can thus only be estimated via detailed FE analysis. Such FE calculations [31, 120-123] considering typical SWATH midship sections loaded in transverse bending have shown that the transverse bulkhead is the main structural element resisting the side load, whereas the midbay plating and decks are lightly loaded (Fig. 1.22). The transverse stress distribution in the bulkhead along the main deck and the outer side shell can be over three times those predicted by single beam theory. The longitudinal distribution of the transverse stresses is more pronounced at larger transverse bulkhead spacing and more uniform at smaller separations. The results of similar studies on an aluminium SWATH [31, 122, 123] are presented in Chapter 5.

Only Sikora et al [120] have published closed form expressions describing the distribution of stresses in the box-structure. These are empirical formulations, based on extensive parametric FE studies varying the longitudinal spacing of the transverse bulkhead for ships with a 45° haunch angle. Hence, the stress distribution in the deck and side plating and the stresses at the transverse bulkheads at their four stress concentration locations due to side loading may be obtained respectively from:

$$\sigma = \sigma_{nom}\, A\, (m\, x^c + B) \qquad \text{and} \qquad \sigma = \sigma_{nom}\, A\, P\, R$$

where σ_{nom} is the nominal bending and axial stress, A is the stress concentration factor (Table 1.10), P is an insert plate factor (Table 1.11) and R is a haunch radius term given by

$$R = 0.35 + 0.0075\,(d/r)^2 \quad \leq 1$$

where r is the haunch radius and d is the depth of the cross-structure. Furthermore, x is the normalised distance in either the transverse or vertical directions while m, B, are functions of the normalised distance, y, in the longitudinal direction (Table 1.10). The stress concentration expression has been obtained from models with 60° haunch angles.

The third problem that needs to be tackled is that of the high shear stresses present in the cross structure. This is due to inability of the non-rigid decks to provide vertical support to the side plating near the corner. As a result, the vertical load arising in the side shell due to the lateral seaway loading is supported by solely the shear stiffness of the transverse bulkhead. Not surprisingly, the upper outboard panel of the transverse bulkhead is found to be in a state of pure shear. Significant shear stresses can also occur in the longitudinal bulkhead above the haunch/wet deck intersection as the primary stresses in the wet deck and haunch plating introduce edge loads.

The stress concentrations on the transverse bulkhead as well as the level of shear stresses present in them, may be reduced by decreasing the bulkhead spacing, at the expense of structural weight. Alternatively, three options are available, the use of (a) insert plates, (b) a radius of curvature at the haunch intersection with the cross deck or (c) partial transverse bulkheads. The optimum from the stress concentration point of view would be to replace the haunch with a large circular arc with tangents at the struts and the cross deck but cost and space allocation considerations in the vessel might not always encourage such an approach.

A more weight efficient approach for reducing both stress concentrations and the peak shear stresses in the transverse bulkhead is the use of partial transverse bulkheads (PTBs) midway between the existing bulkheads. A systematic FE analysis [120] carried out for the T-AGOS 19 design shows that the introduction of PTBs in sections 1, 2 and/or 3 (Fig. 1.23) may reduce the peak stress, at the haunch intersections by 20-45%, while the shear stress

levels in the bulkhead can be reduced by as much as 50%. The stress distribution in the outer shell plating and the main deck also becomes much more uniform. PTBs may also permit the increase of transverse bulkhead spacing, another weight saving measure. Further weight cuts are also possible by the introduction of lightening holes on the PTBs as well as on the deep plate girder forming the cross deck structure.

It is worth noting further, that any overdesign of the wet deck, haunch and the strut inner shell plating will not benefit the ship's structural response under primary loading conditions. Their design is instead dominated by the secondary loads and most importantly by the level of the local slamming loads of the seaway. Hence, their accurate prediction can result in considerable weight savings, and is therefore the subject of experimental investigations described in Chapter 2.

References

1) Foss, B., 'Economy and Speed in Commercial Operations', Proc., 1st Intl. Conf. Fast Sea Transportation (FAST'91), K.O. Holden, O. Faltinsen, T. Moan, June 1991, Trondheim, Tapir Publishers, Norway, 1991.
2) Vederhus, O., Heijveld, H., 'Market Potential for Fast Ferries Between Italy and Greece', Proc. Conf. Cruise and Ferry '93, London, 1993.
3) Lewthwaite, J.C., Stinton, D., Wardale, A.T., 'Likely Developments in Large High-Speed Ferries by the Year 2000', Proc., 10th Fast Ferry International Conference, 22-24 Feb. 1994, Published by High Speed Craft Associates, 1994.
4) Dobler, J.P., 'Growth Prospects of High Speed Car Ferry Utilisation on European Short Sea Routes', Proc., 2nd European Research Round-table Conference on Shortsea Shipping, N. Wijnolst, C. Peeters (Eds.), 2-3 June 1994, Athens, Delft University Press, 1995.
5) Everard, F.M., Boyle, C.P., 'The Single Market and the Removal of Obstacles to the Greater Use of Shortsea Shipping', loc. cit. 4, 1995.
6) Langford, B., 'Car Ferries-Looking to the Future', Proc. Conf. Cruise and Ferry, London, May 1991.
7) Holland, J.R., Kraus, A., 'Performance Standards in Large High Speed Craft', loc. cit. 3, 1994.

8) Akagi, S., 'A Study of Transport Economy and Market Research for High Speed Marine Passenger Vehicles', Proc., 2nd Intl. Conf. Fast Sea Transportation (FAST'93), 12-15th December 1993, Yokohama, The Society of Naval Architects of Japan, 1993.

9) Faulkner, D., Blyth, A.G., Marchant, A., Morrison, B.F.M., Mulligan R.D., Phillips, S.J., 'High Speed Marine Transport', One-Day Seminar on OSTEMS visit to Japan & S. Korea, RINA, London, 30th June 1994.

10) International Ship and Offshore Structures Congress, 'Report of Committee V.8; Weight Critical Structures', Proc. 12th Intl. Ship and Offshore Structures Congress (ISSC'94), N.E. Jeffrey, A.M. Kendrick, (Eds.), Vol. 2, St. John's, Canada, 12-16 Sept. 1994.

11) Blyth, A.G., 'Towards Rational Regulation', Proc. Intl. Seminar Safety for High-Speed Passenger Craft, RINA, London, 7-8 May 1992.

12) Lang, T.G., Slogget, J.E., 'SWATH Developments and Performance Comparisons with Other Craft', Proc., Int. Conf. on SWATH Ships and Advanced Multi-Hull Vessels, RINA, Paper No. 1, London, 1985.

13) Betts, C.V., 'A Review of Developments in SWATH Technology', Proc. Intl. Conf. SWATH Ships and Advanced Multi-Hulled Vessels II, RINA, London, 28-30 Nov. 1988.

14) Kennell, C.G., 'SWATH Ship Design Trends', Proc. Intl. Conf. SWATH Ships and Advanced Multi-Hulled Vessels, RINA, London, 27-19 April 1985.

15) Lang, T.G., Sloggett, J.E., 'SWATH Developments and Performance Comparisons With Other Craft', Proc. Intl. Conf. SWATH Ships and Advanced Multi-Hulled Vessels, RINA, London, 27-19 April 1985.

16) Faulkner, D., 'Classification Societies-Are They up to Date?', Proc., 3d Conf. High Speed Marine Craft, Norwegian Society of Chartered Engineers, Kristiansand, 8-10 Sept. 1992.

17) Faulkner, D., 'Safety of Ships-Risk Assessment Based Design and Operation', Proc., Conf. Safety of Ships, Southampton, 24-25 May 1995.

18) Faulkner, D., 'New Technologies for Ship and Offshore Structural Analysis and Design', Proc., Intl. Symp. Marine Structures (ISMS'91), Shangai, China, 13-14 Sept. 1991.

19) Wiklund, K.M., 'The Future for High Speed Light Craft', loc,cit. 8, 1993.

20) Faulkner, D., 'Building for the Fast Lane', Shipbuilder's Register, Ocean Press.1994-95.

21) Seaspeed Technology Limited, 'Programme Definition Study for Fast Ship Technology Research', Seaspeed Technology Ltd. Report STL/157 /94 Issue 01, prepared for MTD, June 1994.

22) American Bureau of Shipping, 'Preliminary Guide for Building and Classing Small Waterplane Area Twin Hull (SWATH) Vessels', Draft, ABS, New York, Sept. 1990.
23) American Bureau of Shipping, 'Guide for Building and Classing High Speed Craft', ABS, New York, Oct. 1990.
24) Det Norske Veritas, 'Rules for Classification of High Speed Light Craft', DNV, Hovik, 1985.
25) Det Norske Veritas, 'Tentative Rules for Classification of High Speed and Light Craft', DNV, Hovik, Jan. 1991.
26) Lloyd's Register of Shipping, 'Provisional Rules for the Classification of High-Speed Catamarans', LRS, London, 1990.
27) Morlan, C., 'Development of the ABS Guide for Building and Classing High Speed Craft', loc. cit. 8, 1993.
28) Faulkner, D., 'Structural Design Philosophy for Small and Large High Speed Multi-Hull Ferries', Proc., Conf. Safety for High Speed Craft-The Way Ahead, RINA, London, 7-8 May 1992.
29) Plaza, F., Sekemizu, K., 'Towards the Adoption of an IMO High Speed Craft Code', loc. cit. 8, 1993.
30) Cowling, M.J., Burdekin, F.M., Haswell, J., Light, M.F., Xia, Y., Wamuziri, S.C., 'The Impact of Reliability Based Fatigue Assessment and Structural Redundancy on Inspection Planning for Offshore Structures', Proc. 5th Intl. Symp. Integrity of Offshore Structures, Department of Naval Architecture and Ocean Engineering, University of Galsgow, 17-18 June 1993, Emas Scientific Publications, 1993.
31) Burdekin, F.M., Cowling, M.J., Tomkins, B., Light, M.F., 'A New Procedure for Assessing Defects in Offshore Structures',loc. cit. 30, 1993.
32) Pu, Y.C., 'Reliability Analysis and Reliability-Based Optimisation Design of SWATH Ships', Ph.D. Thesis, University of Glasgow, Glasgow, June 1995.
33) Faulkner, D., 'Rule Based and Reliability Based Design for Ship Structures', UETP/COMETT Course on Advanced Design for Ships and Offshore Floating Systems, Dept. of Naval Architecture and Ocean Engineering, University of Glasgow, Glasgow, 21-25 September 1992.
34) Faulkner, D., 'Criteria and Guidance for Good Strength Models', Department of Naval Architecture and Ocean Engineering, Dept. Report No. NAOE-91-15, University of Glasgow, July 1991.
35) Shooman, M.L., 'Probabilistic Reliability: An Engineering Approach', McGraw Hill, New York, 1968.

36) Mansour, A., 'An Introduction to Structural Reliability Theory', Ship Structure Committee, Report No. SSC-351, Washington D.C., 1990.

37) Ayyub, B.M., Haldar, A., 'Practical Structural Reliability Techniques', Jnl. Structural Engineering, ASCE, Vol. 110, No. 8, Aug. 1984.

38) Construction Industry Research and Information Association, 'Rationalisation of Safety and Serviceability Factors in Structural Codes', CIRIA Report, No. 63, 1977.

39) Benjamin, J.R., Cornell, C.A., 'Probability Statistics and Decision for Civil Engineers', McGraw Hill, New York, 1970.

40) Tribus, M., 'Rational Descriptions, Decisions and Designs', Pergamon Press, Oxford, 1969.

41) International Ship and Offshore Structures Congress, 'Report of Committee III.3; Material and Fabrication Factors', Proc. 12th Intl. Ship and Offshore Structures Congress (ISSC'94), N.E. Jeffrey, A.M. Kendrick, (Eds.), Vol. 2, St. John's, Canada, 12-16 Sept. 1994.

42) Frieze, P.A., Das, P.K., Faulkner, D., 'Partial Safety Factors for Stringer Stiffened Cylinders under Extreme Compressive Loads', Proc. 2nd Int. Symp. on Practical Design in Shipbuilding, PRADS' 83, Tokyo and Seoul, 1983.

43) Baker, M.J., 'Variations in the Strength of Structural Materials and Their Effect on Structural Safety', Imperial College, London, July, 1970.

44) Das, P.K., Frieze, P.A., Faulkner, D., 'Reliability of Stiffened Steel Cylinders to Resist Extreme Loads', Proc. 3nd Int. Conf. on Behaviour of Offshore Structures, MIT, Cambridge, 1982.

45) Stiansen, S.G., Faulkner, D, 'Development of a Structural Design Code for Tension Leg Platforms', Proc. Int. Conf. Marine Safety, University of Glasgow, Glasgow, 1983.

46) Mansour, A., 'Approximate Probabilistic Method of Calculating Ship Longitudinal Strength', Jnl. of Ship Research, Sept. 1974.

47) Cornell, C.A., 'A Probability Based Structural Code', Jnl. American Concrete Institute, Vol. 66, No. 12, 1969.

48) Ditlevsen, O., 'Structural Reliability and the Invariance Problem', Solid Mechanics Division, University of Waterloo (Ontario), Research Report 22, March 1973.

49) Hasofer, A.M., Lind, N.C., 'An Exact and Invariant First-Order Reliability Format', Jnl.Eng. Mech. Division, Proc. ASCE, Vol. 100, Jan. 1974.

50) Paloheimo, E., Hannus, M., 'Structural Design Based on Weighted Fractiles', Jnl. Strct. Division, Proc. ASCE, Vol. 100, ST7, 1974.

51) Veneziano, D., 'Contributions to Second Moment Reliability Theory', Dept. Civil Engineering, Massachussetts Institute of Technology, Structures Publication 389, April 1974.

52) Leporati, E., 'The Assessment of Structural Safety', Series in Cement and Concrete Research, Vol. 1, Research Studies Press, Letchworth, England, 1979.

53) Stahl, B., Geyer, E.F., 'Fatigue Reliability of Parallel Member Systems', Jnl. Structural Division, ASCE, Vol. 110, ST 10, Oct. 1984.

54) Kjerengtroen, L., Wirsching, P.H., 'Structural Reliability Analysis of Series Systems', Jnl. Structural Division, ASCE, Vol. 110, July 1984.

55) Madsen, H.O., Krenk, S., Lind, N.C., 'Methods of Structural Safety', Prentice Hall Inc., 1986.

56) Thoft-Christensen, P., Murotsu, Y., 'Applications of Structural Systems Reliability Theory', Springer-Verlag, Berlin, 1986.

57) Schueller, G.I., Stix, R., 'A Critical Appraisal of Methods to Determine Failure Probabilities', Structural Safety, Vol. 4, 1987.

58) Bjerager, P., 'On Computational Methods for Structural Reliability Analysis', Structural safety, Vol. 9, 1990.

59) Pulido, G.E., Jacobs, T.L., Lima, E.C.P., 'Structural Reliability Using Monte Carlo Simulation with Variance Reduction Techniques on Elastic-Plastic Structures', Comp. and Struct., Vol. 43, No. 3, 1992.

60) Freudenthal, A.M., Garretts, J.M., Shinozuka, M., 'The Analysis of Structural Safety', Jnl. Strct. Division, Proc. ASCE, Vol. 92, ST1, Feb. 1966.

61) Mansour, A., 'Probabilistic Design Concepts in Ship Structural Safety and Reliability', Trans. SNAME, 1972.

62) Mansour, A., Faulkner, D., 'On Applying the Statistical Approach to Extreme Sea Loads and Ship Hull Strength', Trans. RINA, 1973.

63) Faulkner, D., Sadden, J.A., 'Toward a Unified Approach to Ship Structural Safety', RINA Spring Meetings, London, 1978.

64) Morandi, A.C., 'Computer Aided Reliability Based Design of Ring-Stiffened Cylindrical Shells Under External Pressure', Ph.D. Thesis, University of Glasgow, September 1994.

65) Rackwitz, R., Fiessler, B., 'An Algorithm for Calculation of Structural Reliability under Combined Loading', Berichte zur Sicherheitsttheorie der Bauwerke, Lab. f. Konstr. Ingb., Munchen, 1977.

66) Faulkner, D., 'Probability-Based Offshore Design for Extreme Lifetime Loads', loc. cit. 33, 1992.

67) Faulkner, D., 'Semi-Probabilistic Approach to the Design of Marine Structures', Proc. Extreme Loads Symposium, SNAME, 19-20 October 1981, Arlington, Virginia, 1981.

68) International Standards Organisation, 'General Principles for the Verification of the Safety of Structures, ISO 2394', ISO, 1973.

69) Comite Euro-International du Beton, 'Common Unified Rules for Different Types of Construction and Material', CEB Bulletin, No. 124E, CEB, Paris, April 1978.

70) European Convention of Constructional Steelwork, 'European Recommendations for Steel Construction', ECCS, 1978.

71) Det Norske Veritas, 'Rules for the Design, Construction and Inspection of Offshore Structures', DNV, Oslo, 1977.

72) Ravindra, M.K., Galambos, T.V., 'Load and Resistance Factor Design for Steel', Proc. ASCE, Jnl. Structural Division, Vol. 104, Sept. 1978.

73) Ellingwood, B., Galambos, T., MacGregor, J., Cornell, C., 'Development of a Probability Based Load Criterion for American National Standard A58', NBS Special Publication SP-577, National Bureau of Standards, Washington D.C., June 1980.

74) National Research Council of Canada, 'National Building Code of Canada', Ottawa, NRCC, 1977.

75) British Standards Institution, 'British Standard Code of Practice BS 5400: Part 3 Steel, Concrete and Composite Bridges', BSI, London, 1982.

76) Faulkner, D., Birrell, N.D., Stiansen, S.G., 'Development of a Reliability Based Code for the Structure of Tension Leg Platforms', Proc. Offshore Technology Conference, OTC' 83, 1983.

77) American Petroleum Institute, 'Recommended Practice for Planning, Designing, and Constructing Fixed Offshore Platforms', API RP2A, API, 12th Edition, Dallas, Texas, 1981.

78) Mansour, A., 'An Introduction to Structural Reliability Theory', Ship Structure Committee, Report No. SSC-351, Washington D.C., 1990.

79) Moses, F., 'Guidelines for Calibrating API RP2A for Reliability Based Design', API Prac. Project 80-22, American Petroleum Institute, Oct. 1981.

80) Mansour, A., Harding, S., Ziegelman, C., 'Implimentation of Reliability Methods to Marine Structures', First Annual Report ABS, University of California, Berkeley, 1983.

81) Det Norske Veritas, 'Structural Reliability Analysis of Marine Structures', DNV, Classification Notes No. 30.6, Hovik, July 1992.

82) Baker, M.J., The Reliability Concept as an Aid to Decision Making in Offshore Engineering', Invited Lecture, 4th Intl. Conf. Behaviour of Offshore Structures, Delft, July 1985.

83) White, G.J., Ayyub, B.M., 'Reliability-Based Design Format for Marine Structures', Jnl. Ship Research, Vol. 31, No. 1, March 1987.

84) Moses, F., 'Load and Resistance Factor Design-Recommended Practice for Approval, Final Report, API PRAC 86-22, American Petroleum Institute, Dec. 1986.

85) Stiansen, S.G., Mansour, A., Jan, H.Y., Thayamballi, A, 'Reliability Methods in Ship Structures', Trans. RINA, Vol. 122, 1979.

86) Wirsching, P.H., 'Fatigue Reliability for Offshore Structures', Jnl. Struct. Division, ASCE, Vol. 110, No. 10, Oct. 1984.

87) Wirsching, P.H., Chen, Y-N., 'Considerations of Probability-Based Fatigue Design for Marine Structures', Jnl. Marine Structures, Vol. 1, No. 1, 1988.

88) Martindale, S.G., Wirsching, P.H., 'Reliability Based Progressive Fatigue Collapse', Jnl. Structural Division, ASCE, Vol. 109, No. 8, Aug. 1983.

89) Flint, A.R., Smith, B.W., Baker, M.J., Manners, W., 'The Derivation of Safety Factors for Design of Highway Bridges', Proc. Conf. on the New Code for the Design of Steel Bridges, Cardiff, Mar. 1980, Granada Publishing, 1981.

90) Nordic Committee on Building Regulations, 'Recommendation for Loading and Safety Regulations for Structural Design', NKB-Report No. 36, Nov. 1978.

91) Parimi, S.R., Lind, N.C., 'Limit State Basis for Cold Formed Steel Design, Proc. ASCE, Jnl. Struct. Division, ASCE, Vol. 102, Mar. 1976.

92) Faulkner. D., 'On Selecting a Target Reliability for Deep Water Tension Leg Platforms', Proc. 11th IFIP Conference on System Modelling and Optimisation, Copenhagen, July 1983, published in Systems Modelling and Optimisation, P. Thoft-Cristensen (Ed.), Springer Verlag, Berlin, 1984.

93) Thoft-Christensen, P., Baker, M.J., 'Applications to Structural Codes', Chapter 11, in 'Structural Reliability Theory and its Applications', Springer-Verlag, Berlin, 1982.

94) Shenoi, R.A., 'Principal Aspects Concerning Structural Design of High Speed Craft', Proc., Intl. Conf. High Speed Passenger Craft-Future Developments and the Nordic Initiative, RINA, London, 15-16 June 1993.

95) Loscombe, R., 'An Exploratory Study of Alternative Structural Materials for Small SWATH Ships', International Shipbuilding Progress, Vol. 35, No. 404, 1988.

96) Faulkner, D., 'Some Aspects of Efficient Structural Design of Future Fast Multi-Hull Ships', loc. cit. 8, 1993.

97) Smith, C.S., Chalmers, D.W., 'Design of Ship Superstructures in Fibre-Reinforced Plastic', Trans. RINA, Vo. 129, 1987.

98) International Ship and Offshore Structures Congress, 'Report of Committee V.4; Novel Design Concepts-High Performance Vehicles', Proc. 11th Intl. Ship and Offshore Structures Congress (ISSC'91), P.H., Hsu, Y.S., Wu, (Eds.), Wuxi, China, 16-20 September 1991, Vol. 1, 1991.

99) Chalmers, D.W., 'The Properties and Uses of Marine Structural Materials', Jnl. Marine Structures, Vol. 1, 1988.

100) Alcan Plate Limited, 'Welding Aluminium, TIG and MIG', 2nd Edition, Alcan, Kitts Green, June 1986.

101) Dean, R.J., Wehner, F., 'Use of Large Aluminium Extrusions in Marine Applications', Proc., Conf. Structural Materials in Marine Environments, 11-12 May 1994, The Royal Society, London, 1994.

102) Sims, E.H., 'Aluminium Boatbuilding', 2nd Edition, Adlard Coles Nautical, London, 1993.

103) Pechiney (Rhenalu), 'Aluminium and the Sea', Pechiney Group, Nanterre, France.

104) Muckle, W., 'The Design of Aluminium Alloy Ships' Structures', The Aluminium Development Association, Hutchinson of London, 1963.

105) Aluminium Federation', The Properties of Aluminium and Its Alloys', ALFED, Birmingham, 1993.

106) Brick, R.M., Pense, A.W., Gordon, R.B., 'Structure and Properties of Engineering Materials', 4th Edition, McGraw-Hill, 1977.

107) Higgins, R.A., 'The Properties of Engineering Materials', Hodder and Stoughton, London, 1977.

108) Bayley, M.J., 'Materials for Aluminium Structures', Proc., Intl. Conf. Steel and Aluminium Structures, 8-10 July 1987, Cardiff, U.K., Elsevier Applied Science, London, 1987.

109) Marchant, A., Pinzelli, R.F., 'The Role for Composite Materials in Future Marine Transportation', Proc., 6th Intl. Conf. High Speed Surface Craft, 14-15 Jan. 1988, Hawkedon International Ltd., 1988.

110) MacGregor, J.R., 'Historical Development of the SWATH Ship Concept', Report NAOE-87-44, Dept. of Naval Architecture and Ocean Engineering, University of Glasgow, Glasgow, Nov. 1987.

111) MacGregor, J.R., 'Computer Aided Design Methods for SWATH Ships', Ph.D. Thesis, University of Glasgow, Nov. 1988.

112) Djatmiko, E. B., 'Hydro-Structural Studies on SWATH Type Vessels', Ph.D. Thesis, University of Glasgow, July 1992.

113) Anonymous, 'Radisson Diamond-A Revolutionary Cruiser Development', Lloyd's Ship Manager, Vol. 13, No. 2, Supplement, 1992.

114) Trillo, R.L., (Ed.), 'Jane's High Speed Marine Craft', Jane's Information Group, London, 1994.

115) Gore. J. L., 'SWATH Ships', Naval Engineers Journal, Feb. 1985.

116) Lovie, P.M., Lang, T.G., 'Commercial Opportunities for SWATH Vessels', Proc. Intl. Conf. SWATH Ships and Advanced Multi-Hulled Vessels II, RINA, London, 28-30 Nov. 1988.

117) MacGregor, J.R., McGregor, R.C., Zheng, X., 'Computer Aided SWATH Ship Design and Seakeeping Analysis', Proc. Intl. Conf. SWATH Ships and Advanced Multi-Hulled Vessels II, RINA, London, Nov. 1988.

118) Gabrielli, G., von Karman, T.H., 'What Price Speed? Specific Power Required for the Propulsion of Vehicles', Mechanical Engineering, October 1950.

119) Report of Committee V.4, 'Novel Design Concepts - SWATH', 10th Intl. Ship and Offshore Structures Congress (ISSC 88), Vol 2, Denmark, Aug.1988.

120) Sikora, J. P., Dinsenbacher, A. L., 'SWATH Structure : Navy Research and Development Applications', Marine Technology, Vol.27, No. 4, July 1990.

121) Stirling, A.G., Jones, G.L., Clarke, J.D., 'Development of a SWATH Structural Design Procedure for Royal Navy Vessels', Proc. Int. Conf. SWATH Ships and Advanced Multi-Hulled Vessels II, RINA, 28-30 Nov. 1988, London.

122) Das, P.K., Pu, Y., 'Finite Element Based Structural Analysis of SWATH', Dept. Report No. NAOE-93-20, Department of Naval Architecture and Ocean Engineering, University of Glasgow, Glasgow, May 1993.

123) Pu, Y., 'On Prediction of Primary Loads on SWATH Ships', Dept. Report No. NAOE-93-21, Department of Naval Architecture and Ocean Engineering, University of Glasgow, Glasgow, May 1993.

124) Anonymous, 'First FBM Marine FDC 400 on Trials', Fast Ferry International, Dec. 1989.

125) Marsh, G., 'SWATH Makes Good on Madeira Route', Ship and Boat International, May 1995.

126) Taylor, C., 'Eurocode 3-Presentation and Calibration', in Constructional Steel Design: World Developments, P.J. Dowling, J.E., Harding, R. Bjorhovde, E. Martinez-Romero (eds.), Elsevier Applied Science, London, 1992.

127) Holden, K.O., 'The Norwegian High Speed Marine Vehicle Research Programme', loc. cit. 8, 1993.

128) Levander, K., 'Fast Slender Monohull Vessels for cargo Transport', loc. cit. 8, 1993.

129) Arena, G., Farinetti, V., 'Introducing Eurofast', loc. cit. 8, 1993.

130) Zhu, L., Faulkner, D., 'Slamming on the Wet-Deck of Twin-Hull Vessels', Proc. Intl. Conf. New Ship Technology, Shangai, China, 22-25 Nov. 1994.

131) Zhu, L., Faulkner, D., 'Design Pressure for the Wet-Deck Structure of Twin-Hull Ships', Proc. 3d Intl. Conf. Fast SeaTransportation (FAST'95), Travemunde, Germany, 25-27 Sept. 1995.

132) Faulkner, D., Das, P.K., Djatmiko, E.B., 'Some Aspects of Structural Design of Fast Multi-Hull Ships', Proc. 5th Intl. Symp. Integrity of Offshore Structures (IOS'93), University of Glasgow, 17-18 June 1993, EMAS Scientific Publications, 1993.

Tables

Table 1.1: The more suitable northern and southern European shortsea routes for application of fast marine vehicles [4].

Area	Crossing	Distance (miles)	Passengers (thousands)	Cars (thousands)
Baltic	Swinoujsie/Copenhagen	120	150	40
	Swinoujsie/Ystad	95	400	100
	Travemunde/Gedser	120	790	122
	Travemunde/Trelleborg	54	1056	165
	Sassnitz/Trelleborg	95	957	135
	Visby/Nynashamn	80	535	123
	Visby/Oscarshamn	65	300	80
	Vasa/Umea	87	625	75
	Ronne/Copenhagen	100	700	70
Belts/Kattegat/ Skagerak	Arhus/Kalundborg	50	1055	240
	Grena/Varberg	64	400	90
	Grena/Halmstad	66	350	77
	Frederikhav/Göteborg	50	3190	486
	Frederikhav/Moss	120	220	45
	Frederikhav/Larvik	105	830	118
	Hirsals/Kristiansan	70	850	163
North Sea	Harwich/Hook of Holland	116	1040	140
	Sheerness/Vlissingue	124	800	125
	Felixtowe/Zeebruge	84	421	60
	Dover/Zeebruge	76	933	141
	Dover/Ostend	61	1891	247
English channel	Dieppe/Newhaven	64	833	137
	Havre/Portsmouth	90	794	209
	Caen/Portsmouth	95	400	100
	Cherbourg/Portsmouth	86	642	192
	Cherbourg/Poole	60	438	114
	St. Malo/Guernsey	55	250	30
	Poole/St. Hélier	100	500	110
	St. Malo/Portsmouth	142	500	127
	Roscoff/Plymouth	96	507	123
Irish Sea	Rosslare/Pembroke	67	400	90
	Rosslare/Fishguard	54	760	170
	Holyhead/Dublin	61	610	115
	Holyhead/Dun Loaghaire	56	1110	190
West Mediter-ranean Sea	Malaga/Almeria/Melilla	114	423	76
	Barcelona/Palma	130	408	67
Corsica	Toulon/Ajaccio	145	107	35
	Nice/Calvi/Ile rousse	98	175	56
	Nice/Bastia	122	163	56
	Genoa/Bastia	108	87	32
	Savona/Bastia	105	175	63
	La Spezia/Bastia	85	240	84
	Leghorn/Bastia	65	355	124
Sardinia	Civittavecchia/Olbia	125	1000	200
Adriatic and Onian Sea	Pescara/Split	114	1000	200
	Bari/Split	145	1000	200
	Bari/Dubrovnic	110	1000	200
	Otrante/Igoumenitsa	100	1000	200
	Brindisi/Corfou	123	1000	200
Aegian Sea	Pireus/Cannea	150	1400	200
	Pireaus/Naxos	120	700	40
	Volos/Stakos/Pelagos	80	700	70

Table 1.2: The number of each of the types of high speed marine vehicles delivered in the period 1988-93 [127].

	1988	1989	1990	1991	1992	1993
Catamaran	33	30	41	43	45	36
Monohull	15	15	21	28	20	10
SES	3	7	10	7	6	7
Hydrofoil	4	11	11	14	8	1
SWATH	0	1	1	0	3	3
Hovercraft	0	2	4	3	0	0
Totals	55	66	88	95	82	57
Norwegian company share:						
- Number	16	12	23	14	15	12
- Percentages	29	18	26	15	18	21

Table 1.3: Transport efficiency values for a number of constructed fast marine vehicle concepts [3].

Type	Designer /Builder (Country)	Loa (m)	Boa (m)	Payload Pass	Payload Cars	Payload Tot. (t)	Installed power (MW)	Service speed (kn)	TE value
Sealet 245 catamaran	NQEA/Danyard (Aust./Denmark)	78	24	450	120	201	23.0	39	0.341
W-9500 catamaran	Westamarin (Norway)	95	29	1000	200	360	30.0	35	0.420
116m SeaCat wavepiercer	Incat (Australia)	116	39	1100	300	500	28.0	38	0.678
W-12000 catamaran	Westamann (Norway)	120	34	1200	275	473	40.0	40	0.478
Stena HSS catamaran	Finnyards (Finland)	124	40	1570	375	645	60.0	40	0.430
SSW 320 swath	Schichau-Seebeckwerft (Germany)	55	23	600	90	177	20.0	36	0.319
69m Regency swath	Swath Ocean (USA)	69	24	450	124	206	30.0	38	0.261
Corsaire 6000 monohull	Emeraude (France)	67	11	400	42	95	12.2	32	0.249
MDV 1200 monohull	Fincantieri (Italy)	89	17	450	126	209	30.0	39	0.271
Mestral 92 monohull	Bazan (Spain)	96	15	450	76	144	20.0	34	0.245
FM-100 monohull	Blohm+Voss (Germany)	111	15	600	180	294	30.9	35	0.330
Seaswift 60 ses	Royal Scheide (Netherlands)	59	18	438	62	124	14.6	43	0.365
Corsair 600 ses	B+V/Cirrus (Germany)	60	17	350	60	113	10.4	47	0.511
SES-300 ses	Fincantieri (Italy)	66	18	450	80	149	9.6	42	0.652
SPS cat hybrid	JCL/MTG (UK/Germany)	120	24	1200	580	874	60.0	40	0.583

Notes:
Payload estimated at 10 pass = 1t and 1 car = 1.3t

$$\text{Transport Effectiveness (TE)} = \frac{\text{Payload (t)} \times \text{Service speed (kn)}}{\text{Installed power (kW)}}$$

Table 1.4: **Transport efficiency values expressed in terms of number of passengers carried for four types of fast marine vehicles [12].**

Craft [Pass. No.]	*Power*	*Speed (Calm Water)*	*T. Eff. (Calm Water)*	*Speed (1m sig. waves)*	*T. Eff. (1m sig. waves)*	*Speed (1.5m sig. waves)*	*T. Eff. (1.5m sig. waves)*
SES HM527-2 [260]	*2825kW*	*36*	*3.31*	*25(h)* *27(b)*	*2.30* *2.48*	*19(h)* *21(b)*	*1.75* *1.93*
ACV AP1-88 [93]	*1277kW*	*52*	*3.79*	*20(h)* *28(b)*	*1.46* *2.04*	*15(h)* *25(b)*	*1.09* *1.82*
Jetfoil [260]	*5532kW*	*44*	*2.07*	*44*	*2.07*	*44*	*2.07*
Mesa80 [446]	*6043kW*	*27.1*	*2.00*	*27.1*	*2.00*	*27.1*	*2.00*

$$\textit{Transport efficiency} = \frac{\textit{(No. of Passengers) x Speed}}{\textit{Installed Power}}$$

Table 1.5: **Range of the main modelling uncertainties as presented by Faulkner [33].**

Item	COV %	Bias ζ_1 %
Factors affecting strength		
Flat panel collapse		
- best	10-15	-5 to 5
- typical codes	15-30	0 to 20
Unstiffened cylinder-codes	20-40	20 to 50[1]
Stiffened cylinders		
- best	12-18[2]	-20 to 40[1]
- typical codes	20-40[2]	0 to 30[1,3]
Submarine Pressure Hull		
- interframe collapse	5-10	-5 to 5
- general instability	15-20	0 to 20
Fatigue strength	30-70	50 to 150[4]
Factors affecting loads		
Dead Loads	5-10	
Hydrostatic Pressure loads	10 (N)	
Dynamic Loads	30 (LN)	
Live Loads	10-20	-10 to -30[5]
Inertia Forces-SWATH ship	15 (N)	
Side force-SWATH ship	20 (Extreme)	
Buoyancy force	15 (N)	
Ship extreme bending		
- initial distribution	5-10	-30 to 0[6]
- extreme distribution	15-25	
Fixed offshore platforms	20-40	-10 to 10[7]
Compliant offshore platforms	15-30	-20 to 50[8]
Fatigue Loads	10-20	-20 to 0

Notes:
(1) 'lower bound' curves are mainly used
(2) for all load combinations
(3) there are some much more extreme examples
(4) large scatter on life predictions
(5) no reliable data available but 'growth factor' essential
(6) relates to overprediction of Linear Strip Theory
(7) based on Morison equation
(8) based on ITTC and ISSC diffraction modelling studies

Table 1.6: **Reliability levels as implied by design codes worldwide for a variety of structural systems and components [16, 33, 66, 126].**

Structural System/Component	β Lifetime average
Marine Structures	
North Sea TLP	5.3
RCC Code for TLP	3.72
Current TLP designs	3.0
NPD for Offshore platforms	3.72
UK DoE (1976) for Offshore Structures	3.72
ISO reccomendations for Offeshore Structures	3.0
Existing Semi-Submersibles	4.4
Columns and Beam-Columns (DnV and API Offshore Rules)	3.3
Fixed Jacket Platforms (North Sea and Golf of Mexico)	2.3*
Fatigue	2.7
Submarines	3.0
ISSC Committee V.2 'Applied Design' (1985) 1709m Products Carrier	3.7-4.9
Merchant ships 160-330m (Deck Collapse)	
Longitudinally Framed	3.2-5.2
Transversely Framed	1.8-4.0
Products tanker	3.7-4.9
Naval Ships 90-150 m (Deck Collapse)	
Faulkner/Sadden (1978)	0.9**-3.5
average value	2.2
Morandi (1994) on externally pressurised cylinders	
Flange yield (MoD)	4.89-5.9
Flange yield (0.5%R)	3.6-4.77
Plate yield (MoD)	3.56-5.01
Plate yield (0.5%R)	3.34-4.91
Tripping	3.71-4.99
Interframe ($1 < p_m/p_{cs} < 2.5$)	3.01-3.74
Interframe ($p_m/p_{cs} > 2.5$)	4.73-7.34
Land Structures	
Eurocode 3 (Steel Structures)	3.8
Eurocode 2 (Concrete Structures)	3.7-4.0
UK Steel Bridges	4.85 av.
German Steel Bridges	3.7 av.
North American Buildings	3.0-4.5
Chinese Buildings	3.2

(**) Ignoring any contibution from superstructure

Table 1.7: Code formats in civil engineering and marine codes [42].

CODE	FORMAT
ISO Standard 2394	function $[\gamma_{c1}, \gamma_{c2}, \gamma_{s1}, \gamma_{s2}, \gamma_{s3}$, effects of $F_k] \leq$ function $[f_k/\gamma_{m1}\gamma_{m2}]$
CEB Model Code	$\{\gamma_D \bar{D} + \gamma_Q [Q_{1k} + \sum_i \psi_{oi} Q_{ik}]\}\gamma_{fj} \leq R_k/\gamma_m\gamma_n$
DnV Offshore Structures	$S_d = S(\sum_i F_i \gamma_{fi}) \leq R_d = R_k \psi/\gamma_m$
LRFD	$\phi R_n \geq \gamma_E(\gamma_D C_D \bar{D} + \gamma_L C_L \bar{L} + \gamma_W C_W \bar{W})$
API RP2A	$\phi_s \phi R_n \geq \{\sum_i \gamma_i F_{in}\}_j$
ANS A58	$\phi R_n \geq \sum_i \gamma_i Q_{ni}$
TLP Rule Case	$\sum_j [(Q_{dj}/\bar{R}_{kj})\gamma_m \gamma_{jm} \gamma_c]^{nj} \leq 1$ where $Q_{dj} = \gamma_s \bar{Q}_{sj} + \gamma_q \bar{Q}_{qj} + \gamma_d \bar{Q}_{dj}$
BS 5400, Part 3	γ_{fj}[effects of $\gamma_{fL} Q_k$] $\leq (1/\gamma_{m2})$ function $[\sigma_y/\gamma_{m1}$, other parameters]

Table 1.8: Typical structural material properties an costs [109].

Material	Matrix	Fibre Weight Fraction	Density Laminate (g/cm^3)	Ultimate Tensile Strength (N/mm^2)	Tensile Modulus (KN/mm^2)	Ultimate Compression Strength (N/mm^2)	Material Cost £/kg
Steel Corten 'A'	-	-	7.75	480	207	340	0.4
Aluminium Alloy N8 (5083)	-	-	2.76	275	69	120	2.1
Aluminium Alloy H30 (6082)	-	-	2.76	295	69	255	2.4
E Glass Random Mat	Polyester	0.33	1.44	80-130	7.3-9.3	140-150	1.6
E Glass Woven Roving	Polyester	0.50	1.63	210-300	12-21	150-270	1.8
S Glass Woven Roving	Polyester	0.50	1.64	440	20	210	5.5
Aramid (Kevlar 49) Woven	Polyester	0.44	1.31	430	26	115	17.1
Carbon Fibre Woven	Polyester	0.40	1.40	460	30	-	35.6
Aramid (Kevlar 49) Woven	Cold cure Epoxy	0.55	1.31	450	30	180	28.5
Carbon Fibre Woven	Cold cured Epoxy	0.59	1.47	550	55	360	37.8

Table 1.9: Structural materials and their degree of application to marine structures [10].

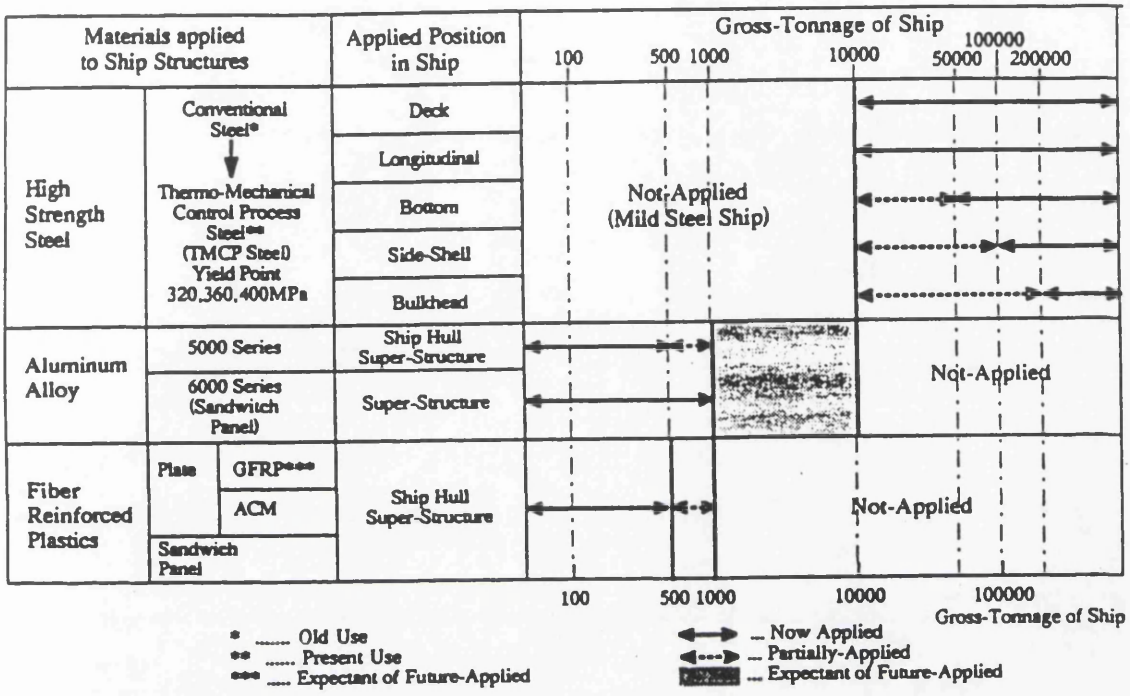

Table 1.10: Design algorithms for the stress distribution in the plating of SWATH vessels as proposed by Sikora et al [120].

Location A
$x = 0$ at $\otimes$ $x = 1$ at longitudinal bulkhead
$A = 0.83 + 2.80\ (b/s)$ $C = 2$
$B = 0.58 - 0.194y$ $\sigma nom = \sigma nom.MD$
$m = 0.41 - 0.625\ \sqrt{y}$

Location B
$x = 0$ at longitudinal bulkhead $x = 1$ at corner
$A = 0.83 + 2.80\ (b/s)$ $C = 1$
$B = 1.01 - 0.806\ \sqrt{y}$ $\sigma nom = \sigma nom.MD$
$m = -B$

Location C
$x = 0$ at main deck $x = 1$ at second deck
$A = 1.20 + 1.784(b/h)$ $C = 1$
$B = 0$ $\sigma nom = \sigma nom.shell$
$m = 0.53 - 0.84y + 0.237y^2$

Location D
$x = 0$ at platform $x = 1$ at second deck
$A = 1.20 + 1.784(b/h)$ $C = 0.5$
$B = 0.94 - 1.96y + 1.12y^2$ $\sigma nom = \sigma nom.shell$
$m = -0.4 + 1.16y - 0.92y^2$

Location E
$x = 0$ strut base $x = 1$ at platform
$A = 1.20 + 1.784(b/h)$ $C = 1$
$B = 0$ $\sigma nom = \sigma nom.shell$
$m = 0.92 - 2.335y + 2.294y^2 - 0.823y^3$

Location F
$x = 0$ at $\otimes$ $x = 1$ at longitudinal bulkhead
$A = 1.83 + 6.114(b/s)$ $C = 2$
$B = 0.276 - 0.187y$ $\sigma nom = \sigma nom.wet\ deck$
$m = 0.716 - 0.754\ \sqrt[3]{y}$

Location G
$x = 0$ at longitudinal bulkhead $x = 1$ at platform
$A = 4.21 - 0.182(b/sh)$ $C = 1$
$B = 0.86 - 1.62y + 0.89y^2$
$\sigma nom = \sigma nom.shell$
$m = 0.186 - 0.44y + 2.51y^2 - 2.035y^3$

Location H
$x = 0$ at strut base $x = 1$ at platform
$A = 4.21 - 0.182(b/sh)$ $C = 1$
$B = 0$
$\sigma nom = \sigma nom.shell$
$m = 1.0 - 0.60\ \sqrt{y}$

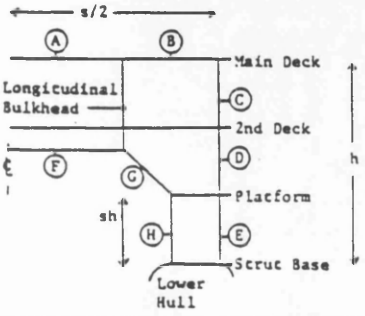

y is in the longitudinal direction
$y = 0$ at transverse bulkhead
$y = 1$ at midbay

Range of Validity
$0.31 < b/s < 0.61$
$1.38 < b/sh < 3.12$
$0.54 < b/h < 1.08$

b = longitudinal spacing between transverse bulkheads

Table 1.11: **Insert plate factor, P, as recommended by Sikora et al for the reduction in the stress concentration levels assumed [120].**

Value of P	Comment
$1.96 - 0.96\sqrt{t/t_o}$	when insert plates exist on the transverse bulkheads, outer shell and longitudinal bulkhead/first platform
$1.57 - 0.57\sqrt{t/t_o}$	when insert plates exist only on the outer shell
$1.75 - 0.75\sqrt{t/t_o}$	when insert plates exist only on the transverse bulkhead

Notes: t thickness of insert plate
t_o thickness of parent material

Figures

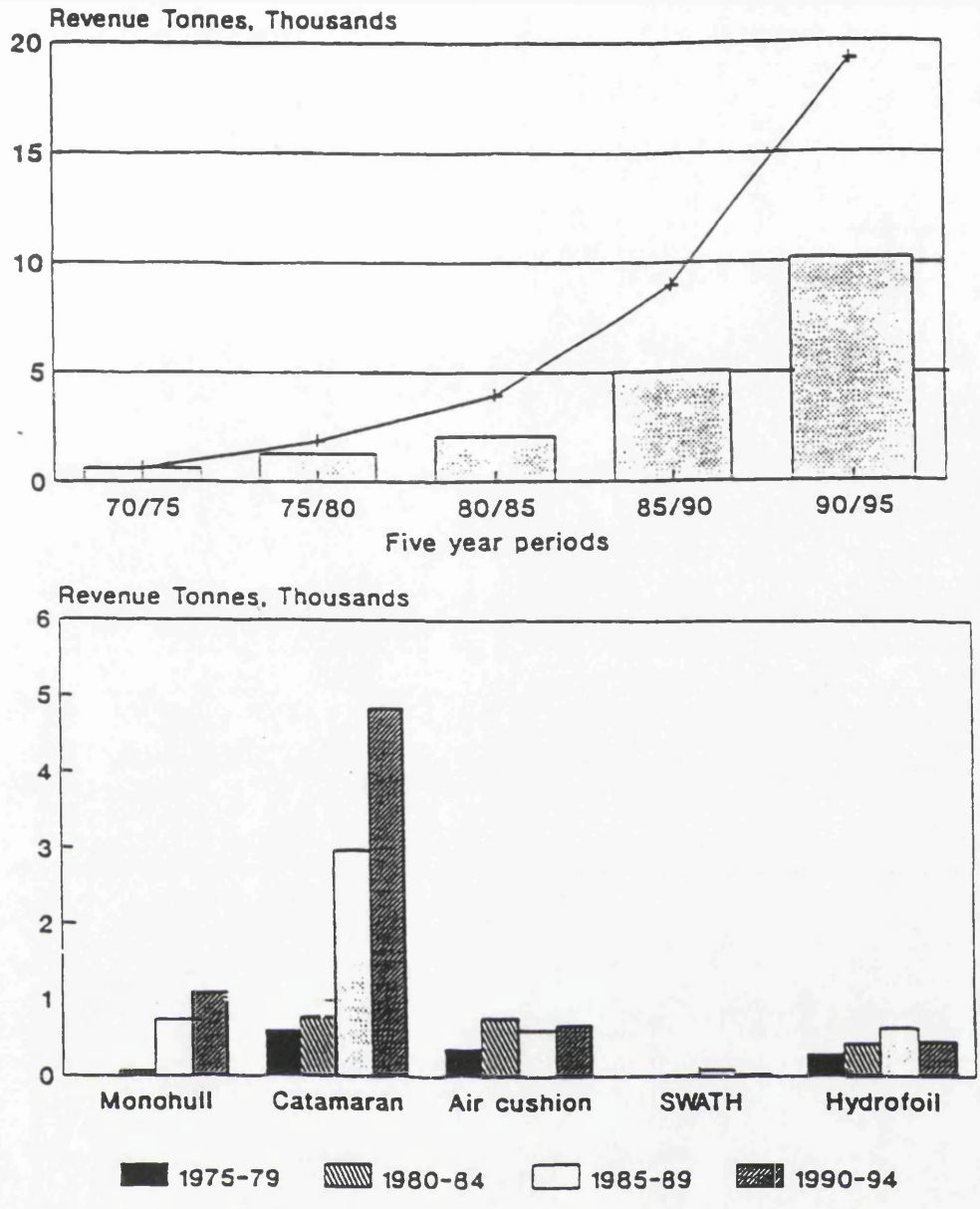

Figure 1.1: The growth in fast ship construction since 1970 [21].

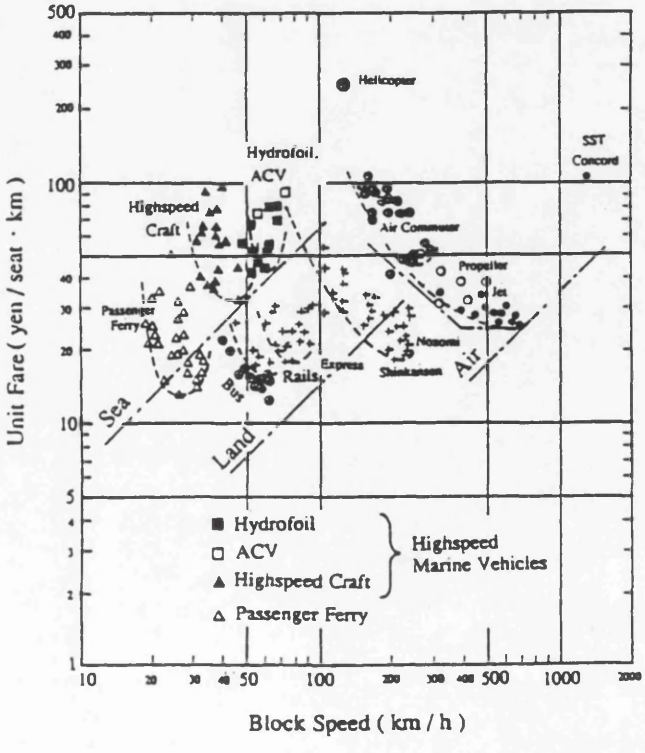

Figure 1.2: Variation of fares with speed for all transportation modes [8].

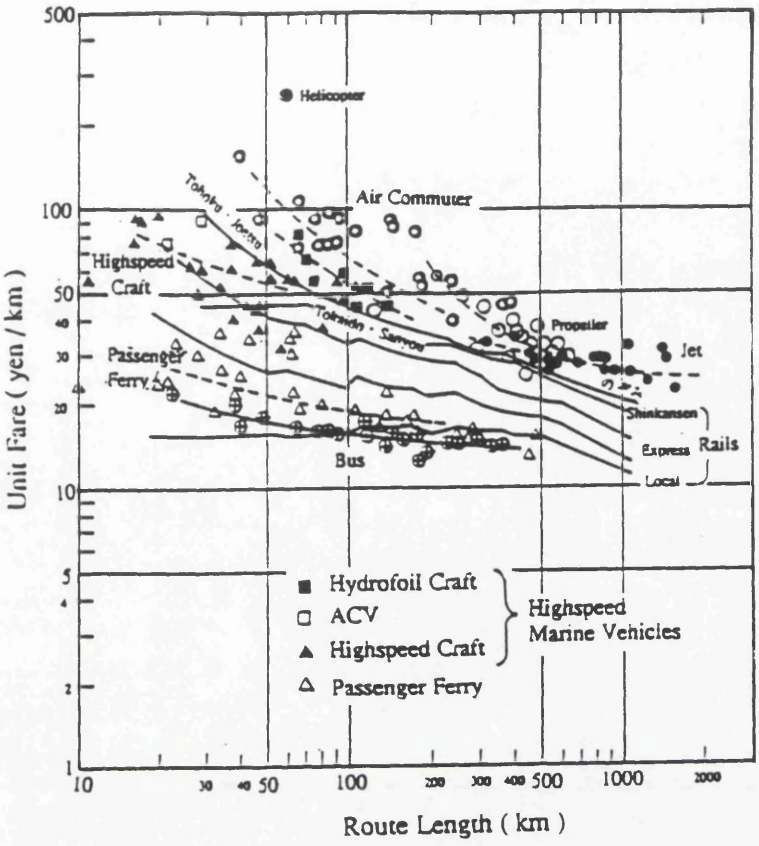

Figure 1.3: **Variation of fares with route length for all transportation modes [8].**

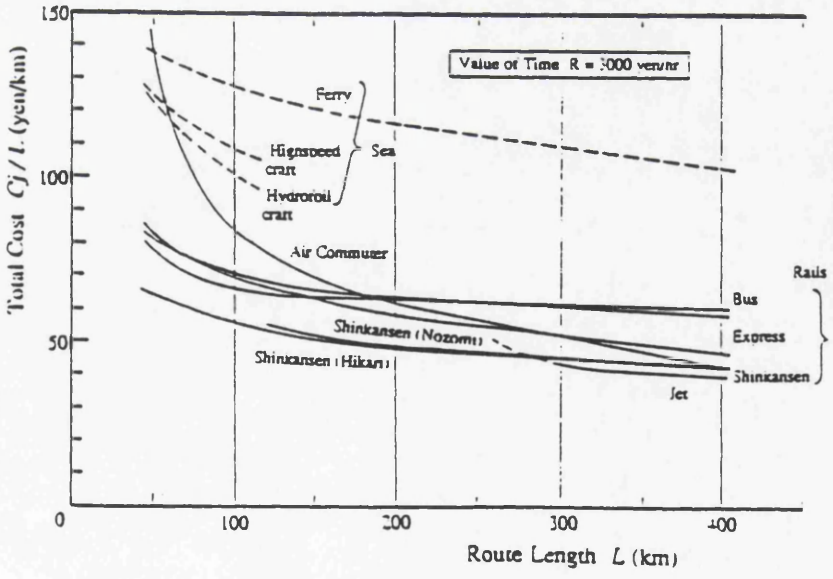

Figure 1.4: **Variation with route length of the operational cost of all transportation modes [8].**

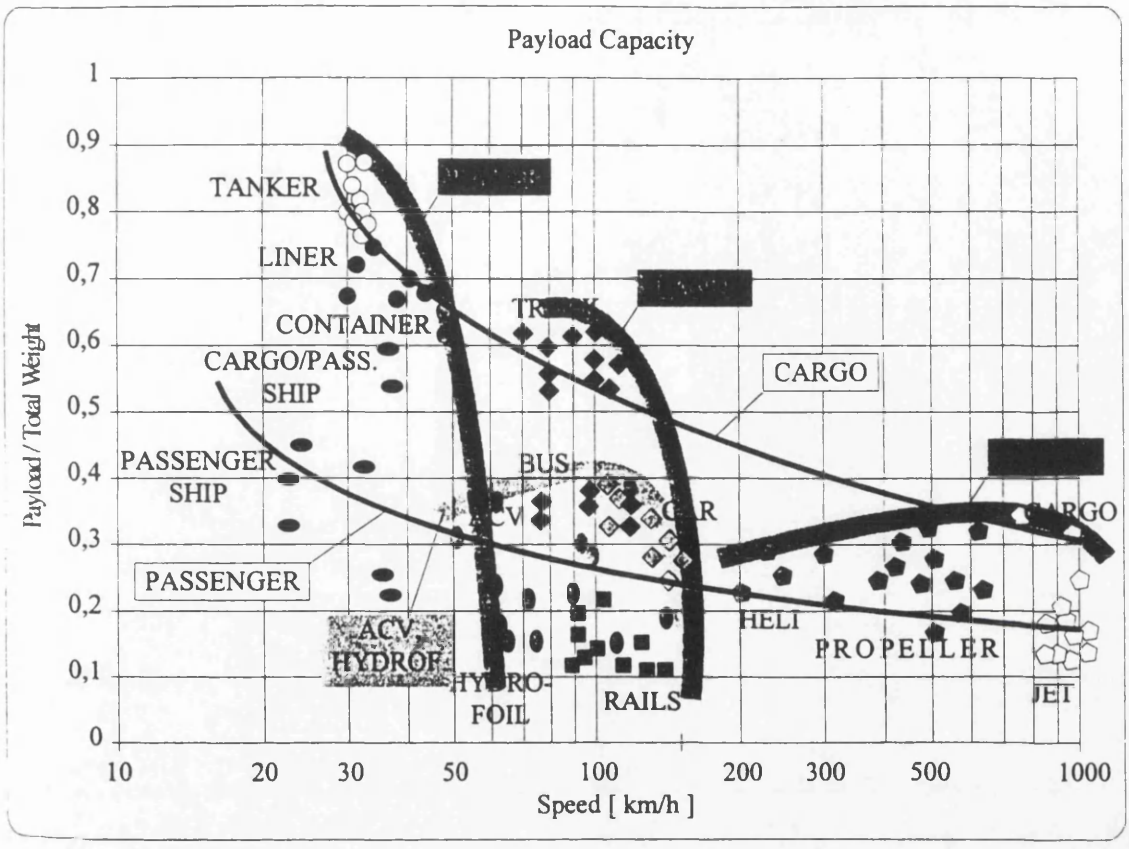

Figure 1.5: **Payload fraction variation with speed of transportation [128].**

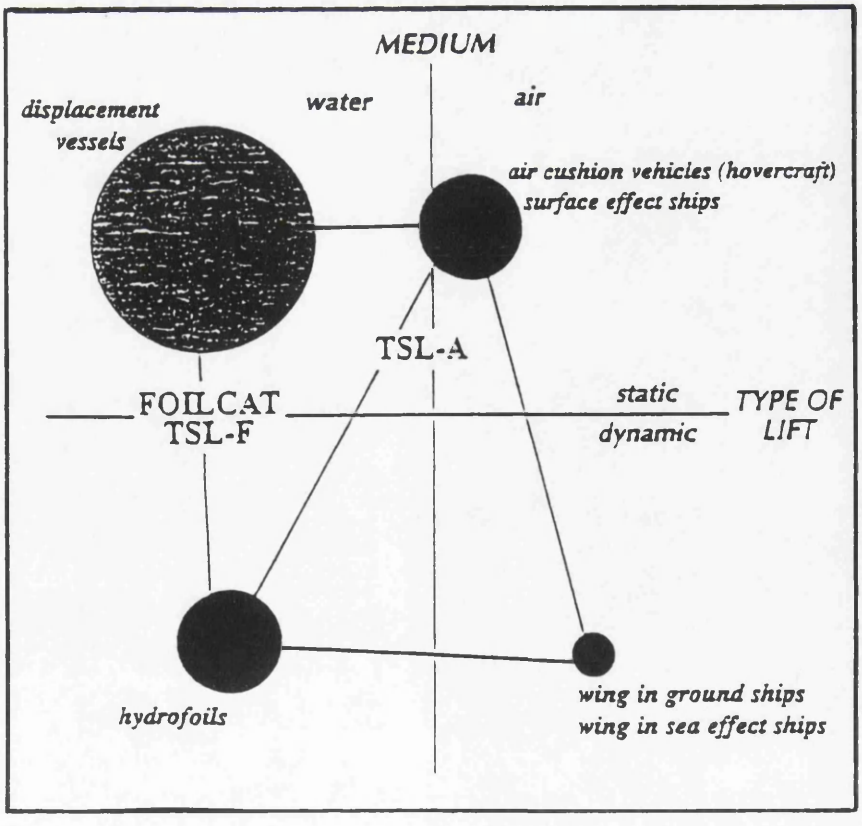

Figure 1.6: **The types of fast marine craft and their sources of lift [20].**

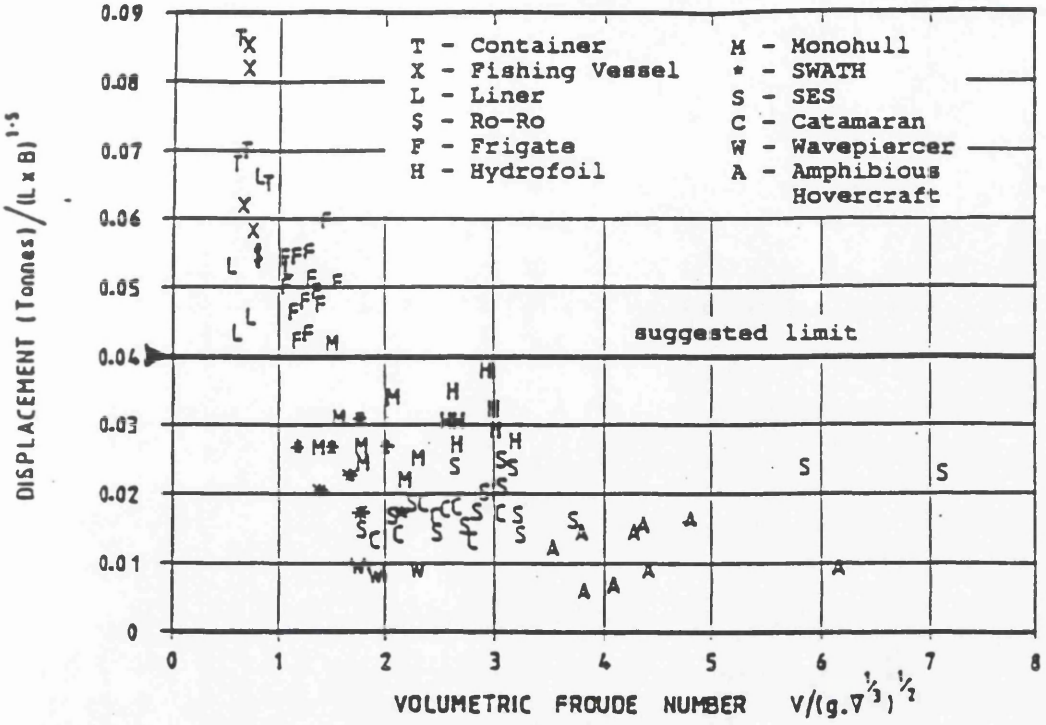

Figure 1.7: Blyth's limits on the definitions of 'small' and 'fast' marine vehicles [10].

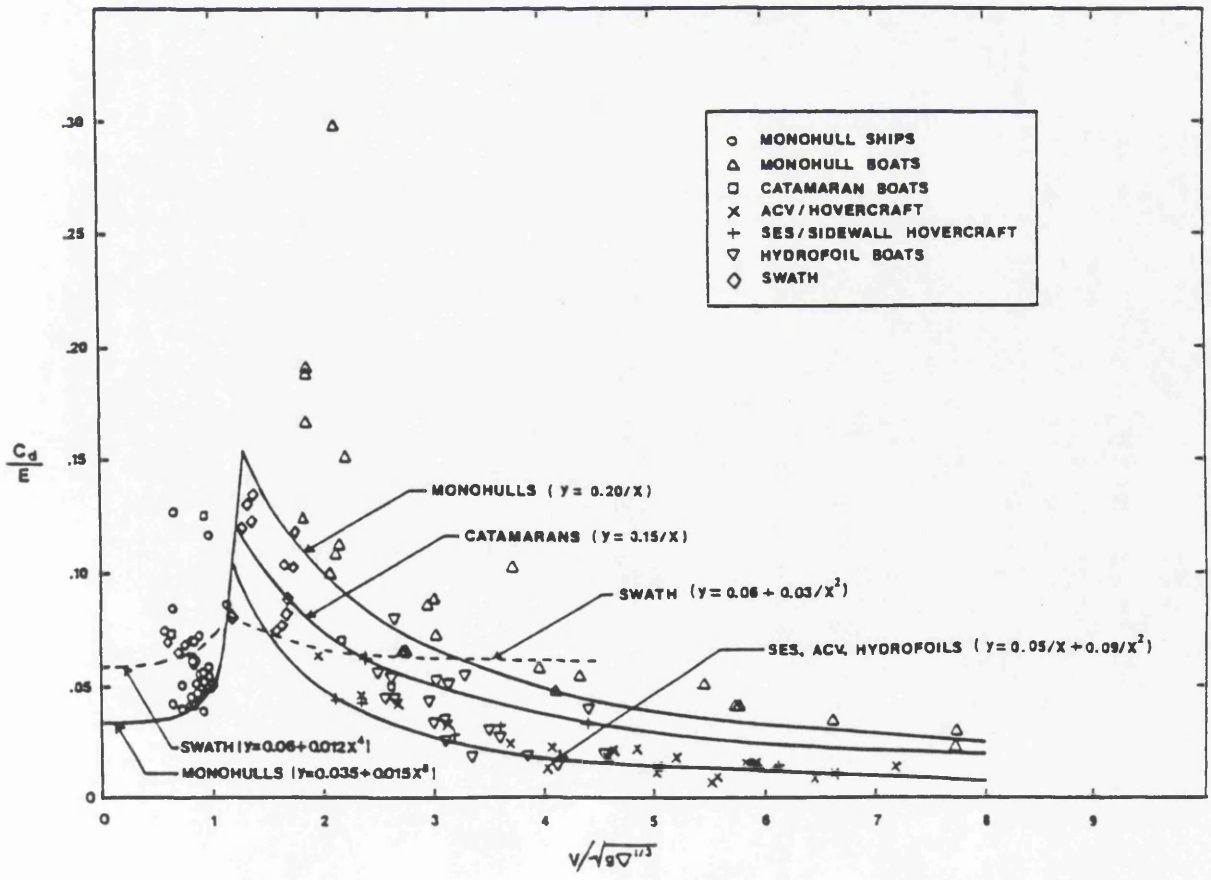

Figure 1.8: Normalised drag coefficient versus Froude number for a number of fast marine concepts in calm water [12].

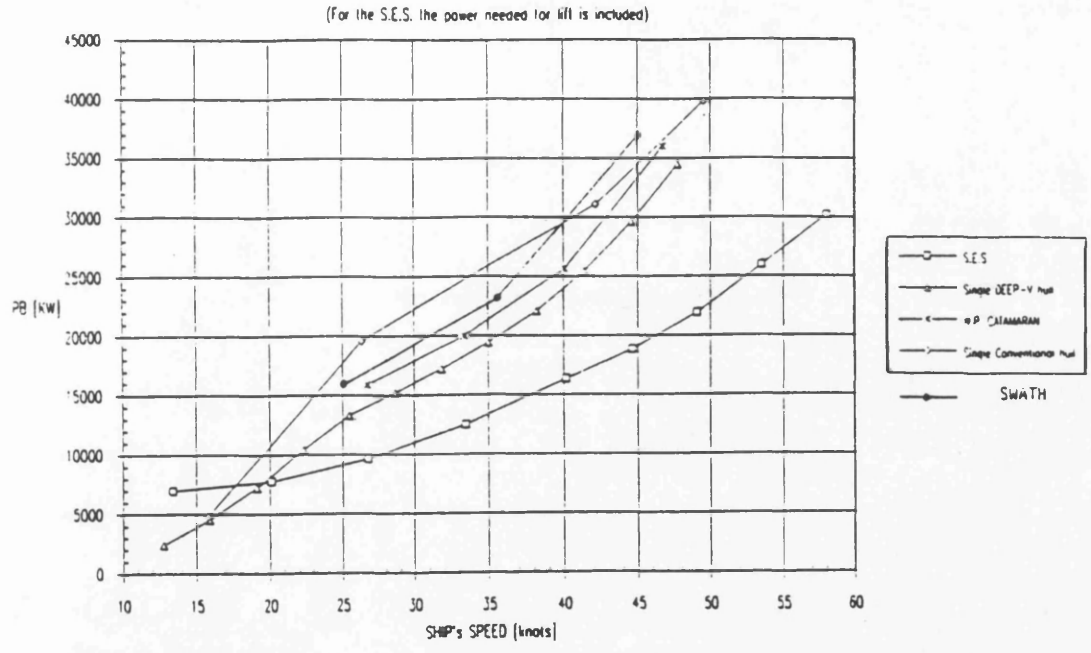

Figure 1.9: Power requirements versus speed for a variety of fast marine vehicles of 1000 t displacement [129].

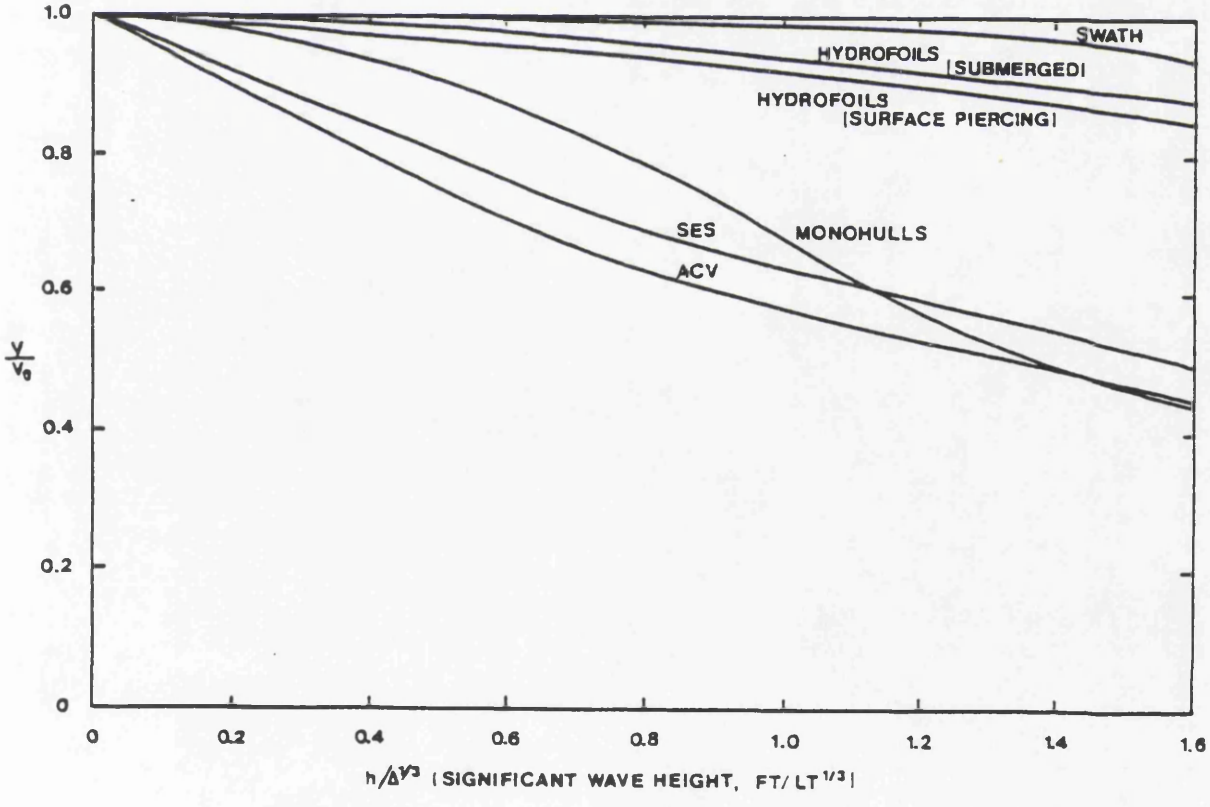

Figure 1.10: The level of speed reduction in waves for a variety of fast marine vehicles [12].

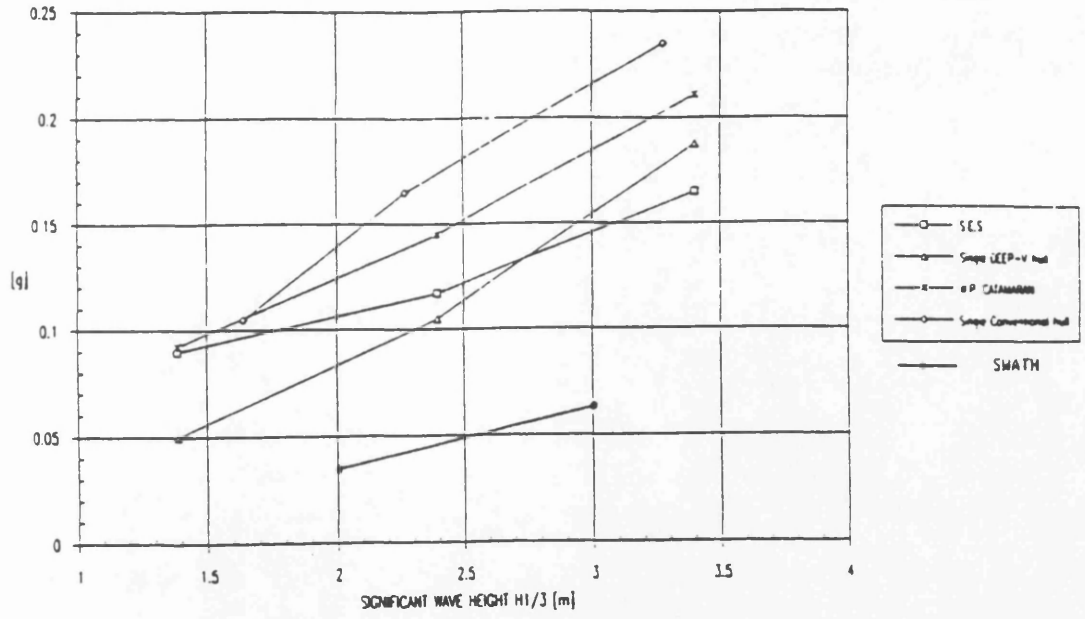

Figure 1.11: Vertical acceleration amidships versus significant wave height at 45 knots for a variety of fast marine vehicles of 1000 t displacement [129].

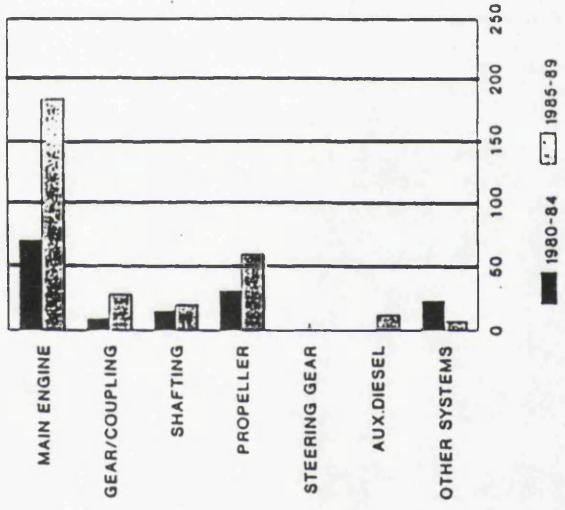

Figure 1.12: Recorded machinery damages on fast craft classed with DNV [19].

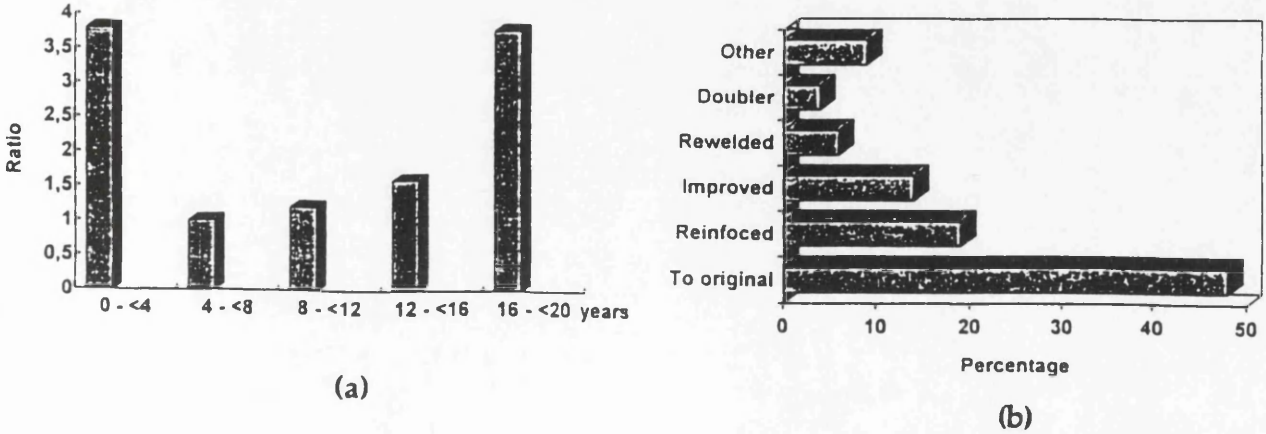

Figure 1.13: (a) Number of damages over the number of all fast craft classed with DNV, (b) Repair method after damage [19].

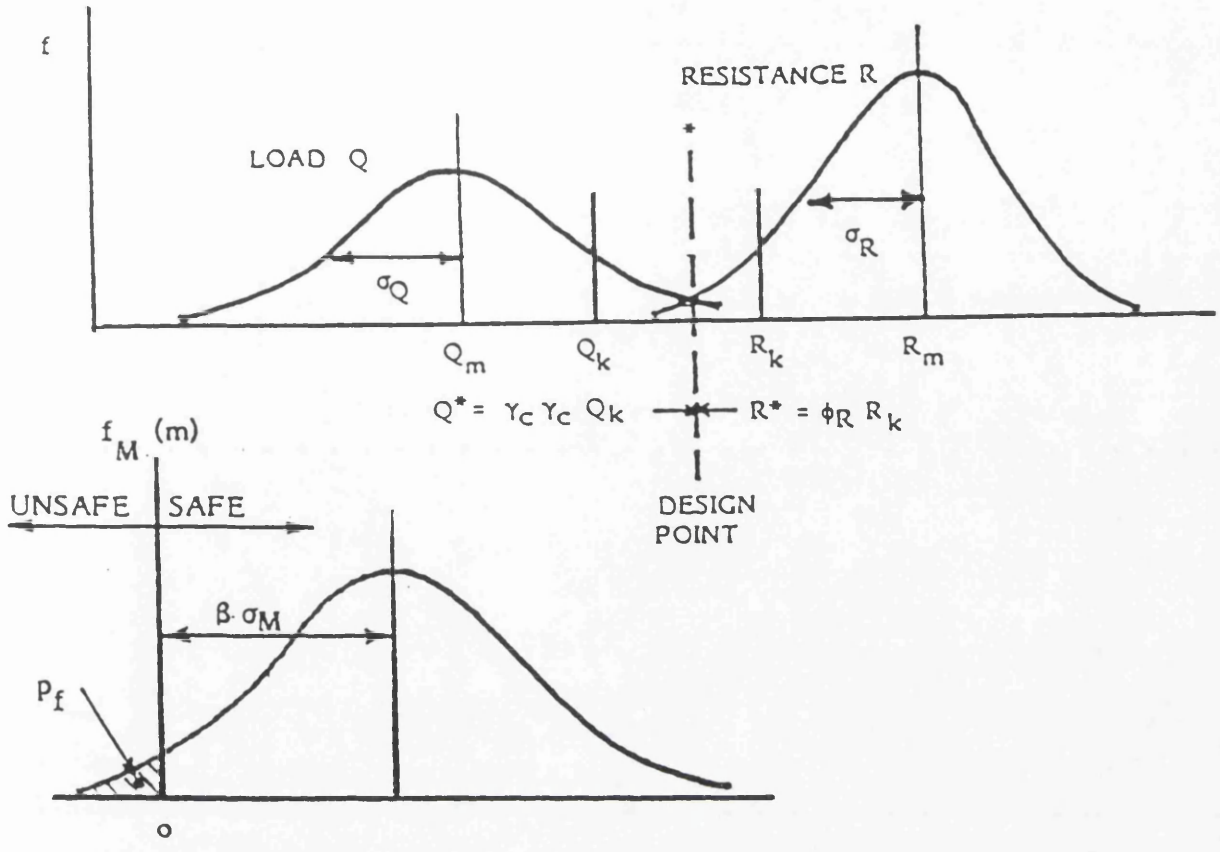

Figure 1.14: **Illustration of (a) the reliability index, partial safety factors and (b) safety margin [33].**

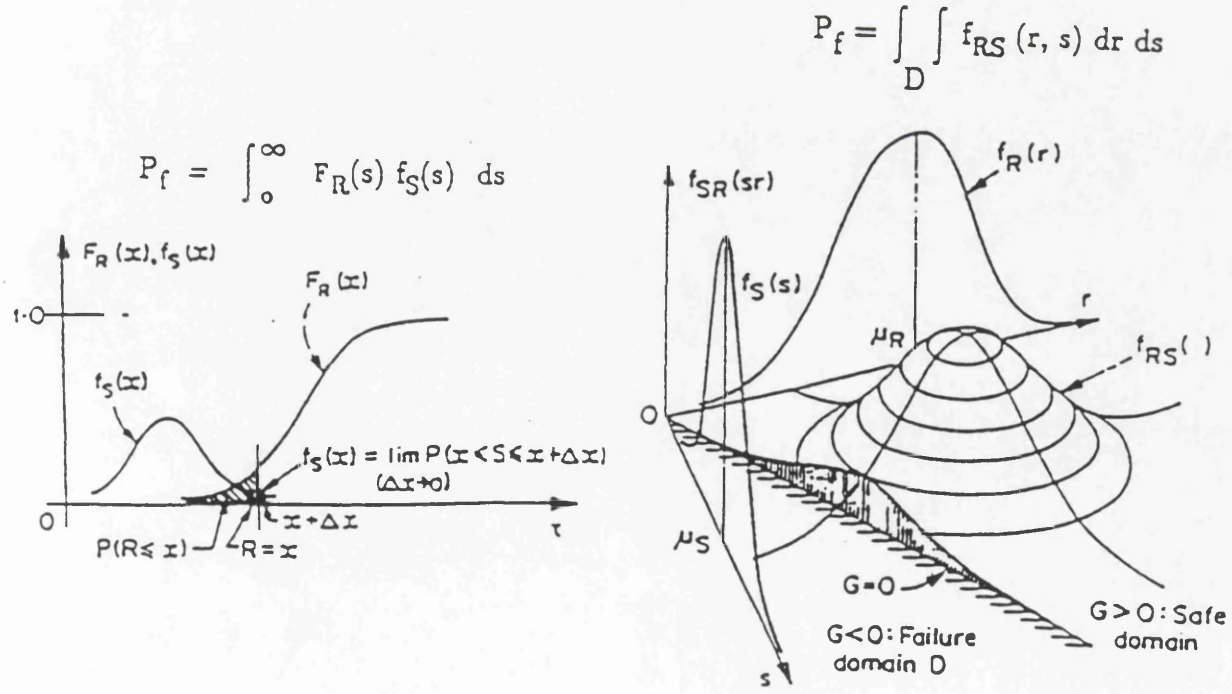

Figure 1.15: **Graphical representation probability of failure estimation by Level 3 reliability methods [33].**

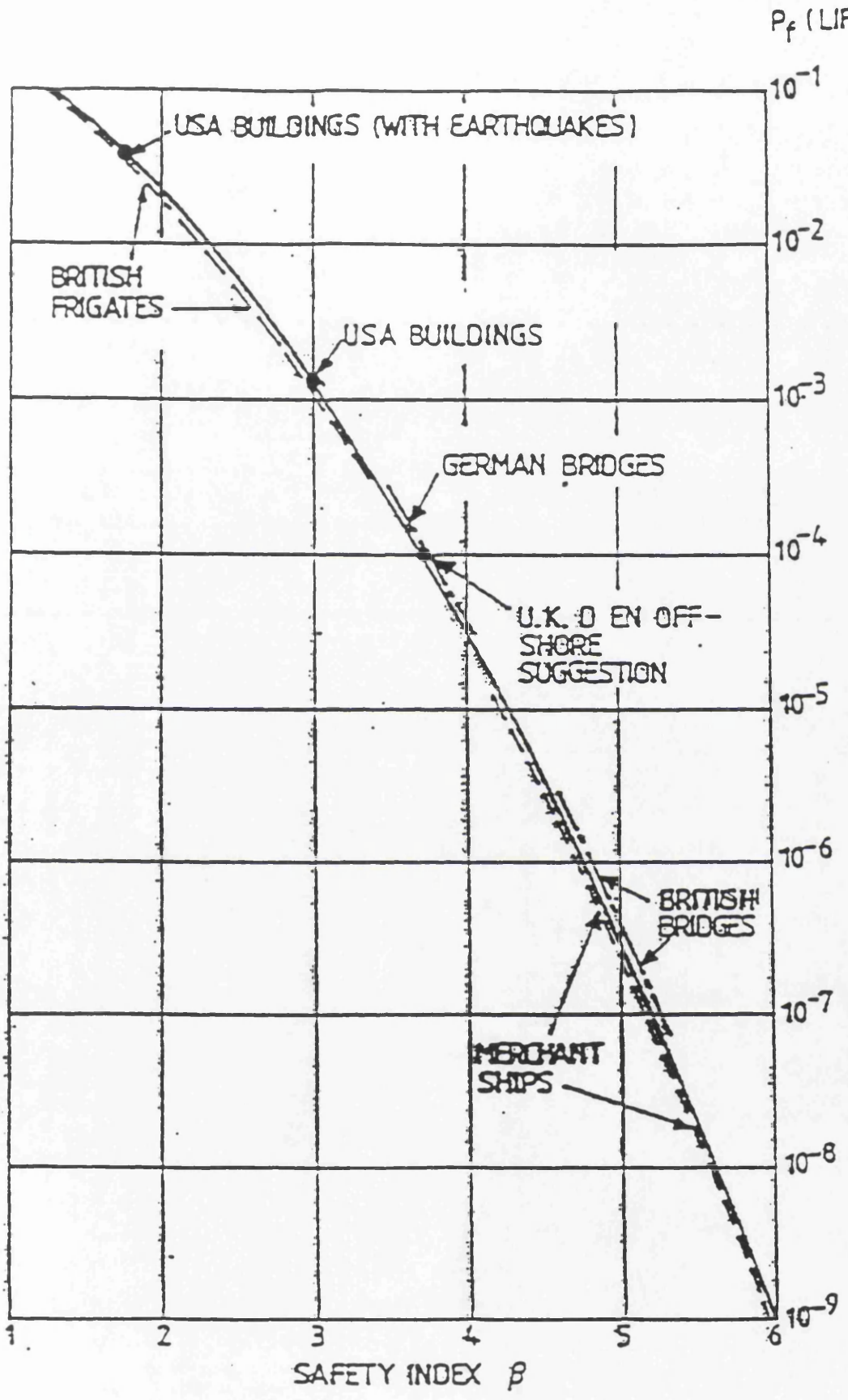

Figure 1.16: Safety index versus failure probabilityas implied by design codes worldwide for a variety of structural systems [33].

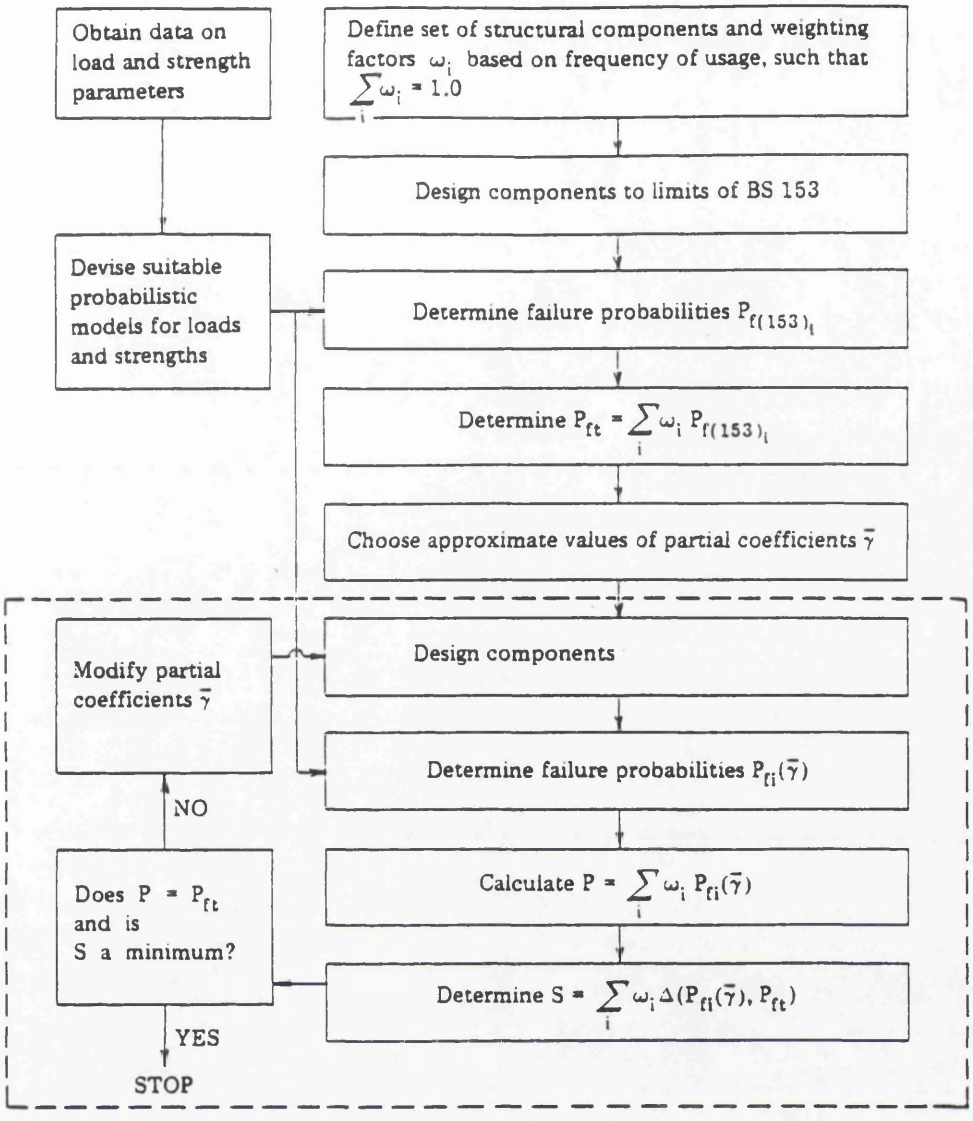

Figure 1.17: **Graphical representation of the procedure for the derivation of β-calibrated partial safety factors [93].**

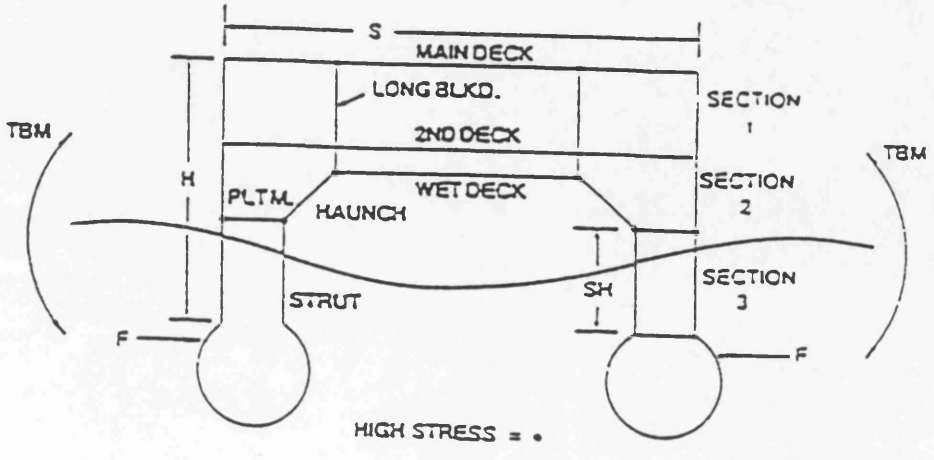

Figure 1.18: **The main structural elements of a SWATH ship.**

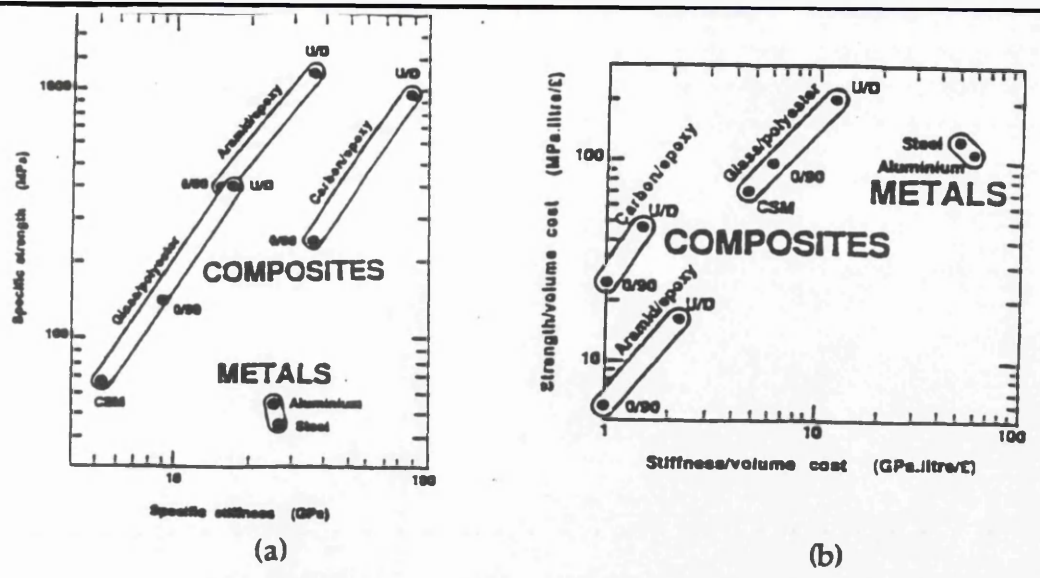

Figure 1.19: (a) Specific strength and stiffness characteristics (b) strength and stiffness characteristics on a volume cost basis, of the main structural materials [94].

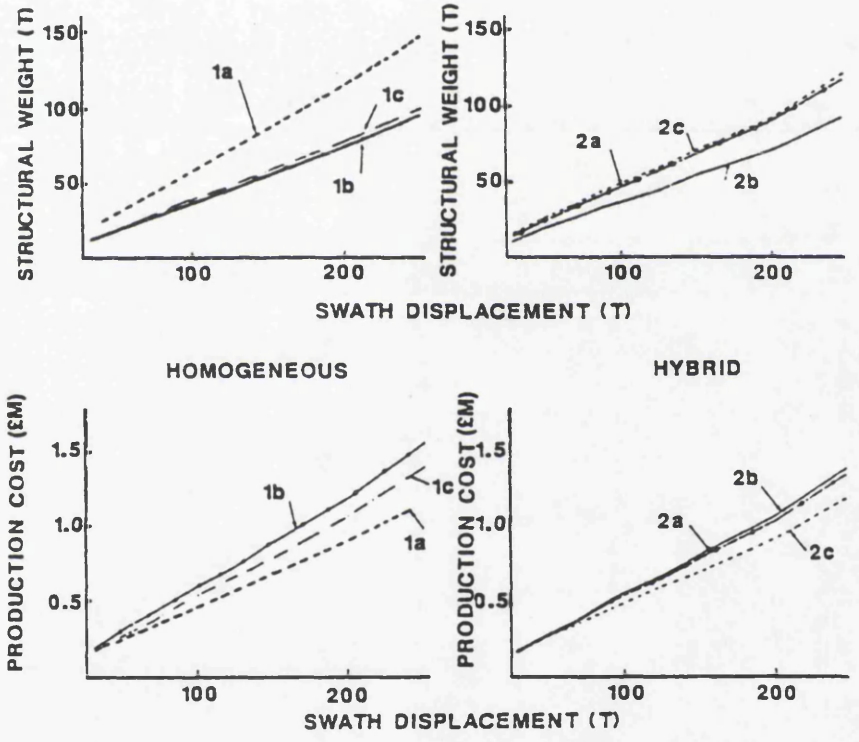

Class	Structural Material			Comments	No.* Built
	Hull	Box	Deckhouse		
1. Homogeneous					
1a	Steel	Steel	Alloy	Heavy	2**
1b	Alloy	Alloy	Alloy	Light	4
1c	FRP	FRP	FRP	Light	1
2. Hybrid					
2a	Steel	Alloy	Alloy	Semi-Heavy	2
2b	FRP	Alloy	Alloy	Light	0
2c	FRP	Steel	Alloy	Semi-Heavy	0

* End 1985.
** One of which has a steel deckhouse.

Figure 1.20: Comparison of structural weight and production cost as functions of displacement of small SWATH ships for different materials [95].

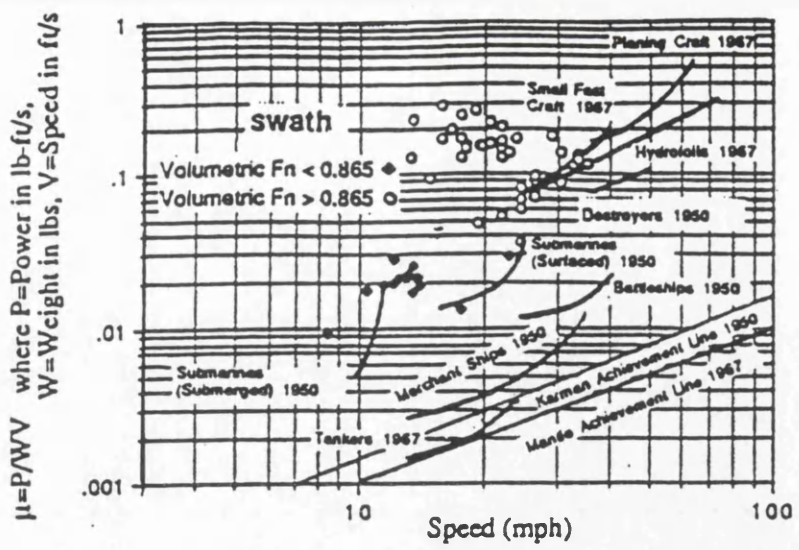

Figure 1.21: Gabrielli and von Karman diagram for SWATH ships [111].

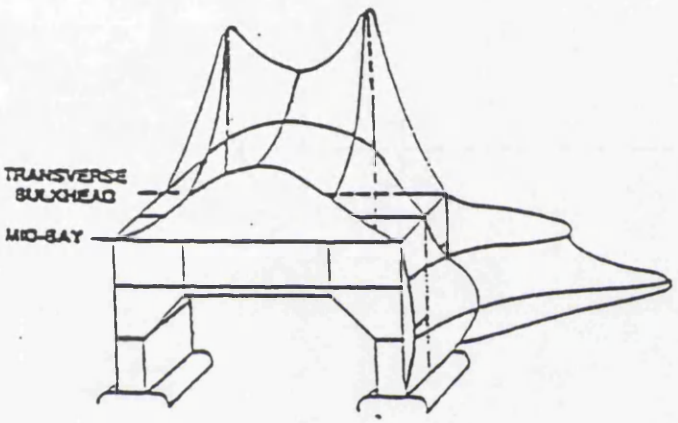

Figure 1.22: Transverse stress distribution in the plating of a SWATH structure [120].

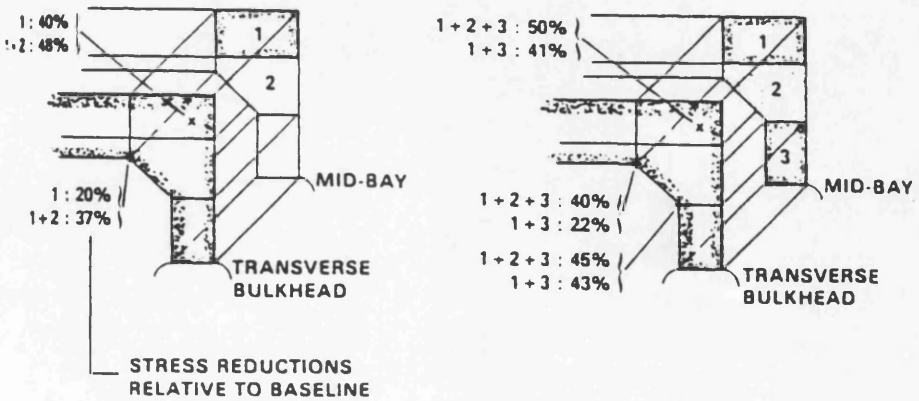

Figure 1.23: Percentage of stress level reduction due to the introduction of partial transverse bulkheads [120].

CHAPTER 2

2.0 Wave Load Considerations in the Design of SWATH Ships

2.1 The Nature of Wave Loads on SWATH Ships

Loading is identified as presenting the largest uncertainty in any design process and strength check formulations [12] and its accurate estimation should be the first step in any structural design procedure. Rational modelling of its effects is hence of tantamount importance if proper use is made of more elaborate ultimate strength modelling of structural response. A probabilistic approach helps to counteract some of this inherent uncertainty.

Overall, there are six components of wave loads acting on the cross deck structure of a SWATH ship due to wave excitation, namely (Fig. 2.1) the vertical bending moment, M_5, the transverse side force, F_2, the vertical shear force, F_3, the longitudinal force, F_1, and the yawing and torsion moments, M_4, M_6. These loads and their effects are generally grouped under the two main headings of *primary loads* and *secondary loads*.

2.1.1 Primary Loads

In contrast, to monohull ships which absorb the primary loading effects in the longitudinal direction, SWATH and multi-hull ships are primarily loaded by the seaway in the transverse direction. Hence, it is not unusual for these structures to be transversely framed. The primary load conditions requiring attention during the vessel's lifetime are, (a) extreme wave induced and still water longitudinal vertical bending moment, (b) extreme wave induced side force and transverse bending moment, (c) fatigue loading, (d) extreme torsional loads, (e) extreme vertical shear loads on the cross-deck.

2.1.1.1 Longitudinal Loads

For a monohull, wave induced vertical hull bending moments are the primary and most important seaway loadings and are most severe in head seas. This loading is also exerted on a SWATH structure and it can be predicted using classical beam theory. But it is generally found not to dominate the structural design procedure as much as the remaining loads

do. Vertical bending in multi-hulled vessels however, becomes more important for multi-thousand tonne designs [5]. Sikora [13] recommends the following empirical algorithm for an approximate estimation of vertical wave bending moments for SWATH ships:

$$M = 0.0011\, B_s\, L_s^{2.5}$$

where M is in feet-tons, B_s is the width between both strut centres (in feet), and L_s is the length of each strut (feet). The superposition of any coexistent static longitudinal loads (e.g. still water bending moments) is also necessary. These loads will be treated no further.

2.1.1.2 Maximum Vertical Shear Loads

Vertical shear loads on the intersections between the haunch and the cross decks in the SWATH structure arise mainly due to the deadweight of the box-structure and differences in inertial heaving amongst the haunch and the cross deck. The shear loads thus introduced due to deadweight remain constant across the span while the inertial forces are maximum at the cross-structure/ strut intersection and drop to zero on the centreline. Chalmers in [14], references unpublished US data suggesting that the total vertical shear force at the cross-deck box structure just inboard of the haunch is given by:

$$V_{max} = 0.25\, F_{max} + 1.25\, g\, M_{b/2}$$

where $M_{b/2}$ is half the box mass and F_{max} is the maximum side force.

2.1.1.3 Side Loads

The most significant primary loads on the SWATH structure are imposed by the wave induced side force, F, and resulting transverse wave bending moment flexing the struts inwards or outwards. The side force, the resultant of an integration of the dynamic pressures, is a maximum at beam seas and zero speed, reduces to about half that magnitude in bow and stern quartering seas and decreases to near zero in head and following seas. Figure 2.2 shows the side load variation with heading [22].

The transverse bending moment causes the main deck to be in tension during the squeeze cycle, forcing it into compression during the pry cycle.

As the resulting transverse stresses do not behave classically because of shear lag of the deck plate elements and stress concentration effects in the haunch/deck connections, a FE analysis must be used to determine the local load distribution in this part of the structure. The value of the bending moment is directly linked to the magnitude and point of application of the side force. Experimental results [15] suggest a vertical point of application of mid-draught for beam sea conditions, and mid-draft to 0.6 of the draft for quartering seas. The Royal Navy assumes a point of load application at mid-draught.

Apart from the importance of the position of the point of application of the side force on the magnitude and the type (torsion etc.) of the transverse bending moment, the longitudinal distribution of the side force can be essential. Sensitivity studies carried out, via FE calculations, [15] using uniform, trapezoidal, and sinusoidal side load longitudinal distributions (with the total load kept constant for every case) show that despite the significant variation of loads locally, the resulting stresses are similar as the loads are redistributed in the structure. Hence, for design purposes a uniform load distribution may be assumed when analysing the complete ship. When analysing a load section a 10% increase in the local load value is considered to be sufficiently safe.

Available model test data [16] demonstrate that the side force and transverse bending moment, increase rapidly with wave height in lower sea states up to some significant side load and then levels off at the peak value (Fig. 2.3). The maximum value of side force is typically in the range 0.2-1.2Δ [5] while in heavy seas the maximum side force to displacement ratio lies in the region 0.5-1.0 depending on geometry. The ratio does not increase further in extreme seas The reasons are:

1. the wavelength of maximum energy tends to increase as the significant wave height grows, while the peak side load response occurs in shorter waves
2. extreme wave conditions occur less frequently than moderate ones.

Exceedence of the design load in storm conditions should therefore need not be of major concern to the designer. Furthermore, research in the U.K. and the U.S. has shown that [2, 4, 9, 11, 15, 17-22] for a given wave height the side force is maximum at wave lengths 3-4 times the underwater beam of

the ship while there is a general trend for the maximum side load to decrease as a fraction of displacement as the displacement increases to values above about 400 tonnes (Fig. 2.4). Furthermore, changes in draft produce the greatest change in the side force and bending moment applied on the cross deck.

2.1.1.4 Fatigue Loads

Due to hull flexing in a seaway, fatigue damage must be expected at the lower hull/strut, strut/haunch and haunch/cross structure welds and any changes in the transverse bulkhead geometry and arrangement that might introduce considerable stress concentrations. The problem is often made worse by the use of high tensile strength materials, as these materials encourage higher stresses and slenderer structures. Proper design of the joints is vital. Paragraph 2.4 describes in reasonable detail the methods currently used for the fatigue load prediction of sea going structures and the implications that increased speeds and variability of headings have on the fatigue loading of fast craft. Chapter 3 describes in more detail the strength considerations that need to be addressed in fatigue strength analysis and pays particular attention to the use of aluminium material.

2.1.1.5 Torsional Loads

The worst case of torsional loading for a SWATH ship is when it is supported at diagonally opposite corners and hence occurs during drydocking or grounding accidents (non-sea-going conditions). The second most important torsional loading is the yaw torsional moment at sea encounter angles between 15° and 45° (bow or stern) off the beam. For design purposes, Sikora and Dinsenbacher [13, 15] propose the estimation of the yaw torsional moment, T:

$$T = K \times \text{Side Force} \times \text{Strut length}$$

where K is a torque arm factor which is a function of heading (Fig. 2.5). The maximum lifetime yaw torsional moment can be obtained by applying the maximum lifetime side force value at a forward or aft eccentricity (trapezoidal distribution assumed by Sikora). The lever arm will vary between 0.05-0.25 of the strut length [13]. Furthermore, Chalmers in [14], reports on unpublished US data giving the maximum torsional loads by:

$$T = 0.13\, F_{max}\, L_s \qquad \text{for the cross deck}$$

$$T = 0.29\, F_{max}\, L_s \qquad \text{for the struts}$$

where L_s is the strut length and F_{max} is the maximum side force. These values are applicable for seas between 15° and 45° off beam.
These loads will be considered no further. For further reading on the subject, references [2, 4, 9, 11, 15, 19-24] may be consulted.

2.1.2 Secondary Loads

The secondary loads applied on a SWATH structure ship are similar to, and of the same severity as those encountered in monohulls. The main secondary load components include:

- slam induced impacts
- wave slapping
- hydrostatic pressures
- docking and berthing
- ice loads
- collision

In SWATH ships slamming loads can be quite severe locally and govern the local structural design, i.e. the design of the scantlings and plate thickness of the wet deck, the haunch, the inner strut shell and the outer strut shell up to the main deck. These loads are generally amplified by ship speed. On the other hand, the design of the lower hulls is normally governed by hydrostatic and drydocking loads.

For slamming pressure loading, experimental test results of models of the T-AGOS 19 in the U.S. [15] support the conclusion that the extreme value slam pressures vary longitudinally on the wet deck plating with maximum value occurring within a distance of 20% of the hull length from the bow, dropping linearly from there onwards to a distance of 40% of the hull length from the bow where the pressure level is at 50% of that encountered at the bow. From that position to the stern of the vessel the level of slamming pressures will remain fixed (50% of the pressure load at the bow). It was further concluded that, the haunch and strut slam pressures are most severe in beam seas and do not vary significantly longitudinally. The inboard strut pressures were found to be approximately half the outboard strut lifetime pressure. It is worth noting that high peak pressures occur

only over very small areas while pressures over larger areas are reduced proportionately. Hence, design pressure must be referenced to a related area and therefore pressures measured at model scale must be scaled to full scale values and adjusted for different panel sizes for use in design. Figure 2.6 provides the variation of slam pressures with area considered.

A trade-off exists between the primary side loads and the local impact loads on the wet deck because an increase of the wet deck clearance to reduce slam loads simultaneously increases the bending loads in the cross-structure. Interaction of side load and wet deck slamming load effects is normally not considered necessary because their maximum values would not occur simultaneously [2, 15, 18, 20]. An experimental investigation into the effects of ramp angles on the level of slamming pressure loads is presented in paragraph 2.5.2 and 2.5.3.

Wave slapping loads on the side shells can be treated in a similar manner to slamming pressure loads.

In turn, for an initial estimate of *hydrostatic loads*, the Royal Navy [14] recommends the use of the same approach as that used for monohulls. That is, to design for a static head of 5m to allow for wave effects superimposed on to the normal hydrostatic pressure head (calm water and no heel angle) and an allowance for rolling and pitching motions (25 and 10 degrees respectively).

2.1.3 Side Load Estimation Procedures

The wave load prediction for SWATH ships is based on the adoption of both analytical and experimental methods whose use is preferred at the detailed design stages. At the concept design stage, however, empirical and semi-empirical formulations for the maximum applied design load will generally be more than satisfactory. The random nature of ocean waves, encourages a stochastic approach to load estimation and therefore long- and short-term statistical analysis of wave spectra is used in deriving the likely extreme load responses for use in fatigue and ultimate strength design. The background and current procedures used by these practices is presented in the following sections.

2.1.3.1 Empirical Side Load Estimation Expressions

In the preliminary design stages, side load values may be estimated using approximate formulae available in the open literature. Empirical formulations derived from experimental data on SWATH models as well as FE estimations of the distributions of loads on the structure prove very useful and are presented next. The expressions are based on the application of the side load at half draught and are of simple, closed-form nature, based on principal dimensions and form coefficients.

The Sikora and Dinsenbacher Proposal: Sikora et al [17] have used a spectra-based method for predicting primary side load fatigue spectra for SWATH ships. A result of this work was the first empirical formulation for side load prediction [17]. This expression was based on a series of fifteen model tests of various SWATH ship geometries whose maximum side load values were obtained via a spectral wave analysis. Parametric studies of wave loads were carried out using the theoretical prediction described by Lee and Curphey [4]. Six basic parameters, namely, the hull and strut lengths, hull separation, draught, metacentric height, waterplane area and displacement, were investigated and it was the length, draught and hull separation that were found to greatly influence the load values. Hence Sikora et al [17] derived the following maximum lifetime side force algorithm for ships in the region of 3,000-30,000 tons, assumed to operate 3,600 days at sea at random headings:

$$F_{max} = \Delta\, D\, T\, L$$

where Δ is the displacement (in tons), d is the draught (in feet) and

$$D = 1.55 - 0.75 \tanh\left(\Delta/11{,}000\right) \qquad T = 0.532\, d/\sqrt[3]{\Delta}$$

$$L = 0.75 + 0.35 \tanh\left(0.5\, L_s - 6.0\right) \qquad L_s = \left(\text{strut length (ft)}\right)/\sqrt[3]{\Delta}$$

This expression presents a mean value with standard deviation of 10.5% when compared with model test results [15]. Stirling et al [18] take the standard deviation of this expression to be 20% for its application to any new SWATH geometry. A characteristic load, which is equal to 0.67 of the maximum expected side load rather than the expected extreme value

provided by the expression above is finally used in SWATH design as has also been the case for monohulls.

The Royal Navy Proposal: The design load practice in the U.K. for both monohulls and SWATH ships requires the use of the higher (than Sikora/US Navy expected value) 1% probability of exceedence load in the vessel's lifetime for both ultimate strength and fatigue strength estimations. Furthermore, for SWATH applications the bending moment for ultimate strength formulations is taken to be 1.1 times higher than the design bending moment predicted by analytical procedures [18]. Normally, theoretical load prediction methods are used which account for the hydrodynamic loads on the structure by means of three dimensional singularity distribution panel methods (computer codes by Glasgow University and Bishop and Price - para. 2.1.3.3). At the concept design level, however, where accuracy of the load prediction is not as important, the Sikora et al [17] closed-form expression is used with changes to account for:

- the need in the U.K. approach to use the higher 1% probability of side load exceedence in the ship's lifetime
- differences in the ships life and operability (30 year life at 70% operability for the US and 25 years at 70% operability for the UK)
- errors in the model load measurements (assumed at 5%)
- differences in the statistics of the sea and the mission profile.

As a result of these changes, the side load modelling uncertainty has a bias of 0.990 and standard deviation of 0.255. The 1% probability of exceedence value corresponds to 2.33 standard deviations above the mean, introducing a factor of 1.584 above the expected value given by the Sikora algorithm. Hence, there seems to be no direct relationship between the UK and the US design loads, but in general the UK values are considerably higher [18]. The effects that other lives or operabilities will have on the factor considered are expected to have negligible effects on its value [18]. The design side load is assumed to act at half draught and uniformly distributed along the length.

Another estimate for expected lifetime side load, F, is given by an empirical formulation derived at *UCL by Betts* from regression analysis of published data [27]. The displacement, Δ, is in tonnes:

$$F_{max} = K \Delta^{0.77}$$

where K id equal to 7.94 for single struts and 4.26 for tandem struts.

All of the above formulations require the ship's main dimensions to be already known before being applied. If this is not the case the design spiral may be initiated with a first shot at the maximum lifetime side load between 0.95 Δ and Δ as proposed by Luedeke et al [25, 26].

Classification Society Expressions: ABS [19] are the only classification society that have published rules specifically for SWATH vessels. The side load estimation expression in these rules has been based on the Sikora and Dinsenbacher approach presented earlier. Besides the side load, ABS [19] also provide simplified empirical formulae to determine the transverse bending moment, longitudinal bending moment, vertical shear force and wave impact to be applied in the design. Other codes applicable to high speed craft in general have been presented by Lloyd's [28] and DNV [29]. The respective expressions may be obtained from the codes themselves. DNV has classed most of the current high speed craft and their rules are comprehensive and widely referenced [5].

Figure 2.7 presents a comparison for the geometry of a 3,500 ton SWATH ship (T-AGOS 19) of various maximum side load predictions with the Sikora and ABS methods. The methods are a short term spectral analysis based on Pierson-Moskowitz sea spectrum (Expt (3) in the figure), a long term spectral analysis carried out by DTNSRDC (Expt (4) in the figure), by a the use of 3-D oscillating source distribution technique which ignores viscous effects (Chan's approach in para. 2.1.3.3), and an approximate approach based on a small body assumption (if incident wavelength λ and D, the characteristic dimension, is such that $D/\lambda < 0.2$ and hence wave diffraction effects are neglected) [12]. The Sikora and ABS predictions are found to lie close to the long-term prediction as their derivation has been based on them. The 3-D method prediction is the most conservative due to the neglect in the calculations of the viscous effects which are the dominant motion dampers in SWATH ships. The approximate method is also conservative due to its failure in high frequencies [12] and the empirical formulations were found to provide conservative estimates. Hence, once the main dimensions become known, Sikora's or the ABS expressions are recommended for use. Prior to the estimation of the main dimensions, the simpler Luedeke or the Betts expression can be used for large SWATH ships (this expression is quite conservative, especially for small vessels).

2.1.3.2 Empirical Formulations for Load Combinations

To account for primary load combination effects empirical relationships have been recommended by Kennel [27] which are presented in Table 2.1. F is the maximum side load, M is the maximum longitudinal bending moment in head seas and T is the maximum torsional moment. A conservative estimate for T is given by [27]:

$$T = 0.15 \times \text{Displacement} \times \text{Strut length}$$

This load combination approach is also recommended by Chalmers in [14].

2.1.3.3 Theoretical Estimations of Wave Loading

In the detailed design stages theoretical approaches to primary load calculation are usually preferred. The existing theoretical predictions of wave loads on SWATH vessels are mostly developed in conjunction with the prediction of motions, since these two problems are closely related.

Lee and Curphey (1977) [4, 21, 30] were the first to estimate analytically the wave loads for SWATH ships. Their method was based on the two-dimensional strip theory to calculate the wave pressure distribution, originally developed for catamaran vessels [21, 30]. The hydrodynamic pressure on any segment of the hull section is determined by applying Bernoulli's equation for the time varying velocity potential, with additional terms representing the change in the static pressure head as the hull experiences heave and roll motion. Five load components must be first evaluated before proceeding with structural response estimation, namely, inertia forces, incident wave or Froude-Krylov force, diffracted wave force, hydrodynamic force due to body motions and the hydrostatic restoring force due to vertical displacement. The total load is derived by integrating the pressure along the submerged structure of the vessel. A more detailed description of the approach is presented by Djatmiko in [31]

The American Bureau of Shipping (ABS) has developed an analytical approach to compute wave loads on SWATH ships similar to the Lee et al approach [32, 33, 34]. The analytical model was initially established to solve the problem of linear response of SWATH ships to wave excitation in five-

degrees of freedom only, but was later modified to account for all six-degrees of freedom ship motions. The hydrodynamic coefficients and wave exciting forces on the twin hulls are computed using strip theory. The hydrodynamic interaction effect between the two submerged hulls was also considered.

The main restriction imposed by the two-dimensional theory strip theory is that load predictions can only be made in the direction in which the section is chosen in. The loading on the cross deck of a SWATH is therefore calculated using an equivalent two-dimensional hull form assumption for only the beam-sea case. The most important advantage of the 3D method, however, is that it allows the inclusion of wave load effects in all directions thus facilitating consideration of the pitch and yaw motion effects which would otherwise be neglected. Therefore, 3-D approaches incorporating the effect of hydro-elasticity on structural responses (Price et al [36]) and accounting for the forward speed effects (translating-pulsating sources - Chan [37]) have also been produced as the next step forward from the 2-D approach.

Work by Price et al into wave loads of SWATH ships resulted in the development of a general linear hydro-elasticity theory for structural response analysis (ie. displacement, distortions, bending moments, shearing forces, torsional moments and stresses) of an idealised flexible SWATH travelling in regular waves [39, 40]. The mass, damping and stiffness properties of the structure in the 'dry' mode are first evaluated (from FE analysis) and the dynamic characteristics of the structure in the absence of external forces is obtained. These properties are then included in the calculation of steady motion under wave excitation. The fluid loads experienced by the ship in waves are then evaluated by use of a three-dimensional singularity distribution panel method considering the influence of forward speed. Price and Wu (1987) [42, 43] improved the method by accounting for non-linear fluid forces effects, and extended the method to tackle time domain response analysis problems. The analytical method developed at Brunel University is one of the most sophisticated and could be expected to produce fairly accurate wave load predictions. It is used by the Royal Navy for analytical estimations of wave loading and structural response.

Work at the Department of Naval Architecture and Ocean Engineering,

University of Glasgow, initially concentrated on the development of a computerised two-dimensional strip theory procedure later extended [45-46] to a three-dimensional sink-source theory and can be used to predict the motion and wave load responses for both twin-hull and monohull vessels. Chan in 1990 [12, 37, 47, 48] improved on these programs by recommending a method, to account for the 3-D and forward ship speed effects on the load levels. Specifically, the wave loads on the structure are estimated from the integration of several pressure components applied onto the oscillating body. These components comprise the motion-induced radiation pressure, the quasi-hydrostatic pressure, the Froude-Krylov and diffraction pressures and are derived from the velocity potential [48]. All six-degrees of motion amplitudes and radiation velocity potentials are considered. In addition, the translating source is added to account for forward speeds. A comparison of this method's prediction with experimental data is presented in [12, 31] demonstrating a very satisfactory correlation. Further developments by the National Technical University of Athens (NTUA) and at NTH, Norway [51, 52] are described by Djatmiko in [31].

2.1.3.4 Experimental Evaluation of Wave Loads

Experimental investigations, whether at full or small (laboratory) scale, aim at providing a better understanding of the structural behaviour, the inherent levels of loading and its distribution on the structure and encourage parametric studies and in enabling the calibration of theoretical/ empirical models describing the loading phenomena.

A summary and review of experimental programs carried out by several research organisations on wave load evaluations of SWATH ships is presented in [31]. This covers tests undertaken in the USA (DTNSRDC) [4, 17, 54], Canada (DREA) and MARIN (the Netherlands) [55, 56], in the U.K. (ARE, Haslar) [18, 57], Japan (Mitsui) [35, 58] and Glasgow University [31, 59].

2.2 Description of the Irregular Seaway and Structural Response

Two ways to calculate the seaway loading and response of a ship structure are identified by the way the seaway is modelled:

1. *a deterministic approach,* using a single (regular) wave represented by a wave period and a wave height assumed to remain unchanged from one cycle to the next, chosen sometimes because of its simplicity and not its accuracy.

2. *a statistical approach* considering the wave spectrum. The most suitable is a design wave spectrum measured at the geographical area(s) under consideration. Since these spectra are rarely available, theoretical spectrum models are chosen, based on the fetch, wind and other meteorological conditions dominant in individual geographical locations. The irregular seaway is hence described by its statistical properties. Wave spectra describe only short term wave conditions.

The statistical description of an irregular seaway and the associated ship structural response can be carried out either in the *short term* or in the *long term*. The *short term statistics* are based on the treatment of short term wave records (usually of 3-6 hour duration) as random processes which are functions of time and are used to define the irregularity of the seaway. On the other hand, *long term statistics* are calculated based on a long-term distribution (usually over the ship's lifetime, 20 years say) of the short term seaway statistics (referring to environmental parameters like the wave height and period, wind speed, etc.). Such an approach is essential as the prediction of the characteristics of long term extreme values accounts for the occurrence of rare events as opposed to the short term statistics which generally describe normal seaway conditions. In addition, the cumulative nature of fatigue damage over the ship's lifetime requires that the estimation of fatigue loading is carried out via a long-term representation of the sea conditions the ship will be expected to experience.

2.2.1 Short Term Statistical Description

The short-term wave statistics that quantify the state of a seaway are the wave height and the wave period. The former is mostly expressed by the significant wave height while the wave period is usually presented in the form of the average zero-crossing period. The estimation of these parameters from the analysis of the wave record in the *time domain* is time consuming and should should therefore be avoided in favour of a frequency domain (spectral) representation. The distribution of wave

elevation follows the shape of a Gaussian (normal) distribution, and the wave height and wave period follow a Rayleigh distribution (for a narrow banded spectrum, developed seas). High and narrow distributions (for period, height, elevation) correspond to a comparatively regular seaway, as the probability of occurrence of specific wave parameter values is large in steadier sea state conditions. Lower and wider distributions correspond to highly irregular, developing seas, (Fig. 2.8).

2.2.1.1 Description of Seaway and Response in the Frequency Domain

The basic advantage of a spectral (frequency domain) representation of an irregular seaway and ship response is that, despite the fact that the wave pattern is never repeated, the statistical characteristics of the sea state will remain the same. This is due to the assumption that the regular wave components chosen to represent a particular sea state remain the same throughout time (differing from one record to the other only in the phase difference), thereby keeping the energy of the wave system constant.

A short-term seastate and structural response, can generally be represented *in the frequency domain* in either of two ways, both based on the spectral representation of the seaway and response:

- by representing its statistical characteristics (significant wave height, zero-crossing period) from the sea-state spectrum (or the response spectrum for response considerations)

- by estimation of extreme values. From the short-term wave record the pdf of the wave elevation is first obtained followed by the probability distribution of the extreme wave heights. It is usually a Gumbel distribution and provides the values for the Extreme Wave Heights and the Most Probable Extreme Wave Heights (para. 2.2.1.2).

In general, short and long term statistics and response is different for the ship and the fixed offshore installation environment. Fixed offshore structures are only dependent on the significant wave height value, while floating structure responses are more sensitive to the values of both the significant wave height and the zero-up crossing period (perhaps more dependent on the period). This sensitivity of ship response to primarily the zero up-crossing wave frequency has been recognised by the deterministic

approaches to ship longitudinal loading by assuming a ship statically poised in waves of wavelengths close to the length of the vessel. Therefore, although response analyses based on extreme wave heights are sufficient for fixed structures, for ship structures a means of combining both the wave height and frequency distributions is essential. This is possible through the wave spectrum (or energy spectrum if multiplied by ρg) representation which accounts for the irregularity of the waves (in both the period or height/amplitude):

$$S(\omega) = \frac{1}{2}\sum_{i}^{n} a_{i,\omega}{}^{2}$$

The shape of a wave spectrum changes continuously as the sea develops until a narrow banded, fully developed sea forms. During this change the contributions from the lower frequencies to the wave energy become predominant as waves of longer and longer wavelengths are produced. The shift towards lower frequencies is usually encouraged even for fully developed seas, by the presence of increasing wind speeds (Fig. 2.9).

The significant wave height and zero-up-crossing period for fully developed seas can then be obtained from the areas under the energy spectral density functions, m_o, m_2, (Rayleigh distributions in this case) as follows:

$$H_s = 4.005\sqrt{m_0} \qquad \text{and} \qquad T_Z = 2\pi\sqrt{\frac{m_0}{m_2}}$$

where $m_n = \int_0^\infty \omega^n\, S(\omega)\, d\omega$. To account for any broadness in the distributions (wave height, and period and hence broad spectrum) the coefficient of the significant wave height expression above must be multiplied by the correction factor:

$$CF = \sqrt{1-\varepsilon^2} \qquad \text{where} \qquad \varepsilon = \sqrt{1-\frac{m_2{}^2}{m_0 m_4}}$$

is the width parameter and is a measure of the rms width of the wave energy spectrum. Narrow-bandedness may be assumed for a value of the width parameter ε below 0.6. The peak period T_o can be obtained from the spectrum as the value of frequency ω_o at which the spectrum peak occurs.

2.2.1.2 Short-Term Extreme Wave Height/Response Estimation

To determine the extreme value of a random process or response, the probability density function of the peak values of the random process (whether this is wave heights, or amplitudes of response) must be known. If this pdf is unknown then one needs to rely on the quantity and nature of the data available.

If the data permits the construction of an approximate probability distribution of the peak values (P(R)) then the extreme value for a longer period can be established by plotting the distribution in the form (1/1−P(R)) and extrapolating the curve (R can be the wave height or the magnitude of response etc.) (as applied, for example, in [99, 110]). This approach is usually used in long-term considerations over the lifetime of a ship. If, on the other hand, the data available is a large number of short-term extreme values then the extreme value to be encountered over a longer period can be estimated by means of asymptotic distributions (para. 2.2.2).

For narrow-banded processes the probability distribution functions of the peak values (whether wave heights or response amplitudes) can be represented by Rayleigh distributions. At such an instance

$$R_{max} = \sqrt{2\, m_o \ln N}$$

where N is the number of records observed. However, usually peak values demonstrate pdfs between Gaussian and Rayleigh distributions. To account for this broad-bandedness, Ochi [81] (based on revised probability density functions for the peak values by Rice) proposed the following formulae for the *Extreme Value* (e.g. wave height) assuming an α probability of exceedence:

$$R_{max} = \sqrt{2\, m_0 \ln\left[\frac{\sqrt{1-\varepsilon^2}}{1+\sqrt{1-\varepsilon^2}}\,\frac{2N}{\alpha}\right]} \qquad \text{for } \varepsilon \le 0.9$$

and the *Most Probable Extreme* value in a record:

$$R_{max,prob} = \sqrt{2\, m_0 \ln\left[\frac{\sqrt{1-\varepsilon^2}}{1+\sqrt{1-\varepsilon^2}}\,2N\right]} \qquad \text{for } \varepsilon \le 0.9$$

where

$$\frac{\sqrt{1-\varepsilon^2}}{1+\sqrt{1-\varepsilon^2}} \qquad \text{and} \qquad \varepsilon = \sqrt{1-\frac{m_2^2}{m_o\, m_4}}$$

is the correction for the case of a wide band spectrum, N is the number of records observed and α is an assumed probability that R_{max} will be exceeded (usually equal to 0.01 i.e. one chance in a hundred). It is notable that if these expressions are presented in terms of time T_S (in hours)

$$R_{max} = \sqrt{2\, m_0 \ln\left[\frac{(60)^2\, T_S}{2\pi\, \alpha}\sqrt{\frac{m_2}{m_0}}\right]} \quad \text{and} \quad R_{max,prob} = \sqrt{2\, m_0 \ln\left[\frac{(60)^2\, T_S}{2\pi}\sqrt{\frac{m_2}{m_0}}\right]}$$

they are independent of the bandwidth parameter ε [62]. They therefore apply to any distribution whether narrow or wide banded.

2.2.2 The Mathematical Description of Wave Spectra

The simplest way to represent a wave spectrum is by the use of theoretical models which have been fitted to real life seaway environments. The mathematical models are generally categorised according to the number of parameters (wave height, period, shape factors, etc.) on which they are based. Spectra which are independent of wind speed, fetch or duration, represent fully developed sea spectra and are usually narrow banded. The existing spectra may be categorised as follows:

Single Parameter Spectrum	-	Pierson-Moskowitz (1964)
Two Parameter Spectra	-	Bretschneider (1969) Scott (1965) ISSC (1964) ITTC (1966)
Five Parameter Spectrum	-	JONSWAP (1973, 1976) Three parameters are normally held constant, i.e. two parameter spectrum.
Six Parameter Spectrum	-	Ochi and Humble (1976)
Additional Spectra	-	Neumann Spectrum (1953) Liu (1971) and Mitsuyasu Spectra (1972)

The Neumann Spectrum has been based on limited data and outdated techniques and is generally neglected. The latter two spectra are fetch dependent and were based on lake and reservoir measurements (not applicable to open seas). For further information on the latter three spectra, references [63, 64, 65] may be consulted.

The Pierson-Moskowitz Spectrum (1964) [66] describes a fully-developed sea and is similar to a Rayleigh distribution. It is determined by one parameter, the wind speed (measured at 19.5 m above the water surface) while the fetch and duration are considered infinite. The formula represents an energy spectrum distribution of a wind generated sea state and is useful in representing a severe storm wave.

The Bretschneider Spectrum (1959, 1969) [67, 68] is also narrow banded and hence the wave heights and periods follow the Rayleigh distribution. Despite this model having been derived for a fully-developed sea, it may also be used (with acceptable accuracy) to partially-developed seas. In turn, the ISSC Spectrum (1964) [69], is a modified form of the Bretschneider spectrum while the ITTC Spectrum (1972) represents a modification of the Pierson-Moskowitz spectrum in terms of the significant wave height and zero crossing frequency. The last of the two-parameter spectra, the Scott Spectrum (1965) is independent of the wind speed, fetch or duration and therefore describes fully developed seas. It is based on data from the North Atlantic. It is not widely used and more information can be obtained from [70]. The general form of these two parameter spectral models can be expressed by:

$$S(\omega)=\frac{A}{4}H_S{}^2\frac{\tilde{\omega}^4}{\omega^5}\exp\left[-A\left(\frac{\omega}{\tilde{\omega}}\right)^{-4}\right]$$

A is dependent on $\tilde{\omega}$ and the area under this energy spectrum corresponds to $(H_S{}^2/16)$ irrespective of the values of the parameter A and the type of the characteristic period chosen for $\tilde{\omega}$. Table 2.2 shows the values of the parameters A, $\tilde{\omega}$ and the relationships between $\tilde{\omega}$ and other statistical wave frequencies for the various two-parameter spectral models.

The JONSWAP spectrum (1973) (Joint North Sea Wave Project) was developed by Hasselman et al [72, 73] and is expressed by a modified P-M formulation to account for the *wide-bandedness* of developing seas. It is

therefore fetch and duration dependent and is usually considered as a two parameter spectrum in terms of γ and ω_o, with the remaining three parameters fixed. There are, however, two difficulties in applying this spectrum. The first is that the peakedness of the spectrum, γ, varies even for a constant wind speed depending on the duration of the wind and the stage of growth/decay of the storm thus following a normal distribution of mean value of 3.3 and standard deviation of 0.79. To account for this variation Ochi suggested the use of a family of JONSWAP spectra for five different values of γ between 1.75 and 4.85 along with their weighting factors based on their probability density spectrum. The response will be calculated for each spectrum of the family and the derived response amplitude calculated by averaging the individual responses and their appropriate weighting factors.

The second difficulty is that, in a design case, it is the significant wave height and average period that are given and not the two spectral parameters γ and ω_o (or T_o). No accurate closed form relationship between them is available except the following parametric expressions, as proposed by Goda in 1979 [61]:

$$H_S = \left(0.11661 + 0.01581\gamma - 0.00065\gamma^2\right) T_o^2 \quad \text{and}$$
$$T_o = \left(1.49 + 0.102\gamma - 0.0142\gamma^2 - 0.00079\gamma^3\right) T_z$$

where T_z is the zero up-crossing period. For γ=1 the JONSWAP spectrum is equivalent to the P-M spectrum.

The Ochi-Hubble Spectrum (1976) [74, 75] accounts for the cases when swell (low frequency) co-exists with wind generated waves (high frequency) and hence double peaks (Fig. 2.10) are observed in a wave energy distribution. The various spectral shapes (degree of sharpness of the spectrum peak) are accommodated by a six parameter spectrum model consisting of a part for the lower and a part for the higher frequency components. This spectrum best expresses the sea conditions in the North Atlantic region and accounts for differences in wind duration, growth and decay-stage of storm and existence of swell, even if the significant wave heights remain unaltered. To cover a variety of stages of the sea, a family of spectra is used consisting of a number of spectra for each (of several) significant wave heights and each of these spectra has the same energy content but different shapes. There are 11 variations of spectra corresponding to any single significant wave height

where one of those spectra acquires 50% probability of occurrence (most probable) and the rest possesses 5% probability of occurrence each (0.95 confidence coefficient) (Table 2.3 and Figure 2.11). In a response analysis each one of the spectra belonging to the family is used and the worst response chosen. The product of the confidence coefficient times the probability of occurrence of the specific significant wave height representing the family of spectra determines the weighting factor.

In conclusion, it may be said that the P-M spectrum is the most widely used despite the fact that the waves of importance are never those in the fully developed sea condition which this spectrum represents. Furthermore, the Bretschneider spectrum is mostly used in the Gulf of Mexico as opposed to the JONSWAP model (γ=3.3) being used in the North Sea to represent a design storm wave. The P-M and JONSWAP spectra are based on wind speeds measured at 19.5m, while the Bretschneider and ISSC wind speeds are measured in the 0-10m range. The Ochi spectrum presents the advantage that it accounts for the presence of swell on wind generated seas and is attractive, although there is no wave spectral model available which is applicable to all sea conditions in all parts of the world. A review of the various spectral formulations was carried out by Ochi and Bales in [76].

2.2.3 Directional Spectra and Frequency of Encounter Correction

All of the aforementioned wave energy models are based on the assumption of *long-crested waves* (except for the JONSWAP spectrum) suggesting one-dimensional spectra. In reality, there exist frequencies of component waves travelling at an angle θ to the original direction. A more complete representation of the seaway would therefore be given by a two-dimensional directional spectrum indicating the direction θ as well as the frequencies of the wave components, thus accounting for the more realistic case of *short-crested waves*. The spectrum thus becomes a joint distribution spectrum:

$$S(\omega,\theta)=S(\omega)\,f(\theta)$$

where ω and θ are assumed independent. The spreading function $f(\theta)$ is given by:

$$f(\theta)=\begin{cases}\frac{2}{\pi}\cos^2(\theta) & (\text{for } -\frac{\pi}{2}\le\theta\le\frac{\pi}{2})\\ 0 & \text{otherwise}\end{cases}$$

Furthermore, it is the forward speed of any marine vehicle (and especially of the fast marine vehicles) that affects the frequency of its encounter with the waves and therefore influences the added mass, damping coefficients and hence its response to external wave loading. In a spectral approach the changes are accommodated by transforming the wave spectrum from an absolute wave frequency spectrum to a frequency of encounter one, thus accounting for the varying ship headings and ship speeds. Short-crestedness should already have been considered in the spectrum type chosen, or by use of the spreading function. In this transformation, the total energy of the original spectrum remains unaltered. The frequency of encounter is thus obtained by the following formulation:

$$\omega_e = \omega_w - \frac{\omega_w^2 V}{g}\cos\theta$$

where

ω_w	is the wave frequency
V	is the ship speed
θ	is the heading angle

This formula provides the abscissa value for the transformed wave spectrum, while the ordinate values $S(\omega_e)$ are given by:

$$S(\omega_e) = S(\omega_w)\,\frac{1}{\sqrt{1-(4\omega_e V/g)\cos\theta}}$$

The change in the ordinate value is necessary so that the total area (and hence energy content) will be the same under the encountering wave spectrum as under the original wave spectrum.

2.3 Long-Term Statistics and Response

Wave spectra are only applicable for short term wave records whose surface is assumed to be a stationary, Gaussian process. However, the prediction of the characteristics of long-term extreme values deals with the occurrence of rare events which cannot be described by a normal distribution because, in a long-term description of the sea, the significant wave height and zero up-crossing period will vary, and are by no means stationary processes. Hence, the definition of a long term distribution for extreme value environmental statistics (wave height, wind speed, etc.) over the lifetime of the vessel (20 years usually) is required.

To construct a long term prediction of the joint frequency (over the vessel's

lifetime) a large number of short term wave records/ship responses (usually of 3-6 hour duration), each described by a pair of H_S and T_Z (or maximum values of wave height or response) values, are obtained and their distributions (or frequency of occurrence) over the lifetime of the vessel established. Assuming them to be independent random variables their joint distribution is obtained by multiplication of their individual distributions resulting in a 3-D surface. If the response of the vessel is dependent on other additional parameters, such as the distribution of the ship heading, ship speed, etc., which is normally the case, then a multi-dimensional probability distribution results presenting all the possible combinations of the individual parameters. In any case, the resulting multi-dimensional spectrum is the input spectrum in a long-term response analysis.

A more helpful way to present the distributions and data is by a scatter diagram in which the frequency of occurrence (in the lifetime of the vessel) of every combination of significant wave height and zero up-crossing frequency relates to a short term sea condition for the geographical area to which the scatter diagram corresponds. Scatter diagrams for various sea locations worldwide are generally available from national and international Hydrographic Services.

The main aim of long-term wave or response analyses is to predict the largest value of the wave height or response for a given probability of this largest value being exceeded. Two methods are available: the Design Sea Load Method and the Lifetime Weighted Sea Method which are now briefly presented.

2.3.1 The Design Sea Load Method

This method first calculates the most probable extreme sea state (in terms of significant wave height) corresponding to the ship's lifetime and then calculates the ship's response to this extreme sea state. A set of other sea states (identified by a significant wave height H_s) is also selected and the responses to these calculated. For each of these sea states the response is calculated for every other combination of environmental parameters (i.e. spectrum family, speed, heading) and out of these responses the largest is kept as representative of the sea state under consideration. A plot of H_s versus response amplitude can thus be drawn (Fig. 2.12). To account for the higher frequency of the presence of seastates of lesser severity than the most

probable extreme sea state (say k times more frequent) then the risk parameter α for each seastate is divided by k to keep the true total risk at the same value for all seastates. k is defined as the ratio of the number of observed wave peaks corresponding to the most probable extreme significant wave height to the number of observed wave peaks for the seastate of lesser severity which is under consideration under any instant. The extreme value of response (characteristic value), R_c, for which there is a probability α of being exceeded is given by:

$$R_c = \sqrt{2\, m_0 \ln\left(\frac{60^2\, T}{2\pi\, \alpha/k}\sqrt{\frac{m_2}{m_0}}\right)}$$

where T is the operational lifetime in hours. Obviously this approach does not lend itself to any serious fatigue damage estimation as it neglects all the load conditions linked to every significant wave height other than that specific combination of heading, frequency and speed that results in the highest response level. The next method is the one most suitable for fatigue analysis.

2.3.2 The Lifetime Weighted Sea Method

This method views the total lifetime response of the ship as the sum of a series of short-term responses appropriately weighted to account for the relative amount of exposure to the various levels of sea severity.

In fact, the probability of the ship operating in a particular mode/seastate (identified by a particular seastate, ship speed and heading and frequency of the particular short term wave spectrum) would be expressed by the product of the probability of it being in the specific range of wave heights, times the probability of operating in the specific speed range, times the probability of having the specific range of headings, times the probability of occurrence of the specific wave spectrum employed. Therefore, the time spent in a specific operation mode is expressed by the product of the probability of the vessel being in that mode times the total operating life at sea of that ship.

It may generally be assumed that all headings are equally probable, whereas the speed probability for SWATHs can be approximated from the data of monohull ships, as proposed by Sikora et al [17] and listed below. The sum

of all of the incremental mode probabilities must be one.

Displacement	<10,000 ton			>10,000 ton		
wave height (m) / ship speed (knots)	0.5	6-10	>10	0.5	6-10	>10
0-10	0.25	0.1	0.6	0.05	0.05	0.4
10-20	0.6	0.8	0.4	0.65	0.85	0.6
>20	0.15	0.1	0.0	0.3	0.1	0.0

In mathematical terms, the probability density function of peak values of response for the ship's lifetime $p_L(R)$ is a weighted sum of the various probability density functions over the ship's lifetime for the *peak values of short-term response.* These pdfs $p_{s-t}(A)_{ijkl}$, are obtained for each of the combination of a sea state, ship heading, ship speed and short-term wave spectrum type. The four weighting factors (probabilities) account for the relative frequency of a particular combination of these conditions:

$$p_L(R) = \frac{\sum_i \sum_j \sum_k \sum_l \overline{N}\, f_i\, f_j\, f_k\, f_l \left(p_{s-t}(A)_{ijkl}\right)}{\sum_i \sum_j \sum_k \sum_l \overline{N}\, f_i f_j f_k f_l} \qquad \text{where} \qquad \overline{N} = \frac{1}{2\pi}\sqrt{\frac{m_2}{m_0}} = \frac{1}{T_Z}$$

is the average number of responses per second *for every individual short term response* considered and T_Z is the zero up-crossing period. f_i are the weighting factors (probabilities) for the sea state, the wave spectrum of the family, the heading and ship speed. Parameter A corresponds to the quantity (the random process investigated like, for example, the most probable extreme response value in the short-term, the extreme wave height, the significant wave height etc.).

Once the lifetime probability density function, $p_L(R)$, has been established, the characteristic (or the most probable-as required) *extreme* value of response is estimated. Based on extreme value analysis, the cumulative distribution of peak values, $P_L(R)$, over the ship's lifetime is:

$$P_L(R) = 1 - \frac{1}{N_L} = 1 - \frac{1}{\left(\sum_i \sum_j \sum_k \sum_l \overline{N} f_i f_j f_k f_l\right) \times T \times 365 \times 24 \times 3600}$$

where R is the probable extreme value of response, N_L is the total number of responses expected in the lifetime of the ship, $1/N_L$ is the probability of exceedence of the extreme value (once in N_L cycles-once in a lifetime), T is is therefore the *return period* in years. If the probability distribution function $P_L(R)$ is known then, from the above equation, the 'T year wave response' is obtained.

To avoid this time consuming and computationally exhaustive general method, the Log-normal, Weibull, Gumbel and the Fisher Tippett II distributions may be used as the probability density function of peak values of response for the ship's lifetime $p_L(R)$. The body of available long-term wave data was found to fit a log-normal distribution quite well with some deviation at the tails. Weibull distributions are also being used widely (in the more special form of the Rayleigh distribution), but Ochi [81] claims that they underestimate the return values. The Gumbel distribution has been found to fit deep-water data around the U.K. very well, while the Weibull distributions are expected to fit shallow water data, but this has not been verified with the available measurements [82]. Appendix 1 of [82] presents all the required parameter relationships for each of the ten distributions mentioned earlier.

2.4 Load Prediction Methods Applicable to Fatigue Design

Static strength design of ships generally concentrates on the maximum expected load that must be withstood by the structure during its operational lifetime. The fatigue damage of marine structures, however, is a cumulative phenomenon whose occurrence and extent depends on all frequencies and amplitudes of wave loads (large or small) encountered during the ship's lifetime. Although the main statistical aspects of maximum lifetime load estimation still apply, fatigue design takes a more detailed and 'continuous' view of the wave loading effects on the structure. The types of loads that are of interest to fatigue design are those that are of cyclic nature. The four main categories of fatigue loading are:

- low frequency wave induced
- high frequency (dynamic
- still water
- thermal.

The low frequency wave induced loads are of irregular nature and their occurrence and magnitude greatly depend on the ship speed, ship heading, and sea conditions. The high frequency, dynamic loading, is of no significance if accounted separately (large number of load cycles but of quite small amplitude), but it becomes important once it is superimposed on the low frequency loading. At that instance the maximum stress range amplitude is raised. High frequency loading can either be transient loading (due to slamming and consecutive hull whipping) or steady-state loading (induced by machinery), or both.

Still water loading is introduced by the pressure/structural weight differential which might be present in the structure. For fast monohull ships additional bending (in the longitudinal direction) may be experienced due to their operating in their own wave pattern. Thermal stresses are introduced by the temperature differentials in the atmosphere and water.

The last two stresses are of no great importance as their frequency of occurrence is quite low and their magnitudes are generally controlled by static strength considerations. The former two are of greater importance since their amplitude and cyclic occurrence can be relatively high ($10^7 - 10^8, 10^6$ respectively). Nibbering [83] has developed a complete fatigue design method for monohulls, accounting for the effects of all the aforementioned stresses by 'correcting' the wave-induced cumulative distribution diagram for slamming effects and effects of corrosion. According to Munse et al [84], Nibbering's fatigue loading curves can be approximated by an exponential distribution (Weibull distribution with $\xi = 1$). References [17, 85] contain detailed information on the application of the method to monohulls. Furthermore, model tests have identified that whipping stresses in SWATH ships are negligible and can thus be neglected [17] in a fatigue analysis.

Fatigue design of ship structures subjected to variable amplitude loading may be carried out either by the use of S-N curves in conjunction with an appropriate damage accumulation rule, or by use of fracture mechanics. By

using Miner's rule and the standard S-N expression the cumulative damage D is derived:

$$D = \frac{N_T}{A} \int_0^\infty S^m \, p(S) \, dS = \frac{N_T}{A} E\left(S^m\right)$$

where $E\left(S^m\right)$ is the expected extreme value of S^m and N_T is the total number of cycles encountered during the ship's lifetime. It is an expression that can be used for both stationary and non-stationary processes [86]. The expression for $E\left(S^m\right)$ depends on the type of distribution assumed for the load and generally the method used for fatigue design. A summary of these distributions and the corresponding expressions for $E\left[S^m\right]$ is given in the following Table:

Distribution	$E\left[S^m\right]$
Beta	$S_{max}^m \left[\frac{\Gamma(q+r)\,\Gamma(m+q)}{\Gamma(q)\,\Gamma(m+q+r)}\right]$
Lognormal	$(E[S])^m \left(1+V_s^2\right)^{m(m-1)/2}$
Rayleigh	$\left(2\sqrt{2}\,\sigma_s\right)^m \Gamma(1+m/2)$
Weibull	$\lambda^m \Gamma(1+m/\xi)$

In this Table, σ_s and V_s represent the standard deviation and COV of the individual stress range distributions. The scale parameter λ and the shape parameter ξ of the Weibull distribution are defined in the next paragraph. q, r are the parameters of the beta distribution identified by:

$$\mu_x = a + \frac{q}{q+r}(b-a) \qquad \text{and} \qquad \sigma_x^2 = \frac{q\,r}{(q+r)^2\,(q+r+1)}(b-a)^2$$

where μ_x, σ_x, a, b, are the mean, the standard deviation and the minimum and maximum limits bounding the distribution.

The modelling of the non-stationary long term seaway stress random process and consequent fatigue load determination can be carried out in two

ways. One is based on the Lifetime Weighted Sea Method, based on the detailed summation of the contributions to fatigue damage of the individual short-term sea states encountered over the ship's lifetime, accounting for heading and speed effects. The second is a simplified approach based on the assumption of a long term distribution of the peak stress range values.

The Lifetime Weighted Sea Approach: In short term response, where the stress is a stationary narrow-band Gaussian process, the stress range follows a Rayleigh distribution [86, 101] and therefore:

$$E(S^m) = (2\sqrt{2})^m \, \sigma^m \, \Gamma\left(\frac{m}{2}+1\right)$$

where σ^m is the rms value of S. The stress range distributions will already include heading and speed effects (para. 2.2.3). In long-term response, N_s sea states (stationary short term Rayleigh processes) may be assumed to be encountered by the structure, each of the seastates being characterised by its own (H_s, f_z). Assuming that T is the ship's operational lifetime (or the time over which the fatigue damage is calculated), N_D is the number of wave directions, t_{ij} is fraction of time spent in the ith seastate and jth direction then the cumulative damage in the structure is given by:

$$D = \frac{T}{A} \sum_{i=1}^{N_s} \sum_{j=1}^{N_D} f_{z,ij} \, t_{ij} \, E(S_{ij}^m) \, C_L(m, S_o/\sigma_s) \, \lambda(\varepsilon, m)$$

More details on the method may be obtained in paragraph 2.3.2. The corrections for wide band load process and for endurance limit considerations (para. 2.4.1) are essential. Three long term seastate distributions in the form of scatter diagrams have also been put forward by RINA, ISSC-88 and GL/IACS for the North Atlantic and are presented in [86].

The Simplified Method, as proposed by Munse et al [95], considers a two-parameter Weibull distribution for the description of the long-term stress-range distribution although ignoring sequence effects. It was found to provide a good fit for the responses in ships and in buoyant offshore platforms, such as semi-submersibles and TLPs [91, 92]. According to the Weibull model the probability density function for the long term (lifetime)

extreme values of the stress range, S, is [91]:

$$p(S)=\frac{\xi}{\lambda}\left(\frac{S}{\lambda}\right)^{\xi-1}\exp\left[-\left(\frac{S}{\lambda}\right)^{\xi}\right]$$

where λ is a scale parameter and ξ is the shape parameter (Fig. 2.13). It should be remembered that this expression stems from a narrow band process assumption. The shape parameter ξ is a function of the type of structure and its dynamic characteristics as well as the location of its operation [5, 92, 93]. Values for ξ may be summarised as follows:

- For small and fast cargo ships operating in the northern or southern seas [84, 94, 95] $1<\xi<1.35$
- For slow ships in equatorial waters [94] (e.g. large tankers and bulk carriers) $0.7<\xi<1.0$
- For shallow water fixed platforms in the Gulf of Mexico [94] $\xi=0.5$
- For template platforms outside the Gulf of Mexico without dynamic amplification [96] $0.5\leq\xi\leq 0.7$
- For deep water platforms in hostile environments (e.g. North Sea) having significant dynamic response [94] $\xi>1.0\,,\xi\approx 1.4$
- For semi-submersibles and gravity platforms [96] $\xi=1.0$

The expected extreme stress range, S_e, occurring *once in a lifetime* of N_T wave encounters (or stress reversals) is given relative to the scale parameter λ by (probability of stress range S_e exceedence is $1/N_T$):

$$S_e=\lambda\left(\ln N_T\right)^{1/\xi}$$

or vice versa, if the required once in a lifetime stress range, S_e, is originally known, then the value of the scale parameter, λ, may be obtained. By

appropriate integration of Miner's rule the damage ratio for a Weibull long-term stress distribution is given by:

$$D = \frac{N_T}{A} \frac{S_e^m}{(\ln N_T)^{m/\xi}} \Gamma\left(\frac{m}{\xi} + 1\right) \Leftrightarrow S_e = \left[\frac{A\,D}{N_T} \Gamma\left(\frac{m}{\xi} + 1\right)\right]^{1/m} (\ln N_T)^{1/\xi}$$

thus permitting the identification of the maximum allowable extreme stress range for any required level of acceptable damage of the ship's lifetime, N_T. The strength of the joint is represented in the expression above by A, m. The parameter A will normally carry the level of safety that will be required and values are generally given for it representing the strength curves through the mean (good for probabilistic analyses) and the minus 1 and minus 2 standard deviations through the experimental data.

This procedure is used by most marine design codes and is also recommended by Moan [97], Faulkner [92], Nordenstrom (DNV) [98]. It is also used in the fatigue design procedure of the Royal Navy monohull and SWATH structures [18, 99]. A Weibull distribution has been used to describe the distribution of long term stress ranges for offshore structures (Wirshing [96]) and for ships (Munse [84, 95]).

2.4.1 Correction for Wide Band Load Processes and Endurance Limit

When a process is wide band, cycle counting becomes complex and especially developed cycle counting methods have to be used. A description of the available methods is presented in [103, 104]. The most popular are the 'rainflow' method put forward by Matsuishi and Endo [105] and the "ordered range" method of Nelson and Fucks [106]:

- *The rainflow method* identifies events in a complex strain sequence which are compatible with constant amplitude fatigue data. It is further able to identify stress range cycles associated with low frequency components and the mean stress associated with each cycle.

- *The ordered range method* (reservoir method) has the advantage of retaining the sequence of loading (useful for crack propagation analyses) and filtering out low level stress ranges causing negligible fatigue damage.

Appendix II of [103] describes the application of these two methods in detail. According to Dowling [104] the rainflow method leads to better prediction of fatigue life.

Wirshing and Light [107] have developed a prediction method for high cycle fatigue damage under wide band Gaussian stresses based on the rainflow method. The transformation algorithm is:

$$E(S^m)_{mod} = \lambda(\varepsilon, m)\, E(S^m) \qquad \text{where}$$

$$\lambda(\varepsilon, m) = a + (1-a)(1-\varepsilon)^b, \quad a = 0.926 - 0.033\,m, \text{ and } \quad b = 1.587\,m - 2.323$$

For typical offshore structures, the spectral width parameter $\varepsilon > 0.5$ and hence $\lambda \approx 0.79$ for m=4.38 and $\lambda \approx 0.86$ for m=3 [94]. This correction is useful when attempting to fit an equivalent Weibull (narrow band) model to wide band long-term wave distributions.

An additional correction is usually required to account for the effect of two segment fatigue strength curves (i.e. the effect of accounting for endurance limits) on fatigue damage. The results of an unpublished study into this question were presented by Wirshing and Chen in [96] and may be summarised by Figure 2.14a and 2.14b for the cases of the UK DEn-T curve and the API-X curve respectively. The long term distribution of stress ranges is Weibull. The reduction in fatigue damage for a two-linear curve is clear, the reduction becoming smaller for increasing shape parameters. This is more notable for high stress ranges. An expression for the fatigue damage reduction coefficient $C_L(m, S_o/\sigma_s)$ is provided in [96], resulting in:

$$E(S^m)_{mod} = C_L(m, S_o/\sigma_s)\, E(S^m)$$

where S_o is the endurance limit and σ_s is the rms of S. Neglect of the endurance limit effects on fatigue damage will certainly simplify the solution and will lead to conservative results.

2.4.2 The US Navy Approach to Fatigue Design

The US Navy approach to fatigue design of SWATH vessels represents an extension to this ship concept of the already existing method for monohull

fatigue design [17]. It uses the Lifetime Weighted Sea method for estimation of maximum load response (para. 2.3.2). The wave spectrum characterising the short-term sea conditions is taken by Sikora et al [17] as Ochi's [76] six-parameter family of spectra:

$$S(\omega) = \frac{1}{4}\sum_{j} \frac{\left(\frac{4\lambda j+1}{4}\omega_{mj}^{4}\right)^{\lambda_j}}{\Gamma(\lambda j)} \frac{H_{sj}^{2}}{\omega^{4\lambda j+1}}$$

where $\Gamma(\lambda_j)$ is the gamma function, λ is a sharpness parameter, H_s is the wave height. Furthermore, ω is the wave frequency (rad/sec), ω_m is a modal frequency parameter and j takes the values of 1, 2 for lower and higher frequency components.

Ochi's family was chosen as it accounts for high frequency rising seas without being over-conservative and was originally developed from North Atlantic wave data [85], a very harsh environment. The values of the six parameters as a function of the wave height are presented in Table 2.3. The method assumes that the individual short-term *response functions* are narrow banded and can be described by Rayleigh distributions.

Model tests have identified that whipping stresses on SWATH ships are negligible and are hence neglected by the design procedure [17]. The reduction in the magnitude of responses with increasing ship speed and heading angle different from those corresponding to beam seas is neglected. The RAO values were experimentally found to be 85% of those in beam seas for the cases of bow and quartering seas (55% for tandem struts). The responses in head and following seas can be neglected. Although RAOs are taken as not affected by ship speed, it is the ship speed, heading and wave frequency that determine the number of cycles the ship will experience and is accounted for in the speed probability. The heading probability will be characteristic to the route of the individual design, and the design method considers that all ship headings are equally probable. Hence, beam seas, bow seas and quartering seas are each being taken to exist 25% of the time, while head and following seas would comprise the remaining 25%. Suitable speed probabilities which may be considered by the designer are presented in paragraph 2.3.2. The probability that a ship would maintain a given speed is a function of ship size and wave height.

Based on the formulation predicting the single maximum lifetime amplitude side force (as derived by Sikora and Dinsenbacher - para. 2.1.3.1), Sikora recommends [15, 17] the following algorithm for constructing a SWATH fatigue load spectrum of side force per displacement versus the common logarithm of the exceedence cycles N:

$$F/\Delta = T\,D\,L\left(1.0 - 0.9\log_{10}(N)\,d^{-1}\,b_i^{-1}\right)$$

where

$$d = 1.0034 - 0.0013\tanh(0.001\,\Delta)$$

$b_1 = 7.085 - 0.017\,C$ for single strut SWATHs

$b_2 = 6.919 - 0.017\,C$ for tandem strut SWATHs

C is the waterline hull separation (ft) per cube root of displacement (ton). This formulation permits both the size and configuration of the vessel to affect the expected lifetime fatigue stress spectra.

The local SCFs should be evaluated either analytically or experimentally for each individual detail. Control over the value of SCF can be obtained by incorporating geometrical radii, insert plate inclusion, smooth thickness transitions and location of welds away from local geometry changes.

The method uses the standard S-N curve characteristics for the joint in question, supported by a Goodman plot correction for stress loading when not fully reversed. In addition, the prediction of fatigue life under variable amplitude loads is carried out by use of Miner's linear cumulative fatigue damage rule.

In the absence of S-N tests in saltwater for the material and joint of interest, Sikora et al [17] recommend biasing the expected fatigue lives 60% towards in-air performance. This is because, despite the fact that sea vessels, and hence SWATHs, operate in a saltwater environment, the actual environment experienced by the various joints will be somewhere between saltwater and air due to coatings and routine maintenance.

2.4.3 The Royal Navy Approach to Fatigue Design

The Royal Navy's approach to fatigue design of SWATH ships employs similar criteria to those for their monohull fatigue design [99]. The wave induced loading estimation approach used is based on the extrapolation of

four hour data measurements on warships [110]. The method is based on the standard fatigue S-N curves derived for steel joints by the Welding Institute and incorporated into the design codes for Steel Bridges [111] and Offshore Structures [112]. The S-N curves used are those two standard deviations below the mean curve providing a probability of fatigue initiation/failure of 2.3% [99], hence, no safety factor is necessary. No allowance is made for an endurance limit at a high cycle number or for residual stress effects.

The Simplified Fatigue Design Method is used. The extreme load long term distribution is expressed by a two parameter Weibull distribution with shape parameter $\xi = 1$ (exponential distribution). Cumulative fatigue damage is accounted for by Miner's Rule with a damage factor $D = \Delta = 1$ at failure. Hence the maximum allowable extreme stress range is given by:

$$S_{ea} = \left[A\Delta / n_o \Gamma(m/\xi + 1)\right]^{1/m} (\ln n_o)^{1/\xi}$$

where Δ is the acceptable damage ratio. Variability in the fatigue life estimation of the joint is accounted for via A in $S^m N = A$ corresponding to the mean minus two standard deviations curve. The design stress value is taken to correspond to a probability of exceedence α of 0.01 in the ship's life and therefore for $\xi = 1$ (exponential distribution) the allowable design stress S_d is [99]:

$$S_d = 21.82\left(\frac{A}{n_o \Gamma(m+1)}\right)^{1/m}$$

where $\Gamma(m+1)=m!$ for integer values of m and n_o is the assumed operational lifetime of the vessel in cycles (in this case assumed equal to $3\ 10^9$ and hence $\ln n_o = 21.82$). Slam induced whipping effects are not considered to be important and are neglected.

The possibility of a major contribution to the fatigue damage from the small number of very high stress cycles has been investigated by Clarke [99] who concluded that such a contribution is small and the damage occurring by stresses up to 10^4 cycles may thus be neglected.

2.5 Secondary Loads Due to Slamming Pressures

Slamming impact, the most important of the secondary loads on a SWATH structure, has long been recognised as one of the major sources of ship structural damage resulting from operation in rough seas. It governs the structural design locally and has thus been the subject of a large number of experimental investigations and theoretical modelling studies. Alleviation of the level of pressure magnitudes due to the slamming phenomenon has been shown over the years to be possible via the introduction of an 'angle of entry' of the structure to the water. Hence, the introduction of a ramp angle will reduce the severity of wet-deck slamming in the wet decks of SWATH ships. Therefore, the study of different impact angles may lead to a decision as to which is the most efficient ramp angle value for implementation in SWATH ships.

The prediction methods for slamming loads can be theoretical, empirical or experimental. The *theoretical methods* predict impact pressures on the wet deck using models determining the relative motions of SWATHs in waves. Such a 3-D motion prediction program developed by Chan [47] has been modified (by Chan) to include slamming theory as part of a more thorough investigation into the structural response of the wet-deck structure of SWATH ships to slamming loads carried out at Glasgow University [114]. In addition, Price et al [36, 43] have presented a linear three-dimensional dynamic analysis of the problem for monohulls and SWATH ships, including the effects of hull elasticity.

Spectral probabilistic estimates of cross-structure impact pressures and loads can also be made by considering the distributions of the amplitudes of the irregular SWATH motions estimated for various headings and ship speeds. Ochi and Motter's [115, 116] method can be adapted to estimate the probability of occurrence of cross-structure impact or the expected number of impacts per unit time. This procedure is demonstrated for a 2,500 ton SWATH in [31].

Sikora et al in [15], based on histograms of results obtained from slamming impact model tests, presented the cumulative probability of exceedence distributions of pressure to be of the form:

$$P(p) = 1 - \exp\left(-1.4\, p/\sqrt{E}\right)$$

where $P(p)$ is the cumulative probability of exceeding pressure p, $\sqrt{E}$ is the rms value of pressure and 1.4 is a coefficient determined from a linear regression of the linearised data distribution. Assuming that the pressure magnitude is directly proportional to the square of the relative velocity υ then the impact pressure distribution can also be described by a Rayleigh distribution and the above expression becomes

$$P(\upsilon) = 1 - \exp\left(-K\,\upsilon^2/\sqrt{E}\right)$$

Hence, the maximum lifetime expected impact pressure is given by:

$$P_{max} = 1.4\sqrt{E}\,\ln\left(N/\alpha\right)$$

where N is the total number of impacts during the life of the ship and is given by the product of the frequency of impacts, times the ship expected time at sea, times the probabilities of the ship being in the headings, speeds and wave heights at which slamming is considered a possibility. α is a risk factor to account for the effect the specific component failure has on the structural integrity and seaworthiness (the risk factor can be seen as increasing the number of impacts N). Sikora et al have used the following α values as representative in the design of T-AGOS 19:

- for plate dishing 0.37
- for stiffener tripping 0.01
- for girder design 0.0001

Peak impact pressures can also be estimated from empirical relationships obtained from drop tests with 2-D and 3-D models and calculated from time histories of the impact pressure distribution, including the extent of the impact area. Comparison between drop test results and seakeeping model test results shows the theoretical predictions to be conservative [2].

Despite the need for well calibrated SWATH slamming pressure data, only four institutions [15, 117 118, 119] have attempted to generate slamming data based on SWATH model tests. However, the accumulated data remains inadequate to formulate an acceptable approach to predict slamming pressures which can be readily adopted for design. Hence, additional slamming data were obtained from two series of drop tests (para. 2.5.2, 2.5.3).

2.5.1 Earlier Investigations

The first to seriously tackle the problem of hydrodynamic impact was von Karman in 1929 [120] with his work on seaplane floater impacts with water during landing. He was the first to introduce the concept of "added apparent mass" thus accounting for the effect of the water being set in motion.

This work was followed up by Wagner [121] who provided a correction to von Karman's formula representing the virtual mass to account for the effect of deadrise (water spray during impact increase the wetted width and apparent mass originally considered). More recently, Payne in 1981 [138] provided a more detailed description of Wagner's 'splash-up' distance. In fact he suggested that the stagnation line is at some fixed fraction η of the 'splash-up' distance, and proposed the expression presented in paragraph 2.5.3 for the stagnation line velocity at an impact angle θ. Both of these analyses were of two-dimensional nature.

Although both of these theories are invalid for a body of zero deadrise angle by predicting an infinite pressure for this case, they and their virtual mass concept were still in use until 1966. Earlier, Egorov [124] and Ogilvie [125] presented theories predicting pressures developed during flat body impact on a compressible fluid. Ogilvie's theory provides explicit predictions of the pressure as a function of time, assuming water compressibility. Full scale tests on USCGC Unimak [126] and other ships demonstrated that the recorded pressures were considerably lower than those predicted by Ogilvie, lasting also for much longer periods of time. The effect of elasticity of the construction on slamming pressures was studied by Sharov [127] who concluded that the magnitude of the initial pressure pulse is equal to the acoustic pressure (shock waves travelling at the speed of sound) and is independent of the elastic properties of the construction.

It was in 1966 that Chuang [128] dictated, through experimental studies of simulated two-dimensional flat bottom slamming, that the maximum pressure at impact was much less than the hydrodynamic impact pressures predicted by Wagner's theory and also not as high as the acoustic pressure of water suggested by von Karman (10 times smaller) and Sharov. This observation was attributed to the cushioning effect of the trapped compressible air in the layer between the falling body and the water surface. In addition, the peak pressure was found to be evenly distributed over the

flat surface at initial impact, while its maximum value when the model was dropped on calm water was not greatly different from the case of drops on rippled water. Based on Chuang's results, Verhagen [129], Johnson [130], and Lewison and Maclean [131], concluded that there is no acoustic pressure, as suggested by von Karman and Ogilvie [125], and that the maximum impact pressure occurred in the layer of air trapped between the body and the free surface. Specifically, in 1967 Verhagen [129] investigated theoretically the impact phenomenon assuming an infinitely long plate dropping vertically on the water surface. He assumed that, as the plate falls, air between the plate and the free surface flows one-dimensionally from the centre to the edge of the plate. Impact was assumed to occur when the deformed free surface of the water touched the edge of the plate. At this instant he found that the air velocity at the edge of the plate was very near to the value of the acoustic velocity. The defining equations were solved numerically. However, Verhagen's theory is applicable only to relatively light models and not to full-scale ships whose inertia is very large. In 1967 Chuang [132], following an experimental study, proposed a set of design equations aiming at predicting the magnitude of the impact pressure on wedge with deadrise angles up to 18°:

$$p = BV^n$$

where B and n are arbitrary constants and n has a limit of $1 \leq n \leq 2$. The results revealed that the peak pressures measured away from the keel are larger (approximately twice) than those at the keel, except for the 1-degree deadrise where the magnitude was on average the same. With respect to the pressures away from the keel, Wagner's predictions were found to be too conservative for low deadrise angles but came more in line with the experimental data with increased deadrise angles.

In 1968, Johnson [130] theoretically examined the case of two-dimensional flow of air between the falling rigid block and a rigid, flat, infinite water surface. Even though he did not extend his solution to the point of impact he concluded that, in order to match the theoretical and experimental results, the deformation of the water free surface had to be taken into account. Johnson's calculations also demonstrated that the velocity of the falling body is almost constant during the time the air acts compressibly. The same year Lewison and Maclean [131] investigated experimentally the impact between a rigid flat plate and the free surface of water. The pressure

distributions along the centreline of the plate (two-dimensional flow) was found relatively uniform, while more distinct variations were observed along the transverse mid-section of the model (Fig. 2.15). The peak pressure distribution in the latter case reaches its maximum at the centre and decreases towards the edges. In view of the variation in impact pressures for different drop heights it was observed that the peak pressure increased linearly with the increasing of drop height and therefore with the square of impact velocity.

In a second experimental programme Lewison conducted a further study on slamming to explore the mechanism for reducing slamming impact on seagoing ships [133]. Two sets of experiments were described. In the first, pressure measurements on a flat plate were made on a large vertical drop test machine where it was shown that the end flanges would sharply reduce the peak pressures because they would encourage air entrapment (Fig. 2.16). The second set of experiments was on a small scale "Mariner" model in head seas which showed that the slamming pressures under the forepeak could be sharply reduced if the air cushion was artificially reinforced.

In 1970, Chuang [134] published further extensive work on the impact of rigid and elastic bodies with water, confirming his previous calculations. When comparing a rigid and a flexible bottom structure he found that the pressure time pulses on the flexible bottom were more highly irregular. Measurements on the magnitude of peak impact pressures showed that, in lower drop heights (6 and 8 ft) the flexible model experienced a local pressure of approximately 25% larger than that of a rigid model, whereas for a 25 ft drop height the pressure was lower, i.e. only about 70% of that measured on the rigid model. Comparison of a flat-bottomed model and a 10 degree deadrise angle model of similar size showed that the latter produces higher local plating pressures and stresses when dropped from the same height.

In 1989, Ando [135] demonstrated that an elastomeric layer of optimal modulus of elasticity could significantly reduce the slamming forces on flat bottoms falling vertically on a water surface. However, such a layer was found to slightly increase the maximum impact forces (relative to rigid bottom impact) when applied to wedge-shaped bottoms due to the cancellation of the cushioning effect by the concave deformation of the elastomeric layers under the action of the compressed air pressure.

However, this increase of impact pressure becomes negligible with increasing deadrise angles.

One of the latest research programmes organised by DnV was the investigation of structural response of fast craft due to slamming loads [136, 137] by performing a series of drop tests on stiffened aluminium and GRP models. The experimental data have been compared with Wagner's [121] and Payne's [138] theoretical approaches. The latter was found to give much better agreement than the former for a 28.8° effective slamming angle. A study into the effects of model flexibility on the maximum impact pressure was rather inconclusive as the presumption that the more flexible structure will induce smaller impact pressures was not proven. On the contrary, the difference was found to be small. The importance of comparing values of pressure integrated over a given area (as is [139]) or a given period of time was stresses, because the pressure peaks are so short in duration that they can have little role to play in the panel response.

A rigorous analysis on the existing impact load data from various model tests was carried out by Sellars in 1976 [140] and resulted in a closed form solution for the pressure load. The inclusion of liquid-gas mixture parameters in the formulation allowed for the effects of entrapped air in reducing the maximum slamming pressure. However, it was found to result in conservative predictions when compared with full scale measurements. In the same year, Stavovy and Chuang [141], refining the assumptions made in previous years by Chuang, proposed an analytical method for determining the wave impact slamming pressures and presented slamming pressure equations applicable to all types of high speed vehicles. Their approach was based on the Wagner wedge theory, the Chuang cone impact theory, and experimental results.

The study of slamming pressure loads by Allen and Jones in 1978 [139] was based on a theoretical approach combined with experimental data. It resulted in a simple formulation allowing structural design-limit pressure values and distributions to be predicted on a number of advanced marine craft, and is currently the most widely acceptable. It is further claimed that the method can be applied even when no extensive knowledge of vehicle motion is available, and can therefore be conveniently used in the early design stages. Furthermore, simple algorithm to predict the underdeck design pressure at the early design stage of SWATHs has also been

developed by Loscombe [23] based on a parametric study using the methods by Sellars [140] and Allen and Jones [139]. Additional formulations on the prediction of both peak and design slamming pressures are provided by Lloyd's Register (LR) [28], Det Norske Veritas (DNV) [29], the American Bureau of Shipping (ABS) [19], and Royal Navy [142]. These expressions are presented and reviewed in [31].

Two more recent investigations were carried out at the Department of Naval Architecture and Ocean Engineering, University of Glasgow, in an attempt to obtain slamming pressure data pertinent to SWATH ships. A better understanding was sought for the slamming phenomenon in multi-hull ships and marine vehicles whose geometry permits the entrapment of air between two side structural elements thus reducing the slam pressures due to "cushioning" effects. These investigations and their conclusions are briefly described in the next paragraph.

Earlier experimental investigations on the slam pressures of SWATH models (T-AGOS 19) in the U.S. [143] concluded that the extreme value slam pressures vary longitudinally on the wet deck, with maximum value at amidships and second highest at the bow. The lowest value occurs at the stern. Furthermore, the haunch and strut slam pressures were found to be most severe in beam seas and not to vary significantly longitudinally. It is useful to note that the inboard strut pressures were found to be approximately half the outboard strut lifetime pressure.

Generally, a trade-off exists between the primary side loads and the local impact loads on the wet deck because an increase of the wet deck clearance (to reduce slam loads) simultaneously increases the bending loads in the cross-structure. A superposition of side load and wet deck slamming load effects is normally not considered necessary because severe values of each would not occur under the same conditions.

2.5.2 The Tolikas/Das Investigation

The first drop test series carried out [144] aimed at generating additional slamming pressure data pertinent to SWATH ships, and acted as a pilot study towards more detailed experimental and theoretical investigations of

the slamming phenomenon. A detailed description of the analysis carried out and tables of all experimental results are included in [144].

The model used accounted for the specific features of SWATH underdeck configuration, such as ramp angle and the presence of the haunches and struts. Reference [144] contains detailed descriptions of the model set up, geometry, test rig installation (Figs. 2.17, 2.18), as well as details on the instrumentation used and its positioning in the model which was designed by Djatmiko [31]. The plate thickness was determined based on the assumption of a panel with edges rigidly clamped and the 3-hinge plastic collapse criterion. The vibrational characteristics and the natural frequency of the model's rectangular bottom plate assumed all edges to be simply supported and were calculated by Djatmiko [31] based on the method proposed by Swindell in [145]. Stiffener sizing was based on a uniform pressure load and the assumption that the beam is simply supported at both ends. A minimum safety factor of 2.0 against yield was set.

Slamming pressures (both peak and post-impact hydrodynamic pressure loading) at 16 individual points on the bottom panels and tensile/ compressive strains at 6 individual points on the web and flange of the largest transverse stiffener were measured. The maximum sampling rate was 2000 samples per second per channel over a period of 10 seconds. Hence, a sampling period of 0.5 milliseconds was deemed sufficient.

The tests consisted of dropping the model from various elevated positions at, and at tilt angles of, 0, 2, 4, 5, 6, 8 and 10 degrees. Since the two bottom panels were inclined at 160° to each other there were 14 variations of impact angles between 0 and 20 degrees which could be investigated. Further, this arrangement allowed two impact angles to be measured simultaneously by pressure transducers located on the two faces of the bottom plate at each run of the test. The model was tested within the range of elastic behaviour. The drop heights were from 0.5 m to 2.5 m in increments of 0.5 m while the tilt angle was varied between 0° and 10° (the slamming angle thus varying between 0° and 20°). For every drop height and drop angle the same test would be repeated 3 to 5 times to limit the unavoidable scatter of experimental results. As a consequence, a minimum of 3,300 test results were recorded and analysed.

2.5.2.1 Analysis of Experimental Results

Although for peak pressure value estimation the time range is not important, when mean and standard deviation results are sought after, it plays an important role in the calculation. The peak pressure time range was defined between the points at which the maximum rate of change started to occur and ending at the point where reversal of the sign of the tangent to the curve occurred. This was the general rule used, but attention had to be paid to avoid local maxima (sign reversal caused by noise). Peak duration was found to be between the 5 and 10 millisecond bands and very rarely outside these limits. The results obtained for every drop height, for every angle of inclination, and for every one of their 22 channels were:

- maximum peak pressure value
- minimum pressure value
- average hydrodynamic pressure value
- standard deviation value of hydrodynamic pressure.

Appendices A and B of [144] contain the tables and plots of data obtained from all six strain gauges mounted on the transverse stiffener of the flat bottom and the pressure transducer data respectively (for the pressure peak range of the time history).

For the model considered, and based on the behaviour of strains, it appears that the boundary conditions for the stiffeners and plating are more towards simply supported than fixed. A more detailed investigation is required to identify the degree of rotational restraint imposed on the plate edges. Numerical modelling for response simulation would benefit from such information.

From observations of pressure transducer data the following apply [144]:

1. Peak pressure values increase linearly with drop height for locations both on the centreline and orthogonal to it.

2. A consistent decrease in peak pressure magnitude moving from the centreline towards the sides occurs. This decrease is more marked between the centreline and mid-width locations, especially for increasing impact angles.

3. The values of peak pressure between mid-width and the sides are close to each other, their proximity and similarity in variation with drop height increasing with increasing angle of inclination.

4. Peak pressure for all transversely positioned pressure transducers occurs at approximately 4° inclinations, irrespective of drop height.

5. For every pressure transducer, as the drop height increases the rate of change of peak pressure with increase in while the peak pressure values level off after a deadrise of 13° to 15° is attained.

6. Centreline pressure transducers obtain their peak values (for a specific drop height) at greater impact angles than the offset pressure transducers. This difference in angle, although small, increases with increasing drop height.

7. The primary objective of any drop test exercise is to obtain a factor of proportionality K relating the slam pressure with the speed at impact, V,

$$p = KV^2$$

Any attempt in establishing a form factor relating the drop height (or square of the impact speed) with pressure should consider that K must be a function of the angle of impact, drop height and the location of the structural element in question (on the centreline and at points off it).

8. All of the empirical models whose predictions are greatly influenced by the angle of inclination (i.e. those for wedge type impacts) demonstrate a considerable decrease in predicted values on and around 4° inclinations. It is then that they approach realistic (wrt experimental data) values.

9. The models by Sellars [140], Loscombe [23], Stavovy and Chuang [141] for 0 degrees condition, have been found to provide very conservative (300-400%) predictions for flat bottom slamming peak pressures. Possible implicit safety factors may be to blame for such a discrepancy. Only Chuang's [128, 132] model is close to the experimental data but their deviation increases for increasing drop height, the model's predictions remaining in the unsafe region relative to the experimental data. Royal Navy's equation is also

unsafe and provides a lower bound to all theoretical and experimental data. This is partly attributed to the inherent safety factor in the formulation. It is worth noting that Royal Navy's formulation is independent of drop height and inclination.

For values corresponding to "wedge" type drops of various input angles:

10. von Karman [120] provides an upper limit prediction for the side pressure values to an angle of 4°. At 4° ABS recommendations [19] for peak pressure may provide a less conservative, but safe prediction to a drop height of 2m. For larger drop heights von Karman should be preferred.

11. For inclinations of 8° to 18°, Stavovy and Chuang's model [141] provides excellent fit (upper limit) to experimental data. At 20° Wagner's formula [121, 122] may be employed.

12. Correlation of pressure readings with the corresponding strain gauge measurements is necessary. This will involve integration of the pressure readings over a specified panel area and the resulting force compared with the force causing the recorded by the strain gauge readings. This correlation will thus enable the identification of an appropriate panel area to be considered for preliminary design against slamming pressures.

The complete results of this investigation were reported in [144]. The main drawback limiting the usefulness of the data was the inadequate response characteristics of the pressure transducers and at times the malfunction of the instrumentation system. As a result, the data obtained were useful only in a qualitative sense permitting only general behavioural conclusions to be drawn.

2.5.3 The Zhu/Faulkner Investigation

As a result of the numerical inadequacy of the first investigation, Zhu and Faulkner [114] carried out a series of drop tests on a small scale model of 1/5 the dimensions of the previous model. The difficulties associated with a harsh outdoor environment and the large scale of the model associated with the first tests were eliminated by running the experiments in the Department's Hydrodynamics Laboratory. Based on the observations and

conclusions of the first investigations [144], Zhu and Faulkner aimed at providing slamming pressure data at the more critical small impact angles for various drop heights, due for correlation with impact flow theory. In addition, the dynamic response due to impact of the bottom panels was investigated via appropriate strain measurements. Attention was paid to the possibility that the proximity of the tank wall to the test model will affect the final pressure readings.

The model was made of steel, of 1/5 the dimensions of the previous large scale model, and weighed 13 kgs (cf. 1000kg of the previous model). Six angles of inclination were investigated (0-20°) between the heights of 0.5-2.5m at 0.5m intervals. Four pressure transducers (3 on the centreline and 1 at quarter width off it) and four strain gauges at the horizontal bottom panel were used. The total sampling period was 3 milliseconds. Two accelerometers provided measurements of the model speed during impact. Complete details of the experimental set-out and details referring to the instrumentation and model geometry may be obtained from [114].

The influence of the drop weight on the peak pressure values was investigated. It was concluded that an increase of 33% in the weight may lead to reductions in peak pressure values for angles of inclination of and around the critical angle of 4° for all drop heights. The phenomenon is reversed for large drop angles (approximately 20°) where the peak pressures seem to increase. At level drops (0°) the picture is unclear as the values for both weights fall within each other's scatter bands.

The study of any 'wall effects' on the peak pressure values was rather inconclusive. There was a clear trend for the wall effects to result in higher peak pressure values for all inclined cases, except for the critical angle of inclination of 4° where the trend is once again reversed. Figure 2.19 (prepared by Zhu) shows the results of an initial investigation into 'heel effects'. The effect on both the shape and peak pressure values recorded by a pressure transducer positioned off the centreline was found to be considerable. According to Zhu, such investigations have the additional advantage that may account for the ships motions in 3-D which will very rarely position the wet-deck level to the seaway during the impact phenomenon (as assumed in all drop test investigations). Further investigations are therefore required.

Figure 2.20 [114] compares the pressure coefficient values C_p as obtained by various experimental procedures (procedures that do not account for air entrapment due to the presence of wall sides), Zhu and Faulkner's data, and the pressure coefficients implied by Wagner [121, 122] and Payne [138, 146, 147]. Note that:

$$p = C_p \frac{1}{2} \rho V_R^2$$

where p is the impact pressure, ρ is the water density and V_R is the relative velocity. Additionally

$$C_p = \begin{cases} \dfrac{1+\pi^2}{4\tan^2\theta} & \text{Wagner} \\ \dfrac{1}{\tan^2\theta} + \left(\dfrac{4\pi\eta f(\theta)}{\cos\theta}\right)^2 + \dfrac{8\pi\eta f(\theta)}{\tan\theta\cos\theta} & \text{Payne} \end{cases}$$

where θ is the deadrise angle, η=0.05 and $f(\theta) \approx 1 - (\theta/\pi)$.

The effect of the air entrapment is obvious in the Zhu/Faulkner test data. Similar qualitative conclusions to those in [144] were drawn and the large scatter in the test data has once again been the main characteristic of the nature of the tests. Work by Zhu and Faulkner will extend to the study of the dynamic response of plates under slamming loads based on numerical simulations. In addition, work is currently underway in the Department of Naval Architecture and Ocean Engineering to modify a 3-D motion prediction program [47] to include slamming theory. Hence, comparison of the experimental data with a time-domain slamming simulation program would be possible. Recommended simplified design formulae can be evaluated in the same manner.

2.5.4 General Comments on Slamming Load Investigations

All researchers are in agreement on the presence of the air cushioning effect, in the case of flat bottom impact, resulting in a significant reduction in the peak impact pressure, and that the pressure developed during flat impact is not evenly distributed over the flat surface. On the evaluation of the effect of structure/model weight variation it is generally agreed that the heavier structure/model (with the same geometrical size) will result in larger in magnitude and shorter in duration impact pressures. This

observation allows the conclusion that the pressure is directly proportional to the square of the drop velocity. At very high mass loading the peak impact pressure tends to fall below the line of proportionality, and may bring about a linear relationship between maximum pressure and drop velocity.

In contrast to the flat bottom impact, the pressure behaviour of wedge shaped bodies is characterised by the larger peak pressure which occurs at a distance away from the keel rather than along the keel. This larger peak pressure is explained as being caused by the splashed up water after impact. Experimental evidence shows the largest impact pressure away from the keel would be experienced on wedge shape bodies with a deadrise angle of about 3-4°. The expectation of larger impact pressure occurring at lower deadrise angles than 3° is not satisfied due to the fact that at such angles the cushioning effect of the entrapped air still exists, although not as intense as in the case of flat bottom impact.

There are some areas that have not been sufficiently incorporated in the slamming investigations by drop test models, like the effects of structural flexibility, disturbed (irregular) water surface, and forward speed. In addition, verification of drop test data should be made against the information from seakeeping tests. The inclusion of the structural flexibility and irregularity of the seaway may well lead to a shift from the current static load criteria to more realistic dynamic load criteria.

References

1) Loscombe, P.R., 'Initial Design Stage Slam Pressure Prediction for Small SWATH Ships', Ship and Boat International, October 1990.
2) Report of Committee V.4, 'Novel Design Concepts - SWATH', 10th International Ship and Offshore Structures Congress (ISSC 88), Vol 2, Denmark, Aug.1988.
3) Gore. J.L., 'SWATH Ships', Naval Engineers Journal, Feb. 1985.
4) Lee, C.M. and Curphey, R.M., 'Prediction of Motion, Stability and Wave Load of Small Waterplane-Area Twin-Hull Ships', Trans. SNAME, Vol. 83, 1977.

5) Faulkner, D., 'Structural Design Philosophy for Small and Large High Speed Multi-Hull Ferries', Proc. Conf. Safety for High Speed Craft-The Way Ahead, RINA, London, 7-8 May 1992.

6) Trillo, R.L., 'Foreword', in Jane's High Speed Marine Craft and Air Cushion Vehicles, Jane's Information Group, London, 1991.

7) Oshima, M., Narita, H., 'Development of Semi-Submerged Catamaran (SSC)', Mitsui Engineering and Shipbuilding Co., Tech. Report No. 115, 1982.

8) Lang, T.G., Slogget, J.E., 'SWATH Developments and Performance Comparisons with Other Craft', Proc. Int. Conf. on SWATH Ships and Advanced Multi-Hull Vessels, RINA, Paper No. 1, London, 1985.

9) Gupta, S.K., Schmidt, T.W., 'Developments in SWATH Technology', Naval Engineers Journal, May 1986. also Discussion: Naval Engineers Journal, Vol. 98, July 1986, pp. 112-122.

10) Waters, R.T., Fein, J.A., 'Maneuvrability of SWATH Ships', Proc. 19th American Towing Tank Conf., Michigan, 1980.

11) Kennel, C.G., 'SWATH Ship Design Trends', Proc. Int. Conf. SWATH Ships and Advanced Multi-Hulled Vessels I, RINA, London, 19th April 1985.

12) Chan, H.S., Djatmiko, E.B., Miller, A.F., Caldwell, L.B., 'Structural Loading Aspects in the Design of SWATH Ships', Proc. 5th Int. Symp. on the Practical Design of Ships and Mobile Units (PRADS'92) Newcastle Upon Tyne,U.K., May 1992.

13) Sikora, J.P., 'Some Design Approaches for Reducing the Structural Weight of SWATH Ships', Proc. 2nd Int. Conf. on SWATH Ships and Advanced Multi-Hulled Vessels, RINA, London, Nov. 1988.

14) Chalmers, D.W., 'Structural Design Aspects of SWATH Ships', WEGEMT Summer School: 'Design Techniques for Advanced Marine Vehicles and High Speed Displacement Ships', Genoa, Italy, 1989.

15) Sikora, J.P., Dinsenbacher, A.L., 'SWATH Structure: Navy Research and Development Applications', Marine Technology, Vol.27, No. 4, July 1990.

16) Kerr, G.D., Anderson, T.A., Kennel, C.G., 'SWATH Ship State of Art', Proc. Conf. Advanced Marine Vehicles, AIAA/SNAME, San Diego, California, 1978.

17) Sikora, J.P., Dinsenbacher, A.L., Beach, J., 'A Method for Estimating Lifetime Loads and Fatigue Lives for SWATH Ships and Conventional Monohull Ships', Naval Engineers Journal, Vol. 95, No. 3, May 1983.

18) Stirling, A.G., Jones, G.L., Clarke, J.D., 'Development of a SWATH Structural Design Procedure for Royal Navy Vessels', Proc. Int. Conf. SWATH Ships and Advanced Multi-Hulled Vessels II, RINA, 28-30 Nov. 1988, London.

19) American Bureau of Shipping, 'Preliminary Guide for Building and Classing Small Waterplane Area Twin Hull (SWATH) Vessels', ABS, Provisional Recommendations, 1990.

20) Liu, D., 'Development and Analysis of SWATH Ships', Presented at the Hellenic Institute of Marine Technology, Piraeus, Greece, 31st October 1989.

21) Lee, C.M., Jones, H.D., Curphey, R.M., 'Prediction of Motion and Hydrodynamic Loads of Catamarans', Marine Technology, SNAME, Vol. 10, No. 4, Oct. 1973

22) Kennel, C., 'SWATH Ships', Technical and Research Bulletin No. 7-5, SNAME, 1992.

23) Loscombe, P.R., 'Key Aspects of the Structural Design of Small SWATH Ships', PhD Thesis, University of Southampton, Dec. 1989.

24) Kennel, C.G., 'The Effect of Transverse Side Load on Small Waterplane Area Twin Hull (SWATH) Structures', Naval Ship Engineering Center Report 6114-041-79, Jan. 1979.

25) Luedeke Jr.G., Montagne, J., Posnasky, H., Lewis, Q., 'The RMI SD-60 SWATH Demonstration Project (HALCYON)', Proc. Int. Conf. SWATH Ships and Advanced Multi-Hulled Vessels I, RINA, London, 19th April 1985.

26) Luedeke Jr.G., Montagne, J., 'RMI's Small Waterplane Area Twin Hull (SWATH) Boat Project', San Diego Section Meeting, SNAME, Nov. 1984.

27) Betts, C.V., 'A Review of Developments in SWATH Technology', Proc. Int. Conf. SWATH Ships and Advanced Multi-Hulled Vessels II, Vol 1, RINA, London, 28-30 Nov. 1988.

28) Lloyd's Register of Shipping, 'Provisional Rules for the Classification of High Speed Catamarans', LRS, Part 1, London, 1990.

29) Det Norske Veritas, 'Tentative Rules for Classification of High Speed and Light Craft', DNV, Oslo, 1991.

30) Curphey, R.M., Lee, C.M., 'Analytical Determination of Structural Loading on ASR Catamaran in Beam Waves', DTNSRDC, Ship Performance Dept. R&D, Report No. 4267, Bethesda, Maryland, USA, Apr. 1974.

31) Djatmiko, E.B., 'Hydro-Structural Studies on SWATH Type Vessels', PhD Thesis, University of Glasgow, July 1992.

32) Reilly, E.T., Shin, Y.S., Kotte, E.H., 'A Prediction of Structural Load and Response of a SWATH Ship in Waves', Naval Engineers Journal, ASNE, May 1988.

33) Reilly, E.T., Ingram, T.J., Arntson, S.G., 'SWATH Vessels for Naval Applications Design and Analysis', American Bureau Shipping, USA, 1990.

34) Shin, Y., Kotte, E., Thayamballi, A., Unger, D., 'Analysis Procedure of Hydrodynamic Load and Fatigue Life Prediction for SWATH Ships in Waves', Proc. Intersociety Conf. Advanced Marine Vehicles, Paper No. 89-1477-CP, Arlington, VA, USA, June 1989.

35) Oshima, M., Narita, H., Kunitake, Y., 'Experiences with 12 Meter Long Semi-Submerged Catamaran (SSC) 'Marine Ace' and Building of SSC Ferry for 446 Passengers', Proc. Conf. Advanced Marine Vehicles, AIAA/SNAME, Paper No. 79-2019, Baltimore, Maryland, USA, 1979.

36) Price, W. G., Wu, Y., 'Structural Responses of a SWATH or Multi-Hulled Vessel Travelling in Waves', Proc. Int. Conf. SWATH Ships and Advanced Multi-Hulled Vessels I, RINA, London, 19th April 1985.

37) Chan, H.S., 'A Three Dimensional Technique for Predicting First- and Second-Order Hydrodynamic Forces on Marine Vehicle Advancing in Waves', PhD Thesis, Dept. of Naval Architecture and Ocean Engineering, University of Glasgow, 1990.

38) Price, W.G., Temarel, P., Wu, Y., 'Responses of a SWATH Travelling in Unidirectional Irregular Seas', Underwater Technology, SUT, Vol. 13, No. 4, 1987.

39) Keane, A.J., Price, W.G., Temarel, P., Wu, X-J., Wu, Y., 'Seakeeping and Structural Responses of SWATH Ships in Waves', Proc. Int. Conf. on SWATH Ships and Advanced Multi-Hulled Vessels II, RINA, London, Nov. 1988.

40) Bishop, R.E.D., Price, W.G., Temarel, P., 'On the Hydroelastic Response of a SWATH to Regular Oblique Waves', Proc. Conf. Advances in Marine Structures, ARE, Dunfermline, Scotland, May 1986.

41) Clayton, B.R. , Bishop, R.E.D., 'Mechanics of Marine Vehicles', E.&F.N. Spon Ltd., London, 1982.

42) Price, W.G., Wu, Y., 'The Influence of Non-Linear Fluid Forces in theTime Responses of Flexible SWATH Ships Excited by a Seaway', Proc. 8th Int. Conf. on OMAE, The Hague, Netherlands, March 1987.

43) Price, W. G., Temarel, P., Wu, Y., 'Fluid Interaction of Multi-Hulled Structures Travelling in Waves', PRADS 83, Tokyo and Seoul, 1983.

44) Atlar, M., 'The SWATH Wave Load Program - Some Aspects of Computer Program SWATHL', Dept. of Naval Architecture and Ocean Engineering, Report, No. NAOE-86-55, University of Glasgow, Dec. 1986.

45) Zheng, X., 'Prediction of Motion and Wave Load of Mono and Twin Hull Ships in Waves', PhD Thesis, Dept. of Naval Architecture and Ocean Engineering, University of Glasgow, June 1988.

46) Zheng, X., 'User's Guide of Program 'SHIPM1.0' - For Twin Hull', Dept. of Naval Architecture and Ocean Engineering, University of Glasgow, 1989.

47) Chan, H.S., 'Prediction of Motion and wave Loads of Twin-Hull Ships', Jnl. Marine Structures, Vol. 6, 1993.

48) Chan, H.S., 'Prediction of Motion and Structural Responses of Mono- and Twin-Hull Ships Advancing in Waves', Dept. of Naval Architecture and Ocean Engineering, Report No. NAOE-91-16, University of Glasgow, July 1991.

49) Papanikolaou, A., Schellin, T.E., Zaraphonitis, G., 'A 3 D-Method to Evaluate Motions and Loads of Ships with Forward Speeds in Waves', Proc. 5th Int. Congress of Marine Technology, HIMT, Athens, 1990.

50) Schellin, T.E., Papanikolaou, A., 'Prediction of Seakeeping Performance of a SWATH Ship and Comparison with Measurements', Proc., 1st Int. Conf. on Fast Sea Transportation (FAST'91), Trondheim, Norway, June 1991.

51) Faltinsen, O., Hoff, J.R., Kvålsvold, J., Zhao, R., 'Global Loads on High-Speed Catamarans', Proc. 5th Int. Symp. on the Practical Design of Ships and Mobile Units, PRADS'92, Vol. 1, Newcastle on Tyne, UK, May 1992.

52) Faltinsen, O.M., 'Sea Loads on Ships and Offshore Structures', Cambridge Ocean Technology Series, Cambridge University Press, Cambridge 1990.

53) Faltinsen, O., Svensen, T., 'Behaviour of Catamarans, Foilcatamarans and SES in Waves', Proc. MARIN Jubilee Meeting, Workshop A: Advanced Vessels, Wageningen, The Netherlands, May 1992.

54) Kallio, J.A., Ricci, J.J., 'Seaworthiness Characteristics of a Small Waterplane Area Twin Hull (SWATH IV) Part II', DTNSRDC, Ship Performance Department, Report No. SPD 620-02, Bethesda, Maryland, USA, May 1976.

55) Nethercote, W.C.E, Schmitke, R.T., 'A Concept Exploration Model for SWATH Ships', Trans. RINA, Vol. 124, 1982.

56) Koops, A., Nethercote, W.C.E., 'An Extended SWATH Concept Exploration Model', Proc. Int. Conf. SWATH Ships and Advanced Multi-Hulled Vessels II, RINA, London, UK, Nov. 1988.

57) Pattison, D.R., Rose, P.H.A., Harris, S.A., 'SWATH - The UK MoD Design and Assessment Programme', Proc. Int. Conf. on SWATH Ships and Advanced Multi-Hulled Vessels II, RINA, London, UK, Nov. 1988.

58) Mabuchi, T., Kunitake, Y., Nakamura, H., 'A Status Report on Design and Operational Experiences with the Semi-Submerged Catamaran (SSC) Vessels', Proc. Int. Conf. SWATH Ships and Advanced Multi-Hulled Vessels, RINA, London, April 1985.

59) Djatmiko, E.B., 'Experimental Investigation into SWATH Ship Motions and Loadings', MSc Thesis, University of Glasgow, Nov. 1987.

60) Bhattacharyya, R., 'Dynamics of Marine Vehicles', John Wiley and Sons Publications, Springer-Verlag, London, 1987.

61) Goda, Y., 'A Review on Statistical Interpretation of Wave Data', Report of the Port and Harbour Research Institute, Vol. 18, No. 1, March 1979.

62) Ochi, M.K., 'On Prediction of Extreme Values', Jnl of Ship Research, SNAME, Vol. 17, No. 1, March 1973.

63) Neumann, G., 'On Ocean Wave Spectra and à New Method of Forecasting Wind Generated Sea', Beach Erosion Board, U.S. Army Corps of Engineers, Technical Memo No. 32, 1953.

64) Liu, P.C., 'Normalised and Equilibrium Spectra of Wind-Wave in Lake Michigan', Journal of Physical Oceanography, Vol. 1, No. 4, 1971.

65) Mitsuyashu, H., 'The One-Dimensional Wave Spectra at Limited Fetch', Proc. 13th Coastal Engineering Conference, ASCE, Vancouver, July 1972.

66) Pierson, W.J., Moskowitz, L., 'A Proposed Spectral Form for Fully Developed Wind Seas Based on the Similarity Theory of S. A. Kitaigorodskii', Jnl of Geophysical Reasearch, Vol. 69, No. 24, Dec. 1964.

67) Bretschneider, C.L., 'Wave Variability and Wave Spectra for Wind Generated Gravity Waves', Beach Erosion Board, U,S. Army Corps of Engineers, Technical Memo No. 118, Washington D.C., 1959.
68) Bretschneider, C.L., 'Wave Forecasting, Handbook of Ocean and Underwater Engineering', Myers, J.J., et al. (Eds), Chapter 11, McGraw Hill Book Co., New York, 1969.
69) Proceedings of the Second International Ship Structures Congress, Delft, Netherlands, 1964.
70) Scott, J.R., 'A Sea Spectrum for Model Tests and Long-Term Ship Prediction', Jnl. of Ship Research, Vol. 9, December 1965.
71) Chakrabati, S., 'Hydrodynamics of Offshore Structures', Computational Mechanics Publishing Company, New York, 1978.
72) Hasselman, K. et al, 'Measurement of Wind-Wave Growth and Swell Decay During the Joint North Sea Wave Project (JONSWAP)', Deutschen Hydrographischen Zeitschrift, Erganzunscheft, Vol. 13, No. A, 1973.
73) Hasselman, K. et al, 'A Parametric Wave Prediction Model', Jnl. of Physical Oceanography, Vol. 6, 1976.
74) Ochi, M.K., Hubble, E.N., 'Six-Parameter Wave Spectra', Proc. 15th Coastal Engineering Conference, ASCE, Honolulu, 1976.
75) Ochi, M.K., Wang, S., 'Prediction of Extreme Wave-Induced Loads on Ocean Structures', Proc. Int. Conf. on Behaviour of Offshore Structures (BOSS'76), Norwegian Institute of Technology, Trondheim, Norway, Aug. 1976.
76) Ochi, M., Bales, S., 'Effect of Various Spectral Formulations in Predicting Responses of Marine Vehicles and Ocean Structures', Proc. 9th Offshore Technology Conference (OTC), ASME, Houston, 1977.
77) Lewis, E.V., 'Predicting Long-Term Distribution of Wave-Induced Bending Moments on Ship Hulls', SNAME Spring Meeting, Montreal, 1967,
78) Hoffman, D., 'Wave Data Application for Ship Response Prediction', Webb Institute of Naval Architecture, October 1975.
79) Ochi, M.K., 'Generalisation of Rayleigh Probability Distribution and its Application', Jnl. of Ship Research, Vol. 22, No. 4, Dec. 1978.
80) Hughes, O.,F., 'Ship Structural Design: A Rationally Based Computer Aided Optimization Approach', SNAME, New Jersey, 1988.
81) Ochi, M.K., 'Stochastic Analysis and Probabilistic Prediction of Random Seas', Advances in Hydrosciences, Vol. 13, 1982.

82) Carter, D.J.T., Challenor, P.G., Ewing, J.A., Pitt, E.G., Srokoszi, M.A., Tucker, M.J., 'Estimating Wave Ultimate Parameters for Engineering Applications', Offshore Technology Report, OTH86 228, DEn, HMSO, 1986.

83) Nibbering, J.J.W., 'Fatigue of Ship Structures', Netherlands Research Centre T.N.O. for Shipbuilding and Navigation, Report No. 55S, Sept. 1963.

84) Munse, W.H., Wilbur, T.W., Tellaliau, M.L., Nicoll, K., Wilson, K., 'Fatigue Characterization of Fabricated Ship Details for Design', Ship Structure Committee Report SSC-318, Aug. 1982, issued by US Coast Guard, Jan. 1984.

85) Sikora, J.P., Beach, J., 'Automated Method for Predicting Maximum Lifetime Loads and Fatigue Lives of Ships', Proc. Conf. Current Practices and New Technology in Ocean Engineering, New Orleans, Louisiana, Feb. 1986.

86) Xue, J., Pittaluga, A., Cervetto, D., 'Fatigue Damage Calculation for Oil Tanker and Container Ship Structures', Jnl. Marine Structures, Vol. 7, No. 6, 1994.

87) Kinra, R.K., Marshall, P.W., 'Fatigue Analysis of the Cognac Platform', Jnl. of Petroleum Technology, March 1980.

88) Maddox, S.J., Wildenstein, A.M., 'A Spectral Fatigue Analysis for Offshore Structures', Proc. of the Offshore Technology Conference (OTC), ASME, May 1975, Vol. 2.

89) Nolte, K.G., Hansford, J.E., 'Closed Form Expressions for Determining the Fatigue Damage of Structures Due to Ocean Waves', Proc. Offshore Technology Conference (OTC), ASME, Vol. 2, May 1976.

90) Wirsching, P.H., Stahl, B.Y-N., Nolte, K.G., 'Probabilistic Fatigue Design for Ocean Structures', Jnl of the Structural Division, ASCE, Vol. 103, ST 10, Oct. 1977.

91) Faulkner, D., 'Ship and Ocean Structures IV: Fatigue and Fracture', Final Year Notes, 1992, Department of Naval Architecture and Ocean Engineering, University of Glasgow, Glasgow, Scotland.

92) Faulkner, D., 'New Technologies for Ship and Offshore Structural Analysis and Design', Proc. Intl. Symposium on Marine Structures (ISMS'91), 12-15 Sept. 1991, Shangai, China.

93) Chen, Y.N., Thayamballi, A.K., 'Consideration of Global Climatology and Loading Characteristics in Fatigue Damage Assessment of Ship Structures', Symp. Marine Structural Inspection, Maintainance and Monitoring, SNAME, Arlington, Virginia, 18-19 March 1991.

94) Wirsching, P.H., 'Fatigue Reliability for Offshore Structures', Jnl of the Struct. Division, ASCE, Vol. 110, No. 10, Oct. 1984.

95) Munse, W.H., 'Fatigue Criteria For Ship Structure Details', Symp. on Extreme Loads Response, SNAME, Arlington, Virginia, USA, 19-20 Oct. 1981.

96) Wirsching, P.H., Chen, Y-N., 'Considerations of Probability-Based Fatigue Design for Marine Structures', Jnl. Marine Structures, Vol. 1, No. 1, 1988.

97) Moan, T., 'Fatigue Design Criteria for Ships', Report MK/R97, Division of Marine Structures, NTH Trondheim, Norway, 1987.

98) Nordenstrom, N., 'A Method to Predict Long-Term Distributions of Waves and Wave Induced Motions and Loads on Ships and Other Floating Structures', Det Norske Veritas, Publ. No. 81, April 1973.

99) Clarke, J.D., 'Fatigue and Crack Initiation and Propagation in Warship Hulls', Proc. Conf. Advances in Marine Structures-2, DRA (Dumfermline), 21-24 May 1991, Dumfermline, Scotland: Elsevier Applied Science Publishers, London, 1991.

100) Ang, A.,H-S., 'Basis for Reliability Approach to Structural Fatigue', Proc. Second International Conference on Structural Safety and Reliability, Munich, Germany, 1977.

101) Pittaluga, A., Cazzulo, R., Romeo, P. 'Uncertainties in the Fatigue Design in Offshore Steel Structures', Jnl. Marine Structures, Vol. 4, No. 4, 1988.

102) Dogliani, M., 'Fatigue Reliability: Modification of the Wirshing Approach for Fatigue Limit', Registro Italiano Navale, Technical Report, No. 18/87, Genoa, 1987.

103) Maddox, S.J., 'Fatigue Strength of Welded Structures', Abington Publishing, Cambridge, England, 1991.

104) Dowling, N.E., 'Fatigue Failure Predictions for Complicated Stress-Strain Histories', Jnl. of Materials, Vol. 7, No. 1, Mar. 1972.

105) Matshuishi, M., Endo, T., 'Fatigue of Metals Subjected to Varying Stress', Japanese Society of Mechanical Engineers, Fukuoka, Japan, 1968.

106) Nelson, D.V., Fuchs, H.O., 'Prediction of Cumulative Fatigue Damage Using Condensed Load Histories', Society of Automotive Engineers, Feb. 1975.

107) Wirsching, P.H., Light, M.C., 'Probability Based Fatigue Design Criteria for Offshore Structures', PRAC Project 79-15, Final Report, API, Dallas, Texas, 1979.

108) Chaudhury, G., 'Spectral Fatigue of Broad-Band Stress Spectrum With One or More Peaks', Proc. Offshore Technology Conference, OTC'86, Vol. IV, No. 5333, 1986.
109) Sigurdsson, G., 'Some Aspects of reliability of Offshore Structures', Structural Reliability Paper, No. 55, University of Aalborg, Denmark, April 1989.
110) Clarke, J.D., 'Wave Loading in Warships', Proc. Conf. Advances in Marine Structures, ARE Dumfermline, 20-23 May 1986, Dumfermline, Scotland, Elsevier Applied Science Publishers, London, 1986.
111) British Standards Institution, 'Specification for Steel Concrete and Composite Bridges: Code of Practice for Fatigue, BS5 400: Part 10', BSI, 1980.
112) British Standards Institution, 'Code of Practice for Fixed Offshore Structures, BS 6235', BSI, 1982.
113) Clarke, J.D., 'Prediction of Fatigue Cracking in Warship Hulls', Proc. 3d Int Symp. Practical Design of Ships and Mobile Units (PRADS 87), Vol. II, Trondheim, Norway, June 1987.
114) Zhu, L., Faulkner, D., 'Slamming Drop Tests for Small Scale SWATH Characteristic Model', Department of Naval Architecture and Ocean Engineering, Report No. NAOE-94-34, University of Glasgow, Nov. 1994.
115) Ochi, M.K., Motter, L.E., 'Prediction of Extreme Values of Impact Pressure Associated with Ship Slamming', Jnl. of Ship Research, Vol. 13, No. 2, June 1969.
116) Ochi, M.K., Motter, L.E., 'Prediction of Slamming Characteristics and Hull Responses for Ship Design', Trans. SNAME, Vol. 81, 1973.
117) Graham, R., 'Slamming Experiment with a Radio-Controlled SWATH Model', Proc. Int. Conf. on SWATH Ships and Advanced Multi-Hulled Vessels II, RINA, London, Nov. 1988.
118) Djatmiko, E.B., 'Comparative Evaluation of Some Slamming Prediction Methods for SWATH Type Vessels', Dept Report, No. NAOE-91-14, Dept. of Naval Architecture and Ocean Engineering, University of Glasgow, June 1991.
119) Hayman, B., Haug, T. and Valsgård, S., 'Response of Fast Craft Hull Structures to Slamming Loads', Proc. 1st Int. Conf. on Fast Sea Transportation (FAST'91), Trondheim, Norway, June 1991.
120) Von Karman, T., 'The Impact of Seaplane Floats During Landing', NACA TN 321, October 1929.

121) Wagner, H., 'Landing of Seaplanes', NACA TN 622, May 1932.
122) Wagner, H., 'Uber Stoss-und Gleituorgange an der Oberflache von Flussigkeiten', Zeitschrift Fur Angewandte Mathematik und Mechanik, Bd. 12, Heft 4, Aug. 1932.
123) Sydow, J., 'Uber den Einfluss von Lederung und Kislung auf den Landestoss', Jahrbuck der Deutchen Luftfahrtforschung, 1938.
124) Egorov, I.T., 'Impact on a Compressible Fluid', NACA TM 1413, Feb. 1958. Translated from Prikladnaia Matematika i Mekhanika, Vol. 20, no. 1, 1956.
125) Ogilvie, T.F., 'Compressibility Effects in Ship Slamming', Schiffstechnik, Bd.10, Heft 53, 1963.
126) Greenpson, J.E., 'Sea Tests of USCG 'Unimak', Part 3: Pressures, Strains and Deflections of Bottom Plating Incident to Slamming', DTMB Report 978, 1956.
127) Sharov, Y.F., 'Slamming Stresses in Ship Bottom Plates', Sundostroenie, Vol. 24, no. 4, 1958.
128) Chuang, S-L., 'Experiments on Flat-Bottom Slamming', Jnl. of Ship Research, Vol. 10, No. 1, March 1966.
129) Verhagen, J.H.G., 'The Impact of a Flat Plate on a Water Surface', Jnl. of Ship Research, Vol. 11, No. 4, Dec. 1967.
130) Johnson, R.S., 'The Effect of Air Compressibility in a First Approximation to the Ship Slamming Problem', Jnl. of Ship Research, Vol. 12, March 1968.
131) Lewison, G., MacLean, W.M., 'On the Cushioning of Water Impact by Entrapped Air', Jnl. of Ship Research, Vol. 12, No. 2, June 1968.
132) Chuang, S-L., 'Experiments on Slamming of Wedge-Shaped Bodies', Jnl. of Ship Research, Vol. 11, No. 3, Sept. 1967.
133) Lewison, G.R.G., 'On the Reduction of Slamming Pressures', Trans. RINA, Vol. 112, 1970.
134) Chuang, S.L., 'Investigation of Impact of Rigid and Elastic Bodies with Water', Report No. 3248, Naval Ship Research and Development Centre, Washington D. C., Feb. 1970.
135) Ando, S., 'Cushioning of Slamming Impact by Elastomeric Layers', Jnl. of Ship Research, Vol. 33, No. 3, Sept. 1989.
136) Boe, A., Hang, T., Hayman, B., 'Slamming Drop Test Arrangement', Det Norske Veritas, Report No. 90-0051, Norway, Sept. 1990.
137) Hayman, B., Hang, T., Valsgard, S., 'Response of Fast Craft Hull Structures to Slamming Loads', Proc. 1st Int. Conf. Fast Sea Transportation (FAST'91), Trondheim, Vol. 1, 17-21 June 1991.

138) Payne, P.R., 'The Vertical Impact of a Wedge on a Fluid', Technical Note, Ocean Engineering, Vol. 8, No. 4, 1981.
139) Allen, R.G., Jones, R.R., 'A Simplified Method for Determining Structural Design-Limit Pressures on High Performance Marine Vehicles', Proc. Conf. Advanced Marine Vehicles, AIAA/SNAME, Paper no. 78-754, San Diego, April 1978.
140) Sellars, F.H., 'Water Impact Loads', Marine Technology, Vol. 13, Jan. 1976.
141) Stavovy, A. B., Chuang, S. L., 'Analytical Determination of Slamming Pressures for High Speed Vehicles in Waves', Jnl. of Ship Research, SNAME, Vol. 20, No. 4, Dec. 1976.
142) Brinkhurst, P.J., 'The Structural Design of SWATHs', CNA Technical Memo 4/90, MoD, Bath, 1990.
143) Dinsenbacher, A. L., Waltz, Kandela, 'SWATH Structural Considerations', ASNE Flagship Section, May 1987.
144) Tolikas, C., Das, P.K., 'Initial Drop Tests to Simulate Slamming Pressures on the Wet Deck of Twin-Hull Vessels', Department of Naval Architecture and Ocean Engineering, Dept. Rept. No. NAOE-93-16, University of Glasgow, 1993.
145) Swindell, R.J., 'Method for Calculating Natural Frequencies of Panels Fluid Loaded on One Side', The Naval Architect, RINA, March 1993.
146) Payne, P.R., 'The Normal Force on a Planing Surface', Jnl. of Hydronautics, Vol. 15, Nos. 1-4, Jan.-Dec. 1981.
147) Payne, P.R., 'The Normal Force on a Flat Planning Plate, Including Low Length to Beam Ratios', Ocean Engineering, Vol. 8, No.3, 1981.
148) Buckley, W.H., Stavovy, A.B., 'Progress in the Development of Structural Load Criteria for Extreme Waves', Extreme Load Response Symposium, SNAME, Arlington, VA, Oct. 1981.
149) Lewis, E.V., 'Structural Dynamics of Ships', Proc. Int. Symp. on the Dynamics of Marine Vehicles and Structures in Waves, IMechE, London, April 1975.

Tables

Table 2.1: Load combination effects on the hull girder as proposed by Kennel [27].

HULL GIRDER COMBINED LOAD			
HEADING	TRANSVERSE LOAD	LONGITUDINAL BENDING	TORSION
BEAM	F	0.15 M	0.25 T
BOW, QUARTERING	0.8 F	0.8 M	T
HEAD, FOLLOWING	0.15 F	M	0.1 T

Table 2.2: Relationship between the two-parameter spectra [71].

Model	A	$\tilde{\omega}$	$\tilde{\omega}/\omega_0$	$\tilde{\omega}/\bar{\omega}$	$\tilde{\omega}/\omega_z$
P–M	5/4	ω_0	1.0	0.772	0.710
Bretschneider	0.675	ω_s	1.167	0.90	0.829
ISSC	0.4427	$\bar{\omega}$	1.296	1.0	0.921
ITTC	5/4	ω_0	1.0	0.772	0.710

A = nondimensional coefficient $\tilde{\omega}$ = mean frequency
$\hat{\omega}$ = characteristic frequency ω_z = zero-crossing frequency
ω_0 = peak frequency ω_s = significant frequency

Table 2.3: The six parameters of Ochi's spectrum as a function of significant wave heights [17].

	H_{s1}	H_{s2}	ω_{m1}	ω_{m2}	λ_1	λ_2
Most probable spectrum	$0.84\,H_s$	$0.54\,H_s$	$0.70\,e^{-0.046 H_s}$	$1.15\,e^{-0.039 H_s}$	3.00	$1.54\,e^{-0.062 H_s}$
0.95 confidence spectra	$0.95\,H_s$	$0.31\,H_s$	$0.70\,e^{-0.046 H_s}$	$1.50\,e^{-0.046 H_s}$	1.35	$2.48\,e^{-0.102 H_s}$
	$0.65\,H_s$	$0.76\,H_s$	$0.61\,e^{-0.039 H_s}$	$0.94\,e^{-0.036 H_s}$	4.95	$2.48\,e^{-0.102 H_s}$
	$0.84\,H_s$	$0.54\,H_s$	$0.93\,e^{-0.056 H_s}$	$1.50\,e^{-0.046 H_s}$	3.00	$2.77\,e^{-0.112 H_s}$
	$0.84\,H_s$	$0.54\,H_s$	$0.41\,e^{-0.016 H_s}$	$0.88\,e^{-0.026 H_s}$	2.55	$1.82\,e^{-0.089 H_s}$
	$0.90\,H_s$	$0.44\,H_s$	$0.81\,e^{-0.052 H_s}$	$1.60\,e^{-0.033 H_s}$	1.80	$2.95\,e^{-0.105 H_s}$
	$0.77\,H_s$	$0.64\,H_s$	$0.54\,e^{-0.039 H_s}$	0.61	4.50	$1.95\,e^{-0.082 H_s}$
	$0.73\,H_s$	$0.68\,H_s$	$0.70\,e^{-0.046 H_s}$	$0.99\,e^{-0.039 H_s}$	6.40	$1.78\,e^{-0.069 H_s}$
	$0.92\,H_s$	$0.39\,H_s$	$0.70\,e^{-0.046 H_s}$	$1.37\,e^{-0.039 H_s}$	0.70	$1.78\,e^{-0.069 H_s}$
	$0.84\,H_s$	$0.54\,H_s$	$0.74\,e^{-0.052 H_s}$	$1.30\,e^{-0.039 H_s}$	2.65	$3.90\,e^{-0.085 H_s}$
	$0.84\,H_s$	$0.54\,H_s$	$0.62\,e^{-0.039 H_s}$	$1.03\,e^{-0.030 H_s}$	2.60	$0.53\,e^{-0.069 H_s}$

Figures

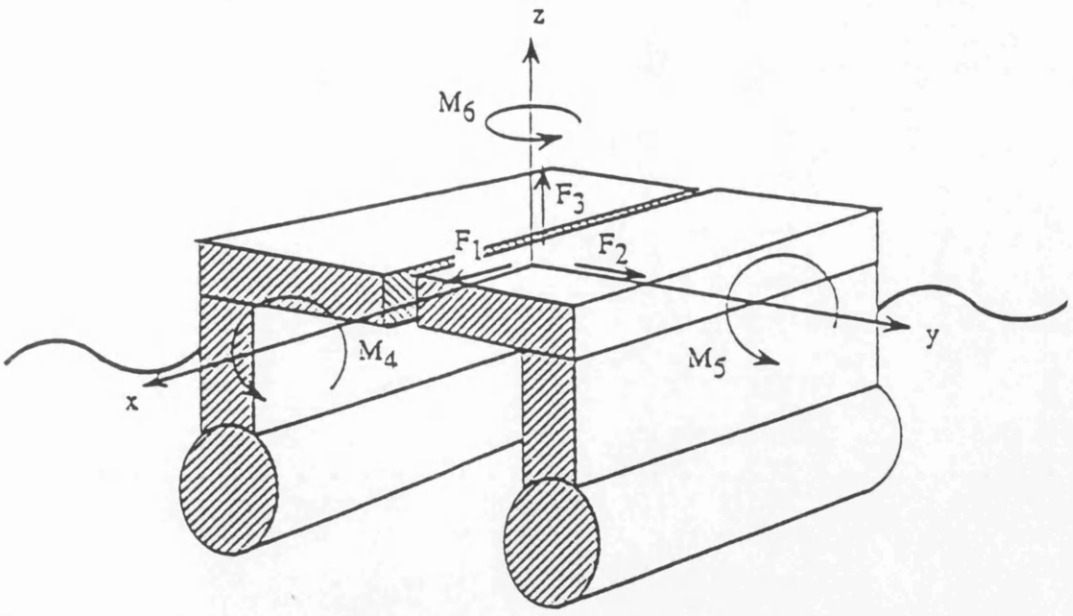

Figure 2.1: The global wave loads on a SWATH ship [12].

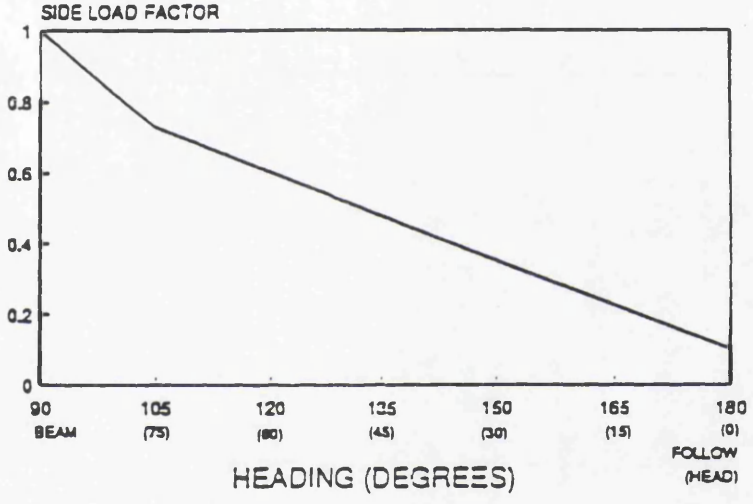

Figure 2.2: Variation of side load factor with heading [22].

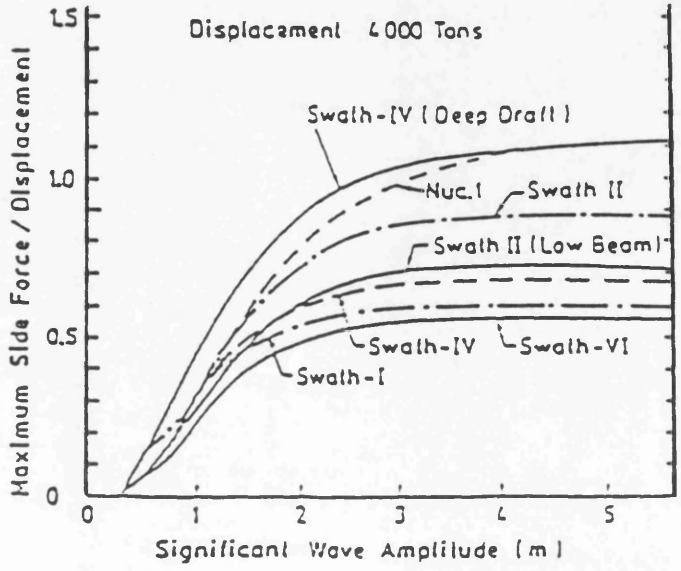

Figure 2.3: Side load variation with significant wave height [2].

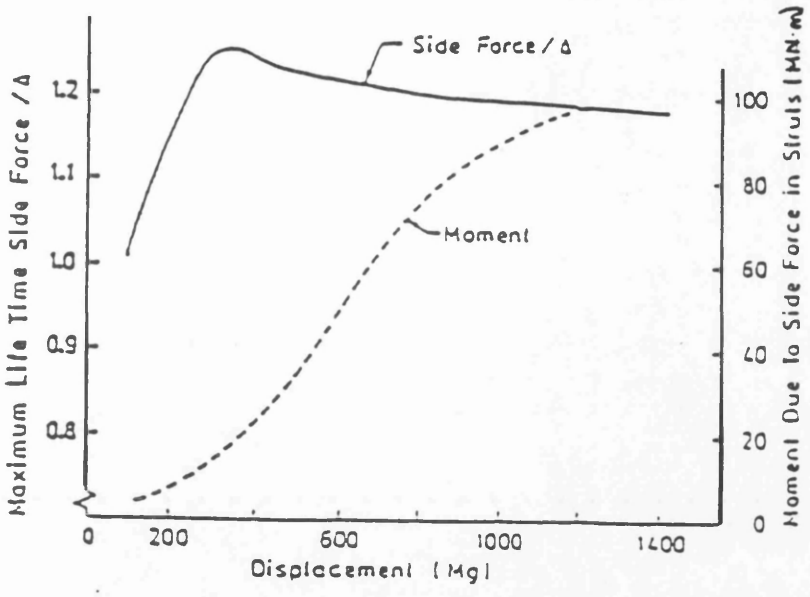

Figure 2.4: Variation of the side load with ship displacement [2].

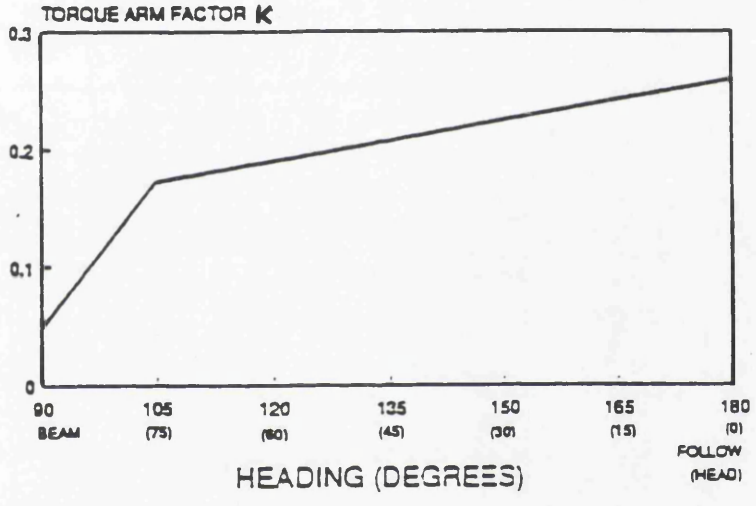

Figure 2.5: Torque arm factor variation with heading as proposed by Sikora et al [2].

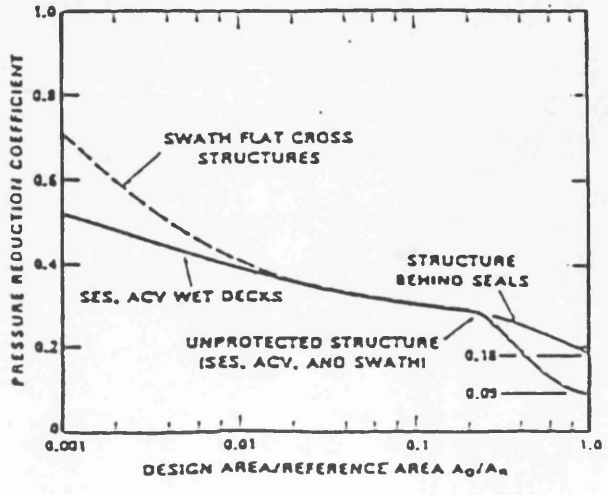

Figure 2.6: Percentage of slamming pressure reduction as a function of relative area for SES, ACV and SWATH ships [15].

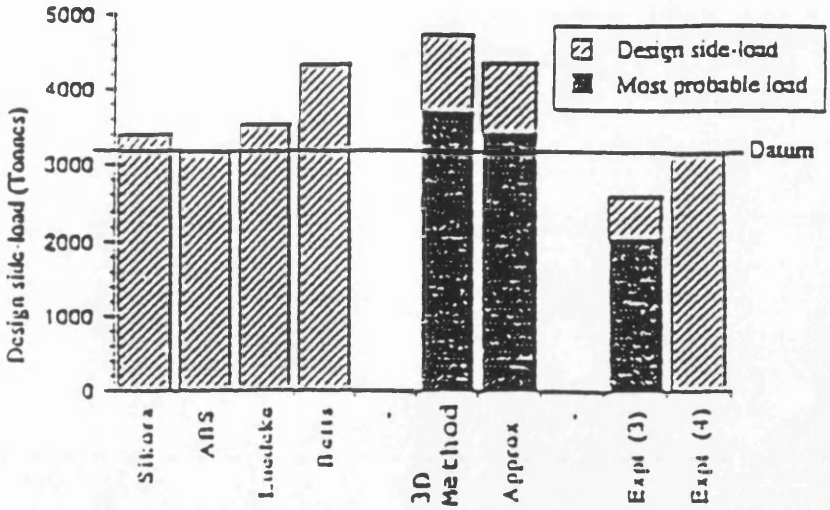

Figure 2.7: Comparison of experimentally, analytically and empirically derived side force on T-AGOS-19 [12].

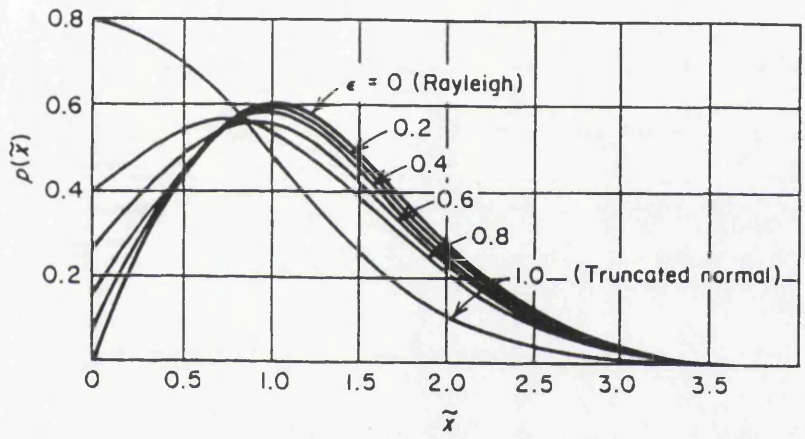

Figure 2.8: Wave height probability density functions for developing and fully developed seas.

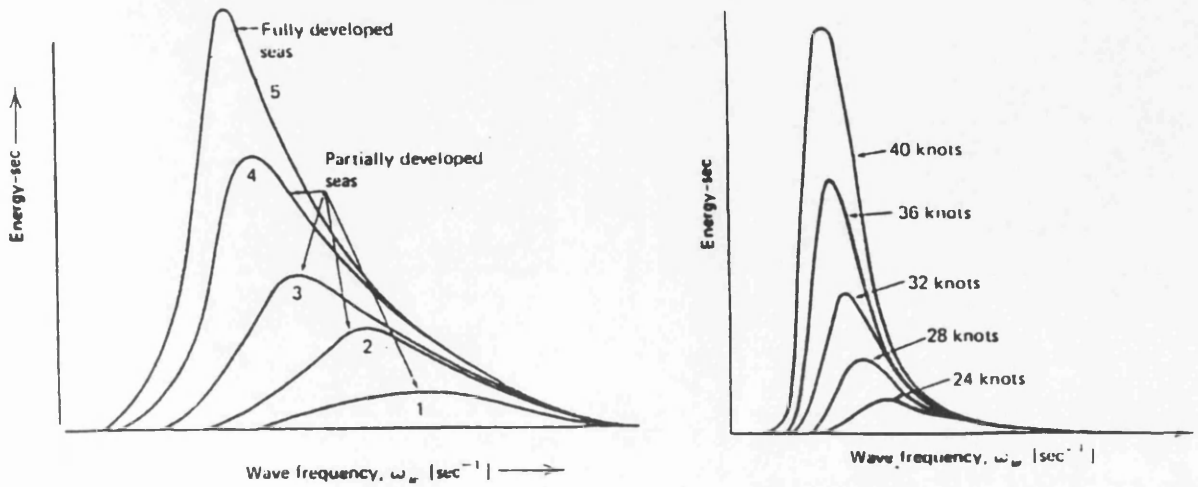

Figure 2.9: Energy build-up in (a) partially and fully-developed seas (b) fully developed seas for various wind speeds.

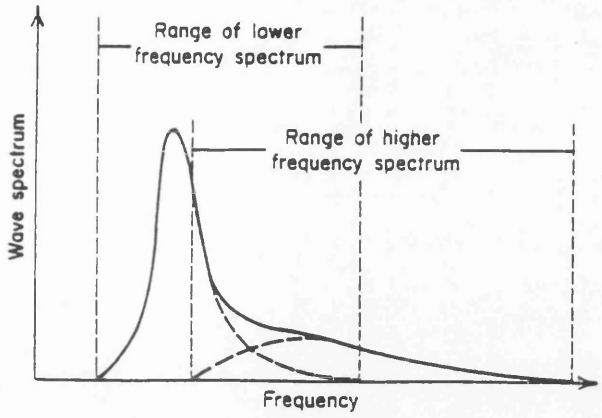

Figure 2.10: Two-peak spectrum representing swell and wind generated seas.

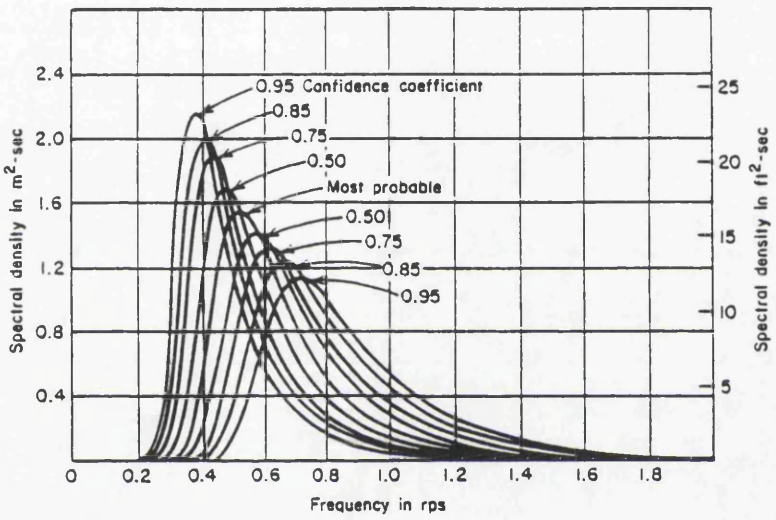

Figure 2.11: Ochi's family of two-parameter wave spectra [80].

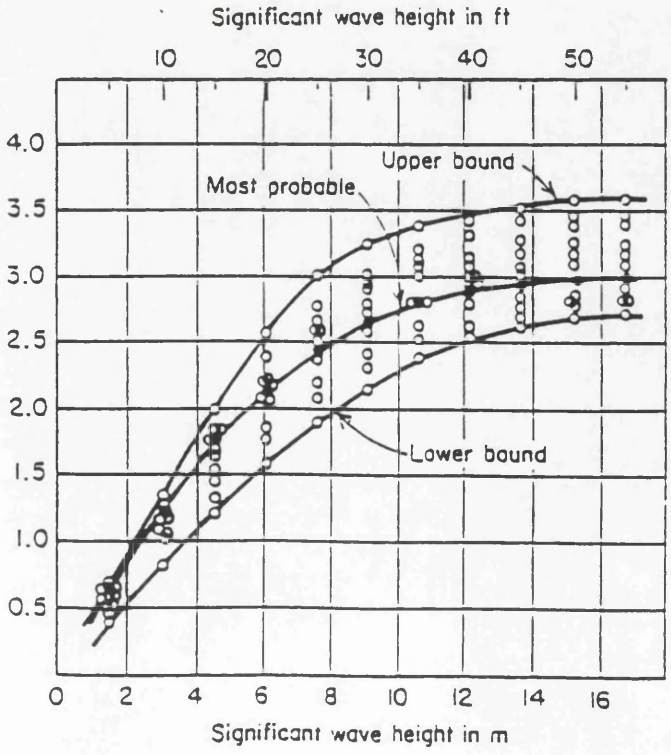

Figure 2.12: The Design Sea Load method [80].

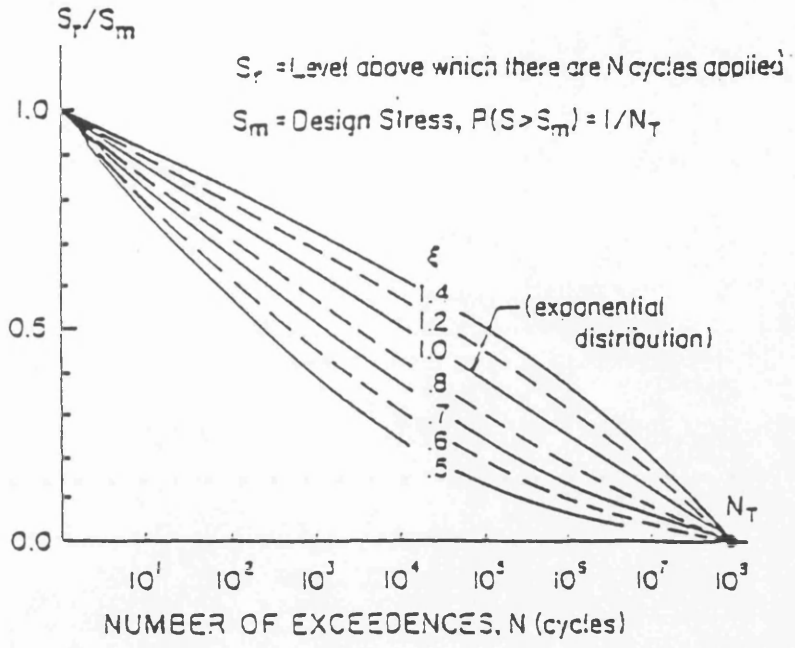

Figure 2.13: **Weibull lifetime ship loading histories for various values of the shape parameter.**

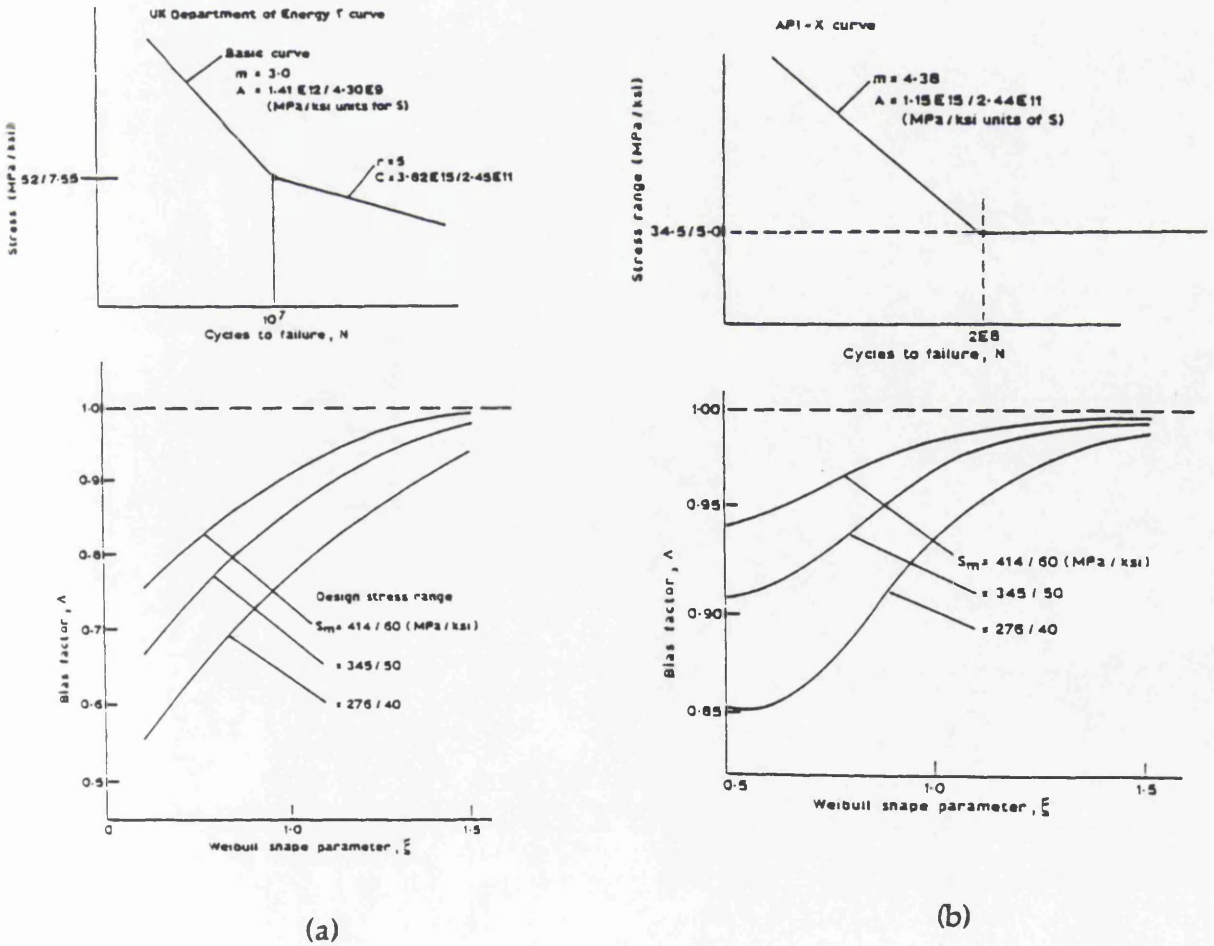

Figure 2.14: **Fatigue damage correction factor versus the shape parameter for a variety of stress ranges for (a) the DEn-T curve and (b) the API-X curve [96].**

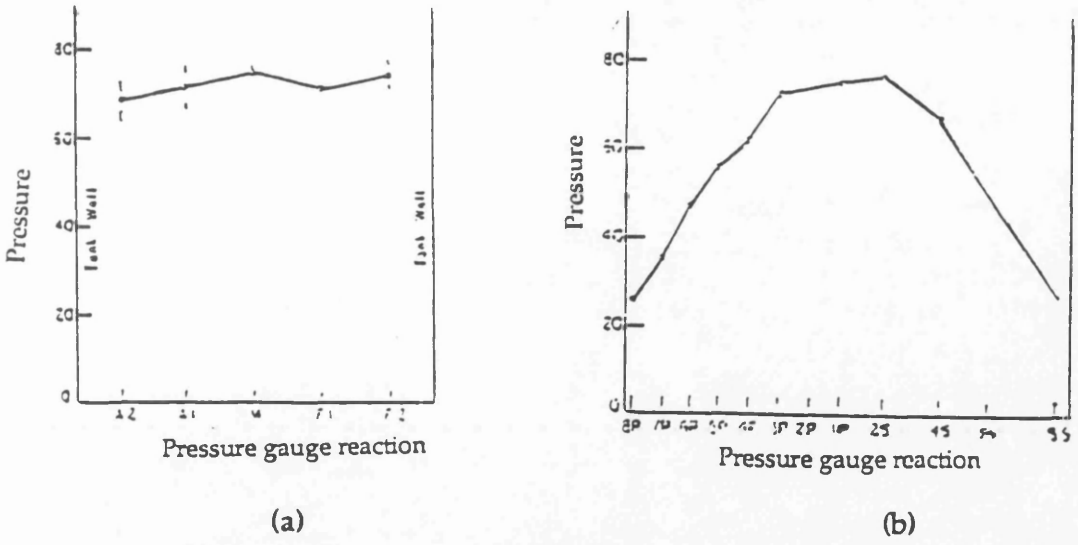

(a) (b)

Figure 2.15: Peak pressure distribution along (a) the model centreline and (b) the model transverse mid-plane [131].

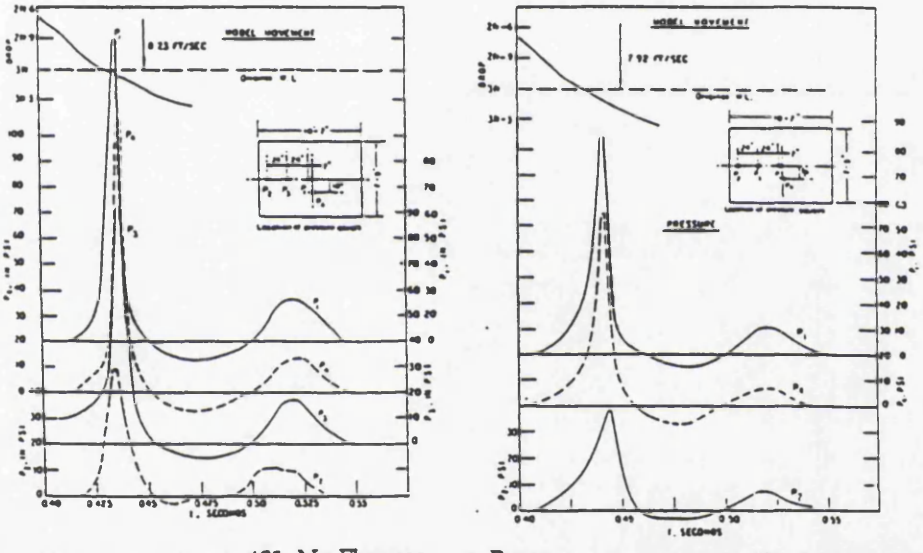

Pressure curves, mass=481, No Flanges

Pressure curves, mass=481, 1.5 in flanges

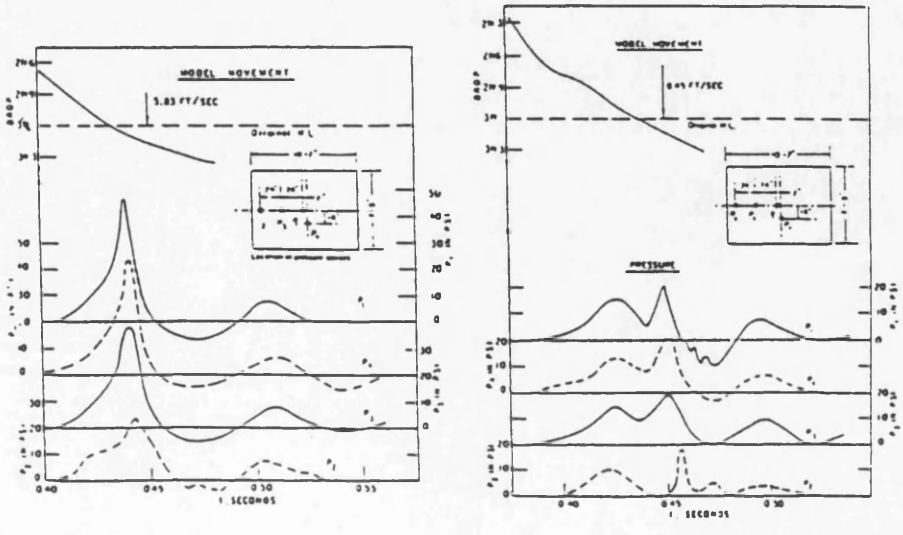

Pressure curves, mass=287, 1.5 in flanges

Pressure curves, mass=287, 3 in flanges

Figure 2.16: Impact pressure time series with and without air-entrapping flanges on a flat bottomed model [133].

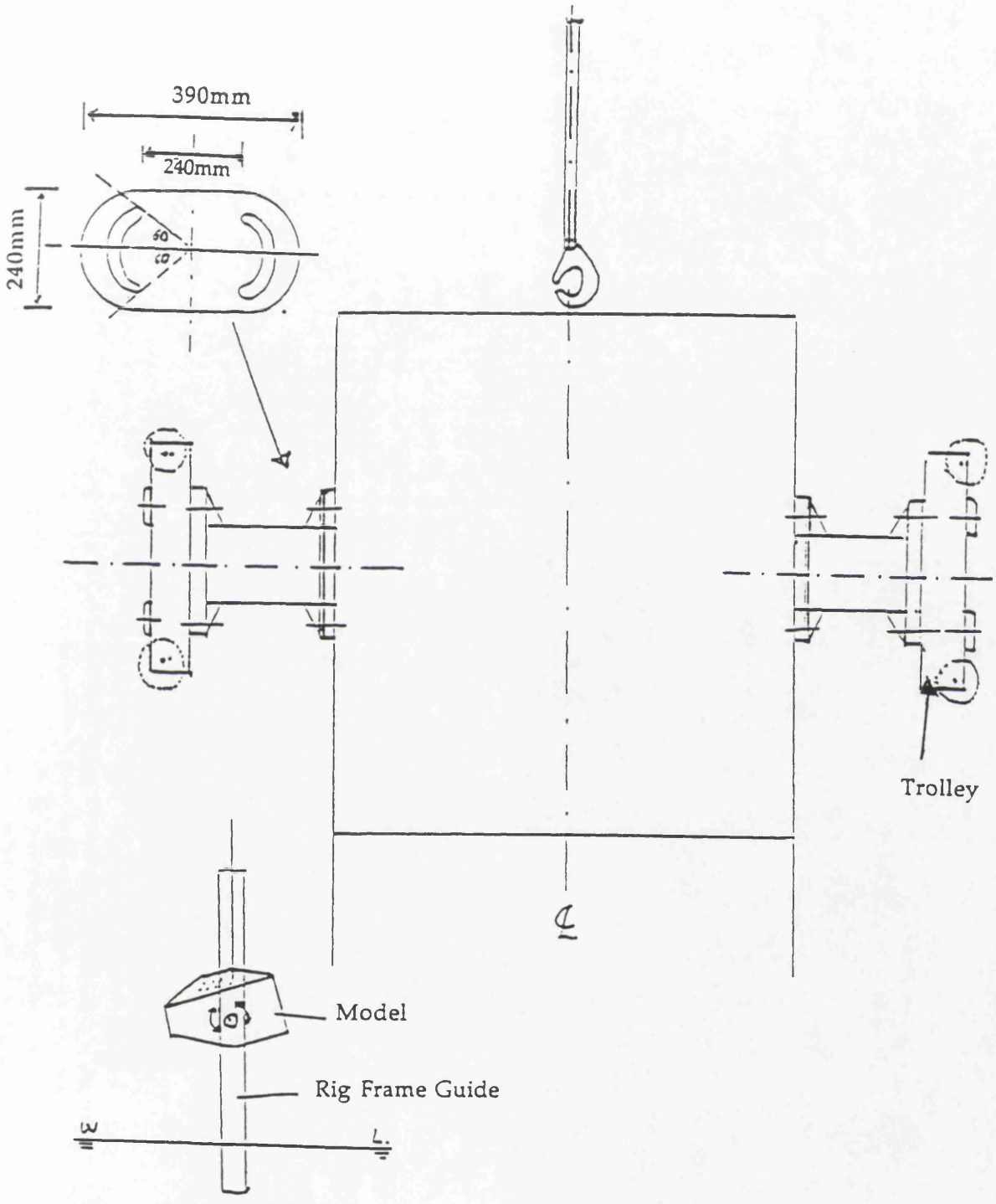

Figure 2.17: **Model and trolley configuration in the Tolikas/Das/ Djatmiko tests [144].**

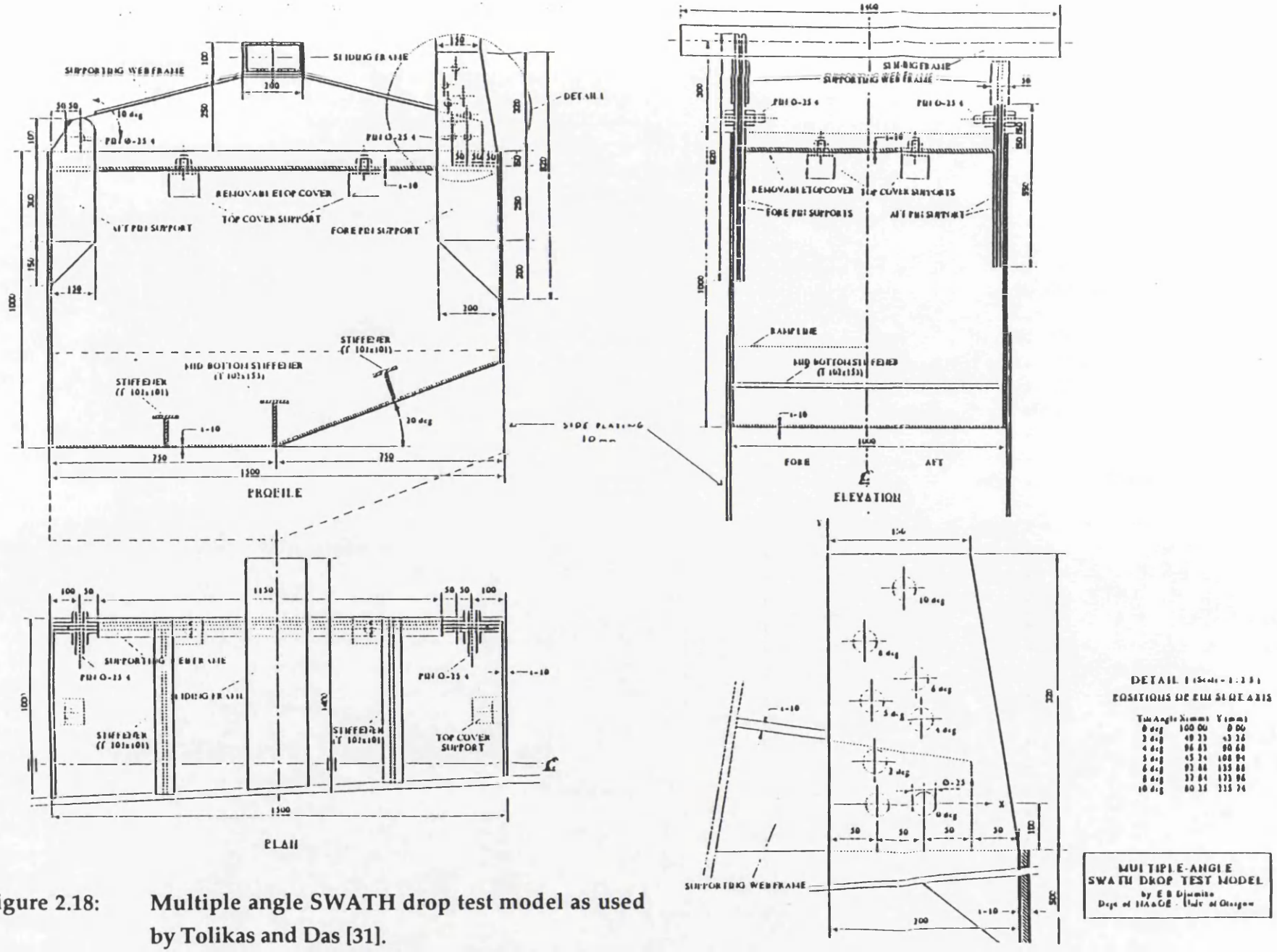

Figure 2.18: **Multiple angle SWATH drop test model as used by Tolikas and Das [31].**

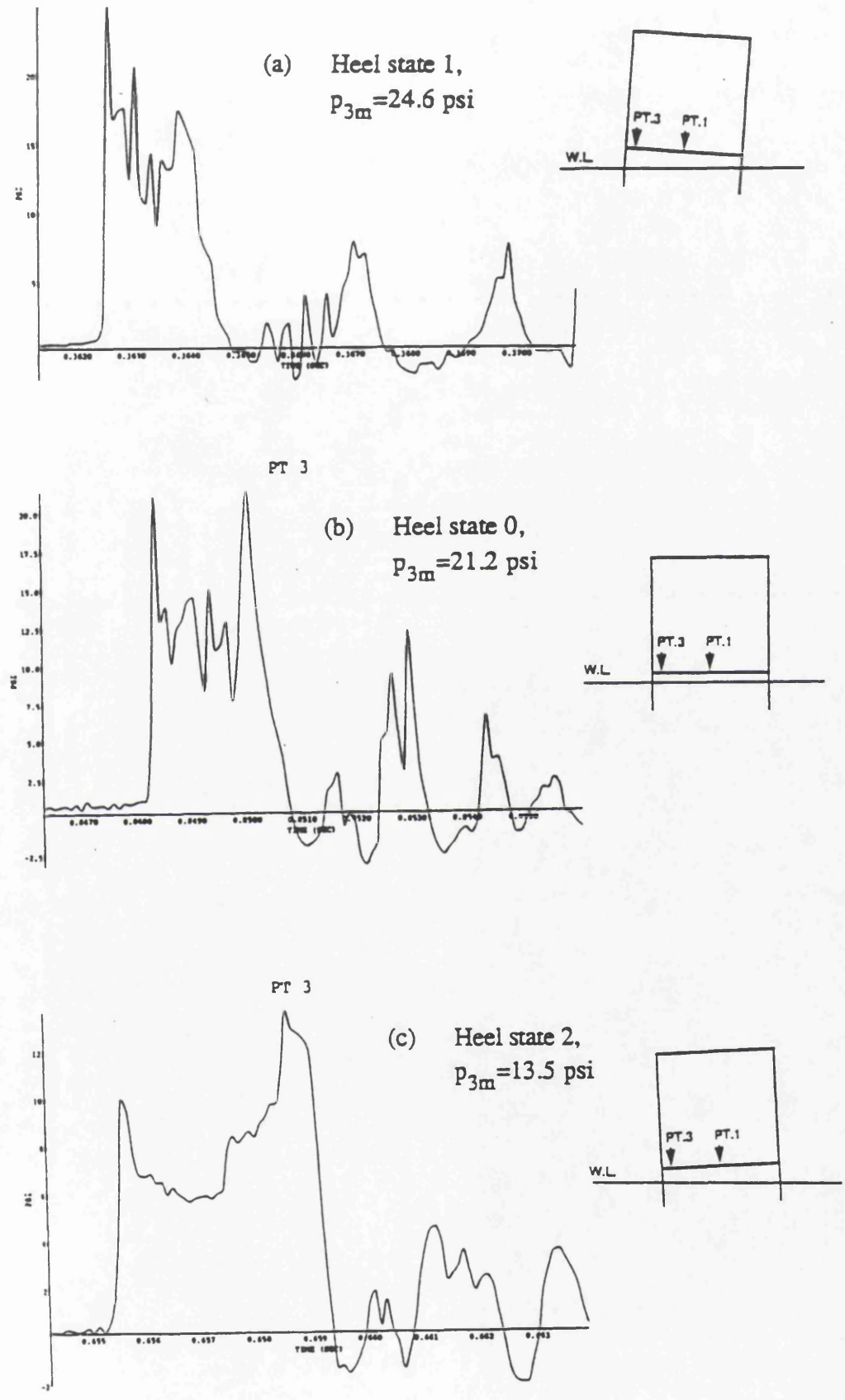

Figure 2.19: Influence of heel on slamming pressure readings [114].

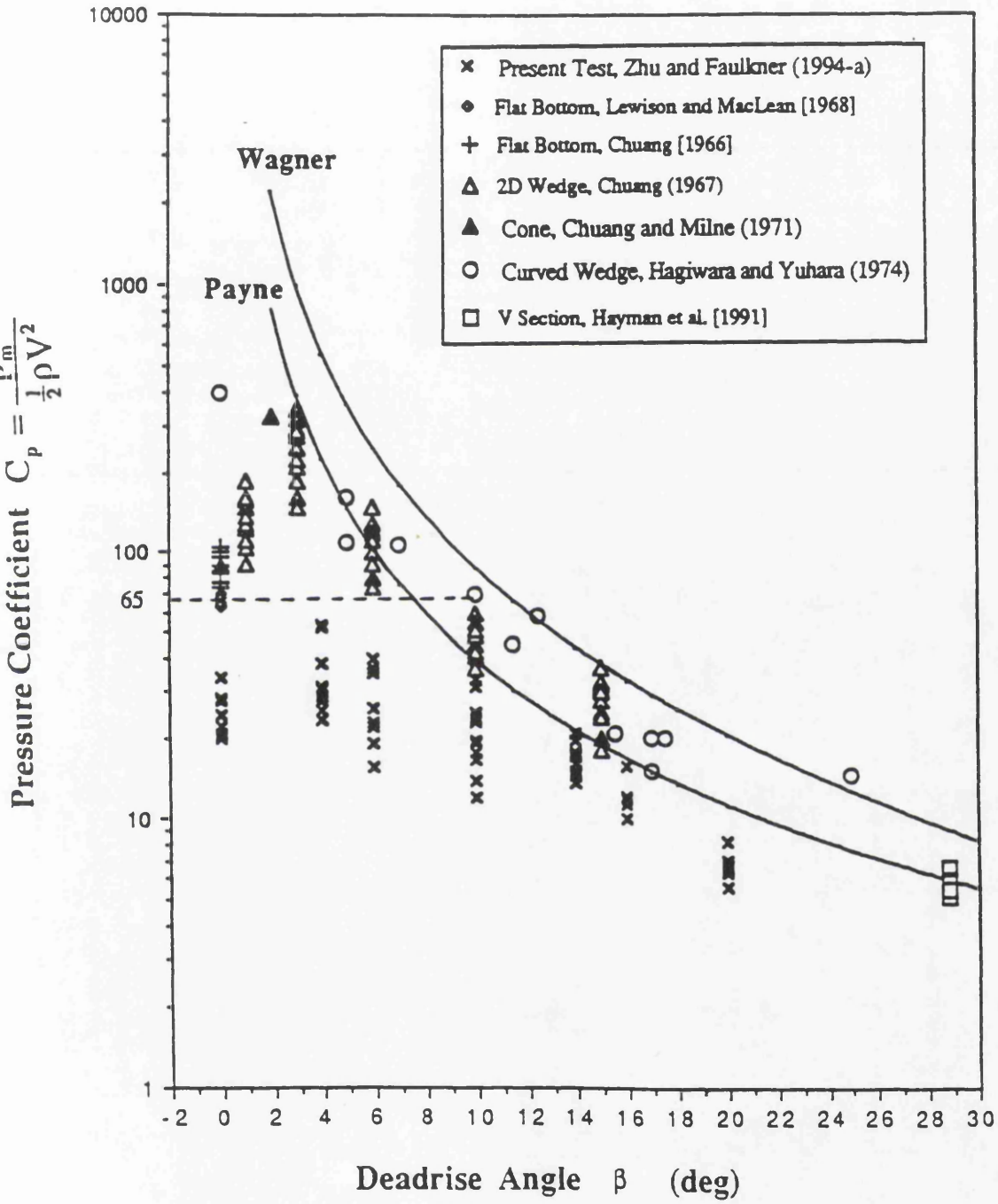

Figure 2.20: Comparison of the Payne and Wagner theoretical methods with Zhu's experimentl data [114].

CHAPTER 3

3.0 Aspects of Fatigue Design of Monohull and Multi-Hull Vessels

3.1 Introduction

Viability of the use of Fast Craft Transportation over the current conventional means of sea transportation demands a combination of high speed, high payload and low operating costs, all at commercially acceptable levels. Because these requirements can only be achieved by lightweight structures, slender sections and structural components then become prone to fatigue damage thus rendering the development of rational fatigue design procedures even more essential than for conventional ships. The presence of discontinuities and cut-outs in the structural components, further adds to the problem. The restrictions on limits of present generation fast craft operation imposed by environmental conditions, maintain the stress range values experienced over their lifetime to relatively low values with respect to those experienced by similar monohull vessels. This factor, in addition to the higher operating speeds involved, means that more waves of smaller load amplitude should be expected to act on the structures. These craft hence become more prone to fatigue as their operating envelope is moved towards the low stress-range/high cycle area of the fatigue strength spectrum. Future fast sea transportation vessels for unrestricted open sea operation will experience higher stress ranges which can exacerbate fatigue cracking.

The proper material selection is likely to affect the level of damage experienced in the structures. Competing lightweight materials for application in the fast craft construction are aluminium and FRP and, for larger craft sizes, steel (mild and high strength). A comparison of relative fatigue strengths for these materials is shown in Figure 3.1.

May and Barltrop point out [1] that current fatigue design codes do not provide adequately for the complex load paths present in typical ship connections and hence are found to overpredict fatigue strength. This problem exists due to the lack of a unified code for the fatigue design of all types of fast craft which is anyway very difficult to develop for the following reasons [1]:

- the rapid development of fast craft technology
- the numerous and different types of vessels being designed
- the new materials and construction details being considered.

What remains common despite all these differences, is the type of loading which remains that of the seaway. The longitudinal bending moment is of lesser importance for catamarans, and generally for multi-hull vessels, for which the worst loading occurs at beam/quartering seas, which in turn introduces significant bending moment and torsional actions in the cross-structure. It is essential that any estimation of fatigue life should take into account the variable nature of the loading, and the heading and ship speed, over the vessel's lifetime. Fatigue damage is after all a cumulative phenomenon. The variability of the seaway parameters is best treated probabilistically, with the load modelled by means of spectra. Deterministic methods usually lead to conservative results when compared with a full spectral analysis, although this depends on how the deterministic loading history is derived and applied. Load modelling considerations for a fatigue analysis are treated in detail in section 2.4, Chapter 2. Additional sources of fatigue loading are machinery/propeller/impeller vibrations, whipping loads (due to slamming on the the hull and underdeck/wet deck regions of the ships) and tank pressure fluctuations, which have not been considered in this work.

Fatigue generally occurs at a high ratio of dynamic to static load and at a place where high stress concentrations occur, e.g. at welded connections. Complex joints are often used to resist buckling and high static loads, and the abrupt geometrical changes and high stress concentrations introduced by these joints in the cross section, considerably reduce the fatigue strength of the structure. Therefore, the requirements to resist buckling are frequently in conflict with those providing a long fatigue life. Designing for both is important.

This Chapter aims at highlighting the difficulties involved in the fatigue design of both steel and aluminium joints, with a strong bias towards aluminium applications. No excuse is made for such a choice, as this material is widely used in secondary structural components of marine applications and its extensive application to primary components is only a matter of time as fast marine craft construction moves towards larger displacements. Attention is paid to the more general aspects which affect

the fatigue strength of welded joints, irrespective of material type. When, however, the material becomes an issue, then this is appropriately clarified. The need for more rational, reliability based limit state checks (para. 1.4, Chapter 1) is also expected to affect the way fatigue damage and safety will be assessed and communicated, and shift it away from the currently applicable lower bound strength solutions. Therefore, the method of deriving partial safety factors to a pre-specified level of safety for the fatigue strength check is described in some detail. This is carried out for two cases: where the safety margin is expressed through empirical S-N curves, and through the more theoretical approach of fracture mechanics. Due consideration is paid to the inaccuracies inherent in the current cumulative damage rules, and levels of uncertainties for their variables are recommended based on extensive work carried out by the offshore industry. A rather extensive description of the background and recommendations of the current aluminium fatigue codes is carried out followed by their comparisons, in an attempt to inform the reader of the current state-of-the-art in the aluminium industry.

The last part of this chapter dwells on aspects of weldability of aluminium, and weld repair methods. The main reason for this was to satisfy the author's curiosity arisen due to worries expressed by the marine construction industry over the welding options available to the designer and the problems associated with his final choice. It is hoped that paragraph 3.8.3 throws some light on the subject.

3.2 Aspects Affecting the Fatigue Strength of Welded Connections

Welded joints in any metal construction may be categorised into any of the following group types:

(a) transverse butt welds
(b) longitudinal butt welds
(c) fillet welded connections - load and/or non-load carrying.

The fatigue behaviour of *transverse butt welds* depends mainly on the stress concentration at the toe of the weld metal (e.g. weld profile and misalignment). Hence, welds with minimum "overfill" and a smooth transition at the weld toe (by machining or grinding) give the highest fatigue strengths. Fatigue failure for this joint type consists of crack

initiation (at the weld toe) followed by crack propagation through the thickness of the plate and normal to the direction of loading. One sided butt welds require, in addition, careful control of the root penetration and of the shape of the root bead. Generally the fatigue strength of a joint in a plate edge is lower as the stress concentration is higher and the weld shape is poorer than normal.

Longitudinal butt welds have the advantage that the weld metal lies in a direction parallel to the load and therefore does not introduce a geometrical discontinuity to the stress flow. Even the detrimental to strength stop/start positions and ripples on the surface of the weld tend to be eliminated by the application of automatic welding techniques. Any variation in weld penetration resulting in a rough weld bead for both double and/or single sided welds will, however, reduce the longitudinal weld fatigue strength. Generally speaking, good fatigue strength of longitudinal butt welds can be obtained only if they are continuous and the effect of the weld ends can be avoided.

Fillet welds are generally weaker in fatigue loading because of the more abrupt geometrical discontinuity they introduce in the stress flow (e.g. brackets). These welds are particularly sensitive to size effects (Fig. 3.2) arising from:

(a) attachment length L (in the direction of loading)
(b) main plate thickness.

An increase in any of these variables results in a decrease of fatigue strength of the joint [2]. For double fillet welded transverse attachments, cracking is expected to initiate at one of the weld toes and propagate through the plate. For single fillet welds, however, cracking might occur at either the weld toe or root. Root cracking is unlikely to be detected prior to final failure and must therefore be designed out.

Specifically, the location of failure in fillet welds depends on the ratio leg length/plate thickness (H/B) (Fig 3.3) [2]. Optimum weld (joint) performance is achieved when there is just enough weld metal to ensure that failure would occur at the weld toe (where it is easy to detect) instead of the root of the weld. This requirement generally translates to $H \approx B$. Increasing the plate thickness immediately implies a larger weld size.

Noting that the weld metal volume, and hence costs, rise proportionately to H^2, H should be kept to the minimum possible value. By taking advantage of partial root penetration welds (Fig. 3.3b) it is possible to achieve a given throat dimension with a smaller than normally required leg length. Increasing the weld area to a value greater than that representing optimum design (by use of larger or partial penetration welds) will not improve in fatigue strength. What it does, however, is to make sure failure is limited to the weld toe.

Summarising, longitudinal fillet welds have higher fatigue strength than those transversely orientated to the direction of loading. Continuous welds based on automatic welding processes are preferred instead of tack welds even if the latter are sufficient to successfully carry the static load.

3.2.1 Sources of Fatigue Strength Reduction in Welded Joints

The fatigue life of the aforementioned types of welded joints is influenced by any or all of the following:

- environmental effects - corrosion
  - low/high temperatures
- alloy type (for aluminium joints)
- residual stresses and stress relief actions
- discontinuity effects
- weld quality
- geometrical misalignment
- size effects
- weld shape and orientation to the direction of loading

Column 1 in Table 3.1 lists the main factors affecting fatigue strength which are normally controlled by the designer via the specification. The degree of dependency of these factors on production procedures and their consequent effect on fatigue strength are summarised in Columns 2 and 3 of the Table respectively.

Geometrical Misalignment presents a source of fatigue strength reduction *in transversely loaded welds only* due to the resulting superposition of additional local secondary bending stresses on the nominal stress field. This reduction may arise from (a) axial and/or angular misalignment of the

parent elements, (b) axial misalignment arising from different thicknesses on either side of the weld. It is worth remembering that it is only in the presence of nominal axial stresses that misalignment should be considered. Geometrical misalignment is generally accounted for by multiplying the *nominal applied axial stress* by the factor, K_m [2]:

$$S' = K_m S \qquad \text{where} \qquad K_m = 1 + \left(\frac{S_b}{S_a}\right)$$

S_b being the secondary bending stress and given by Table 3.2 while S_a is the axially applied stress range. Maddox suggests [2] that a 1° angular misalignment may be considered as equivalent to a 10% (e/B=0.1) axial misalignment. The use of this correction to the stress range values, would introduce a small degree of conservatism in the S-N life predictions, as the S-N curves have themselves been based on the data from specimens which are obviously not always perfectly aligned.

The fatigue strength of a joint decreases with an increase in the *size of the attachment* i.e. with an increase in (Fig. 3.2):

- attachment length, L, (in the direction of loading)
- plate thickness, B
- width of the stressed member

which all influence the stress concentration at the weld toe. This stress concentration affects the stress intensity factor, K, and hence the rate of crack propagation da/dN as the crack propagates in the stress concentration region. The stress analysis of weld toe cracks in a range of fillet and butt-welded joints has revealed the following relationship between the crack size, the welded joint geometry and the crack geometry function Y(a) (para. 3.5.2 for definitions) [2]:

$$Y(a) = M_K Y_U \quad \Leftrightarrow \quad Y = \alpha\left(\frac{a}{B}\right)^{\beta} Y_U$$

where the constants α and β are both functions of L/B. a is the instantaneous crack depth. The values of α and β are included in BS PD 6493 [3]. A particular feature of this relationship for weld toe cracks is that M_K decreases with increase in a/B, as the crack tip moves away from the

region of stress concentration, until it reaches unity. Therefore, for a given crack depth, a, the stress intensity factor of a crack in a thick plate is higher than in a thin plate, and hence the former demonstrates a lower fatigue life.

Although the aforementioned correction is not included in the estimations, an adjustment to the stress range predictions needs to be made to account for the different specimen thicknesses which have formed the basis of the individual code recommendations. Hence, a thickness correction factor to the *nominal stress range* is recommended by the U.K. DEn [4, 5, 6]:

$$S_r = S_B \left(\frac{t_B}{t}\right)^{0.25} \qquad \text{where} \quad \begin{array}{ll} \text{For tubular joints} & t_B = 32\,\text{mm} \\ \text{For other joint types} & t_B = 22\,\text{mm}. \end{array}$$

The aluminium codes (BS 8118 and Alcan) do not mention anything about thickness corrections and therefore may be assumed as not requiring such a check. t is the joint thickness, S_B is the fatigue strength of the joint using the S-N curve, t_B is the thickness corresponding to the S-N curve data. This factor is applicable irrespective of whether the load is axial and/or bending stresses. Bridge structure tests, forming the basis of BS 5400 fatigue design rules, have used 16mm thickness models. In addition, the level stress concentration at the weld toe depends on the proportions of the joint L/B such that a small attachment to a thick plate results in a lower stress concentration factor than a long attachment to a thin one. The effect of *attachment size and magnitude* is introduced in the rules as part of the joint classification system.

Discontinuities at both the root and toe of welds result in unwanted stress concentrations. In *weld toes* discontinuities are introduced due to undercutting of the plate surface and sometimes due to the abrupt convex profile which a weld bead may adopt. Crack-like intrusions may also exist at the weld toe as a result of conditions introduced by arc welding processes. In *weld roots*, lack of sufficient weld penetration introduces crack-like discontinuities at which the stress-concentration will be *higher* than that at the weld toes. Cracking will hence first occur at this position and propagate through the weld throat. Because of their location they are almost impossible to detect prior to final failure. Weld toe and root discontinuities are implicit in the specimens used to derive the S-N curves, and therefore no corrections on the nominal stress range need be applied.

The potential increase in fatigue strength with *tensile material strength* obtained from the use of high tensile strength materials is directly related to the *crack initiation process* which forms the larger part of the fatigue life of any *unwelded* structural element. The fatigue strength of *welded joints*, however, being dominated by the weld residual tension stresses and the crack propagation stage, does not benefit, as the tensile strength of the material does not affect the rate of crack propagation. However, the reduction in ductility, which is common in high strength steels, may lead to premature brittle fracture. This dominance of fatigue crack propagation in the lives of welded joints may be used to support the fact that the fatigue strengths of joints of different metals are generally in the ratio of their elastic moduli ($da/dN \propto S \propto E$). So, not surprisingly, the fatigue strength of an aluminium alloy weld is taken to be approximately one third of the same joint in steel. On the other hand, use of high strength material enables a higher fatigue (as well as static) design stress to be withstood, which is beneficial for low cycle designs. High cycle designs, like fast marine craft, will then have a problem. A higher class of joint (different joint design and orientation to load) will then have to be used.

As most of the fatigue design data have been obtained in air and at ambient temperature, they do not allow implicitly for the effects of the environment, namely (a) corrosion, and (b) high/low temperatures.

In steel structures the onset of corrosion results in an increase in the rate of crack propagation, especially at the lower stress-high cycle operating levels. The applied stress ranges increase due to the increased value of the stress concentration, including those which were originally neglected as being below the endurance limit. Reduction or omission of the endurance limit threshold is a simple but conservative solution. Little data exists on fatigue tests of steel joints in corrosive environments. A limited study undertaken in the North Sea environment [2] observed a reduction in the fatigue strength of freely corroding steel welded joints by a factor of 2 approximately depressing the endurance limit so much that it could be neglected. More research is required on the topic and the effects of cathodic protection.

There are four types of corrosion attack affecting the fatigue behaviour *of aluminium structures*, (a) weathering corrosion (pitting), (b) galvanic corrosion, (c) exfoliation, (d) stress corrosion. The better corrosion resistance of aluminium over mild steel is demonstrated in Figure 3.4 [7, 8].

Weathering corrosion occurs when aluminium is exposed, unprotected, to a corrosive environment such as seawater. The oxides formed concentrate on the base metal and protect it against any further oxidisation. Relative corrosion ratings (in decreasing order of merit) of aluminium alloys are given in Table 3.3. The choice of 5000 series material for plating and 6000 series materials for stiffening arrangements is hence obvious and common (Figure 3.5 for *unwelded* specimens). The higher magnesium content of the 5000 series is credited with this difference. Painting or anodised coatings should be used only if the oxide's appearance is unwanted. Otherwise, the structural efficiency of the material is in no danger.

Galvanic corrosion occurs in the presence of dissimilar metals (usually steel and aluminium) coupled with the presence of an electrolyte. The aluminium components then act as sacrificial anodes with their cross-section geometry diminishing as time elapses. The essential isolation of the materials is hence obtained either by painting the steel components with a zinc-based primer or by isolating the electrolyte components away from the other metals using a proper sealant (e.g. silicone). The use of galvanised or stainless steel at an extra cost is also a precautionary solution.

Exfoliation delaminates the material parallel to the surface when heating is imposed over a period of time. Together with *stress corrosion* they only occur in some 5000 series alloys (alloys of high Mg content only).

Stress corrosion results from tensile stresses (e.g residual stresses) or electrochemical reactions and reduces the crack formation threshold (sensitisation). In the annealed state, the Mg containing alloys may be considered as non-sensitive to stress corrosion up to Mg levels of 7%. However, increasing the cold forming or annealing at temperatures greater than 60°C, increases the sensitivity with Mg contents greater than 2.7% (5052, 5454) [9]. Hence, 5000 series alloys containing over 3% magnesium (5083, 5086 and 5456) and subjected to elevated temperatures are susceptible to both exfoliation and stress corrosion. It is worth noting that stress-corrosion susceptibility of rolled alloy products is directionally controlled, the susceptibility being greater in the through-the-thickness direction [10]. Specifically, Bilgram and Winkler concluded that stress corrosion is not a problem for *unwelded* 5083 alloy structures while for *welded* construction, the fatigue crack threshold values are 60% of the yield

strength when stressed in a direction transverse to that of rolling and are therefore not of great importance. Thermal stresses in the plate thickness direction should always be avoided in the case of welded structures, as the threshold limits were found to fall to less than 10% of the yield strength.

Another investigation by Engh et al in [11] investigating the effect of saltwater and saline atmosphere on *welded* details of 6000, 5000 alloys at R=0.1 and R=0.5, showed that the effect of the corrosive environment is dependent on the alloy type as well as on the R-ratio of the applied load. The corrosive environment strength values were found to be less than the 'air' strength values by approximately the following percentages [11]:

	Butt Weld		**Butt Weld with backing strip**		**T-Fillet Weld**	
Cycles	10^5	10^6	10^5	10^6	10^5	10^6
5052 (R=0.1)	20%	25%	0%	0%	0%	0%
5083						
R=0.1	16%	8%	-	-	18%	11%
R=0.5	40%	40%	-	-	48%	53%
6063 (R=0.5) saline atm. only	30%	53%	-	-	32%	22%

It is obvious that the major differences occur at R=0.5 when the cracks are expected to be open to the effects of the corrosive environment. These results agree well with fatigue test results for *welded* butt joints of 6061-T6 and 5083-H321 alloys [12] and the fatigue strength of small 5456 plate butt weld specimens [13]. The Alcan/Canadian Codes [14, 15] advise that uncoated surfaces prone to corrosion should have their non-welded nominal fatigue strengths reduced by 50%. BS 8118, [16] however, make no specific mention of any corrosion corrections required.

According to Kohler [17] who investigated the effects of shot-peening on the corrosion resistance of aluminium transverse butt joints (7020 alloy), post-weld treatments may reduce the susceptibility to corrosion. Shot-peening was found to benefit the corrosion strength of aluminium welded details

(Fig. 3.6). Five details for each set of conditions were tested. The different levels of fatigue strength improvements obtained by using glass or steel shots is also demonstrated. Benefits are possible for unwelded details (work by Hanley reported in [17]) for which 13 times improved corrosion strengths were obtained.

The fatigue strength of *steel joints* decreases with *increasing temperature.* If however, the temperature is close to the creep zone then creep should dominate the design considerations. On the other hand, the *reduction in temperature* to below ambient reduces the crack propagation rate, thus increasing fatigue life for steel joints. However, if the material fracture toughness is low, low temperatures will almost certainly result in brittle fracture. Aluminium is different as it is well known for its cryogenic properties. A study at temperatures as low as -196°C [8] showed the fatigue strengths of a number of specimens (machined, round specimens of base metal, welded panels, sharply notched) to be always higher than those at room temperature by factors of 15-60%. On the other hand, elevated temperatures (300°C and 400°C) were found to reduce the fatigue strength values by factors up to 50% for both smooth and notched specimens. As a result, the design codes permit their application without any procedural changes for the cases of [2]:

- structural carbon-manganese steels at temperatures up to 375°C.
- austenitic stainless steels at temperatures up to 430°C.
- aluminium alloys at temperatures up to 100°C.

At temperatures within or outside the ranges just quoted, specialist advice or individual testing is recommended.

With regard to the *effects of alloy type,* significant difference has been detected in the case of parent materials between the 5000/6000 and the 7000 series alloys. The latter were found to exhibit 44% higher strength on average than the former [18]. In addition, significant differences have been observed between the 5000 and 6000 series alloys in the low cycle-high stress range (Fig. 3.7). Little difference in the high cycle range (which is of more interest in marine structures) is generally observed, and therefore the same fatigue design curves are usually recommended and used by the current design codes for all aluminium alloys sections. The designer, however, should be aware of the differences occurring in the low cycle range.

Residual Stresses and their Effect on R-Ratio Considerations: Residual stresses are characterised by a tensile stress (at filler material yield level) in the weld zone with adjacent bands of compressive stresses maintaining equilibrium in the cross-section, in contradiction to steel applications for which the tensile strength of the weld and parent metal are closely matched.

Consideration of the effects of a fully tensile repeated loading (0 to S_{max}) and of a fully compressive repeated loading (0 to $-S_{max}$) on the residual stress distribution of a longitudinal weld is made in Figures 3.8a and 3.8b respectively. It is observed that for the case of repeated tensile loading on the weld (0 to S_{max}) the weld will cycle between a minimum value of $S_{y,filler} - S_{max}$ and a maximum value of $S_{y,filler}$, i.e. it will cycle in the same stress range as the nominal range applied but with a mean value different from $S_{max}/2$ and hence different stress ratio R. The same applies (Fig. 3.8b) for the case of fully compressive repeated loading (0 to $-S_{max}$) with a mean value different than $-S_{max}/2$. Note that R is related to the mean stress and stress range by the following expression [24]:

$$\sigma_m = \frac{\sigma_r}{2}\left(\frac{1+R}{1-R}\right) \qquad \text{where} \qquad R = \frac{\sigma_{min}}{\sigma_{max}}$$

Stress relief of residual stresses is fruitful only if partly or wholly compressive loads and mostly in the high-cycle fatigue zone of the S-N curve are applied. For fully tensile applied stresses the results for as-welded and stress-relieved joints have been found [6] to demonstrate little difference (15% on stress range at 2×10^6 cycles). In this latter case, the extra cost of stress relieving the locked in stresses would not be justified. Figure 3.9 confirms that if a joint contains low residual stresses (stress relieved) and is subjected to partly compressive loading, the fatigue strength is increased. Hence, there may well be a case for increasing design stresses for joints under compression-compression loading only. Guerney [6] suggests that it could be safe for stress relieved joints subjected to partially compressive loading to increase the design stress range to a value equal to the tensile component of stress, plus 60% of the compressive component. However, detailed design rules for stress-relieved joints do not exist. What is currently assumed is that as-welded joints will contain tensile residual stresses of yield strength magnitude, a conservative assumption.

The treatment of R-ratio effects in design codes has varied in the past with the data available and/or the viewpoint of those drafting the respective recommendations (Table 3.4). Earlier recommendations are mostly found to accept the R-ratio dependent fatigue strength values as they are based on small specimen test results (with no significant residual stress values). Recent fatigue design rules, however, are based on re-evaluation of those older small scale test results as well as on new tests carried out on full scale specimens containing significant residual stress. Hence, the latter codes do not account for any beneficial effect of the R values near or below zero. Although not explicitly stated, experimental evidence suggests that fatigue strength values at R=0.5 values have formed the basis of the currently used design rules [19]. ISSC advises [20] the use of an unaltered stress range strength in complex structures and only in the cases where the residual stresses are known should the stress ratio effect be considered. The same view is held by ERAAS whose recommendations, which allow for the R-correction only if the designer knows clearly the level of the residual stresses in his structure and can use them effectively to his benefit (Fig. 3.10). In this figure the multiplicative factor f(R) increasing the fatigue strength value varies with the R-ratio values. Line I applies only to base material and wrought products where there are no residual stresses or where such stresses can be fully taken into consideration in the design stages. Line II should be used for all connections including welded ones where knowledge of the residual stresses is available and is considered in the design. Line III covers the cases where significant residual stresses exist but cannot be estimated and thus considered in the design. This line, providing no allowance for an enhancement factor is applicable to most of the welded details in general practice. Two or three-dimensional more complex structures with global residual stresses are not allowed any enhancement, unless they have been adequately stress-relieved. The diagram assumes that the f(R) values are relative to the fatigue strength for R=0.5, the latter being estimated for every structural detail in question at 2×10^6 cycles. Figure 3.11 provides the f(R) values assumed by the Aluminium Association in the USA [21] (also relative to R=0.5). In general, whenever the stress loading is not fully reversed i.e. whenever $R \neq -1$, the Goodman plot correction might be used on the nominal S-N curve strength predictions by design codes:

$$\sigma_{an} = \sigma_n \left(1.0 - \frac{\sigma_m}{\sigma_u}\right)$$

where σ_{an} represents the fatigue strength at a given stress ratio, σ_n is the fatigue strength for R=-1, σ_m is the mean value of alternating stress and σ_u is the ultimate material strength in tension.

3.3 The Background to Current Fatigue Design Codes

Fatigue failures occur because there are no accurate load spectra and life prediction techniques available, especially for new aluminium applications. In addition, most of the fatigue design techniques available are two-dimensional and determine nominal stresses in components only. Three-dimensional behaviour and local stresses resulting from load combinations have not been given proper treatment. There are three general approaches for fatigue design, the use of:

- S-N curves of typical joints
- crack propagation and fracture mechanics techniques
- strain controlled fatigue methods.

It is the S-N curves for the relevant weld details that currently form the basis of available fatigue rules. As the design stresses recommended by the code S-N curves should be the nominal stress ranges in the vicinity of the joint detail, correction is essential via the elastic stress concentration factor K_t:

$$S' = K_t S$$

References [22-24] provide some SCF data. Furthermore, in the presence of *load combinations* the maximum principal stress range should be used, calculated as the greatest algebraic difference between principal stresses occurring during the whole loading event [2]. The co-existence of normal and shear stresses is treated in the latest 1992 ERAAS guidelines [25] by a single formulation. The maximum principal stress considered, both in the fatigue assessment and the static strength analysis of any weld, is estimated by [26]:

$$\sigma_p = 0.5\left[\sigma + \sqrt{\sigma^2 + 4\tau^2}\right]$$

The orientation of the welded joint with respect to the principal stress directions is also important. As the maximum principal stress range may not act in a direction which corresponds to the lowest classification of the

joint it is recommended that a continuous weld should be classified as 'longitudinal' with respect to stresses acting within 30° of the weld axis and transverse for other directions. For load-carrying welds, the stress in the weld should be the vector difference between the maximum and minimum vector sum of the stresses on the weld throat [2].

3.3.1 The Development of Steel Fatigue Codes

Fatigue design rules for *steel joints* have evolved and developed in the last twenty years. Following a review and statistical analysis of published fatigue data, the Welding Institute was first to publish [27] a set of rules. Further effort was concentrated in the area of steel bridges and BS 5400 [23] fatigue rules resulted from this work having been based upon the earlier Welding Institute suggestions. What followed was a number of European research projects providing design data for tubular structures which together with the welded plate data contained in BS 5400 formed the basis of fatigue rules for Offshore Structures [4, 5, 28, 29]. Generally, the same rules have also been adapted for application in pressure vessel design [30, 31] and for considering fatigue of aluminium alloy welded structures [16, 32].

All steel design rules and codes are based on the general argument that fatigue cracks in welded joints result from already existing welding flaws and therefore the fatigue life consists primarily of the propagation of a crack. For unwelded material, the fatigue life predictions correspond to the period of crack initiation. The basis for design is usually taken as the S-N curve two standard deviations below the mean. If a lognormal distribution of fatigue life is assumed then their S-N curve represents the lower 95.4% confidence limit and represents approximately 2.3% probability of failure or a 97.7% survival limit. In such curves, the stress values quoted refer to permissible stress ranges, irrespective of the applied stress ratio and mean stress values. Mean stress effects should, however, be separately accounted for (para. 3.2.1), a correction which is particularly necessary for joints containing significant residual stresses.

3.3.2 The Development of Aluminium Fatigue Codes

Many problems which generally hinder the selection of a procedure for fatigue design have also been evident for aluminium design fatigue code development. Firstly, contradictions exist between early (1970's) small scale

experimental data and more recent full scale tests on structural components of corresponding geometries [33], the latter showing lower fatigue strengths (para. 3.7). Furthermore, despite the large number of experimental data, not all cases of direct interest to the designer are experimentally covered and supported. This is primarily due to the significant spread of the use of aluminium alloys in many, and frequently novel, structural applications. As a result, and despite extensive research, the design codes are based on different principles and their correlation is relatively poor. Their main discrepancies are related to the (a) selection of specified materials, (b) classification of joint types (c) strength parameters. These problems are aggravated by possible unaccounted stress concentrations and residual stresses present in the code fitting data. Two approaches to aluminium design exist:

(a) an analytically (fracture mechanics) formulated code (e.g. Aluminium Association), and

(b) an empirically derived S-N expression calibrated to available experimental data (e.g. BS 8118).

In addition, there are codes which assume the stress-ratio R significantly affects the fatigue strength (e.g. UNI 8634, Alcan, ECCS) and introduce an appropriate amplification factor correcting the S-N curve values. The BS 8118 and Aluminium Association recommendations, on the other hand, neglect the stress-ratio effects. Paragraphs 3.2.1 and 3.6 should also be consulted further on R-ratio effects.

3.3.3 Empirically Derived Fatigue Strength Prediction Models

There are three strength prediction models generally available characterising the stress (or strain)-cycle relationship, the S-N curves, the Low Cycle fatigue model and the Langer model.

The S-N curves are applicable to the medium to high cycle range as they assume that the overall structural behaviour remains elastic. The general form of the S-N relation:

$$S^m N = K$$

Constants K, m take empirical values based on experimental data while the

value of K is chosen depending the degree of pessimism introduced in the strength expression (1 or 2 standard deviations below the mean).

Under variable amplitude loading conditions, damage estimation must account for stresses lower than the endurance limit. This is due to the fact that the higher stresses in the spectrum will propagate the cracks and flaws to such an extent that they cannot be neglected any further in the cumulative damage estimation. Therefore a reduction in any endurance limit is carried out using the Haibach correction [34]. Hence BS 5400 [23] recommends a bi-linear S-N curve so that its slope is 1/m for stress ranges above S_0 and 1/(m+2) for stress ranges below S_0. The slope changes from m=1/3 to a slope of m=1/5 at 10^7 cycles. However [35] quotes the reduced Haibach slope as being instead 1/(2m-1), an unimportant difference if m=3. For other m values Faulkner advises the use of 1/(2m-1) for $N > 10^7$. The most conservative approach, of course, would be to extrapolate the curve with no slope change.

Low cycle fatigue ($<10^4$) is generally associated with a certain degree of plasticity. The approach to fatigue design involving macroscopic yielding at the point of stress concentrations is complicated and a list of techniques in the strain range domain (e.g. Coffin-Manson Law) to tackle the problem is referenced in [36]. In this high stress range, fatigue analysis is carried out in the *strain* range domain. Considering the fact that marine structures are most vulnerable to high cycle fatigue ($N>10^5$-10^6 cycles), low cycle fatigue is not of primary consideration in this type of structures and is hence not treated any further.

Langer's model [37] on the other hand, covers both the elastic and plastic strain ranges and has been used in the development of the ASME Boiler and Pressure Vessel Code [31].

3.3.4 Cumulative Fatigue Damage Rules

As a ship is exposed to a random repeated loading throughout its service life, it is important that the relevant stress spectrum is accurately determined, especially as the fatigue life is proportional to the stress range raised to the power of m. Since the load stress spectrum identifies, in number and magnitude, the individual load cycles constituting the stress

sequence may be described in terms of number of cycles n_i, applied at different stress ranges S_i. The fatigue life is then estimated based on the accumulation of the fatigue damage arising from each block of cycles using an appropriate cumulative damage rule.

Some researchers like Schilling and Klippstein [38] and Albrecht and Yamada [39] suggest that the results of variable amplitude fatigue tests can be correlated to the results of an equivalent stress range of constant amplitude producing the same degree of fatigue damage as the variable amplitude stress range distribution it replaces:

$$S_{re} = \left[\sum_{i=1}^{k} p_i S_{ri}^{\,m} \right]^{\frac{1}{m}}$$

where p_i is the frequency of occurrence of the ith stress range S_{ri}. This expression may be viewed as a calculation of the root-mean-square or the root-mean-cube equivalent stress range if m is equal to 2 or 3 respectively. Maddox, however, demonstrated in [40] that fatigue life is a function of the spectrum shape, the block length and the peak stress and that neither the rms nor the cube root mean cube stress represents a unique parameter for defining fatigue behaviour.

The most widely used cumulative damage rule is attributed to Palmgren and Miner [41]:

$$D = \sum_{i=1}^{k} D_i = \sum_{i=1}^{k} \frac{n_i}{N_i} = \sum_{i=1}^{k} \frac{S_i^{\,m} n_i}{A} \leq 1$$

n_i is the total number of cycles at a stress range level S_i, while N_i is the number of cycles to failure under S_i. k is the total number of blocks of constant stress range values. Values of N_i are obtained from the appropriate design S-N curve for each value of S_i.

3.3.4.1 The Validity of Miner's Rule

It is widely accepted that Miner's rule provides a safe, if not always conservative, means of estimating cumulative fatigue damage of joints. However, it has been shown that Miner's rule does not always provide the degree of safety against failure that is envisaged and that its efficiency is entirely dependent on [36, 39, 42, 43]:

- *The form of the loading spectrum*: Miner's rule has been found to be reasonably accurate for an applied stress spectrum resembling narrow-band random loading (e.g. loads due to resonance induced vibration of the structure, developed seas) as more gradual stress range changes occur for this type of loading.

- *Block Lengths*: short block lengths tend to make Miner's rule unsafe

- *Mode of stress application*: Miner's rule does not account for the effects occurring due to any interaction of high to low stress range sequencing in loading. The rule has also been found to be unsafe in the cases where high frequency small amplitude cycles are superimposed on to a lower frequency high amplitude stress fluctuation. Tests in which the applied stress spectrum contains occasional overloads have demonstrated that under this type of loading Miner's rule is over-conservative due to the resulting retardation of crack growth.

A block length is defined as the number of cycles between successive applications of the largest stress range (Fig. 3.12). 'Block' loading contains the same mix (in magnitude and number) of load cycles as the expected stress ranges but these are applied in blocks of constant stress range starting with the lower amplitude stress ranges and applying the higher ones successively.

To avoid these problems, Webber and Guerney [40, 44] recommended the following empirical rule as providing better predictions of fatigue lives of steel (and therefore for aluminium) joints:

$$N_B = \prod_i^n \left| \frac{N_{E_{i-1}}}{N_E} \right|^{p_i} N_C$$

where N_B is the number of 'blocks' to failure, N_C is the constant amplitude life at the greatest stress range in the spectrum, S_{max}, p_i ($S_i = p_i S_{max}$) for each stress range in the load spectrum and N_{E_i} number of cycles per block at stresses greater or equal to $p_i S_{max}$.

One of the most extensive investigations on the cumulative damage prediction of aluminium alloy joints, using both Miner's and the Guerney

rules, was carried out by Harrison et al at the Welding Institute in the late 1960's [45]. These tests were complemented by Webber and Guerney [44] investigating the degree of dependency on block length of fatigue strengths of 7019 fillet welds (symmetrical, longitudinal and transverse fillet welds as well as single non-symmetrical transverse fillet welds). This study concluded that for aluminium fillet welds:

- a Rayleigh stress range distribution at R=0 increases Miner's damage rapidly with block length
- Miner's damage prediction is less than the value of 1.0, sometimes reaching the value of 0.47. No effect of block length was observed in this case
- Miner's rule gives sufficient predictions of fatigue life for R=0 while the 'Guerney Rule' was more accurate at higher mean stresses
- tests at R=0 suggest that the presence of occasional overloading in the spectrum increases the fatigue life.

Irrespective of the comments above, Miner's Rule is preferred for its inherent simplicity by accepting a summation value less than unity (D<1). A probabilistic approach to fatigue damage helps to alleviate some of the discrepancies described above (paras. 3.4, 3.5).

3.3.5 The Use of Equivalent Steel Recommendations in the Fatigue Design of Aluminium Details

Based on work presented in [46] Maddox concludes [47] that the fatigue life of many aluminium welded joints is dominated by fatigue crack growth, implying that the aspects influencing the fatigue behaviour of steel and aluminium joints should be the same. Since crack growth data rates for steel and aluminium correlate on the basis of $\Delta K/E$ this implies that the fatigue strength for steel could be divided by 3 to obtain aluminium fatigue strength. Such an assumption is not always true for higher strength joints for which fatigue crack initiation occupies a large part of the fatigue life.

A comparison of fatigue values at 2×10^6 cycles between aluminium and steel design codes is shown in Table 3.5. The last column of the Table shows the ratio of steel to aluminium fatigue strengths when comparing the European Steel specifications (EC3, ECCS TC6) to the ERAAS (1992) Recommendations. Out of 27 details, only 1 exhibited a value higher than

3.0. There were 4 cases with values higher than 2.5 and in 11 cases the ratio was found to be lower than 2.0 [19]. These results hence question whether steel fatigue design strength estimates may be used in aluminium structures by simple division of their predictions by a factor of 3. The view that direct transfer of fatigue strength values for steel sections to corresponding aluminium ones is not always valid is also supported by [48, 49] as well as by test data obtained by British Rail [50] which support the view that for longitudinal non-load carrying fillet welds factorisation by 3 is satisfactory in contradiction to other joint classes which generally fail to follow this trend.

3.4 Reliability Based Fatigue Design of Steel and Aluminium Joints

The randomness in the prediction of initiation and propagation of fatigue cracks is due to the following sources of uncertainty:

- the fatigue data is characterised by statistical scatter
- modelling inefficiencies existing in the strength expressions
- unpredictable/uncontrollable weld defects
- inaccurate wave load modelling
- approximate stress analysis procedures introduce inaccuracies in the values of stress range acting on any joint
- corrosion and cathodic protection effects on fatigue strength are unclear.

The random nature of these factors therefore encourages a probabilistic approach to fatigue design. The main drawback of the original deterministic strength expressions is that extrapolation to structural configurations and environmental conditions, other than those for which their safety factors have been derived, is difficult. On the other hand, the more elaborate, limit state design codes use partial safety factors to account for parameters influencing the loading and fatigue strength values. Partial safety factors can be determined via reliability based analysis and their final values are obtained relative to a pre-determined level of safety expected of the joint/structure.

3.4.1 Derivation of Partial Safety Factors

In a reliability procedure the statistical distribution of loads is compared to that of the resistance. Assuming that the fatigue strength check is given by

$$\frac{R}{\gamma_R} \geq \gamma_Q Q \quad \Leftrightarrow \quad \log(R) - \log(Q) - \left[\log(\gamma_R) + \log(\gamma_Q)\right] \geq 0$$

then the determination of fatigue design specifications is normally based on the concept of the safety margin Z. The RHS of the expression above represents the linearised form of the strength check criterion. The safety margin is nothing else but the failure function which identifies the distance between a prespecified level of resistance (below the mean) and identified by the partial safety factor γ_R and a prespecified level of load (above the mean) identified by the partial safety factor γ_Q:

$$Z = \log(R) - \log(Q) - \left[\log(\gamma_R) + \log(\gamma_Q)\right]$$

At failure, Z=0, and hence

$$\log(R) - \log(Q) = \log(\gamma_R) + \log(\gamma_Q)$$

The two partial safety factors, γ_R and γ_Q reflect the uncertainties of the fatigue strength predictions and the uncertainties in estimation of the fatigue loading in the strength estimation and are always greater or equal to 1. The probability of failure is expressed as:

$$P_f = \Phi(-\beta) = P(Z \leq 0)$$

For *log-normal basic variables,* for both the resistance and the load Albrecht's formula for the safety index applies [51]:

$$\beta = \frac{\log(R) - \log(Q) + 2\,\sigma_{\log R}}{\sqrt{\left(\sigma_{\log R}\right)^2 + \left(\sigma_{\log Q}\right)^2}} \quad \Leftrightarrow \quad \beta = \frac{\log(\gamma_R) + \log(\gamma_Q) + 2\,\sigma_{\log R}}{\sqrt{\left(\sigma_{\log R}\right)^2 + \left(\sigma_{\log Q}\right)^2}}$$

while for *normally distributed basic variables,* the safety index is expressed in the form:

$$\beta = \frac{\log(R) - \log(Q)}{\sqrt{\left(\sigma_{\log R}\right)^2 + \left(\sigma_{\log Q}\right)^2}} \quad \Leftrightarrow \quad \beta = \frac{\log(\gamma_R) + \log(\gamma_Q)}{\sqrt{\left(\sigma_{\log R}\right)^2 + \left(\sigma_{\log Q}\right)^2}}$$

The mean safety factors on life, N, and stress range are therefore:

$$SF_N = \frac{N}{N_d} = 10^{\beta\sqrt{(\sigma_{\log R})^2 + (m\,\sigma_{\log Q})^2}} \qquad SF_S = 10^{\frac{\beta}{m}\sqrt{(\sigma_{\log R})^2 + (m\,\sigma_{\log Q})^2}}$$

For the necessary comparison of fatigue resistance and load curves to take place, and the consequent identification of the safety margin, both resistance and load must be plotted along the same base line, i.e. they should both be expressed either in terms of N or in terms of stress-range. For the reliability-based design of structures, both resistance and load are normally expressed in terms of stress. This facilitates the design process, in that it gives a target value of stress to which the structure can be designed. However, using the S-N curve, the distribution and statistics of the resistance is usually known in terms of fatigue cycle life and not in terms of stress as is the case for the load part of the strength check. Hence, the need exist to 'transform' the resistance from cycles to failure into stress. Figure 3.13 shows graphically such a transformation. The following points must be borne in mind though:

(a) The standard deviation, $\sigma_{\log N_R}$, of fatigue cycle random variable, $\log N_R$, is connected to the standard deviation of the stress range random variable, $\sigma_{\log R}$, by the following expression derived from similar triangle properties (Fig. 3.13):

$$\sigma_{\log R} = \frac{\sigma_{\log N_R}}{m}$$

(b) the standard deviation, $\sigma_{\log N_R}$, of the distribution of fatigue cycles, $\log N_R$, in the strength expression is assumed to be constant throughout the strength stress range.

Based on the standard S-N expression, the following relationships apply:

$$R^m\, N_R = K \Leftrightarrow m\log(R) + \log(N_R) = \log(K) \Leftrightarrow \log(R) = -\frac{1}{m}\log(N_R) + \log(K)$$

$$Q^m\, N_Q = K \Leftrightarrow m\log(Q) + \log(N_Q) = \log(K) \Leftrightarrow \log(Q) = -\frac{1}{m}\log(N_Q) + \log(K)$$

and hence $$\log(R) - \log(Q) = \frac{1}{m}\left[\log(N_Q) - \log(N_R)\right]$$

By substituting into the expressions for β for both normally, as well as log-normally distributed random variables:

For normally distributed random variables

$$\beta = \frac{\frac{1}{m}\left[\log(N_Q) - \log(N_R)\right]}{\sqrt{\left(\sigma_{\log R}\right)^2 + \left(\sigma_{\log Q}\right)^2}} = \frac{\frac{1}{m}\left[\log(N_Q) - \log(N_R)\right]}{\sqrt{\left(\sigma_{\log N_R}/m\right)^2 + \left(\sigma_{\log Q}\right)^2}} = \frac{\left[\log(N_Q) - \log(N_R)\right]}{\sqrt{\left(\sigma_{\log N_R}\right)^2 + \left(m\,\sigma_{\log Q}\right)^2}}$$

Similarly, *for log-normally distributed random variables*

$$\beta = \frac{\frac{1}{m}\left[\log(N_Q) - \log(N_R)\right] + 2\,\sigma_{\log R}}{\sqrt{\left(\sigma_{\log R}\right)^2 + \left(\sigma_{\log Q}\right)^2}} \quad \Leftrightarrow \quad \beta = \frac{\left[\log(N_Q) - \log(N_R)\right] + 2\,\sigma_{\log N_R}}{\sqrt{\left(\sigma_{\log N_R}\right)^2 + \left(m\,\sigma_{\log Q}\right)^2}}$$

and *in terms of partial safety factors,* for normally distributed variables

$$\beta = \frac{\log(R) - \log(Q)}{\sqrt{\left(\sigma_{\log R}\right)^2 + \left(\sigma_{\log Q}\right)^2}} \quad \Leftrightarrow \quad \beta = \frac{\log(\gamma_R) + \log(\gamma_Q)}{\sqrt{\left(\sigma_{\log N_R}/m\right)^2 + \left(\sigma_{\log Q}\right)^2}}$$

and for log-normally distributed variables

$$\beta = \frac{\log(R) - \log(Q) + 2\,\sigma_{\log R}}{\sqrt{\left(\sigma_{\log R}\right)^2 + \left(\sigma_{\log Q}\right)^2}} \quad \Leftrightarrow \quad \beta = \frac{\log(\gamma_R) + \log(\gamma_Q) + 2\left(\sigma_{\log N_R}/m\right)}{\sqrt{\left(\sigma_{\log N_R}/m\right)^2 + \left(\sigma_{\log Q}\right)^2}}$$

The safety factors vary with type or detail because the standard deviation of the resistance $\sigma_{\log R}$ varies. The assumed value of safety index β the designer will wish to inherit in his structure should be based on his experience or the level of safety implied by previous codes and/or designs. Design diagrams relating allowable stress $\Delta\sigma_{eq}$ vs β, allowable stress $\Delta\sigma_{eq}$ vs $\gamma_R * \gamma_Q$, and safety index β vs $\gamma_R * \gamma_Q$, may hence be derived based on these expressions. Safety index values normally used refer to values corresponding to the end of the service life of the structure or joint. The reliability-based derivation of partial safety factors for fatigue check has been used by the European Aluminium Recommendations [25] on the assumption that the random variables follow a log-normal distribution.

3.4.2 Application to Miner's Rule

Under *spectrum* loading, fatigue failure is usually determined assuming linear cumulative damage expressed by the Miner-Palmgren Rule:

$$D = \sum_{i=1}^{k} \frac{n_i}{N_i} = \frac{N_T}{K} E[S^m]$$

where the D is the damage ratio (= Δ at failure), N_T is the total number of cycles in time T, S is the applied stress range (the random variable), $E[S^m]$ is the expected mean, or average value of S^m and depends on the assumed distribution of stress range (lognormal, Weibull, Beta etc.) (Table in section 2.4, Chapter 2) and n corresponds to the lifetime stress cycle number. If Wirshing et al's [52] representation is used then the above expression becomes:

$$D = \frac{N_T B^m E[S^m]}{K} = \frac{T B^m \Omega}{K} = \Delta \text{ (at failure)}$$

where f_o (= N_T/T) is the lifetime zero up-crossing frequency of the stress range, $\Omega = f_o E[S^m]$ and B ($S_a = B S$) is a random variable quantifying the uncertainty in fatigue stress load estimates. Note that K=A where A is one of the experimentally derived constants of the standard S-N expression. In this case K should correspond to the mean value strength line and not the mean-1 or mean-2 standard deviations. Expressions of Ω for various load distributions can be derived information presented in the Table of section 2.4 (Chapter 2).

The safety index then becomes $\beta = \frac{\ln \tilde{T} - \ln T_S}{\sigma_{\ln T}}$ where $\sigma_{\ln Z} = \sigma_{\ln T}$

and $$\ln \tilde{T} - \ln T_S = \ln\left[\frac{K\Delta}{B^m \Omega}\right] - \ln T_S = \ln K + \ln \Delta - m \ln B - \ln T_S$$

$\tilde{T}$ corresponds to the median or mean (depending whether the distribution is lognormal or normal) of the time of exposure of the joint to fatigue loading.

Two methods are available for the reliability based fatigue design of structural joints. One attributed to Wirsching et al, assumes that the

random variables and hence the fatigue strength model are all log-normally distributed. The second method, attributed to Munse et al is based on the other hand, on a Weibull distribution of the fatigue strength model.

3.4.2.1 API/Wirsching et al Method

Wirshing et al [52] have assumed lognormal distributions for all the random variables of the fatigue strength expression above, namely Δ, K and B. Therefore, the time of exposure of the joint to fatigue loading, T, is a random variable with a lognormal distribution itself. Transforming, this distribution into a normal one, the probability of failure may be expressed as:

$$P_f = \Phi(-\beta) = P(T \leq T_S)$$

where the safety margin is set as $Z = T - T_S = \frac{K\Delta}{B^m \Omega} - T_S$

T_S is the intended service life of the structure, having no distribution. The safety index β is hence defined as

$$\beta = \frac{\ln \tilde{T} - \ln T_S}{\sigma_{\ln T}} \qquad \text{since} \qquad \sigma_{\ln Z} = \sigma_{\ln T}$$

where $\tilde{T}$ is the median value of T (assuming a log-normal distribution). In addition, the standard deviation of lnT is given by [52]:

$$\sigma_{\ln T} = \sqrt{\ln\left[\left(1 + C_\Delta{}^2\right)\left(1 + C_K{}^2\right)\left(1 + C_B{}^2\right)^{m^2}\right]}$$

where the C_is denote the COVs for each of the random variables (para. 3.4.2.3).

3.4.2.2 Munse et al SSC Method

The Munse et al method [53] is a result of work funded by the Ship Structure Committee aimed at ship structures. Munse et al have assumed the Weibull distributions to describe the stress range loading on the structural joints of ships. From Miner's rule:

$$\frac{N B^m E[S^m]}{K} = \Delta \quad \Leftrightarrow \quad N = \frac{\Delta K}{B^m E[S^m]} \text{ (at failure)}$$

where for this method B=1. The probability of failure may then be expressed as:

$$p_f = \left[N_S E[S^m] \Gamma(1 + C_N^{-1.08})/K\right]^{C_N^{-1.08}}$$

The shape and scale parameters of the distribution are given respectively by (para. 2.4, Chapter 2):

$$\xi = \bar{N}/\Gamma(1/\lambda + 1) \qquad \text{and} \qquad \lambda = C_N^{-1.08}$$

The random variable N is assumed to have a Weibull distribution and therefore the COV accounting for the uncertainty in life cycle predictions is given by

$$C_N = \sqrt{C_K^2 + C_\Delta^2 + m^2 C_S^2 + C_C^2}$$

where C_S is the COV accounting for the uncertainty in stress range predictions, C_Δ is the COV for the uncertainties involved in Miner's Rule predictions, C_K is the COV representing scatter inherent in S-N data and C_C is the COV value for the uncertainty in workmanship, usually taken equal to 0.

3.4.2.3 The Statistical Uncertainties in the Cumulative Fatigue Damage Model

The random variable B (accounting for the uncertainties in the stress range load predictions) is the most important element of the fatigue strength expression because it possesses high variability and its influence is magnified due to the presence of m as an exponent to both its mean and COV values. Assuming that the uncertainty in stress estimates stems from manufacturing and assembly operations (M), the seastate statistical models used (S), the wave force prediction methods from wave data (F), the nominal structural component load calculations given wave forces (N) and the calculation methods of fatigue stress at joints from nominal structural component forces (H), then the mean and COV values of the random variable B may be defined as follows [54]:

$$\overline{B} = \prod_i \overline{B}_i \qquad \text{for i=M, S, F, N, H} \qquad \text{and} \qquad C_B = \sqrt{\prod_i \left(1 + C_i^2\right) - 1}$$

Table 3.6 provides appropriate values for the bias and COV values of these variables, reflecting the experience of the offshore industry. Generally values of $\overline{B}$=0.7 and C_B=0.5 are considered to be reasonable for general application [52]. Wirshing et al [54] assume a lognormal distribution of this variable.

The random variable K is, together with m, derived from regression analysis of experimentally obtained S-N fatigue data and accounts for the uncertainties in the strength prediction estimates. Wirshing et al [55] assume a lognormal distribution for the values of A. Values for the mean value of K and C_K are presented in Table 3.7 for 5 sets of data.

For *the random variable N*, the estimation of its COV value, C_N, should consider all sources of uncertainty in fatigue behaviour (e.g. scatter in test data, errors in stress analysis, effects of fabrication and workmanship, sampling and measurement). Experimental investigations on over 11,000 aluminium and steel specimens [52] indicate that the variance may be assumed constant for all values of S_i. Wirshing et al [55] assume a lognormal distribution for the values of N. Table 3.8 presents Whittaker's recommendations on the COV values who collected and summarised fatigue data from a number of experimental studies [42, 56, 57]. Ang and Munse in [57] indicate an average COV value of 0.52 based on data by Guerney and Maddox [42]. In addition, Whittaker and Besuner [56] and Jacoby and Novack [58] found that the scatter in fatigue data under spectrum loading is usually less than that for constant amplitude loading.

The *cumulative damage ratio at failure* Δ is also a random variable with values ranging from 0.5 to 1.6 [24] sometimes reaching values as low as 0.2 and as high as 5.0. From tests on tubular joints an average value of Δ=1.7 has been derived. Wirshing et al's attempts [54] to identify the variability in the amplitude fatigue estimates using Miner's Rule, concluded that a model of Δ having a log-normal distribution with a median of 1.0 and COV of 0.65 is acceptable for design purposes (Tables 3.9, 3.10).

3.5 Fracture Mechanics in Fatigue Design

The second of the two methods available for establishing rules predicting the fatigue behaviour and strength of any metal joint is that based on the theory of fracture mechanics. The main attraction of such a theoretical approach is that it does not rely on any expensive and time consuming experimental investigations as the S-N approach does. This approach instead, simulates, using appropriate fracture mechanics laws, the stages leading to fatigue failure, namely crack initiation and crack propagation (both stable and unstable). Its probabilistic treatment is briefly described next.

3.5.1 The Fracture Mechanics Model

In both cases Paris' law applies [59], requiring the most accurate definition possible of the following four parameters (Fig. 3.14):

- crack growth rate (da/dN)
- local stress-range values ΔK $(= Y(a)\,\Delta S\sqrt{\pi\, a})$
- the instantaneous crack geometry (identified by a,Y)
- the R-ratio.

where a is the instantaneous crack length, ΔS is the nominal stress acting normal to the crack, and Y(a) is a function that depends upon the instantaneous geometry of the crack (para. 3.5.2). It must be borne in mind, that in the sections referring to fracture mechanics based fatigue design, K bears no relation to the similarly defined S-N curve material constant which is merely determined by curve-fitting to experimental fatigue data. Hence, *for stable crack growth,* (between $a_{threshold}$ and a_{crit}) the rate of crack propagation according to Paris-Erdogan is given by:

$$da / dN = C[\Delta K]^n$$

where C and n are material constants (depending on the mean cycling stress, test environment, cycling frequency) and ΔK is the stress intensity factor. Values of K_C (the fracture toughness of the material) for common flaws are given in [60], and are obtained by crack opening displacement tests (CODTs).

The number of cycles required to propagate a crack from initial size a_i to final size a_f is obtained by integrating the relationship between ΔK and N [36]:

$$N_f - N_i = \int_{a_i}^{a_f} da / C[\Delta K]^n = \int_{a_i}^{a_f} da / \left(Y(a)\sqrt{\pi a}\right)^n$$

For Y(a) assumed constant during the crack propagation process and constant values of a_i and a_f the expression reduces to the S-N format ($\Delta S^n N = constant$). Provided the value of K (i.e. the value of Y) for the joint and the values of C and m in the crack propagation equation are known, one of the remaining four parameters, a_i, a_f, ΔS and N can be calculated given the other three. For example, if the applied stress range, S, and Y(a) are assumed constant during the crack propagation process then:

$$a_f = \left[a_i^{\left(1-\frac{n}{2}\right)} + \left(1-\frac{n}{2}\right) C \left(Y S \sqrt{\pi}\right)^n \left(N_f - N_i\right) \right]^{\left(\frac{2}{2-n}\right)}$$

Reference [61] presents ways of *correcting Paris' equation for stress ratio effects*. Clarke in [62] accounted for this correction by:

$$da / dN = C[\phi \Delta K]^n \qquad \text{where} \qquad \phi = \begin{cases} 1/(1-R) & R<0.50 \\ 1.0 & R \geq 0.50 \end{cases}$$

When the loading is of variable amplitude (S_i stress range), an incremental form of the crack growth equation must be used as defined in [63]:

$$a_{i+1} = a_i + \Delta a_i = a_i + C\left(Y(a_i) S \sqrt{\pi a_i}\right)^n$$

Due to the complexity of such an approach, an alternative approach would be to consider an equivalent ΔK that will provide the same rate of crack propagation under variable and constant amplitude loading. Working along these lines Barsom in [43] recommended the use of ΔK_{rms} is the rms value of ΔK. Yang and Trapp [64] recommended the substitution of ΔK_{rms} with the average of the nth power of ΔK.

Employing the stress intensity factor range expression it may be concluded that damage accumulates approximately as $(\text{stress})^n$ and $(\text{crack size})^{n/2}$. Final

failure may be assumed to occur when:

- the crack length (or depth, depending on the position and shape of the initial crack flow) becomes equal to the chosen size a_{crit}, or
- $a_{crit} = t$ for through thickness cracking, or
- unstable crack growth occurs, or
- the component reaches the yielding or tearing level.

The final choice of one of the above modes of failure as a design criterion primarily depends on the redundancy of the structure, the material properties, the structural geometry and ease of inspection.

Specifically, for reliability based fatigue design using AFOSM methods, the designer has a choice of two failure functions to control the fatigue crack propagation [65]:

(a) one limiting the stress intensity factor, K, at the leading edge of the crack to that of the fracture toughness of the material, K_C:

$$g = K_C - Y(a)\, S \sqrt{\pi a} \qquad \text{or} \qquad \gamma_C K_C - Y(\gamma_a a)\,(\gamma_S S)\sqrt{\pi (\gamma_a a)} = 0$$

where $\gamma_C, \gamma_a, \gamma_S$ are partial safety factors applied to the nominal design variables. The values of mean and COV values for a, are obtained by non-destructive testing techniques, while estimates of the mean and COV values for K_C can be obtained from fracture tests conducted in the environment of interest. The COV value for S depends on the load history. Assuming log-normal distributions, and by small variance approximations, i.e. median $\ln x_i \approx \ln \tilde{x}_i$, $\sigma_{\ln x_i} \approx \mathrm{COV}_{x_i}$ then the relation between β and K_C, a, S is given by:

$$\beta = \ln\left[\frac{\tilde{K}_C}{0.637\, \tilde{S} \sqrt{\pi \tilde{a}}}\right] \Bigg/ \sqrt{C_{K_C}^2 + C_S^2 + \frac{C_a^2}{4}}$$

(b) One based on restricting the crack size, a, to below a preset critical size, a_{crit}, set from serviceability considerations [65]:

$$g = a_{crit} - a$$

The uncertainty in da/dN values stems from two sources; scatter inherent in the material (COV=15%-25% [66]) and scatter due to experimental techniques (log-normal distribution and COV is app. 50% [66]). Clarke in [62], sets the standard deviation in crack growth rate to a value of 15%.

3.5.2 The Empirical Coefficients in the Paris-Erdogan Law

Reference [6] suggests that the following empirical formula relating n and C applies for steels:

$$C = \frac{1.315 \times 10^{-4}}{895.4^{n}}$$

For structural steels the values for n lie in the range of 2.4-3.6 with an average value of 3 [6]. As a useful approximation and in the absence of test data $n \approx m$. Due to the difficulty in predicting the values of m and C, it is generally assumed [6] that m=3 and $C = 1.83 \times 10^{-13}$ will correspond to the mean strength.

The crack geometry function, Y(a), varies by crack type as well as during crack propagation. This function is usually expressed by the Linear Elastic Fracture Mechanics (LEFM) model of which the most frequently used is the surface crack by Newman [67]. The Y function may also be expressed as [6] $Y = M_K Y_U$ where Y_U is the value of Y for the same crack geometry in a plate with no weld and M_K is a correction factor allowing for it. Values for Y_U are provided in [68], while values for M_K are presented in [69, 70] for various joint geometries. Y(a) includes the stress concentration factor effects. For a circularly shaped crack embedded in an elastic, infinite plate Y=1.13, while for an edge crack Y becomes 1.98. For an elliptical surface crack in the same plate environment, Y varies from 1.2 to 1.98 depending on its aspect ratio. Finite plate correction factors for plate thicknesses and width have also been derived by Newman.

3.6 Current Aluminium Fatigue Code Recommendations

3.6.1 The Aluminium Association Recommendations

The recommendations in [21] (1986) were the first to tackle aluminium

fatigue design in the USA and were based on small scale fatigue tests. They assume that the fatigue strength is unaffected by stress ratio R while the applied stress range, number of cycles, and structural detail type identify the required strength level.

The design strength values are based on the 95% confidence limit (5% probability of failure) hence requiring no additional safety factor. Miner's rule is recommended for the cases of variable amplitude loading. The final design lines have the form presented in Figure 3.15. The maximum allowable stress range is kept constant for N in the ranges $0\text{-}10^5$, $10^5\text{-}5\times10^5$, $5\times10^5\text{-}2\times10^6$ and greater than 2×10^6. There is still a log-log relation between the stress range and the number of cycles. Low/high cycle fatigue limits are also imposed. The recommendations are not affected by alloy type even though significant differences between alloys at the lower cycle range are observed [18], the higher strength alloys having higher fatigue strengths. At the low cycle range no great difference is observed. Twenty structural details are considered (Fig. 3.15) whose categorisation is based only on the joint configuration, while environmental, geometrical factors and weld quality should be judged by the designer. The databank forming the basis of the development of this code was the one jointly formed at Iowa State University and the University of Munich under the auspices of ECCS and CAFDEE [19, 71].

3.6.2 The ALCAN/Canadian Standard Recommendations

These recommendations [14, 15], present the designer with seven classes of joints (Classes A, B, B', C, D, E and F) according to their mechanical and geometrical features (Fig. 3.16). No distinction is made between the different alloy types and the strength is expressed in a log-log linear form relating the number of cycles with the 'semi-range' stress. The effects of stress ratio R are also accounted for by correcting the basic strength data with appropriate magnification factors obtained as shown in (Fig. 3.16). Miner's rule is recommended for multiple amplitude loading cases. The code advises that uncoated surfaces prone to corrosion should have their non-welded nominal fatigue strengths reduced by 50%. No safety factors or general safety requirements (lower bound curves etc.) are presented, while the test data supporting the choice of curves remain unknown.

3.6.3 The BS 8118 Recommendations

The BS 8118 recommendations [16] do not discriminate between the various alloys and are thus universally applicable. They cover 3000, 5000, 6000 series alloys and the 7020 alloy in various product forms including sheet, plate and extrusions. Design curves are given for plain material with different finishes, welded, and for mechanically fastened joints, but not for adhesively bonded joints. The joint classes are divided in three categories and 29 separate detail types (Fig. 3.17):

(a) non-welded details (7 classes)
(b) welded details on surface of the loaded member (11 classes)
(c) welded details at the end connections (11 classes).

The potential crack location is a key factor in defining classification together with the direction of applied loading relative to the weld. The classification in the form of Tables (Fig. 3.17) enables the designer to identify rapidly the low strength details at the conceptual stage of the design.

Figure 3.18 shows the form of the S-N strength curves put forward. The lower five curves have a common slope of m=3. For consideration of variable amplitude loading, the design curves demonstrate a change of slope to m+2 at 5×10^6 cycles and a horizontal cut-off at 10^8 cycles. The detail types are given in terms of nine (9) class reference numbers in the range of 14 to 60. The reference number is the design stress range corresponding to 2×10^6 cycles. Stress ratio, R, effects are not accounted for and the basic strength is expressed in a log-log linear form relating the maximum allowable stress range with the number of cycles. The S-N curves represent the mean minus two standard deviations on laboratory data to account for the discrepancies present in the small scale laboratory tests (Appendix 3.1). It is recommended that no reliance is made upon any fatigue life improvement technique. Hence conservative loadings are encouraged and the fatigue strength predictions are assured by using lower bound data (mean minus 2 standard deviations) and an attainable weld quality.

3.6.4 The ECCS Recommendations

The ECCS 1991 recommendations [25], are considered in [72] to be the most up-to-date, due to the wider number of cases accounted for, as well as the large theoretical/experimental background they were based on. The code makes no distinction between the various alloy types, except in the case of rolled or extruded details. A 'life' design criterion, as well as a serviceability criterion are available. Multiple amplitude loading is tackled either by Miner's rule or by calculating the constant amplitude equivalent stress-range. The joints are divided into 6 main classes according to mechanical and geometrical features of the joint (Fig. 3.19). These classes are further sub-divided to a total of 32 sub-classes depending on constructional aspects. The S-N curves are parallel but not equidistant to each other with two different slope values for all 27 welded details (Fig. 3.20). The fatigue strength is expressed in S-N form and the values are valid for R=0.5. The influence of the stress ratio R is accounted for via a diagram in which an appropriate enhancement factor for the basic stress range is provided by a linear relationship.

3.6.5 Aluminium Fatigue Design Code Comparison

Mandara et al [72] compared the fatigue design codes by Alcan, UNI, BS 8118, Aluminium Association and ECCS. This comparison was based on 11 structural details (Table 3.11) and the stress range was evaluated for $N=10^5$ and $N=10^7$, constant loading conditions and R=0.5. The comparison demonstrated that:

- In the low cycle range, the Alcan, BS and Aluminium Association rules provide the highest design stresses. The Italian Code is more conservative with the ECCS predictions lying in between.

- In the high cycle range, BS 8118 is more conservative, and Alcan and UNI codes are most optimistic. The ECCS recommendations lie once again in between.

- The worst disagreement between the codes was for the cases of the base metal and transverse butt welds. In the case of less resistant details the agreement is better.

- The Aluminium Association code shows a discontinuity in predictions for $N=10^5$ and 2×10^6.

- BS 8118 is in good agreement with the ECCS and Alcan codes especially for low N values.

Figure 3.21 shows that for a number of basic joints at 10^7 cycles, BS 8118 predictions are clearly conservative with the ALCAN recommendations tending to be optimistic for some of the weld types. The Aluminium Association, UNI and ECCS codes provide relatively similar predictions.

Kosteas presents an even more detailed comparison between the two most developed aluminium fatigue codes with fatigue design strengths provided by ERAAS and BS 8118 at 2×10^6 and 10^5 cycles respectively [19] (Fig. 3.22). For parent material, BS 8118 demonstrates lower values without distinguishing between alloys. In the case of welded details good agreement was generally observed over a large number of classes. The agreement was found to be more pronounced at shorter lives. The derivation of the design S-N curves, as well as the categorisation of details in classes, is different in the two codes due to the different sets of experimental data used in either case (different slope values). The lack of a standardised detail categorisation between the two codes hindered the comparison by forcing the use of equivalent details.

Finally, the main features of the five latest aluminium fatigue design codes, namely, the Alcan [14], BS 8118 [16], UNI8634 [73], the Aluminium Association [21] and the ECCS [25] recommendations are presented in Table 3.12.

3.7 Experimental Investigations into the Fatigue Strength of Steel and Aluminium Weldments

The main drawback in the development of fatigue codes is that the small scale fatigue data generally prove to be inconsistent to that obtained by the fewer large-scale tests. The reasons leading to these discrepancies are varied. Firstly, small scale tests do not contain realistic representations and values of residual stresses and secondary bending stresses that might be present in the structure. The larger the test specimen the greater the constraint to expansion and contraction during fabrication. As a result the locked-in

residual stresses developed in the large scale specimens are greater and therefore the associated decrease in fatigue strength is expected to be greater. On the other hand, small scale specimens do not represent satisfactorily the effects of joint preparation, welding process, welding procedure, post-weld treatments, environment and loading history. In addition, full scale tests contain more and larger flaws resulting in smaller fatigue lives.

Fatigue data sources for *steel joints* in the form of S-N curves are published in references [4, 5, 16, 23, 24, 27, 28, 29, 74, 75, 76]. Munse et al [53, 77] present a wealth of fatigue data on steel ship details. However, the limited number of data per joint and limited range of N tested, restrict their usefulness. Accurate values of the slope of the S-N curves were hence difficult to obtain and might better have been obtained from fracture mechanics considerations.

The development of the more recent aluminium fatigue design codes (e.g. BS 8118, ERAAS) has demanded (a) the re-evaluation of old fatigue data usually carried out in small scale and (b) the generation of new data, more 'application specific' and in larger scale. The experimental research projects aimed to satisfy both of these goals for *aluminium joints* are described in greater detail in Appendix 3.1.

Few experimental investigations into the fatigue strength of welded *aluminium ship details* have been found in the open literature. Beach et al in [78] report on a number of fatigue tests of full-scale, ship details (Fig. 3.23). The material was 5086-H116 with 5356 filler metal. The loading conditions addressed were hull girder bending and slamming pressures. It was concluded that the fatigue life of a continuous longitudinal is approximately twice that of a discontinuous one. Approximately the same drop in fatigue strength was observed due to the introduction of brackets and the geometrical discontinuity thus introduced. In addition, large improvements in fatigue life were obtained by sniping the bulkhead stiffener (e.g. configurations 7 and 8 - Fig. 3.23) with concurrent benefits in the fabrication costs.

Further tests on welded aluminium ship details were presented by Niemi et al in [79] on small and large scale specimens constructed of 5083 and 6061 alloys. The small scale tests were executed at constant amplitude loading

and at various R-ratio values while the large scale specimens were modelled in accordance with the design of the main deck of a Finnish patrol vessel in operation and consisted of a 5083 alloy flat plate with two T-shaped 6061 alloy longitudinal stiffeners.

The properties of aluminium-steel, explosively bonded, transition joints used in ship structures have been studied by Terazawa et al and reported in [80, 81].

3.8 The Static Strength of Aluminium Welded Joints, Fabrication and Aspects of Inspection/Repair

3.8.1 The Effects of Post-Weld Repair Treatments

The decision on whether a weld discontinuity should be repaired or not depends on whether the repair action will eventually improve or worsen the fatigue performance of the joint. The types of weld discontinuities generally considered are porosity, excessive/lack of penetration, weld reinforcement, edge misalignment, angular contraction, root concavity and cracks.

All improvement methods interfere with the mechanisms of crack initiation and propagation usually at the weld toe transition where this type of failure is usually expected to initiate. However, as they are expected to increase the construction cost they should be avoided unless necessary. Different structural details are expected to respond differently to the various post-weld treatments but generally, post-weld treatments are more effective at smaller stress ranges [82]. Information and specific guidance for the fabrication and protection aspects of aluminium alloy structures is provided by Bayley in [83].

The two improvement techniques available are (a) weld toe dressing (reducing stress concentrations) and (b) residual stress techniques (reducing the tensile residual stresses). The former act favourably on the fatigue crack initiation period but the benefit of the latter spurs from the reduction of their crack growth rate.

Weld toe dressing techniques (hammer peening, shot peening, disc grinding or, machining) reduce the level of stress concentrations by

smoothing out the weld bead and removing all crack-like flaws to a depth of at least 0.5 mm below any undercut. The two other non-mechanical methods, TIG dressing and Plasma dressing require the remelting of the weld toe but being expensive options they are generally avoided. After all, they do not guarantee the absence of any additional weld defects. The resulting improvement in fatigue strength of a welded fillet joint, both in terms of slope of the S-N curve and endurance limit, is demonstrated in Figure 3.24. Such an improvement is due to a shift from a crack propagation to a crack initiation condition for the joint.

The residual stress techniques superimpose high compressive residual stresses where high applied tensile stresses are expected. The most common technique is that of *cold working of the material surface* (hammer peening, needle peening and shot peening), producing a layer of compressive stress at the surface, balanced by a tensile stress within the material thickness. Hammer peening provides the greatest improvement while needle and shot peening are less noisy but do not provide any major strength improvements (Fig. 3.25). Of the two remaining methods, *prior overloading* introduces high tensile stresses in stress concentration areas so that consequent tensile fatigue loads will have no effect on the fatigue life of the joint. The danger of deformation however, remains great. *Spot heating* introduces local radial (from the centre of the heat spot) tensile residual stress at every stress concentration position (Figs 3.26a and 3.26b). The compressive stress components in a tangential direction act outside the spot area. The residual stresses thus introduced, clamp the crack tip and hence reduce or even prevent further crack growth.

Indications exist that the application of high strength material will greatly enhance the beneficial effect of the improvement techniques [2]. However, insufficient data are available in this respect and therefore no secure guidance is currently available.

For aluminium joints, the effectiveness of the individual post-weld improvement techniques has been reviewed and improvement factors recommended by Hobbacher in [82]. Table 3.13 presents his recommendations on the most appropriate and efficient post-weld treatments for four types of welded aluminium details. The enhancement factor of 1.4 (once proper post-weld treatment has been applied) on the fatigue strength of these welded aluminium details is not excessive

considering that, for most of the structural design cases, an improvement of 40% to 50% was observed. In addition, Kruger and Priesnitz in [84] investigated the effect of discontinuities on the fatigue strength of transverse butt welds connecting two aluminium plates of 6061 aluminium alloy under axial loading. It was concluded that tungsten inclusions have no detrimental effect and that pores up to 30% of the weld volume were found to reduce the fatigue strength by 20%. Overwelded crater cracks reduced the fatigue strength by about 10%.

Following a series of inconclusive experimental investigations [85], the US Navy carried out a number of fatigue investigations on repaired and unrepaired plate specimens containing transversely and longitudinally loaded butt joints, all made of 5456 aluminium alloy, in an attempt to provide an answer to the benefit of repair [13]. It was concluded that although the use of filler wire that reduces porosity improved the fatigue life of reinforced welds, that did not happen for the unreinforced ones. It was the surface pore size and not the number of pores that seemed to determine their fatigue life. Polishing was not found to increase the fatigue life any more than grinding. The porosity did not affect the fatigue lives of longitudinal welds at all. Furthermore, lack of penetration did not affect the fatigue performance of reinforced welds, leading to the conclusion that, although weld reinforcement is generally considered to be detrimental to the fatigue performance, it can negate some of the the lack of penetration effect. Repaired welds were found to have lives in the range of 30% to 75% of those of sound welds. Little benefit was found by pre- or post-heating of repairs.

Addressing the concern over the poor fatigue performance demonstrated by SES ships, Hardy et al [86] investigated the effect on the fatigue performance of 5086 aluminium joints of Gas and Electron Beam Welding. Transverse flat-plate butt and T-fillet weld details were tested under bending loading of R=-1. The investigation demonstrated that Gas-MIG and TIG welding reduces the fatigue strength of butt welds by 50% compared to 67% for fillet welds. Brush shot peening gives an improvement to fatigue performance of at least 50% reaching 100% for the case of butt-welds. Values that would be best applied as variables in the various peening techniques are recommended in [86]. On the other hand, the study of the effectiveness of Electron Beam welding was inconsistent. The fatigue life determined using

beam specimens was equivalent to that for the parent metal. However, the fatigue life determined using flat plate specimens showed no improvement over the Gas-welded butt welds.

Polmear in [87] investigated the relative merits of shot peening and TIG dressing on the fatigue strength of aluminium butt welded and fillet welded plates of 5000 series alloy. It was concluded that the average increase in fatigue lives due to TIG dressing ranged between 1.9 to 3.3 times for butt-welded plates and between 2.8 and 7.2 for fillet welded plates. The variations occur for different load values (mean and stress range values).
The shot peening investigations concluded that peened specimens (peened before preloading) tested with low preload and high cyclic stress up to 10^6 cycles, could accommodate approximately 40% higher stress levels than the unpeened ones. If the specimens were peened after preloading the percentage increases to 60%. For fillet welds 30% improvements were recorded. Previous investigations into the question of post-weld treatment of aluminium joints is referenced and discussed in [87].

Crack Repair is usually carried out by using insert plates. Although this is initially an expensive operation it is cheaper in the long run because repair welds generally crack in a shorter time than the original. Alternatively, a method very popular in aluminium superstructure repairs is based on the use of adhesively bonded steel or carbon fibre reinforced plastic patches. Application of this technique as well as more general applications of adhesives are outlined in [88, 89]. The main advantages of this method are that cables and lagging do not have to be removed and that the stress transition to the adjoining structure is less severe than welded inserts.

For temporary crack growth arrest the traditional method is to drill a hole at the crack tip. Insertion of a highly torqued bolt in the hole has been shown to increase the fatigue life by a factor 4 to 5 in both steel and aluminium [62, 90]. This enhancement is due to the introduction of compressive stresses at the edge of the hole.

3.8.2 The Static Strength and Inspection Schemes for Aluminium Joints

General guidance for the static design of aluminium welds is included in [91] while Soetens in [92] presents the results of an extensive three year (1981-1984) numerical and experimental investigation into the static

strength of aluminium welded joints whose conclusions were introduced into the ERAAS and BS 8118 proposals. The background information on the development of the BS 8118 design recommendations for the static design of aluminium joints is provided by Cullimore in [93]. Furthermore, the layout and background to the guidance by the Aluminium Association [21] concerning inspection, welding and manufacturing processes are provided in [94]. More detailed information and experimental data on the behaviour of various types of fastening systems, including the welding process, is provided by Sharp in [95]. The recommendations have been based on the respective steel ones with some adaptations to accommodate for the special features of the aluminium material. The BS 8118 weld quality, inspection and acceptance criteria, are described in detail in [96]. Possible inspection schemes and their optimisation based on the use of structural reliability techniques are described in [97].

3.8.3 The Weldability of Aluminium Alloys

As knowledge about welding of aluminium is not widespread, many people unfamiliar with aluminium alloys would consider them to be non-weldable or in the worst case would choose an inappropriate welding process resulting in premature failure. To encourage the proper selection of the aluminium alloy for the job in question, one needs to know the:

- property data and characteristics of the aluminium alloy
- weldability of the alloy finally chosen.

The first aspect is satisfied by the publicly available databank called ALUSELECT [98] which is the result of an European Aluminium Association (EAA) project in association with eight major aluminium companies aimed at forming a unified databank of aluminium alloy property data. The main difficulty overcome was the need to harmonise the different property data presented by the various companies due to differences in production technologies. In ALUSELECT, basic mechanical and physical properties, as well as technological properties on corrosion, brazing, cold forming machining, soldering, surface treatment and welding were harmonised (a total of 50 properties).

Weldability is the ability of a material to be welded without cracks or other defects being formed to the extent that the integrity of the joint is

threatened [98]. Indices are used (e.g. A to D or 1 to 5) to compare the weldability levels which are generally empirically derived. This approach is mostly driven by personal opinion. Supporting decision making data are scarce [98]. As a result weldability data for the following five welding processes were analysed by Sandstrom [98] and his colleagues (in the same EAA project of the ALUSELECT development) namely MIG/TIG, Oxy-gas, Electron Beam, Spot welding (hard and soft). The results of this evaluation are presented in Table 3.14 out of a scale of 6 for 28 EAA alloys with the general conclusions summarised in Table 3.15. Furthermore, guidance on the possible and recommended combinations of parent metal and filler metal alloys is given in Table 3.16 obtained from BS 8118.

Hot tearing and solidification cracking are considered to be the main causes of low weldability in aluminium alloys. Hot tearing occurs when cracks form in the grain boundaries of the material when they are exposed to stress due to solidification shrinkage and thermal contraction during welding. Tearing sensitivity is at a maximum for an alloy content between 1% and 3% [98] (e.g. AlCu-2000 series, AlMg-5000 series alloys). Copper is the element that has the largest negative influence on MIG/TIG weldability.

Liquifaction in the HAZ can give cracking in alloys (e.g. 6082) which are not considered susceptible to tearing. The weld metal compositions can be such that the level of alloying elements in the weld metal is higher than in the HAZ. Thus in certain temperature intervals (liquid to solid state temperature difference) the stresses from the solidification shrinkage in the weld metal will directly act on the weaker HAZ which cracks.

As hot tearing is primarily controlled by grain boundary liquifaction, a large solidification temperature should have a negative influence on the weldability the value of which has been found in [98] to reduce when the solidification interval is increased. Generally copper and elements like lead and bismuth, which are added to improve machining characteristics, have the largest deteriorating effect on the MIG/TIG weldability. Gas weldability is also adversely influenced by lead and bismuth in addition to silicon, manganese and magnesium alloying elements. Finally, a list of ten references on the background and previous investigations relating to the effect of special alloying elements on the weld cracking behaviour of aluminium filler alloys and parent materials, is provided in [99].

References

1) May, R., Barltrop, N., 'Fatigue in Fast Craft', Ship and Boat International, Sept. 1993, pp. 35-37.
2) Maddox, S.J., 'Fatigue Strength of Welded Structures', Abington Publishing, Cambridge, England, 1991.
3) British Standards Institution, 'British Standard Code of Practice BS PD6493: Guidance on Methods for Assessing the Ability of Flaws in Welded Structures', BSI, London, 1991.
4) HMSO, 'United Kingdom Offshore Steels Research Project (UKOSRP) -Phase II', Summary and Recommendations, OTH 87-265, Techword Services, HMSO, London, 1987.
5) United Kingdom Department of Energy, 'Offshore Installations, Guidance on Design and Construction', HMSO, London, 1984.
6) Guerney, T.R., 'Fatigue Design', Chapter 5.4 in Constructional Steel Design: An International Guide, P.J. Dowling, J.E. Harding, R. Bjorhovde (Eds.), Elsevier Applied Science, London, 1992.
7) Van Horn, Kent, R., (eds.), 'Aluminium: Properties, Physical Metallurgy and Phase Diagrams', Volume 1, American Society of Metals, Metals Park, Ohio, 1967.
8) Paauw, A.J., Bardahl, E., 'Fatigue Crack Growth in Aluminium Alloy AlMgSi1 in Air and Seawater', Proc. 3d Int. Conf. on Aluminium Weldments, D. Kosteas, (ed.), Munich, 15-17 April 1985, Aluminium Verlag GmbH, Dusseldorf, 1985.
9) Sharp, M., 'Special Design Problems', Chapter 12 in Behaviour and Design of Aluminium Structures, McGraw-Hill Inc., New York, 1992.
10) Bilgram, E., Winkler, P-J., 'Stress Corrosion Behaviour and Welded Aluminium Alloy AlMg4,5Mn (5083)', loc. cit. 8, 1985.
11) Engh, B., Solli, O., Aabo, S., Paauw, A.J., 'The Influence of the Corrosive Environment on the Fatigue Life of Aluminium Weldments', loc. cit. 8, 1985.
12) Nordmark, G.E, Kelsey, R.A., 'Fatigue Tests of Weathered Aluminium Bolted and Welded Joints', Proc. 1st Intl. Conf. Aluminium Welding, American Welding Society, Cleveland, 8th April 1981.
13) Nordmark, G.E., Dickerson, P.B., Herbein, W.C., Montemarano, T.W., 'Discontinuities in Aluminium Weldments - Should They be Repaired?' Proc. Int. Conf. on Fatigue of Welded Constructions, S.J. Maddox (ed.), Brighton, England, 7-9 April 1987, The Welding Institute, Abington, 1988.

14) Marsh, C., 'Strength of Aluminium', Alcan Canada Products Limited, Fifth Edition, Canada, 1983.
15) Canadian Standards Association, 'Strength Design in Aluminium', CAN3-S 157-N83, Rexdale, Ontario, 1983.
16) British Standards Institution, 'British Standard Code of Practice BS8118: The Structural Use of Aluminium', BSI, London, 1992.
17) Kohler, W., 'Improvement of Stress Corrosion Resistance of Aluminium Weldments by Shot Peening', Proc. 2nd Int. Conf. on Aluminium Weldments, D. Kosteas, (ed.), Munich, 24-26 May 1982, Aluminium Verlag GmbH, Dusseldorf, 1982.
18) Sharp, M., 'Fatigue', Chapter 11 in Behaviour and Design of Aluminium Structures, McGraw-Hill Inc., New York, 1992.
19) Kosteas, D., 'European Recommendations for Fatigue Design of Aluminium Structures', Proc. 5th Int. Conf. on Aluminium Weldments, D. Kosteas, R. Ondra, F. Ostremann, (eds.), Munich, 27-29 April 1992, Aluminium Verlag GmbH, Dusseldorf, 1992.
20) Report of Committee III.2, 'Fatigue and Fracture', Proc. 12th Int. Ship and Offshore Structures Congress (ISSC), N.E. Jeffrey, A.M. Kendrick (eds.), Vol. 1, Newfoundland, Canada, 12-16 September 1994.
21) Aluminium Association, 'Specifications for Aluminium Structures', Aluminium Construction Manual, Section 1, Washington D.C, 1986.
22) Violette, F.L.M., 'Calculation Procedure for Fatigue Damage Assessment of Ship Structural Details', TPDD Report No. 88/3, Lloyd's Register of Shipping, London, Nov. 1989.
23) British Standards Institution, 'British Standard Code of Practice BS5400: Specification for Steel Concrete and Composite Bridges', BSI, London, 1980.
24) Almar-Naess, A. (Ed.), 'Fatigue Handbook-Offshore Steel Structures', Tapir, Trondheim, 1985.
25) European Convention for Constructional Steelwork, 'European Recommendations for Aluminium Alloy Structures-Fatigue Design', Committee TC2-TG4, 1991.
26) Ondra, R., Kosteas, D., 'Evaluation of Welded Attachments Under Combined Fatigue Loads', Proc. Int. Conf. on Steel and Aluminium Structures, ICSAS'91, S.L. Lee and N.E. Shanmugam, (eds.), Singapore, 22-24 May 1985, Elsevier Applied Science, London, 1985.
27) Olivier, R., Ritter, W., 'Catalogue of S-N Curves of Welded Joints in Steel, Parts 1-5', Deutscher Verband fur Scweisstechnik, Dusseldorf, Germany, 1979-1982.

28) British Standards Institution, 'British Standard Code of Practice BS6235: Code of Practice for Fixed Offshore Structures', BSI, London, 1982.
29) American Petroleum Institute, 'API Recommended Practice for Planning, Designing and Construction of Fixed Offshore Platforms', API RP2A: API, Washington D.C., 1990.
30) British Standards Institution, 'British Standard Code of Practice BS5500: Specification for Unfired Fusion Welded Pressure Vessels', BSI, London, 1988.
31) American Society of Mechanical Engineers, 'Boiler and Pressure Vessel Code for Design by Analysis', Sections III and VIII, Division 2, ASME, 1969.
32) British Standards Institution, 'British Standard Code of Practice CP118: The Structural Use of Aluminium', BSI, London, 1968.
33) Kosteas, D., Saunders, W.W., 'Fatigue Design Format for Welded Aluminium Structures', Proc. Int. Conf. on Steel and Aluminium Structures, R. Narayanan (ed.), Cardiff, UK, 8-10 July 1987, Vol. 2, Elsevier Applied Science, London, 1987.
34) Haibach, E., 'The Allowable Stress Under Variable Amplitude Loading of Welded Joints', Proc. Conf. on Fatigue of Welded Structures, The Welding Institute, 6-9 July 1970.
35) Takashima, H., Machida, S., 'Reliability Analysis of Fatigue Damage of Offshore Structures', Jnl. Society of Naval Architects of Japan, Vol. 163, June 1988.
36) The Committee on Fatigue and Fracture Reliability of the Committee on Structural Safety, 'Fatigue Reliability: Variable Amplitude Loading', Jnl. Structural Division, ASCE, Vol. 108, ST 1, Jan. 1982.
37) Langer, B.F., 'Design of Pressure Vessels for Low Cycle Fatigue', Jnl. Basic Engineering, ASME, Vol. 84, No. 3, Sept. 1962.
38) Schilling, C.G., Klippstein, K.H., 'Fatigue of Steel Beams by Simulated Bridge Traffic', Jnl. Structural Division, ASCE, Vol. 103, ST 8, Aug. 1977.
39) Albrecht, P., Yamada, K., 'Simulation of Service Fatigue Loads for Short Span Highway Bridges', Proc. Symp. Service Fatigue, Loads Monitoring Simulation and Analysis, American Society for Testing and Materials, STP 671, Atlanta, Nov. 1977.
40) Guerney, T.R., 'Some Variable Amplitude Fatigue Tests on Fillet Welded Joints', loc. cit. 13, 1988.

41) Palmgren, A. 'Die Lebensdauer von Kugellagern', Zeitschrift des Vereines, Deutsches Ingenieure, Dusseldorf, Germany, Vol. 68, No. 14, 1924.
42) Abtahi, A., Albrecht, P., Irwin, G.R., 'Fatigue Behaviour of a Periodically Overloaded Transverse Stiffener Detail', Jnl. Structural Division, ASCE, Vol. 102, ST 11, Nov. 1976.
43) Barsom, J.M., 'Fatigue Crack Growth Under Variable Amplitude Loading in A514-B Steel', Proc. Conf. Progress in Flow Growth and Fracture Toughness Testing, American Society for Testing and Materials, STP 536, 1973.
44) Webber, D., Guerney, T.R., 'The Effect of Some Programme Variables on Fillet Weld Cumulative Fatigue Damage Tests Results', loc. cit. 19, 1992.
45) Harrison, J.D., Guerney, T.R., Smith, B., 'Cumulative Damage of Fillet Welded Joints in AlZnMg Alloy', Proc. Conf. on Fatigue of Welded Structures, Welding Institute, Brighton, July 1970.
46) Maddox, S.J., Webber, D., 'Fatigue Testing of Weldments', Proc. ASTM, STP 648, 1978.
47) Maddox, S.J., 'Fatigue Design of Welded Aluminium Alloy Structures', loc, cit. 17, 1982.
48) Maddox, S.J., 'British Fatigue Design Rules for Welded Aluminium', loc, cit. 17, 1982.
49) Kosteas, D., '14 Structural Welded Details in Aluminium-Comparison of Regressional Parameters', Draft Doc. ECCS-TC2, ECCS-TG4 Committee Meeting, Cardiff, England, July 1987.
50) Armstrong, R., 'Design and Fatigue Life Prediction Techniques for Welded Aluminium Joints', loc. cit. 8, 1985.
51) Albrecht, P., 'S-N Fatigue Reliability Analysis of Highway Bridges', Proc. ASTM, STP 798, 1983.
52) Wirsching, P.H., 'Fatigue Reliability for Offshore Structures', Jnl. Struct. Division, ASCE, Vol. 110, No. 10, Oct. 1984.
53) Munse, W.H., Wilbur, T.W., Tellaliau, M.L., Nicoll, K., Wilson, K., 'Fatigue Characterization of Fabricated Ship Details for Design', Report SSC-318, Ship Structure Committee, US Coast Guard, 1983.
54) Martindale, S.G., Wirsching, P.H., 'Reliability Based Progressive Fatigue Collapse', Jnl. Structural Division, ASCE, Vol. 109, No. 8, Aug. 1983.

55) Wirsching, P.H., Chen, Y-N., 'Considerations of Probability-Based Fatigue Design for Marine Structures', Jnl. Marine Structures, Vol. 1, No. 1, 1988.

56) Whittaker, I.C., Besumer, P.M., 'A Reliability Analysis Approach to Fatigue Life Variability of Aircraft Structures', Technical Report AFML-TR-69-65, Wright-Patterson Air Force Base, Ohio, Apr. 1969.

57) Ang, A.,H-S., Munse, W.H., 'Practical Reliability Basis for Structural Fatigue', Proc. Conf. National Structural Engineering, ASCE, New Orleans, April 1975.

58) Jacoby, G.H., Novack, H., 'Comparison of Scatter Under Program Random Loading and Influencing Factors', Probabilistic Aspects of Fatigue, ASTM, STP 511, Dec. 1974.

59) Paris, P.C., 'Stress Analysis of Crack', Proc. ASTM, STP 381, 1970.

60) Rolfe, S.T., Barsom, J.M., 'Fracture and Fatigue Control in Structures', Prentice Hall Inc., N. Jersey, 1977.

61) International Ship Structures Congress, Report of Committee III.1, Genoa, Italy, 1985.

62) Clarke, J.D., 'Fatigue and Crack Initiation and Propagation in Warship Hulls', Proc. Conf. Advances in Marine Structures-2, DRA (Dumfermline), 21-24 May 1991, Dumfermline, Elsevier Applied Science Publishers, London, 1991.

63) Schivje, J., 'Observations on the Predictions of Fatigue Crack Growth Under Variable Amplitude Loading', Fatigue Crack Growth Under Spectrum Loads, American Society for Testing and Materials, STP 595, 1976.

64) Yang, J.N., Trapp, W.J., 'Reliability Analysis of Aircraft Structures under Random Loading and Periodic Inspection', AIAA Jnl., Vol. 12, No. 17, Dec. 1974.

65) The Committee on Fatigue and Fracture Reliability of the Committee on Structural Safety, 'Fatigue Reliability: Development of Criteria for Design', Jnl. Structural Division, ASCE, Vol. 108, ST 1, Jan. 1982.

66) The Committee on Fatigue and Fracture Reliability of the Committee on Structural Safety, 'Fatigue Reliability: Introduction', Jnl. Structural Division, ASCE, Vol. 108, ST 1, Jan. 1982.

67) Newman, J.C., 'A Review and Assessment of the Stress-Intensity Factors for Surface Cracks', Proc. ASTM, STP 687, 1979.

68) Rooke, D.P., Cartwright, D.J., 'Compendium of Stress Intensity Factors', HMSO, London, 1976.

69) Guerney, T.R., Johnston, G.O., 'A Revised Analysis of the Influence of Toe Defects on the Fatigue Strength of Transverse Non-Loading Carrying Fillet Welds', Weld. Res. Int., Vol. 9, No. 3, 1979.
70) Smith, I.J., Hurworth, S.J., 'The Effect of Geometry Changes upon the Predicted Fatigue Strength of Welded Joints', Report No. 244/1984, Welding Research Institute, 1984.
71) Saunders, W.W., Ondra, R., Kosteas, D., 'State of the Art of the ALFABET Project', loc. cit. 19, 1992.
72) Mandara, A., Mazzolani, F.M., Mele, E., 'Fatigue of Aluminium Alloy Joints-Comparison of Codification', loc. cit. 19, 1992.
73) UNI 8634, 'Strutture in Leghe d'alluminio-Istruzioni per il calcolo e l'esecuzione (Aluminium Alloy Structures-Instructions for Design and Construction)', UNIMET, Milano, 1985.
74) Saunders, W.W.Jr., 'Fatigue Behaviour of Aluminium Alloy Weldments', Welding Research Council Bulletin, 1972, No. 171 and 1983, No. 286, Welding Research Council, New York, U.S.A.
75) Guerney, T.R., Maddox, S. J., 'A Re-analysis of Fatigue Data for Welded Joints in Steel', Welding Research International, Vol. 3, No. 4, 1973.
76) National Research Institute for Metals, 'NRIM Fatigue Data Sheets', National Research Institute for Metals, Tokyo, Japan.
77) Park, S.K., Lawrence, F.V., 'Fatigue Characterization of Fabricated Ship Details for Design-Phase II', Report SSC-346, Ship Structure Committee, 1990.
78) Beach, J.E, Johnson, R.E., Koehler, F.S., 'Fatigue of 5086 Aluminium Weldments', loc, cit. 17, 1982.
79) Niemi, E., Nurkkala, P., Knuttila, E., 'Fatigue Testing of Welded Aluminium Ship Details', loc. cit. 8, 1985.
80) Terazawa, K., Kurino, I., Kubota, A., 'Studies on the Properties of Aluminium Alloy Steel Transition Pieces for Structural Transition Joints (STJ) of Ship Structure', loc, cit. 17, 1982.
81) Terazawa, K., 'Studies on the Properties of Aluminium Alloy Steel Transition Pieces for Structural Transition Joint (STJ) of Ship Structure-I', loc. cit. 12, 1981.
82) Hobbacher, A., 'The Benefit of Fatigue Improvement Techniques at Welded Aluminium Joints in Context of Scatter of Non-Improved Welds', loc. cit. 19, 1992.

83) Bayley, M.J., 'Fabrication and Protection', Proc. Seminar on 'The Structural Use of Aluminium', The Institution of Structural Engineers, London, 1st October 1985.
84) Kruger, U., Priesnitz, U., 'The Effects of Discontinuities on the Fatigue Behaviour of Aluminium Welds', loc, cit. 17, 1982.
85) Slater, G., 'The Effect of Repair Welds on Service Performance', Welding Journal, March 1985.
86) Hardy, R.R., Wells, M.E., 'The Effect of Fabrication Methods on the Fatigue Performance of Welded 5086-H116 Aluminium Alloy', loc, cit. 17, 1982.
87) Polmear, I.J., 'Post-Weld Treatments to Improve Fatigue Performance of Aluminium Alloy Weldments', loc, cit. 17, 1982.
88) Allan, R., Bird, J., Clarke, J., 'Use of Adhesives in Repair of Cracks in Ship Structures', Materials Science and Technology, Vol. 4, Oct. 1988.
89) Hashim, S.A., Cowling, M.J., Winkle, I.E., 'Design and Assessment Methodologies for Adhesively Bonded Structural Connections', Int. Jnl. Adhesion and Adhesives, Vol. 10, No. 3, July 1990.
90) Hugill, P.N., Sumpter, J.D.G., 'Fatigue Crack Growth Arrest by Stop-Crack Hole Drilling Techniques', Unpublished Report, ARE Dumfermline, Scotland.
91) Marsh, C. 'The Ultimate Limit State for Aluminium Welds', loc, cit. 17, 1982.
92) Soetens, F., 'Connections in Aluminium Alloy Structures', loc. cit. 33, 1987.
93) Cullimore, M.S.G., 'Static Design of Welded Joints to BS8118: Structural Use of Aluminium', loc. cit. 19, 1992.
94) Saunders, W.W., Rager, D.D., 'New American Structural Welding Code for Aluminium Structures', loc, cit. 17, 1982.
95) Sharp, M., 'Joint Behaviour', Chapter 10 in Behaviour and Design of Aluminium Structures, McGraw-Hill Inc., New York, 1992.
96) Ogle, M., Blewett, R.V., 'Weld Quality, Inspection and Acceptance Specification Recommended by BS8118, Part 2', loc. cit. 19, 1992.
97) Cowling, M.J., Burdekin, F.M., Haswell, J., Light, M.F., Xia, Y., Wamuziri, S.C., 'The Impact of Reliability Based Fatigue Assessment and Structural Redundancy on Inspection Planning for Offshore Structures ', Proc. 5th Int. Symp. on Integrity of Offshore Structures, D. Faulkner, M.J. Cowling, A. Incecik, P.K. Das, (eds.), Glasgow, June 1993, EMAS, 1993.

98) Sandstrom, R., 'Harmonisation of Weldability Data for Aluminium Alloys', loc. cit. 19, 1992.
99) Tanaka, T., Yoshida, S., Kambayashi, K., 'Effect of Alloy Composition on Weld Cracking in AlZnMg Alloy Welds', loc, cit. 17, 1982.
100) Ogle, M.H., Maddox, S.J., 'Design Rules for Fatigue of Aluminium Structures According to BS8118 Part 1', loc. cit. 19, 1992.
101) Poalas, K., Kosteas, D., 'Considerations for Reliability-Based Fatigue Life Estimations of Structural Parts in Aluminium', loc. cit. 8, 1985.
102) Jaccard, R., 'Fatigue Life Prediction of Aluminium Components Based on S-N Curve Simulation', loc. cit. 17, 1982.

Tables

Table 3.1: Factors affecting the fatigue life of welded joints and their influence [100].

Factors Effecting Fatigue Life			Degree of Influence According to Situation				
Primary Factors	Sub Group	Detailed Factors	1. Degree of Control by Designer	2. Dependency on Production Procedures	3. Effect on Fatigue Life	4. Degree of Reporting in S-N Test Literature	5. Degree of Differentiation in Current Design Rules
MATERIAL PROPERTIES	Composition	parent	●	0	0	●	0
		HAZ	0	•	0	0	0
		weld metal	●	0	0	•	0
	Strength	parent	●	0	0	●	0
		HAZ	0	●	0	0	0
		weld metal	0	•	0	0	0
	Grain Structure	parent	0	0	•	0	0
		HAZ	0	●	•	0	0
		weld metal	0	●	•	0	0
GEOMETRY	Member(s)	Shape	●	-	•	●	0
		Size and thickness	●	0	•	●	•
		Straightness and flatness	•	●	•	0	0
	Joint	Type	●	-	●	●	●
		Orientation w.r.t member	●	-	●	●	●
		Relative proportions	●	0	●	•	•
		Fit-up	•	●	●	0	0
	Weld	Type	●	-	●	●	●
		Orientation w.r.t joint	●	-	●	●	●
		Size	●	•	•	•	•
		Quality *	0	●	●	O	•
LOADING EFFECTS	Static stress	Primary	●	0	●	●	0
		Secondary	•	•	•	0	0
		Residual **	0	●	●	0	0
	Dynamic stress	Primary	●	0	●	●	●
		Secondary	•	•	●	0	0
		Hot spot	0	•	●	0	•
		Stress Intensity	0	●	●	0	0
	Stress orientation		●	0	●	●	●
ENVIRONMENT	Chemical		•	0	•	•	•
	Protection		•	●	•	0	0

Key: ● High • Medium 0 Low - Nil

* includes profile and other discontinuities

** weld shrinkage and assembly stresses

Table 3.2: Expressions for estimating the secondary bending stress due to misalignment [2].

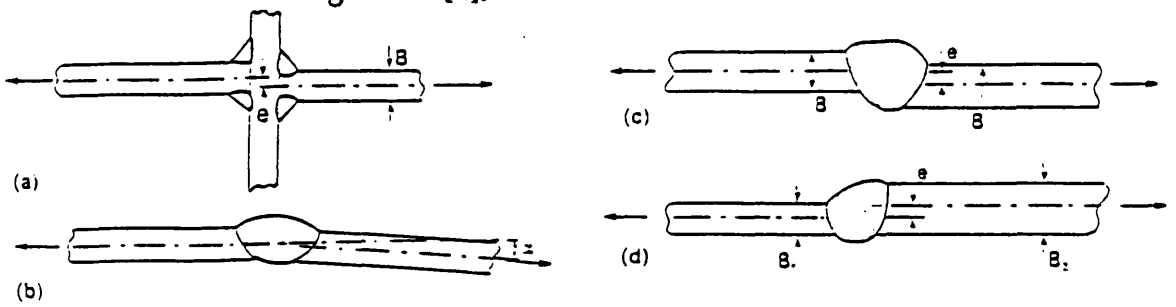

Type	Bending stress. S_b
Axial misalignment in butt or cruciform joints between flat plates:	
- of equal thickness	$\frac{3e}{B} \cdot S_a$
- of unequal thickness	$\frac{6e}{B_1}\left[\frac{B_1^{1.5}}{B_1^{1.5}+B_2^{1.5}}\right]S_a$ $B_1 < B_2$
Axial misalignment in fillet welded cruciform joints *	$\frac{e}{B+H} \cdot S_w$ where S_w = stress on weld throat H = weld leg length
Axial misalignment in butt welded seam of pressurised vessel or pipe †	$\frac{6e}{B_1(1-\nu^2)}\left[\frac{B_1^{n}}{B_1^{n}+B_2^{n}}\right]S_a$ where ν = Poisson's ratio $B_1 = < B_2$
Angular misalignment in butt or cruciform joints between flat plates. Boundary conditions equivalent to:	
- fixed ends	$\frac{3}{4}\alpha \frac{L}{B} \cdot S_a$
- pinned ends	$\frac{3}{2}\alpha \frac{L}{B} \cdot S_a$
Angular misalignment in seam of pressurised vessel or pipe ‡	$\frac{6d}{B} \cdot S_a$

Key: * Relevant to fatigue failure in weld throat from root
† n = 1.5 for circumferential seams and seams in spheres
n = 0.6 for longitudinal seams
‡ d = deviation from true circular shape. Assumes pinned end boundary conditions

Table 3.3: Relative corrosion ratings of aluminium alloys [18].

Alloy class	Commercial alloy example	Major alloying elements	General corrosion rating*
	Wrought, Strain-Hardened		
1XXX	1100	Unalloyed	A
3XXX	3003	Manganese	A
5XXX	5052, 5154	Magnesium	A
	Wrought, Heat-Treated		
6XXX	6061, 6063	Magnesium, silicon	B
2XXX	2027, 2017, 2024	Copper	D
7XXX	7075, 7178	Zinc, magnesium, copper	C

*Relative ratings are in decreasing order of merit. Alloys with B ratings can be used in industrial and seacoast atmosphere; alloys with lower ratings generally should be protected, especially on faying surfaces.

Table 3.4: R-dependent and R-independent aluminium fatigue design codes [19].

R-independent	R-dependent
Ontario Highway Bridge (1983)	DVS 1608 (1969)
Aluminium Association (1985)	ALCAN (1983)
BS8118 (1985, 1989)	UNI 8634 (1985)
ERAAS Fatigue Design (1985)	Austrian Code (1988)
	Assc. American Railways (1980)
	CP 118 (1969)
	ERAAS (1992)

Table 3.5: Comparison of fatigue predictions between aluminium and steel design codes (at 2×10^6 cycles) [19].

Steel: DIN 15018, DIN 4132, DS 804, DASt Ri 011, EC 3, ECCS TC6
Aluminium: ERAAS Fatigue Design Final Document

Detail	Aluminium	Steel		Ratio St/Al	
		range of recomm.	EC 3 ECCS TC6	range	EC 3 ECCS TC6
A1	130	116-194	160	**0,89-1,49**	**1,23**
A2	85	116-194	160	**1,39-2,28**	**1,88**
A3	95	116-194	160	**1,22-2,04**	**1,68**
A4	70	116-194	160	**1,66-2,77**	**2,28**
A5	0.9*A	87-143	0,88*A	**0,74-2,27**	**1,20-2,23**
B1	55	93-194	125	**1,69-3,52**	**2,27**
B2	50	(77-90)	(90)	**(1,54-1,80)**	**(1,80)**
B3	45	76-90	80-40 (?)	**1,69-2,00**	**1,79-0,89**
B4	40	52-64	71-50	**1,30-1,60**	**1,78-1,25**
B5	45	93-194	125	**2,07-4,31**	2,78
B6	40	(77-90)	(90)	**(1,93-2,25)**	**(2,25)**
B7	35	76-90	80	2.17-2,57	**2,29**
B8	30	52-64	40	**1,73-2,13**	**1,33**
B9	40	93-194	125	2,32-4,85	3,12
B10	35	69-90	90	**1,97-2,57**	2,57
B11	30	52-64	40	**1.73-2,13**	**1.33**
C1	60	93	---	**1,55**	---
C2	45	86-107	100	**1.91-2,38**	**2,22**
D1	45	77-100	100	**1,71-2,22**	**2,22**
D2	40	77-100	100	**1,92-2,50**	2,50
D3	35	58-80	80	**1,66-2,29**	**2,29**
E1	35	50-80	80-71	**1,43-2,29**	**2,29-2,03**
E2	23	39-64 (?)	---	**1,70-2,78**	---
E3	35	52-90	90	**1,49-2,57**	2,57
E4	18	39-51	45	**2,17-2,83**	2,50
E5	35	50-76	50 (?)	**1,43-2,17**	**1,43**
E6	23	39-51	(?)	**1,70-2,22**	---
E7	18	(?)	(?)	---	---
E8	23	(?)	(?)	---	---
F1	30	59-90	71	**1,97-3,00**	2,37
F2	25	36-39	36	**1,44-1,56**	**1,44**
F3	20	39-58	50-36	**1,95-2,90**	**2,50-1,80**

(?): questionable or problematic classification
(-): no special classification for extruded shapes in steel

Table 3.6: Bias and COV values for the components of B [52].

Random variables representing sources of uncertainty in fatigue stress estimates	Bias[a]	COV[b]
B_M	0.90–1.30[c]	0.10–0.30[c]
B_S	0.60[d]–1.20	0.40[d]–0.60[e]
B_F	0.60[f]–1.10	0.10–0.30
B_N	0.80–1.10	0.20–0.40[g]
B_H	0.80[g]–1.20	0.10–0.50[g]

[a]Bias = actual load or stress/load or stress estimated by current analysis procedure; for each B_i, the bias can be interpreted as the median value $\breve{B}_i$.

[b]COV = $\sqrt{\exp(\sigma^2) - 1}$, in which $\sigma = \ln(X_U/X_L)/6$; and X_U and X_L = upper and lower limits of X.

[c]$\breve{B}_S = \breve{B}_P \cdot \breve{B}_D = (0.9)(0.7) \cong 0.60$ in which P = percent occurrence of each seastate; and D = directionality.

[d]This relatively large figure, which dominates C_B, is due to the sensitivity of the dynamic response to small variations in T_O. The figure of 0.40 is due to this effect only.

[e]This figure was obtained by Eq. 10 by assuming "maximum" COV's of 0.4 for dynamic response, and 0.3 each for directionality and percent occurrence effects. The resulting figure of 0.60 is considered to be the largest reasonable value.

[f]This bias occurs when wave spreading is not considered in the development of the response spectra.

[g]These extreme values should be used only when supporting evidence exists.

Table 3.7: Evaluation of fatigue damage modelling uncertainties using different data sets [52].

Design factors		Data Set A	B	C	D	E	F
S-N curve, in kips per square inch units	m	4.38[a]	4.38[a]	4.42[a]	3.00[c]	3.22[d]	3.00[f]
	$\bar{K}$	4.6E12	4.6E12	1.55F12	5.25E10	1.29E11	1.46E10
	C_K	0.73	0.73	1.35	0.73	1.25	0.67
Rainflow correction	λ	0.79	0.79	0.79	0.86	0.85	0.86
Damage ratio	Δ	1.00	1.00	1.00	1.00	1.00	1.00
	C_Δ	0.30	0.30	0.30	0.30	0.30	0.30
Stress modeling error	$\breve{B}$	0.80[e]	0.70[f]	0.70[f]	0.70[f]	0.70[f]	0.70[f]
	C_B	0.17	0.50	0.50	0.50	0.50	0.50
Average frequency, f_0, in hertz		0.25	0.25	0.25	0.25	0.25	0.25
Safety index implied by[g] RP2A design wave peak stress rule (60 ksi rule), β		5.34[h]	2.78	2.09	2.62	2.57	1.83

[a]Data from Commentary of API RP2A, p. 81, Fig. C2.5.3-2. (13).

[b]AWS-X data, elastic range only. See Ref. 14.

[c]T and K joint data provided by member of Technical Advisory Committee (20).

[d]T and K joint data: an "improved" version of data set *D*.

[e]Values provided by member of Technical Advisory Committee. Value of C_B now thought to be low.

[f]Values provided by member of Technical Advisory Committee. Numbers are now considered reasonable for "worst case" analysis in which wave spreading and wave directionality are not considered.

[g]As computed by solving for β_0 in Eq. 8.

[h]Relatively high value due to small value of C_B. See superscript e above.

[i]The "T-curve" from Ref. 11.

Note: For a 20-year life, S_R = 53.2 ksi; ξ = 0.69 for 20 year-wave. (Same structure would have S_R = 100 ksi and ξ = 0.57 for 100-year wave climate.)

Table 3.8: COV values of cycles to failure, V_N, as suggested by Whittaker for design purposes [66].

Material	V_N, as a percentage
Steel, $S_u \leq 240$ ksi	36
Steel, $S_u > 240$ ksi	48
Aluminum Alloys	27
Titanium Alloys	36

Table 3.9: Statistics of damage at failure, Δ, assuming a lognormal distribution (n is the number of specimens) [36].

Variables	$\bar{\Delta}$ Mean of Δ	$\tilde{\Delta}$ Median of Δ	s Standard deviation of Δ	Coefficient of variation of Δ
Crichlow, et al. (12); an amalgamation of test data of many configurations and materials of flight vehicle structures including full scale *P*-51 and *C*-46 airplane wing test ($n = 266$)	1.53	1.30	0.962	0.627
Schijve (50); amalgamation of results from 19 reports; all specimens 2024 and 7075 aluminum	1.72	1.23	1.68	0.980
Richart and Newmark (47); axially loaded large (3 1/2 × 1/2 in.) specimens of ASTM-A7 ($n = 31$)	1.27 (1.79)*	1.23	0.341	0.269
Richart and Newmark (47); rotating beam small specimens (dia. = 0.160 in.) of ASTM-A7 ($n = 29$)	1.47 (2.06)*	1.39	0.519	0.353
Topper, Sandor, and Morrow (62); strain controlled tests on 2024-T4 aluminum ($n = 18$)	1.15	1.14	0.186	0.161
Dowling (15); 2024-T4 specimens; mostly in the elastic range, but some with large plastic strains; rainflow method used to count cycles ($n = 83$)	0.863	0.823	0.271	0.314
Topper and Sandor (63); strain controlled tests on 2024-T4 aluminum with tensile and compressive mean stresses ($n = 11$)	0.836	0.809	0.219	0.262
Miner (36); tests run at two or more stress levels on 24S-T Alcad ($n = 11$)	0.980	0.949	0.251	0.256
Schilling (52); welded cover plated beam specimens of A36 and ASTM A514 under simulated random bridge loading ($n = 36$)	1.44	1.25	0.78	0.54
SAE Fatigue Design & Evaluation Committee; tests on Man-Ten & RQC-100; notch specimen with cyclic plasticity at notch root; See Table III; ($n = 54$)	1.46	1.09	1.30	0.889
Swanson (60); an amalgamation of random fatigue test data ($n = 671$); Values based on an assumption that $C_\Delta = 0.60$, and $F_\Delta(1.0) = 0.47$	1.21	1.04	0.726	0.60

*Esumates of μ_Δ using a "minimum SN curve."

Table 3.10: Statistical summary of models of composite data [36].

Variable	Mean $\bar{\Delta}$	Median $\tilde{\Delta}$	C.O.V. (V_Δ)	Percentage less than 1.0
Composite (all data; n = 537)	1.35	1.13	0.643	42
Smooth specimen composite (all data except Crichlow Schilling, and SAE; n = 183)	1.06	0.997	0.380	51
Composite (all data except Crichlow's 266 points; n = 271)	1.17	1.01	0.612	49
Aluminum (all data; n = 389)	1.33	1.11	0.650	43
Steel (all data; n = 148)	1.37	1.16	0.638	40
Full scale structural components (Crichlow & Schilling's data, n = 300)	1.50	1.27	0.620	34

Table 3.11: Mandara et al's comparison of the equivalent detail categorisation of the Alcan, UNI, BS8118, Aluminium Association and ECCS fatigue design codes [72].

	ALCAN	UNI	BS	A.A.	ECCS	DETAIL DESCRIPTION
1	A	A	50	A	A3	Base metal
2	B'	B	41	B	B1	Butt weld transverse with overfill ground flush
3	C	D	30	C	B2	Butt weld transverse with overfill
4	C	C	30	B	C2	Longitudinal butt weld with overfill
5	C	-	41	B	D1	Longitudinal fillet weld without interruptions
6	D	-	30	-	D2	Longitudinal fillet weld with interruptions
7	E	D	27	F	E8	Transverse attachment
8	D	F	23	E	F1	Butt or fillet weld cruciform joint
9	E	F	20	E	F1	Butt or fillet weld cruciform joint
10	E	G	23	F	E6	Flange attachment
11	E	G	17	D	E4	Flange attachment

Table 3.12: The main features the Alcan, BS8118, UNI8634, Aluminium Association and the ECCS recommendations [72].

	ALCAN	UNI	BS	A.A.	ECCS
1 Type of alloy	rules apply to 3000, 5000, 6000 and 7000 alloy series, but without any distinction.	rules apply to 5000, 6000 and 7000 alloy series; material influence on strength parameters is taken into account.	rules apply to 3000, 5000, 6000 and 7000 alloy series, but without any distinction; other alloy types can be also used.	no difference is made among the type of alloys.	rules apply to all alloys listed in ERAAS; distinction among 5000, 6000 and 7000 alloy series is made for the base metal only.
2 Safety concept	the safety concept is not discussed.	rules are based on the safe-life limit state.	rules are based on the safe-life limit state (or damage tolerant fail-safe limit state if economically justified).	the safety concept is not discussed.	rules are based on the safe-life limit state even if a procedure is supplied for fail-safe limit state design.
3 Safety factor	no safety factor is supplied.	rules provide two values of the safety factor ν_1 and ν_2 for static and cyclic loads respectively.	rules provide two values of the safety factor γ_{mf} and γ_L for fatigue inspection and design life respectively.	no safety factor is supplied.	no safety factor is supplied.
4 Details	6 joint classes are defined according to their mechanical and geometrical features.	7 joint classes are defined according to their mechanical and geometrical features.	29 joint classes are defined, divided into: 1. non welded details 2. welded details on loaded members 3. welded details at end connections.	20 structural details are defined belonging to 6 strength categories.	32 joint details are defined belonging to 6 classes, according to their mechanical and geometrical features.
5 S-N curves	for each detail class the $\Delta\sigma/2$-N curves are provided in graphic form.	for each detail class the fatigue strength $f_{d,\mu}$ is provided as a function of: - cycles number N - alloy type - stress ratio μ - load versus.	for each detail class the $\Delta\sigma$-N curves are provided in graphic and tabular form.	for each strength category the $\Delta\sigma$-N curves are provided in tabular form; these curves are not continuos.	for each detail class the $\Delta\sigma$-N curves are provided in graphic and tabular form.
6 influence of thickness	it is not taken into account.	it is not taken into account.	it is not taken into account.	it is not taken into account.	for t>25mm fatigue strenght is reduced according to the formula $\Delta\sigma_R(t) = \Delta\sigma_R(25/t)^{0.25}$
7 influence of the stress ratio R	a suitable diagram is supplied to take into account the influence of the stress ratio R.	the dependence of the design strength on R is expressed by means of Moore diagrams and tables.	$\Delta\sigma$ values do not depend on R.	$\Delta\sigma$ values depend on R for mechanically fastened joints only.	for R < 0.5, an enhancement factor of $\Delta\sigma$ is considered.

Table 3.13: **Hobbacher's recommendations on the most appropriate and efficient post-weld treatments for four types of welded aluminium details and relative improvement factors [82].**

Structural detail	Treatment method	Factor
transverse butt weld	laser dressing TIG dressing brush peening shot blasting	1.4
cruciform joint fillet welds	hammer peening	1.4
longitudinal stiffener	grinding and hammer peening	1.4
transverse stiffener	brush peening (no rolled lips)	1.4

Table 3.14: **Results of Sandstrom et al's evaluation of the weldability of EAA (ALUSELECT) alloys for five welding processes (least preferred=2, most preferred=6) [98].**

Alloy	Composition (wt. %)	MIG/ TIG	Electron Beam	Gas	Spot	
					Hard	Soft
AA2030	Al 3.9Cu 1.2Pb 0.9Mg 0.6Mn	2		2	4	
AA2017A	Al 4.0Cu 0.7Mn 0.7Mg 0.5Si	3	5	2	5	5
AA2007	Al 4.0Cu 1.2Pb 1.1Mg 0.8Mn	2		2	4	
AA2024	Al 4.4Cu 1.5Mg 0.6Mn	3	5	2	5	5
AA2014A	Al 4.5Cu 0.8Mn 0.7Si 0.5Mg	3	5	2	5	5
AA2014	Al 4.5Cu 0.9Si 0.8Mn 0.5Mg	3	5	2	5	5
AA2011	Al 5.5Cu 0.4Bi 0.4Pb	2		2	3	
AA6060	Al 0.5Mg 0.5SiFe	6	5	5	5	
AA6005A	Al 0.6Mg 0.7SiMnCr	6	5	5	5	
AA6063	Al 0.7Mg 0.4Si	6	5	5	5	
AA6082	Al 0.9Mg 1.0Si 0.7Mn	6	5	5	5	4
AA6061	Al 1.0Mg 0.6SiCuCr	6	5	5	5	4
AA7020	Al 4.5Zn 1.2MgMnCrZr	5	5	5	5	
AA7075	Al 5.6Zn 2.5Mg 1.6CuCr	3	5	3	5	5
AA7010	Al 6.2Zn 2.4Mg 1.8CuZr	3	5	3	5	
AA5005	Al 0.8Mg	6	6	5	6	5
AA5005A	Al 0.9Mg	6	6	5	6	5
AA5251	Al 2.0Mg 0.3Mn	6	6	5	6	5
AA5052	Al 2.5MgCr	6	6	5	6	5
AA5454	Al 2.7Mg 0.8MnCr	6	6	4	6	5
AA5754	Al 3.1MgMnCr	6	6	4	6	5
AA5154A	Al 3.5MgMnCr	6	6	4	6	5
AA5086	Al 4.0Mg 0.5MnCr	6	6	4	6	5
AA5083	Al 4.5Mg 0.7MnCr	6	6	4	6	5
AA3103	Al 1.2Mn	6	6	6	5	4
AA3003	Al 1.3MnCu	6	6	6	5	4
AA1200	Al99.0	6	6	6	5	4
AA1050A	Al99.5	6	6	6	5	4

Table 3.15: Identification of the most appropriate welding techniques for individual aluminium alloys.

Welding Process	Preferred	Avoided
MIG/TIG	6000 series, Non-hardened, 7000 series (no copper)	2000, 7000 (with Cu), lead alloys
Gas	Pure, 3000, 6000 series	Copper alloys
Electron Beam	All alloys	-
Spot*	High strength alloys, -H, -T tempers	Low strength alloys -O, -F tempers

(*) Temper dependent weldability.-O (annealed), -F (untreated, as hot worked),-H (hard cold worked), -T (aged).

Table 3.16: Combinations of parent metal and filler metal as recommended by BS8118 [16].

Selection of filler wires and rods for inert-gas welding

Parent metal combination[1]

1st part	2nd Part							
	LM5 castings	LM6 LM5 castings	3103 3106	1200	7020	6061 6063 6082	5154A 5251 5454	5063
5063	Type 5 Type 5 Type 5	NR[3]	Type 5 Type 5 Type 5	Type 5 Type 5 Type 5	5556A Type 5 5556A	Type 5 Type 5 Type 5	Type 5 Type 5 Type 5	5556A Type 5 Type 5
5154A 5251 5454	Type 5 Type 5 Type 5	NR[2]	Type 5 Type 5 Type 5	Type 5 Type 5 Type 5	Type 5 Type 5 Type 5	Type 5 Type 5 Type 5	Type 5 Type 5[3] Type 5	
6061 6063 6082	Type 5 Type 5 Type 5	Type 4 Type 4 Type 4	Type 4 Type 4 Type 4	Type 4 Type 4 Type 4	Type 5 Type 5 Type 5	Type 4/5 Type 4 Type 4		
7020	Type 5 Type 5 Type 5	NR[2]	Type 5 Type 5 Type 5	Type 5 Type 5 Type 5	5556A Type 5 Type 5			
1200	Type 5 Type 5 Type 5	Type 4 Type 4 Type 4	Type 4 Type 3/4 Type 4	Type 1[4] Type 1 Type 1[4]				
3103 3106	Type 5 Type 5 Type 5	Type 4 Type 4 Type 4	Type 3[4] Type 3 Type 3[4]					
LM6 LM25 Castings	NR[2]	Type 4 Type 4 Type 4						
LM5 Castings	Type 5 Type 5 Type 5							

Welding filler metals

Filler metal group	BS alloy designation[1]	ISO alloy designation[2]	Durability rating
Type 1	1080A 1050A	Al99,8 Al99,5	A
Type 3	3103	Al Mn1	A
Type 4	4043A 4047A[3]	Al Si5(A) Al Si12(A)	B
Type 5	5056A 5356 5556A 5183	Al Mg5 Al Mg5Cr(A) Al Mg5,2MnCr Al Mg4,5Mn	A A

[1] See BS 2901 : Part 4 for chemical composition.

[2] Or nearest equivalent.

[3] 4047A is specifically used to prevent weld metal cracking in joint involving high dilution and high restraint. In most cases 4043A is preferable.

[1] Filler metals for parent combination to be welded are shown in one box, which is located at the intersection of the relevant parent metal row and column. In each box, the filler metal for maximum strength is shown in the top line; in the case of 6* * * and 7020 alloys, this will be below the fully heat-treated parent metal strength. The filler metal for maximum resistance to corrosion is shown in the middle line. The filler metal for freedom from persistent weld cracking is shown in the bottom line.

[2] NR = Not recommended. The welding of alloys containing approximately 2 % or more of Mg with Al-Si (5 % to 12 % Si) filler metal (and vice versa) is not recommended because sufficient Mg_2Si precipitate is formed at the fusion boundary to embrittle the joint.

[3] The corrosion behaviour of weld metal is likely to be better if its alloy content is close to that of the parent metal and not markedly higher. Thus for service in potentially corrosive environments it is preferable to weld 5154A with 5154A filler metal or 5454 with 5554 filler metal. However, in some cases this may only be possible at the expense of weld soundness, so that a compromise will be necessary.

[4] If higher strength and/or better crack resistance is essential, type 4 filler metal can be used.

NOTE 1. Table derived from BS 3019 : Part 1 and BS 3571 : Part 1.

NOTE 2. For particular filler metal alloys in each alloy type see table

Figures

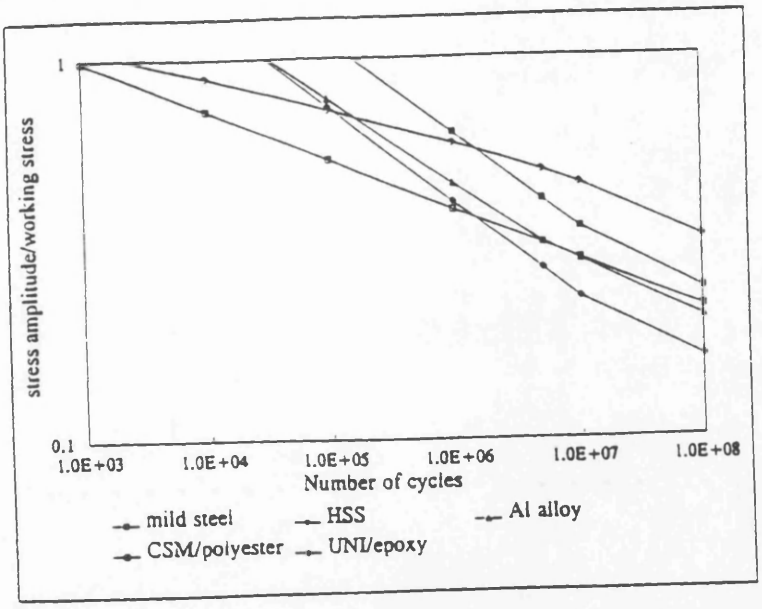

Figure 3.1: Comparison of relative fatigue strengths of lightweight materials [1].

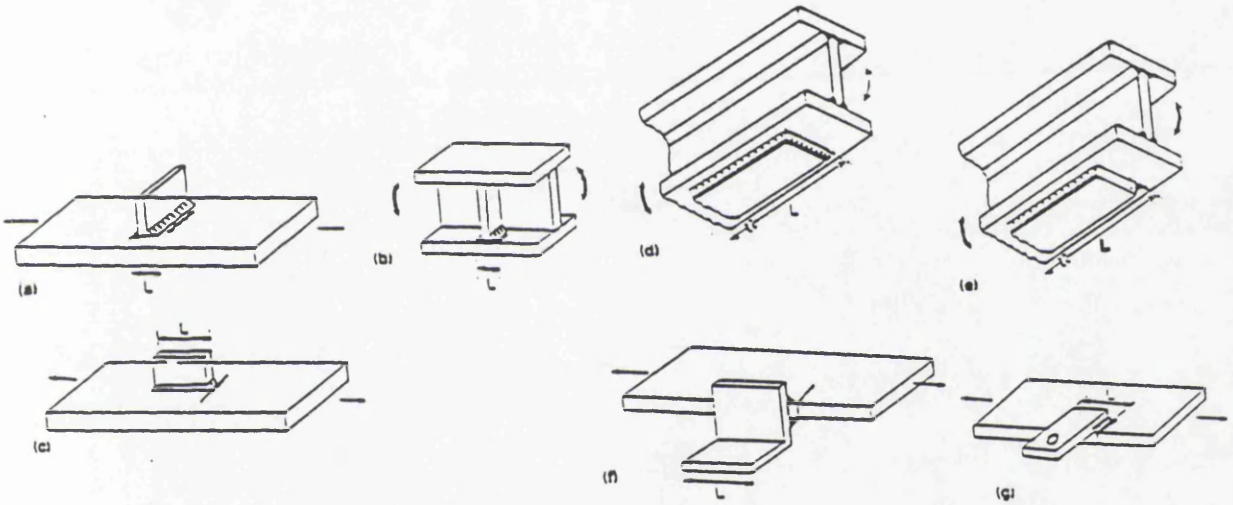

Figure 3.2: Dimensions relevant to size effects in transverse and butt welded joints [2].

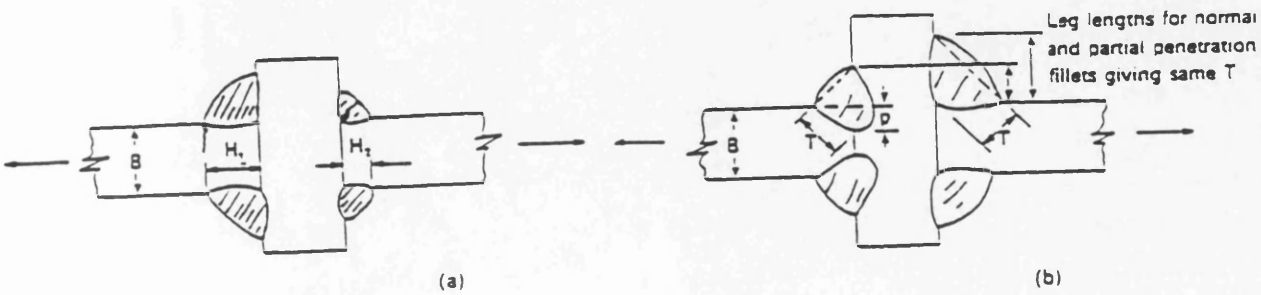

Figure 3.3: Penetration effects on the fatigue crack location on a transversely loaded fillet weld [2].

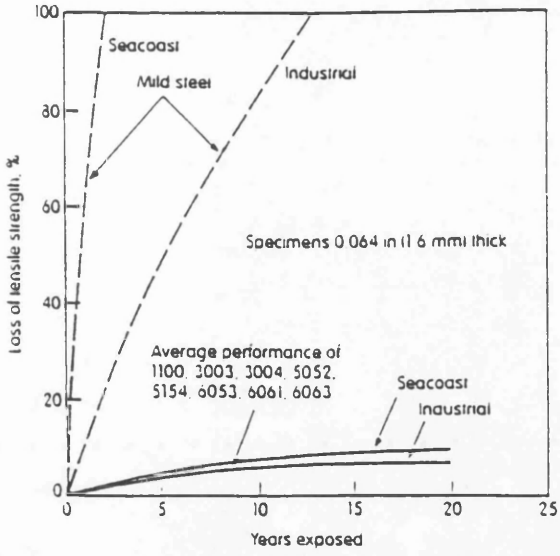

Figure 3.4: **Loss of strength due to weathering corrosion [9]**

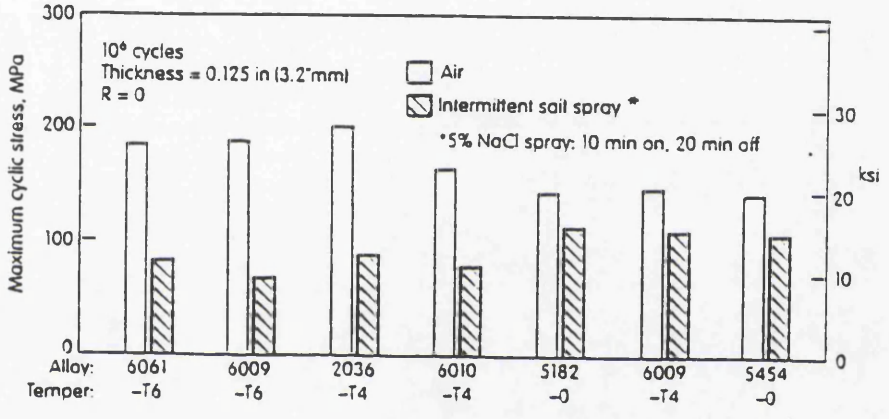

Figure 3.5: **Effect of environment on axial fatigue strengths on unwelded aluminium alloys [18].**

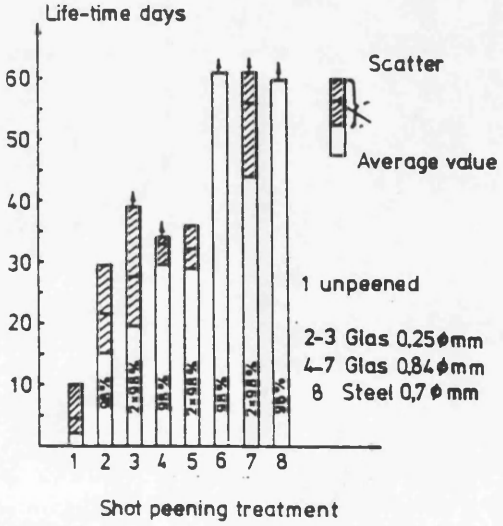

1) unpeened
2) glass beads 0,25 Ø mm, 98 %
3) glass beads 0,25 Ø mm, 2 x 98 %
4) glass beads 0,84 Ø mm, 98 %
5) glass beads 0,84 Ø mm, 2 x 98 %
6)
7) glass beads 0,84 Ø mm with optimized parameters
8) steel shot 0,7 Ø mm, 98 % + wet peened by glass beads

Figure 3.6: **The beneficial effects of different shot-peening methods on the corrosion strength of aluminium joints [17].**

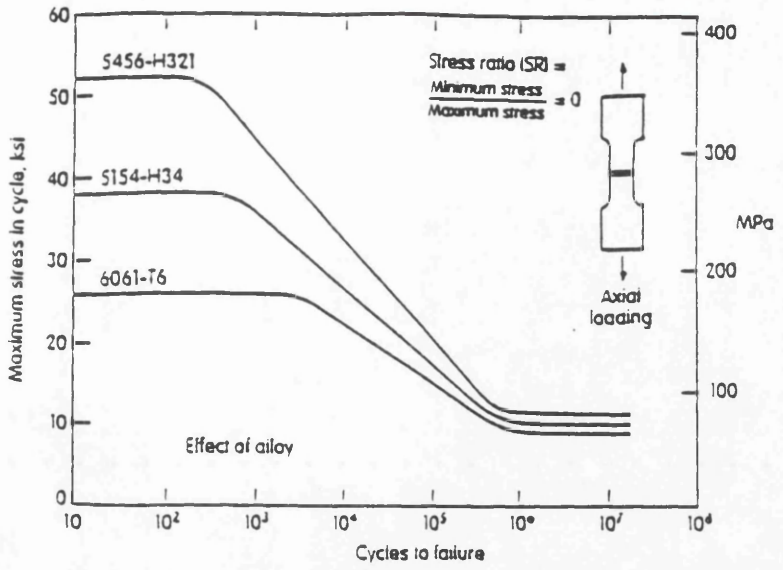

Figure 3.7: Effect of alloy type on the fatigue strength of butt welds [18].

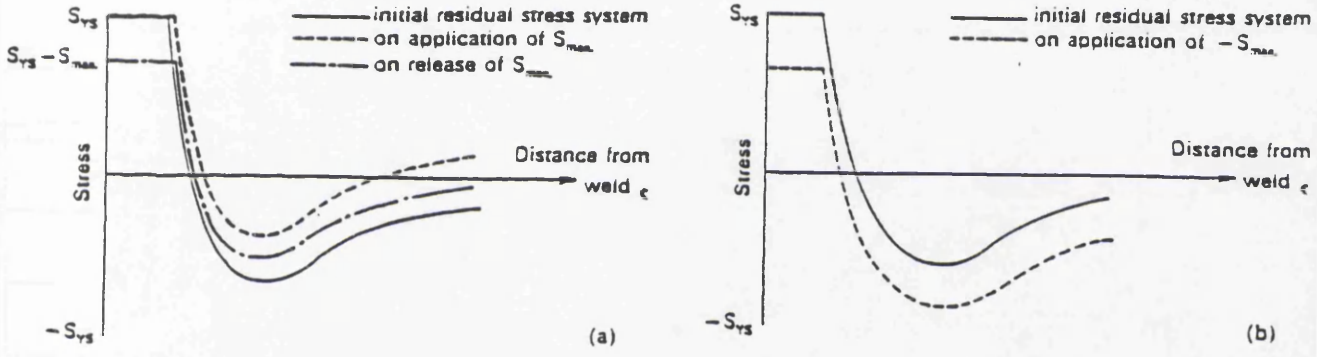

Figure 3.8: Effect of cyclic (a) tensile and (b) compressive loads on the residual stresses and fatigue strength of a welded joint [2].

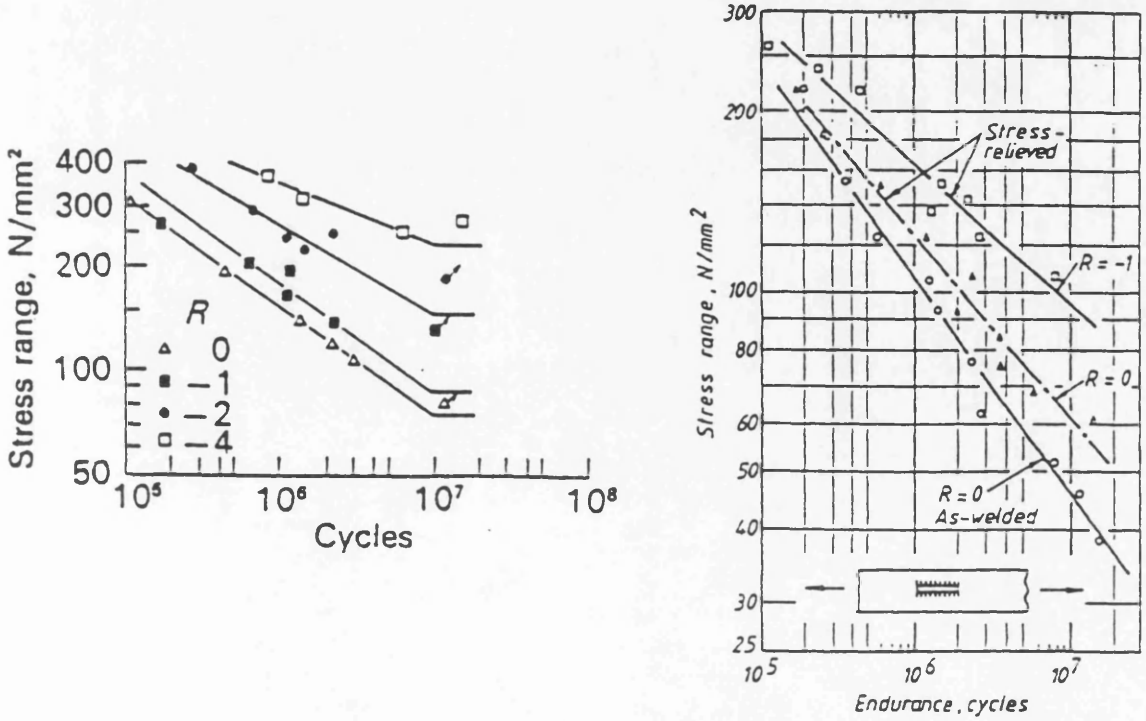

Figure 3.9: Influence of stress ratio and stress relief on fatigue strength of steel fillet [6].

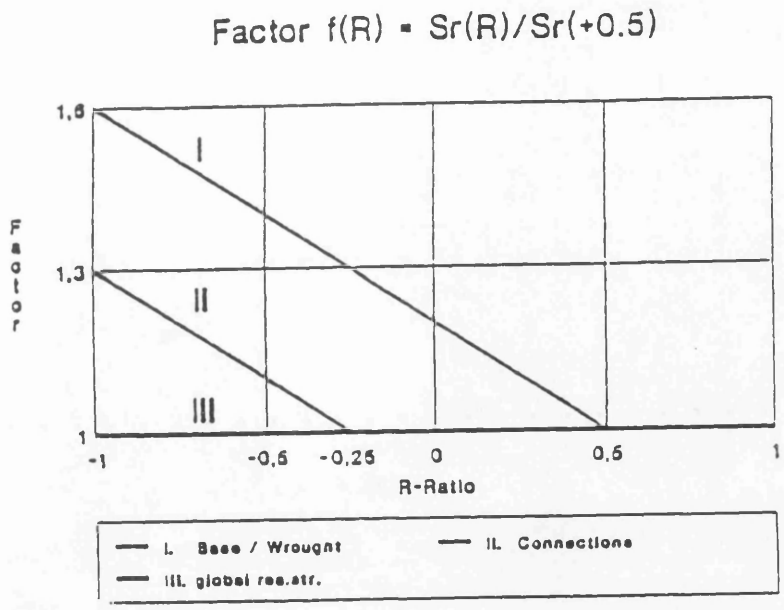

Figure 3.10: R-ratio enhancement factor in the ERAAS code [19].

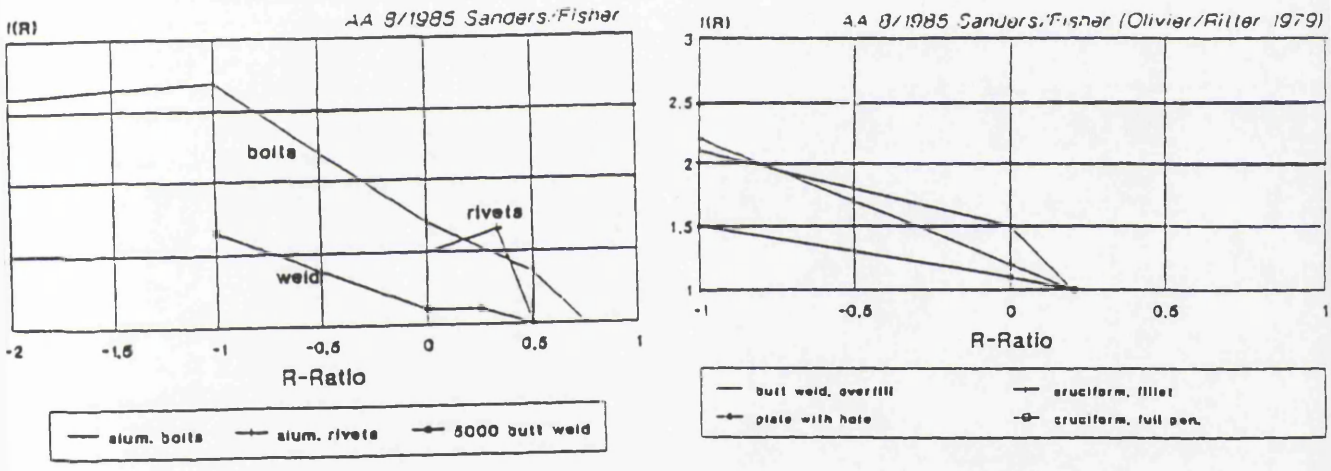

Figure 3.11: R-ratio enhancement factor in the Aluminium Association recommendations [19].

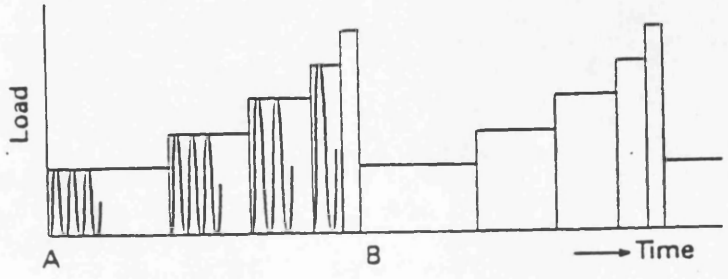

Figure 3.12: Description of a 'block' type load sequence employed in experimental techniques and Miner's Rule evaluations [2].

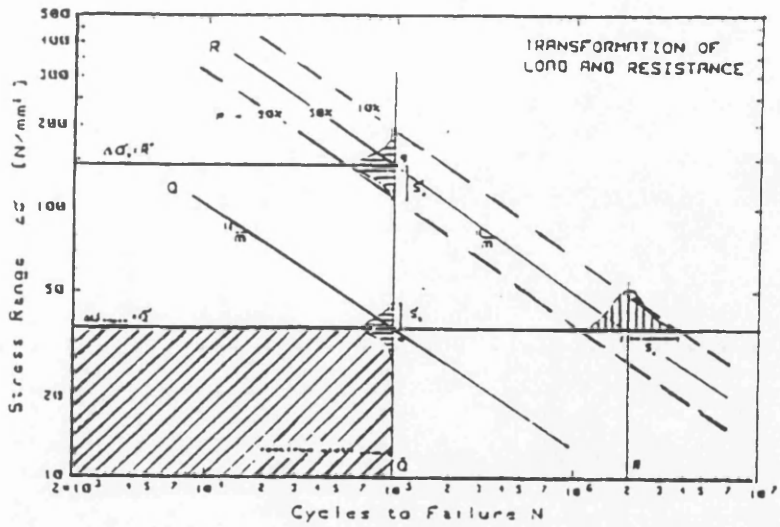

Figure 3.13: Graphical representation of the load and resistance fatigue curve transformation [101].

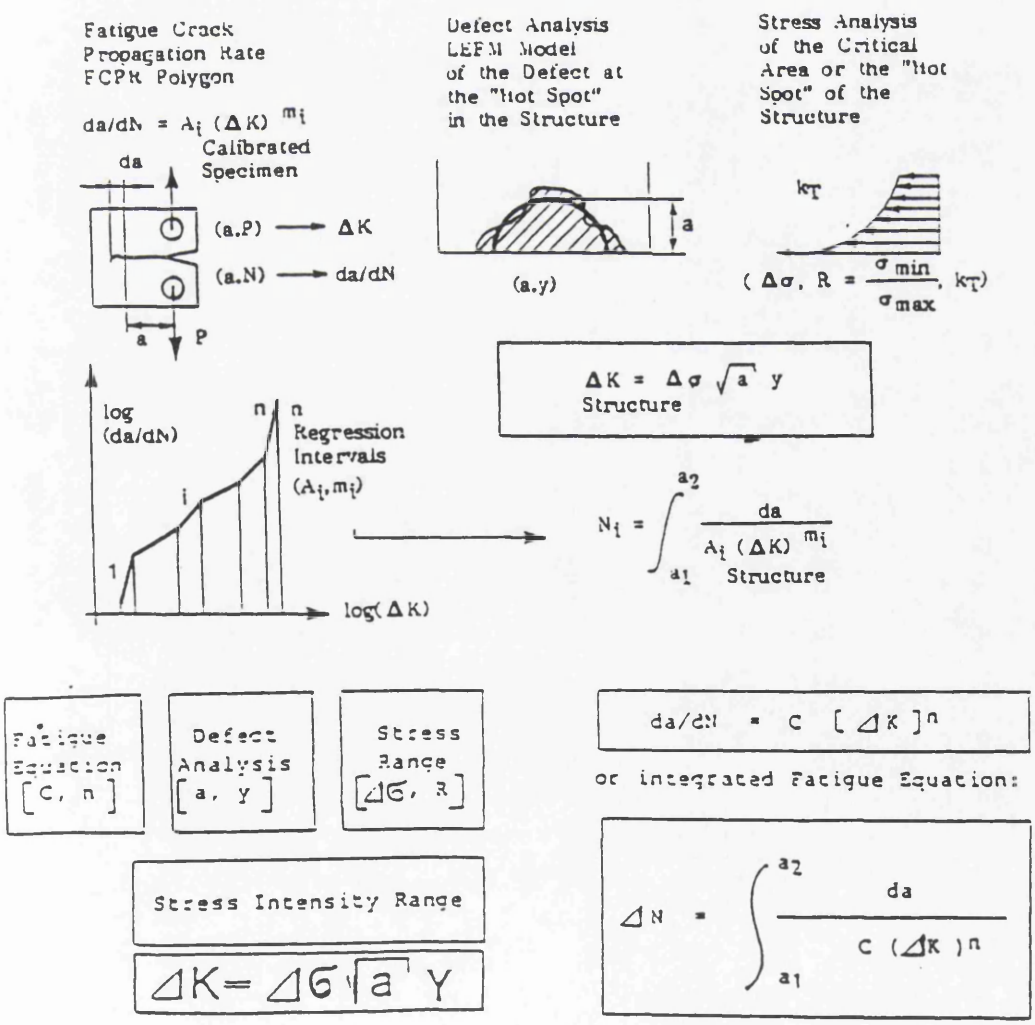

Figure 3.14: Fatigue life prediction of joints based on LEFM models [102].

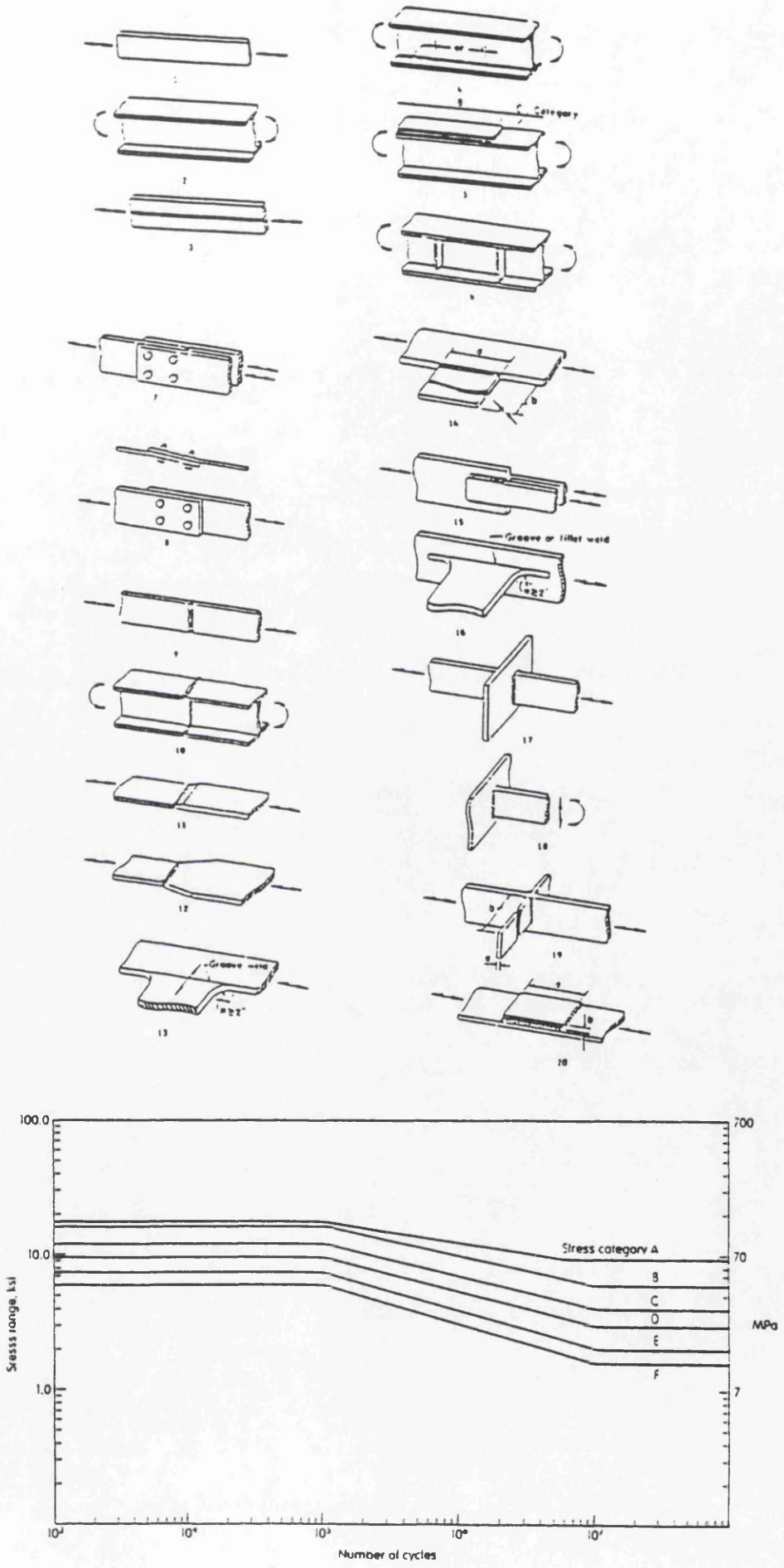

Figure 3.15: The Aluminium Association S-N curves and the structural details considered [18].

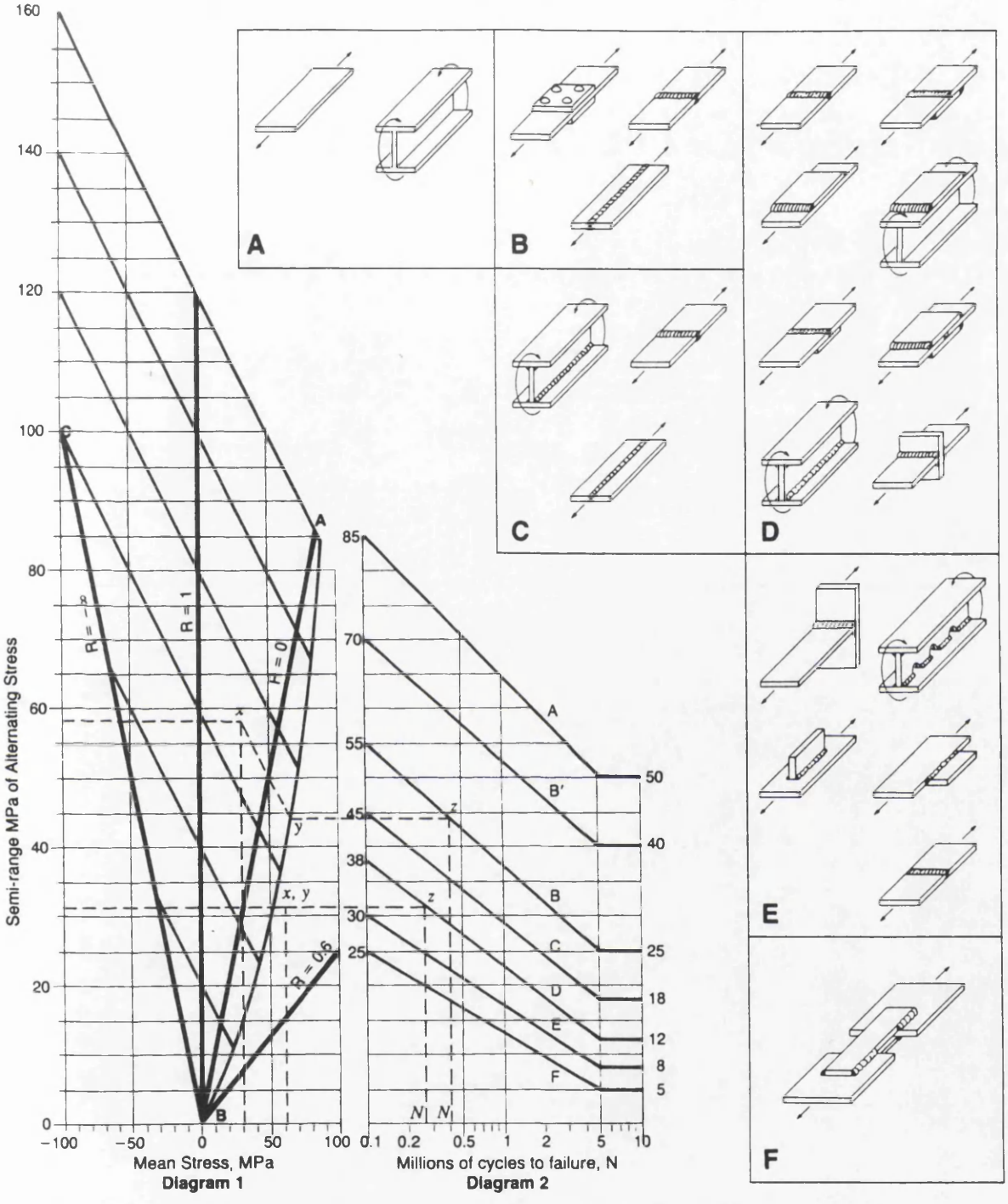

How to use the curves

1. In diagram 1, draw a vertical line from the value on the mean stress scale to meet the horizontal line from the value of the semi-range of fluctuating stress scale at x, (or use the appropriate stress ratio line; see (5) below). If x is to the left of the line $R = -\infty$, fatigue is not important.
2. If x falls between lines $R = -\infty$ and AB, draw a line parallel to the sloping lines to meet AB at y. If x falls to the right of line AB, x and y are a common point.
3. From y draw a horizontal line to meet the appropriate curve for the class of joint at z in diagram 2.
4. A vertical line from z gives the cycles to failure, N.
5. A stress ratio line, or R line, is the locus of all points having the same value for the ratio,

$$R = \frac{\text{minimum stress}}{\text{maximum stress}}$$

$$= \frac{\text{mean stress} - \text{semi-range of fluctuating stress}}{\text{mean stress} + \text{semi-range of fluctuating stress}}$$

Tension stresses are positive, compressive stresses are negative.

Figure 3.16: The Alcan S-N curves with correction for R-ratio effects [14].

Type 1 classifications: non-welded details

Product form	Rolled or extruded sections						
Location of potential crack initiation	Away from all welding						
	Away from all structural connections or parts				At a lapped or spliced connection fastened with:		
	On a member of constant or smoothly varying cross-section	At any external or internal edge		At a small hole (may contain bolt for minor fixtures)	Friction grip bolts	Rivets	Bearing bolts
Dimensional requirements	No holes or re-entrant corners	Any aperture or re-entrant corner radius $\geq t$		Hole diameter $\leq 3t$			
Manufacturing requirements	All surfaces rolled, extruded or machined to a smooth finish in direction of f_r		Surfaces machined or ground in direction of f_r	Holes drilled or removed			
					Torqued to proof load of bolt	Cold driven	Nuts secured mechanically or by sealant
Special inspection requirements	Surfaces proved free of defects by penetrant dye testing						
Design stress area		Net cross-sectional area					
Special design stress parameter		Use stress concentration factor for apertures or re-entrant corners					
Type number	1.1	1.2	1.3	1.4	1.5	1.6	1.7
Maximum permitted class	60	60	50	36	29	29	17

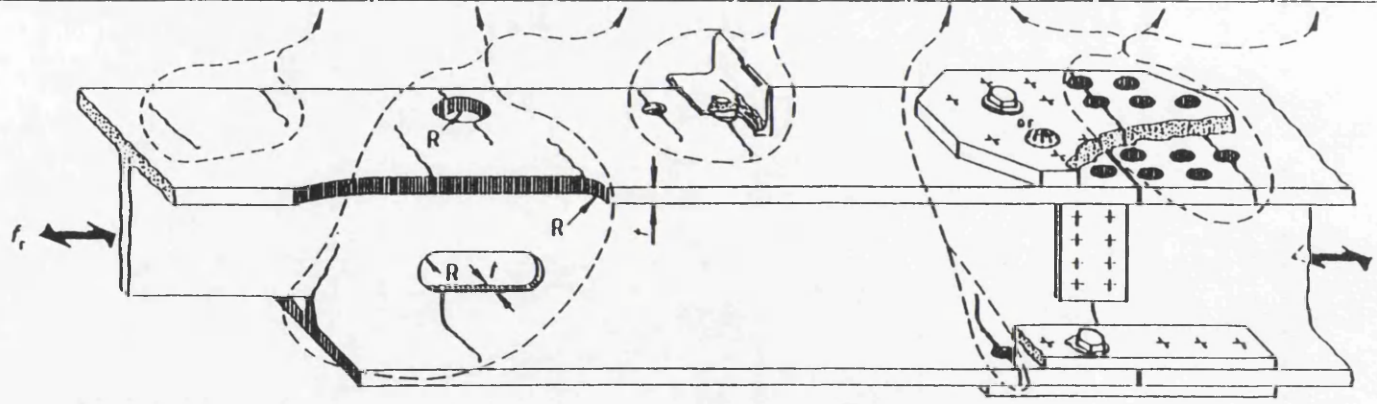

Keys

Typical crack location —— Cut edge ▬ Fastener ○ Direction of stress fluctuation ⟷

Figure 3.17: The BS8118 joint detail classification (continued) [16].

Type 2 classifications: welded details on surface of member

Product form	Rolled or extruded sections or built up members										
Location of potential crack initiation	At a long welded attachment (in direction of f_r)								At a short welded attachment		At any attachment
	Away from weld end			At an intermediate gap in a longitudinal weld	At a cope hole	At a weld end					
					Narrow attachment		Wide attachment				On edge of member
							On one side only	On both sides symmetrically			
Dimensional requirements	Butt weld full penetration			Fillet weld		Weld not on member edge					Weld on member edge
				Intermittent $\frac{m}{h} \leq 2.5$		Weld length (parallel to f_r) $l > 50$ mm			$50 \geq l > 25$ mm	$l \leq 25$ mm	
					Attachment width $w \leq 50$ mm		$w > 50$ mm				
Manufacturing requirements (see also BS 8118 : Part 2)	Grind smooth any undercut on member edges										Grind any undercut
	Dress overfill flush	Automatic no stop starts	Stop-starts free of lack of fusion								Avoid weld returns round laps (see z)
Special inspection requirements (see also BS 8118 : Part 2)	Weld surfaces proved free of cracks and lack of fusion by penetrant dye testing										
	Radiography										
Design stress area	Minimum transverse cross section of member at location of potential crack initiation										
Special design stress parameter							Stress dispersal angle 1 in 2 both sides				
Type number	2.1	2.2	2.3	2.4	2.5	2.6	2.7	2.8	2.9	2.10	2.11
Maximum permitted class	50	42	35	29	21	20	17	20	24	29	17

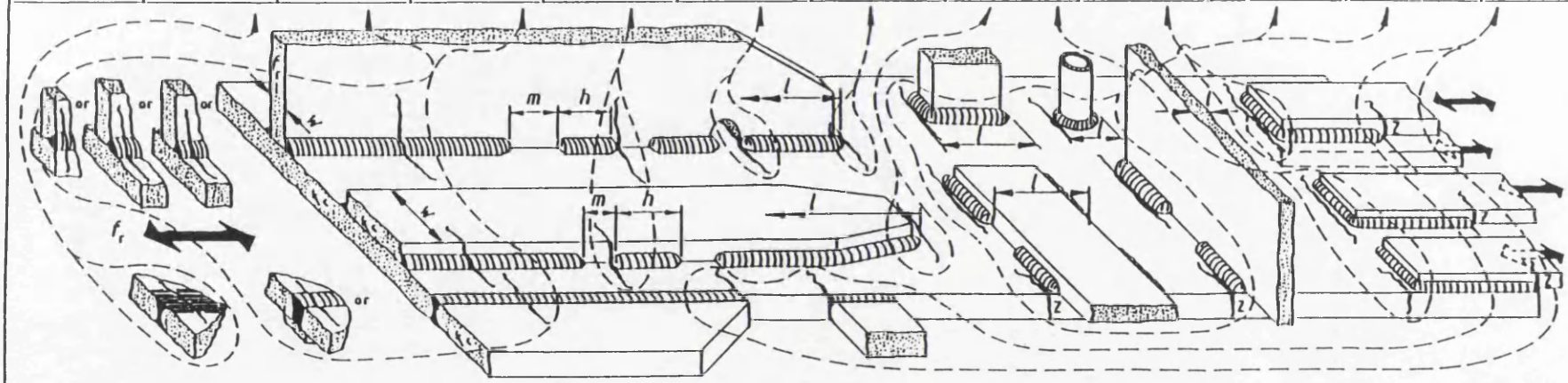

Figure 3.17: The BS8118 joint detail classification (continued) [16].

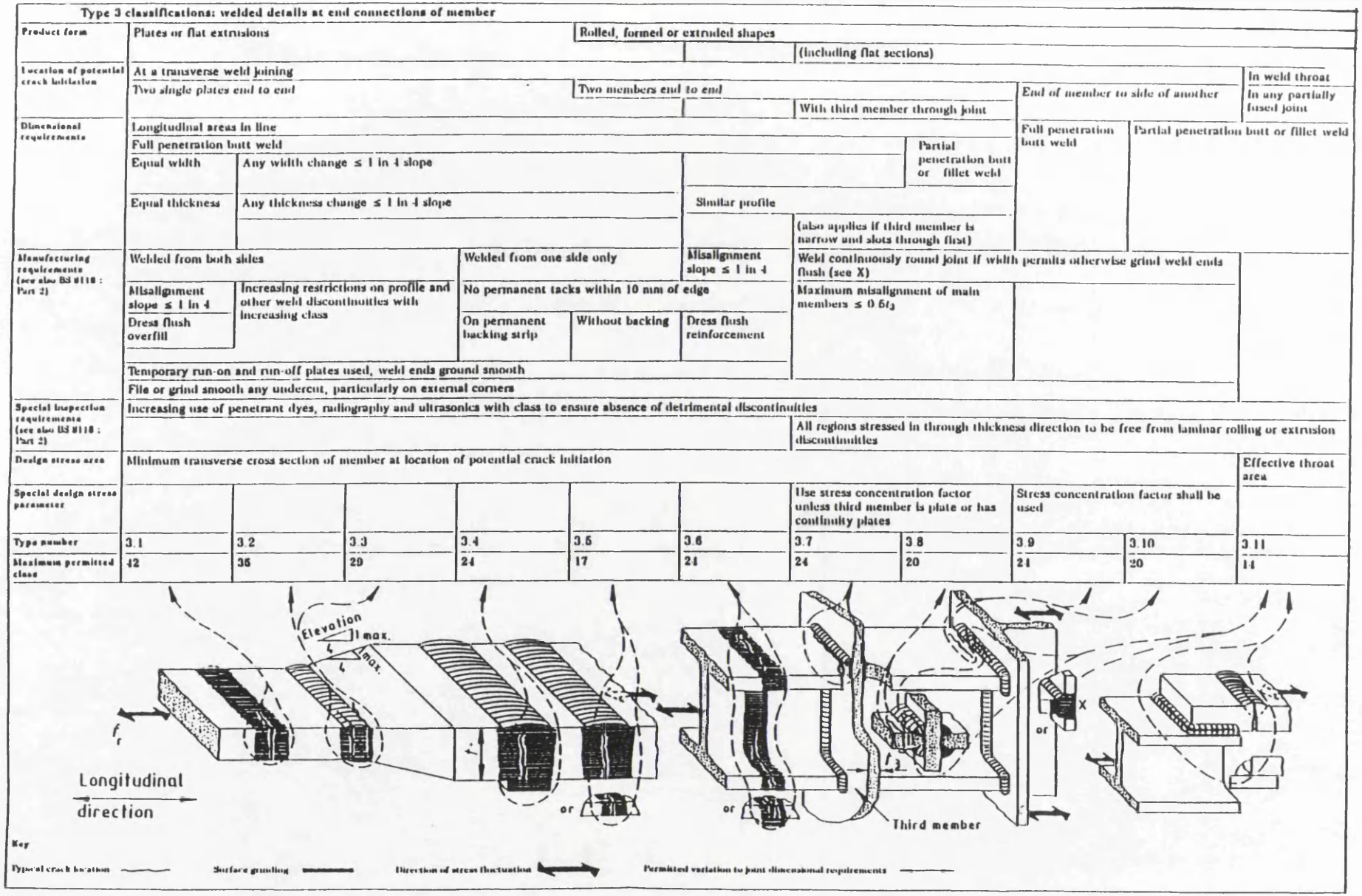

Figure 3.17: The BS8118 joint detail classification (final) [16].

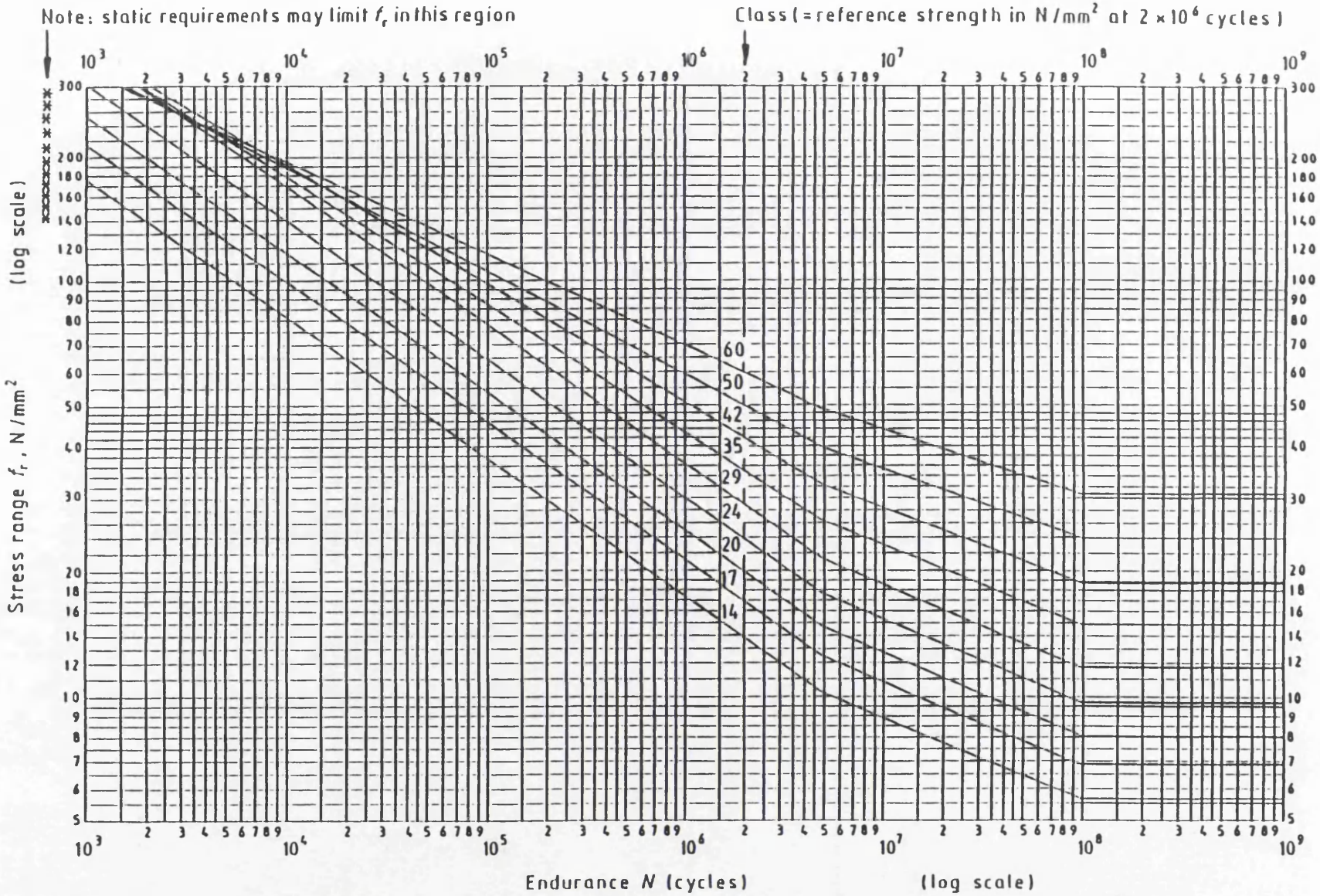

Figure 3.18: The BS8118 S-N design curves [16].

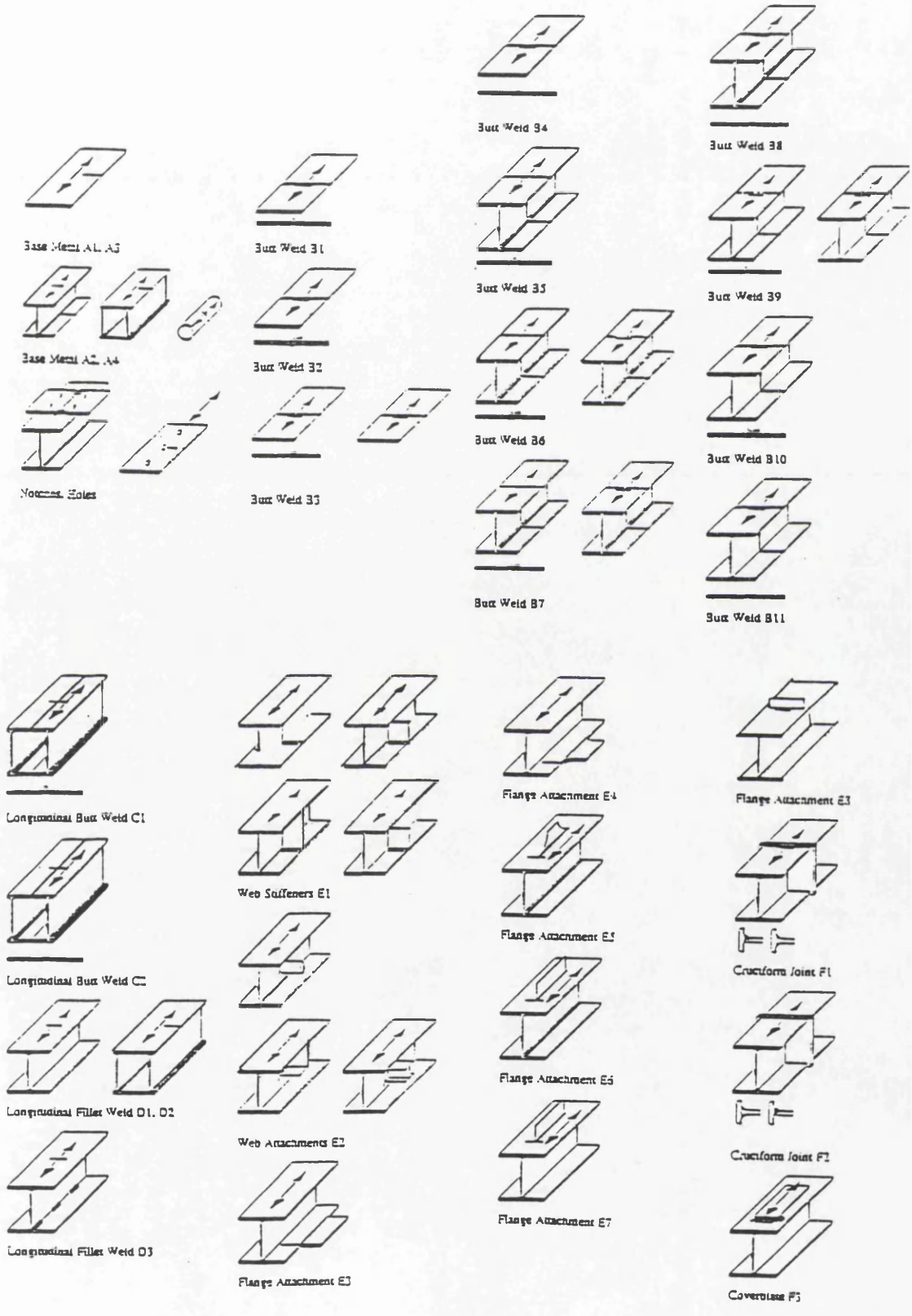

Figure 3.19: The ERAAS joint detail classification [19].

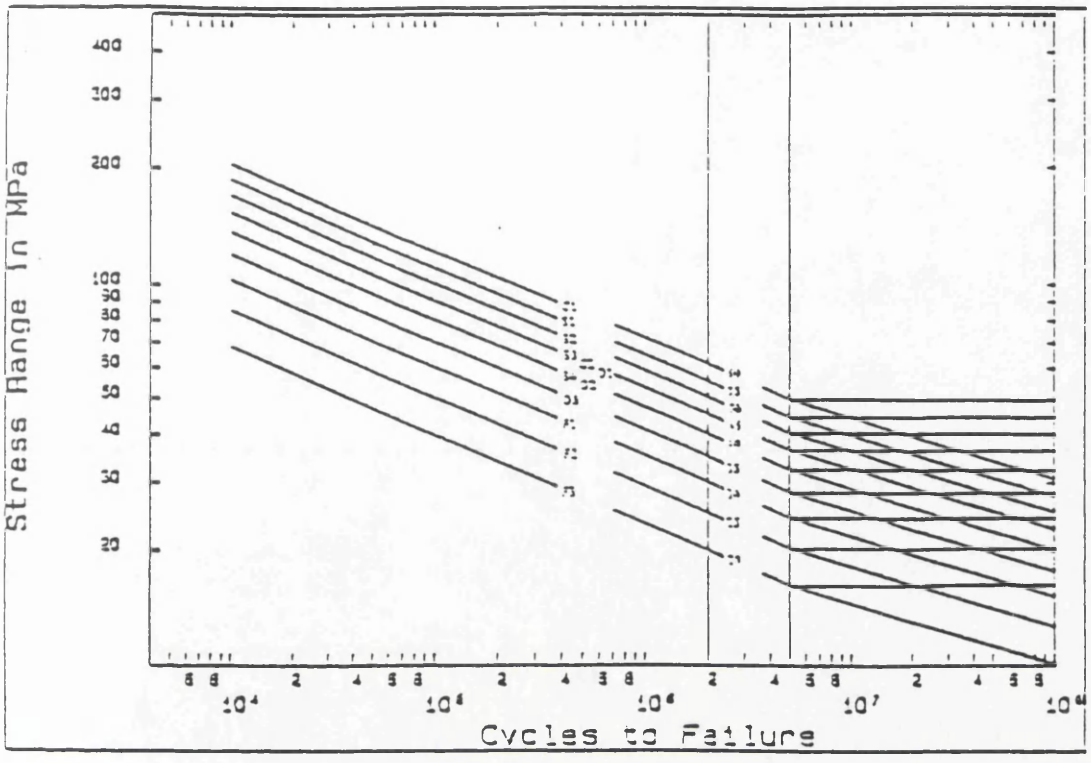

Figure 3.20: The ERAAS, S-N design curves [19].

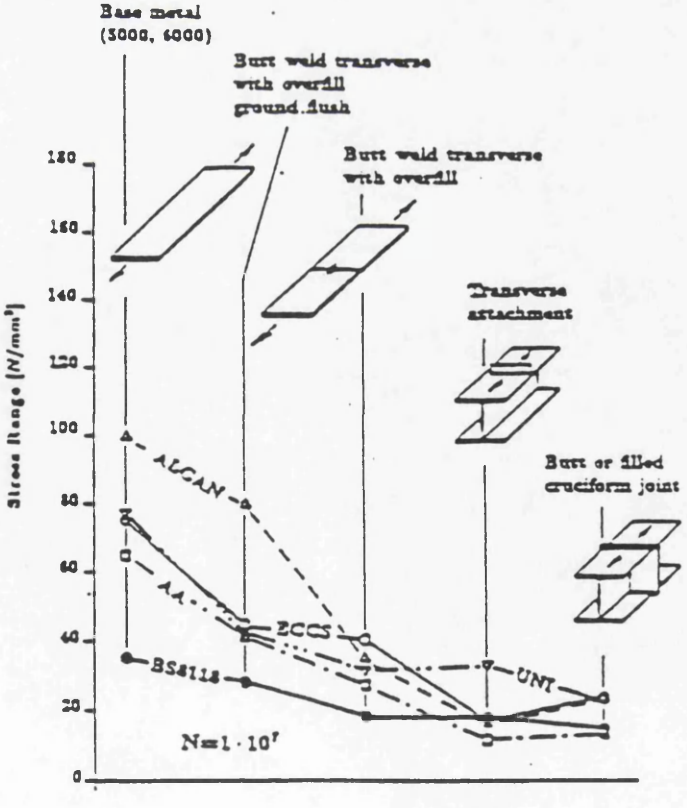

Figure 3.21: Comparison of fatigue design strength of five joint types for a number of fatigue design codes [20].

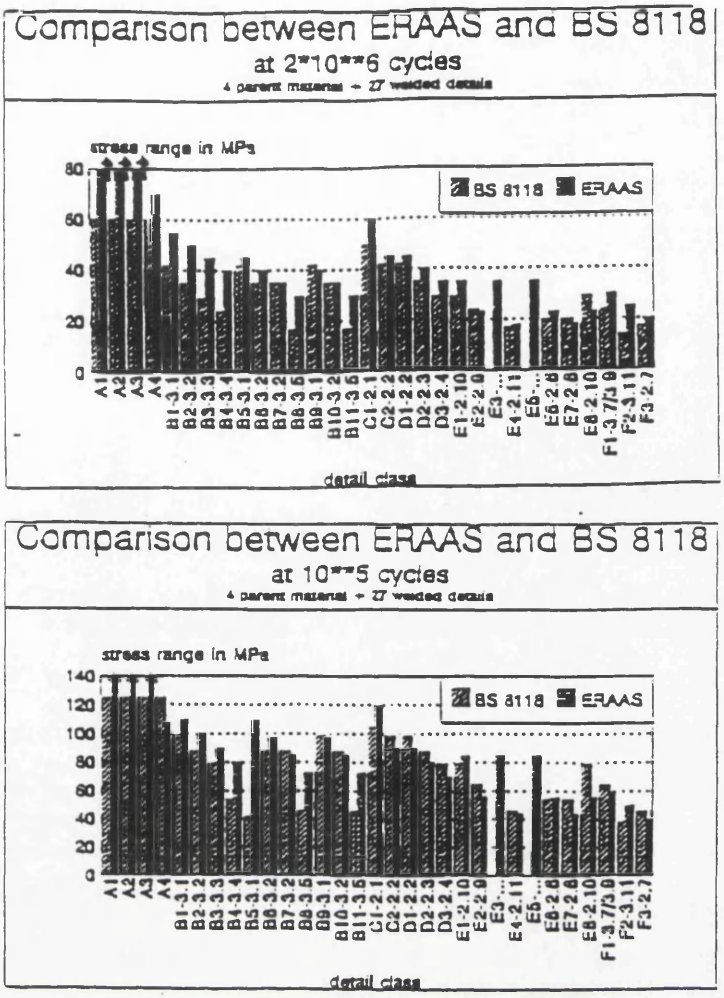

Figure 3.22: **Comparison of the fatigue design strengths provided by ERAAS and BS8118 at 2×10^6 and 10^5 cycles [19].**

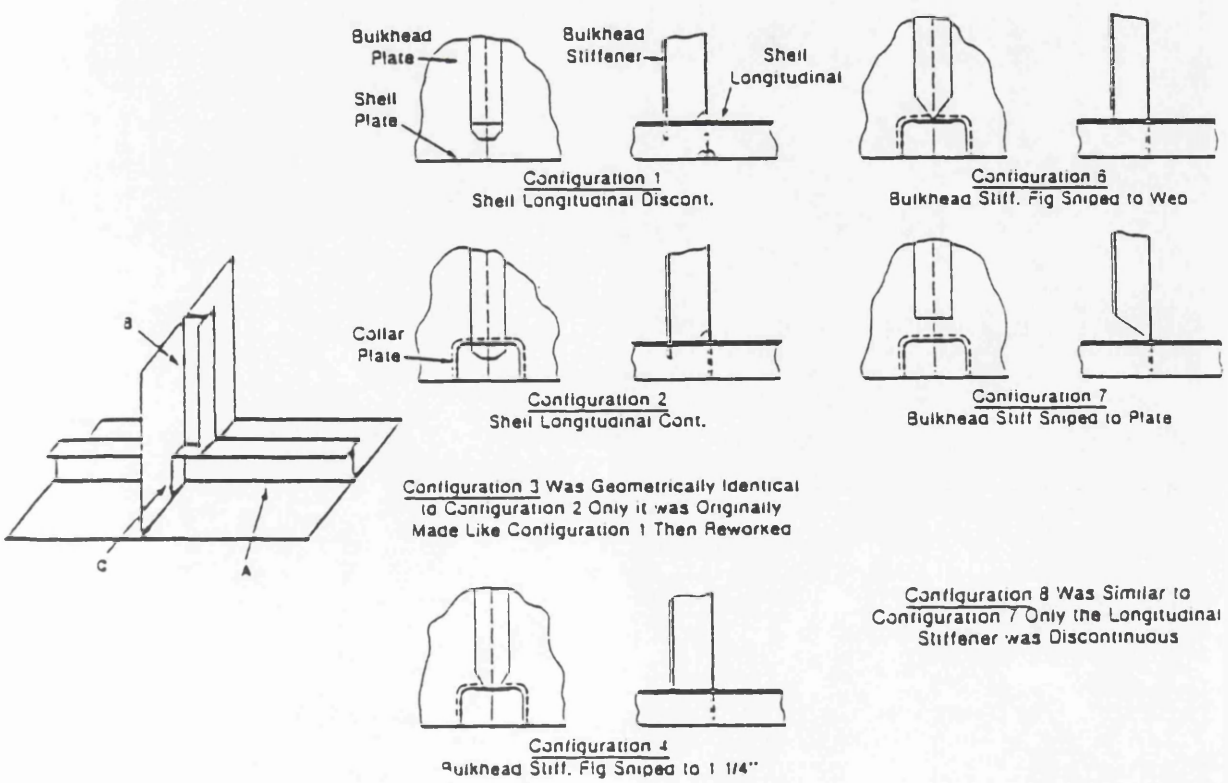

Figure 3.23: **Aluminium ship structural details tested by Beach et al [78].**

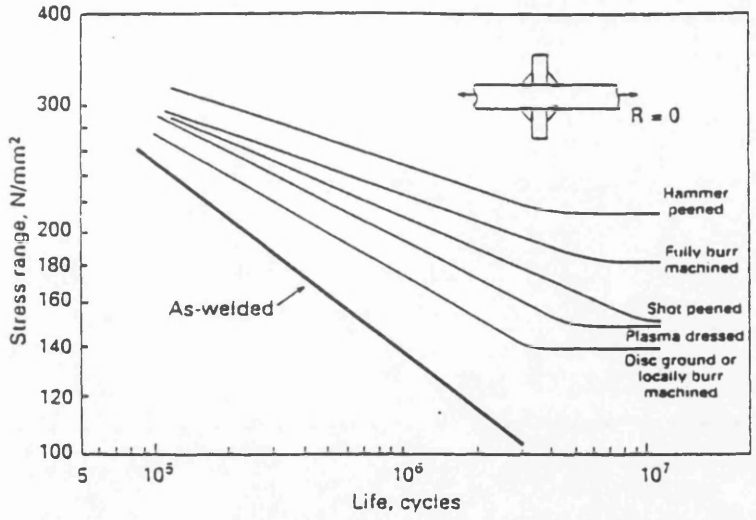

Figure 3.24: **Effect of weld improvement techniques on the fatigue strength fillet welded joints [2].**

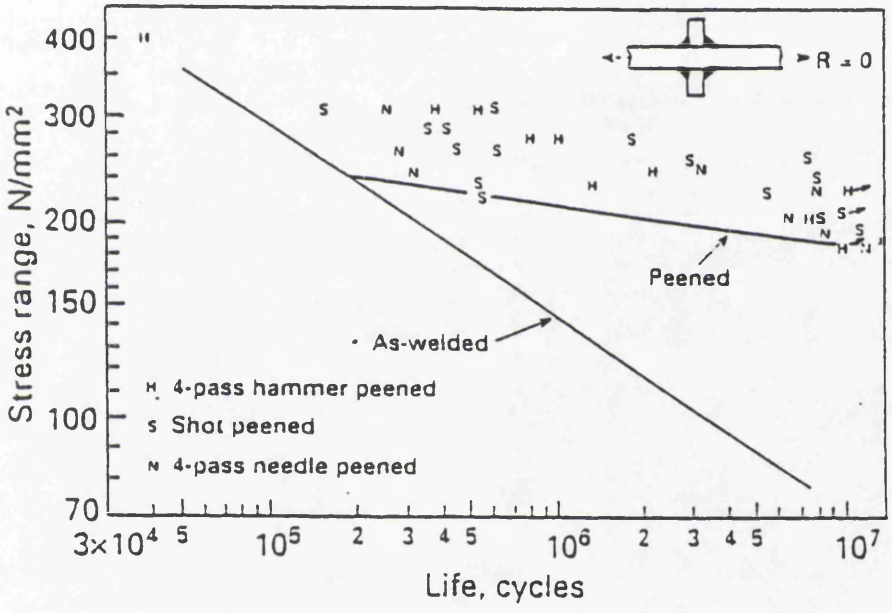

Figure 3.25: **Comparison of fatigue life improvement due to hammer, needle and shot peening [2].**

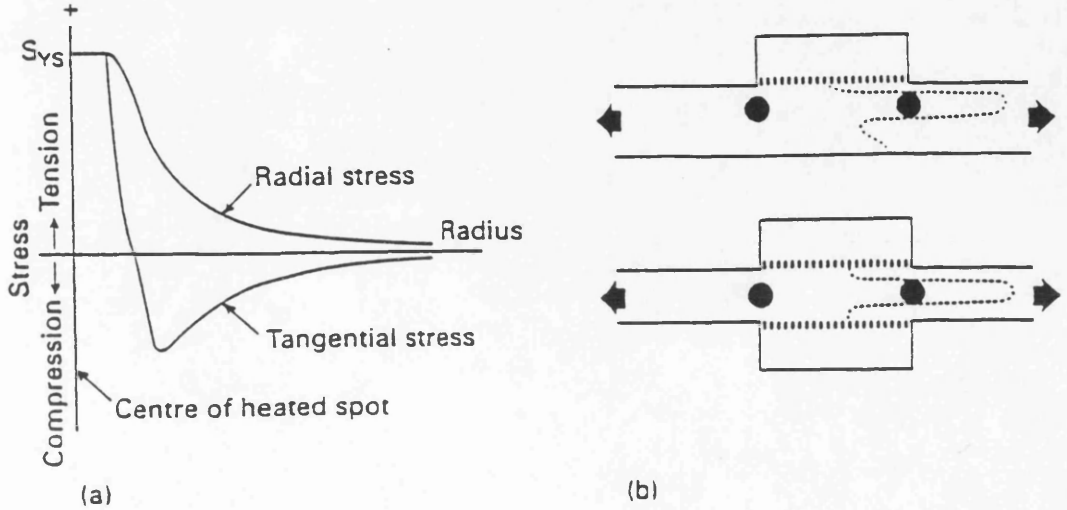

Figure 3.26: **Spot heating residual stress distribution [2].**

CHAPTER 4

4.0 Ultimate Strength Modelling of the Behaviour of the Main Structural Components

4.1 Welding Effects in Steel and Aluminium Structures

Two types of mechanical imperfections generally affect the capacity of a structural element:

- residual stresses
- HAZ effects (only in aluminium welded structures).

The former result in a reduction in compressive strength of the welded section due to the introduction of compressive 'locked-in' stresses in the section. The effect of the latter is, however, of different nature as it reduces the strength of the parent material at zones adjacent of the weld. Due to the micro-structure changes it introduces in the material, its effects are considerable for aluminium alloys drawing their strength from heat-treatment (e.g. 6000 series alloys) and negligible for the 5000 series alloys unless they are in their work-hardened temper. A key factor in welded aluminium design is the ability to accurately account for the effects of HAZ softening, especially for heat-treated aluminium alloys.

4.1.1 Residual Stresses

4.1.1.1 Residual Stresses in Steel and Aluminium Sections

Residual stresses are caused by *thermal processes* such as cooling of extrusions and welding, and *mechanical processes* like cold rolling and straightening.

For extrusions, the intensity of residual stresses, due to thermal processes is strongly related to the rate of non-homogeneity of plastic deformation during the cooling stage of the extrusion process. This rate is higher if the thermal conductivity k is lower and is threfore inversely proportional to the specific heat c, the thermal expansion coefficient α and the specific weight of the material γ, all forming the thermal diffusion factor $k/\gamma c$. In aluminium alloys this factor is ten times higher than steel [1].

It is therefore not surprising that studies on the residual stresses in *extruded aluminium sections and hot rolled steel profiles* [2, 3] have concluded that for steel hot-rolled profiles, the residual stresses due to cooling may reach values between 0.3-0.5 of the yield limit compared to extruded aluminium profiles for which the residual stresses are negligible and may therefore be neglected.

For welded sections, however, the 'locked-in' stresses cannot be neglected. The intensity of the heat input, and therefore the magnitude of the residual stresses, is related to the type of welding process used, the weld sequence, the pass size and the weld penetration. Their relation with the thermal diffusion factor of the material means that they are lower in aluminium than in steel structures (higher thermal conductivity, and smaller specific weight for aluminium). Experimental investigations by Mazzolani [4] and Gatto et al [5] have concluded (see [6]) that the effect of welding residual stresses in lowering the resistance of welded compression bars of aluminium alloys is smaller to the corresponding effect in steel bars by approximately 40%.

4.1.1.2 Residual Stress Models

The nature and distributions of locked-in residual stresses during hot and cold forming and during welding of steel sections and plates are described in great detail by Faulkner in [7]. They are therefore not tackled herein.

For residual stresses in aluminium structures, there are mainly two models, describing their extent and strength, and are the results of two extensive experimental investigations. One is attributed to the ECCS [8] and is the result of work carried out in Italy, while the second is the result of extensive work at Cambridge University [9, 10] which has later been promoted by the BS 8118 guidelines. Based on the investigations by Mazzolani and Gatto [4, 5], ECCS recommend the use of three empirical models describing the residual stress distribution in three specific built-up aluminium sections (I sections with fillet welds, I sections with butt welds, box sections respectively).

The BS 8118 (Cambridge) model is to be preferred over the ECCS as their comparison [1] showed that despite the fact the ECCS models are closer to experimental results and the magnitude of the residual stress predictions of

the two models is comparable, the British models allow extrapolation to all types of joints.

The Cambridge University model is based on the Tendon Force Concept first developed to model the residual stresses and their effects in welded steel sections and was later extended by Wong [9, 10] to the case of non-linear materials (e.g. aluminium). The tendon force F_t is defined by the area AACC (Fig. 4.1), and is insensitive to the width of the tension zone, plate dimensions, material yield stress and actual stress pattern on the cross section. This force is resisted by the whole cross section and when is divided by the total plate area, it gives the overall compression stress on the whole plate. Wong provided detailed expressions [10] of the magnitude of the force relative to Q/υ, *the heat input per unit length of weld and* A_w, *the cross sectional area of the weld deposit* and not relative to the yield stress of the parent of filler materials. The weld deposit and the reduced-strength area A_{HAZ} were thus related by the empirical relation:

$$A_{HAZ} = 10\, A_w$$

It was on this work by Wong that BS 8118 based its approach providing two different values for the residual compressive force depending on the hardening method of the alloy:

For 5000 series alloys	$F_t = A_{HAZ}/2$	In Newtons
For 6000, 7000 series alloys	$F_t = A_{HAZ}/4$	In Newtons

In other words, the value of the compressive residuals (tendon force) in heat-treated alloys is half of that for non-heat-treated alloys. Approximate A_{HAZ} values are provided in BS 8118 and are presented in Table 4.1.

4.1.2 HAZ Effects in Welded Aluminium Structures

The effects of heating generated by the welding process is to alter the heat treatment of the aluminium alloy material and introduce softened zones of reduced material strength in the vicinity of the welds. This softening is more significant in the 6000 and 7000 series alloys and in the 5000 series alloys only when these are at a work-hardened temper. It is the extent and strength of this reduction that investigators and codes have attempted to model as accurately as possible.

4.1.2.1 The Strength and Extent of HAZ Effects

The first attempt to identify and model the extent and strength of the HAZ effects was by Hill et al [6] in 1962 in the USA. The "reduced-strength zone" model (HAZ) was then introduced for the first time and consisted of a uniformly softened zone adjacent to a weld, with a sudden jump to full parent strength (Fig. 4.2). This rule, however had the disadvantage that it identified the extent of the HAZ irrespective of parent alloy, plate thickness, welding parameters or welding process considerations to 25 mm on either side of the weld (from the centre-line of a butt-weld or the root of a fillet weld).

This 'one-inch' rule persisted up until a decade ago (1983) with the French specifications [11] and CP118 promoting it. It was, in 1977 with the experimental investigations of Gatto [5] that it was observed that the extent of the HAZ region could take values below 20 mm on either side of the weld and led to the ECCS recommendations of 1978 (ERAAS) [8], and its more modern versions (Figs. 4.3 and 4.4) which refer to butt-welded joints and built-up welded sections respectively. Parts (a) and (b) of the figures refer to residual stress models and the elastic limit variation $\sigma_{0.2}$ respectively). These recommendations are however only restricted to the sections shown in the figures.

Experimental plots of the strength variation within the HAZ have been presented by Kelsey [12], Pirner [13], Wong [9, 10], Mazzolani [5, 14], Soetens [15] and Robertson [16] mostly in the form of hardness surveys. All these investigations, with the exception of those by Wong and Robertson, do not relate the extent of the HAZ to the welding parameters namely the weld deposit area A_w and the arc heat input Q/υ per weld unit length (J/mm).

In 1985 work at Cambridge University by Robertson and Dwight [16, 17] tackled the question of HAZ effect representation in the most comprehensive way to date. Their work concentrated in providing accurate estimates of the extent and the strength of the HAZ softening using Kelsey's [12] earlier description (Fig. 4.5). It was shown that the *extent* of the HAZ is affected by:

- the metal temperature at the beginning of welding
- effect of the plate thickness
- the built-up of temperature in multi-pass welds
- neighbouring parallel welds; if these are laid simultaneously the extent of their combined HAZ increases
- the positioning of the weld too near to a free edge. The HAZ softening increases as in this case the heat dispersal is by far less efficient. In this case the effect was found to depend on the ratio between the distance of the weld to the free edge and the extent of the HAZ calculated disregarding the free edge effect.

The model is described in more detail in Appendix 4.1. This work was however restricted to 6000 series alloys and was later (1988) extended to 5000 series alloys for use in the development of BS 8118 by Shercliff [18].

4.1.2.2 The BS 8118 Approach

According to *BS 8118* [19] the HAZ is assumed to extend a basic distance z_o *in any direction* from a weld (Fig. 4.6) given by *the lesser of*:

Alloy series	All weld types
7000	$z_o = 30 + (t_A/2)$ mm
other alloys	$z_o = 20 + (t_A/3)$ mm

OR

Alloy series	In-line butt welds	Other butt-weld types/ all fillet weld types
7000	$z_o = 4.5\, t_A$ mm	$z_o = 4.5\, t_B^2/t_A$ mm
other alloys	$z_o = 3\, t_A$ mm	$z_o = 3\, t_B^2/t_A$ mm

t_A is the lesser of $0.5(t_B + t_C)$ and $1.5\, t_B$. t_B, t_C are the thickness of the thinnest and thickest elements welded together respectively. Elevated material temperatures prior to welding are accounted for via a magnification factor α while the 'free edge' effects and additional heat concentrations due to adjacent welds are accounted for via the magnification factor η:

$$z = \alpha \eta z_o$$

The values are given in tabular form in the BS 8118 document itself, but the main trends *for a single, straight, continuous weld* are as follows:

weld deposit area	t_c	α
<50 mm^2	<25 mm	1.0
>50 mm^2	>25 mm	2.0

It is suggested therefore, that for very large welds, the basic HAZ width is doubled. η can be as high as 1.33 and 1.5 in the worst of cases. Proper temperature control during fabrication is therefore essential to restrict the extent of the HAZ softening. Table 4.4 presents the level of parent material strength reduction due to HAZ softening for a number of aluminium material alloys, as recommended in BS 8118 and herein.

4.2 The Design of Steel and Aluminium Flat Plates

4.2.1 Introduction

Plate elements can be found in several structural systems such as those of built-up sections, stiffened panels and shells and can be stiffened by longitudinal and/or transverse stiffeners. Plates/panels subjected to compression have to be checked against:

- buckling of the plate element between stiffeners under all the possible load combinations and destabilising the latter

while the strength of the stiffening system has to be checked against:

- plate induced interframe stiffener collapse
- tripping failure of the stiffener (due to lack of sufficient lateral stiffness)
- overall grillage collapse
- local buckling of stiffener elements
- insufficient rigidity and stiffness of the stiffeners.

The effects of coexistent lateral pressure, in plane shear loads, and biaxial compression should also be properly accounted for.

Generally, the main type of framing found in ships is longitudinal, presenting 'long' plates in the direction of the main compressive loading. The main function of the transverse stiffeners/frames is to resist the hydrostatic and hydrodynamic loads acting on the wet decks and side shell of the structure.

The overall grillage collapse mode consists of the global deflection of both longitudinal and transverse stiffeners, and is unlikely to be encountered in practice except for lightly stiffened panels found in superstructure decks. Stiff transverse frames and bulkheads would insure that this failure mode is avoided. Generally, the weakest mode of failure is inter-stiffener plate buckling. Once the plate has buckled and stops being fully effective, interframe, plate induced stiffener (and associated effective plating) collapse is expected to occur. This is the failure mode forming the basis of stiffened plate design.

4.2.2 Types of Buckling Models

In tackling the buckling question of plate elements as well as stiffened elements (stiffener/plate section), it is widely accepted to treat them as columns. *The plate element* is easily converted by means of an 'equivalent' slenderness to a column of the length equal to the length of the plate in the direction of in-plane loading and cross sectional properties equal to those of the plate. Boundary conditions can be considered in detail but pinned boundary conditions are more widely acceptable as a simplifying and simultaneously conservative assumption.

For *stiffened plates*, the same approach as for the plates apply, only this time the 'equivalent' column cross section is assumed to consist of the sectional area of the stiffener and the effective width of the plating as calculated from post-buckling considerations of the plate in-plane strength.

Since the buckling behaviour of structural elements can be modelled by the behaviour of an 'equivalent' pin-ended column, it is important that some attention is paid to the general trends in modelling their strength. These can be categorised in two groups:

(a) a group that concentrates more on the effects of initial imperfections and does not directly account for the effects of residual stresses in the ultimate strength of the plate/stiffened plate (Perry-Robertson approach)

(b) a group which concentrates in the effects of residual stresses but does not account implicitly for the effects of initial imperfections (tangent modulus approach).

The former category would be most appropriate for structural components whose ultimate strength is very much dependent on the level of initial imperfections, like for columns whose reserve strength in the post-critical region is minimal. On the other hand, the latter category is particularly attractive for structural elements with considerable post-buckling strength (e.g. plates/stiffened plates). Although their critical buckling strength is considerably affected by the presence of initial imperfections, the ultimate strength level will be affected more by the presence of residual stresses (and HAZ effect in the case of heat-treated aluminium alloys) than from initial imperfections.

The most popular of the former category is the Perry-Robertson equation and its consequent variations. In 1886 that Ayrton and Perry [20] put forward their basic strut formulation. Robertson's 1925 [21] variation of Perry's expression, mostly known as the Perry-Robertson expression, has formed the basis of British and ECCS steel and aluminium column design codes. Godfrey [22] has introduced a variant to this model while a variation of this expression is used in France and was based on work by Dutheil [23]. *Perry's original formulation* was [24]:

$$(\sigma_E - \sigma)(\sigma_y - \sigma) = \eta\, \sigma_E\, \sigma$$

where $\sigma_E, \sigma_y, \sigma$, are the Euler stress, material yield stress (for steel) and average applied failure stress respectively. This expression was based on the assumption of pinned boundary conditions, the existence of an initial sinusoidal out-of-straightness, Δ, the absence of any residual stresses and the restriction of behaviour and failure to the elastic limit.

The original 'Perry constant', η, is given by $\eta = (\Delta y/r^2)$. r is the radius of gyration and y the distance of the extreme fibre of the cross-section from the

neutral axis. It is obvious that the value of η will influence the final shape of the strut curves and this is where the variations on Perry's approach are introduced.

Robertson assumed that the initial out-of-straightness is proportional to the strut length i.e.:

$$\eta = \alpha \frac{L}{r}$$

and calibrated the curve to steel experimental results so that $\alpha = 0.003$.
Godfrey's 1962 variation assumed that the initial out-of-straightness is proportional to L^2 and proposed

$$\eta = 0.3\left(\frac{L}{100r}\right)^2$$

Dutheil, not only assumed that the initial out-of-straightness depends on L^2, but that it decreases as the yield stress of the material increases:

$$\eta = 0.38\left(\frac{\sigma_y}{250}\right)\left(\frac{L}{100r}\right)^2$$

Dutheil's expression leads to stresses below the Godfrey curve.

Dwight in 1975 [24] put forward the *modified Perry-Robertson* expression, calibrating the original Ayrton-Perry expression to the european steel strut data. The value of the Perry constant, η, was hence proposed as:

$$\eta = \begin{cases} 0 & \text{for} \quad \dfrac{L}{r} < S_o \\ \alpha\left(\dfrac{L}{r} - S_o\right) & \text{for} \quad \dfrac{L}{r} > S_o \end{cases} \qquad \text{and} \qquad S_o = 0.2\pi\sqrt{\frac{E}{\sigma_y}}$$

In other words, $\lambda_o = 0.2$ at which the limit of low slenderness is set. α is a data fitting parameter. This work has formed the basis of the ECCS steel column curves currently in use.

In general, residual stress effects would be accounted for by the use of empirically derived, higher, values of η in the various code proposals.

The only advantages of the Perry-Robertson formulation, and its variations, stem from its simplicity and the ability to account for the stress magnification occurring due to the inherited out-of-straightness. The disadvantages, however,may be considerable and are therefore summarised as follows:

(a) it is a pessimistic approach as it reduces failure to first yield without considering the shape factor of the cross-section
(b) ignores strain hardening
(c) ignores residual stresses (were accounted for by an increased out-of straightness assumption in design codes)
(d) it is curve fitted to available experimental/numerical data and therefore its accuracy depends on the quality of this data.

The aforementioned methods tackle the effect of magnification of load in the presence of initial imperfections. In addition, there are three ways to account for the interaction of yielding and elastic buckling in the elasto-plastic buckling range. By means of:

1. the circular Merchant-Rankine formulation,

$$\left(\frac{\sigma}{\sigma_{cr}}\right)^2 + \left(\frac{\sigma}{\sigma_y}\right)^2 = 1$$

where σ_{cr} is the critical buckling stress for imperfect structures.

2. the Perry-equation, where δ is a curve-fitting coefficient to test data,

$$(\sigma_{cr} - \sigma)(\sigma_y - \sigma) = \delta\, \sigma_{cr}\, \sigma$$

3. the η-method, or tangent modulus method, where η is a plasticity reduction factor,

$$\sigma = \eta\, \sigma_{cr}$$

The main drawback of the former two approaches is that they do not allow implicitly for the effects of residual stresses and HAZ effects (in the case of aluminium alloys). For the Merchant-Rankine formulation this problem is overcome by the introduction of 'elastoplastic knockdown factors' as used by Odland [25], Cho and Frieze [26] and Odland and Faulkner [27]. The

introduction of an appropriate correction factor, δ, for these effects is the solution to the problem for the Perry formulation.

However, it is the detailed consideration of residual stress effects and the potential to extend this method to account for HAZ strength reductions that makes the tangent modulus approach most attractive. It is therefore recommended and adopted in the work that follows.

The tangent modulus approach is widely accepted in North American design codes and the 'unified' buckling formulae prescribed are based on it. Although residual stress effects and material non-linearities (i.e. aluminium) are easily accounted for by this method the effect of any initial imperfections has to be accommodated empirically, in the form of reduction coefficients which have been derived from calibration of these strength curves to appropriate experimental data.

Figure 4.7 demonstrates the relationship between the critical stress of an ideal steel column and the slenderness. It is observed that the shape of the curve is controlled by three parameters, the modulus of elasticity E (defining the Euler Hyperbola) the proportional limit σ_p and the yield stress σ_y which identify the inelastic part of the curve AB. *The inelastic curve* AB, derived from the tangent modulus concept is generally expressed by the quadratic parabola:

$$\sigma_c = \sigma_y - \frac{\sigma_p(\sigma_y - \sigma_p)}{\pi^2 E}\left(\frac{l}{r}\right)^2$$

This expression can be simplified in two forms:

(a) a form that is generally used in the 'unified' North American codes for both steel and aluminium structures

$$\sigma_c = a - b\left(\frac{l}{r}\right)^2$$

where the coefficients a and b depend on the yield stress, proportional stress, the type of section and the mode of buckling failure considered (e.g. in-plane compressive loads, flexural-torsional buckling etc.), or

(b) in the form of the Ostenfeld-Bleich parabolae given by:

$$\frac{E_t}{E} = \frac{\sigma_c\left(\sigma_y - \sigma_c\right)}{\sigma_p\left(\sigma_y - \sigma_p\right)}$$

This approach has been promoted by Faulkner [28] in modelling the inelastic buckling behaviour of unstiffened/stiffened steel plates and shells. A brief historical review of the development of the tangent modulus approach is given next.

4.2.3 The Tangent Modulus Approach

Considere and Engesser (in 1889) were the first to use Euler's critical buckling formulation for the description of inelastic buckling strength, by introducing a variable modulus of elasticity, $\eta = E_t/E = d\sigma/d\varepsilon$ of the material stress-strain curve. Although Considere did not recommend an expression for the variable modulus of elasticity, he recognised that as an axially loaded column stressed beyond the proportional limit starts to bend, the stresses on the concave side increase according to the compressive stress strain curve whereas the stresses on the convex side decrease proportionally to the strain. Engesser in 1895, accounted for Considere's concept by presenting the double-modulus theory [29] according to which, the variable modulus of elasticity, $\overline{E}$, is given by:

$$\overline{E} = E\frac{I_1}{I} + E_t\frac{I_2}{I} \qquad \text{and hence} \qquad \eta = \frac{I_1}{I} + \frac{E_t}{E}\frac{I_2}{I}$$

where I is the moment of inertia of the cross-sectional area about the neutral axis of the section, and I_1, I_2 are the moments of inertia of the cross-sectional areas separated by an axis parallel to the neutral axis and positioned in such a way so as the cross sectional stress developed prior to deflection remains unchanged. The moments of inertia of these two areas of the cross-section are taken about this axis. The position of this axis is identified by equilibrium of external and internal forces to the section. Hence, the value of $\overline{E}$ depends on the shape of the cross-section and the properties of the material. In 1912 Southwell also presented the same theory as a result of his own work, apparently not being aware of the work by Considere and Engesser.

Bleich in [29] concludes that the tangent modulus approach is more

conservative than the double-modulus concept as η is smaller for the tangent modulus approach. In addition, in the tangent modulus theory, and hence the inelastic buckling strength of the column, is not affected by the shape of the column section and depends only on the elasto-plastic behaviour of the material.

It was not until 1947, that Shanley challenged the correctness of the double-modulus concept and its main assumption that until the reduced critical buckling load is reached, the column remains straight. Based on experimental results showing that the double-modulus concept overpredicted the inelastic critical buckling strength, Shanley accounted for the fact that once the tangent modulus load is reached (less than the reduced load estimated by the double-modulus approach) the column will start deflecting with increasing axial load, and therefore the column buckling strength will in reality be between the tangent modulus and the double-modulus predictions. Detailed expressions for various structural elements were presented (Table 4.2 and Figure 4.8). As it is observed, although the tangent modulus does not accurately define the actual buckling load, it provides a lower limit of the buckling load, which for most structural metals is only slightly below the actual critical column load [29]. So Engesser's original formulation is preferable for its simplicity and sufficient accuracy.

4.2.4 The Ultimate Strength of Longitudinally Loaded, 'Long', Plates

The subject of post-buckling behaviour and ultimate strength of steel plate elements in uniaxial compression has received a large amount of attention in the last 15-20 years. The formulations used in the analysis of plates have changed emphasis with time mainly due to the wider applications of computers and numerical methods. Hence, the studies started off as being analytical in nature and then moved on to numerical and then to semi-empirical approximate formulations for design which were mainly concerned with the effects of large deflections, post-buckling behaviour, imperfection sensitivities, residual stress and plastic deformations on the behaviour of the plates.

Researchers like Moxham and Little in Cambridge, Ueda et al in Japan, Crisfield, Frieze, Harding, Hobbs and Dowling in London all developed *numerical procedures* (Finite Element and Finite Difference) to construct

the complete load-shortening curves and determine the ultimate strength of unstiffened flat plates as affected in every case by the conditions just described above. According to Guedes Soares' detailed review of these approaches [30], the differences between these procedures are of the order of a few percent and therefore it is very difficult to pinpoint one approach as being the best.

The *approximate formulations* avoided the detailed description of all aspects affecting the post-buckled behaviour of plates, in favour of a simple, designer orientated, method that would only account for the more dominant features of response and could easily be calibrated to experimental and/or numerical results. The most popular of these approaches is the *effective width* concept based on the form of the actual stress distribution at the edges of the plate in the post-buckled phase. Faulkner in [31] provides an extensive review of the effective width formulations in use and applicable to the ultimate strength of stiffened plates.

One of the most widely used by the marine industry effective width approaches to analysing the ultimate compressive strength of simply supported plate elements is that by Faulkner first presented in 1965 and later extended and adopted in a method for predicting the strength of stiffened plates [28]. The approach takes in due consideration the effects of residual stresses via using the tangent modulus of elasticity thus accounting for the development of plasticity. No explicit account is however taken of initial imperfections.

The effect of initial distortions is considered in more detail by Carlsen's [32] proposed method. This method is similar to Faulkner's recommendations in the way the unwelded plate strength is calculated and on the level of residual stresses locked in the structure after welding is applied. An additional term accounts for the distortion effects.

Soreide and Czujko's proposal added a third term to Faulkner's formulation for the ultimate strength of unwelded and perfect plates. The effect of initial distrortions and residual stresses is accounted for via an multiplicative reduction factor which is a function of the plate cross sectional dimensions, maximum initial deflection and is restricted to values between 0.01 b/t and 0.1 b/t. For smaller distortions, the expression does not apply.

More recently, Ueda and Yao [33], based on a series of finite element calculations on the strength of rectangular plates with initial imperfections, put forward an expression for the design of compressed flat rectangular plates. No residual stresses were considered however.

Vilnay's 1981 design procedure [34], generated the effective width at any strain using the load-shortening curves from well controlled numerical analysis. Two different formulations were presented depending on the presence of residual stresses. Detailed numerical studies were also used to derive the Imperial College method [35, 36] which accounts for the effects of various, but predetermined, levels of residual stresses and initial imperfections on the ultimate strength capacity of compressed flat plates.

Finally, in 1988 Guedes Soares [37] presented a re-evaluation against a larger population of experimental and numerical results of Faulkner's method and extended it to account explicitly for the effect of initial deflections by the use of an appropriate 'curve-fitting' factor.

Five of the aforementioned models have been tested against existing numerical and experimental results by Pu [38] and the modelling uncertainties thus calculated are presented below.

	Faulkner	**Carlsen**	**Imp Col.**	**G. Soares**	**Vilnay**
Bias (Exp.)	1.159	1.117	0.893	1.031	0.990
COV (Exp.) (pop. 200)	0.163	0.138	0.200	0.101	0.147

The Guedes Soares method is clearly the best in terms of bias and COV values and is preferable.

The analysis of *stiffened plates* over the years has also been carried out via analytical, numerical approaches and semi-empirical approximations. Most of the initial *analytical formulations* do not account for the post-buckling behaviour or local component buckling and are often restricted to elastic behaviour. They generally concentrate on two main idealisations. One is to consider the stiffened plate as an orthotropic plate by smearing the stiffeners

along the plate (Schade [39], Mansour [40]), Smith [41], and the other is to consider the plate as a grillage of intersecting beam columns for which the plate is assumed to be the flange of the stiffeners. Mansour assumed that the stiffeners in either direction are equally stiff and equally spaced, with the spacing small enough for the plate elements to be considered fully effective. Under these circumstances, an homogeneous, orthotropic plate of constant thickness equivalent to the plate-stiffener combination was assumed by calculating the appropriate rigidity factors in both directions. The validity of orthotropic plate formulations depends primarily on the number of stiffeners in each direction, the uniformity of the overall stiffened panel and the boundary conditions. The correlation with experimental data of these analyses improves as the boundary conditions move closer to the simply-supported case and the number of stiffeners increases.

The second idealisation considering the stiffened plate as a grillage of intersecting beam columns for which the plate is assumed to be the flange of the stiffeners, has been used in the past by Chang and Michelsen, Wittrick (see [30] for more information). Closed form solutions have been obtained for uniform grillages subjected to uniaxial and biaxial loading by Faulkner [42] and Adamchack [43] which has been found to agree well [30] with a matrix formulation by Smith [41].

A number of *numerical formulations* presented over the years describing the behaviour of stiffened flat plating has been reviewed by Guedes Soares in [30]. *Approximate formulations*, on the other hand, centre around *column or beam-column methods* since these have proven to be fairly accurate over a large range of parameters, and provide the basis for accounting for residual stress, initial imperfection and mode interaction effects.

4.2.5 The Ultimate Strength of Stiffened Plates in Uniaxial Compression

The strength of stiffened plates depends on three variables, as identified by Little [44]; the plate slenderness β, the stiffener/plate column slenderness λ, and the level of residual stresses locked in the plate (HAZ effects would also affect the strength of aluminium columns). An increase in these variables results in a decrease in stiffened plate strength. Noting that it is both the plate and the stiffener that contribute to the slenderness and rigidity of the 'column', a decrease in β would be beneficial only if it is associated with a

small (or no) increase in λ. Despite the fact that residual stresses decrease the column strength, they result in a less peaked load-shortening curve for the plate and therefore improve the load redistribution in the structure.

The reduction in column strength due to residual stresses is significant for low β values ($\beta \approx 0.8$) as they cause the plate to loose stiffness at lower strain levels due to earlier compressive yielding of its central region. At intermediate values of plate slenderness ($\beta \approx 1.4$) the plate behaviour is imperfection sensitive and an increase in residual stresses causes a significant decrease in plate strength. At high column slendernesses ($\lambda > 1$) the residual stresses become less important due to the increasing dominance of elastic buckling. At high plate slenderness values ($\beta \approx 2$), an increase in residual stresses causes a reduction of column strength which is independent of λ.

The main feature of the beam-column method is that one isolated stiffener with an associated width of plating, is considered as representative of the whole panel behaviour. A number of such methods have been proposed. Of these, methods by Faulkner [28], Carlsen [32], Pu [38] and Imperial College/Smith [35, 36] are marine structures orientated. Others, such as those by Dwight and Little [45], Horne and Narayanan [46], Chatterjee and Dowling [47] and Murray [48] have been developed for steel box girders in bridges. These are based on Perry-Robertson and effective width formulations. Their main differences are the values used to account for the effects of residual stresses, initial imperfections and assumed load eccentricity due to loss of plate effectiveness.

Faulkner's method is based on a Johnson-Ostenfeld accountability of inelastic effects, while the post-buckled plate strength is modelled via an effective width approach (para. 4.2.5.1). Carlsen in turn, proposed a Perry-Robertson formulation together with an effective width formulation for the plate strength. This approach accounts in more detail of initial deflections in the plate and the stiffener, and accounts for magnification effects that occur due to the shift in neutral axis once the plate has buckled in plate induced interframe collapse. Plate induced and stiffener induced failures are treated separately. The Imperial College proposal [35, 36], is also based on a Perry-Robertson formulation accounting for initial imperfections for the plate and the stiffener components. The main drawback of the proposal, is that the final formulations have been calibrated to numerical data, which although

extensive, contain assumed definitions of the level of residual stresses and initial deflections expected in stiffened steel plated structures. Pu's proposal is based on Faulkner's method for stiffened plates. The sole difference is that the plate's ultimate strength is described by Guedes Soares' calibrated (to experimental data) expression of Faulkner's original effective width model.

Pu in [38] compared these four methods against 203 experimental and numerical data with his conclusions summarised by the following Table:

	Faulkner	Carlsen	Imperial Col.	Pu
Bias (Exp.) (pop. 63)	1.039	1.148	1.012	0.992
COV (Exp.)	0.143	0.137	0.151	0.099
Bias (Num.) (pop. 140)	1.041	1.197	0.901	0.983
COV (Num.)	0.104	0.171	0.118	0.129
Bias (All) (pop. 203)	1.041	1.182	0.931	0.986
COV (All)	0.117	0.163	0.132	0.120

This Table supports the view that Faulkner's method is the best in terms of bias and COV values and is therefore also recommended herein in the design of stiffened steel flat plating. This column approach will also form the basis for a new design approach of aluminium stiffened flat plates in uniaxial compression presented in paragraph 4.2.5.4.

4.2.5.1 Faulkner's Model for Unstiffened and Stiffened Steel Plating

The best example of application of the Tangent modulus approach to the description of the buckling strength of unstiffened and stiffened steel plates has been provided by Faulkner [28]. Faulkner's column treatment of the ultimate strength of a 'long' uniaxial plate in compression is based on an effective width approach, b_e. The ultimate strength capacity is given by:

$$\frac{\sigma_a}{\sigma_e}=\frac{b_e}{b}=\begin{cases}\left(\frac{2}{\beta}-\frac{1}{\beta^2}\right)R_r\,R_m & \text{for} \quad R_r=\begin{cases}1-\frac{\sigma_{rc}}{\sigma_y}\frac{E_t}{E}\left(\frac{\beta}{2\beta-1}\right) & \text{for } \beta\geq 1\\ 1 & \text{for } \beta<1\end{cases}\\ R_r\,R_m\end{cases}$$

σ_e is the edge stress when this is less than the yield stress ($0.75\leq\sigma_e\leq\sigma_y$) and σ_a is the equivalent average stress over the complete section. R_r is a plate strength reduction ratio accounting for the detrimental effect of residual stresses. R_m is defined later and accounts for biaxial loading effects. σ_{rc} is the compressive residual stress in the structure which for equilibrium considerations in the plating cross section is given by:

$$\frac{\sigma_{rc}}{\sigma_y}=\frac{2\,n}{(b/t)-2\,n}$$

Values of n=4.5-6 are typical for as-welded ships but values of 3-4.5 are more appropriate after allowing for shakedown. E_t is the structural tangent modulus for the stiffened plate in compression. For flat-yield type materials the ratio E_t/E is approximated using the Ostenfeld-Bleich parabolae [28]:

$$\frac{E_t}{E}=\frac{\sigma(\sigma_y-\sigma)}{\sigma_{ps}(\sigma_y-\sigma_{ps})}=\begin{cases}\left(\frac{3.62\beta^2}{13.1-p_r(1-p_r)\beta^4}\right)^2 & \text{for } 0\leq\beta\leq 1.9\sqrt{\frac{\sigma_y}{\sigma_{ps}}}\\ 1.0 & \text{for } \beta\geq 1.9\sqrt{\frac{\sigma_y}{\sigma_{ps}}}\end{cases}$$

where σ_{ps} is the structural proportional limit in compression. Expressions for 'clamped' boundary conditions [28] are used when the lateral pressure is greater than $\sigma_y^2/E\beta^2$.

'Wide' plating is treated in a similar manner, using an effective width approach and the final ultimate strength expression is based on the French Bureau Veritas/Faulkner solution for a pinned plate:

$$\sigma_{ym}=\sigma_y\left[\frac{0.9}{\beta^2}+\frac{1.9}{\alpha\beta}\left(1-\frac{0.9}{\beta^2}\right)\right] \qquad \text{for } \beta\geq 1 \text{ and } \alpha\beta\geq 1.9$$

Outside the stated limits the plate slenderness is sufficiently small as to justify the assumption of a stocky plate and the change of failure mode from

buckling to material yielding. No residual stress effects are accounted for and the edge stress is always expected to reach yield stress levels.
Biaxial loading of long plates is accounted for by means of a parabolic interaction relationship [28]:

$$\frac{\sigma_x}{\sigma_{x,ult}} + \left(\frac{\sigma_y}{\sigma_{y,ult}}\right)^2 = 1 \qquad \text{or} \qquad R_m = 1 - \left(\frac{\sigma_y}{\sigma_{y,ult}}\right)^2$$

where $\sigma_{x,ult}$ and $\sigma_{y,ult}$ are the ultimate strengths of the plate in uniaxial compression in the longitudinal and transverse directions respectively, when the compressive load is acting separately in each direction. For the case of *combined pressure and compression* a linear interaction between the compressive strength of a wide plate and lateral loading is conservatively assumed. The beneficial effect of lateral loading on 'long' plating is neglected.

The design of *flat stiffened panels* has been based on interframe plate induced buckling failure. Faulkner used a reduced effective width approach to account for the continuous stiffness loss of the plating as load increases in the post-buckling regime. Hence, the plating breadth assumed to act with the stiffener as a column is taken at the reduced value of:

$$\frac{b_e'}{b} = \begin{cases} (1/\beta_e) R_r & \text{for } \beta_e \geq 1 \\ 1 & \text{for } \beta_e \leq 1 \end{cases}$$

with the critical buckling load of the column given by :

$$\frac{\sigma_{cr}}{\sigma_y} = \begin{cases} 1/\lambda_{ce}^2 & \text{for } \lambda_{ce}^2 \geq 1/p_r \\ 1 - p_r(1-p_r)\lambda_{ce}^2 & \text{for } \lambda_{ce}^2 \leq 1/p_r \end{cases} \quad \text{where } \lambda_{ce} = \frac{a}{\pi}\sqrt{\frac{\sigma_y (A_s - b_e t)}{E I_{xe}'}}$$

is the non-dimensional column slenderness and $p_r = \sigma_{ps}/\sigma_y$ is the structural proportional limit stress ratio, I_{xe}' is the moment of inertia of the combined section with the plating width of b_e'. When biaxial stressing is present, then b_e' is reduced by a factor of R_m, $b_e' = b_e' R_m$.

In the presence of *lateral pressure loading* a linear interaction is assumed

between critical compressive 'column' buckling and lateral load:

$$\frac{\sigma_{ce}}{\sigma_{cr}} + \frac{q_x}{q_{xp}} = 1$$

where q_x is the equivalent pressure load per unit width on the plating and q_{xp} is the pressure load per unit length required to cause full plasticity in the cross section.

4.2.5.2 A Model for the Ultimate Strength of Unstiffened Aluminium Flat Plates

Current design code approaches generally opt for a Perry-Robertson type of expression to estimate the strength of unstiffened/stiffened aluminium plates in compression (mainly in Europe, ERAAS, BS 8118) and a 'unified' column approach in the case of North American recommendations. However, they do not account so for residual stresses, having to rely on curve fitting to experimental data for this purpose (e.g. work in Cambridge by Dwight). As most of the current steel design codes (e.g. ECCS, BS 5400) use the Perry-Robertson approach, it is perhaps not unusual that this expression has found its way, in one form or the other, in current aluminium design codes too (e.g. ERAAS, BS 8118). The efficiency of such expressions and hence the accuracy of their strength predictions, are of course dependent on the the quality and quantity of the data on which the derivation of their coefficients has been based, which is not always yield the right result.

Good models based on proper understanding of the phenomenon, and followed by consistent modelling of its effects on the structural behaviour (para. 1.5.3, Chapter 1) are bound to withstand the test of time and agree with, rather than adjust to, experimental data. Faulkner's effective width approach to 'long' plate strength [28]:

$$\Phi_B = \frac{\sigma_a}{\sigma_e} = \frac{b_e}{b} = \begin{cases} \left(\frac{2}{\beta} - \frac{1}{\beta^2}\right) & \text{for } \beta \geq 1 \\ 1 & \text{for } \beta < 1 \end{cases}$$

has proved to be one such model, and has thus been chosen as the basis for its extension to aluminium plate buckling behaviour. Its validity and

efficiency for steel plates has been proved consistently over the years (para. 4.2.4) and provides mean predictions relative to experimental data. The main difference of the model relative to the various design approaches currently in use is that it accounts in detail for the effects of locked-in residual stresses in steel plate buckling behaviour neglecting any direct reference to any existing initial imperfections in the plate. Their effect can later be accounted for by curve fitting (if necessary) to experimental data.

4.2.5.3 Application of Faulkner's Model to Unstiffened Aluminium Flat Plating

The substitution of steel by aluminium in a welded flat plated structural element requires that proper account is taken of the initial out-of-flatness, residual stresses, HAZ softening and the curvature of the material stress-strain curve. Initially, the approach already described for steel has been used in the past [51]. Residual stress considerations remained unchanged (n=3.0 taken for both steel and aluminium) to those of Faulkner, the 0.2% proof stress was used in the place of the material yield stress. Material properties as applicable to aluminium were also used. The use of 0.2% proof stress in a theory that assumes elastic-perfectly plastic behaviour of the structural material (steel) is conservative, as the inherent strain hardening in aluminium material is neglected. HAZ softening was introduced as a reduction in the reduced effective plating width assumed to act with the stiffener in column collapse. The calculation of the extent and strength of the heat affected zone was based on the BS 8118 proposals [19]. However, such an arbitrary approach to HAZ effect modelling on plate behaviour resulted in a formulation that was independent of the overall plating breadth (or stiffener spacing). As a result, the actual extent of the HAZ was taken as a proportion of the reduced effective width as follows:

$$b_e' = b_e' - (\text{Area HAZ} / b\,t)\, b_e'$$

Proportioning of the HAZ with b_e' protected against unacceptably small values of the reduced effective width in addition to relating the HAZ and its effect to the plate geometry. Such a model, perhaps not surprisingly, proved unsatisfactory [51] and was followed by a more thorough investigation.

More recently, the accuracy of strength predictions of the basic Faulkner expression presented in the previous paragraph was originally tested against

the 22 available experimental data for unwelded plates (11 tests for each of the 6082 and 5083 alloy cases) [52, 54]. Table 4.3 presents the results of such a comparison. The bias is defined as the ratio of the experimental values over the theoretical predictions. Although the population of data is quite small, the applicability of this model to unwelded aluminium plates of both the 6082 and 5083 aluminium alloys, is justified. It is found to be slightly unconservative for the 5083 alloys and providing slightly conservative estimates for the 6082 alloys. Hence, a small scalar correction, B_{imp}, of

$$B_{imp} = \begin{cases} 1.056 & \text{for 6082 alloys} \\ 0.959 & \text{for 5083 alloys} \end{cases}$$

will reduce the error and leave the COV values unaffected. If on the other hand, a linear variation with the plate slenderness ratio β of the imperfection correction factor, B_{imp}, is assumed, regression analysis of the bias has resulted in the following coefficients for the linear relationships:

$$B_{imp} = \begin{cases} 0.002\beta + 1.004 & \text{for 6082 alloys} \\ -0.002\beta + 0.962 & \text{for 5083 alloys} \end{cases}$$

It is obvious that the bias is effectively unaffected by the plate slenderness (Table 4.3). Hence, a linear correction factor is considered no further, in favour of the scalar ones as presented earlier. Therefore, for *unwelded* aluminium plates the ultimate strength prediction expression becomes:

$$\Phi_B = \frac{\sigma_a}{\sigma_e} = \frac{b_e}{b} = \begin{cases} \left(\frac{2}{\beta} - \frac{1}{\beta^2}\right) B_{imp} & \text{for } \beta \geq 1 \\ B_{imp} & \text{for } \beta < 1 \end{cases} \quad \text{for} \quad B_{imp} = \begin{cases} 1.056 & \text{for 6082 alloys} \\ 0.959 & \text{for 5083 alloys} \end{cases}$$

When a plate is *welded*, two additional aspects require particular attention, the:

- residual, locked-in stresses reducing the compressive strength of the cross section
- strength reduction in the parent material strength adjacent to the welds due to HAZ softening.

The different natures of the sources of reduction in these two cases is worth

noting. In the first instance, the reduction is due to 'external' factors, i.e. due to locked-in stresses in the section, whose level although dependent on the parent metal/weld metal strength is not directly influenced by the microstructure and treatment of the material. In the second case however, the reduction is solely due to changes in the microstructure of the material occurring due to the considerable heat input of the welding process. It is therefore suggested herein, that the degrading effects of the HAZ softening and the residual stresses are treated as follows:

(a) to firstly account for the localised material strength reduction (due to HAZ softening) by means of a plate of 'equivalent' strength, and then
(b) to account for the residual stress reduction in a manner similar to that used by Faulkner in the steel flat plate model.

By 'plates of equivalent strength' it is implied that the geometrical dimensions of the plate will remain unchanged while the material proof stress will be altered in such a way so as to accommodate the HAZ reduced strength values on the plate edges. In other words, the reduction in strength on the two edge regions (see Figure below) will be proportionately (to the heat affected over heat unaffected areas of the plate cross section) evenly spread over the complete width of the plate, b.

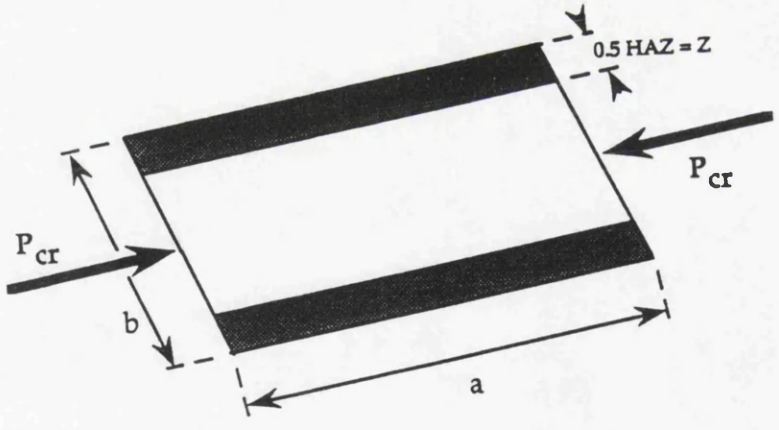

The criterion for such an action is that, *at the elastic critical stress level*, the stiffness of the complete plate will be equal to the summation of the stiffnesses of the three individual 'elements' in the section, i.e. the two heat affected zones and the heat unaffected zone in between. Hence the equality of stiffnesses at the critical buckling stress level may be expressed

$$\left(\frac{P_{cr,el}}{\varepsilon}\right)_{(b-HAZ)} + \left(\frac{P_{cr,el}}{\varepsilon}\right)_{(HAZ)} = \left(\frac{P_{cr,el}}{\varepsilon}\right)_{(\sigma_{0.2})}$$

$$\frac{\sigma_{cr,el}\,(b-2z)\,t}{\frac{\sigma_{cr,el}}{E}+0.002\left(\frac{\sigma_{cr,el}}{\sigma_{0.2}}\right)^{n}}+\frac{\sigma_{cr,el}\,2z\,t}{\frac{\sigma_{cr,el}}{E}+0.002\left(\frac{\sigma_{cr,el}}{\sigma^{*}_{0.2}}\right)^{n}}=\frac{\sigma_{cr,el}\,b\,t}{\frac{\sigma_{cr,el}}{E}+0.002\left(\frac{\sigma_{cr,el}}{\sigma'_{0.2}}\right)^{n}}$$

where w ($=k_z$) and 2z are the magnitude and extent of the HAZ reduction as identified in the BS 8118 recommendations. For details on these values, paragraph 4.1.2, Table 4.4, Figure 4.6 and reference [19] should be consulted. Solving for $\sigma'_{0.2}$, the 'equivalent' material proof stress for the heat-affected plate, the following expression is obtained

$$\sigma'_{0.2}=\left(\frac{0.002\,E\,\sigma^{n}_{cr,el}}{\left(\frac{b}{A+B}\right)-\sigma_{cr,el}}\right)^{1/n}$$

where $$A=\frac{b-2z}{\sigma_{cr,el}+0.002\,E\left(\frac{\sigma_{cr,el}}{\sigma_{0.2}}\right)^{n}} \qquad B=\frac{2z}{\sigma_{cr,el}+0.002\,E\left(\frac{\sigma_{cr,el}}{w\,\sigma_{0.2}}\right)^{n}}$$

$\sigma_{cr,el}$ is the elastic critical buckling stress for a 'long', 'pinned', plate of dimensions a, b in uniaxial, in-plane, compression given by:

$$\sigma_{cr,el}=\frac{4\pi^{2}E}{12\left(1-\upsilon^{2}\right)}\left(\frac{b}{t}\right)^{2}$$

In accounting for the *residual stress reduction* effects and inelastic behaviour, Faulkner's tangent modulus concept is used and adopted for use in aluminium alloy applications. The main difference between the mild steel and aluminium alloy stress-strain curves is that the former demonstrate clearly a point above which the material behaviour changes from purely elastic to purely plastic. Such a behaviour, permits the application of proportional limit concept accounting for the effects of residual stresses. Material non-linearities will hence commence at stress levels above the proportional limit as that is identified by the welding process. In aluminium however, material non-linearities characterise the curve throughout the stress-strain range. Hence, the arbitrary assumption of yielding occurring at the 0.2% proof stress level. Application of residual stresses in the model hence becomes more complex.

In steel the structural tangent modulus accounting for the geometrical and material non-linearities is assumed to be given by the Ostenfeld-Bleich parabolae (para. 4.2.5.1):

$$\frac{E_t}{E} = \frac{\sigma(\sigma_y - \sigma)}{\sigma_{ps}(\sigma_y - \sigma_{ps})}$$

Herein, however, it is assumed that in *welded* aluminium structures the structural stress-strain curve is assumed to follow, over the complete stress-strain range, the already modified (for HAZ effects) Ramberg-Osgood material curve which in turn is appropriately modified to account for the effect of residual compressive stresses (see Figure below).

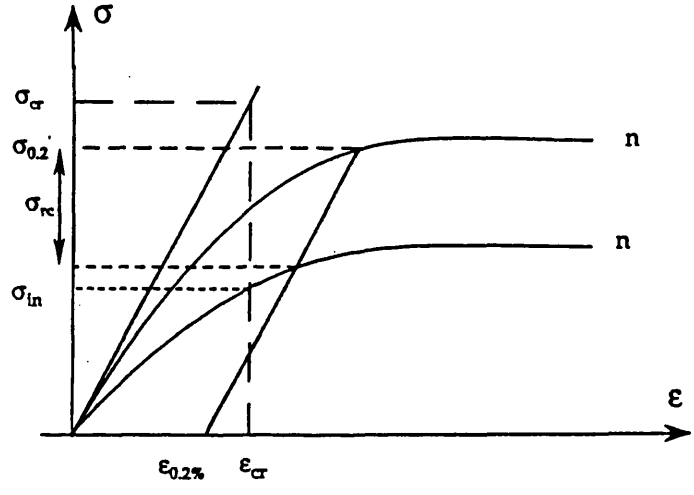

Faulkner's assumptions used for steel [28] are assumed to apply for aluminium too:

1. the plate buckles elastically or inelastically at the same critical strain
2. the 'inelastic' plate buckling stress is assumed to be given by:

$$\sigma_{in} = \sigma_{cr.el}\sqrt{\frac{E_t}{E}}$$

3. the reduction in plate strength will be equal to the reduction in the 'inelastic' buckling stress

$$\Delta\sigma_m = \sigma_{rc}\frac{E_t}{E}$$

The first assumption relating the inelastic strain $\varepsilon_{cr,in}$ to the elastic strain $\varepsilon_{cr,el}$ may be expressed as

$$\varepsilon_{cr,in} = \varepsilon_{cr,el} \quad \Leftrightarrow \quad \frac{\sigma_{in}}{E} + 0.002\left(\frac{\sigma_{in}}{\sigma_{0.2}' - \sigma_{rc}}\right)^n = \frac{\sigma_{cr,el}}{E}$$

which results in the following nth degree equation in σ_{in}:

$$k_1 \sigma_{in}^n + k_2 \sigma_{in} + k_3 = 0$$

where

$$k_1 = 0.002\,E, \qquad k_2 = \left(\sigma_{0.2}' - \sigma_{rc}\right)^n, \qquad k_3 = -\sigma_{cr,el}\,k_2$$

σ_{rc} is the residual compressive stress introduced in the section due to welding. Its level and extent is calculated as recommended by Wong [9, 10] and presented in paragraph 4.1.1 and Table 4.1 and Figure 4.1. As this expression requires an numerical solution, the Newton-Raphson procedure was found to be adequate and convergence was quite fast.

Having established σ_{in}, the value of the assumed tangent modulus E_t is obtained based on the second of Faulkner's assumptions:

$$\frac{E_t}{E} = \left(\frac{\sigma_{in}}{\sigma_{cr,el}}\right)^2$$

As the reduction in plate strength will be equal to the reduction in the 'inelastic' buckling stress (third assumption)

$$\Delta\sigma_m = \sigma_{rc}\frac{E_t}{E} = \left(\frac{\sigma_{in}}{\sigma_{cr,el}}\right)^2 \qquad \text{and hence} \qquad R_r = 1 - \frac{\Delta\sigma_m}{\sigma_{0.2}\,\Phi_B}$$

Therefore, *for welded aluminium plates* the ultimate strength model becomes:

$$\frac{\sigma_a}{\sigma_e} = \frac{b_e}{b} = \begin{cases} \left(\dfrac{2}{\beta} - \dfrac{1}{\beta^2}\right) C_1\, C\, R_r & \text{for } \beta \geq 1 \\ C_1\, C & \text{for } \beta < 1 \end{cases}$$

where C, R_r, refer to correction for imperfection effects, and welding effects (residual stress and HAZ effects) respectively.

The evaluation of the accuracy of the proposed model was based on an

detailed experimental study carried out by Mofflin and Dwight [52]. The buckling strength of individual, unstiffened, aluminium plates loaded in uniaxial compression, having unloaded edges simply supported and free to slide, was investigated. The plate thickness was restricted to 6 mm and the aspect ratio was fixed to 4. The b/t ratio varied from 20 to 85 and the slenderness ratio β from 1.11 to 5.5. The experimental program consisted of 76 specimens in two aluminium alloys:

6082-TF	Fully heat treated material having a relatively abrupt knee on its stress strain curve. n varied between 25 and 28
5083-M	Non-heat-treatable material with a rounded material stress-strain curve. -M is the hot-rolled condition
5083-O	A number of test data (12 in number) used an annealed material. n varied between 8 and 18.

The exponent n of the Ramberg Osgood law is characteristic of the material strain hardening rate of the inelastic portion of the stress-strain diagram. It can be expressed relative to the 0.2% and 0.1% proof stresses by [53]:

$$n = \frac{\ln 2}{\ln(\sigma_{0.2}/\sigma_{0.1})}$$

Initial imperfections were introduced mechanically in all specimens. Although, the magnitude of these imperfections was not accurately controlled due to plating 'springback, the final measurements concluded that the magnitude of these imperfections was in the range

For unwelded plates	0.0005-0.006 b
For longitudinally welded plates	0.0010-0.0075 b
For transversely welded plates	0.001-0.0023 b
For longitudinally and transversely welded plates	0.001-0.005 b

Out of 76 tests, 22 tests were on unwelded plate specimens in both alloys (11 tests from each alloy). In addition, 33 of the remaining specimen population (19 tests -5083 and 14 tests of 6082) were welded along the long edges to introduce residual stresses and HAZ softening. Some of the remaining specimens (2 tests in 5083 and 3 tests in 6082 alloys) were welded solely in

the transverse direction while 4 (1 test in 6082 and 3 tests in 5083 tests) were transversely welded and longitudinally welded. The results confirmed Wong's earlier predictions [9, 10] that the heat treated alloys (e.g. 6082) suffer less residual stress than the 5083 alloys. These experimental results have shown that unwelded plates are fairly insensitive to the degrees of geometrical imperfections but the effects of welding are by far the most dominant on the plate strength level. As Mofflin and Dwight commented [52], although the absolute strengths of the 5083 plates are well below those of the 6082 plates, when these are non-dimensionalised relative to the material proof stress the difference reduces to only 10-15% below the 6082 plate strengths. Another observation by Mofflin and Dwight was that transverse centrally positioned welds seem to have negligible effects on the 5083 alloy plates, but seem to reduce the strength of the 6082 alloy plates by 20-30% due to HAZ softening.

Tables 4.5 and 4.6 present a comparison of the proposed model for 5083 and 6082 alloy plates respectively, with the experimental data of Mofflin and Dwight [52, 54]. In the comparison C and C_1 are both taken equal to 1. The accuracy of the model predictions for various welding arrangements is also carried out by checking separately the bias (expr/pred) and COV values for longitudinally welded plates, transversely welded plates and longitudinally /transversely welded plates. The comparisons, for the latter two cases particularly, should be treated cautiously due to the extremely limited number of data. Caution should also be exercised for the comparison of the longitudinally welded plates, but the initial results are very encouraging. The effects of including the imperfection correction (as derived for unwelded plates) on the accuracy of the predictions was also investigated.

For the 5083 longitudinally welded alloys and for a population of 19 tests (Table 4.5) the accuracy of the model is satisfactory with a bias of 0.955 and COV of 6% for the case when no imperfection correction is introduced in the model. The model prediction draws a mean curve to experimental data if the imperfection correction is applied and a small change is observed in the COV values. Corrections with the scalar factor of 0.955 (for no imperfection correction) or a factor of 0.9995 (when imperfection correction is included) is to be preferred over a correction factor which varies linearly with the plate slenderness ratio. Although in the latter case an improvement is observed in the COV values, they are not considered as worth implementing bearing in mind the limited number of data available.

The accuracy of the model has also been tested and proved against data for 6082, longitudinally welded plates. For the case where no imperfection corrections is used, the predictions form a mean to experimental data and present a small COV value of 5.3%. If the imperfection correction is included however, the relative accuracy of the model breaks down by underpredicting the strength and increasing the COV value. The dominance of the welding effects over the effects of initial imperfections for heat-treated alloy plate behaviour could be the cause. Scalar corrections provide negligible improvements on the modelling prediction, while a linear variation of the correction factor make the predictions conservative and establishes a COV value of approximately 5% for both cases of accounting for imperfection corrections or not.

Following the above discussion the following values for the correction factor C (includes the coefficient of B_{imp}) are proposed:

For Longitudinally Welded Plates	
For 5000 Series Plates	C=0.9585
For 6000 Series Plates	$C=0.034\beta+0.9953$
For Transversely Welded Plates	
For All Alloy Plates	C=1.0

The reduction factor C_1 accounts for the effects of positioning the welds elsewhere but at the toe of the stiffeners (i.e. elsewhere except the geometrical boundaries of the plates under consideration). The use of extrusions encourages the positioning of welds away from the geometrical boundaries of the plate. Hence:

For Longitudinal Welds	
$C_1=1.0$	For All Alloy Plates
C	As described earlier

For Transverse Welds

$C = 1.0$ and

$$C_1 = \begin{cases} 0.8 & \text{for } 0.2\,b \le x \le 0.8\,b \\ 1.0 & \text{for } x < 0.2\,b \text{ or } x > 0.8\,b \end{cases} \quad \text{for 6000 Alloy Plates}$$

$$C_1 = \{1.0 \quad \text{for 5000 Alloy Plates}$$

The welds orientated in the direction of compressive loading) are identified as longitudinal welds above. x denotes the distance (orthogonal to the line of application of the load) of the welds from the loaded edges of the plates and does not correspond to the length of the weld. The use of the reduction coefficient C_1 attempts to account for the detrimental effects of transversely positioned welds and also allows due account to be taken of the possibility of using extruded sections, requiring welded connections to be made at places other than at the stiffener toe. The values for C_1 recommended above were chosen rather arbitrarily, bearing in mind the following:

(a) Experimental observations of the strength of transversely welded aluminium plates (welds centrally located, i.e. x=0.5 a) by Mofflin and Dwight [52] record minimal reduction in strength for 5083 alloy plates and reductions in strength of the level of 20-30% for the 6082 alloy plates (hence the reduction coefficient of 0.8 above).

(b) Extensive numerical and experimental investigations on the effect on the strength of the position of transverse welds relative to the loaded edges for aluminium columns (reviewed by Tolikas in [55] supported this dependence and was generally found that positioning the welds in the regions 0-0.2a, and 0.8a-1.0a, does not affect the column strength considerably. Their effect may therefore be neglected. The worst case was observed for the cases where the welds were positioned centrally on the plate. Such results therefore limit the applicability of extrusions.

It is worth noting the approach adopted by Kendrick in using well established procedures developed for steel submarine design to the design of the ALUMINAUT, an aluminium submarine constructed by Reynolds Metals in the early 1960s. The equivalence came by replacing σ_y with the

0.2% proof stress, $\sigma_{0.2}$, and by replacing Young's modulus E, by the secant modulus, E_s, defined at the 0.2% proof stress by $\sigma_{0.2} / \varepsilon_{0.2}$. The comparison of this proposal against the aluminium flat plate data presented earlier has not been carried out, but its general effect would be to increase the plate slenderness, β, resulting in reduced compression strength.

4.2.5.4 Application of Faulkner's Model to Stiffened Aluminium Flat Plating

The design of *stiffened flat aluminium panels* should be based on interframe plate induced buckling failure. In tackling the problem for steel structures as essentially a column under compression, Faulkner [28] used a reduced effective width approach to account for the continuous stiffness loss of the plating as load increases in the post-buckling regime (para. 4.2.5.1). In extending this approach to aluminium stiffened plating the following points need to be addressed which arise as a result of HAZ softening:

(a) the possibility of different alloy materials used for plate and stiffener.

(b) the need to account for construction aspects arising from the use of extruded sections. At such instances, the model should be able to adjust readily to the possibility that welding would occur at the stiffener toe (if the stiffener is extruded and the plating rolled separately) or to the case where welding would be prescribed at a position away from the toe of the stiffener (in the case where the stiffener and part of the plating would be extruded together in one section).

(c) the effect that the position along the length of the stiffener of a possible transverse weld will have on the overall column strength.

In tackling these questions, the approach used for the flat plate case is very useful, as will be demonstrated. If a section is assumed, consisting of the stiffener (A_s is the stiffener cross-sectional area) and the plate (of dimensions b_e and t - note that the proof stress is assumed as the original parent material strength), the equality of stiffnesses at the critical buckling stress level for the complete section may be expressed by:

$$\left(\frac{P_{cr,el}}{\varepsilon}\right)_{(plate)} + \left(\frac{P_{cr,el}}{\varepsilon}\right)_{(stiffener\ HAZ)} + \left(\frac{P_{cr,el}}{\varepsilon}\right)_{(unaffected\ stiffener)} = \left(\frac{P_{cr,el}}{\varepsilon}\right)_{(all\ section)}$$

$$\frac{\sigma_{cr,el}\,(b_e' t)}{\frac{\sigma_{cr,el}}{E} + 0.002\left(\frac{\sigma_{cr,el}}{\sigma_{0.2,pl}}\right)^{n_p}} + \frac{\sigma_{cr,el}\, z_w\, t_w}{\frac{\sigma_{cr,el}}{E} + 0.002\left(\frac{\sigma_{cr,el}}{\sigma_{0.2,st}^{*}}\right)^{n_{st}}} +$$

$$\frac{\sigma_{cr,el}\left(A_s - z_w\, t_w\right)}{\frac{\sigma_{cr,el}}{E} + 0.002\left(\frac{\sigma_{cr,el}}{\sigma_{0.2,st}}\right)^{n_{st}}} = \frac{\sigma_{cr,el}\left(A_s + b_e\, t\right)}{\frac{\sigma_{cr,el}}{E} + 0.002\left(\frac{\sigma_{cr,el}}{\sigma_{0.2}'}\right)^{n}}$$

where $\sigma_{cr,el}$ is the elastic critical buckling stress for the column in compression given by:

$$\sigma_{cr,el} = \frac{\pi^2\, E\, I}{L_e^2\, A}$$

$n = \min\left(n_p, n_s\right)$ where n_p, n_s are the Ramberg-Osgood exponents for the plate and stiffener materials respectively, A_s is the full stiffener area, $\sigma_{0.2,s}, \sigma_{0.2,p}$, are the proof stresses of the stiffener and plate materials respectively and t_w is the web thickness of the stiffener. In addition, w $(=k_z)$ and $2z_w$ are the magnitude and extent of the HAZ reduction *in the stiffener web only* as identified in the BS 8118 recommendations. For details on these values, paragraph 4.1.2, Table 4.4, Figure 4.6 and reference [19] may be consulted. Solving for $\sigma_{0.2}'$, the 'equivalent' material proof stress for the complete section, the following expression is obtained

$$\sigma_{0.2}' = \left(\frac{0.002\, E\left(\sigma_{cr,el}\right)^n}{\left(\frac{A_s + b_e' t}{C_1 + C_2 + C_3}\right) - \sigma_{cr,el}}\right)^{1/n}$$

$$C_1 = \frac{b_e' t}{\sigma_{cr,el} + 0.002\, E\left(\frac{\sigma_{cr,el}}{\sigma_{0.2,p}}\right)^{n_p}}$$

$$C_2 = \frac{z_w\, t_w}{\sigma_{cr,el} + 0.002\, E\left(\frac{\sigma_{cr,el}}{w\,\sigma_{0.2,s} - \sigma_{rc}}\right)^{n_s}}$$

$$C_3 = \frac{\left(A_s - z_w\, t_w\right)}{\sigma_{cr,el} + 0.002\, E\left(\frac{\sigma_{cr,el}}{\sigma_{0.2,s} - \sigma_{rc}}\right)^{n_s}}$$

Hence a section of 'equivalent' proof stress is obtained which can be used

with no reduction in its original geometrical characteristics.

Using (as was done for aluminium plates earlier) Faulkner's assumption that columns buckle elastically or inelastically at the same critical strain and hence relating the inelastic strain $\varepsilon_{cr,in}$ to the elastic strain $\varepsilon_{cr,el}$ by

$$\varepsilon_{cr,in} = \varepsilon_{cr,el} \quad \Leftrightarrow \quad \frac{\sigma_{in}}{E} + 0.002\left(\frac{\sigma_{in}}{\sigma'_{0.2}}\right)^n = \frac{\sigma_{cr,el}}{E}$$

the following nth degree equation in σ_{in} results:

$$\sigma_{clm} = \begin{cases} \sigma_{cr,el} & \text{for} \quad \sigma_{cr,el} < \sigma'_{0.2} \\ k_1 (\sigma_{in})^n + k_2\, \sigma_{in} + k_3 = 0 & \text{for} \quad \sigma_{cr,el} \geq \sigma'_{0.2} \end{cases}$$

where $k_1 = 0.002\, E$ $\qquad k_2 = (\sigma'_{0.2})^n$ $\qquad k_3 = -\sigma_{cr,el}\, k_2$

The benefits of this approach are demonstrated by applying it to the specific problems mentioned above and for which it has been developed. Hence,

For Non-Welded Stiffeners or Extrusions

Extrusions contain their welds away from the stiffener toe. As a result the effects of welding (residual stresses and HAZ strength reduction) will only be present in the plate. The stiffener cross section characteristics will not be affected. Hence the aforementioned expressions still apply incorporating though the following changes:

$$\sigma_{rc} = 0, \quad w = 1, \quad z_w = 0$$

For Welded Stiffeners at Their Toes

The extent ($z_w = \alpha\, \eta\, z_o$) and magnitude (w) of reduction in the HAZ for the stiffener portion of the column cross section should be obtained according to the BS 8118 recommendations (para. 4.1.2) For *longitudinally welded* columns all the aforementioned expressions apply. Heat-treated and non heat-treated materials are accounted for via n and w. For *transversely welded* columns, the positioning of the weld along the stiffener length is of primary importance and greatly affects the final strength result. Hence for x being the distance of the weld from the column ends:

• For $0.1L > x$ and/or $x > 0.9L$: The approach for non-welded stiffeners and extrusions presented earlier should be followed.

• For $0.1L \leq x \leq 0.9L$: The approach for non-welded stiffeners and extrusions presented earlier should be followed i.e. use of $\sigma_{rc} = 0$, $w = 1$, and $z_w = 0$, and the final result reduced by the factor w (as recommended by ERAAS [56]. Hence

$$\sigma_{clm}^{red} = \begin{cases} w\,\sigma_{clm} & \text{for } \bar{\lambda} < 1.25 \\ \sigma_{clm} & \text{for } \bar{\lambda} \geq 1.25 \end{cases} \qquad \text{where} \qquad \bar{\lambda} = \sqrt{\sigma_{0.2}/\sigma_{cr}}$$

Justification of this formula is available in the following paragraph. However, the approach has not been tested against experimental data. It is presented herein as a rational extension to the unstiffened aluminium plate approach presented in paragraph 4.2.5.3. Appropriate experimental data are very limited (5 data points in [123]) and thus more thorough investigation and evaluation is recommended as further work.

4.2.5.5 The Effect of Transverse Welds on the Buckling Strength of Aluminium Columns

Extensive experimental and numerical studies on the instability of extruded and welded aluminium alloy columns has been carried out since 1970 under the auspices of the ECCS [1, 53] and the BS 8118 [57, 58] development committees and by Hong [59]. All of these studies have concentrated, among others, on the study of the effects on column strength of the position of transverse welds relative to the column slenderness ratio. It was generally concluded that *for centrally located transverse welds* and stocky columns ($\bar{\lambda} < 1.25 - 1.5$) the column strength is reduced by a factor approximately equal to w ($=\sigma_{0.2}^{*}/\sigma_{0.2}$), which is the worst strength reduction scenario. For slender columns ($\bar{\lambda} \geq 1.5$) the strength reduction becomes insignificant implying that over this slenderness range, it is the cross-section geometry that governs the strength level. $\bar{\lambda}$ is the normalised slenderness ratio of the column.

On the other hand, for *non-centrally located transverse welds* it has been established that the reduction in strength is significant if the welds are placed in the region of 0.2 to 0.8L from either ends. So it is unhelpful to

weld at one-third points instead of at midspan. Positioning of the welds at distances less or equal to 0.2L from the ends (simply supported) is only beneficial. For positions between these limits, Hong [59] recommends either the conservative approach of treating the columns as having a centrally placed weld or by interpolation using a sinusoidal function:

$$P_3 = P_2 - (P_2 - P_1)\sin\left(\frac{\pi X}{L}\right)$$

where X/L is the position of the weld from the column ends, L is the effective column length, P_1 is the column strength estimated by assuming the material to be fully HAZ softened (i.e. $\bar{\lambda}$ calculated based on $w\,\sigma_{0.2}$) and P_2 is the column strength estimated by entering the column strength curves by with a normalised slenderness ratio, $\bar{\lambda}$, calculated assuming the material proof stress to be given by $\sigma'_{0.2} = \sigma_{0.2} - 0.5\,w\,\sigma_{0.2}$. The agreement with numerical and experimental data was found in [59] to be 'remarkably good'. Simply supported end conditions are implied.

Figure 4.9 provides a comparison between the buckling curves for columns of the same shape consisting of either base material, or base material and longitudinal welds, or base material and cross-weld midspan, or pure HAZ material. The advantages of longitudinally welding a section (over cross-welding) are obvious especially for $\bar{\lambda} < 1.5$. At high slendernesses ($\lambda \geq 1.5$) the reduction is negligible while at low slenderness values the ratio between the capacities of longitudinally welded and extruded (unwelded) columns tends to the value of A^* / A.

4.2.6 Ultimate Strength of Transversely Loaded 'Wide' Plates

At 'wide' plate compressive loading, the plate elements in the central region of the plate do not experience the restraining effect that the short edges do, and thus behave like a column. As column behaviour is characterised by the lack of postbuckling strength, it is inevitable that transversely loaded plates have smaller postbuckling strength that if loaded in the 'long' direction. In addition, in this case, the influence of weld induced residual stresses in the direction of loading may be neglected as these are located at a position in the plate which is away from the critical buckling zone of the element. Also, the detrimental effects of initial imperfections are more dominant for 'wide' plates and will adversely affect their ultimate strength.

It was Blanc in 1965 [60] who first attempted to model the post-buckling strength of plates in transverse compression by assuming that the two edge strips of plating will carry the load in the post-buckled regime with a middle zone carrying the simple column buckling stress. Eight years later in 1973, Faulkner [28] presented an effective width approach to the plate's ultimate strength estimation by assuming that Blanc's two edge strips are at material yield stress level, for final plate collapse to occur. The model is formulated as:

$$\frac{\sigma_{yu}}{\sigma_o} = \frac{a_e}{a} = \frac{0.9}{\beta^2} + \frac{1.9}{\beta\alpha}\left(1 - \frac{0.9}{\beta^2}\right) \qquad \text{in the range} \quad \beta \geq 1 \quad \text{and} \quad \alpha\beta \geq 1.9$$

This formula has also been employed in the Bureau Veritas regulations [61] and the DNV rules for offshore structures [62].

An effective width approach was also promoted by Becker in 1977 [63], who introduced a degradation coefficient (1-C) in his expression to account for initial shape imperfections:

$$\frac{\sigma_{yu}}{\sigma_o} = \frac{a_e}{a} = 0.923\left\{\frac{2}{\alpha}\left(\frac{b_e}{b}\right) + \left[1 - \frac{2}{\alpha}\left(\frac{b_e}{b}\right)\right](1-C)\gamma\frac{\sigma_{y,cr}}{\sigma_o}\right\} + 0.077$$

where $\gamma = \left[(\alpha - 1)^2 + 1\right]^{-1}$ and C is zero for a perfect plate and 1 for a plate with large initial deformations. $\sigma_{y,cr}$ is the transverse critical buckling stress.

Based on Finite Differences Valsgard [64] concluded that Faulkner's formulation overestimates the stocky plate strength while it underestimates the strength of the more slender plates. As a result, he adjusted Faulkner's effective width formulation for 'wide' plates to the following:

$$\phi_V = \frac{\sigma_{yu}}{\sigma_o} = \frac{a_e}{a} = \frac{\phi_x}{\alpha} + 0.08\left(1 - \frac{1}{\alpha}\right)\left(1 + \frac{1}{\beta^2}\right)^2 \leq 1 \qquad \text{where} \qquad \phi_x = \frac{2}{\beta} - \frac{1}{\beta^2}$$

This expression gives very low transverse strengths for long panels ($\alpha \to \infty$) [65]. The two terms in the expression above represent the sources of plate strength assumed by the model in the post-buckling region. The first component of strength is assumed to arise from that part of the plate

adjacent to the edges, having square dimensions and providing strength equal to ϕ_x. The second strength term is provided by the remaining of the plate. Blanc and Faulkner have assumed that the strength provided by the remaining of the plating is equal to its critical buckling strength, but Valsgard simply altered this value to match his numerical results. This expression is also used by the DNV Classification Note 30.1 [66].

Most ultimate strength formulations for plates in compression, whether for longitudinal or transverse loading, are based on the assumption of long plates i.e. for plates with $\alpha \geq 3$ [67]. To account for the effects of the more realistic limits of $1 \leq \alpha \leq 2$ the model that follows has been presented [68]. It is important to note that the *transverse* ultimate strength of a plate with aspect ratio in the range $1 \leq \alpha \leq 2$ may be viewed as the *longitudinal* ultimate compressive strength of a plate of aspect ratio $0.5 \leq \alpha \leq 1$. This view was taken by Guedes Soares and Faulkner who in 1987 presented the following expression for the transverse strength of plates:

$$\phi_x = \left(\frac{2}{\beta} - \frac{1}{\beta^2}\right) R \qquad \text{for} \qquad 1 \leq \beta \leq 3.5$$

where $$R = 1 + (0.55 - 0.16\beta)(1 - \alpha)$$

R accounts for the effects of slenderness and aspect ratio. Its value becomes 1 for an aspect ratio of 1 and reduces for higher β values.

In 1990, Guedes Soares and Gordo [67] modified Valsgard's proposal to account for its dependency on the plate aspect ratio and plate slenderness levels to:

$$\phi_y = \phi_V B_y \qquad \text{where} \qquad B_y = 0.589 + 0.13\alpha + 0.252\beta - 0.069\alpha\beta$$

The model parameter B_y was derived from regression analysis with numerical (Valsgard's) data only. A very good agreement with the numerical results is demonstrated (see Table below), while the agreement of the model with experimental results, as perhaps is expected, remains poor.

Davidson et al [35] have proposed their own numerically derived strength curves. The strength implied consists of a 'long' plate model (of square dimensions) for the end regions of the plate with a polynomial model (σ_c')

applied to the central region. The central region contribution is modified by an imperfection sensitivity factor K_{pr} based on a Perry-Robertson approach.

The BS 5400 Bridge code uses two different approaches (segments) for stocky and slender plates. For stocky plates, the plate behaviour is modelled as that of a column consisting of a section across the width of the plate. The aspect ratio of the plate (considering a 'wide' column) is not accounted for, rendering the approach as conservative. For the slender plates, the plate strength is modelled by the strength of an equivalent square plate of width equal to the plate length, and an effective width (load redistribution on the edges permitted) approach as used for 'long' plates is adopted.

The ABS Recommendations [69] limit their buckling strength design to the critical buckling limit of the plate as defined by the Bryant equation. Inelastic buckling effects are accounted for by the Johnson-Ostenfeld parabola approach. The same approach is used by the DNV High Speed Craft Rules [70] who propose a classically derived elastic buckling coefficient to account for linearly varying compressive loading on the edges. As these approaches are not limit state design formulations they are considered no further.

The Aluminium Association, BS 8118, and Alcan design guidelines do not seem to tackle the case of a 'wide' plate loaded compressively in its plane, mainly because of the smaller frequency by which this structural arrangement is preferred for application. Two approaches can thus be applied in this case; either to treat the plate as a 'long' plate with small (less than 1) aspect ratio or to approach the subject just as BS5400 does (see above).

Figure 4.10 compares the transverse strengths obtained from several design rules and guidelines for a plate of aspect ratio of 4. It may be concluded that the DNV offshore structure guidelines are close to the critical buckling curve for all plate slenderness values, contradicting the more general experimental and numerical evidence wanting the plate strength to reduce in the stocky plate region due to the presence of initial imperfections. In addition, Valsgard's formulation is seen to provide very low transverse strengths for long panels ($\alpha \rightarrow \infty$).

In 1990, Guedes Soares and Gordo [67] compared the ABS, Faulkner,

Valsgard and Guedes Soares-Gordo expressions with the available experimental and numerical data for steel plates. Data by Becker et al [63, 71] (1970 and 1977), Bradfield and Porter Goff [72] (1975), Fischer and Harre [73] (1978), Dowling, Harding and Slatford [74] (1979) and Valsgard in 1980 [75] (numerical simulations) were considered, a total of 20 experimental and 16 numerical results. The results of this comparison [67] are presented in the following Table,

Tests		ABS	Faulkner	Valsgard	Soares	Srs/Flkner
Expts	**Bias**	0.77	0.83	1.07	1.05	0.99
(20 tsts)	**COV**	0.17	0.24	0.16	0.19	0.12
Num.	**Bias**	0.77	0.78	1.06	1.04	1.0
(16 tsts)	**COV**	0.22	0.21	0.09	0.067	0.14
All	**Bias**	0.77	0.81	1.07	1.05	0.99
	COV	0.19	0.23	0.13	0.15	0.13

The Soares/Faulkner expression accounting for 'wide' plates as if the were 'long' plates with aspect ratios less than one looks the best and is to be preferred. In applying this model to aluminium 'wide' plates, it is suggested that the approach presented in paragraph 4.2.5.3 is used with the exception that this time the effect of residual stresses can be neglected.

4.2.7 The Design of Steel and Aluminium Plates Under Lateral Pressure

As approximately 65% to 90% of ship midship sections comprise of plating, rational selection of its thickness has a significant influence on design efficiency for weight critical structures. The capital cost of the structure will also be influenced through the material cost. Considering that minimum plating thicknesses are normally set based on the maximum levels of initial imperfection and/or maximum acceptable deformations under lateral load (serviceability considerations), it is inevitable that a rational approach to design against pressure loading is essential. The main design approaches are presented next and final recommendations made.

4.2.7.1 Elastic Small Deflection Theory

A plate under lateral loadings generally draws its strength from (a) bending, occurring at small deflections and (b) from membrane stresses arising from large deflections. Prior to 1962, when Clarkson presented his elasto-plastic proposals on the design of plates under pressure, a number of theoretical approaches were put forward tackling the problem and reviewed in [76, 77]. This early work was confined to linear elastic small deflection theory assuming that no membrane stresses are present due to excessive plate stretching and/or initial plate deflections. Edges free-to-slide were thus assumed. As a guideline, initial plate deflection may be assumed as small if $w_{max} \leq 0.75\,t$. This neglect of membrane stresses, has resulted in the past to the design of plating with excessive plate thicknesses.

In elastic design of plates under lateral pressure, plate bending generally occurs in the two orthogonal directions. The maximum *elastic* deflection is given by:

$$w_{max} \cong \begin{cases} 5\,k_1\,C & \text{for simply supported edges} \\ k_1\,C & \text{for clamped edges} \end{cases} \qquad \text{where} \quad C = \frac{p\,b^4\left(1-\upsilon^2\right)}{32\,E\,t^3}$$

while the maximum stress in the plate is given by $\sigma_{max} \leq k_2\,p\,(b/t)^2$.

The coefficients k_1, k_2 depend on the plate boundary conditions, the plate aspect ratio and the position of the point at which the stress is required. For simply supported boundary conditions, maximum stress (and deflection) occurs at mid width of the plate, while for clamped boundary conditions it occurs on the plate edges.

For *long plates* under lateral pressure however, bending becomes one-dimensional. When however, the aspect ratio of the plate is small enough (*short plates*, $\alpha < 3$), then interaction of bending in the x and y directions is accounted for via a biharmonic deflection expression [78]

$$w = \sum_{m=1}^{m=\infty} \sum_{n=1}^{n=\infty} A_{mn} \sin\left(\frac{m\,\pi\,y}{l}\right) \sin\left(\frac{n\,\pi\,x}{b}\right)$$

resulting in bending moments (stresses) in the x and y directions given by

$$m_x = -D\left(\frac{\partial^2 w}{\partial x^2} - \frac{\upsilon\,\partial^2 w}{\partial y^2}\right) \qquad \text{and} \qquad m_y = -D\left(\frac{\partial^2 w}{\partial y^2} - \frac{\upsilon\,\partial^2 w}{\partial x^2}\right)$$

This approach leads to the following correction coefficients applied to maximum deflection, k_1, and maximum stress, k_2, (Fig. 4.11):

$$k_1 = \begin{cases} \text{simply-supported} & \\ -0.0269\,\alpha^4 + 0.3409\,\alpha^3 - 1.599\,\alpha^2 + 3.296\,\alpha - 1.517 & \text{for } 1 \le \alpha \le 2.4 \\ 1 & \text{for } \alpha > 2.4 \\ \text{clamped} & \\ 0.0052\,\alpha^3 - 0.5275\,\alpha^2 + 1.781\,\alpha - 0.98224 & \text{for } 1 \le \alpha \le 2.6 \\ 1 & \text{for } \alpha > 2.6 \end{cases}$$

and for the maximum stress, the correction factor becomes (Fig. 4.12):

$$k_2 = \begin{cases} \text{simply-supported} & \\ -0.018\,\alpha^4 + 0.1736\,\alpha^3 - 0.599\,\alpha^2 + 0.8389\,\alpha - 0.1054 & \text{for } 1 \le \alpha \le 3 \\ 0.25 & \text{for } \alpha > 3 \\ \text{clamped} & \\ -0.0162\,\alpha^4 + 0.188\,\alpha^3 - 0.813\,\alpha^2 + 1.552\,\alpha - 0.603 & \text{for } 1 \le \alpha \le 1.6 \\ 0.34 & \text{for } \alpha > 1.6 \end{cases}$$

The elastic design of plates under lateral pressure when based on small deflection theory neglects any yielding and the eventual spread of plasticity in the section further to not allowing for the membrane stresses which arise when the deflection becomes large and/or when the edges are rigidly held apart. Design to first yield should therefore be avoided, unless fatigue is a problem.

4.2.7.2 Plate Failure in the Elasto-Plastic Range

Elastoplastic analysis as employed in beam bending may be extended to plates under uniform lateral pressure by representing the latter as a 'strip' beam of unit-width. This theory is strictly applicable to infinitely long plates, but may be employed with small error [79] to rectangular plates of aspect ratios less or equal to 3. Clarkson [79] estimated that by reducing the aspect ratios from 3 to 2, the deflection calculated employing the infinite plate

approach will be 2.5% higher than the actual ones. Significant errors occur when the aspect ratio approaches the value of 1 suggesting that proper account must be taken of shape hardening effects. References, [79, 80] demonstrated that the elasto-plastic behaviour depends on:

- the plate boundary conditions
- the aspect ratio α, which defines whether the approach used is a short or long plate approach
- the plate slenderness β, which defines whether the design approach is elastic, elasto-plastic or plastic.

As a general guideline, ship plating subjected to large lateral loads (deck and shell plating) is generally within the range $30 < b/t < 80$ whereas superstructure plating in smaller and lightweight vessels is more slender having $b/t > 80$. Guedes Soares' detailed review [81] of aspect ratios and b/t ratios of tankers and frigates concluded that:

	Aspect Ratio		b/t Ratio	
	Mean	**COV**	**Mean**	**COV**
Tankers	4.7	0.16	46	0.25
Frigates	3.2	0.32	60	0.42

Membrane effects in stocky plates are quite small as the deflections involved are small in addition to the presence of edges free to slide. *Small deflection* elasto-plastic theory will therefore be sufficient for estimating the serviceability limits of stocky plates. For slender plates ($\beta > 2.5$), deflections are greater and hence the membrane effects are more influential. In this case *large deflection* elasto-plastic theory would be required for serviceability requirements. According to Hughes [78] membrane stresses (or membrane action) become significant when:

$w > 1.5\,t$ for edges rigidly held apart

$w > t$ for edges free to pull in.

It was Hovgaard in 1940 [82] who first designed laterally loaded plates on a permanent set basis, by providing design data curves for no permanent set and for a permanent set equal to 1/5 of the total deflection. These curves were based on limited experimental data by the German Navy carried out in

1908 which however gave no indication of material yield stress used.

Clarkson [79] in 1956, extended Hovgaard's work to the design of plates under lateral loads past the elastic limit and into the elasto-plastic range by means of an extensive theoretical and experimental investigation [83, 84]. The effect of *in-plane boundary conditions* (edges free-to-slide or rigidly held apart) on the lateral stiffness of the panel was found to be considerable (Fig. 4.13). In practice, edges free-to-slide conditions are more applicable to grillage plating.

The effect of *edge plasticity* on the central deflection under load was found to be quite small, especially for thin plates. This is due to the fact that slender plates behave more like membranes for which the degree of edge clamping is less important. Thus for slender plating the pressure-deflection curve may be calculated ignoring edge plasticity but employing large deflection theory.

Stocky plates ($\beta < 2.5$) were found to demonstrate only small deflections and edge boundary conditions closer to edges free to slide. Hence small deflection elasto-plastic theory is preferred for estimating their serviceability limits. It presents the designer with three design expressions corresponding to the three steps in the failure of the plate, (Fig. 4.14):

- First Yield of the surface of the plate edges $$p_y = \frac{2\sigma_y}{\sqrt{1-\upsilon+\upsilon^2}}\left(\frac{t}{b}\right)^2$$
- Two hinge (at the edges) collapse $$p_{2h} = \frac{3\sigma_y}{\sqrt{1-\upsilon+\upsilon^2}}\left(\frac{t}{b}\right)^2$$
- Three hinge collapse $$p_{3h} = \frac{4\sigma_y}{\sqrt{1-\upsilon+\upsilon^2}}\left(\frac{t}{b}\right)^2$$

Up to the two-hinge collapse pressure the permanent set will be negligible. So any plasticity effects are ignored until the edge plastic hinges have formed. Once this pressure is attained, a rapid increase in permanent set occurs. Complete collapse occurs with the formation of a third plastic hinge at mid-width of the strip. Work hardening occurring during the spread of plasticity from the edge centres to the corners is usually ignored in the analysis. Stocky plates can carry larger pressures but the boundaries do not provide the stiffness for the membrane tension stresses to develop.

For slender plates ($\beta \geq 2.5$), deflections are greater and hence the membrane effects are more influential. In this case *large deflection* elasto-plastic theory was used by Clarkson [79] for the derivation of the following serviceability requirements:

- Elastic membrane behaviour (no permanent set) limiting the membrane stress to 2/3 of the yield stress

$$p_{2/3} = \frac{8}{3}\sqrt{1-\upsilon^2}\sqrt{\frac{\sigma_y^2}{E}}\left(\frac{t}{b}\right)$$

- Inelastic membrane behaviour with permanent set ($\beta > 2.5$) assuming fully plastic membrane tensions [79]:

$$p_m = 9.0\,\sigma_y \frac{t}{b}\left(\frac{w_{pt}}{b}\right)$$

w_{pt} is the maximum acceptable plastic deformation. P_m will never really be achieved as the stiffening system would have failed first.

Clarkson [79] recommended for stocky plates ($\beta \leq 2.5$) the 3 hinge collapse criterion while for slender plates either the $P_{2/3}$ or a maximum allowable permanent set value $(\delta/b)\sqrt{E/\sigma_y}$ (in the form of design curves) (Fig. 4.15). However, the $p_{2/3}$ membrane stress approach recommended by Clarkson has never been popular. The reasons are that the restriction of the stress to 2/3 of the yield stress was totally arbitrary, and indeed conservative as it neglects any 'shape hardening' effects of the smaller plate aspect ratios.

In correcting for shape hardening the plate thickness, t, in the formulations above should be substituted by, $\tau\, t$, where τ is a correction factor given for clamped plates by:

$$\tau = \begin{cases} -0.0144\,\alpha^4 + 0.19244\,\alpha^3 - 0.9011\,\alpha^2 + 1.782\,\alpha - 0.2803 & \text{for } 1 \leq \alpha \leq 2 \\ 1 & \text{for } \alpha > 2 \end{cases}$$

A permanent set criterion with edges free to slide should be preferred when serviceability considerations prevail (i.e. pressure acts alone), while the p_{3h} approach should be preferred where the magnitude of the lateral load

controls design over maximum deflection considerations. Permanent set is undesirable if in-plane compression is also present as the buckling mode can be easily triggered. It is argued by many that at the centre of any grillage structure the compressive loads are not high and that continuity of the plating in those regions renders the rigidly held apart edge condition more attractive. However, for reasons of complexity and conservatism, it is better to assume edges free to slide.

In 1974, Faulkner [42], based on experimental data by Clarkson [84] on plates with edges free to slide (Fig. 4.16), presented the following expressions for elastoplastic design of laterally loaded plates. According to these expressions, which account implicitly for the 'shape hardening' effect of the aspect ratio, the allowable pressure, p, is expressed in terms of an acceptable permanent set, w_{pt}, defined in paragraph 4.2.7.4:

$$p = \begin{cases} \dfrac{6\sigma_y}{\sqrt{\alpha}}\left(\dfrac{t}{b}\right)^2\left(1+\dfrac{2w_{pt}}{\alpha t}\right) & \text{for } \beta < 2.5 \\ \dfrac{6\sigma_y}{\sqrt{\alpha}}\left(\dfrac{t}{b}\right)^2\left(\dfrac{4}{3}+\dfrac{w_{pt}}{\alpha t}\right) & \text{for } \beta \geq 2.5 \end{cases} \qquad \text{for} \quad 1 \leq \alpha \leq 5 \quad \text{and} \quad 2 \leq \beta \leq 6$$

This expression presents a discontinuity at the changeover point i.e. for $\beta = 2.5$ and for $w_{pt}/\alpha t = 1/3$, for no obvious explanation. Figure 4.17 underlines the approximate agreement of this expression with Clarkson's experimental data. According to Faulkner [42], this approximation is good enough considering the uncertainties inherent in test data and has been used by API, Bulletin 2V. Another expression for elastoplastic design of plating with edges free to slide has also been presented by Hughes [85] who also based his empirical formulation on a regression analysis of Clarkson's experimental data [84].

4.2.7.3 Large Deflection Analysis

At large lateral loads, where material yielding is expected to proceed the development of considerable deflections *elastoplastic large deflection analysis*, is more applicable. The non-linearities introduced in the analysis are due to yielding, large deflections (the membrane effects) and the restraint from edge in-plane movements as deflections become large. As a result of these non-linearities there is no direct analytical method that would result

in reliable solutions. Accurate load-deflection values may be obtained only by use of finite element analyses.

An approximate closed form solution to this problem was suggested by Wood in 1961 [86] and accounts of shape hardening, as it is limited to plates of $\alpha < 2.5$. Hence for stocky plates, $\beta < 2$, (and $\alpha < 2.5$), a failure mechanism analogous to 3-hinge collapse i.e. *bending mechanism* has been recommended. For slender plates, $\beta \geq 2$, (and $\alpha < 2.5$) an approach accounting for *membrane stresses* and shape hardening effects has been recommended by Greenspon and referenced by Jaeger in [90]:

$$p = \begin{cases} 12\, C_{bc}\, \sigma_y \left(\frac{t}{b}\right)^2 \left(\sqrt{3+\frac{1}{\alpha^2}} - \frac{1}{\alpha}\right)^{-2} & \text{for } \beta < 2 \quad \text{(Wood)} \\ 8\, C_{bc}\, \sigma_y \left(\frac{t}{b}\right)^2 \left(\frac{w_{pt}}{t}\right) \left(1 - \frac{32}{\pi^3} \operatorname{sech}\left(\frac{\pi\alpha}{2}\right)\right)^{-1} & \text{for } \beta \geq 2 \quad \text{(Greenspon)} \end{cases}$$

where C_{bc} *is equal to 1 for clamped plates and equal to 0.5 for simply supported plates.* For 'long' plates ($\alpha \geq 2.5$) 3-hinge collapse may be used. Since the theory neglects membrane effects, this clamped plate solution is also applicable as an upper bound for roof-top collapse for edges free to slide.

An extension of Wood's expression above, was presented by Sawczuk in 1964 [87] for clamped and simply supported plates. The edges are assumed to be completely restrained from in plane movement, so that large deflection and hence membrane stresses dominate. The expression between uniform lateral pressure p and permanent plate deflection w_{pt} is as follows [88]:

$$\frac{p}{p_c} = \begin{cases} 1 + \frac{(A\, w_{pt})^2}{3\, t^2} \left[\frac{\zeta_o + (3 - 2\zeta_o)^2}{3 - \zeta_o}\right] & \text{for } \frac{A\, w_{pt}}{t} \leq 1 \\ \frac{2\, A\, w_{pt}}{t} \left[1 + \frac{\zeta_o (2 - \zeta_o)}{3 - \zeta_o} B \left(\frac{t^2}{3 (A\, w_{pt})^2} - 1\right)\right] & \text{for } \frac{A\, w_{pt}}{t} > 1 \end{cases}$$

where $\zeta_o = \frac{1}{\alpha}\left(\sqrt{3 + \left(\frac{1}{\alpha}\right)^2} - \frac{1}{\alpha}\right)$ and $p_c' = 2\, \sigma_y \left(\frac{t}{b}\right)^2 \left(\sqrt{3 + \left(\frac{1}{\alpha}\right)^2} - \frac{1}{\alpha}\right)^{-2}$

$$p_c = \begin{cases} p_c' \\ 0.5\,p_c' \end{cases}, \quad A = \begin{cases} 1 \\ 2 \end{cases}, \quad B = \begin{cases} 1 & \text{for clamped plates} \\ -1 & \text{for simply supported plates} \end{cases}$$

p_c is the collapse strength of clamped plate with unrestrained edges. This expression is unconservative for ship plates of typical slenderness [89]. Reference [78] has demonstrated that a better choice for a threshold load is the pressure to cause two edge hinges only. This model has been based on bending stress considerations with subsequent plastic hinge formation but neglecting any membrane stress effects.

Experimental and theoretical studies into the behaviour of long, rectangular, laterally loaded plates have been conducted by Clarkson [79, 80], Jaeger [90], Young [91], and Wah [92, 93]. Hooke and Rawlings [94] have reported results of an extensive experimental study into the static behaviour of uniformly loaded, fully clamped rectangular plates with aspect ratios within the range $1 \le \alpha \le 3$.

Figure 4.18 compares the plate strength requirement as set by the DNV-Offshore structures Code, the API recommendations, Faulkner's elasto-plastic recommendations (para. 4.2.7.2) and Wood's expression (para. 4.2.7.3). It is observed that Faulkner's elastoplastic formulation (used also by API [95] for elastoplastic design) provides the most conservative predictions. Scawzuck and Greenspon's rigid-plastic expressions neglect any membrane stress effects and are based on the assumption of edges rigidly held apart, assumption which is not realistic in ship structures.

4.2.7.4 Initial and Final Permanent Set Values

Based on the review presented in Appendix 4.2, *initial deflections* of plate elements due to welding should be restricted to :

$$w_{pi}/t = \begin{cases} 0.12\,\beta^2\,(t_w/t) & \text{for } \beta \le 3 \\ 0.15\,\beta^2\,(t_w/t) & \text{for } \beta > 3 \end{cases} \qquad \text{for} \quad t_w > t$$

where t_w,t are the web and plate thicknesses respectively. An additional check should be carried out for these deflections, making sure that they do not exceed the value of

$$w_{pi}/t = 0.0094\,(b/t) - 0.205$$

Stiffener initial permaset deflections should be limited to $w_{stiffener}/l \approx 0.001$ where l is the stiffener length. Furthermore, the *maximum permissible deflection* of the plating under lateral loads, for serviceability should be $w_{pt}/b = 1/75$.

In addition, the maximum permissible deflection in the plating should be restricted relative to the plate thickness to:

- $w_{pt}/t = 0.25\beta$ for bottom plating and strength deck
- $w_{pt}/t = 0.5\beta$ for decks, bulkheads and remaining structure

to protect against reductions in plate buckling strengths.

4.2.7.5 Application to Aluminium Plates

According to Clarkson [79], the theory presented for steel plates is equally applicable to plates of aluminium alloys as well as other material that do not display a well defined yield point. The material must not however be brittle.

In applying the approach to aluminium or material of rounded material stress-strain curve, the 0.2% proof stress must be used instead of the corresponding yield stress [79] and the material Young's modulus should be replaced by the the secant $E_{0.2}$.

It should perhaps be more conservative to use the reduced material strength $w\,\sigma_{0.2} = \sigma^{*}_{0.2}$ for those alloys whose strength is more affected by HAZ phenomena. However, since HAZ reduction occurs only at the surroundings of welds, only the design approaches based on the bending strength of plates (by the formation of plastic hinges) should be affected. Design strength values based on a membrane approach should not however be affected. Extruded sections, for which the welds are based in the zones of membrane tension formation, the full reduction in strength should be conservatively applied. The final recommended procedure for the design of flat plates under lateral pressure is presented in Appendix 4.3.

4.2.8 Ultimate Strength of Plates Under In-Plane Biaxial Loading

The available interaction equations accounting for biaxial loading on flat

stiffened/unstiffened plating can all be expressed in the form of a generalised parabolic (Von Mises) expression given by:

$$R_x^a - \eta R_x R_y + R_y^b \leq 1$$

The coefficients a, b, η for the main models currently in use are summarised in the Table below. Of all these expressions, the Dier/Dowling and the Odland/Faulkner proposals are able to tackle tensile loads as well.

	a	b	η	Comments
ABS [69]-DNV [62]* BS5400 [96]	2	2	0	Circular
Faulkner [28]	1	2	0	Parabolic
Stonor et al [97]	1.5	1.5	0	Lower bound
Valsgard [75]	1	2	0.25	Parabolic
Dier+Dowling [98]	2	2	-0.45	For tensile loads
DNV-Fast Craft [70]*	1	n	η	η, n vary with β
Odland-Faulkner [99] (cylinders)	2	2	η	For comp. and tensile loads
ABS-TLP Committee [100]	2	1	0	(cylindrical sectns)
Davidson et al [35] Imperial College	2	2	η	η varies with β

(*) implies that the normalising strengths are critical, elastic/inelastic strengths

All these expressions were derived by calculating the ultimate strengths of the plate under compressive loads in each direction separately, and finally combining their effects through an interaction expression. Curve fitting to experimental data normally identifies the values for the coefficients and exponents. Furthermore, the ultimate strength values of σ_{xu} and σ_{yu} used for R_x, R_y in the interaction models, are based on individual (for each load direction) ultimate strength formulations as assumed by the researchers that have proposed them. This is a point that must be born in mind whenever

comparisons of interaction expressions is undertaken.

The most 'mechanically correct' interaction expression is the one that accounts for both the aspect ratio as well as slenderness effects on the plate behaviour. As Bradfield at al point out in [65], the use of a single interaction curve would require a compromise between the required reduction in longitudinal strength when transverse strength is applied first, and the large combined loadings which may be carried near the change in mode shapes.

The Faulkner expression (based on Becker's data) is found [67] to form a lower bound to the remaining curves. The DNV Offshore Structure rules [62], in turn, propose a circular approach to interaction and have partly been based on the numerical investigations of Harding, Frieze, Dowling et al [74, 98, 101] but mainly on the numerical investigations of Valsgard [75]. However, the latest DNV Code for the design of High Speed and Light Craft [70] settles more for a generalised parabolic expression which varies from elliptical to parabolic depending on the plate aspect ratio. This code is not a limit state code and hence normalisation of the loads is carried out relative to the critical buckling stresses for the individual load components.

The BS 5400 circular interaction has also been based on the Imperial College numerical investigations and does not reflect the effect of slenderness or mode changes on plate behaviour. Despite this fact, analysis of the data in [67] has demonstrated that for slender plates of $\beta \geq 1.3$ the BS 5400 curve predicts the collapse strength more satisfactorily than the remaining of the expressions while for stocky plates ($\beta < 1.3$) the Von Mises criterion is closer to the results than any interaction curve. Valsgard's expressions do not intersect the yield ellipse (not very accurate for stocky panels) and they do not describe the effect of mode changes (not accurate for rectangular panels).

To account for residual stresses and initial deformations on plate behaviour, Guedes Soares and Gordo [67] modified their original proposal by introducing a data calibrated factor $R_{r\delta}$ as follows:

$$R_x^2 - R_x R_y + R_y^2 = R_{r\delta}^2 \qquad \text{for} \qquad \beta < 3$$

$$R_x^2 + R_y^2 = R_{r\delta}^2 \qquad \text{for} \qquad \beta \geq 3$$

where the correction factor is given by

$$R_{r\delta} = \begin{cases} 1.11 - 0.16\,T_r - 2.01\,\delta + 0.27\,R_x^* & \text{for} \quad \beta < 3 \\ 1.12 - 0.58\,T_r - 0.07\,\delta + 0.04\,R_x^* & \text{for} \quad \beta \geq 3 \end{cases}$$

while $$T_r = \frac{\sigma_r}{\sigma_y} \qquad \text{and} \qquad R_x^* = \frac{R_x}{\sqrt{R_x^2 + R_y^2}}$$

Inclusion of residual stress and initial deformation correction will improve the model uncertainty to a mean value of 1.0 and a COV of 13%.

Odland and Faulkner's proposal is however proving to be the most attractive due to its accuracy and relative simplicity. The model has benefited from a large number of experimental data obtained from a test program of Conoco-ABS [102, 103] as part of their TLP development research and specially sponsored tests by DNV [104, 105] closely related to the American program. Faulkner generalised (for the purposes of the TLP Committee) Odland's earlier interaction formulation [25] which had been developed for unstiffened and ring-stiffened shells. Odland's expression combined linear interaction for elastic buckling with a quadratic interaction between elastic buckling and yielding, in addition to accounting for tensile stresses. Faulkner avoided the slenderness parameters in λ and used instead ϕ parameters for each individual load component [99]:

$$\left(\frac{R_x}{\phi_x}\right)^2 + R_x\,R_\theta\left(\frac{2\sqrt{\left(1-\phi_x^2\right)\left(1-\phi_\theta^2\right)}}{\phi_x\,\phi_\theta} - 1\right) + \left(\frac{R_\theta}{\phi_\theta}\right)^2 = 1$$

where $\phi_x = \sigma_{xu}/\sigma_o$ and $\phi_\theta = \sigma_{\theta u}/\sigma_o$. In addition, σ_{xu} and $\sigma_{\theta u}$ are the ultimate collapse values for each of the loading cases individually and $R_x = \sigma_x/\sigma_o$, $R_\theta = \sigma_\theta/\sigma_o$ are the load components normalised relative to the material yield (proof) stress. Although this expression strictly applies to axial and hoop stresses in cylindrical structures, they can be applied just as well to flat stiffened structures too. For shell structures, this model has demonstrated good uncertainty characteristics. The bias and COV were found to be 0.99 and 13.1% respectively [99].

Following a lengthy but very detailed numerical investigation into the ultimate strength of flat plates in a number of in-plane load conditions,

Imperial College has put forward a model for the case of combined biaxial compression, lateral pressure and shear. Square and rectangular plates are treated separately. This expression which is also applicable to biaxial loading cases is described in detail in [35]. Davidson et al's [35] strength curves offer the useful feature of allowing a two segment curve thus improving the agreement with the tests at the higher ultimate transverse strength values. Each segment has the form:

$$R_x^2 + \eta_q R_x R_y + R_y^2 \leq \zeta^2 R_{xq}^2$$

where η varies with slenderness and ζ accounts for shear load effects and R_{xq} for the presence of lateral loads.

In 1990, Guedes Soares and Gordo [67] carried a comparison of most of the aforementioned models with available experimental data for steel. Data from the following sources was considered:

(a) Becker et al [63, 71] who conducted in 1970 and 1977 a series of tests on mild (18 test points) and stainless steel plates (8 test points) under biaxial compression. The test specimens included residual stresses and in some cases they were stress relieved. Bradfield et al [65] express reservations on whether the intended boundary conditions have been achieved, due to the fact that the specimens were small square tubes and interactions between adjacent sides would be inevitable

(b) Stonor, Bradfield, Moxham and Dwight [97] in 1983 studied the overall behaviour of plates under biaxial loading, paying particular attention to the mode of failure by measuring the out-of-plane deflections. Residual stresses were welded onto the plates and initial imperfections were introduced mechanically (16 tests points)

(c) Dowling, Harding and Slatford in 1979 [74] carried out numerical simulations of plate failures under biaxial loading. Varying levels of residual stresses and initial imperfections were present in the test specimens (233 numerical data points). This numerical study was complemented by 110 experimental tests by Dier and Dowling carried out in 1980 [98].

(d) Bradfield et al [65] in 1993 presented the results of large scale tests

measuring the strengths of long, rectangular stocky plates under biaxial in-plane compressive loads. Plates with aspect ratios of 4-6 were tested containing residual stresses and initial deformations. These tests were not considered in the comparison of models by Guedes Soares and Gordo.

In total the study by Guedes Soares and Gordo [67] considered 385 data points. Figure 4.19 presents the relative accuracy of the BS5400 (circular) predictions and the Von Mises criterion. The values of σ_{xu}, σ_{yu} used to normalise the strength values on the axes were taken as those recommended by Faulkner [28] without any residual stress corrections.
Figure 4.20 [67] presents a comparison of these expressions.

In terms of uncertainties, the ABS (BS5400, DNV-Offshore) formulation was found [67] to demonstrate a mean of 0.79 and COV of 31%. Faulkner's method demonstrated a bias of 0.94 and a COV of 24%. In addition the use of the Von Mises criterion to describe the behaviour of the stocky plates and the circular interaction of BS5400 (ABS) for more slender plates will result in an improvement for the model uncertainty. The mean will then be 0.99 and the COV equal to 19% [67]. Odland and Faulkner's proposal is hence recommended for use in both steel and aluminium structures to account for biaxial in-plane loading.

4.2.9 Ultimate Strength of Plates Under In-Plane Biaxial Loading and Lateral Pressure

Any lateral pressure loading acting on a plate already loaded in-plane, will, in general, introduce deflections that will be in phase with the buckling modes of a transversely compressed 'wide' plate, thus significantly reducing its in-plane strength in that direction. On the contrary, 'long', uniaxially compressed plates have their strength rarely reduced. Their strength will in fact be increased due to the beneficial effect of the circularity that the deformed plating will present to the axial load.

The available experimental and numerical results existing on this type of loading are due to:

(a) Steen and Valsgard who in 1984 [106] presented a design method based on the derivation of simplified non-linear elastic response curves for the in-plane and pressure load cases separately, and combining the local stresses

into an equivalent stress criterion. Both linear and non-linear types of behaviour were assessed by using an equivalent Von Mises stress as a criterion. Initial yield was the criterion for elastic behaviour while the ultimate collapse load was the limit for non-linear plate behaviour. As a result of this work, interaction curves were provided for square plates of various slenderness and initial imperfection levels under a variety of lateral pressure loads.

(b) Dier and Dowling who in 1980 [98] carried out numerical studies on both square plates and plates of aspect ratio of 3 with different slenderness ratio, initial imperfection and residual stress values. The biaxial strengths were demonstrated in the form of interaction curves for different levels of lateral pressure.

(c) Becker et al who in 1977 [71, 107] conducted tests on square tubes with internal pressure acting as the lateral load.

(d) Japanese researchers [108-111] who conducted tests on plates under uniaxial compression and lateral pressure only.

(e) American investigators who undertook experiments [112] on stiffened panels with heavy stiffeners which experienced local plate failure. Numerical results are also available from work by Lee [113].

(f) Aalami et al [114] and Kilford [115] who carried out tests on plates under uniaxial compression and lateral load conditions.

These tests, with the exception of (e) and (f), were reviewed Guedes Soares and Gordo [67]. Following this review (235 data points), determined that lateral load results in a significant reduction in the biaxial strength of the plate, the level of this reduction being dependent on the plate slenderness and the intensity of the pressure loading. Hence Guedes Soares and Gordo proposed to account for both of these aspects by:

$$\sqrt{R_x^2 + R_y^2} + R_Q = 1$$

where $R_Q = 0.116\, Q_L\, \beta^2$ and $Q_L = \frac{q\, E}{\sigma_y^2}$

R_Q was assumed as a linear function of Q_L and β and the coefficients were hence obtained from regression analysis. The modelling uncertainty was found to be characterised by a bias of 0.99 and a COV 11% when compared to all 235 data. A linear relationship between the 'equivalent' (in the case of in-plane biaxial loading) uniaxial load and lateral pressure is also recommended by Faulkner [28].

The only design code that seems to include recommendations for load combinations that include lateral pressure is the DNV design guidelines for Offshore Structures [62] and the DNV High Speed Craft Design guidelines [70]. The main problem with the offshore proposals is that they should mainly be used in load cases where the lateral pressure loads dominate the effects of the in-plane loads. As a result the model fails to predict experimental trends and was found [116] to be non-conservative for the more realistic cases of in-plane compression loads being the dominant over any lateral pressure actions. Hence, this model is not considered any further. The DNV High Speed Craft Design guidelines on the other hand account for lateral load effects approximately by the use of a strength reduction factor (usage factor) on the final value of strength derived whose value varies depending on the global position of the plate on the ship.

The Imperial College model [35], accounting for the case of combined biaxial compression, lateral pressure and shear can be used in this instance too, but its accuracy is greatly dependent on the assumptions made in the numerical study relative to initial imperfections, boundary conditions and residual stresses. The Guedes Soares/Gordo proposals should be preferred in the first instance on the grounds of accuracy and reduced model uncertainty

4.2.10 Ultimate Strength of Plates Under Uniaxial/Biaxial Loading and In-Plane Shear

Guedes Soares and Gordo [67], based on 42 numerical data by Harding et al [117], have opted in 1990 for the following circular interaction expression to account for the effects of coexistent uniaxial loads (compression or tension) and in-plane shear loads in flat plates:

$$R_x^2 + R_\tau^2 = 1$$

where $R_\tau = \tau/\tau_y = \sqrt{3}\,\tau/\sigma_y$ and $R_x = \sigma_x/\sigma_{xu}$ where σ_{xu} is the ultimate strength of the plate in uniaxial compression as recommended by Faulkner [28] without any residual stress correction. The bias and COV were found to be equal to 1.19 and 16% respectively. However, when the evaluation of the model was concentrated to those data points (21 in number) for which there was a significant degree of load combination i.e.

$$-1 \le \frac{R_x}{\sqrt{R_x^2 + R_\tau^2}} \le 0.8$$

then the bias and COV dropped to 1.07 and 6% respectively. Restrained boundary conditions were assumed (as being representative of those met at orthogonally stiffened plating in ships) which according to [117] do not result in a significant reduction in shear strength due to plate slenderness. Hence the ultimate strength in shear was taken as equal to the shear load to cause yield in the material τ_y.

The expressions suggested by BS 5400 [96] and DNV-Offshore Structures [62] are based on numerical investigations by Harding et al [117, 118] and Carlsen [32] respectively. They are both of the form:

$$R_x^2 + R_y^2 + R_\tau^2 \le 1$$

where R_x, R_y, R_τ are normalised by the characteristic uniaxial/shear stresses.

The latest DNV Rules for the Classification of High Speed and Light Craft [70] use a generalised Von Mises (parabolic) expression whose shape depends on the plate aspect ratio. This expression may be used for solely biaxial loading as well:

$$\frac{R_x}{q} + c\beta^a \frac{R_x R_y}{q} + \left(\frac{R_y}{q}\right)^n \le 1$$

where the reduction factor q accounts for coexistent in-plane shear and is given by:

$$q = 1 - (\tau/\tau_c)^2$$

R_x, R_y refer to load ratios of the longitudinal and transverse in-plane compressive loads respectively over the critical buckling stresses for each of

these loading cases. These design rules do not imply limit state structural design. The effect of coexistence of lateral pressure loads on the plate strength is accounted for by the use of a strength reduction factor (usage factor) on the final value of strength derived whose value varies depending on the global position of the plate on the ship. The dependency of interaction on plate aspect ratio is demonstrated by the Table below, which provides the appropriate values of c, a, n in the interaction expression.

Aspect ratio	c	a	n
$1<\alpha<1.5$	0.78	-0.12	1.0
$1.5\leq\alpha<8$	0.80	0.04	1.2

In the presence of uniaxial compression, in-plane bending loads and shear loads in the panel the following expression is recommended to describe the plate behaviour in the pre-buckling as well as the post-buckling region (if necessary):

$$\frac{\sigma_x}{\sigma_c}+\left(\frac{\sigma_{x,b}}{\sigma_b}\right)^2+\left(\frac{\tau_s}{\tau_\tau}\right)^2=1$$

This expression was first derived by Horne et al [119] for critical buckling behaviour and its applicability to an ultimate limit state approach to design was verified by the numerical investigations of Harding et al [117] in 1976 and Harding and Hobbs [118] in 1979.

Biaxial compression can also be incorporated by finding an 'equivalent' uniaxial compression the biaxial load as follows (as recommended by Harding and Dowling in [120]):

$$\sqrt{\left(\frac{\sigma_x}{\sigma_{c,x}}\right)^2+\left(\frac{\sigma_{yy}}{\sigma_{c,yy}}\right)^2}+\left(\frac{\sigma_{x,b}}{\sigma_b}\right)^2+\left(\frac{\tau_s}{\tau_\tau}\right)^2=1$$

This expression has been used by the ECCS recommendations on steel structures.

An alternative approach for the interaction of bending and shear would be to use a tension field approach when shear load is dominating. This

approach accounts for the pre-buckling shear strength and the post-buckling tension field reserve strength of the plate. It is normally considered in the design of deep plate girder webs including the effects of flange rigidity and is described in paragraph 4.4.2.2.

4.2.11 Application of Steel Plate Ultimate Strength Models to Aluminium Structures

In parallel to Imperial College (numerical) and AMTE (experimental and numerical) tests theoretical and experimental work was carried out on the development of weld induced residual stresses and distortions at Cambridge University [10] and on plate buckling at the same place [52, 54, 121].

In 1981 an extensive numerical study investigating the possibility of extrapolating steel plate data and ultimate strength results to aluminium plate applications, was completed by Dier and Dowling for AMTE [122]. The behaviour of square plates under uniaxial compression, rectangular and square plates under biaxial loading and biaxial loading with coexistent pressure loading and the case of aluminium plating under uniaxial compression and coexistent shear, were investigated. Although no HAZ effects were accounted for (5083 alloy assumed), residual stresses were accounted for in addition to initial geometrical imperfections.

In parallel to the aforementioned study, experimental and numerical work was carried out at AMTE [123] aiming in monitoring the post-buckling behaviour of stiffened flat aluminium plating constructed from 5083 aluminium alloy failing by interframe collapse under uniaxial compression. The effect of HAZ softening on the strength of the five specimens was therefore not studied.

In 1982, Little presented theoretical predictions of the collapse behaviour of thin rectangular aluminium plates under uniform uniaxial, in-plane compression [124, 125] but took no account of residual stresses and HAZ softening effects. This work was followed up by theoretical and experimental work on the development of weld induced residual stresses and distortions at Cambridge University [10] as well as extensive experimental and numerical studies carried out by Mofflin and Dwight [52, 54, 121] into the behaviour of individual, unwelded and welded aluminium plates in

uniaxial compression made of 5000 and 6000 series alloys. It was generally concluded that, results obtained for steel plates can be used for aluminium plates (5000 series) by applying non-dimensional factors. This statement was found to be true except in the cases of

- stocky plates loaded transversely
- plates with small imperfections

for which cases the maximum reduction in strength observed was not greater than 5%.

In addition, aluminium plates were found to be less imperfection sensitive than their steel equivalents and their load-deflection curves in the post-buckling range are flatter than steel thus enabling plate grillages to sustain greater loads (smaller load shedding).

For plates of slendernesses of $\beta < 1.383$, the plate's *uniaxial compression* strength is enhanced by strain hardening (low n value alloys) but for plates of $\beta > 2.766$ there is not much strength variation (except perhaps for plates with small imperfections). Between these values it is possible, depending on the failure criterion (which is the $\varepsilon_x/\varepsilon_{0.2}$ value chosen), to get some loss of strength for rounded material stress/strain curves. This loss was found in [122] to be of the order of 5%. For all slendernesses and levels of imperfections, conservative estimates of strength can be made by referring to the non-hardening case ($n = \infty$).

For plates in *biaxial compression* it was observed that work hardening is beneficial mostly for longitudinally loaded stocky plates while the rounded material stress-strain curve was found to weaken the stocky plates in the transverse direction by approximately 5%. Biaxially loaded aluminium plates, like plates under uniaxial compression, were found to be less imperfection sensitive than steel plates over the complete range of slendernesses. In other words, for small imperfections the aluminium plate is relatively weaker than the corresponding steel plate while for severe imperfections the aluminium plate is stronger. The more rounded material stress-strain curve (low n) will give a stronger interaction curve.

For plates under *combined biaxial and lateral loading* a linear interaction between the biaxial strength and the lateral load was recommended.

Aluminium plates under this loading condition are found to be at least as strong as their steel equivalents. In addition, aluminium plates *under combined compression and shear* were found to be relatively stronger than steel ones over most of the range of load combinations.

The beneficial effect of strain hardening is most evident for plates of high aspect ratio (say 3) and reducing as the aspect ratio drops to 1. The main benefit is obtained in the longitudinal direction for both stocky and slender plates. Strain hardening was also found to be beneficial for square plates but the enhancement of strength was not great, thus highlighting the dependence of strain hardening effects to geometrical factors (i.e. slenderness, aspect ratio).

Centrally positioned transverse welds on the plate were found to have no weakening effect on the strength of the 5083 plates. On the other hand, for 6082 alloy plates the weakening effect is of the order of 30% for unwelded (longitudinally) plates and 20% for welded (longitudinally too) plates. 5083 alloy unwelded plates were found to unload more slowly than the 6082 ones due to the better strain-hardening characteristics the former material possesses.

The lower material strength of the 5083 alloy implies an earlier loss of axial stiffness in unwelded plates than would be observed for the 6000 alloy plates (in the low to medium slenderness range, the strengths are approximately 10-15% lower). The introduction of longitudinal welds will lead to an even earlier loss in axial stiffness for the 5083 plates, the unloading curves becoming even more flatter. In 6082 alloy plates, longitudinal welds reduce the plate strength without having any influence on the shape of the load-shortening curve. A transverse weld does not seem to have a significant effect on the load -shortening behaviour of 5083 plates. For 6082 plates it leads in loss of axial stiffness at a stress corresponding to $\sigma^*_{0.2}$ of the softened material.

In addition, for 5083 plates the difference between strengths of heavily and lightly welded plates is small indicating that overwelding (during fabrication) does not significantly affect the plate buckling strength. Furthermore, the difference in strengths between welded and unwelded plates is small for $\beta > 1.5$. For 6082 the buckling strengths between welded and unwelded is small throughout the β range as the welding residual

stresses in 6082 alloys are considerably less than 5083 alloy plates [54] as predicted by Wong [9].

The study carried out at AMTE demonstrated that, although the weld induced plating distortion was found to be greater than for equivalent steel structures, the distortion values expressed as a ratio of plate thickness had a similar relationship with β. A value of $\delta_o/t = 0.15\beta$ was indicated as a reasonable assumption of the level of imperfection [122]. A similarity in non-dimensionalised stresses and stiffeners distortions was also observed. However, when the measured stiffened plate strength values were compared against predicted values using Faulkner's method, the bias and COV values were found to be 0.865 and 0.19 respectively. It must, however be noted that the data population available was quite small (5 data points).

4.3 Aspects of Stiffener Design

Any stiffened panel or shell between frames subjected compression of its stiffeners may fail either by *primary failure* (i.e.plate induced interframe buckling of the stiffeners and associated plating, tripping of the stiffener about its line of attachment with the plating) or by *secondary failure* (i.e. plate buckling between stiffeners, local buckling of the stiffener web, and/or, local buckling of the stiffener flange.

Interframe buckling of the stiffeners will be in the form of a column under the action of the local loading system which would consist of the stiffener and an effective width of the plating. This effective width accounts for the premature buckling of the plate under any form of compressive load. Premature secondary collapse will result in the lowering of the effectiveness of the cross section to resist primary collapse.

This section describes the methods currently available to design efficient and adequate stiffeners under a variety of loading systems.

4.3.1 The Design of Efficient Stiffeners Based on Orthotropic Plate Theory

The design of every stiffened plated structure, is based on the assumption that the stiffening arrangements (both transverse and longitudinal, single or double-sided) remain effective over the loading range the structure is

expected to experience. Generally, stiffener design is based on empirical relationships which tend to be conservative [127] and require an accurate estimation of the:

(a) loads imposed upon the transverse stiffener
(b) rigidity of the stiffener
(c) strength of the stiffener especially in limit state design
(d) number and positioning of the stiffeners.

This paragraph attempts to provide guidance tackling the above points.

A measure of the load carrying capability of stiffeners is their relative (to the plate) flexural rigidity given by $\gamma = E I_s / D d$ where d is the stiffener spacing, or the width of the plate associated with the stiffener. If the criterion for design is inelastic buckling of the plate element between the stiffeners, Timoshenko [29, 128] suggests the following alteration to the rigidity of the stiffener, for the latter to continue to behave elastically:

$$\gamma = \frac{E I_s}{\left(\sqrt{E_t/E}\right) D d}$$

The estimation of I_s should contain (in the post-buckling range) the effective width of the plate contribution. A further increase in the rigidity of the stiffener beyond the optimum γ^*, will not result in an increase of the critical buckling strength and will thus be uneconomical. The critical buckling stress σ^*_{cr} in this case is that of the weakest (depending on the load condition) subpanel.

4.3.1.1 Optimum Rigidity Values for Various Stiffening and Loading Types

A number of studies have tackled the problem of determination of the optimum rigidity γ^* for various stiffening systems under a number of load combinations based on linear buckling theory. Timoshenko made the greatest contributions to the development of this theory for stiffener design. Additional data were obtained by NACA, Dubas, Kloppel, Massonnet, Rockey, Skaloud [129-132] etc.. The most detailed studies have been those of Kloppel and his collaborators [133, 134] which resulted in a large number of closed form formulae and charts on the subject. Table 4.7 presents the

formulae for γ^* for the most frequently encountered cases of stiffened webs, plates and flanges. Such values can also be found in the form of tables in [135]. The values of γ^* generally depend on, the

(a) aspect ratio of the longitudinally stiffened plate
(b) relative cross-sectional area of the stiffener ($\delta = A_s / d\,t$)
(c) relative torsional rigidity of the stiffener, the effect of which is usually disregarded
(d) number and stiffener positions
(e) load combinations acting on the plate edges.

It was Massonnet [136, 137] who first pointed out that stiffeners which were proportioned on the basis of γ^* would buckle with the plating in the post-critical range and in order to avoid this happening the optimum flexural rigidity of the stiffeners should be factored up 3 to 8 times depending on the distance between the horizontal stiffener and the compressed flange. These observations were later verified by both theoretical (Massonnet at al [138-140]) and experimental investigations (Massonnet et al [136, 137], Owen et al [141], Dubas [142] and Meszaros and Djubek [143]). These tests have also concluded (Fig. 4.21 for the case of pure bending) that for stiffener rigidities greater than approximately $4\gamma^*$ the gain in the load carrying capacity is relatively small. Hence, slightly slenderer (and hence lighter) stiffeners of $4\gamma^*$ rigidities can still satisfy the load carrying requirements. This conclusion is generally applicable to all stiffening arrangements under various loading types.

4.3.1.2 Maquoi's Recommendations

Following a review of the aforementioned theoretical and experimental data, Maquoi et al [144] put forward the following recommendations for the design of rigid stiffeners which account for the effect of *initial imperfections* and *post-buckling behaviour*:

$$\gamma = m_t\,\gamma_t^* \qquad \text{and} \qquad \gamma = k\,m_l\,\gamma_l^*$$

for transverse and longitudinal stiffeners respectively. k=0.8 when the plate is stiffened by more than one longitudinal stiffeners. Otherwise k=1.0. γ^* is then taken from Table 4.7. The values of the amplification factors m_t, m_l

are a function of the type of stiffeners (longitudinal/transverse), the type of stiffener cross-section (open/closed), and the depth to thickness ratio of the plate. Maquoi recommends the following values for the amplification factors m_t, m_l:

For Transverse Stiffeners:
$$m_t = \begin{cases} 1 & \text{for } d/t \le 75 \\ \frac{2}{75}(d/t) - 1 & \text{for } 75 < d/t < 150 \\ 3 & \text{for } d/t \ge 150 \end{cases}$$

For Longitudinal Stiffeners:

(a) For open cross sections (flats, angles, Ts etc)
$$m_l = \begin{cases} 1.25 & \text{for } d/t \le 120 \\ \frac{2.75}{120}(d/t) - 1.5 & \text{for } 120 < d/t < 240 \\ 4 & \text{for } d/t \ge 240 \end{cases}$$

(b) for closed sections
$$m_l = \begin{cases} 1.25 & \text{for } d/t \le 120 \\ \frac{1.25}{120}(d/t) & \text{for } 120 < d/t < 240 \\ 2.5 & \text{for } d/t \ge 240 \end{cases}$$

There is dispute about the need for the amplification factors, m, primarily in Germany although its use does not seem to result in a proportional increase in the cross-sectional area and weight [145].

When the plate is subjected to a *load combination* of compression σ_c, bending σ_b, and shear τ, Maquoi recommends that the value for the longitudinal stiffeners is calculated by the following interaction expression

$$\gamma_l^* = \sqrt{\left(\gamma_{l,\sigma_c}^* \frac{\sigma_c}{\sigma_{c,ult}} + \gamma_{l,\sigma_b}^* \frac{\sigma_b}{\sigma_{b,ult}}\right)^2 + \left(\gamma_{l,\tau}^* \frac{\tau}{\tau_{ult}}\right)^2}$$

where $\sigma_{c,ult}, \sigma_{b,ult}, \tau_{ult}$ are the ultimate strengths in compression, bending and shear of the plate respectively and $\gamma_{l,\sigma_c}^*, \gamma_{l,\sigma_b}^*, \gamma_{l,\tau}^*$ are the optimum rigidities for pure compression, bending or shear of the longitudinal stiffener respectively. This expression should be applied to each of the two adjacent panels of the stiffener and the larger value finally selected.

For transversely (to the direction of load application) stiffened plates, it is the shear loading that is only of importance, irrespective of the presence of other longitudinal loads and the value of γ^* is taken from Table 4.7 according to the specific design conditions. The presence of longitudinal stiffeners is accounted for by assuming an 'equivalent' plate thickness, t_e, so that the critical shear load of the substituted plate is equal to the critical shear load of the original stiffened plate. Then for transverse stiffeners on longitudinally stiffened plates [145]

$$\gamma^* = \gamma^*_{t,o}\left(\frac{t_e}{t}\right)^3 \qquad \text{where} \qquad t_e = \sqrt[3]{k_{\alpha_{max}}/k_\alpha}\,(d/d_{sub,max})^{2/3}$$

and $k_{\alpha_{max}}$, k_α are the shear buckling coefficients for aspect ratios α_{max} and α respectively. $\gamma^*_{t,o}$ is the optimum rigidity for a similar plate without longitudinal stiffeners. $d_{sub,max}$ is the depth of the largest unstiffened sub-panel as identified by the stiffening arrangement. α_{max} is the aspect ratio of the largest unstiffened sub-panel.

The main disadvantage of the rigidity approach γ^* to stiffener design is that the recommendations apply only to the stiffener spacing and load cases for which they were derived and cannot be generalised to the more unpredictable requirements of the designer. Hence a strength criterion is also generally introduced to account for such inefficiencies. Strength criteria for the web stiffeners of deep plate girders will be presented next followed by recommendations for the design of stiffeners against tripping.

4.3.2 The Design of Transverse (Vertical) Stiffeners in Deep Plate Girders

The stiffeners on the web of a deep plate girder, can be intermediate transverse stiffeners (which, apart from increasing the buckling resistance of the web and offering support to the tension field, they also keep the flanges well apart from each other), transverse bearing stiffeners (which, apart from carrying out the functions of the intermediate transverse stiffeners, they need to support an externally applied load), and end bearing stiffeners which also have to withstand the lateral loading imposed upon them by the horizontal component of the tension field forces in the adjacent web panel. The latter are of greater use in the civil engineering profession and will not be discussed any further. Longitudinal stiffeners may also be present, which have to remain straight and efficient throughout the girder collapse stages.

Transverse stiffeners only influence the shear capacity and not the bending resistance of the plate girder web sections. They increase the shear buckling resistance of the web and must therefore be rigid enough and effective up to the ultimate shear load when compressed by the tension field vertical component. In addition, they must prevent any tendency for the flanges to move towards one another as a result of the tension field component acting on them. The presence of longitudinal stiffeners may result in destabilising transverse forces on these stiffeners. At such an instance, a combined compression and bending load condition will apply.

Up until 1980, little was known of the behaviour of transverse stiffeners in the post-buckled range of girder web panels, loaded primarily in shear. It was in 1981 that Rockey et al [146] established a semi-empirical approach to their design by providing a means of establishing the load being imposed upon them by the tension field in the post-critical range of webs loaded in shear. Further experimental investigations by Tang and Evans [147] showed that Rockey's approach leads to the design of safe and slightly conservative transverse stiffeners. hence it is recommended and is described next.

4.3.2.1 The Loads on Transverse Stiffeners

The move towards limit state design procedures, has introduced the need for a more rational and 'mechanically' correct approach to the load estimation on stiffeners, an approach that would obey the physics of the problem. Rockey et al [146] were the first to propose such a procedure for the load estimation on transverse stiffeners in deep plate girders.This approach was latter adopted with slight modifications in BS 5400 [96] as it was shown [147] to provide a conservative envelope to experimental load readings. It assumes that the stiffener has to withstand:

(a) the compression loads due to the vertical force components of the tension fields in the adjacent to the stiffener sub-panels, V_1, V_2 (Fig. 4.22). These loads act only in the regions of non-overlapping of the tension fields namely CG and DH,

$$V_1 = -\sigma^y_{t,1}\, t\,(CG)\sin(\theta_1)\cos(\theta_1) \quad \text{and} \quad V_2 = \sigma^y_{t,2}\, t\,(HD)\sin(\theta_2)\cos(\theta_2)$$

(b) the compression loads introduced by the tension fields' anchoring on the flanges (W_1C, DY_2) thus resulting in forces V_C, V_D;

$$V_C = -\sigma^y_{t,1}\, t\,(W_1C)\sin^2(\theta_1) \qquad \text{and} \qquad V_D = \sigma^y_{t,2}\, t\,(DY_2)\sin^2(\theta_2)$$

(c) the difference in critical shear forces of the two adjacent sub-panels assumed to act over the complete length of the stiffener $(\tau_{cr,1} - \tau_{cr,2})\, d\, t$.
$\sigma^y_{t,1}, \sigma^y_{t,2}$ are the stresses to cause yielding in the corresponding tension bands and are therefore obtained from tension field theory (para. 4.4.2.2).

Maquoi in [145] recommends an identical approach for estimating the loads on intermediate transverse stiffeners not carrying any direct compressive loads (e.g. patch loads). The load actions assumed are:

- compression forces equal to $(V_d - 0.8V_{cr})$, the difference in the design shear strength of the girder and 0.8 of the critical buckling strength of the web panel in shear. The critical buckling shear strength is to be the least of the values of the subpanels adjacent to the stiffener in question

- bending moment loads introduced by the eccentricity of application of the compression loads to the stiffener's neutral axis

- destabilising bending moments (superimposed on the moment due to eccentricity) introduced on the transverse stiffeners by the out-of-straightness of the longitudinal stiffeners (in the compression zone only). It is recommended [145] that the intensity of each transverse force on the transverse stiffener is taken as 1% of the compression load existing in the longitudinal stiffener (without any web effective width).

The British Standard for structural design in aluminium, BS 8118 assumes the compressive load acting with the vertical stiffeners to be:

for an intermediate stiffener $\qquad P = V/3$

for a bearing stiffener $\qquad P = P_1 + V/3$

where P_1 is any *external* concentrated load acting on the stiffener and V is the average value of the ultimate shear force arising in the web panels on either side of the stiffener.

4.3.2.2 Checking the Rigidity and Strength of Transverse Stiffeners

The rigidity of transverse stiffeners should be checked as described in paragraph 4.3.2.1 making the necessary corrections for the presence of any longitudinal stiffeners. An effective width of plating should be assumed to act with the stiffener as described later. The strength check, in turn should pay due to (a) the estimation of the effective width of the web plating that may be assumed to act with the stiffener, (b) the application of the loading in the web plate and thus eccentrically to the position of the neutral axis of the combined (stiffener-plate) section, (c) any initial imperfections on the stiffener and (d) the destabilising action of the buckled web on the stiffener.

The experimental study of Rockey et al [146] has shown that a width of web of forty times the web thickness could be empirically assumed to act with the stiffener and has been adopted by the steel British Structural design code (BS 5400). BS 8118 assumes, in both checks, an effective width of web plating to act with the stiffener given by $b_e = 0.27\,b$ or $30\,t\sqrt{\sigma_{0.2}/250}$ whichever is less.

The moments arising from the eccentricity of the compressive loads P and the neutral axis of the section as well as due to any initial imperfections of the stiffener, δ_o, are magnified by the standard amplification factor $1/(1-P/P_e)$ where the Euler buckling load of the stiffener is calculated assuming the effective column length to be equal to the length GH (Fig. 4.22) i.e. the length over which the the tension fields in the adjacent panels overlap. BS 8118 assumes the effective strut length to be:

$$l = \begin{cases} d & \text{for } \alpha \geq 1.5 \\ d/\sqrt{1.6 - 0.4\,\alpha} & \text{for } \alpha < 1.5 \end{cases}$$

When the panel dimensions are different on opposite sides of the stiffener, an average value of l should be considered.

The destabilising action of the buckled web may be accounted for as recommended in BS 5400 [96] by assuming an 'equivalent' axial load to act in addition to the actual compressive loads. According to Chatterjee [148] this load may be taken as

$$\frac{4\,d^2\,t}{\pi^2\,b^2\,t_s}\,\tau_{cr} \times (\text{plate / stiffener area})$$

Hence the stiffener is to be designed as a strut under combined axial loads and bending moments. Tang and Evans [147] have found that Horne's expression for such an interaction [149]

$$\frac{M}{M_{ps}} + \frac{\sigma_y\,t_s\,0.5\left(b_s + b\,t/t_s\right)^2}{M_{ps}}\left(\frac{P}{P_s}\right)^2 = 1$$

was more than adequate in providing strong transverse stiffeners. M_{ps} is the full plastic moment capacity of the section when there is no axial loading and P_s is the axial squash load of the section.

Maquoi, in turn, [145], agrees that the transverse stiffener should be checked by a Perry-Robertson type of interaction expression (used in ECCS proposals for both steel and aluminium [145, 150]). He recommends the use of an effective width of the web b_e taken as $b_e = t\sqrt{E/\sigma_y}$ to act with the stiffener [145, 150]. These curves however, should be altered to account for the effects of out-of-straightness by assuming this out-of-straightness to be (1/500) of the stiffener length. The buckling length is safely and economically recommended to be 70% of the stiffener depth [145].

4.3.3 The Design of Longitudinal Stiffeners in Deep Plate Girders

Longitudinal stiffening systems provide an attractive alternative to increasing the plate thickness, in terms of load to weight ratio but can be disadvantageous in terms of fabrication costs. It is therefore of extreme importance for the designer to have guidance on the number and positioning of any longitudinal stiffeners he chooses to apply to limit this cost penalty.

Longitudinal stiffeners are expected to support the load shedding due to buckling of adjacent web sub-panels, in addition to maintaining the nodal lines in the buckled web up to its ultimate limit. A rigidity and a stability check would then permit the proper selection and sizing of their dimensions. These aspects are discussed next.

4.3.3.1 The Number and Positioning of Longitudinal Stiffeners

When pure shear loading is applied on the panel, the optimum spacing for the stiffeners is obtained by placing them at equidistant intervals along the web depth as all the sub-panels will then present the same critical buckling resistance. When dominating bending moments and shear loads coexist, the stiffener spacing must be adjusted so that the panels subjected to the highest compressive stresses are the smallest. From theory (Timoshenko [128, 133]) the optimum position of an horizontal stiffener of a panel subjected to pure bending is at a distance equal to d/5 from the compressed flange. As soon as shear is present, the stiffener must be placed in a lower position. This is required to reduce the height of the larger web panel that is below the stiffener and to increase the stability of the web against shear buckling. In addition, this will move the stiffener to positions nearer the neutral axis of the section, thus reducing the bending stresses acting upon it. For the extreme case of a panel that is subjected to pure shear, the optimum location of an horizontal stiffener is at mid-depth.

For girders primarily loaded in shear, guidance on the choice of an optimum number of stiffeners for any given web slenderness is available. Design curves have been developed by Ardali in 1980 [151] as a result of a parametric, numerical study of 15,000 girders employing the tension field mechanism. These curves are of the type shown in Figure 4.23 (for a web plate aspect ratio of 1.5) and present the percentage increase in ultimate load capacity of the web plate against the web plate slenderness as a function a number of longitudinal stiffeners (up to eight in total). It is observed, that the benefits in ultimate strength obtained by an increase in the number of stiffeners is a function of the web slenderness. For every web slenderness ratio there is an optimum number of stiffeners that will provide the maximum increase in ultimate load. There is no real benefit in increasing the number of stiffeners to a value higher than the optimum (unless the web slenderness is increased appropriately).

Furthermore, Massonnet [138] put forward a chart (Fig. 4.24) which enables the identification of the optimum positioning on a web of a longitudinal stiffener, under the action of different shear to bending stress ratios ($\xi = \tau/\sigma$). Values of σ/σ_e and τ/τ_{cr} are plotted as abscissae and ordinate respectively. The stress σ_e is given by [138]:

$$\sigma_e = \frac{\pi^2 E}{12(1-\upsilon^2)}\left(\frac{t}{b}\right)^2$$

To use the chart, the aspect ratio α of the complete panel is first computed followed by the determination of the ratio $\xi = \tau/\sigma$ identified by the design loads. Once the intersection of the radial lines (representing ξ) and the aspect ratio curve is established, its position in one of the areas 2, 3, 4, 5 of the graph is noted. These areas are identified by the dotted lines on the graph. Depending on whether the point lies on areas 2, 3, 4, 5, the optimum position for the stiffener is at d/2, d/3, d/4 and d/5 from the compressed flange.

4.3.3.2 The Loads on Longitudinal Stiffeners

Evans and Tang's proposal [152, 153] for estimating the *loads* on longitudinal stiffeners in the post-buckling range is based on the assumption that the tension field in longitudinally stiffened webs acts over the complete web depth, and therefore the tension field is not expected to add significantly to the stiffener loading in the post-buckling range. Hence, these stiffeners are assumed to be solely loaded by the destabilising effect of the shear buckling stress. This is converted into an equivalent axial compression on the stiffener (para. 4.3.2.1), with any additional compression arising from direct bending loads superimposed.

4.3.3.3 Checking the Rigidity and Strength of Longitudinal Stiffeners

The rigidity of longitudinal stiffeners should be checked as described in paragraph 4.3.2.1. As to the effective width of plating that should be assumed to act with the stiffener the following apply.

BS 8118 prescribes both a rigidity and a stability check both requiring an effective width of web plating to act with the stiffener given by [127]:

$$b_e = 0.27\, d'_{av} \qquad \text{or} \qquad 30\, t\sqrt{\sigma_{0.2}/250} \qquad \text{whichever is less}$$

where d'_{av} is the average depth of the two sub-panels lying either side of the longitudinal stiffener. BS 5400 [96] recommends the design of longitudinal stiffeners by a procedure very similar to that of Rockey et al [146] for

transverse stiffeners (para. 4.3.2.2). This procedure is discussed in some detail by Chatterjee in [148].

Maquoi in [145] agrees with the general view that either the strength or the rigidity criterion is sufficient when designing normally straight longitudinal stiffeners except for the case when the longitudinal direct stress in the stiffener exceed 2/3 of the direct stress in the nearest compression flange. Both requirements are then necessary. When in need for a strength criterion for longitudinal stiffeners, Maquoi recommends [145] the use of a Perry-Robertson type of expression which accounts for compressive and lateral loads in a beam column approach. In applying the beam-column strength check it is advised that an initial out-of-straightness of 1/500 of the stiffener length is employed and that an effective width of plate is assumed to act with the longitudinal stiffener ($b_e = t\sqrt{E/\sigma_y}$).

Evans and Tang proposed a new approach to the ultimate load capacity estimation of longitudinal stiffeners. Following an initial proportioning according to linear buckling theory, the ultimate load capacity should then be checked assuming an effective width of the web panel to act with the stiffener. As the tension field in longitudinally stiffened webs is assumed to act over the complete web depth, the tension field is not expected to add significantly to the stiffener loading in the post-buckling range. Hence, the loading carried by the stiffener is assumed to be primarily due to the destabilising effect of the shear buckling stress. This is converted into an equivalent axial compression on the stiffener (para. 4.3.2.1), with any additional compression arising from direct bending loads superimposed. An effective width of web of 40 times the web thickness is assumed to act with the stiffener. The additional bending moment introduced by the eccentricity of the load from the neutral axis of the section is also accounted for in the form of Horne's interaction diagram (para. 4.3.2.2). This expression will readily provide the plastic moment capacity of the stiffener/effective plate section.

4.3.4 Designing Stiffeners Against Tripping

Most of the design recommendations currently available on design against buckling, are based on the assumption that the stiffener web is 'pinned' onto the plating an assumption which is generally true for the boundary

conditions of beam-columns, plates and shell elements. However, when tripping is concerned an interaction of the tripping modes of the stiffener with the buckled modes of the plate panel should be expected, providing a variable rotational restraint along the length of the stiffener-plate connection, and making the modelling of the boundary conditions and stiffener toe restraint difficult.

Tripping failures may be avoided by appropriate proportioning of the stiffener dimensions, introduction of symmetry in the stiffener cross-section and the introduction of tripping brackets. The benefits of the latter measure are questionable. The assumption of pinned boundary conditions, makes the use of tripping brackets worthwhile, as the tripping strength *about the line of attachment of the stiffener to the plate* then becomes length dependent:

$$\sigma_T I_o = G J + \frac{\pi^2 E \left(I_z \bar{z}^2 + \Gamma \right)}{l^2}$$

where l is the stiffener length. The use of brackets is expected to increase the fabrication cost and add hard spots making the structure more fatigue prone. There is also the danger of the brackets actually precipitating tripping if inappropriately placed at possible positions of buckling antinodes. However, as Faulkner points out [154], for the majority of structures, tripping failure is independent of the unsupported length as the plating provides a stabilising (or destabilising) rotational restraint to the stiffener.

A limited number of studies into the stiffener tripping phenomenon have been made and the number of experimental and or numerical investigations into this failure mode is even more limited. Winderburg [155] and Faulkner [156] have recommended approximate formulae for elastic tripping stresses for axial compression cases and these were later extended by Adamchak [157] to end-moment and lateral loading cases. More general elastic solutions exist using folded-plate or finite element analysis [158-160]. Inelastic tripping has been tackled in the past for steel, using a modified tangent modulus [156, 161] but the assumed tripping modes were found not to resemble those observed experimentally [154]. Incremental inelastic finite element analyses are an alternative approach to inelastic tripping studies. It was Faulkner [154, 156] who first considered the effect of stiffener/plate interaction, and did so for flat grillage structures ignoring the flexural stiffness of the web. Faulkner later extended his proposal to

stiffened cylinders [162]. On the other hand, Adamchack in [157] has treated the tripping problem taking due account of the web deformation, with limited account of any web/plate interaction though.

4.3.4.1 The Effect of Rotational Restraint of the Plating on the Stiffener Tripping Strength

In response to the pessimistic criterion of BS 5500 prescribing elastic tripping of a stiffener pinned at its toe, Faulkner in [154, 156], accounted for the rotational restraint of the plate on the stiffener tripping in two possible ways. Firstly by assuming a constant restraint value C_s and then by taking the restraint to vary linearly. Based on beam theory (Fig. 4.25):

$$\sigma_T = \frac{G J + \dfrac{m_T^2 \pi^2 E\left(I_z \bar{z}^2 + \Gamma\right)}{l^2} + \dfrac{C_s l^2}{m_T^2 \pi^2}}{I_o} \qquad \text{where} \qquad C_s = \frac{E t^3}{3\left(1-\upsilon^2\right) b}$$

The minimum value of tripping strength is obtained for the following tripping modes:

for flat bars [157] $$m_T = (l/\pi)\sqrt[4]{12\left(1-\upsilon^2\right) 3 C_s / E t_w^3 d^3}$$

for T-bars [154, 156, 157] $$m_T = (l/\pi)\sqrt[4]{C_s / E\left(I_z \bar{z}^2 + \Gamma\right)}$$

d is the depth of the stiffener. For $C_s = 0$, the critical tripping mode m_T becomes 1. The independence of the tripping strength from the stiffener length, when substituting for m_T, is noteworthy.

Recently, Morandi has demonstrated [163] that the torsional parameter $(I_z \bar{z}^2 + \Gamma)$ can be approximated with little loss of accuracy by $I_z d_c^2$ where d_c is the distance of the shear centre from the stiffener toe. Longitudinal warping Γ is neglected as its values were found to be considerably smaller than those of transverse warping. This substitution in the above expression and all expressions that follow is thus recommended.

In order to account for the possible destabilising of the stiffener due to plate buckling, the following linear variation of the rotational restraint with the axial load was proposed by Faulkner [154]

for stiffeners [154] $$C = C_s\left(1-\frac{\sigma}{\sigma_{cr}}\right) \qquad \text{for} \qquad \sigma \le 2\,\sigma_{cr}$$

for ring frames [162] $$C = C_{on}\left(1-\frac{p}{p_{mn}}\right) \qquad \text{for} \qquad p \le 2\,p_{mn}$$

where σ_{cr} is the critical buckling strength of the plate panel in compression given by:

$$\sigma_{cr} = \frac{\pi^2 E}{12\left(1-\upsilon^2\right)}\left(\frac{t}{b}\right)^2\left(\frac{m_p\, b}{l}+\frac{l}{m_p\, b}\right)^2$$

m_p is the mode number for critical buckling of the plate in compression (number of half waves along the length of the stiffener). For $\sigma/\sigma_{cr} > 1$ (or $p/p_{mn} > 1$) the restraint value becomes negative accounting for shell/plate destabilisation effects. Hence the tripping stress becomes [154]:

for stiffeners [154] $$\sigma_T = \frac{G\,J + \dfrac{m_T^2\,\pi^2\,E\left(I_z\,\bar{z}^2+\Gamma\right)}{l^2} + \dfrac{C_s\,l^2}{m_T^2\,\pi^2}}{I_o + \left(k\,C_s\,l^2/\left(m_T^2\,\pi^2\,\sigma_{cr}\right)\right)}$$

for ring frames [162] $$p_{Tn} = \frac{G\,J + E\left(I_z\,\bar{z}^2+\Gamma\right)\left(\dfrac{n}{R}\right)^2 + C_{on}\left(\dfrac{R}{n}\right)^2}{I_o + \left(\dfrac{C_{on}}{\xi\,p_m}\right)\left(\dfrac{R}{n}\right)^2}$$

The Notation section provides a description of all the parameters used above. m_T is the mode number for critical tripping of the stiffener in compression (number of half waves along the length of the stiffener). Coefficient k has been introduced by Faulkner to cater for plate buckling/stiffener tripping mode interaction. Based on experimental investigations [164], Faulkner proposes the following values:

m_p/m_T	1	2	3	>3
k	1	0.25	0.5	0

The accuracy of this approach has been tested against experimental results in

[165]. For *ring frames* the third term in the numerator is the addition arising from the stable shell constraint C_{on} for mode n, and the last term in the denominator represents the destabilising effect arising from shell buckling for the same mode n. Morandi in [166, 167] verified (for ring frames) that the solution gives accurate predictions for $n \approx 2-4$, but for $n \approx 5-10$ the accuracy breaks down requiring consideration of the web deformation effects. For $n > 10$, tripping was found to be no longer a problem as interframe shell collapse and/or local buckling of the frames seem to take over as a main failure criterion.

As a result of the inaccuracies occurring due to the neglect of the web deformation effects, Morandi [163, 167] adapted Adamchack's previous theoretical approach for flat stiffened panels [157] accounting for web deformations, to the case of ring frames. Morandi's expression does not tackle tripping failures in the inelastic range and is of the following form for both T- and flat-bar stiffeners:

$$\sigma_T = \frac{b - \sqrt{b^2 - 4\,a\,c}}{2\,a}$$

The values of the coefficients a, b, c, vary depending on whether the stiffeners are T- or flat-bars and whether they are applied straight or in the form of ring-frames. These are presented in Appendix 4.4. This formulation has been tried against FE analyses of ring stiffened cylindrical structures [163]. Despite its accuracy, the complexity of the coefficients renders its use prone to computational errors and should therefore benefit more from further simplifications prior to its widespread application in design.

Irrespective of the method used to estimate the tripping stress, the *average limiting tripping stress* used in design would be

$$\sigma_u = \sigma_T \left(\frac{A_s + b_e\,t}{A_s + b\,t} \right)$$

where b_e (s_e) is the effective width of the plating (shell) as determined by an ultimate strength approach to the plates post-buckling behaviour, A_s is the stiffener sectional area, t is the plating thickness and b (s) its width.

Adamchak in [157] also recognised the need to account for the rotational restraint and also used the same linear variation of the of rotational

restraint as Faulkner above. However, this variation was limited only up to $\sigma/\sigma_{cr} \leq 1$ implying that it was only the beneficial stabilising effect that was considered. For $\sigma/\sigma_{cr} > 1$ the stiffener was assumed pinned to the plating implying a condition of no rotational restraint thus neglecting any destabilising effects.

4.3.4.2 Tripping Strength Under the Influence of End-Moments or Lateral Loads

Based on an energy approach, Adamchak [157] derived expressions for the elastic, critical tripping stresses for flat and T-bars under end bending moment and lateral load conditions. For stiffeners under *end bending*, the end-moment to cause tripping on stiffeners is given by:

for flat-bars
$$M_{cre} = \left(\frac{I}{S}\right)\left(\frac{1}{3}\frac{E\,t_w^3\,d}{12\left(1-\upsilon^2\right)}\left(\frac{m_T^2\,\pi^2\,d^2}{l^2} + 6\left(1-\upsilon\right)\right) + \frac{C_s\,l^2}{m_T^2\,\pi^2}\right)$$

for T-bars
$$M_{cre} = \left(\frac{I}{S}\right)\left(G\,J + \frac{m_T^2\,\pi^2\,E\left(I_z\,\bar{z}^2 + \Gamma\right)}{l^2} + \frac{C_s\,l^2}{m_T^2\,\pi^2}\right)$$

As mentioned earlier, the torsional parameter $\left(I_z\,\bar{z}^2 + \Gamma\right)$ can be approximated with little loss of accuracy by $I_z\,d_c^2$ [163]. The critical tripping mode values m are identical to those given for the axial compression case above. I is the vertical moment of inertia of the stiffener and its associated effective width of plating about the neutral axis of the section and S is a grouping of variables relating to the geometry of the stiffener given by:

$$S = 0.25\left[t_w\,d^4 - 4\left(h - 0.5\,t\right)I_o + 4\,d_c\left(A_f\,d_c^2 + I_{zf}\right)\right]$$

where I_{zf} and A_f are the moment of inertia of the flange about the web plane and the cross sectional area of the flange respectively.

For stiffeners under *lateral pressure loading*, the load per unit length, q, to cause tripping on the stiffeners is for flat-bars and T-bars respectively:

$$q_{cre} = -\left(\frac{4\,I\,d\,E\,t_w^3}{12\left(1-\upsilon^2\right)S\,l^2}\right)\frac{\overline{H}_m(K)}{F_m(K)} \quad \text{and} \quad q_{cre} = -\left(\frac{12\,I\,G\,J}{S\,l^2}\right)\frac{H_m(K)}{F_m(K)}$$

where $\overline{H}_m(K)$, $H_m(K)$, $F_m(K)$ are quadratic functions in K. These functions may be obtained in full from [157]. The coefficient K results from the underlying energy considerations and assumption of the shape of deformation of the stiffener/plate beam under lateral load.

4.3.4.3 Tripping Strength Under Combined Loading

For tripping under combined loading, Adamchak [157] opts for the more conservative linear interaction expression, in the absence of detailed theoretical, experimental or numerical investigations. Hence load interaction effects on the tripping strength of a stiffener are given by:

$$\frac{\sigma_e}{\sigma_T}+\frac{M}{M_{cre}}+\frac{q}{q_{cre}}=1$$

In case that the sign of loading is such so as to stabilise the stiffener (i.e. tensile loading, negative end moments M) then introduction of these quantities with their appropriate sign in the expression above will guarantee that the stabilisation effects are accounted for appropriately.

4.3.4.4 Inelastic Tripping

For stiffeners in steel, Faulkner [154, 156, 162] and Adamchak [157] favour the structural tangent modulus approach E_t, when accounting for inelastic effects. E_t is defined by the Ostenfeld-Bleich parabolae (para. 4.2.5.1). Faulkner recommends for *flat stiffened plating*, Stowell's relationship between inelastic and elastic critical tripping strengths:

$$\sigma_{Ti}=\sqrt{E_t/E}\,\sigma_{Te} \quad \Rightarrow \quad \sigma_{Ti}=\begin{cases}\sigma_y\left[1+p_r\left(1-p_r\right)\dfrac{\sigma_y}{\sigma_T}\right]^{-1} & \text{for} \quad \sigma_T>p_r\sigma_y \\ \sigma_T & \text{for} \quad \sigma_T\le p_r\sigma_y\end{cases}$$

where $p_r=\sigma_{ps}/\sigma_y=0.8$ or 0.5 if the stiffeners are fabricated or cold bent respectively. Adamchak [157] takes the more conservative view setting this relationship equal to $\sigma_{Ti}=\left(E_t/E\right)\sigma_{Te}$.

According to Adamchak [157] and in the absence of any detailed studies, the same expressions may be used to calculate the inelastic tripping moment.

This is done by simple substitution of σ_T by M_{cre} and σ_y by M_p in the expressions above.

For *ring frames* in stiffened shell structures, tripping failure is more sensitive to local bending effects than for flat plated structures. As Faulkner points out [162, 168], this sensitivity increases with shorter the number of buckling wavelengths (i.e. smaller mode number n). He therefore proposed the following expression for the external pressure to cause inelastic tripping which is dependent on the mode number n and leading to different tangent moduli approaches:

$$p_{Tin} = \begin{cases} \frac{E_t}{E} p_{Te} = p_{fy}\left[1 - r(1-r)\lambda_T^2\right] & \text{for } \lambda_T \le 1/\sqrt{r} \text{ and } n \le \pi R/3d \\ \sqrt{\frac{E_t}{E}}\, p_{Te} = p_{fy}\left[1 + r(1-r)\lambda_T^4\right]^{-1} & \text{for } \lambda_T \le 1/\sqrt{r} \text{ and } n > \pi R/3d \\ p_{Te} & \text{for } \lambda_T > 1/\sqrt{r} \end{cases}$$

where $\lambda_T = \sqrt{p_{fy}/p_{Te}}$ and $r = \begin{cases} 0.8 & \text{fabricated frames} \\ 0.5 & \text{cold bent frames} \end{cases}$

p_{Te} is the elastic tripping external pressure for the ring frames and is obtained in terms of the elastic tripping stress σ_T by the following expression:

$$p_{Te} = \sigma_T/\xi \qquad \text{where} \qquad \xi = (1 - 0.5\upsilon - \gamma)\left(\frac{R}{t}\right)\left(\frac{R}{R_s}\right)$$

and R_s is the radius to the centroid of the ring frame, while γ is given in the notation for the design of stiffened shell structures. p_{fy} is the external pressure at which the circumferential stress in the flange of a ring frame reaches yield level.

4.3.4.5 Inelastic Tripping of Aluminium Stiffeners

The approach proposed in paragraph 4.2.5.4 for the design of stiffened aluminium plating can be extended for tackling the inelastic tripping strength problem of *aluminium* stiffeners and ring frames. The procedure would remain essentially the same with the sole change being the substitution for the critical tripping stress. However this remains a suggestion awaiting further and more detailed investigations.

4.3.5 Local Buckling Criteria

Proportioning the stiffener dimensions to avoid local buckling of the cross section components (flange and web) is based on the need to make full use of the material properties thus forcing any buckling to occur in the inelastic range. Hence, each of the section components, is treated as a long, uniformly compressed flat plate with pinned boundary conditions. Assuming a safety factor of SF against yielding of the material ($\sigma_{cr} \geq SF\,\sigma_y$) then for the *web plate* of dimensions d_w, t_w,

$$\sigma_{cr} = 3.62\,E\left(\frac{t_w}{d_w}\right)^2 \geq SF\,\sigma_y \;\Rightarrow\; \frac{d_w}{t_w} \leq \sqrt{\frac{3.62}{SF}}\sqrt{\frac{E}{\sigma_y}} \;\Rightarrow\; \frac{d_w}{t_w} \leq C_w\sqrt{\frac{E}{\sigma_y}}$$

while for the *flange plate* of dimensions $b_f\,(w_f = b_f/2), t_f$

$$\sigma_{cr} = 0.385\,E\left(\frac{t_f}{w_f}\right)^2 \geq SF\,\sigma_y \;\Rightarrow\; \frac{w_f}{t_f} \leq \sqrt{\frac{0.385}{SF}}\sqrt{\frac{E}{\sigma_y}} \;\Rightarrow\; \frac{w_f}{t_f} \leq C_f\sqrt{\frac{E}{\sigma_y}}$$

Faulkner proposes the additional restriction for the *flange* dimensions:

$$\frac{b_f}{t_f} \leq \sqrt{\frac{0.385}{SF}}\sqrt{\frac{E}{\sigma_y}} + \frac{t_w}{t_f} \qquad \text{where} \qquad \frac{t_w}{t_f} \approx 0.6$$

The safety factor values against yield and the corresponding coefficient C implied by the major marine and civil engineering codes are presented below. C_w and C_f refer to the web and flange elements:

	SF	C_w	SF	C_f
API	3.62	1.0	2.75	0.375
DNV	2.0	1.35	2.4	0.4
BS 5500	3.0	1.1	1.54	0.5
Recommended	3.0	1.1	3.0	0.36

A very good overview of the stiffener proportioning requirements in the civil engineering codes worldwide is available in [169].

4.4 Ultimate Strength of Unperforated Deep Plate Girders

The question of the ultimate strength of plate girders in 'pure' shear, pure bending and combined shear and bending loading conditions first came to the attention of researchers worldwide after the steel box-girder bridge failures in the U.K., Australia, and Germany in the late sixties. The resulting international research effort in response to these failures has lead to the publication of numerous analytical and some numerical models all attempting to provide the most efficient and effective solution to the design of these structures. Interestingly enough this research has been mainly initiated and conducted by the civil engineering profession.

In designing a deep plate girder, the distribution of shear and bending stresses characteristic to the loading system being imposed on it, should be appropriately accounted for and each of the subpanels determined by the intermediate vertical stiffeners has to be designed by the specific load combination acting along its edges. When the web is vertically (transversely) stiffened, the shear load along its edges is assumed constant and equal to the average shear value within the panel. When bending becomes more significant than shear, failure occurs by either general yielding of the flanges or by their inward collapse. The behaviour and design of deep plate girders under these loading conditions are examined next.

4.4.1 The Design of Deep Plate Girders Under Dominating Bending Loads

When the bending loads become more significant than shear effects, the need to distinguish between the shear mechanism type occurring at high shear load and the various forms of flange failure occurring at dominating bending loads arises. The failure modes that must be designed out under dominating bending loads are:

(a) general yielding of the tensile flanges,

(b) inward collapse of the compression flanges

(c) buckling of the web plate between the two flanges.

In the design of the *flanges*, local instability phenomena (e.g. local plate buckling and resulting column buckling) occurring in the elastic range govern the design of the *compression flange*, while the material yield stress will determine the limiting value for the *tensile flange* stresses for plate girders under solely direct and bending loads.

In order to account for the reserve strength of a deep-plate girder once the web has buckled, and hence allow for the resulting load shedding from the web to the flanges three methods are generally available:

1. the web 'effective depth' concept,
2. the 'effective stress' approach,
3. a Pratt truss approach, preferred in the presence of considerable shear loads.

The web 'effective depth' concept is generally preferred [150], permitting the use of a linear stress distribution in the section and providing more accurate values of extreme fibre stresses. The concept of a fully effective cross-section using an 'effective stress' approach is less popular, leading to limiting stresses that are lower than those used by the 'effective width' approach. Alternatively, the Pratt truss approach assumes that the flanges alone resist direct and bending stresses while the the web material remains fully effective in resisting the shear loads. The latter approach avoids the determination of the effective section of the web, is simpler and conservative.

The *effective cross-section concept* requires η (= $(1\text{-}0.005\ (3+\psi)/\lambda_p)/\lambda_p$), the 'efficiency' of the web compression zone which depends on the normalised web slenderness, λ_p, and the stress ratio, ψ. Values for the critical buckling coefficients of the web elements under various edge loading conditions (i.e. ψ values) are shown in Figure 4.26. This expression for η is a general form of the Winter formula and is recommended by [150]. Other formulae have been proposed by [150, 170, 171] but the differences in the final results are relatively small [145]. This method may also be employed for the case of longitudinally stiffened webs with the difference that each of the subpanels thus formed must be considered separately [150]. In addition, Cooper's formula [172] seems to be in popular use for doubly symmetric I sections (e.g. North America) in calculating the ultimate bending moment of a girder and is used in the Cardiff approach (para. 4.4.2.2). The bias and

COV values relating to Cooper's model for steel girders subjected to pure bending have been estimated [173] as:

Number of tests	18
Mean value of ratio (obs/prd)	1.008
Standard deviation	0.045
Minimum value of ratio	0.89
Maximum value of ratio	1.06

This evaluation has been based on experimental data presented in [172, 174, 185].

4.4.2 The Design of Deep Plate Girders Under Dominating Shear Loads

Two approaches to the design of plate-girder webs under dominating shear loads are generally considered:

(a) design based on critical buckling as a limiting condition, with a relatively low safety factor to allow for post-buckling effects
(b) design based on yielding or ultimate strength as a limiting condition.

The design procedure will generally involve finding a combination of plate thickness and stiffener spacing that will be economical in terms of material and fabrication.

Critical buckling was accepted as a basis for design of plate-girder webs almost exclusively until the early 1960's. Such design recommendations (a good review in [169]) usually express separate restrictions in terms of web depth to web thickness ratios to control the web buckling under bending or shear.

The more detailed consideration of the post-critical behaviour and reserve strength of a deep plate girder in shear loading is generally based on the Tension Field Modelling approach. This general approach assumes that failure occurs in three stages (Fig. 4.27):

Stage 1: The web plate is subjected to pure shear until the shear stress equals the critical buckling shear stress. Until this stage, equal tensile and compressive direct stresses inclined at 45°and 135° to the flanges (direction of principal stresses) develop in the web.
Stage 2: Following critical buckling, a tension band forms, the shape and inclination of which is the area of difference between the various ultimate strength models developed to date. If the flanges have a very high flexural rigidity, this membrane stress field will develop uniformly across the depth and length of the web plate acting at an angle of approximately 45° to the flanges. If however, the flanges are weaker, both the inclination and the width of the membrane field decrease with decreasing flange rigidity. As a result of this truss action the web imposes lateral and axial loading on the flanges and stiffeners. The tension field contribution will be reduced accordingly by the presence of web perforations.
Stage 3: Final failure will occur via a frame mechanism assuming plastic hinge formation on the flanges which is accounted for by some models only. If however, the flanges are rigid enough so that plastic hinges cannot occur (flanges remain elastic), the web yields completely. Any additional load is then carried by a framework comprising of the flanges and stiffeners and failure occurs either by weld failure, or rapture of the yielded web, or by the creation of an overall frame failure mechanism operating as a Vierendeel frame. The effect of additional plastic hinges forming on the reinforcements of any web perforations must also be accounted for.

Hence, the ultimate shear capacity of a plate girder may be computed by summing up three components, the elastic critical load of the web, the load carried by the post-critical tension field and the load carried by the flanges and any perforation reinforcement at the instant of plastic hinge formation. Figure 4.28 depicts the contribution of these three individual strength terms to the total ultimate strength for an example girder web plate. A brief review of the available theoretical models to date follows.

4.4.2.1 Review of the Available Theoretical Tension Field Models

The first studies on transversely stiffened web plates under 'pure' shear loading conditions were carried out in the aeronautical field [175, 176] and have highlighted the beneficial influence of increased flexural rigidity of the flanges and the stiffness of the transverse stiffeners on the post-buckled

behaviour of a shear panel. However, these theoretical solutions were not directly applicable to the marine field and certainly not in the civil engineering sector. This is due to the very rigid flanges and stockier webs, $h/t \leq 80$, used in the aeronautical field versus the less rigid flange and more slender web $200 \leq h/t \leq 350$ applications employed elsewhere.

In 1958 Rockey [177] demonstrated that by simply increasing the flexural rigidity of the flange it was possible to increase the ultimate shear strength of the web by approximately 60% and proposed an expression to account for this effect.

However, the first ultimate load method based on a *tension field approach* for predicting the failure load of slender plate girders in pure shear was that proposed by Basler and Thurlimann [178, 179]. Assuming flexible flanges and based on experimental observations, it was postulated that the girder fails when the web panel develops an off-diagonal yield band anchored on the transverse stiffeners while the stresses in the adjacent triangular web panel wedges remain at the critical shear stress level. Neglecting the contribution of the flanges, Basler's ultimate strength formulation consists of the contribution of the critical stress and the contribution of the tension field only:

$$V_{ult} = \tau_{cr}\, h\, t + \frac{\sigma_t^y\, h\, t}{2\sqrt{1+\alpha^2}} \qquad \text{where} \qquad \sigma_t^y = \sigma_y \left(1 - \frac{\tau_{cr}}{\tau_y}\right)$$

It was later pointed out by Gaylord [180], Fujii [181] and Selberg [182], that the shear strength predicted by the original Basler formulation corresponds to that of a complete tension field instead of the limited tension band assumed by the model. The aforementioned expression was therefore corrected to:

$$V_{ult} = \tau_{cr}\, h\, t + \frac{\sigma_t^y\, h\, t}{2\sqrt{1+\alpha+\alpha^2}}$$

The corrected Basler approach is still used by some specifications mainly in the USA (e.g. AISC, API Bul2V, [183]) because of its implicit conservatism.

Following Basler, many different theories for the ultimate shear capacity of plate girders were produced. Most notable were those by Fujii, Komatsu,

Ostapenko and Chern, Steinhardt and Valtinat, Herzog, Bergfelt, Hoglund, Rockey and Skaloud, Porter et al and Dubas. They differed, in the boundary conditions assumed for the web, the inclination and the width of the tension band, and the tensile stress distribution within the tension band. These models are reviewed in some detail in [150, 184]. Their main characteristics are presented in Figure 4.29 and Table 4.8 while their verification with experimental results is presented in Table 4.9. The most important improvement to Basler's model was suggested by Rockey, Porter et al at Cardiff [185] and is described in paragraph 4.4.2.2.

Specifically, it was Rockey and Skaloud [186] that considered the effect of the flexural rigidity of the flanges on the ultimate load-carrying capacity of plate girders for the first time explicitly. It was shown that the girder shear collapse mode involved the development of plastic hinges in the tension and compression flanges with simultaneous yielding of the tension band in the web. The position of the plastic hinges on the flanges and hence the width of the tension band varied with the flange rigidity but the main weakness of the model was the assumption that the plastic tension band was inclined along the web plate diagonal. In addition, it was proposed that the collapse of plate girders could be represented by the summation of the critical shear force and the vertical component of the tension field force, thus neglecting any additional load carried by the plastic hinges of the flanges. Full details of the theoretical approach are presented in [187].

In 1969 Fujii [181] in Japan, presented a solution which considered the web to fail by the development of plastic hinges at the central mid panel positions under the action of a uniformly distributed tensile field. Tresca's yield condition was used to determine the magnitude of the tension field. Although the solution recognised the part played by the flanges in the collapse of the girder, it did not take specific account of the influence of the flange rigidity on the position of the plastic hinge and hence on the width of the tension band.

The model assumed by Ostapenko and Chern [188] in 1969 was similar to that employed by Basler, except that it allowed for a variation of the membrane stresses across the web diagonal (Fig. 4.29). The web plate was assumed to be clamped at the longitudinal edges and simply supported at the transverse stiffeners while the contribution of the tension band to the ultimate strength was independent of the flange rigidity (no formation of

internal plastic hinges in the flanges only at the web plate corners). The only contribution of the flanges to the strength of the girder was via a Vierendeel frame action a concept first introduced at the time. The variation of the ultimate strength with the angle of inclination of the tension field was allowed for and the maximum strength value obtained by trial and error. This model was later (1971) extended [189] to cover the combined shear and bending load case based on a numerical parametric study.

In 1971, Komatsu [190] postulated a tension band as shown in Figure 4.29. The inner band was assumed to yield under the combined action of the buckling stress and the post-buckling tension field, while the smaller tension in the outer bands is at the level that can be supported by the girder flange as a beam mechanism with the interior hinge at the distance c determined by an empirical formula. The inclination of the yield band is determined by trial and error so as to maximise the shear capacity. This model together with Fujii's and Ostapenko and Chern's model assumes a web fixed at the flanges and simply-supported at the transverse stiffeners.

Calladine's [191] and Hoglund's models [192] tackled the cases of stocky webs and unstiffened plate girders respectively and are hence of no direct interest. Bergfelt's model (1977) [193] allows the evaluation of the ultimate load capacity of a girder in *shear and bending*. It combines Basler's initial model and the assumption of the Cardiff (1975) model that the tension band is anchored to the flanges within the plastic hinge distances.

Dubas's model (1974) [194], assumes the formation of two 'gussets' at the two corners where the tension field anchors, thus allowing the development of the tension band between them. The size of each gusset is taken to be a rectangle with the same aspect ratio as the shear panel, and are considered to act as simply supported plates under pure shear. A third component in the total ultimate strength accounting for the flange contribution and and which depends on the plastic moment capacity of the flanges, is also included:

$$V_{ult} = h\,t\,\tau_{cr} + h\,t\,\tau_y\left(1-\tau_{cr}/\tau_y\right)\sqrt{\tau_{cr}/\tau_y} + \frac{4\,M_p}{b\left(\sqrt{\tau_{cr}/\tau_y}-\tau_{cr}/\tau_y\right)}$$

However, the Cardiff model [185] (para. 4.4.2.2) is to be preferred for use in

the ultimate strength design of deep plate girders and eventually to the design of the cross-structure of fast marine vessels because:

1. it covers many of the other models as special cases (Basler [178], Ostapenko [188, 195], Calladine [191], Komatsu [190]) and is the most complete theory to plate girder shear ultimate strength to date
2. its effectiveness has been proven via its implementation in BS 5950 (steel buildings) [196], BS 5400 (steel bridges) [96], Eurocode 3 [170], BS 8118 [19] and and the German DASt 015 structural design code
3. according to [197] it provides a mean value of 0.98 and standard deviation of 0.06 for transversely stiffened girders while for longitudinally stiffened girders the mean is 1.00 and the standard deviation 0.07 (Table 4.9)
4. it provides the only analytical basis for the approach to the ultimate strength of perforated girders subjected to shear
5. it is the only model whose application has been tested against numerical and experimental data for aluminium girders and recommendations based on it have been put forward and used in BS 8118.

For these reasons it is recommended herein, and has been adopted in the analysis example presented in Chapter 5. A description of its main assumptions and modelling considerations follows next.

4.4.2.2 The Cardiff Tension Field Model

Porter, Rockey and Evans' 1975 model [198], referenced herein as the 'Cardiff model', assumes a rectangular tension zone to form in the post-buckling range which is inclined at an angle θ to the horizontal and not along the panel diagonal. The formation of hinges occurs simultaneously with the plastic yielding of the tension band area and the structure then fails as a mechanism (Fig. 4.30). In reality, the yielding in the web extends beyond the assumed tension band boundaries, but it is a modelling requirement that this web band must at least yield. The web panels are assumed simply supported along their boundaries while cases of unsymmetrical girders may be accommodated relatively easy. The ultimate strength in shear of a girder is assumed to consist of three terms (Figs. 4.27, 4.28) describing the collapse phases during its loading [185, 198]:

1. the resistance to elastic critical buckling of the web, V_1
2. the resistance to the load carried by the post-critical tension field, V_2
3. the resistance to the load carried by the flanges during plastic hinge formation, V_3.

Figure 4.28 presents graphically the variation and contribution of each of these individual strength components to the final ultimate strength value relative to the web slenderness. Furthermore, Figure 4.31 demonstrates graphically the effect on the individual strength components of the aspect ratio and slenderness of the web plate. The relations between the ultimate shear stress, the optimum value of angle of inclination of the tension band, and the positions of the plastic hinges on the flanges, with flange rigidity $M_p^* (= M_{pf}/h^2\, t\, \sigma_y)$, for a square panel of h/t equal to 200 are also shown in Figure 4.32.

In estimating the critical buckling stress, V_1, the critical buckling coefficient, k_o, for a rectangular simply supported plate is classically given by:

$$k_o = \begin{cases} 5.34 + 4/\alpha^2 & \text{for } \alpha > 1 \\ 4 + 5.34/\alpha^2 & \text{for } \alpha < 1 \end{cases}$$

where α is the web plate aspect ratio. To restrict the elastic critical shear buckling stress to a value smaller than the shear yield stress τ_y the following limit in the web slenderness is recommended (neglecting the postbuckling reserve of the web):

$$h/t \le 1.57\sqrt{k_o}\sqrt{E/\sigma_y}$$

Possible formulae for inelastic shear buckling are:

from [150]: $$\tau_{cr}' = \sqrt{0.8\,\tau_y\,\tau_{cr}}$$

from [170, 199]: $$\tau_{cr}' = \tau_y\left(1 - 0.625\left(\sqrt{\tau_y/\tau_{cr}} - 0.8\right)\right)$$

from [185]: $$\tau_{cr}' = \tau_y\left[1 - 0.68\left\{\sqrt{\tau_y/\tau_{cr}} - 0.33\right\}^2\right]$$

The variation in the predicted postbuckling strength will not be significant by applying either of these expressions [145]. The latter has been used and is

only applicable in the range of $1/\sqrt{3} < \sqrt{\tau_y/\tau_{cr}} < 1.118$. The method does not account for the effect of direct and bending stresses on the critical buckling strength of the web panel assuming that these loads are carried only by the flanges.

The contributions of the tension band, V_2, and the flanges (via plastic hinge formation), V_3, in the post-critical region, are obtained from vertical equilibrium in the web element (Fig. 4.30), and energy considerations in the flange. The ultimate load capacity of the plate girder is then given by [198]:

$$V_{ult} = V_{cr} + 0.5\,\sigma_t^y\, t \sin(2\theta)\,(h - b\tan\theta) + \sigma_t^y\, t\,(c_c + c_t)\sin\theta$$

$$V_{ult} = V_1 + V_2 + V_3$$

The stress to cause yielding of the web material *in the tension band*, σ_t^y, is obtained by resolving the total state of stress in the web plate in the post-critical stage (i.e. the critical shear stress and the tension band stress σ_t) in the direction of the tension band, θ (using the stress transformation expressions) and setting the equivalent Von Mises stress equal to the web material yield stress. σ_t^y is eventually given by:

$$\frac{\sigma_t^y}{\sigma_y} = -\frac{\sqrt{3}}{2}\frac{\tau_{cr}}{\tau_y}\sin 2\theta + \sqrt{1 - \left(\frac{\tau_{cr}}{\tau_y}\right)^2\left(1 - \frac{3}{4}\sin^2 2\theta\right)}$$

From energy considerations of the flange behaviour under the action of the vertical tension field component, *the positions* c_c, c_t *of the plastic hinges* on the compressive and tensile flanges respectively are obtained as:

$$c_c = \frac{2}{\sin\theta}\sqrt{\frac{M_{pc}}{\sigma_t^y\, t}} \quad \text{and} \quad c_t = \frac{2}{\sin\theta}\sqrt{\frac{M_{pt}}{\sigma_t^y\, t}}$$

where M_{pc} and M_{pt} are the plastic moment capacities of the compression and tension flanges respectively ($M_{pf} = 0.25\, b_f\, t_f^2\, \sigma_{yf}$). The only unknown parameter in the final ultimate strength expression is the angle of inclination of the tension band θ at which collapse as a mechanism will occur. The solution being an equilibrium one, suggests an iterative procedure in evaluating θ although the approximate value of $\theta = 0.67\,\theta_d$ provides either the optimum or yields conservative strength results [185,

200, 201]. The variation of ultimate strength with θ is demonstrated in (Fig. 4.33).

The ultimate shear force equation is subject to the empirical rigid flange control:

$$M_{pf} < 0.125\, b^2\, t\, \sigma_y \left\{ -\frac{\sqrt{3}}{2}\frac{\tau_{cr}}{\tau_y} + \sqrt{1 - 0.25\left(\frac{\tau_{cr}}{\tau_y}\right)^2} \right\}$$

where for the case of unequal flanges, M_{pf} is considered to be the largest of the two values for the flanges. In the case that the flange plastic moment capacity is greater than that assumed by the expression above, the flanges are very rigid and hence plastic hinge formation will occur at the corners of the web panel. The ultimate shear strength of the girder is then given by:

$$\frac{V_s}{V_y} = \frac{\tau_{cr}}{\tau_y} + 4\sqrt{3}\frac{M_{pf}}{bht\sigma_y} + \left\{ -\frac{3}{4}\frac{\tau_{cr}}{\tau_y} + \sqrt{\frac{3}{4} - \frac{3}{16}\left(\frac{\tau_{cr}}{\tau_y}\right)^2} \right\}$$

with the inclination of the tension band θequal to 45°.

4.4.2.3 The Effect of Longitudinal Web Stiffeners

For a web subjected to shear the optimum location of a longitudinal stiffener is at mid-depth, so that the two panels buckle simultaneously. For the case of a differently positioned longitudinal stiffener, the larger web sub-panel will buckle at a lower critical stress. Once the panel buckles, the adjacent panels will have to support a greater share of any additional shear load. The in-plane membrane tension thus applied to the adjacent panels, tends to increase their buckling resistance. As a result, various approaches have been put forward throughout the years [172, 174, 185, 188, 198, 199] to account for the beneficial effect of longitudinal stiffeners (Fig. 4.34).

Cooper [172, 174] in 1967 assumed that each of the sub-panels develops its own tension band after buckling independently of the others, in the direction of the sub-panel diagonal. The shear strength of the complete panel was assumed to be the sum of the individual sub-panel shear strengths (Model 1).

Chern and Ostapenko (1969) [188] is based on the original assumption for the tension band distribution for unstiffened longitudinally girders with each sub-panel treated independently (like Cooper) but accounts for the plastic bending moments of the flanges and stiffeners and the axial force reduction for the flange plastic moment capacity (Model 3).

Rockey's model (1971) [202] considered the total shear strength of the panel to be equal to the sum of the ultimate strengths of the individual sub-panels assuming that each subpanel acts as a very rigid flange to the adjacent one (plastic hinge formation at mid panel). Simple summation of the ultimate strength of each sub-panel provides the overall strength (Model 4).

In contradiction to the above 'summation' methods, the Cardiff proposal [198], considers the buckling resistance of the weakest subpanel (identified by the longitudinal stiffeners) as the critical stress of the whole web panel. There is no direct effect of the presence of longitudinal stiffeners in the values of V_2 and V_3, the primary and only role of the longitudinal stiffener(s) being to increase the critical buckling resistance of the web.

In 1980 Ostapenko [203] presented a comparison (based on 40 test data) between these four approaches to the problem of ultimate strength of longitudinally stiffened plate girders. It was concluded that Model 1 is the least accurate while the Cardiff approach (Model 2), although not the most accurate, was recommended for the case of one longitudinal stiffener because of its simplicity. Reference [150] suggests caution in the use of these conclusions as being 'non-proven' but considers the Cardiff model as adequate for design.

4.4.2.4 The Effect of Bending and Direct in-Plane Loads

The presence of any direct and bending stresses in girder section, in coexistence with dominating shear loads, will normally affect, the critical buckling stress of the web plate, the membrane stress field σ_t^y, and the plastic moment capacity M_{pf} of the flanges.

The first two reductions are neglected, as the model assumes that the direct

and bending loads are absorbed by the flanges while the web remains fully effective to absorb the shear loads. However, the plastic moment capacity M_{pf} of the flanges is affected by any set of axial stresses σ_f on their cross-section as follows:

$$M_{pf\,mod} = M_{pf}\left[1-\left(\frac{\sigma_f}{\sigma_{yf}}\right)^2\right]$$

These axial stresses can be direct stresses, bending stresses and even the horizontal component of the membrane tension flange. The Cardiff model does not account for the detrimental effect of the horizontal tension field component on the flange rigidity. The question on whether this should be considered as a flange axial load still remains. The use of the Cardiff model allowing for this horizontal component is promoted in Germany [197, 204] while elsewhere, its effect on the bending capacity of the flanges is disregarded. Experimental data presented in [198] support the following modelling uncertainties for the case where the tension field component is included in the calculation:

	Transv. stiff only	**1 Longl.+transv. stiff**
Number of tests	11	16
Mean value of ratio (obs/pred)	0.996	1.006
Standard deviation	0.063	0.054
Minimum value of ratio	0.820	0.740
Maximum value of ratio	1.710	1.710

The way these stresses may be incorporated is presented in [185]. No experimental or numerical data exist on the post-buckling behaviour of plate girders in coexistent shear, bending, and uniform compression loads.

To account for the detrimental effect of the coexistence of shear and bending loads in the plate girder cross-section, the Cardiff model proposes [185] a simplified interaction curve (Fig. 4.35). The approach is originally not allowing for direct stresses but these can easily be accommodated by superimposing them on the bending stresses. Other models are presented in [178, 195, 199]. Two failure modes are possible:

(a) Failure with a shear type mechanism (Region S-C on the curve) on which the shear load dominates and is only reduced by the presence of bending (and direct if any) stresses and

(b) Failure with a bending mechanism (C-B on the curve) at which the dominating bending stresses are affected by the presence of shear loading (and any direct stresses if any). Change over in the failure mode occurs at point C at which the applied bending moment is assumed to be carried solely by the flanges.

Part S-C of the curve is governed by the analysis already presented. Parametric studies in [185] have shown that applied bending moments of magnitude less or equal to M_s' would not affect the 'pure' shear strength. M_s' ($=V_s\, b<0.5\, M_F$) is the maximum bending moment at the edge of the subpanel assuming it is simply supported. V_s is the ultimate strength of the girder in 'pure' shear reduced for any direct stresses present. Furthermore, the change from a web to a flange failure mode was found to occur [185] at applied bending moments approximately equal to the plastic moment of resistance of a section consisting of the flanges only, M_F. The shear load capacity in this case is provided by the following empirical formula:

$$\frac{V_c}{V_y}=\frac{\tau_{cr}}{\tau_y}+\frac{\sigma_t^y}{\sigma_y}\sin\left(\frac{4\theta_d}{3}\right)\left(2-\left(\frac{b}{h}\right)^{\frac{1}{4}}\right)\left(0.554+\frac{36.8\, M_{pf}}{M_F}\right)$$

Note that τ_{cr} and σ_t^y relate to the 'pure' shear case, while θ_d is the angle of inclination of the diagonal of the web panel to the horizontal. For the case of unsymmetrical girders the M_{pf} value of the weakest flange is employed in the approach. Between point S' and C the curve may be represented by a parabola. A linear representation simplifies the procedure with little loss of accuracy and is thus preferred.

Part C-D corresponds to the bending dominated failure mode. In this case, due to the high web slenderness the girder is unable to develop its full plastic moment capacity $M_{fl,plastic}$ but it instead buckles with consequent load shedding to the flanges. Inward collapse of the compression flange is expected to occur at an applied bending moment M_u which is approximately equal to the moment required to produce first yield in the extreme fibres of the compression flange. Cooper's expression [172, 174] provides a simple, and sufficiently accurate estimate of this moment (para. 4.4.1):

$$\frac{M_u}{M_y} = 1 - 0.0005\frac{A_w}{A_f}\left(\frac{d}{t} - 5.7\sqrt{\frac{E}{\sigma_{yf}}}\right) \quad \text{for} \quad M_u < M_{fl,plastic}$$

where A_w, A_f, are the sectional areas of the web and flange respectively. M_y represents the bending moment required to produce yield in the extreme fibre of the compression flange assuming a fully effective web. This formula has been derived for symmetrical and uniform material girders having one longitudinal stiffener, but may be used for multiple stiffeners. Therefore, its application to unsymmetrical as well as non-uniform girders demands a choice of A_f and σ_{yf} that will yield the lowest M_u value. As M_u will never exceed M_y, then the corresponding stresses in the web plate will be below yield and therefore the web can support a certain amount of coexistent shear loading (defined as V_B in the interaction diagram) given by the empirical formula:

$$\frac{V_B}{V_C} = \sqrt{\left(\frac{M_{fl,plastic} - M_u}{M_{pw}}\right)}$$

where M_{pw} $(=0.25th^2\sigma_y)$ is the plastic resistance of the web plate. A linear interaction may be assumed between point B and C without any great loss of accuracy [200]. Other models are presented in [145, 150].

4.4.3 Design Code Proposals on the Design of Steel Deep Plate Girders

4.4.3.1 The Eurocode 3 Recommendations

Two design approaches are used by EC3 [170] for the estimation of the ultimate strength of transversely stiffened girder webs in predominant shear depending on the aspect ratio of the panel to be analysed:

(a) *the Simple post-critical method,* is employed for the webs of I section girders provided that the web has transverse stiffeners at the supports and is applicable for $\alpha \leq 1.0$ and $\alpha \geq 3.0$, i.e. for girders which are unstiffened or the web panel aspect ratios are sufficiently high for the girder to be considered as unstiffened. The method is based on Dubas's model [194] and assumes pinned boundary conditions throughout.

(b) the Tension field approach employed for webs with transversely stiffened web plates provided adequate anchorage for the tension fields is available. It is valid only for $1.0 < \alpha < 3.0$, $h \leq 1500\text{mm}$, $h/t \leq 400$ and is based on the Cardiff model (para. 4.4.2.2) and accounts for the contribution of the flanges together with the contribution of the tension field formed in the post-buckled range. Pinned boundary conditions are once again assumed.

EC3 also assumes that the bending moment is taken by the flanges with the shear force transmitted to the web, but the case of longitudinally stiffened web panel is not tackled.

To account for the interaction between shear force, bending moment and axial forces, the *simple post-critical method* assumes an interaction diagram as shown in Figure 4.36a. M_f is the plastic moment resistance of the girder cross-section consisting of the flanges only, taking into account of the effective width of the compression flange while V_{ba} is the 'pure' shear strength of the web panel as defined by Dubas. If the applied moment is less than M_f, the method neglects the effect of the bending moment on the shear strength. Similarly, if the applied design shear is less than $0.5\,V_{ba}$, no allowance for bending and axial forces is required. A parabolic interaction is proposed otherwise. The effect of any direct axial forces is introduced through a reduction in the value of M_f and a reduction of the plastic moment resistance M_{pl} of the cross-section.

The *tension field model* assumes the interaction diagram shown in Figure 4.36b. V_{bo} is the ultimate web strength under shear loading, V_{bw} is the contribution of the web only to the shear strength neglecting any contributions to the strength from the flanges. Similar arguments as for the simple post-critical method apply with respect to the necessity to account for the effects of any bending or direct stresses in the girder cross section.

4.4.3.2 The BS 5400 Recommendations

BS 5400 proposes two different approaches for the cases of transversely and longitudinally stiffened web plates. The estimation of the shear resistance of a girder web with transverse stiffeners is based on the Cardiff (1978) [185] model. A linear reduction with the height of the largest cutout present in the web is recommended.

For the case of combined bending and shear loads (Fig. 4.37), BS 5400 neglects the effect of the shear force on the bending capacity of the girder if the former is less than $0.5\,V_R$, where V_R is the ultimate shear capacity of the girder in 'pure' shear neglecting the contribution of the flanges. Furthermore, M_D is the plastic bending moment resistance of an 'effective' part of the complete girder cross-section which accounts for any premature buckling in the flange or web. Similarly, if the applied bending moment is less than $0.5\,M_R$, then the ultimate shear strength of the girder remains unaffected by the presence of bending stresses and is given by the value of V_D, the ultimate shear capacity of the girder in 'pure' shear inclusive of the contribution of the flanges. M_R is the bending moment to cause yielding in a girder cross-section consisting only of the two flanges. A linear interaction is assumed otherwise (Fig. 4.37).

The Cardiff tension field approach, has been adopted by the British design codes for steel bridges (BS 5400-1982) and steel buildings (BS 5950-1985) *only* for transversely stiffened girders. For the case of longitudinally stiffened webs, BS 5400 has been based instead on numerically derived design curves (by Harding and Hobbs [118, 120]) while BS 5950 refers the designer to BS 5400. This is due to the lack of information on longitudinal stiffener behaviour at the time when the codes were developed. More recent experimental results [201] confirm the accuracy of the use of the tension field theory for longitudinally stiffened girders, even for the combined loading cases. For longitudinally stiffened webs, the ultimate shear strength is obtained from the sum of the strengths of the individual web sub-panels.

4.4.3.3 The BS 5950 Recommendations

BS 5950, being limited to transversely stiffened girders only, allows one of the following three methods to be used for the determination of ultimate strength capacity under any combination of shear, bending and direct loads:

(a) the moment may be assumed to be resisted by the flanges alone and the web designed for shear only,
(b) the moment may be assumed to be resisted by the whole section, the web being designed for combined shear and longitudinal stresses,
(c) a proportion of the loading may be assumed resisted by the first method and the remainder by the second.

Although the first method is slightly conservative it leads to considerable simplification and is the one most commonly used (the other two methods are included in Appendix H of the code). Panels with an opening having a dimension greater than 10% of the minimum panel dimension are designed based on critical buckling strength criteria. Unequal flanges are catered for by considering the dimension of the smallest flange in the tension field calculations. No specific attention to girders with longitudinal stiffeners is paid. For such girders the designer is referred to BS 5400 where numerically derived design curves are provided for this purpose.

4.4.3.4 Evaluation of the Design Code Proposals

A study presented in [201, 205] provides a detailed comparison of the BS 5400, BS 5950 and EC3 design codes. A large number (197) of experimental results was considered, out of which 133 tests on transversely stiffened girders and 64 on longitudinally stiffened ones. Of the 133 reported tests on transversely stiffened girders, 31 have been discounted on account of premature failures (e.g. stiffener failures, end post failures) with the comparison of the remaining 102 girders summarised in the following Table. Comparison of the codes for the case of unstiffened girders (i.e. $\alpha \geq 3.0$) has also been carried out in [205].

	Transversely stiffened			*Long. stiffened*
	BS 5400	**BS 5950**	**EC3**	**BS 5400**
No. of tests	102	102	102	51
Mean value (obs/prd)	1.140	1.130	1.100	1.60
St. deviation.	0.180	0.164	0.159	0.57
Min. value of ratio	0.667	0.820	0.740	1.07
Max. value of ratio	1.660	1.710	1.710	3.02

In general, the results, for transversely stiffened girders, predicted by all three codes are observed to be in reasonably good, if not conservative, agreement with the experimental data, with the BS 5400 providing the more pessimistic predictions. The EC3 proposals are more accurate and were found by the study to almost invariably lie within (±10%) of the measured values.

Of the 64 reported tests [206] on longitudinally stiffened girders, 13 have been discounted because of premature stiffener failures. The results obtained from BS 5400 for this case are very conservative as the mean value of 1.6 is high. Note that BS 5400 does not allow the application of tension field theory to longitudinally stiffened girders. BS 5950 refers the designer to BS 5400, and EC3 does not have an approach for longitudinally stiffened girders yet. A more detailed investigation of the BS 5400 proposals has been carried out by Sen in [206].

4.4.3.5 Code Proposals as Used in the Marine Industry

Of the available marine codes, only the API Bul 2V [95] proposes an ultimate strength approach, based on tension field modelling. The proposals follow closely, Basler's modified ultimate strength formulation (para. 4.4.2.1) due to its inherent conservatism. A circular interaction between uniaxial compression and shear is assumed.

On the other hand, the DNV recommendations [62, 66, 70, 207, 208] restrict the design of girders to either elastic or inelastic critical buckling and are considered no further. Critical buckling criteria are also proposed by the ABS preliminary guidelines for building and classing SWATH ships [209]. Pinned boundary conditions are assumed and the effect of any rectangular web perforation is accounted for by multiplication of the critical shear strength with a reduction factor, r, given by:

$$r = 1 - (h_{cutout}/h)$$

where h_{cutout} is the depth of a rectangular perforation with any circular perforations converted to their rectangular equivalents. The coexistence of shear and compression loads is accounted for by circular interaction.

4.4.4 The Design of Aluminium Deep Plate Girders

As the significantly reduced material stiffness of aluminium results in premature (relative to steel) buckling, it is important to allow for the post-buckling web capacity in aluminium girders. Aluminium girders present the additional problem that they seem to fail by 'brittle' fracture instead of a

more ductile form of failure. Tests in aluminium alloy plate girders [210-215] have demonstrated that although their mode of failure is similar to that for steel plate girders loaded primarily in shear (shear mechanism), fractures usually occur in the Heat Affected Zones adjacent to the perimeter welds at the stage when the shear sway mechanism is developing. The question therefore arises on whether or not the contribution to strength of the formation of plastic hinges on the flanges should more appropriately be neglected altogether, but no signs of such an action in the available design models and codes have been observed. Most of the research effort into the behaviour of aluminium deep plate girders, has once again concentrated, perhaps not surprisingly, at Cardiff and has moved along similar lines as for their earlier steel model [127, 210, 212, 215, 216].

4.4.4.1 The Cardiff Recommendations

The application of the Cardiff Tension Field Model for steel plate girders to aluminium girders has been investigated in references [210, 212, 213, 216] where the results of tests on aluminium plate girders in the range of 100-300 web slenderness ratios, loaded in pure shear are presented. These studies have concluded that the theory applicable to steel, does not fully represent the failure modes of aluminium girders, but provides very unconservative predictions [216] (eg. 17% overestimation of strength of the 6082 alloy). As a result, a conservative approach to design has been proposed in [216] assuming that the *complete* web area suffers a reduction in strength due to HAZ softening. Hence, the reduction in ultimate strength will be to the reduction of the contribution of its post-buckling components, V_2, V_3 (para. 4.4.2.2):

$$V_{ult} = V_1 + w\left(V_2 + V_3\right)$$

The critical buckling strength contribution to ultimate strength remains unaffected. w $(=k_z)$ is the percentage of material strength reduction as recommended in paragraph 4.1.2. As the case of predominant bending loads has not been tackled, it can be assumed that Cooper's formula is also valid for aluminium girders. The case of longitudinally stiffened aluminium plate girders is also not tackled in the literature and hence the approach employed for steel girders should be used.

4.4.4.2 Code Proposals on Aluminium Deep Plate Girders

The three different types of plate girders identified by the *BS 8118 proposals* are (a) unstiffened girders ($\alpha > 2.5$) which are treated by limiting their capacity to the critical buckling load, (b) transversely stiffened girders ($0.5 \leq \alpha \leq 2.5$) whose treatment is based on the tension field approach accounting for HAZ effects, and (c) longitudinally stiffened girders which are also designed by the tension field approach.

These design recommendations apply for web slenderness ratios (h/t) up to 300 as for higher slendernesses no supporting experimental data exist. The procedures adopted by BS 8118 have been based on those originally developed for steel girders [200] (paras. 4.4.2.2, 4.4.3) taking due account of the effect in material strength of the HAZ adjacent to the welds (as adapted by Burt et al [213, 216] and described earlier).

An upper limit to the plastic moment capacity of the flanges is imposed on the flanges

$$M_{pf} < M_{pw} (\alpha \sin\theta)^2 (\sigma_t^y / \sigma_{0.2})$$

to identify the limiting case for which the flange rigidities are so high that the plastic hinges form at the extreme ends of the panel and failure occurs in a 'picture frame' collapse mechanism. Longitudinally stiffened webs are treated in the same way as webs with transverse stiffeners, on the assumption that the main effect of longitudinal stiffeners is to increase the initial buckling resistance of the web. After buckling, the tension field is assumed to develop over the complete web depth and hence the critical buckling strength of the weakest subpanel is used in the ultimate strength expressions throughout.

In BS 8118 the capacity of a girder to sustain *the combined effects of shear and bending* is expressed by the simplified interaction diagram shown in Figure 4.38. V_{RS} represents the pure shear capacity of the girder (para. 4.4.4.1), V_{RW} is the web shear capacity of the web only ($V_{RW} = V_1 + V_2$) and M_{RF} represents the moment capacity of a section consisting only of the flanges and assuming first yield in the outmost flange fibres. M_{RS} in turn, represents the pure moment capacity of the girder to the level of causing first yield in the out-most flange of the section. The section is assumed as semi-compact by assuming it to consist of a web plate of reduced thickness to

account for premature buckling effects and HAZ reduction effects. A linear interaction is assumed for the cases where shear and bending moment interaction occurs.

The effects of perforations in the web plate are not adequately treated by both the steel (BS 5950, BS 5400) and aluminium (BS 8118) design codes. In both cases the capacity is limited to the critical buckling strength reduced linearly with the diameter or the width/height of the perforation.

Experimental data by Evans and Hamoodi [210] and Seah [211] on 6082 alloy girders have been used by Evans [127] to check the modelling uncertainty of the BS 8118 proposals. A small number (13) of experimental results was considered for transversely stiffened girders while only 7 test data were used for the case of longitudinally stiffened web plates. For all 20 data points the value of the bias was found to be greater than 1.0 and at some cases the experimental strength values were found to be between 1.5 and 2.0 times greater than the strength predictions of the code, indicating a considerable level of conservatism inherited in the latter. However, considering the 'brittle' nature of failure of girders made of heat-treated material, such a conservatism may be justifiable. The modelling uncertainties of the code were derived to be [210]:

	Transv. stiffened	*Longit. stiffened*
No. of tests	13	7
Mean value (obs/prd)	1.742	1.514
COV	0.116	0.064
Min. value of ratio	1.460	1.370
Max. value of ratio	2.030	1.620

The Alcan design manual [217] adopts the same approach as the Canadian Aluminium Structural code [218] in the estimation of the ultimate strength in shear of deep plate girders by using a tension field approach. They also account for the additional shear capacity associated with the formation of plastic hinges on the flanges prior to collapse. The ultimate shear force is given by [217]:

$$V = \left[2\sqrt{\tau_{cr}\,\tau_y} - \tau_{cr}\right] h\,t + \sqrt{3\,M_p\,t\,\tau_y}$$

The critical buckling stress τ_{cr} is calculated via an 'equivalent slenderness' approach by [217]:

$$\tau_{cr} = \left(\frac{0.6\,\pi^2\,E}{\lambda^2} \right) \frac{h}{b} \qquad \text{where} \qquad \lambda = \frac{1.1}{\sqrt{1 + 0.75\,(b/h)^2}} \frac{b}{t}$$

is the equivalent slenderness λ for pinned edges. Any coexistent bending stresses in the plate is tackled via a circular interaction equation. Longitudinal stiffeners are assumed to only affect the critical buckling shear stress and are therefore tackled by choosing the 'equivalent slenderness' ratio as identified by Table 4.10.

The *Aluminium Association recommendations* (USA) [219] take account of the post-buckling reserve strength of the stiffened deep-plate aluminium girders. The maximum shear capacity is given by [219]:

$$\tau_s = \tau_{cr} + C_1 \frac{\sqrt{3}}{2} \sqrt{\tau_y - \tau_{cr}}$$

The coefficient C_1 (Fig. 4.39) accounts for the effect of flange rigidity on the extent of the tension field zone, but the beneficial effect of plastic hinge formation on the flanges is neglected. Instead, Figure 4.40 demonstrates that this formulation gives conservative values compared to aluminium test data by Evans and Burt [216]. The critical shear buckling strength, τ_{cr}, is calculated by entering the 'unified' column curves using the following equivalent slenderness ratio:

$$\lambda = \frac{b}{t} \sqrt{\frac{1.6}{1 + 0.7\,(b/h)^2}}$$

The boundary conditions assumed are half way between simple and fixed supports.

On the other hand, the *European Convention for Constructional Steelwork* restricts the design methodology to critical buckling stress levels, thus neglecting any post-buckling strength components for both the steel and aluminium girders. The method proposes the calculation of the ideal critical stress or an 'equivalent critical stress' in the case of a multi state of stress stress field and is of no further interest to this work.

4.5 Ultimate Strength of Plate Girders with Web Perforations Under 'Pure' Shear In-Plane Loading Conditions

Thin webs containing cutouts are often to be found in double bottoms of ships, the cross-structures in multi-hulled vessels and in the webs of perforated deep plate girders. Their main purpose is to provide services and access, allow inspection and reduce structural weight. These openings can be circular, rectangular or extended circular and can be situated in the web plate centrally, eccentrically or at a corner. In addition, they can either be reinforced or unreinforced.

Since it is advantageous to make the webs of plate girders as deep and as thin as possible (to reduce the axial bending stresses in the flanges and the amount of material in the web) very slender webs result, which buckle at relatively low shear loads. Although cutting a hole in the web plate reduces its shear buckling resistance and ultimate strength considerably, the reduction in *bending strength* is small because the flanges carry most of the bending moment if the size of the opening is limited to avoid torsional and lateral buckling of the compression flange above the hole. Therefore, when non-central openings are used, it is preferable to place them adjacent to the tensile flange or at least clear of the compression flange. Suitable reinforcements could be designed (para. 4.5.5) to restore the strength of the girder to that of an unperforated web.

As already mentioned, the ultimate shear capacity of plate girders with unreinforced web cutouts consists of the sum of the elastic critical load the membrane tension load and the load carried by the flanges. Once the critical shear stress is reached, the web cannot sustain any further increase in the primary compressive stresses and therefore buckles, with any additional load supported by a tensile membrane stress developed in the web. The extent and inclination of the membrane stresses is influenced by the rigidity of (a) the flanges and (b) the reinforcement (if any) of the cutouts. The final stage in the loading sequence is reached when the tensile membrane stress has reached yield levels and hinges are formed on the flanges and the reinforcement, if any (Fig. 4.41). The contribution to the web plate strength made by the reinforcement consists of two terms, the:

1. formation of 4 extra plastic hinges on the reinforcement itself
2. extension of the tensile band relative to the unreinforced case.

A rectangular reinforcement is only efficient if adequate end fixity is provided to it which is guaranteed via a minimum requirement on its length. If the anchorage length is inadequate then plastic hinges cannot form on the reinforcement (Fig. 4.42) and localised web yielding will occur over an area of the web associated with the reinforcement length l. The reinforcement will then rotate about its end and failure will occur as shown in Figure 4.42b.

The positioning of an opening at the centre of the web results in the biggest reduction of the width of the post-buckling tension band thus reducing the ultimate shear capacity of the girder. Therefore, where possible, the cutout should be placed eccentrically to the centre. The extreme case of positioning the perforation in a web corner (and away from the anchoring corners of the tension band) offers the advantages of an increased critical buckling shear stress and an increased tension band width and thus an increased ultimate shear strength relative to the values obtained for the centrally located cutout cases. In the cases where alternating loads exist, the openings can only be placed centrally on the web.

Work on the ultimate strength of uniformly compressed square and rectangular plates with central circular holes has been presented by Ritchie and Rhodes [220] while Narayanan and Chan [221] published the only reference to date for the case of varying in-plane edge loading of plates containing circular holes. Methods of obtaining design charts for practical plates with varying sizes of diameters and locations of openings were proposed. However, no work or formulations had been published as yet, (except perhaps the numerical based proposals in [222] which have major limitations) on the ultimate strength of perforated girder webs under *combined bending and shear loading*. On the contrary, as concluded elsewhere [184], there is a considerable treatment of the subject of ultimate strength formulations for deep plate ($200 \leq h/t \leq 350$ app.) steel girders containing perforations (eg. [223-227]), under *solely* shear loading with very low axial bending stresses and only for vertically stiffened plate girders containing one cutout-per panel. No horizontally stiffened and/or aluminium girders have been treated.

The first published work of relevance to slender webs was by Hoglund in 1971 [224] who reported on statically loaded plate girders with circular and

rectangular holes. Twelve tests were carried out on girders with web plates of slenderness in the region 200-300 thus ensuring web buckling prior to failure. However, it was not until 1977 that the theoretical and experimental investigations aimed at tackling the problem of shear ultimate strength of slender web girders with web cutouts were initiated at University College for the U.K. Department of Transport. The first design approach was put forward by Rockey and Narayanan in 1981 [228]. These recommendations and their products, were based, and follow suit, the tension field theory predicting the collapse behaviour of conventional, unperforated deep plate girders by Porter et al [185, 198]. These will be described next.

4.5.1 Critical Buckling Shear Strength of Perforated Web Plates

The presence of a perforation in the web will evidently reduce the critical buckling strength of the plate in shear. The positioning of the perforation is also important, with the worst possible scenario being that of *a centrally located opening*. It was Rockey et al [229] who first showed that the critical buckling shear stress of a panel decays linearly with the diameter of a centrally situated circular cutout, an observation which was later confirmed by Redwood and Uenoya [230] and Shanmugam and Narayanan [231] for the cases of rectangular cutouts (of dimensions b_o, h_o). A series of FE investigations by Narayanan and Der Avenessian into the critical shear buckling strengths of web plates with reinforced rectangular or circular perforations [223, 232-234], followed these initial observations. These demonstrated the effects of hole size, width and thickness of reinforcement and anchorage length of rectangular openings. Figure 4.43 shows the effects of the size of reinforcement on the value of the critical buckling coefficient.

The restoration of the critical buckling coefficient back to its unperforated value is possible if the following criterion for the minimum reinforcement dimensions applies [234]:

$$\left(\frac{t_r}{t}\right)^2 \left(\frac{w_r}{h}\right) \geq 2.76 \sqrt{\frac{b_o\, h_o}{b\, h}}$$

Any further increase in the cross sectional area of the reinforcement is not expected to improve the critical buckling strength. The additional dependency (improvement) of the the critical buckling strength on the value of the reinforcement length, especially for lengths larger than $1.5\, b_o$,

is accommodated by the following empirical formulation [223, 233]:

$$k_1 = \begin{cases} k_o\left[1-1.25\sqrt{\frac{A_c}{A}\left[1-\frac{0.44L_r^{\,2}}{b_o^{\,2}}\right]}\right] & \text{when } b_o > h_o \\ k_o\left[1-1.25\sqrt{\frac{A_c}{A}\left[1-\frac{0.88L_r^{\,2}}{b_o^{\,2}+h_o^{\,2}}\right]}\right] & \text{when } b_o \le h_o \end{cases}$$

These formulae are only applicable for $b_o / b \le 0.5$ and $h_o / h \le 0.5$. k_o is critical buckling coefficient for an unperforated web plate in shear with clamped boundary conditions (as supported by numerical investigations). For $L_r = 0$, the expression reduces to that applicable for the case of webs with unreinforced rectangular, centrally located openings [223, 233].

The case of the critical buckling coefficient for a web plate with *central, circular reinforced cutout* of diameter d in the web, was also tackled by Narayanan and Der Avanessian [223] who from FE parametric studies proposed the following empirical formulation for the purpose:

$$k_1 = k_o\left(1-\frac{1.5d}{\sqrt{h^2+b^2}}\right)\left[1+6\left(\frac{t_r}{t}\right)^2\left(\frac{w_r}{h}\right)\sqrt{\frac{d}{\sqrt{h^2+b^2}}}\right]$$

with an upper limit of $$k_1 \le k_o\left(1-\frac{1.5d}{\sqrt{h^2+b^2}}\right)\left[1+\left(\frac{w_r}{h}\right)^{1/4}\frac{17.0\,d^2}{h^2+b^2}\right]^3$$

These formulae are only applicable for $d / h \le 0.5$. The assumed thickness of reinforcement, t_r in the expression above should consist of the web plate thickness and that of the single/double sided reinforcement. The unreinforced case is simply accounted for by setting $w_r = t_r = 0$.

Based on observations of rectangular/circular, reinforced and unreinforced openings showing that the elastic critical stress in shear improves as the cutout is moved away from the centre and along the compression diagonal, Narayanan and Der Avanessian [233] recommend the conservative approach of using the equivalent elastic buckling coefficients applicable to the centrally located cutout cases for *eccentrically located unreinforced perforations*. No experimental, numerical investigations or analytical models have been published on eccentrically located, reinforced openings.

Clearly treating such perforations as unreinforced, would only lead to conservative estimates of the critical buckling strength.

The only published formulation for the critical buckling coefficient of *corner located* openings is that by Narayanan and Der Avanessian [225] focusing only on circular openings of varying diameter:

$$k_1 = k_o\left[1-\left(\frac{d}{h}\right)\right]$$

This approximation is sufficiently close to a simplified expression for centrally located holes presented in [232], and is therefore conservative for eccentrically positioned openings.

Reinforced and unreinforced extended circular openings have not been adequately studied and presented in the open literature, and are hence treated no further.

4.5.2 Ultimate Shear Strength of Webs with Centrally Located Openings

The first systematic study of the ultimate behaviour of slender plate girders containing holes was undertaken by Narayanan and Rockey in two series of tests with *centrally located circular openings* [228]. It was observed that the distance between the plastic hinges on the flanges increases at a large rate for increasing cutout diameter (Fig. 4.44) but levels off after the d/h ratios become greater than 0.5. For d/h ratios approaching 1.0 only a small depth of web plate will act with the flange and the girder will thus fail via a Vierendeel type mechanism action. This observation coupled with the apparent linear reduction of ultimate load capacity with increasing cutout diameter has thus resulted in the following ultimate capacity assessment by linear interpolation between the unperforated ultimate strength, V_u, and the Vierendeel load, V_v:

$$V_{ult} = V_v + (V_u - V_v)\left(1-\frac{d}{h}\right) \qquad \text{where} \qquad V_v = \frac{2}{0.5\,b}\left(M_{pc} + M_{pt}\right)$$

The bias and COV for this model may be obtained from Table 4.11.

It was Narayanan and Der Avanessian who took Rockey's results one step

further by extending the Cardiff tension field model for the ultimate strength of unperforated girders to account for the ultimate strength behaviour of *unreinforced* perforated web plates in shear with rectangular [232] and circular openings [235]. As a consequence of their work in the area of unreinforced, perforated web plates, Narayanan and Der Avanessian looked into the ultimate strength analysis and design of web plates with *reinforced circular openings* [223]. The tensile membrane stress across the cutout was substituted by a tension band of equivalent width b_e, to account for the variation in tension field strength across the reinforced opening (Fig. 4.41). The final stage in the loading sequence is reached when the tensile membrane stress has reached yield levels and hinges are formed on both the flanges and the reinforcement. From force equilibrium considerations across a quarter of the ring reinforcement (Fig. 4.41), the value of the effective width is given by:

$$M_{pr} = \sigma_{yr}\, t_r \left[\frac{w_r^{\,2}}{4}\right] \quad \text{and since} \quad M_{pr} = \sigma_t^y \frac{b_e^{\,2}\, t}{16} \quad \text{then} \quad b_e = \sqrt{\frac{16\, M_{pr}}{\sigma_t^y\, t}}$$

Note that b_e is considered only in the case of a reinforced circular opening. From vertical force equilibrium:

$$V_{ult} = \tau_{cr,mod}\, ht + 2ct\, \sigma_t^y \sin^2\theta + \sigma_t^y\, th\left(\cot\theta - \cot\theta_d\right)\sin^2\theta - \sigma_t^y\, td\left[1 - \frac{b_e}{d}\right]\sin\theta$$

σ_t^y is obtained via the same expression as for the unperforated girder case by substitution of the reduced (due to the perforation) value of the critical buckling stress, $\tau_{cr,mod}$. The following points apply:

1. the maximum value of V_{ult} is obtained by trial and error for various for various values of the angle of inclination of the tension field θ. A parametric study [226] of plate girders containing various cutout diameters shows that the optimum angle θ drops linearly with an increase in the cutout diameter. An approximation to its value may be obtained by $(2/3)\,\theta_d\,(1 - d/h)$ [235] (Fig. 4.45)

2. the introduction of the reinforcement may permit the perforated web panels to develop 85-90% of their unperforated ultimate strength

3. for unreinforced circular cutouts b_e=0 with the resulting expression

being valid only [226] for cutouts with diameters $d \le h\cos\theta - b\sin\theta$ (Fig. 4.41). Larger cutouts, although unlikely to be met in practice, can be tackled by adjusting the positions on the flanges at which the plastic hinges form as follows [236] (Fig. 4.46):

$$a = 0.5\left(b - \left(h - \frac{d}{\cos\theta}\right)\cot\theta\right) \qquad \text{and hence} \qquad c = \sqrt{a^2 + \frac{4\,M_p}{\sigma_t^y\, t \sin^2\theta}}$$

The ultimate shear strength for this case will then be:

$$V_{ult} = 2\,t\,\sigma_t^y\,(c-a)\sin^2\theta + \tau_{cr,mod}\,h\,t$$

4. for b_e=d the ultimate strength equation reduces to the unperforated girder case.

The presence of an *unreinforced rectangular opening* will also reduce the extent of the tension field as shown in Figure 4.47 thus adversely affecting the ultimate strength of the plates. The extent of width reduction in the tension field is dependent on the dimensions of the opening and is given by (Fig. 4.47):

$$\delta = \sqrt{h_o^{\,2} + b_o^{\,2}}\,\sin(\alpha+\theta) \qquad \text{where} \qquad \alpha = \arctan(h_o/b_o)$$

Figure 4.48 demonstrates the effect of an unreinforced cutout depth d_o on the value of ultimate strength prediction values V_{ult}. Therefore, *for cutouts with* $h_o \le h-(b+b_o)\tan\theta$ the positions of the plastic hinges on the girder flanges and the reinforcements (if present) are (Figs. 4.47, 4.48, 4.49):

no reinforcement [232] $\qquad c = (2/\sin\theta)\sqrt{M_p/\sigma_t^y\, t}, \quad c_r = 0$

adequate reinforcement [223, 234] $\qquad c_r = \dfrac{2}{\sin\theta}\sqrt{\dfrac{M_{pr}}{\sigma_t^y\, t}} \le b_o + l$

inadequate reinforcement [223, 234] $\qquad c_r = \dfrac{1}{\sin\theta}\sqrt{\dfrac{2\,M_{pr}\left[1+(\beta l/c_{ro})^2\right]}{\sigma_t^y\, t}}$

where $\dfrac{M}{M_{pr}} = \beta^2\left(\dfrac{l}{c_{ro}}\right)^2 \le 1.0$ and $\beta = b_o/l$ [223, 234].

The reinforcement is however, efficient only if adequate end fixity is provided to it. If the anchorage length is inadequate then plastic hinges on the reinforcement cannot form (Fig. 4.42) and localised yielding will occur over an area of the web associated with the reinforcement length l. The reinforcement will then rotate about its end and failure will occur as shown in Figure 4.42b. Any inadequacy in length of the reinforcement should properly be accounted for in the ultimate strength formulation. Experiments [223] have shown that the anchorage length, l should be at least $0.25\,b_o$ for the reinforcement to be fully effective. M ($=\beta^2 M_{pr} (l/c_{ro})^2$) is the moment at which premature reinforcement rotation occurs.

From vertical force equilibrium and assuming *adequate reinforcement* (Figs. 4.47, 4.48), the ultimate shear capacity of a girder web plate with a reinforced rectangular cutout is given by:

$$V_{ult} = \tau_{cr,mod}\, h t + 2 c t\, \sigma_t^y \sin^2\theta + \sigma_t^y\, t h(\cot\theta - \cot\theta_d) \sin^2\theta - \\ - \sigma_t^y\, t \delta \sin\theta + 2 c_r\, \sigma_t^y\, t \sin^2\theta$$

σ_t^y is obtained via the same expression as for the unperforated girder case by substitution of the 'perforated' critical buckling stress value, $\tau_{cr,mod}$. An iterative procedure with respect to θ is required to obtain the ultimate shear strength. Reinforced rectangular webs were found to develop 75-80% of the strength of the their equivalent unperforated webs.

For cutouts with $h_o \geq h - (b + b_o)\tan\theta$ the tension field of *unreinforced web plates* will not extend to the transverse (vertical) stiffener but will be a distance, a, short of it given by (Fig. 4.47b):

$$a = 0.5\left(b + b_o - (h - h_o)\cot\theta\right) \qquad \text{and hence} \qquad c = \sqrt{a^2 + \frac{4 M_p}{\sigma_t^y\, t \sin^2\theta}}$$

and hence the ultimate shear strength for this case will be:

$$V_{ult} = 2\, t\, \sigma_t^y\, (c - a) \sin^2\theta + \tau_{cr,mod}\, h t$$

Such large cutouts are unlikely to be met in practice and have therefore not been considered for the reinforced web cases. The bias and COV values for the models of both the *unreinforced* and *reinforced* rectangular perforation cases may be obtained from Table 4.11.

Reinforced and unreinforced extended circular openings have not been adequately studied and presented in the open literature and are hence treated no further.

4.5.3 Ultimate Shear Strength of Webs with Corner Located Openings

Compared with a web having a central circular cutout, locating the opening in a corner results in an increase in the critical buckling shear stress and an increase in the tension band width, and should therefore be preferred. However, in the cases where alternating loads exist, the openings can only be placed centrally on the web.

For *circular openings*, when the diameter of the cutout is small ($d/h \leq 0.33$) and its location is at the extremity of the compression diagonal, the reduction of the ultimate strength value is only due to the reduction in the critical buckling stress (para. 4.5.1). As the tension field component is not significantly affected, any reductions in its contribution are neglected. The ultimate shear strength is therefore calculated by using the expression for ultimate shear strength of an unperforated girder, after making appropriate allowance for the reduction in the critical buckling strength [225]:

$$V_{ult} = \tau_{cr,mod}\, ht + 2ct\,\sigma_t^y \sin^2\theta + \sigma_t^y\, th\left(\cot\theta - \cot\theta_d\right)\sin^2\theta$$

σ_t^y is obtained via the same expression as for the unperforated girder case by substitution of the reduced (due to the perforation) value of the critical buckling stress, $\tau_{cr,mod}$. This expression is valid only if the 'extent', g, ($g = b - 0.5\,d\left(\cot\theta + 1\right)$), of the tension flange (Fig. 4.50) is larger than the hinge distance i.e. $g > c_t$.

For large diameter cutouts ($d/h \geq 0.33$), the hinge positions will be different and especially the hinge position on the tension flange will be totally independent of the extent of the tension band on the compression flange (Figs. 4.50, 4.51). The width of the tension band assumed to contribute towards the ultimate strength capacity is determined for the compression flange by c_c (coinciding with the position of the plastic hinge) and for the tensile flange by c_t:

$$c_t = \begin{cases} b - 0.5\,d & \text{(circular opening)} \\ b - b_o & \text{(rectangular opening)} \end{cases}$$

In this case, from vertical force equilibrium the ultimate shear strength of the web plate with a corner located circular opening is given by [225]:

$$V_{ult} = \tau_{cr,mod}\, h t + \frac{1}{2} c_c\, t\, \sigma_t^y \sin^2\theta - 0.5\sigma_t^y \frac{t}{c_t}\left(b - \frac{d}{2}\left(\cot(0.5\theta)+1\right)\right)^2 \sin^2\theta$$
$$+ \sigma_t^y\, t\left(h\cot\theta - \frac{d}{2}\left(\cot(0.5\theta)+1\right)\right)\sin^2\theta + 2M_p\left(\frac{c_c + c_t}{c_c\, c_t}\right)$$

which is valid only for $(g < c_c)$. V_{ult} is evaluated by maximising the above expression with respect to θ in the usual iterative way. σ_t^y is obtained via the same expression as for the unperforated girder case by substitution of the reduced value of the critical buckling stress, $\tau_{cr,mod}$. The bias and COV for this model may be obtained from Table 4.11.

Figure 4.52 demonstrates that diameters up to 0.3h, do not affect the extent of the tension band and hence $c_c = c_t = c$ but for larger cutout diameters this is not the case. Furthermore, parametric variations in panel geometry [225] showed that for cutout diameters up to 0.3h a marginal drop of approximately 5% in ultimate shear strength compared to an unperforated web would result (Fig. 4.53). The rate of strength reduction for centrally located cutout cases is considerably larger.

No specific design methodology has been published for the case, of *rectangular perforations and extended circular perforations.*

4.5.4 Ultimate Shear Strength of Webs with Eccentrically Located Openings

Figure 4.54 depicts the idealised tension band formed in the post-critical stage in a web containing a *circular cutout eccentrically placed on the compression diagonal* and the type of panel failure involved. Using the method of virtual work and vertical force equilibrium, Narayanan and Darwish [227] proposed the following ultimate strength formulation for eccentrically located web cutouts (Fig. 4.54):

$$V_{ult}^e = \tau_{cr,mod}\, h t + \frac{1}{2} c_c\, t\, \sigma_t^y \sin^2\theta - \sigma_t^y\, t \frac{h_1}{c_1} g \sin^2\theta + \sigma_t^y\, t L \sin\theta + 2M_p\left(\frac{c_c + c_t}{c_c\, c_t}\right)$$

where g is the effective width of the tension band at the tension flange, L is the width of the tension band that is effective between points B and C and

will be reduced appropriately to account for any cutout located within the band. σ_t^y is obtained via the same expression as for the unperforated girder case by substitution of the reduced (due to the perforation) value of the critical buckling stress, $\tau_{cr,mod}$. The hinge distance c_c on the compression flange is given by the usual unperforated expression ($=[2/\sin\theta][\sqrt{M_p/\sigma_t^y\, t}]$) and V_{ult} is finally obtained from maximisation of the above expression with respect to θ.

Respecting the designer's need for simplified design formulae, Narayanan et al put forward the following approximate formula [227]:

$$V_{ult}^e = V_{ult} + (0.9\,V_u - V_{ult})\left(\frac{r}{r_{max}}\right) \qquad \text{for} \qquad 0.8 \le h/b \le 1.25$$

where r, r_{max}, (Fig. 4.55), are the distance and maximum distance (when at the corner) of the centroid of the opening (whether circular or rectangular) from the centroid of the web panel. For a circular cutout:

$$r_{max} = \sqrt{(0.5\,b)^2 + (0.5\,h)^2} - \left(\frac{d}{\sqrt{2}}\right)$$

V_u is the ultimate strength of the unperforated web with the same geometry and V_{ult} is the ultimate strength of a girder with a central hole calculated by the simplified approach of Narayanan and Rockey's first study. Rectangular cutouts may be treated as circular, once their 'equivalent' diameter is obtained by:

$$D = \sqrt{h_o + b_o}\,\sin(\theta + \theta_o) \qquad \text{where} \qquad \theta_o = \tan^{-1}(h_o / b_o)$$

where θ_o is the slope of the geometrical diagonal of the cutout. No research results has been published for the cases of webs with reinforced circular or rectangular eccentrically placed perforations.

4.5.5 Design of Reinforcements for Web Plate Cutouts

There are three ways of reinforcing a cutout, namely by using (a) 'lips', (b) single sided rings, and (c) double sided rings.

Usually procedures for the design of reinforcements for web cutouts aim in determining the cross section $w_r \times t_r$ of the reinforcement. Note that the thickness of the reinforcement usually includes the thickness of the web plate. Such procedures, based on the ultimate strength formulations reviewed above are presented for the case of centrally located circular and rectangular cutouts in [223], and for eccentrically located circular perforations in [237]. This subject is treated no further.

4.5.6 Application of Design Methodology to Aluminium Perforated Plate Girders

No research has been carried out or published for the case of aluminium plate girders with web perforations. Furthermore, due to the lack of detailed experimental as well as theoretical models of the cases of direct interest to marine applications (shear and bending loading, with the presence of direct stresses on aluminium girders) it is recommended that a conservative method should be used instead. For this approach, Rockey's initial proposal is recommended (para. 4.5.2)

$$V_{ult} = w\left[V_v + (V_u - V_v)(1 - d/h)\right]$$

reduced by a factor w ($= k_z$) to account for HAZ effects (para. 4.1.2). The w-reduction approach, although very conservative, has been recommended for unperforated aluminium girders (para. 4.4.4.1) [216] and has been used in the BS 8118 guidelines (for unperforated girders). The beneficial effect of horizontal stiffeners is not considered, so is any effect of reinforcements of perforations. In the case of coexistent bending and direct stresses, the aforementioned strength reduction could be used directly in reducing the values of V_s and V_c in the interaction diagrams. The value of V_B is indirectly affected via V_c (para. 4.4.2.4).

4.6 The Design of Deep Plate Knee Joints

As pointed out in the Introduction (para. 1.8.3), the use of partial transverse bulkheads (PTBs) may result in a more efficient structure in terms of weight. This is due to the fact that although the peak and shear stresses increase with bulkhead spacing, the presence of PTBs will bring them back to acceptable levels. This section attempts to transfer the principles involved

in the design of the plating at deep-plate girder corner joints of civil engineering structures, to the design of those panels in the transverse bulkheads which lie at the cross-deck strut intersection. The application of the method to the design of Partial Transverse Bulkheads is equally possible.

Knee joints of portal frames are generally designed based on their critical buckling load. Higher loading conditions are traditionally catered for, either by the introduction of haunches of by the insertion of 'doubler' plating to increase the web thickness. However, concentration on an ultimate strength approach to design would lead to a more weight efficient structure.

Most of the investigations (theoretical and experimental) have been carried out in the U.S. in the late 30s and especially by the American Bureau of Standards and Lehigh University [238]. However, that research was limited to the critical buckling of the web plate having no consideration of its postbuckling strength. Recent research in Germany [197, 239, 240] on the ultimate strength of square panel knee-joints of portal frames with thin webs made of steel, provides the state of the art in ultimate strength design of such structural arrangements. The theoretical model bases the post-buckling behaviour of the structure on a tension field approach (Figs. 4.57, 4.58) similar to that used for deep plate girders [185, 198]. The inclination of the tension bands and the internal forces for the deep plate girder and the knee joint cases are demonstrated in Figure 4.56. In addition, Bodarski [241] has investigated the post-buckling behaviour of frame joints made of plastic material with different stiffener arrangements (Fig. 4.57). The tension field formation is clearly visible and current work in Braunschweig aims in extending their tension field recommendations to these type of structural arrangements. Steel is the material used in the latest studies.

4.6.1 Critical Buckling Strength Estimation

Figure 4.58 presents the force and moment distribution (due to external load actions) on a flat rectangular corner plate of uniform thickness t, and dimensions 2a and 2b. Pinned boundary conditions are assumed throughout. Buckling and consequent failure will occur by rotation about point (i) of the structure. Hence the moment about point (i), to cause critical buckling of the web panel is given by (Fig. 4.58) [197, 239, 240]:

$$M_{cr} = M_{actual}\left(\frac{\tau_{cr}}{\tau_{actual}}\right)$$

where τ_{cr} is the critical buckling of the web panel under purely shear loading as given in the classic theory for pinned boundary conditions. Furthermore, the existing maximum shear stress is determined by the Airy Stress Function and according to Scheer et al [239] is given by:

$$\tau_{actual} = \left(2\,a\,F_{xy} + a\,F_y + M_x + 3\,M_y\right)/\left(2\,a\,b\,t\right)$$

where the the loads and moments applied at the edges of the rectangular plate were derived by Osgood et al to be [238, 242] (Fig. 4.58):

$$M_o = V\left(a + A\right) = H\left(b + B\right) \qquad M = M_o - V\,a = V\,A$$

$$F_x = -\left(1 - k - j\right)H - \left[\frac{m}{1-k+j} - \frac{n}{1+k-j}\right]\frac{M}{b} \qquad F_y = -\left(1 - 2\,p\right)V$$

$$F_{xy} = \left(1 - p\right)V - \frac{1}{a}\left(M_o - H\,b\right) \qquad F_{yx} = \left(1 - j\right)H - \frac{n\,M}{\left(1 + k - j\right)b}$$

$$M_x = -\left(1 - \frac{m}{1-k+j} - \frac{n}{1+k-j}\right)M \qquad M_y = -\left(1 - 2\,r\right)H\,B$$

The coefficients p and r above are the proportion of V and M respectively which are taken by each flange of the *column* at the edge y=b:

$$p, (j) = \frac{\text{Area of one flange of column, (beam)}}{\text{Total sectional area of column, (beam)}}$$

$$r, (n) = \frac{\text{I of one flange of column, (beam) about N.A. of section}}{\text{Total I of column, (beam)}}$$

where I stands for the second moment of inertia of the flange or section (as appropriate). Similarly, k and j are the proportions of H and m and n are the proportions of M taken by the top and bottom flanges of the *beam portion* of the knee at the edge x=a. It is important to stress that k, m are used to account for the possibility that the flange is not continuous at the knee (e.g. riveted) and will thus partially transmit stress across the discontinuous section. *For welded sections k=j and m=n.*

4.6.2 Ultimate Strength Estimation

As already mentioned the Braunschweig model [197, 239, 240] calculates the moment carrying capacity of the knee joint from two components. The critical buckling component and the post-buckling component which obtains its contribution from the formation of a tension band in the direction of the diagonal of the web plate. The tension field contribution is very similar to that described for the Cardiff model (Fig. 4.30) [185, 198]. The main difference between the girder and the knee-joint models is that for the former the angle of inclination of the tension field is approximately equal to two thirds of the angle of the panel diagonal, while for the latter the angle of the tension field is limited to the angle of the panel diagonal. However, in both models, the direct and bending loads are assumed to be resisted solely by the flanges, while the shear loads are taken up by the web plate.

Figure 4.58 demonstrates the failure mode of a rectangular knee joint. Once the critical buckling shear stress has been reached, a tension zone is formed along the diagonal of the plate. Any consequent increase in the load will be carried by the tension field whose stress amplitude increases till the yield stress of the web material is reached. At this instance plastic hinges are assumed to occur at the points A, B, C, D and the structural arrangement fails as a mechanism as shown in Figure 4.58. The positions of the plastic hinges depend on the rigidities of the flanges which in turn depend on the loads, material, and geometrical considerations. Experimental observations [197, 239, 240] have supported the assumption that edges Ai and Ci will remain straight throughout the load application up to the moment of failure. Hence no plastic hinges are assumed to form on them.

With reference to Figure 4.58, zone g_2 has been empirically set to $0.5\,h_2$ while the extent of zone g_1 is dependent on the rigidity of the flanges AB and CD and hence on the plastic hinge positions. Therefore,

$$g_1 = \max\left(l_{AB}\sin\theta_r,\ l_{CD}\sin\theta_c\right) \qquad \text{and} \qquad g_2 = 0.5\,h_2$$

where

$$l_{AB} = \sqrt{2\left(M_A + M_B\right)/\left(\sigma_y^t\, t \sin^2\theta_r\right)} \le a$$

$$l_{CD} = \sqrt{2\left(M_C + M_D\right)/\left(\sigma_y^t\, t \sin^2\theta_c\right)} \le b$$

$$\theta_r = \arctan(b/a), \qquad \theta_c = \arctan(a/b)$$

The beam (AB) and column (CD) flange rigidities M_A, M_B, M_C, M_D, are reduced by any direct and/or bending stresses acting externally on them (Appendix 4.5) while the tensile stress to cause yield in the web material σ_t^y is given by:

$$\sigma_t^y = \sqrt{\sigma_y^2 - 3\,\tau_{cr}^2 + d^2} - d \quad \text{where} \quad d = \frac{3}{2}\tau_{cr}\sin 2\theta_r$$

The lengths l_{AB} and l_{CD} must be determined iteratively (Appendix 4.5) as the maximum moments acting on the knee will affect the individual bending stresses acting on the flanges and hence will affect their bending rigidity. The lengths l_{AB} and l_{CD} should therefore account for these increased loads as the ultimate bending moment is iteratively approached. The load carrying capacities of the two zones expressed in the form of the bending moment about point i are given by

$$M_1 = \sigma_t^y\, t_w\, g_1 \left(h_2 + 0.5\, g_1\right) \quad \text{and} \quad M_2 = \sigma_t^y\, t_w\, g_2 \left(h_2 - 0.5\, g_2\right)$$

and hence the total moment carrying capacity of a knee joint about point i is [239]:

$$M_u = M_{cr} + M_1 + M_2$$

i.e. the contributions of the moment to cause critical buckling plus the moments carried by the structural arrangement in the post-buckling region.

4.6.3 Experimental Verification of the Model

The aforementioned theoretical model has been compared with the results of experimental data carried out in Braunschweig and reported in [239, 240]. Ten steel square knee joint plates were tested with b/t ratios ranging from 130 to 300. Osgood's critical buckling formulation was found to constantly underpredict the strength by approximately 40%. Furthermore, the ultimate strength predictions by Scheer at al's model were found to overestimate strength by about 10%. Specifically, the model uncertainty was found to contain a bias of 0.91 and a COV of 11.5% for a population of only 9 tests.
No experimental or numerical tests for rectangular plates other than square plates were found from the literature survey and therefore the same modelling uncertainties as for the square plates are recommended.

4.6.4 The Effect of Vertical/Horizontal Web Stiffeners

In the presence of horizontal web stiffeners, the use of the critical buckling shear strength of the weakest subpanel as the only change in the ultimate strength formulation is recommended (para. 4.4.2.3). No proposals and/or experimental have been published along these lines, and therefore such an approach should be treated with caution. A conservative approach would be to neglect the influence of the stiffeners and consider the complete web depth of the corner panel in the strength analysis.

4.6.5 Accounting for the Effect of Web Perforations

In the absence of appropriate research and indeed of any design proposals, a similar approach to that used for steel plate girders loaded in shear (para. 4.5.2) is recommended, although caution in its application is advised due to the untested nature of the expression in this context. Therefore, it may be assumed that the moment capacity of the joint plate will vary linearly with diameter between the moment capacity of the section assuming that only the four flanges are effective and that no web material is present, M_{hinge}, and the case at which there are no perforations and the web is fully efficient, M_u:

$$M_{ult} = M_{hinge} + \left(M_u - M_{hinge}\right)\left(1 - \frac{D}{2b}\right)$$

where 2b is the plate depth, D is the diameter (or equivalent diameter - para. 4.5.2) of the perforation, $M_{beam,top}$, $M_{beam,bot}$, $M_{col,left}$, $M_{col,right}$ are the plastic moment capacities of the beam (top and bottom) flanges and the column (left and right) flanges respectively and M_{hinge} is given by the summation of these capacities. The diameter (or equivalent diameter) of the perforation should be restricted to 2/3 of the web depth.

4.6.6 Applying the Model to Aluminium Knee Joints

In the absence of any theoretical and experimental investigations into the ultimate strength behaviour of aluminium knee-joints, and considering the similarity of analysis to that of plate girders in shear, it is possible to assume that the reduction in ultimate bending moment will occur in a similar manner to the reduction of ultimate shear strength (para. 4.4.4.1). Hence, the total moment carrying capacity of a knee joint about point i may given by:

$$M_u = M_{cr} + w\left(M_1 + M_2\right)$$

Paragraph 4.1.2 may be referenced for details on the value of the reduction factor w ($= k_z$).

4.6.7 The Design of Knee Joints with Tapered or Curved Flanges

In order to reduce the high stress concentration values associated with knees having their beam and column components at right angles to each other, it is possible to opt for a haunched knee with tapered flanges or for a haunched knee with curved flanges.

A tension field approach has not yet been developed for this type of problem, although experimental investigations by Bodarski [241] suggest that this is possible and research at Braunschweig heads along these lines.

Current design procedures aim to maintain the maximum stresses at the various sections of the knee at levels below the material yield stress. Evaluation of these stresses at these locations not only provides a safety check but permits the evaluation of the local forces and their components against which any stiffening system would have to be designed.

Two methods are currently most popular for the estimation of the stress level in the knees:

(a) Vierendeel's Tapered Beam Formulae [242]

(b) Olander's Formulations [243].

Figure 4.59 demonstrates the notation for *Vierendeel's method*. The method consists of calculating the stresses (shear, direct and bending) at different locations in the knee identified by the distances a_o and a_i from the neutral axis and the angle of the tangent to the curved flange ϕ. Hence the forces in any section A-A are given by [242]:

$$f_o = \frac{P_o}{A} - \frac{M\,a_o}{I} \qquad f_i = \frac{P_o}{A} + \frac{M\,a_i}{I} \qquad v = \frac{1}{t_w\,d}\left(V + f_i\,A_i\,\sin\phi\right)$$

where v is the shear stress, f_o, f_i are the mean stresses in the outer and inner flanges respectively, a_o, a_i distances of the centroids of the outer and

inner flanges respectively from the neutral axis *of the specific section* and A_o, A_i are the cross-sectional areas of the outer and inner flanges. Furthermore, M, V, P are the bending moment, shear force, and axial force at section A-A, t_w, d are the web thickness and depth respectively while A $(= t_w\, d + A_o + A_i \cos\phi)$ and I $\left(= \left(t_w\, d^3/12\right) + A_o\, a_o^2 + A_i \cos\phi\, a_i^2\right)$.

These expressions are also applicable to tapered knees.

Olander's method considers a number of circular sections (e.g. A-B) that cut the extreme fibres of the flanges at right angles (Fig. 4.60). Each section is then developed to its true length and hence its area A and moment of inertia I are obtained. All forces to the right of the section A-B are then resolved into the values P_o and M_o about point O, the centre of the arc. P_o passes through the neutral axis of the section and M_o is the moment of the forces about O (i.e. due to the eccentricity of the forces from the neutral axis). The stresses are then calculated as for a beam-column:

$$f = \frac{P_o}{A} \pm \frac{M\,c}{I}$$

The shear force V in the chosen section is calculated from M_o by $V = M_o/r$ (Fig. 4.60) and the geometrical properties of the circular sections are obtained by:

$$r = \frac{h + R\left(1 - \cos 2\phi\right)}{\sin 2\phi} \qquad a = R \sin 2\phi$$

$$b = r \cos 2\phi - a \qquad c = \phi\, r \quad (\phi \text{ in rads})$$

$$d = r \cos\phi \qquad e = r \sin\phi - g$$

The resolution of the forces into the values P_o and M_o and practical examples of both methods are presented in greater detail in [242]. Since, the optimum from the stress concentration point of view would be to replace the right angle haunch with a large circular arc with tangents at the struts and the cross deck, or a tapered haunch, Vierendeel's and Olander's methods become attractive. The use of such structural arrangements might be hindered by cost and space allocation considerations in the vessel, despite their structural benefits and the possibility of reducing the slamming damage on the wet-deck.

These two methods can also be used for the design of stockier beam to frame connections (depth on thickness of web plates less than 80) in ship structures. Although of no direct interest to the above presentation, it is worth mentioning that they were both initially considered by the Royal Navy for the design of haunched beam-frame connections. However, they were later rejected on the grounds of insufficient experimental evidence and complexity and a simpler approach (by use of doubler plates) was chosen, as reported by Faulkner [245]. This latter reference provides useful information on the design of beam to frame, longitudinal to bulkhead and grillage connections.

4.7 The Design of Stiffened Cylindrical Structures Under Pressure Loads

The advantage of axisymmetric structures to resist external (as well as internal) uniform pressure loading, is best put to use in the design of submerged structures and structures under the action of mainly hydrostatic loading. The hulls of submarines, semi submersibles as well as the underwater structural components of SWATH vessels are some examples of the application of cylindrical sections in the marine environment and Figure 4.63 demonstrates the variety of shapes and sizes that such components can be encountered in. These are:

(a) ring or ring/stringer stiffened cylindrical elements
(b) conical elements acting as transition joints
(c) spherical elements acting as end closures.

It is the ring frames and internal bulkheads that stabilise the shell. Longitudinal stringers are usual only when axial compression loads are significant. Their design aims to provide sufficient scantling and shell thickness dimensions to ensure that the structure will be able to resist any axial loads, external pressure loads or their combination.

The use of ring stiffened cylinders to withstand high axial loads is considered to be unrealistic and its treatment herein is omitted. For these, references [95, 99, 208, 245] may be consulted. Furthermore, the case of ring stiffened cylinders under axial compression and external pressure usually occurs in offshore structures and work by Faulkner [27, 99] and Cho and Frieze on interframe shell collapse provide accurate interaction equations

for this purpose (paras, 4.2.8, 4.7.4.3). Hence, the cases of ring framed cylinders under hydrostatic pressure loading as well as under a combination of axial and lateral pressure loading are initially reviewed followed by consideration of the strength models for orthogonally stiffened cylinders. Recommendations for the design of conical transitions as well as dome ends under hydrostatic pressure loads are also presented.

4.7.1 The Design of Ring-Framed Cylindrical Structures Under Hydrostatic Pressure

The need for structural weight efficiency in marine vessels having small waterplane areas, requires a more rational approach to structural design. Kendrick in [246] suggests general guidelines leading towards a more weight efficient cylindrical structure when it is externally pressurised, underlying the necessary trade off between the following considerations:

- the shell thickness and hence weight decreases with decreasing frame spacing L_s,
- high strength material is advantageous only when high external pressures are expected,
- the ring frame cross sectional area A_s increases with increasing L_s,
- the structural weight is not proportional to the level of external pressure loading. This is the case only for large pressures, because of the buckling penalty introduced to the structure at shallow depths.

Specifically, as the operating depths of hulls of SWATH ships are bound to be relatively (to submarine hulls) small, these structures are more prone to interframe shell buckling (as the thickness will be small) rather than interframe shell yielding which is a characteristic of stockier, deep-diving cross sections.

In ring stiffened cylinders, the weight of the frames is a small percentage of that of the shell (app. 25-30%). Hence, for a given level of external pressure, material and radius, the shell thickness (and structural weight) is determined mainly by the stiffener spacing and to a smaller extent by the stiffener size. Hence, the aim of any design procedure should be to establish the level of hydrostatic pressure for interframe collapse and require that the

frames are adequate to avoid premature overall collapse. Since in this case, the design is based on collapse instead of elastic buckling criteria, the shape imperfections, residual stress effects and material stress-strain characteristics become important.

Two main modes of failure are of concern in the design of externally pressurised cylindrical structures (Fig. 4.64):

- Interframe Collapse (basis for design)
- Overall Collapse (avoided by large safety factors)

The former can occur in the form of shell yielding at mid-bay, or elastic shell buckling between frames. Interframe collapse is usually an interaction between these two conditions. Elastic shell buckling occurs for the more slender geometries and appears in the form of a number of circumferential waves with one-half wave between frames ($n>10$, $m=1$). Interframe yielding (axisymmetric plastic deformation) is a characteristic of stocky shells and should be preferred for deep diving structures, because it would permit greater use of the material strength and because shape imperfections will then be less important.

Overall collapse is *frame induced*. Frame failure can occur either by frame yielding ($n \approx 2-5$), shell yielding ($n \geq 6$), or frame tripping (interacting with shell buckling). General instability is sensitive to shape imperfections and its prediction is therefore less certain. Hence it is designed out by dimensioning the ring frames against o-o-c bending stresses and by providing them with adequate rigidity against tripping.

Interaction between these two failure modes is avoided by proper choice of safety factors, which ensure that general instability is preceded by bay instability and eventual interframe shell collapse. Hence, in the design of cylindrical externally pressurised structures of a given radius:

- the stiffener spacing is governed by interframe shell collapse,
- the stiffener size is governed by general instability and volume requirements in the cylinder, while
- the proportions of the frames are governed by tripping and local buckling considerations.

The detailed theoretical background and derivation of the closed form expressions describing the load capacity against these failure modes is covered in detail in [246]. Only the main formulations will be presented herein to the degree necessary for highlighting the parameters affecting strength. It must be noted that the strength formulations that follow are based on the assumption of equal frame spacing (uniformly stiffened cylinders). A small degree of non-uniformity in the frame spacing may be tackled by using an average bay length [246]. If it is the size of the ring-frames that is not uniform, then the average combined moment of inertia should be used. An accurate treatment of the case of unequal stiffeners is presented in [246].

The mostly used design codes for the design of externally pressurised ring and/or stringer stiffened cylinders are the British Standard BS 5500 [247] (which is also the basis for most other codes), the ECCS [248] proposals for cylinders under external pressure only, the DNV Classification Notes 30.1 [66, 208], the API Bulletin on Stability Design of Cylindrical Shells for Floating Offshore Platforms ($R/t \geq 150$) [95] and the API code for Fixed Offshore Platforms $R/t < 150$ [249]. Of these codes it is the later [249] that is reliability based, while the remaining support a deterministic approach to the derivation of their safety factors.

The most popular design method currently in use is that proposed by BS 5500 and has stemmed from the pioneering work of Kendrick and his colleagues for the Royal Navy (reviewed in [168, 246, 250-253]). These proposals have also formed the basis for the ECCS guidelines and where coupled with research efforts carried out in Norway [25] to result in the DNV formulations [208, 66]. API based its approach on earlier RCC work [254, 255] thus not directly benefiting from the Royal Navy's experience. A comparison of these codes with experimental data is presented in [116].

4.7.1.1 Designing Against Interframe Shell Collapse

Interframe shell collapse is associated with the shell thickness and frame spacing and the available formulations for design are described next.

The BS 5500 proposal against interframe shell collapse suggests the use of a lower bound curve to within about 1% of experimental data (Fig. 4.65)

relating the collapse pressure, p_c, to the pressure to cause yielding at the shell at mid-bay, p_{c5} and to the pressure for mid-bay elastic shell buckling p_m. This interaction curve between elastic and inelastic behaviour has been expressed in a closed-form by Faulkner [255] :

$$p_c/p_{c5} = \begin{cases} 1 - p_{c5}/2\,p_m & \text{for } p_m/p_{c5} \geq 1 \\ p_m/2\,p_{c5} & \text{for } p_m/p_{c5} < 1 \end{cases}$$

and is used with a safety factor of 1.5 against collapse. The accuracy of the approach has been tried in the range of $5.9 < R/t < 250$ and $0.04 < L/R < 50$. A closed form expression for the mean curve through the experimental points is not available although its derivation using the data presented in Table 4.12 is possible. Such a curve would ensure a safety factor of 1.75 against collapse. For probabilistic design it is the mean curve is preferred.

p_m is the elastic buckling pressure for the unsupported shell between ring frames (see Notation) and is attributed to Kendrick [246] who slightly modified von Mises' original solution to give correct answers for small values of n. The expression derived for p_m, ignores the ring frame area, an acceptable approximation The minimised (wrt n) form of the expression as derived by Windenburg for hydrostatic pressure is used. The pressure at which the applied circumferential compression stress at shell mid-bay and mid-thickness reaches the shell yield stress, p_{c5}, (see notation), has been based on a linear simplification of Wilson's formula for elastic deformations of perfect uniformly framed cylinders [257]. The product γG accounts for the beneficial effect of the presence of ring frames, as it depends on the stiffener geometry, stiffener spacing, shell thickness and shell radius. Its value is usually between 0 and 0.2.

Generally speaking, when p_m is much smaller than p_{c5} and p_{yf} and the o-o-c is very small, the collapse pressure will be close to p_m. When p_m is greater than $6p_{c5}$ and much larger than p_{yf}, the collapse pressure will be close to $1.15p_{c5}$ [252] and predictions can be made within 10%. Furthermore, in the region $p_m \approx p_{c5}$ the greatest scatter is observed (Fig. 4.65) as it is the area of greatest interaction between yielding and buckling [252]. In this case, the collapse is influenced by geometry, Young's modulus, material yield stress and the level of o-o-c. Collapse at pressures close to p_m will be lobar in appearance while collapse at pressures close to $1.15p_{c5}$ will be axisymmetric

in appearance. The BS 5500 expression is applicable to all ductile materials and the associated modelling uncertainty is shown in Table 4.13. For application to *welded aluminium structures,* Faulkner [255] recommends the safe substitution of Young's modulus with the secant modulus at 0.2% proof stress to account for the reduced material stiffness and the HAZ strength reduction.

In 1984, *Cho and Frieze* [26, 258] presented a modified version of the BS 5500 approach, which represented the whole range by one curve. The pressure to cause yielding in the shell at mid-bay, p_{c5}, was substituted by p_{ym}, the hydrostatic pressure at which the von Mises equivalent stress in the shell reaches the material yield stress and p_m refers to the critical buckling pressure of the shell under hydrostatic pressure. A quadratic Merchant-Rankine formulation was used to account for elasto-plastic effects resulting in:

$$\left(\frac{p_c}{\rho_h\, p_m}\right)^2 + \left(\frac{p_c}{p_{ym}}\right)^2 = 1.0 \qquad \text{and} \qquad \rho_h = 0.134\left(\sqrt{LR}/t\right)^{0.407}$$

where ρ_h is a hydrostatic knockdown factor and p_c is the mean hydrostatic collapse pressure. This expression is found to demonstrate better values on the modelling uncertainty than BS 5500 (Table 4.13) but the BS 5500 should be used on the basis of conservatism and wider acceptance.

4.7.1.2 Designing Against General Instability

This mode of failure is associated with weak frames and widely spaced bulkheads. Weakness of the ring frames can be expressed by either frame yielding or shell induced tripping, while large spacing would trigger yielding in the shell in the immediate vicinity of the frames. For this failure mode, attention concentrates on the overall behaviour of a cylindrical compartment, of length L_c, between two rigid bulkheads or heavy frames. The structure is assumed imperfect in the analysis and any initial imperfections are magnified under external pressure loading.

The first theory for elastic general instability of perfect structures was presented by Kendrick in 1953 [246] who assumed a half-sine wave over the compartment length L_s with allowance for shell distortions between frames (Fig. 4.64). Currently, it is Bryant's two term approximation [259] for the

overall buckling pressure, p_n, that is widely accepted and used in BS 5500:

$$p_n = p_{nf} + p_{ns} \qquad \text{where}$$

$$p_{nf} = \left(n^2 - 1\right) E\, I_c / R^3\, L_s \qquad \text{and} \qquad p_{ns} = \left(E\, t/R\right) \Big/ \left(\left(n^2 - 1 + k\,\lambda_c^2\right)\left(n^2/\lambda_c^2 + 1\right)^2\right)$$

k=0.5 for hydrostatic pressure and k=0 for radial pressure. Pressure p_n indirectly governs the size of the ring frames. The first term, p_{nf}, expresses the elastic collapse pressure for the shell and frame combination (frame buckling term) of an infinitely long cylindrical structure (attributed to Bresse [128]) while the second term, p_{ns}, is a shell buckling term which accounts for the fact that the structure is not of infinite length but is restricted between rigid bulkheads/frames. This forces the shell to deform with significant membrane actions which increase as L_c reduces and decrease as n increases. This expression is the first term in the von Mises expression [260] (see Notation) for the elastic shell buckling pressure of a closed cylinder with simple support conditions, p_m. The second shell bending term of the von Mises expression is omitted because it is generally small. The following apply for the Bryant expression above [252]:

- the frame term increases with increasing n and the shell term decreases. The optimum n value usually lies in the region of n=2-6 for most compartment lengths [255].

- p_n reduces with increasing L_c

- the value of n for which p_n is a minimum increases as L_c decreases.

The expression ignores interframe deformation which can be accounted for by assuming a reduced effective length, L_e (see Notation) of shell acting with the ring frame when evaluating I_c. The Bijlaard expression for L_e is recommended on grounds of accuracy and relative simplicity.

One end	Other end	L_c
Bulkhead	Dished Head	$2\,L_c$
No diaphragm	No diaphragm	$L_c = \infty,\ p_n = p_{nf}$

In the event that non-rigid (or no) structural elements are placed at either end of the compartment, the approximations to the length of L_c shown in the Table above may be made (as recommended by BS 5500):

4.7.1.3 Ring Frame Design

Ring frames should be proportioned in such a way so as to withstand:

(a) the total stresses arising from the 'as constructed' o-o-c bending plus direct hoop stresses [246].

(b) any sideways tripping tendencies that might arise by the slenderness of their dimensions and the destabilising effect of shell buckling.

The maximum stress in the frame is calculated (by BS 5500, ECCS, and DNV) in terms of a Perry-Robertson type expression, as the sum of the hoop stress at the centroid of frame (first term) and the bending stress arising from the worst o-o-c, C_n, magnified under pressure by a factor $p/(p_n - C^* p_d)$

$$\sigma_{tf} = A^* \frac{p_d \sigma_{yf}}{p_{yf}} + B^* \frac{E \bar{x} C_n (n^2 - 1) p_d}{R^2 (p_n - C^* p_d)} \leq D^* \sigma_{yf}$$

where p_d is the design pressure and A^*, B^*, C^*, D^*, have the following values for the individual design codes:

Code	A^*	B^*	C^*	D^*
BS 5500/ECCS				
hot formed/fabricated frames	1.8	1.8	1.8	1.0
cold bent frames	2.0	2.0	2.0	1.0
DNV	2.0	2.0	2.0	0.9

A number of values for n between 2 and 6 need to be tried before a maximum value for σ_{tf} is obtained. For n=2 the magnitude of the bending stress is very sensitive to the value of the compartment length L_c, while for n=6 this phenomenon reverses [252]. Most codes assume C_n is the same for all modes (0.005R) which is pessimistic for higher n. BS 5500 requests the

evaluation of σ_{tf} for n=2-6 and for $C_n = 0.005R$. It was Kendrick [168] who showed that overall collapse is close to the pressure causing first yield at the frame flange. The statistical uncertainties involved in the modelling of strength against this failure mode, are presented in Table 4.13.

The importance of *tripping induced general instability* resulting from the loss of the radial and bending stiffness of the frames should not be overlooked. A characteristic of tripping failure is that it can happen without any loss of circularity at the stiffener/shell connection. Elastic sideways tripping for flanged ring frames is tackled by BS 5500 and ECCS with the very conservative criterion (by Kendrick [246, 250-253]):

$$\sigma_T = \frac{E I_z}{A_s R \bar{z}} > \frac{p_d \sigma_{yf}}{p_{yf}}$$

where σ_T acts at the frame centroid and pinned boundary conditions are assumed at the frame toe. Small changes in the flange width of the frame have considerable effects on I_z and hence σ_T. Increasing the flange width increases the tripping strength. Any geometrical changes in the frames should, however, satisfy the limits imposed by slenderness and minimum thickness requirements. The modelling uncertainty associated with this failure mode is presented in Table 4.13. Additional design approaches against tripping accounting for the more realistic cases of shell/stiffener interaction are described in paragraph 4.3.4.

Local buckling of ring frames should be avoided by appropriate proportioning of the stiffener section. BS 5500 recommends that the lowest instability pressure associated with local stiffener instability is at least 4 times the design pressure. The factor of 4 was chosen because the design curve for interframe collapse requires that $p_m \geq 3 p_d$ and it is desirable to avoid interaction between the various buckling modes [252]. Guidance on the design against local buckling of stiffener sections is provided in paragraph 4.3.5.

4.7.1.4 Initial Imperfection and Residual Stress Effects

The two types of initial imperfections affect the behaviour of ring frames are (a) geometrical imperfections (o-o-c on shell and/or frames, frame tilt) and (b) residual stresses.

Out-of-Circularity: Local indentations on the shell (corresponding to high n) introduce bending stresses in the shell which can be calculated using interframe buckling pressures [246]. The effect however, of the shell indentations on the ring frames is small (small circumferential wavelengths) and hence negligible bending stresses are introduced in the shell and frames. Imperfections of longer wavelength generally involve both the frame and the shell.

Out-of-circularity of frames is far more important and greatly affects the strength of the structure against general instability but has little effect on interframe shell collapse [246, 251]. The resulting stress in the frame flange (hoop stress plus bending stress arising from o-o-c) is obtained via a Perry-Robertson type interaction (para. 4.7.1.3) and with an appropriate safety factor is restricted to below yield stress levels. The allowable levels of frame out-of-circularity permitted by the various codes are shown below.

Code	O-o-c assumed
BS 5500, ECCS, DNV,API Bul 2U	0.005 R
API RP2A	0.002 R or 0.125 t if t<2in then 0.25 t

The use of a specific value of o-o-c irrespective of the mode number n, is conservative and is based on the unrealistic assumption that high n values are associated with large magnitudes of o-o-c and hence induced bending stresses. In an attempt to connect the amplitude of the o-o-c to the value of half cycles of deformation in the circumference, the following expression was recommended from an MoD study (a, b are in millimetres and R in metres) [165, 261]. This reduces the amplitude of the o-o-c as n increases:

$$C_n = \frac{a + b\,n}{n^2 - 1} \qquad \text{where} \qquad \bar{a} = 3.15\,R, \quad a_k = 8.38\,R \qquad \bar{b} = 1.20\,R, \quad b_k = 3.31\,R$$

The bar denotes mean values and the subscript k the upper 3 standard deviation values. The shape imperfections can be assumed normally distributed with a very high COV of 50%. Das et al in [261] have demonstrated that the COV values involved with this expression vary

between 51.3 % and 54.6% for n values varying between 2 and 6 respectively. When use is made of the worst level of o-o-c in the worst possible mode (e.g. 0.5%R), Morandi [163] recommends a less conservative COV value of 20%. Faulkner, in turn, proposed the following compromise between the BS 5500 and MoD recommendations:

$$C_n = \frac{0.005\,R}{n-1}$$

which also recognises the dependence of the magnitude of the o-o-c to the shell radius and the number of circumferential shell lobes.

Generally, o-o-c's in the hoop direction are more serious than lengthwise imperfections and hence no information is available on the latter.

Effect of Initial Tilt on Ring Frame Strength: Any initial tilt of the ring frames away from the plane through the toe of the web which is perpendicular to the cylinder axis will:

(a) magnify the tilt by approximately $\sigma_{mean}/(\sigma_T - \sigma_{mean})$ where σ_{mean} is the mean applied stiffener stress,
(b) introduce additional bending stresses in the ring frame flange. For axisymmetric tilts (n=0) these bending stresses are small and may be neglected.

Initial tilts should be avoided by proper control of the construction process. In any case, Louca and Harding [262] demonstrated that any initial frame tilt, however slender the frame is, has no major effect on the frame collapse pressure. In support of this, Morandi's FE investigation [163] concluded that a 4° initial tilt is less harmful than a 0.005R o-o-c on the frame strength and that the reduction in tripping strength associated with this tilt angle is approximately 8%.

The Effect of Residual Stresses: Although residual stress effects in interframe shell collapse are indirectly accounted for by calibration to experimental data of welded specimens, for general instability considerations larger safety factors are used. Specifically, *cold-rolling of the shell* and the resulting through the thickness stress distribution (Fig. 4.66) have been found [7, 246, 263, 264] to have little effect on the shell's collapse

pressure. However, the apparent decrease in Young's modulus that results (Fig. 4.66), increase the shell deflections and therefore indirectly increases the load on the ring frames (even by 25% [246]).

Cold bending of frames introduces a large region of compressive residuals in the outer fibres of the flanges (Fig. 4.67) ensuring an early loss in the compression stiffness as well as a loss in the bending rigidity at outward anti-nodes for internal ring frames (e.g. 40% [7]). O-o-c bending will further aggravate the problem. BS 5500 implicitly allows lower safety factors for stress-relieved, hot-bent or fabricated frames. Smith and Kirkwood [266], have observed reductions of 30% and 7% on the overall buckling strength due to ring frame cold bending and shell cold rolling respectively.

Residual stresses due to *hot-rolling* (Fig. 4.67) are independent of the material yield strength. The flange tips and midweb regions are usually in compression while the flange/web intersections are in tension. As bending of these sections to a circular shape introduces tensile stresses which counterbalance the deleterious effects of the compressive stresses in the flanges, their effect may be neglected.

Weld induced residual stresses depend on the weld process, the rate of heat input and the welding sequence. Although radial shrinkage effects are small and are neglected, this is not possible for the residual stresses introduced from *along the weld* and *across the weld* contractions. The shrinkage occurring along the weld introduces a tensile yield zone over a width $2\eta t$ of the shell and a depth ηt_w in the stiffener web, which are both balanced by a compressive stress in the remaining of the cross section. For the shell the mean compressive stress is σ_{rc1}.

The shrinkage occurring across the weld, distorts the cross-section by producing inwards interframe corrugations of the shell with internal frames. It is important to note, that the distortion of the plating radially towards the stiffener, induces hoop stresses in the shell σ_{rc2}, which are balanced by circumferential stresses of opposite sign (tensile) in the frame, σ_{rf} and in the adjoining shell which move radially in the opposite direction (Fig. 4.68). Hence, the mid-bay shell compression stress is given by [7]:

$$\sigma_{rc} = \sigma_{rc1} + \sigma_{rc2} \quad \text{where}$$

$$\frac{\sigma_{rc1}}{\sigma_{ys}} = \frac{\left(2+(t_w/t)^2\right)\eta}{(L_s/t)\left(1+(A_s/L_s\,t)\right)-\left(2+(t_w/t)^2\right)\eta}$$

$$\sigma_{rc2} = \sigma_{rf} - \frac{\delta_p E}{R} = \frac{\delta_p E}{R}\left(\frac{2}{\pi\left(1+A_s/L_s\,t\right)}-1\right) \quad \text{and} \quad \delta_p \approx 0.1\,t$$

A thorough review of the subject is carried out by Faulkner [7] and more recently by Morandi in [163] but validation is limited to measurements on one ring frame of a full scale submarine.

4.7.2 The Design of Conical Transitions Under External Pressure Loads

The approach to design of ring stiffened, conical transition sections under external pressure loads is dependent on the extent of the conical section as well as on the taper ratio involved. For small taper ratios Niordson's 'equivalent cylinder' approach [267] for cones simply supported at their ends has proved to be quite accurate in design. The very good aggreement of this approximate method with more detailed studies and theories presented in the aeronautical field by Seide [268] and Singer et al [269, 270] have justified its attraction and its use is recommended in BS 5500 [247].
Niordson proposes the use of the same strength formulations and criteria as for cylindrical elements under external pressure, by accounting for the taper angle, θ, by the following modifications:

t	by	$t\cos\theta$	E	by	$E\cos^2\theta$
R	by	R_m (mean radius)	L	by	generator length

Mean frame dimensions should be used and the frames have been assumed in the analysis to be normal to the axis of the cone and not to the shell. Criteria to avoid over-conservatism in the design of cone-cylinder combinations have been presented by Kendrick in [250].

4.7.3 The Design of Dome Ends Under External Pressure Loads

Spherical dome ends are usually unstiffened and their behaviour is sensitive to initial imperfections and boundary conditions when loaded under external pressure. The effects of inaccuracies in manufacturing will

normally restrict the beneficial effect on strength obtained by the double curvature and hence render the classical buckling pressure for perfect spherical shells, p_{cl}, too optimistic.

As the diameter of the dome ends is normally dictated by the radius of the adjacent cylindrical structure and considering that no stiffening is present, the only way to secure failure by yielding is by raising the shell thickness considerably. A review of a number of theories attempting to predict the collapse pressure load by Thomson [271], proved the inefficiency of analytical procedures to properly account of the initial imperfection effects. Tests and parametric studies were carried out by Dixon on welded torispheres (reported in [272]), and Newland [273] and Kiernan/Nishida [274] on hemispheres (Fig. 4.69) concluded that the hemisphere results fell entirely within the scatter band of the torispheres. Analysing this data, Faulkner [275] proposed a *Merchant-Rankine interaction* between elastic and inelastic sphere collapse pressures as a *mean* curve through the data:

$$\overline{p}_c = 2\,p_b \Big/ \sqrt{1+\left(2\,p_b/0.3\,p_{cl}\right)^2}$$

where $2\,p_b$ $(=p_{ys})$ is the membrane yield pressure. This expression was found to be accurate within 3% over the complete slenderness range $(1.0 < p_e/p_{ys} < 6.5)$ of 60 test data and can be put in a form useful for design:

$$\left(\frac{R}{t}\right)^4 + \frac{E^2}{30.4\,\sigma_y^2}\left(\frac{R}{t}\right)^2 - \frac{E^2}{7.6\,\overline{p}_c^2} = 0$$

The relative bias and COV values are shown in Table 4.13.

BS 5500 [247] accounts only for spheres that are spherical to within 1% of the radius and for which the radius of curvature (based on an arc length of $2.4\sqrt{R\,t}$) does not exceed the nominal value by more than 30%. The design curve (Fig. 4.69a) proposed by BS 5500 forms a lower bound to experimental data. This choice was due to the large scatter and the fact that the test results for large dome ends tend to plot towards the lower bound curve and was underlined by a safety factor of 1.5 on these lower bound predictions (implying a safety factor of 2.35 when compared with the mean curve through the test data). The 'proposed design curve' is roughly equivalent to the mean curve for ring stiffened cylinders.

4.7.4 The Design of Orthogonally Stiffened Cylindrical Structures

When high axial loads and bending moments have to be resisted by cylindrical shells with the possible presence of external pressure, the most efficient stiffening system is that consisting of longitudinal stringers supported laterally by ring frames and/or bulkheads. Generally, the load carrying capacity of such a structure would consist of that of the stringer stiffened shell (carrying all the loads acting in the longitudinal direction) and of the load capacity of the ring frame stiffened shell to withstand any radially applied loads. Application of such structural arrangements to offshore structures is considerable but not widely used for the underwater hull elements of SWATH ships as the load fields acting on the structure do not justify such an action.

Ring and stringer stiffened cylinders under the action of any combination of the above loads may collapse in any of the following failure modes:

(a) buckling of shell element between the stiffeners,
(b) interframe column buckling,
(c) tripping of stringers and/or ring frames,
(d) general instability.

General instability is designed out by the choice of conservative dimensions for the ring frames and based on procedures described in paragraph 4.7.1.2. Hence, the design of orthogonally stiffened cylinders proceeds as if it were stringer stiffened only for the failure modes (a), (b), (c) above.

4.7.4.1 Post-Buckling Strength of Orthogonally Stiffened Shell Elements Under Axial Compression

Shell buckling in axial compression is dependent on s/t and L/s ratios which correspond to b/t and aspect ratio respectively in flat panel buckling theories. Similarly to flat panels, long narrow shells present little shape sensitivity while for short wide shells post-buckling is unstable and very imperfection sensitive.

The critical buckling stress of shells in axial compression are given by the following formula attributed to Koiter [276]:

$$\sigma_{cr} = k_c \frac{\pi^2 E}{12(1-\upsilon^2)}\left(\frac{t}{s}\right)^2 \qquad \text{where} \quad k_c = \begin{cases} 4 + \left(3 Z_s^2/\pi^4\right) & \text{for } Z_s \le 11.4 \\ 0.702\, Z_s & \text{for } Z_s > 11.4 \end{cases}$$

The first term in the expression for k_c corresponds to the buckling coefficient of long simply supported flat plates while the second term allows for the beneficial curvature effects. A knockdown factor, $B\rho_n$, is recommended by the RCC proposals [100] to account for initial imperfection and residual stress effects:

$$\sigma_{icr} = B\,\rho_n\,\sigma_{cr} \qquad \text{and} \qquad \lambda = \sqrt{\sigma_y/\sigma_{icr}}$$

where B converts the lower bound knockdown factor, ρ_n, to a mean one. Expressions for B and ρ_n are presented in Appendix 4.6.

By analogy with flat plate effective width formulations presented in [31] (para. 4.2.5.1), and by introducing the shell curvature effect via the slenderness parameter λ, the following expression has been derived by RCC to model the ultimate strength of a curved plate in uniaxial compression. Hence, the effective shell width, s_e, and reduced effective width s_e', assumed to act with the stringer in postbuckling estimations [277] are:

$$\frac{s_e}{s} = \begin{cases} \left[\dfrac{1.05}{\lambda\sqrt{\sigma_y/\sigma_e}} - \dfrac{0.28}{\lambda^2\left(\sigma_y/\sigma_e\right)}\right] R_r & \text{for } \lambda \ge 0.53 \\ 1 & \text{for } \lambda < 0.53 \end{cases} \qquad \text{and}$$

$$\frac{s_e'}{s} = \begin{cases} \left[\dfrac{0.53}{\lambda\sqrt{\sigma_y/\sigma_e}}\right] R_r & \text{for } \lambda > 0.53 \\ 1 & \text{for } \lambda \le 0.53 \end{cases}$$

The residual stress reduction factor, R_r, has been based on the assumptions used by Faulkner for flat unstiffened plates (para. 4.2.5.2) and is hence calculated based from the Ostenfeld-Bleich parabolae to represent the structural tangent modulus. The expression for this factor is presented in Appendix 4.6. The welding parameter η required in the determination of the level of residual stress reduction of strength in the structure, is generally taken as 4.5 for continuous fillet welds, 3.0 for light fillet welds, and 0 for stress relieved shells.

Modelling of *interframe column buckling* would have to account for both the behaviour of the stringer and associated plating as a column, as well as, for the beneficial effect of the shell curvature on the effective width of the shell. At failure, a number of half-waves around the circumference of the shell and one-half wave between ring-frames is expected to occur. It was Faulkner at Glasgow [100, 254], who, influenced by the Bryant two term approach for pressure collapse of perfect ring framed cylinders, proposed the following expression [277]:

$$\sigma_{ss} = \frac{\pi^2 E I_{ec}}{L^2 (A_s + s_e t)} + \frac{\rho_s 0.605 E}{1 + (A_s / s t)} \left(\frac{t}{R}\right)$$

The first term is the column term while the second presents the contribution of the unstiffened shell element (i.e. the effect of shell curvature). The assumed knockdown factor is ρ_s=0.75. The Ostenfeld-Bleich tangent modulus expression is used to determine the inelastic buckling stress given by:

$$\frac{\sigma_{ic}}{\sigma_y} = \begin{cases} 1 - r(1-r)(\sigma_y/\sigma_{ss}) & \text{for } \sigma_{ss} \geq r\sigma_y \\ \sigma_{ss}/\sigma_y & \text{for } \sigma_{ss} < r\sigma_y \end{cases}$$

just as it was carried out for stiffened flat plates (para. 4.2.5.1). The average ultimate collapse stress is then obtained via:

$$\sigma_u = \sigma_{ic} \left[(A_s + s_e t) / (A_s + s t) \right]$$

where the effective width of the shell s_e is obtained from the expression for the effective width in compression of an axially loaded curved shell for $\sigma_e = \sigma_{ic}$ and therefore an iterative calculation is necessary.

API Bulletin 2U proposes a discrete and an orthotropic method for checking against interframe column buckling. As the orthotropic theory has advantages only for closely stiffened shells (and flat plates) (e.g. aircraft structures) when used for lightly stiffened shells, frames and stiffeners it may not adequately represent practical marine structures. Discrete beam solutions should hence be preferred for marine applications. API's discrete solution is based on Faulkner's approach just presented above.

In a critical review of the available formulations (RCC [254, 255], DNV [66,

208], API Bul 2U [103], ECCS [248], for the design orthogonally stiffened cylindrical structures under axial compression the accuracy and robustness of the RCC model has been proved [277, 278] and is hence recommended for use herein. Tables 4.14 provides details of the modelling uncertainties of these expressions. Following a review of the RCC work, minor adjustments were made to the value of the knockdown factor assumed, which led to only a small improvement in the modelling uncertainty (identified as 'Glasgow' in Table 4.14).

4.7.4.2 Strength of Orthogonally Stiffened Shell Elements Under External Pressure

Models for bay instability in orthogonally stiffened shells, have been presented by DNV, API and RCC. The API Bulletin 2U procedure has been based on work by Miller et al [103]. and present a bias and COV value as demonstrated in Table 4.14. Das et al [277] have improved the uncertainty by changing the adjustment coefficient K_p to $K_p = 0.98 + 0.12g/500$ when g>500. However, as pointed out by Faulkner et al [277], the API has the drawback that it combines the purely elastic shell behaviour with totally plastic stringer behaviour. In addition, the original RCC proposal as presented in [254] has the disadvantage that its good accuracy (Table 4.14) stems from the choice of good 'curve-fitting' factors (f_1, f_2, f_3) and not from detailed modelling of the structural behaviour. Such an approach is still pending. For the time being, a recent critical review of the RCC work [277, 278] proposed the API-2U discrete procedure for design with a more detailed expression for the the effective pressure correction factor

$$K_p = \begin{cases} 0.25 + 0.85\, g/500 & \text{for } g \le 500 \\ 0.98 + 0.12\, g/500 & \text{for } 500 < g \le 2500 \end{cases}$$

which provides only a small improvement to the statistical uncertainty of the model in Table 4.14. Appendix 4.6 may be consulted for further information on the model and the parameters used in the expression above.

4.7.4.3 Modelling of Combined Axial Loading and External Pressure Effects

The expression presented by the RCC [99, 254, 255] to account for load

interaction on cylindrical structures, is widely accepted to possess a better theoretical basis than any other existing proposals (which are semi-empirical in nature anyway). Odland's von Mises based method [25] for unstiffened and ring-framed shells was extended by Faulkner and Warwick [99] to stringer stiffened shells and is of quadratic nature (para. 4.2.8 and Notation):

$$\left(\frac{R_x}{\phi_x}\right)^2 + R_x R_\theta \left(\frac{2\sqrt{\left(1-\phi_x^2\right)\left(1-\phi_\theta^2\right)}}{\phi_x \phi_\theta} - 1\right) + \left(\frac{R_\theta}{\phi_\theta}\right)^2 = 1.0$$

The advantage of this model, and indeed of the original Odland proposal, is that for stocky shell geometries it tends towards the von Mises yield criterion while for very slender structures it approaches a linear interaction between elastic buckling and yielding modes of failure. For some geometries it is possible to have combined collapse strengths higher than the material yield stress. This phenomenon occurs in tests but has not been modelled previously [277]. Comparisons with tests have yielded the bias and COV values presented in Table 4.14. The RCC model has also formed the basis for the API Bulletin 2U proposals on combined load interaction.

References

1) Mazzolani, F.M., 'Aluminium Alloy Structures', Pitman, London, 1985.
2) Mazzolani, F.M., 'Residual Stress Tests on French Profiles 63X63X4 in Aluminium Alloys', ECCS Committee 16, Doc. 16-74-3, 1974.
3) Mazzolani, F.M., 'Residual Stress Tests on Aluminium Alloy Austrian Profiles', ECCS Committee 16, Doc. 16-75-1, 1975.
4) Mazzolani, F.M., 'Les Imperfections Structurales dans les Asseblages Suodees en Aluminium', Revue de l' Aluminium, No. 431, 1974.
5) Gatto, F., Mazzolani, F.M., Morri, D., 'Experimental Analysis of Residual Stresses and of Mechanical Characteristics in Welded Profiles of Al-Si-Mg (type 6082), ECCS Committee 16, doc. 16-77-5, 1977. Also in Italian Machinery and Equipment, Vol. 11, No. 50, March 1979.
6) Hill, H.N., Clark, J.W., Brungraber, R.J., 'Design of Welded Aluminium Structures', Trans. ASCE, Vol. 127, No. II, 1962.

7) Faulkner, D., 'Effects of Residual Stresses on the Ductile Strength of Plane Welded Grillages and of Ring Stiffened Cylinders', Jnl. Strain Analysis, Vol. 12, No. 2, 1977.
8) ECCS, 'European Recommendations for Aluminium Alloy Structures', 1st Edition, 1978.
9) Wong, M,P., Dwight, J.B., 'Longitudinal Weld Shrinkage in Materials Having Rounded Stress-Strain Curve', Proc., Conf. Joints in Structural Steelwork, Pentech Press, 1981.
10) Wong, M.P., 'Weld Shrinkage in Non-linear Materials ', Ph.D. Dissertation, Cambridge University, 1982.
11) DTU 32/2, Regles de Conception et de Calcul des Charpentes en Alliages d'Aluminium, Travaux de Batiment, Paris, 1976.
12) Kelsey, R.A., 'Effect of Heat Input on Welds in Aluminium Alloy 7039', Welding Journal Research Supplement, 1971.
13) Pirner, M., 'Properties of Gas Shielded Arc Welded Joints in Heat-Treatable Al-Mg-Si and Al-Zn-Mg Alloys', Colloquim on Aluminium and its Alloys in Welded Construction, Porto, 1981.
14) Mazzolani, F.M., 'Structural Imperfections in Wedled Aluminium Structures', CECM 1-1, 73-1, 1973.
15) Soetens, F., 'Welded Connections in Aluminium Alloy Structures, Heat Affected Zone Effects', TNO Report No. BI-84-17/63.4.3181, 1984.
16) Robertson, I., 'Strength Loss in Welded Aluminium Structures', Ph.D. Dissertation, Cambridge University, 1985.
17) Robertson, I., Dwight, J.B., 'HAZ Softening in Welded Aluminium', Proc. 3d Int. Conf. on Aluminium Weldments, Munich, 15-17 April 1985.
18) Shercliff, H.R., 'Strength Loss in the Heat-Affected Zones of Welds in Non-Heat-Treatable Aluminium Alloys', Cambridge University Engineering Department Report, No. CUED/C-Mats/TR149, Oct. 1988.
19) British Standards Institution, 'British Standard Code of Practice BS 8118: The Structural Use of Aluminium', BSI, London, 1992.
20) Ayrton, W.E., Perry, J., The Engineer, Vol. 62, 1886.
21) Robertson A., 'The Strength of Struts', Instn. Civ. Engrs., Selected Engineering Paper No. 28, 1925.
22) Godfrey, G.B., 'The Allowable Stress in Axially Loaded Steel Struts', The Structural Engineer, Vol. 40, No. 3, 1962.
23) Galambos, T.V., 'Structural Members and Frames', Prentice Hall, 1968.

24) Dwight, J.B., 'Use of the Perry Formula to Represent the European Column Curves', Steel Construction, Australian Institute of Steel Construction, Vol. 9, No. 1, 1975.

25) Odland, J., 'Buckling Resistance of Unstiffened and Stiffened Circular Cylindrical Shell Structures', Norwegian Maritime Research, Vol. 6, No. 3, 1978.

26) Cho, S.R., Frieze, P.A., Faulkner, D., 'Strength of Ring Stiffened Cylinders Under Combined Loads', Proc. Offshore Technology Conference, 16th Annual OTC, Paper No. 4714, Houston, 1984.

27) Odland, J. Faulkner, D., 'Buckling of Curved Steel Structures-Design Formulations', Proc. Integrity of Offshore Structures, IOS' 81, Glasgow, Applied Science Publishers, London, 1981.

28) Faulkner, D., Adamchak, J.C., Snyder, G.J., Vetter, M.F., 'Synthesis of Welded Grillages to Withstand Compression and Normal Loads', Computers and Structures, Vol. 3, No. 2, 1973.

29) Bleich, F., Ramsey, L., 'Buckling Strength of Metal Structures', McGraw-Hill Book Company, London, 1952.

30) Guedes Soares, C. 'Survey of Methods of Prediction of the Compressive Strength of Stiffened Plates', Report MK/R 57, Department of Marine Technology, Norwegian Institute of Technology, University of Trondheim, August 1981.

31) Faulkner, D., 'A Review of Effective Width Plating for Use in the Analysis of Stiffened Palting in Bending and Compression', Jnl. Ship Research, Vol. 19, No. 1, 1975.

32) Carlsen, C.A., 'Simplified Collapse Analysis of Stiffened Plates', Norwegian Maritime Research, Vol. 5, No. 4, 1977.

33) Ueda, Y., Yao, T., 'The Influence of Complex Initial Deflection Modes on the Behaviour and Ultimate Strength of Rectangular Plates in Compression', Jnl. Const. Steel Research, Vol. 5, 1985.

34) Vilnay, O., Rockey, K.C., 'A Generalised Effective Width Method for Plates Loaded in Compression', Jnl. Const. Steel Research, Vol. 1, No. 3, 1981.

35) Chapman, J.C., Smith, C.S., Davidson, P.C., Dowling, P.J., 'Recent Developments in the Design of Stiffened Plate Structures', Proc. Intl. Conf. Advances in Marine Structures -2, Admiralty Research Establishment (ARE), Dunfermline, Scotland, 21-24 May 1991, C.S. Smith, R.S. Dow (Eds.), Elsevier Applied Science, London, 1991.

36) Chapman and Dowling Associates, 'Model Code Study: Design of Flat Stiffened Plating, Phase 1 Report' Engineering Structures Laboratories, Civil Engineering Department, Imperial College, CESLIC Report SP9, (Confidential), December 1991, London.
37) Guedes Soares, C., 'Design Equation for the Compressive Strength of Unstiffened Plate Elements with Inital Imperfections', Jnl. Const. Steel Res., Vol. 9, 1988.
38) Pu, Y., Das, P.K., 'Ultimate Strength and Reliability Analysis of stiffened Plates', Report No. NAOE-94-37, Dept. of Naval Architecture and Ocean Engineering, University of Glasgow, Dec. 1994.
39) Schade, H.A., 'The Effective Breadth of Stiffened Plating Under Bending Loads', Trans. SNAME, Vol. 59, 1951.
40) Mansour, A., 'On the Non-Linear Theory of Orthotropic Plates', Jnl. of Ship Research, Dec. 1971.
41) Smith, C.S., 'Elastic Buckling and Beam-Column Behaviour of Ship Grillages', Trans. RINA, Vol. 110, 1968.
42) Faulkner, D., 'Strength of Welded Grillages Under Combined Loads', Chapter 22 in Ship Structural Design Concepts, H.R. Evans (Ed.), Cornell Maritime Press, 1975.
43) Adamchak, J., 'A Rapid Technique for Predicting the General Instability of Ship Grillages with Elastically Constrained Edges', Report No. 4604, Naval Ship Research and Development Centre, 1975.
44) Little, G.H., 'Rapid Analysis of Plate Collapse by Live-Energy Minimisation', Int. Jnl. of Mechanical Science, Vol. 19, 1977.
45) Dwight, J., Little, G.H., 'Stiffened Steel Compression Flanges-A Simpler Approach', The Structural Engineer, Vol. 54A, 1976.
46) Horne, M.R., Narayanan, R., 'Design of Axially Loaded Stiffened Plates', Jnl. Structural Division, ASCE, Vol. 103, 1077.
47) Chatterjee, S., Dowling, P.J., 'The Design of Box-Girder Compression Plates Under Combined In-Plane and Lateral Loading', Steel Plated Structures, P.J. Dowling, J.E. Harding, P.A. Frieze (Eds.) Crosby Lockwood and Staples, London, 1977.
48) Murray, N.W., 'Analysis and Design of Stiffened Plates for Collapse Load', The Structural Engineer, Vol. 53, 1975.
49) Guedes Soares, C. Soreide, T.H., 'Behaviour and Design of Stiffened Plates under Predominantly Compressive Loads', Intl Shipbuilding Progress, Vol. 30, 1983.

50) Gordo, J.M., Guedes Soares, C., 'Approximate Load Shortening Curves for Stiffened Plates Under Uniaxial Compression', Proc. Conf. on Integrity of Offshore Structures-5, Glasgow, EMAS Publishers, 1993.

51) Tolikas, C., Morandi, A.C., Das, P.K., Faulkner, D., 'Reliability-Based Multiple Criteria Optimisation of a Fast SWATH Ship', Proc. 2nd Int. Conf. Computational Stochastic Mechanics, Rice University/AISC, Athens, Greece, 13-15 June 1994.

52) Mofflin, D.S., Dwight, J.B., 'Buckling of Aluminium Plates in Compression', in Behaviour of Thin-Walled Structures, J. Rhodes, J. Spence (Eds.), Elsevier Applied Science Publishers, London, 1984.

53) Mazzolani, F.M., Valtinat, G., De Luca, A., De Martino, A., Faella, C., Dangelmaier, P., 'Bars, Beams and Beam Columns', Chapter 2 , Aluminium Structural Analysis, Recent European Advances, P.S. Bulson (Ed.), Elsevier Applied Science, London, 1992.

54) Mofflin, D.S., Dwight, J.B., 'Tests on Individual Aluminium Plates under In-Plane Compression', CUED Tech. Report No. CUED/D-Struct/TR.100, Cambridge University, 1983.

55) Tolikas, C., 'A Review of the Design of Aluminium Columns, Beams and Beam-Columns', Progress Report, Confidential, ALCAN, Oct. 1994.

56) Mazzolani, F.M., Frey, F., 'ECCS Stability Code for Aluminium Alloy Members, Present State and Work Progress', Proc., 3d Int. Col. on Stability of Metal Structures, Paris, Nov. 1983.

57) Nethercot, D.A., 'Behaviour and Design of Aluminium Beams, Columns and Beam Columns', Proc. Int. Conf. on Steel and Aluminium Structures (ICSAS 91), Singapore, 22-24 May 1991.

58) Lai, Y.F.W., Nethercot, D.A., 'Design of Aluminium Columns', Engineering Structures, Vol. 14, No. 3, 1992, pp. 188-194.

59) Hong, G.M., 'Effects of Non-Central Transverse Welds on Aluminium Columns', Proc. Int. Conf. on Steel and Aluminium Structures (ICSAS 91), Singapore, 22-24 May 1991.

60) Blanc, F., 'Discussion to Ultimate Longitudinal Strength', Trans. RINA, Vol. 107, 1965.

61) Bureau Veritas, 'Reglement du Bureau Veritas pour la Classification des Navires de Longeur Superieure a 65m', Paris, 1987.

62) Det Norske Veritas, 'Rules for the Design, Construction and Inspection of Offshore Structures', DNV, Oslo, Norway, 1982.

63) Becker, H., 'Instability Strength of Polyaxially-Loaded Plates and Relation to Design', Steel Plated Structures, P.J. Dowling, J.E. Harding, P.A. Frieze (Eds.) Crosby Lockwood and Staples, London, 1977.
64) Valsgard, S., 'Ultimate Capacity of Plates in Transverse Compression', DNV Report 79-104, Feb. 1979.
65) Bradfield, C.D., Stonor, R.W.P., Moxham, K.E., 'Tests of Long Plates Under Biaxial Compression', Jnl. Constr. Steel Research, Vol. 24, 1993.
66) Det Norske Veritas, 'Buckling Strength Analysis', Classification Note 30.1, DNV, Oslo, Norway, May 1992.
67) Guedes Soares, C., Gordo, J.M.M., Compressive Strength of Ship Plates Under Combined Loading', Report, Dept. of Naval Architecture and Marine Engineering, Technical University of Lisbon, Lisbon, Oct. 1990.
68) Guedes Soares, C., Faulkner, D., 'Probabilistic Modelling of the Effect of Initial Imperfections on the Compressive Strength of Rectangular Plates', Proc. 3d Intl. Symp. on Practical Design of Ships and Mobile Units (PRADS), Vol. 2, Trondheim, 1987.
69) American Bureau of Shipping, 'Rules for Building and Classing Steel Vessels', 1988.
70) Det Norske Veritas, 'Tentative Rules for Classification of High Speed and Light Craft; Part 3', DNV, Hovik, Norway, 1991.
71) Becker, H., 'Compressive Strength of Ship Hull Girders, Part 1: Unstiffened Plates', Ship Structure Committee, Rept. No. SSC-217, Washington D.C., 1970.
72) Bradfield, C.D., Porter Goff, R.F.D., 'Compressive Tests on Steel Plates of Low Aspect Ratio', Dept. of Engineering, Report No. CUED/C-Struct/TR48, University of Cambridge, 1975.
73) Fischer, M., Harre, W., 'Experimental Determination of the Ultimate Load Curves of Uniaxially Compressed, Structural Steel Rectangular Plates of Aspect ratio $\alpha \leq 1$, Part 1 and 2', Stahbau, Vol. 47, 1978, pp 199-204 and 239-247.
74) Dowling, P.J., Harding, J.E., Slatford, J.E., 'Plates in Biaxial Compression-Final Report', Department of Civil Engineering, Imperial College, London, CESLIC Report SP4, 1979.
75) Valsgard, S., 'Numerical Design Prediction of the Capacity of Plates in In-Plane Compression', Computers and Structures, Vol. 12, 1980.
76) Lamble, J.H., Shing, L., 'A Survey of Published Work on the Deflection of and Stress in Flat Plates Subject to Hydrostatic Loading', Trans INA, 1947.

77) Lamble, J.H., Choudhary, J.P., 'Support Reactions, Stresses and Deflections for Plates Subjected to Uniform Transvesre Loading', Trans. INA, 1953.
78) Hughes, O.F., 'Plate Bending', Chapter 9 in Ship Structural Design; A Rationally Based Computer-Aided Optimisation Approach, SNAME, New Jersey, 1988.
79) Clarkson, J., 'A New Approach to the Design of Plates to Withstand Lateral Pressure', Trans. INA, Vol. 98, 1956.
80) Clarkson, J., 'Strength of Approximately Flat, Long Rectangular Plates Under Lateral Pressure', Trans. North East Coast Inst. Eng. Shipbuild., Vol. 74, 1958.
81) Guedes Soares, C., 'A Code Requirement for the Compressive Strength of Plate Elements', Jnl. Marine Structures, Vol. 1, 1988.
82) Hovgaard, W., 'Structural Design of Warships', U.S. Naval Institute, Annapolis, Maryland, 1940.
83) Clarkson, J., 'Tests on Flat Plated Grillages Under Uniform Pressure', Trans. RINA, Vol. 105, 1963.
84) Clarkson, J., 'Uniform Pressure Tests of Plates With Edges Free to Slide Inwards', Trans. RINA, Vol. 104, 1962.
85) Hughes, O.F., 'Design of Laterally Loaded Plating-Uniform Pressure Loads', Jnl. Ship Research, Vol. 25, No. 2, June 1981.
86) Wood, R.H., 'Plastic and Elastic Design of Slabs and Plates', Ronald Press, 1961.
87) Sawczuk, A., 'On the Initiation of the Membrane Action in Rigid-Plastic Plates', Jnl. Mecanique, Vol. 3, No. 1, 1964.
88) Intl. Ship and Offshore Structures Congress, 'Report of Committee III.I; Ductile Collapse', Proc. 11th Intl. Ship and Offshore Structures Congress (ISSC'91), Hsu, P.H., Wu, Y.S., (Eds.), Wuxi, China, 16-20 September 1991, Vol. 1, Elsevier Applied Science, London, 1991.
89) Jones, N., Walters, R.M., 'Large Deflections of Rectangular Plates', Jnl. Ship Research, Vol. 15, No. 2, June 1971.
90) Jaeger, L.G., 'An Approximate Analysis for Plating Panels Under Uniformly Distributed Load', Proc. Inst. Civil Engineers, Vol. 10, 1958.
91) Young, A.G., 'Ship Plating Loaded Beyond the Elastic Limit', Trans. INA, Vol. 101, 1959.
92) Wah, T., 'A Theory for the Plastic Design of Ship Plating Under Uniform Pressure', Jnl. Ship Research, Vol. 4, 1960.
93) Wah, T., 'Design of Long Rectangular Elasto-Plastic Plates', Jnl. Ship Research, Vol. 5, 1961.

94) Hooke, R., Rawlings, B., 'An Experimental Investigation of the Behaviour of Clamped Rectangular Mild Steel Plates Subjected to Uniform Transverse Pressures', Proc. Instn. Civil Engrs., Vol. 42, 1969.

95) American Petroleum Institute, 'Bulletin on Design of Flat Plate Structures', API Bulletin 2V, First Edition, May 1987.

96) British Standards Institution, 'British Standard Code of Practice BS 5400: Part 3 Steel, Concrete and Composite Bridges', BSI, London, 1982.

97) Stonor, R.W.P., Bradfield, C.D., Moxham, K.E., Dwight, J.B., 'Tests on Plates Under Biaxial Loading', Engineering Department, Cambridge University, Report CUED/D-Struct/TR98, 1983.

98) Dier, A.F., Dowling, P.J., 'Plate Under Combined Lateral Loading and Biaxial Compression', Department of Civil Engineering, Imperial College, London, CESLIC Report SP8, Final Report for the British Ship Research Association, Sept. 1980.

99) Faulkner, D., Warwick, D.M., 'Predicting the Strength of Welded Stiffened Cylinders', Proc. Symp, Deeper Waters, RINA, London, Oct. 1986.

100) Rule Case Committee, 'Model Code for Structural Design of Tension Leg Platforms', Conoco-ABS Rule Case Committee, ABS New York, 1983.

101) Frieze, P.A., Dowling, P.J., Hobbs, R.E., 'Ultimate Load Behaviour of Plates in Compression', Proc. Conf. on Steel Plated Structures, P.J. Dowling, J.E. Harding, P.A. Frieze (Eds.), Crosby Lockwood Staples, London, 1977.

102) Miller, C.D., Frieze, P.A., Zimmer, R.A., Jan, H-Y., 'Collapse Tests of Fabricated Stiffened Cylinders Under Combined Loads', Proc. Conf. Portland, Oregon, June 1983.

103) Miller, C.D., Grove, R.B., Vojta, J.D., 'Design of Stiffened Cylinders for Offshore Structures', Proc. Conf. Offshore Structures, American Welding Society, New Orleans, Dec. 1983.

104) Agelidis, N.A., Harding, J.E., Dowling, P.J., 'Buckling Tests on Stringer Stiffened Cylinder Models Subject to Load Combinations', DNV Report, No. 82-0298, 1982.

105) McCall, S., Walker, A.C., 'Buckling Tests on Stringer-Stiffened Cylinder Models Subject to Load Combinations', DNV Report, No. 82-0299, 1982.

106) Steen, E., Valsgard, S., 'Simplified Buckling Strength Criteria for Plates Subjected to Biaxial Compression and Lateral Pressure', Proc. Symp. Extreme Load Response, SNAME, 1984.
107) Becker, H., Colao, A., 'Compressive Strength of Ship Hull Girders, Part III: Theory and Additional Experiments', Ship Structure Committee, Rept. No. SSC-267, Washington D.C., 1977.
108) Okada, H., Oshima, K., Fukumoto, Y., 'Compressive Strength of Long Rectangular Plates Under Hydrostatic Pressure', Jnl. Society Naval Architects of Japan, Vol. 146, Dec. 1979.
109) Yamamoto, Y., Matsubara, N., Murakami, T., 'Buckling Strength of Rectangular Plates Subjected to Edge Thrusts and Lateral Pressure', Jnl. Society Naval Architects of Japan, Vol. 127, June. 1970.
110) Yoshiki, M., Yamamoto, Y., Kondo, H., 'Buckling of Rectangular Plates Subjected to Combined Lateral and Edge Loads', Jnl. Society Naval Architects of Japan, No. 118, Nov. 1965.
111) Fujita, Y., et al, 'Ultimate Strength of Rectangular Plates Subjected to Combined Loading - Rectangular Plates Under Compression and Lateral Pressure', Jnl. Society of Naval Architects of Japan, Vol. 146, 1979.
112) Kondo, J., Ostapenko, A., 'Tests on Longitudinally Stiffened Plate Panels with Fixed Ends; Effect of Lateral Loading', Fritz Engineering Laboratory Report, Rept. No. 248.12., Lehigh University, 1964.
113) Lee, T-T., 'Elastic-Plastic Analysis of Simply Supported Rectangular Plates Under Combined Axial and Lateral Loading', Fritz Engineering Laboratory Report, Rept. No. 248.7., Lehigh University, 1961.
114) Aalami, E., Moukharzade, A., Mahumti-Satti, P., 'On the Strength Design of Ship Plates Subjected to In-Plane and Transverse Loading', Trans. RINA, Vol. 114, 1972.
115) Kilford, J.T., 'The Ultimate Strength of Steel Plates Under Combined In-Plane and Normal Loads; tests on Pressurised Box Columns', Civil Engineering Dept. Report to BSRA, Imperial College, London, 1972.
116) Ellinas, C.,P., Supple, W.J., Walker, A.C., 'Buckling of Offshore Structures', Prepared for the U.K. Department of Energy by J.P. Kenny & Partners Ltd., Granada, London, 1984.
117) Harding, J.E., Hobbs, R.E., Neil, B.G., 'Ultimate Load Behaviour of Plates Under Combined Direct and Shear In-Plane Loading', Proc. Conf. on Steel Plated Structures, P.J. Dowling, J.E. Harding, P.A. Frieze (Eds.) Crosby Lockwood and Staples, London, 1977.

118) Harding, J. E., Hobbs, R. E., 'The Ultimate Load Behaviour of Box Girder Web Panels', The Structural Engineer, Vol. 57B, 1979.

119) Horne, M.R., Dowling, P.J., Ogle, M.H., 'Report to Steering Group on Plated Structures', Committee B116/3, British Standards Institution, London 1976.

120) Harding, J.E., Dowling, P.J., 'The Basis of the Proposed New Design Rules for the Strength of Web Plates and Other Panels Subjected to Complex Edge Loading', in Stability Problems in Engineering Structures and Components, Applied Science Publs, London,1979.

121) Mofflin, D.S., 'A Finite Strip Method for the Collapse Analysis of Compressed Plates and Plate Assemblages', CUED Tech. Report No. CUED/D-Struct/TR.101, Cambridge University, 1983.

122) Dier, A.F., Dowling, P.J., 'Aluminium Plated Structures', Final Report for the Admiralty Marine Technology Establishment, Engineering Structures Laboratories, CESLIC Report APS2, Department of Civil Engineering, Imperial College, London, July 1981.

123) Clarke, J.D., 'Buckling of Aluminium Alloy Stiffened Plate Ship Structure', Proc. Int. Conf. on Steel and Aluminium Structures, R. Narayanan (ed.), Cardiff, UK, 8-10 July 1987, Vol. 2, Elsevier Applied Science, London, 1987.

124) Little, G.H., 'Collapse Behaviour of Aluminium Plates', Int. Jnl. of Mechanical Science, Vol. 24, No. 1, 1982.

125) Little, G.H., 'Collapse Analysis of Plates with Strain Hardening', Int. Jnl. of Mechanical Science, Vol. 23, 1981.

126) Royal Aeronautical Society, 'Structural Principles and Data', Handbook of Aeronautics No. 1, New Era Publishing Co. Ltd., London, 1952.

127) Evans, H.R., 'Shear Webs and Plate Girders', Chapter 4 , Aluminium Structural Analysis, Recent European Advances, P.S. Bulson (Ed.), Elsevier Applied Science, London, 1992.

128) Timoshenko, S.P., Gere, J.M., 'Theory of Elastic Stability', 2nd Edition, McGraw Hill, 1977.

129) Skaloud, M., 'Optimum Rigidity of Stiffeners of Webs and Flanges', Chapter 4, Plated Structures, Stability and Strength, R. Narayanan (Ed.), Elsevier Applied Science Publishers, London, 1983.

130) Skaloud, M., Kristek, V., 'Folded Plate Theory Analysis of the Effect of the Stiffener Configuration Upon the Buckling of Longitudinally Stiffened Compression Flanges', Acta Technica CSAV, No. 5, 1977.

131) Skaloud, M., Kristek, V., 'Stability Problems of Steel Box Girder Bridges', Trans. Czech. Acad. Sci., Techn. Ser., Vol. 91, Pt. 1, 1981.
132) Skaloud, M., Zornerova, M., 'Linear Buckling Theory Optimum Rigidity of the Longitudinal Stiffeners of the Compression Flanges of Steel-Box Girder Bridges', Acta Technica CSAV, No. 1, 1977.
133) Kloppel, K., Scheer, J., 'Beulwerte Ausgesteifter Rehteckplatten', Band 1,Wilhelm Ernst and Sohn, Berlin, 1960.
134) Kloppel, K., Moller, K.H., 'Beulwerte Ausgesteifter Rehteckplatten', Band 2, Wilhelm Ernst and Sohn, Berlin, 1968.
135) Ballio, G., Mazzolani, F.M., 'Theory and Design of Steel Structures', Chapman and Hall, London, 1983.
136) Massonnet, C., 'Essai de Voilement Sur Poutres a Ame Raidie', Memoires de l'AIPC, Vol. 14, 1954.
137) Massonnet, C., Mas, E., Maus, H., 'Essai de Voilement sur Deux Poutres a Membrures et Raidisseurs Tubulaires', Memoires de l'AIPC, Vol. 22, 1962.
138) Massonnet, C., 'Stability Considerations in the Design of Steel Plate Girders', Jnl. Structural Division, ASCE, Vol. 86, ST1, Jan. 1960.
139) Massonnet, C., Skaloud, M., Donea, J., 'Comportement Postcritique d'une Plaque Caree Raidie Cisaillee Uniformement. Deuxieume Partie: Repartition des Contraintes et Analyse de l'Etat Limite', Memoires de l'AIPC, Vol. 28, 1968.
140) Skaloud, M., Massonnet, C., Donea, J., 'Comportement Postcritique d'une Plaque Caree Raidie Cisaillee Uniformement. Premiere Partie: Solution Generale et Deformee de la Plaque', Memoires de l'AIPC, Vol. 27, 1967.
141) Rockey, K.C., Cook, I.T., 'The Buckling Under Pure Bending of a Plate Girder Reinforced by Multiple Longitudinal Stiffeners', Int. Jnl. of Solids and Structures, Vol. 1, 1965.
142) Dubas, C., 'Le Voilement de l'Ame des Poutres Flechies et Radies au Cinquieme Superieur', Memoires de l'AIPC, Vol. 14, 1954.
143) Meszaros, I., Djubek, J., 'Vplyv Tuhosti Vystuh na Deformativ Nost Stien', Stavebnicky Casopis, SAV X1V3, Bratislava, 1966.
144) Maquoi, R., Massonnet, C., Skaloud, M., 'Design of Stiffened Webs', Stavebnicky Casopis, No. 2, 1981.
145) Maquoi, R., 'Plate Girders', Chapter 2.6, 'Constructional Steel Design; An International Guide', Dowling, P, J., Harding, J.,E., Bjorhovde, R., (Eds), Elsevier Applied Science, London, 1992.

146) Rockey, K.C., Valtinat, G., Tang, K.H., 'The Design of Transverse Stiffeners on Webs Loaded in Shear-An Ultimate Strength Approach', Proc. Instn Civ. Engrs, Vol. 71, Part 2, Dec. 1981.
147) Tang, K.H., Evans, H.R., 'Transverse Stiffeners for Plate Girder Webs-An Experimental Study', Jnl. Construct. Steel Research, Vol. 4, 1984.
148) Chatterjee, S., 'Design of Webs and Stiffeners in Plate and Box Girders', The Design of Steel Bridges, Granada Publishing, St. Albans, 1981.
149) Horne, M.R., Plastic Theory of Structures. Pergamon Press, Oxford, 1979.
150) Dubas, P., Gehri, E., (Eds.), 'Behaviour and Design of Steel Plated Structures', ECCS-CECM-EKS, Publication No. 44, Brussels, Jan. 1986.
151) Ardali, S., 'A Parametric Study of the Effect of Longitudinal Web Stiffeners on the Behaviour of Plate Girders', M.Sc. Thesis, University College Cardiff, 1980.
152) Rockey, K.C., Evans H.R., Tang, K.H., 'An Investigation of the Rigidity of Longitudinal Web Stiffeners for Plate Girders', Report, University College Cardiff, 1979.
153) Evans, H.R., Tang, K.H., 'Longitudinal Stiffeners for Girder Webs; Their Behaviour and Design', Jnl. Construct. Steel Research, Vol. 6, 1986.
154) Faulkner, D., 'Towards a Better Understanding of Compression Induced Stiffener Tripping', Proc. Intl. Conf. Steel and Aluminium Structures, R. Narayanan (Ed.), Vol. 1, Cardiff, U.K., 8-10 July 1987, Elsevier Applied Science, London, 1987.
155) Windenburg, D.F., 'The Elastic Stability of Tee Stiffeners', United States Experimental Model Basin Report 457, Nov. 1938.
156) Faulkner, D., 'Compression Strength of Welded Grillages', Chapter 21 in Ship Structural Design Concepts, H.R. Evans (Ed.), Cornell Maritime Press, 1975.
157) Adamchak, J.C., 'Design Equations for Tripping of Stiffeners Under Inplane and Lateral Loads', DTNSRDC Report No. 79/064, Maryland, October 1979.
158) Smith, C.S., 'Elastic Analysis of Stiffened Plating Under Lateral Loading', Trans. RINA, Vol. 108, 1966.
159) Smith, C.S., 'Bending, Buckling and Vibration of Orthotropic Plate-Beam Structures', Jnl. Ship Research, Vol. 12, No. 4, Dec. 1968.
160) Wittrick, W.J., 'General Sinusoidal Stiffness Matrices for Buckling and Vibration Analyses of Thin Flat-Walled Structures', Int. Jnl. of Mechanical Science, Vol. 10, 1968.

161) Sharp, M., Clark, J.W., 'Thin Aluminium Shear Webs', Proc. ASCE, Jnl. of the Structural Division, April 1971.
162) Faulkner, D., 'Application of Reliability Theory in Submarine Design', in Advances in Marine Structures-2, C.S. Smith, R.S. Dow (Eds.), Elsevier Applied Science, 1991.
163) Morandi, A.C., 'Computer Aided Reliability Based Design of Ring-Stiffened Cylindrical Shells Under External Pressure', Ph.D. Thesis, University of Glasgow, September 1994.
164) Trizna, J.R., Miller, C.D., 'Buckling Tests on Ring and Stringer Stiffened Cylindrical Plastic Models Under Combined Loadings', Final Report to ABS, Conoco, etc. by CBI Indstries Ltd., Plainfield, April, 1984.
165) Faulkner, D., Das, P.K., 'Application of Reliability Theory to Structural Design and Assessment of Submarines and Other Externally Pressurised Cylindrical Structures', Proc. Int. Symp. Integrity of Offshore Structures-4, D. Faulkner, M.J. Cowling, A. Incecik (Eds.), Elsevier Applied Science, 1990.
166) Morandi, A.C., Das, P.K., Faulkner, D.F., 'An Investigation on the Application of Alternative Materials to Externally Pressurised Vessels', Proc. Int. Conf. Structural Materials in Marine Environments, London, 11-12 May 1994.
167) Morandi, A.C., Das, P.K., Faulkner, D.F., 'An Outline of the Application of Reliability Based Techniques to Structural Design and Assessment of Submarines and Other Externally Pressurised Cylindrical Structures', Jnl. Marine Structures, Vol. 7, 1994.
168) Kendrick, S.B., 'Vessels to Withstand External Pressure', Developments in Pressure Vessel Technology-4, R.W. Nicholls (ed.), Applied Science Publishers, London, 1983.
169) Beedle, L. C., (ed.)., 'Stability of Metal Structures, A World View', National Science Foundation and U.S.A. International Development Cooperation Agency,1991.
170) Commission of the European Communities, 'Eurocode 3: Design of Steel Structures, General Rules and Rules for Buildings-Part 1', Volume 1, Brussels, February. 1992.
171) DASt-Richlinie 015: 'Trager mit Schlanken Stegen', Deutcher Auscschuss fur Stahlbau, 1990.

172) Cooper, P. B., 'The Ultimate Bending Moment for Plate Girders', Proc. of IABSE Colloquim, London, 1971. Massonnet et al (Eds), IABSE, Zurich, 1972.
173) Tolikas, C., 'Report to ISSC Committee V.1', (private communication), 1994.
174) Cooper, P. B., 'Strength of Longitudinally Stiffened Plate Girders', Proc. Jnl. of Stl. Div., ASCE, ST. 2, 1967.
175) Leggett, D.M.A., Hopkins, H. G., 'The Effect of Flange Stiffness on the Stresses in a Plate Web Spar under Shear', H.M. Stationary Office, R & M No. 2434.
176) Bergman, S.G.A., Hopkins, H.G., 'Behaviour of Buckled Rectangular Plates Under the Action of Shearing Forces', Stockholm, 1948.
177) Rockey, K.C., 'The Influence of Flange Stiffness Upon the Post-Buckled Behaviour of Webplates Subjected to Shear', Engineering, Vol. 184, Dec. 1957.
178) Basler, K., Thurlimann, B., 'Strength of Plate Girders in Bending', Jnl of the Struct. Division, Proc. ASCE, No. 2913, ST.6, Aug. 1961.
179) Basler, K., 'Strength of Plate Girders in Shear', Jnl of the Struct. Division, Proc. ASCE, No. 2967, ST.7, Oct. 1961.
180) Gaylord, E.H., 'Discussion on 'Shear Strength of Plate Girders', Trans. ASCE, Vol. 129, 1963.
181) Fujii, T., 'On an Improved Theory for Dr. Basler's Theory', Proc. 8th Congress, IABSE, New York, Sept. 1968.
182) Selberg, A., 'On the Shear Capacity of Girder Webs', University of Trondheim, 1973.
183) American Institution of Steel Construction, 'Load and Resistance Fatcor Design (LRFD); Specification for Structural Steel Buildings', AISC, Chicago, 1986.
184) Tolikas, C., et al., 'Integrated SWATH Structural Design-Progress Review', University of Glasgow, Department of Naval Architecture and Ocean Engineering, Limited Distribution Report NAOE-92-14, April 1992.
185) Rockey, K.C., Evans, H.R., Porter, D.M., 'A Design Method Predicting the Collapse Behaviour of Plate Girders', Proc. ICE, Vol. 65, Part 2, March 1978.
186) Rockey, K.C., Skaloud, M., 'Influence of Flange Stiffness Upon the Load Carrying Capacity of Webs in Shear', Proc. 8th Congress, IABSE, New York, Sept. 1968.

187) Rockey, K.C., Skaloud, M, 'The Ultimate Load Behaviour of Plate Girders Loaded in Shear', The Structural Engineer, Vol. 50, No. 1, Jan. 1972.

188) Chern, C., Ostapenko, A., 'Ultimate Strength of Plate Girders Under Shear', Fritz Engineering Laboratory, Report No. 328.7, Lehigh University, USA, Aug. 1969.

189) Ostapenko, A., Chern, C., Parsanejad, S., 'Ultimate Strength Design of Plate Girders', Proc. Intl. Conf. Developments in Bridge Design and Construction, University College, Cardiff, 1971, Crosby Lockwood Publishers, 1971.

190) Komatsu, S., 'Ultimate Strength of Stiffened Plate Girders Subjected to Shear', Proc. Col. Design of Plate and Box Girders for Ultimate Strength, IABSE, London, 1971.

191) Calladine C.R., 'A Plastic Theory for Collapse of Plate Girders Under Combined Shearing Force and Bending Moment', The Structural Engineer, Vol. 51, April 1973.

192) Hoglund, T., 'Design of Thin Plate I Girders in Shear and Bending with Special Reference to Web Buckling', Institutionen for Bug-gnadsstatik, KTH Stockholm, Medd., No. 94, 1973.

193) Bergfelt, A., 'Slender Plate Girders, Especially Girders with Stiffeners at the Supports Only', ECCS TWG 8.3, Doc 3.2/5.1, 1974, and CHT Division of Steel and Timber Structures, Int. skr. S74:3, Goteborg 1974.

194) Dubas, P., 'Zur Erschopfungslast Schubbeanspruchter Stehblesche', Professor Steinhardt, Festschrift, Karlsruhe, 1974.

195) Ostapenko, A., Chern, C., 'Ultimate Strength of Longitudinally Stiffened Plate Girders under Combined Loads', Proc. Colloquim on Design of Plate and Box Girders for Ultimate Strength, IABSE, London, 1971.

196) British Standards Institution, 'British Standard Code of Practice BS 5950: Part 1 The Structural Use of Steelwork in Buildings', BSI, London, 1985.

197) Sheer, J., Pasternak, H., 'Zum Nachweis vonVollwandtragern mit dunnen Stegen und Quer-sowie auch Langssteifen in Regelwerken, Bauingenieur, Vol. 64, 1989.

198) Porter, D. M., Rockey, K. C., Evans, H. R., 'The Collapse Behaviour of Plate Girders Loaded in Shear', The Structural Engineer, Vol. 53, No. 8, Aug 1975.

199) European Recommendations for the Design of Longitudinally Stiffened Webs and of Stiffened Compression Flanges, Publication no. 60, ECCS, Brussels, 1990.
200) Evans, H.R., 'Longitudinally and Transversely Reinforced Plate Girders', Chapter 1 , Plated Structures, Stability and Strength, R. Narayanan (Ed.), Elsevier Applied Science Publishers, London, 1983.
201) Evans, H. R., Moussef, S., 'Design Aid for Plate Girders', Proc. Instn Civ. Engrs, Part 2, Vol 85, March 1988.
202) Rockey, K.C., 'An Ultimate Load Method of Design for Plate Girders', Proc. Intl. Conf. Developments in Bridge Design and Construction, University College, Cardiff, 1971, Crosby Lockwood Publishers, 1971.
203) Ostapenko, A., 'Shear Strength of Longitudinally Stiffened Plate Girders', Proc., Structural Stability Research Council, New York, 1980.
204) Zur Berechnung der Tragfahigkeit augesteifter Vollwandtrager mit schlanken Stegen under Schub-und Biegebeanspruchung in Eurocode 3-Bericht 6057, T.U. Braunschweig, Institut fur Stahlbau, July 1988.
205) Evans, H. R., 'Assessment of Eurocode 3 - Determination of Model Factors for Plate Girders', Report CAR/BRE, Civil Engineering Department, University College, Cardiff, 1985.
206) Sen, R., 'Evaluation of BS 5400 Plate Girder Rules', Proc. Instn Civ. Engrs, Part 2, Vol 81, Sept. 1986.
207) Det Norske Veritas, Rules for Classification of Ships', DNV, Oslo, 1992.
208) Det Norske Veritas, 'Buckling Strength Analysis of Mobile Offshore Units', DnV, October 1987.
209) American Bureau of Shipping, 'Preliminary Guide for Building and Classing Small Waterplane Areal Twin Hull (SWATH) Vessels', ABS, Draft, Sept. 1990.
210) Evans, H.R., Hamoodi, M.J., 'The Collapse of Welded Aluminium Plate Girders-an Experimental Study', Thin Walled Structures, Vol. 5, 1987.
211) Seah, H.A., 'The Behaviour of Welded Aluminium Alloy Plate Girders Reinforced with Carbon Fibre Reinforced Plastics', M.Sc. Thesis, University College, Cardiff, 1984.
212) Burt, C.A., Evans, H.R., Vilnay, O., 'Further Experimental Studies of the Collapse of Welded Aluminium Plate Girders', Thin Walled Structures, Vol. 8, 1989.
213) Burt, C.A., 'The Ultimate Strength of Aluminium Plate Girders', Ph.D. Thesis, University College, Cardiff, 1987.

214) Hamoodi, M.H., 'The Behaviour of Reinforced Aluminium Alloy Web Plates in Shear Loading', M.Sc. Thesis, University College, Cardiff, 1983.
215) Brown, K.E.P., Evans, H.R., 'Theoretical and Experimental Investigation of the Collapse Behaviour of Transversely Stiffened Aluminium Alloy Plate Girders', Thin Walled Structures, Vol. 18, 1994.
216) Evans, H.R., Burt, C.A., 'Ultimate Load Determination for Welded Aluminium Plate Girders', Proc. Int. Conf. on Steel and Aluminium Structures, R. Narayanan (ed.), Cardiff, UK, 8-10 July 1987, Vol. 2, Elsevier Applied Science, London, 1987.
217) Marsh, C., Strength of Aluminium', Alcan Canada Products Limited, Fifth Edition, Canada, 1983.
218) Canadian Standards Association, 'Strength Design in Aluminium, CAN3-S 157-N83, Rexdale, Ontario, 1983.
219) Sharp, M., 'Stiffened Flat Plates', Chapter 8 in Behaviour and Design of Aluminium Structures, McGraw-Hill Inc., New York, 1992.
220) Ritchie, D., Rhodes, J., 'Buckling and Post-Buckling Behaviour of Plates with Holes', Aeronautical Quarterly, Vol. 26-27, 1975-1976.
221) Narayanan, R., Chan, S. L., 'Ultimate Capacity of Plates Containing Holes under Linearly Varying Edge Displacements', Computers and Structures, Vol. 21, No. 4, 1985.
222) Lee, M. M. K., 'A Theoretical Model for Collapse of Plate Girders with Perforated Webs', The Structural Engineer, Vol. 68, No. 4, Feb. 1990.
223) Narayanan, R., Der Avanessian, N. G. V., 'An Equilibrium Method for Assessing the Strength of Plate Girders with Reinforced Web Openings', Proc. Instn Civ. Engrs, Vol. 77, Part 2, June 1984.
224) Hoglund, T., 'Strength of Thin Plate Girders with Circular or Rectangular Web Holes without Web Stiffeners', IABSE Colloqium, London, March 1971.
225) Narayanan, R., Der Avanessian, N. G. V., 'Strength of Webs with Corner Openings', The Structural Engineer, Vol. 62B, No. 1, 1984.
226) Narayanan, R., 'Ultimate Shear Capacity of Plate Girders with Openings in Webs', Plated Structures: Stability and Strength, R. Narayanan (Ed.), Chapter 2, Applied Science Publ., London, 1983.
227) Narayanan, R., Darwish, I. Y. S., 'Strength of Slender Webs Having Non-Central Holes', The Structural Engineer, Vol. 63B, No.3, 1985.

228) Narayanan, R., Rockey, K. C., 'Ultimate Load Capacity of Plate Girders with Webs Containing Circular Cut-outs', Proc. Instn Civ. Engrs, Vol. 71, Part 2, Sept. 1981.

229) Rockey, K.C., Anderson , R.G., Cheung, Y.K., 'The Behaviour of Square Webs Having a Circular Hole', Symp. Thin Walled Structures - Their Design and Use In Building, University College, Swansea, Sept. 1967, K. C. Rockey, H.V. Hill (Eds.), Crosby Lockwood Publishers, London, 1967.

230) Redwood, R.G., Uenoya, M., 'Critical Loads for Webs with Holes', Jnl of the Struct. Division, Proc. ASCE, Vol. 105, ST10, Oct. 1979.

231) Shanmugam, N.E., Narayanan, R., 'Elastic Buckling of Perforated Square Plates for Various Loading and Edge Conditions', Proc. Int. Conf. Finite Element Methods, Paper No. 103, Shangai, 1982, University of Hong Kong, 1982.

232) Narayanan, R., Der Avanessian, N.G.V., 'Equilibrium Solution for Predicting the Strength of Webs with Rectangular Holes', Proc. Instn Civ. Engrs, Vol. 75, Part 2, June 1983.

233) Narayanan, R., Der Avanessian, N.G.V., 'Elastic Buckling of Perforated Plates Under Shear', Thin Walled Structures, Vol. 2, 1984.

234) Der Avanessian, N.G.V., 'Ultimate Strength of Plate Girders Containing Openings in Webs', Ph.D Thesis, University of Wales, Cardiff, 1983.

235) Narayanan, R., Der Avanessian, N.G.V., 'Strength of Webs Containing Circular Cut-Outs', IABSE Periodica, Vol. 3, 1983.

236) Narayanan, R., Der Avanessian, N.G.V., 'A Theoretical Method for the Prediction of Ultimate Capacity of Webs with Circular Cutouts', Report, Dept. of Civil Engineering, University College, Cardiff, 1981.

237) Evans, H.R., Narayanan, R., 'Simplified Procedures for the Design of Plate Girders with Web Stiffeners or Openings', Proc. Int. Conf. Steel Structures, Recent Research Advances and their Application to Design, M.N. Pavlovic (Ed.), Budva, Yugoslavia, 29 Sept.-1 Oct. 1986, Elsevier Applied Science Publishers, London, 1986.

238) Stang. A., Greenspan, M., Osgood, W.R., 'Strength of a Riveted Steel Rigid Frame Having Straight Flanges, Jnl. of Research, R.P. 1130, U.S. National Bureau of Standards, 1938.

239) Scheer, J., Pasternak, H., Schween, T., 'Zum Tragverhalten Ausgeteifter Rahmenecken mit Schlanken Stegen', Stahlbau, Vol. 60, 1991.

240) Scheer, J., Pasternak, H., Schween, T., 'On the Load Capacity of Stiffened Knee Joints with Thin Webs', Proc. Int. Conf. Steel and Aluminium Structures (ICSAS'91), S.L. Lee, N.E. Shanmugam (Eds.), Singapore, 22-24 May 1991, Elsevier Applied Science, London, 1991.
241) Bodarski, Z., 'Der Spannungszustandim Ausgesteiften Stegblech einer Dreischenkligen, Unsymmetrischen Rahmenecke mit Gekrummten Inneren Gurten', Dissertation TU Breslau, (Polnisch), 1965.
242) Constructional Steel Research and Development (CONSTRADO), 'Steel Designer's Manual', Crosby Lockwood, London, 1972.
243) Olander, H.C., 'A Method of Calculating Stresses in Rigid Frame Corners', Proc. ASCE, Aug. 1953.
244) Faulkner, D., 'Welded Connections Used in Warship Structures', Trans. RINA, Vol. 106, 1964.
245) Warwick, D.M., Faulkner, D., 'Strength of Tubular Members in Offshore Structures', Department of Naval Architecture and Ocean Engineering, University of Glasgow, Report NAOE-88-36, Glasgow, June 1988.
246) Kendrick, S., 'Externally Pressurised Vessels', Chapter 9, 'The Stress Analysis of Pressure Vessels and Pressure Vessel Components', S.S. Gill (Ed.), Pergamon Press, Oxford, 1970.
247) British Standards Institution, 'British Standard Code of Practice BS 5500: Specification for Unfired Fusion Welded Pressure Vessels', BSI, London, 1991.
248) European Convention on Constructional Steelwork, 'European Recommendations for Steel Construction', London, The Construction Press, 1981.
249) American Petroleum Institute, 'Recommended Practice for Planning, Designing, and Constructing Fixed Offshore Platforms, API Bulletin RP 2A, Draft, 1989.
250) Kendrick, S.B., 'Design for Extrernal Pressure Using General Criteria', Int. J. Mech. Sci., Vol. 24, No. 4, 1982.
251) Kendrick, S.B., 'The Technical Basis of the External Pressure Section of BS 5500', Proc. 4th National Congress of Pressure Vessels and Piping Technology, Portland, Oregon, June 1983.
252) Kendrick, S., 'Ring-Stiffened Cylinders Under External Pressure', Chapter 3, 'Shell Structures: Stability and Strength', R. Narayanan (Ed.), Elsevier Applied Science Publishers, London, 1985.

253) Kendrick, S.B., 'Design of Submarine Structures', Proc. Advances in Marine Structures, Paper 20, C.S. Smith and J.D. Clarke (eds.) Elsevier Applied Science Publishers, 1986.
254) Faulkner, D., Chen, Y.N., de Oliveira, J.G., 'Limit State Design Criteria for Stiffened Cylinders of Offshore Structures', Proc. 4th National Congress on Pressure Vessel and Piping Technology, ASME, Portland, USA, 1983.
255) Faulkner, D., Birrel, N.D., Stiansen, S.G., 'Development of a Reliability Based Code for the Structure of Tension Leg Platforms', OMAE Special Symposium, New Orleans, Feb. 1986.
256) Faulkner, D., 'The Collapse Strength and Design of Submarines', Proc. Symp. Naval Submarines, Royal Institution of Naval Architects, May 17-20, 1983, London.
257) Wilson, L.B., 'The Elastic Deformation of a Circular Cylindrical Shell Supported by Equally Spaced Ring Frames Under Uniform External Pressure', Trans. RINA, Vol. 108, 1966.
258) Cho, S.R., Frieze, P.A., 'Strength Formulation for Ring-Stiffened Cylinders Under Combined Axial Loading and Radial Pressure', Jnl. Constructional Steel Research, Vol. 9, 1988.
259) Bryant, A.R., 'Hydrostatic Pressure Buckling of a Ring Stiffened Tube', NCRE Report R306, October 1954.
260) von Mises, R., 'Stodola Festschrift', Zurich, 1929.
261) Das, P.K., Garside, J.F., Faulkner, D., 'Pilot Study into the Application of Reliability Analysis to a Structural Design Code for Externally Pressurised Vessels', BMT Report No. W1868, February 1988.
262) Louca, L.A., Harding, J.E., 'Torsional Buckling of Ring-Stiffeners in Cylindrical Shells Subjected to External Pressure', Proc. ICE, Vol. 104, 1994.
263) Lunchick, M.E., 'The Influence of Residual Rolling Stresses on the Strength of Cylindrical Pressure Vessels Under External Loading', Jnl. Eng. Ind., ASME, May 1970.
264) Bushnell, D., 'Computerised Buckling Analysis of Shells', Martinius Nijhoff Publishers, Dordecht, 1985.
265) Khaw, T.K., 'Buckling Strength of Imperfect Ring-Stiffened Cylinders Under Combined Loads', PhD Thesis, University of Glasgow, 1980.
266) Smith, C.S., Kirkwood, W., 'Influence of Initial Deformations and Residual Stresses on Inelastic Flexural Buckling of Stiffened Plates and Shells', in Steel Plated Structures, P.J. Dowling, J.E. Harding, P.A. Frieze (eds.), Crosby Lockwood Staples, London, 1977.

267) Niordson, F.I.N., 'Buckling of Conical Shells Subjected to Uniform External Lateral Pressure', Trans. R. Inst. Technol., No. 10, Stockholm, 1947.

268) Seide, P., 'On the Buckling of Truncated Conical Shells Under Uniform Hydrostatic Pressure', Proc. IUTAM Symposium on the Theory of Thin Elastic Shells, Delft, Aug. 1959, North-Holland Publishing Co., Amsterdam, 1959.

269) Hoff, N.J., Singer, J., 'Buckling of Circular Conical Shells Under External Pressure', Proc. IUTAM Symposium on the Theory of Thin Elastic Shells, Delft, Aug. 1959, North-Holland Publishing Co., Amsterdam, 1959.

270) Singer, J., 'Buckling of Circular Conical Shells Under Axisymmetric External Pressure', J. Mech. Eng. Science, Vol. 3, No. 4.

271) Thomson, J.M.T., 'Elastic Buckling of Thin Spherical Shells', Symp. on Nuclear Reactor Containment Buildings and Pressure Vessels, Glasgow, Butterworth, 1960.

272) Cloud, R.L., 'Pressure Vessel Ends', Chapter 4, 'The Stress Analysis of Pressure Vessels and Pressure Vessel Components', S.S. Gill (Ed.), Pergamon Press, Oxford, 1970.

273) Newland, C.N., 'Collapse of Domes Under External Pressure', Proc. Conf. Vessels Under Buckling Conditions', IMechE, Paper C192/72, London, Dec. 1972.

274) Kiernan, T.J., Nishida, K., 'The Buckling Strength of Fabricated HY80 Steel Spherical Shells', DTMB Report No. 1721, July 1966.

275) Faulkner, D., 'The Safe Design and Construction of Steel Spheres and End Closures of Submersibles, Habitats and Other Pressurised Vessels', Proc. Int. Conf. BOSS'79, ICST London, 1979.

276) Koiter, W.T., 'Buckling and Post-Buckling of a Cylindrical Panel Under Compression', Trans. National Aeronautical Research Institute, Amsterdam, Vol. 20, No. 71, 1956.

277) Das, P.K., Faulkner, D., Zimmer, R.A., 'Selection of Robust Strength Models for Efficient Design of Ring and Stringer Stiffened Cylinders Under Combined Loads', Proc. OMAE '92, Calgary, June 1992.

278) Das, P.K., Faulkner, D., Guedes da Silva, A., 'Limit State Formulations and Modelling for Reliability Based Analyses of Orthogonally Stiffened Cylindrical Shell Structural Components', Department of Naval Architecture and Ocean Engineering, Report No. NAOE-91-26, University of Glasgow, Aug. 1991.

279) Rockey, K. C., 'The Design of Web Plates for Plate and Box-Girders - A State of the Art Report', Proc., Int. Symp. on Steel Plated Structures, P. J. Dowling, J. E. Harding, P. A. Frieze (Eds.), Imperial College, London, 1976, Crosby Lockwood Staples, London, 1977.

280) Johnston, B.G., (ed.) 'Guide to Stability Design Criteria for Metal Structures', 3d Edition, John Wiley, New York, 1976.

Tables

Table 4.1: A_{HAZ} used in BS8118 for residual stress estimation [1].

Straight butt welds	
Single pass	$2t^2$
Two pass (single V)	$5t^2$
Two pass (double V)	$2.5t^2$
n passes (single V)	$7t^2/\sqrt{n}$
n passes (double V)	$3.5t^2/\sqrt{n}$
T butt (one pass per side)	
Consecutive passes	$2.5t^2$
Simultaneous passes	$5t^2$
Corner weld	
(Depending on penetration)	$3t^2$ to $7t^2$

Fillet welds	*Automatic*	*Manual*
Single fillet	$6t_1^2$	$10t_1^2$
T fillet (sequential)	$t_1(6t_1 + t_2)$	$t_1(10t_1 + t_2)$
T fillet (simultaneous)	$12t_1^2$	$20t_1^2$
Cruciform	$t_1(7t_1 + t_2)$	$t_1(11t_1 + t_2)$

For butt welds, when the thicknesses (t_1 and t_2) differ, replace t^2 by t_1t_2.
For fillet welds, t_1 is the greater thickness and t_2 the lesser.

Table 4.2: Reduced tangent moduli assumed by Stowell for inelastic buckling of flat plates in compression [1].

l = length of plate, b = width of plate

Boundary Conditions of Plate	$\eta = \frac{E_s}{E}$	Curve in Fig. 4.8
Long Flange One unloaded edge free, the other simply supported	$\frac{E_s}{E}$	A
Long Flange One unloaded edge free, the other built-in	$\frac{E_s}{E}\left[0{\cdot}428 + 0{\cdot}286\left(1 + 3\frac{E_t}{E_s}\right)^{\frac{1}{2}}\right]$	B
Long Plate Both unloaded edges simply supported	$\frac{E_s}{E}\frac{1}{2}\left[1 + \frac{1}{2}\left(1 + 3\frac{E_t}{E_s}\right)^{\frac{1}{2}}\right]$	C
Long Plate Both unloaded edges clamped	$\frac{E_s}{E}\left[0{\cdot}352 + 0{\cdot}324\left(1 + 3\frac{E_t}{E_s}\right)^{\frac{1}{2}}\right]$	D
Short Plate Loaded as a column ($l/b \ll 1$)	$\frac{E_s}{E}\frac{1}{4}\left(1 + 3\frac{E_t}{E_s}\right)$	E
Square Plate Loaded as a column ($l/b = 1$)	$\frac{E_s}{E}\left(0{\cdot}114 + 0{\cdot}886\frac{E_t}{E_s}\right)$	F
Long Column ($l/b \gg 1$)	$\frac{E_t}{E}$	G

Table 4.3: Comparison of Faulkner' ultimate strength model for unwelded steel plates in uniaxial compression with experimental aluminium data.

	6082 ALLOY		5083 ALLOY	
	BIAS	COV	BIAS	COV
Faulkner	1.056	3.60%	0.959	4.70%
Scalar Correction	1	3.63%	1	4.71%
Linear Correction	1.0065	3.53%	1.0011	4.72%
	0.002*beta+1.004		-0.002*beta+0.962	
Population: 11 tests				

Table 4.4: HAZ softening factor w as identified in BS 8118 [19].

. HAZ softening factor $k_z = w$			
Alloy	**Condition**	**Product** (see note 1)	**w**
Non-heat-treatable			
1200	H14	S	0.13
3103	H14	S	0.18
	H18	S	0.13
3105	H14	S	0.17
	H16	S	0.15
	H18	S	0.13
5083	O, F	E, S, P, DT	1.00
	H22	S, P	0.45
5154A	O, F	E, S, P	1.00
	H22	S, P	0.40
	H24	S, P	0.29
5251	F	WT	0.20
	F	F	1.00
	H22	S, P	0.35
	H24	S, P	0.24
5454	O, F	E, S, P	1.00
	H22	S	0.35
	H24	S	0.30
Heat-treatable			
6061	T6	E, DT	0.50
6063	T4	E	1.00
	T4	DT	0.65
	T4	F	0.80
	T5	E	0.75
	T6	E, F	0.50
	T6	DT	0.45
6082	T4	E, S, P, DT, F	1.00
	T6	E, S, P, DT, F	0.50
7020	T4	E, S, P	0.80(A) 1.00(B)
	T6	E, S, P	0.60(A) 0.80(B) (see note 2)

NOTE 1. In the product column, E, S, P, DT, WT and F refer respectively to extrusion, sheet, plate, drawn tube, welded tube and forgings.

NOTE 2. For 7020 material refer to 4.4.2.2, for the applicability of the A and B values.

Table 4.5: **Comparison of proposed ultimate strength model for welded aluminium plates in 5083 alloy in uniaxial compression with experimental aluminium data.**

	LONG. WELDS		TRANS. WELDS		LONG+TRANS		ALL WELDS	
5083 ALLOY	BIAS	COV	BIAS	COV	BIAS	COV	BIAS	COV
Original								
No Imp. Correction	0.955	5.96%	0.969	3.56%	1.004	*	0.913	7.48%
With Imp. Correctn	1	6.07%	1.011	3.55%	1.048	*	0.959	4.70%
Scalar Correction								
No Imp. Correction	1	5.96%	1	3.38%	1	*	1	5.58%
With Imp. Correctn	1	6.07%	1	3.56%	1	*	1	5.67%
Linear Correction								
No Imp. Correction	0.996	5.13%	1.04	3.44%	1.075	*	1.003	5.17%
With Imp. Correctn	0.996	5.11%	1.04	3.42%	1.074	*	1.003	5.15%
Population:	19 tests		2 tests		1 test		22 tests	

Table 4.6: **Comparison of proposed ultimate strength model for welded aluminium plates in 6082 alloy in uniaxial compression with experimental aluminium data.**

	LONG. WELDS		TRANS. WELDS		LONG+TRANS		ALL WELDS	
6082 ALLOY	BIAS	COV	BIAS	COV	BIAS	COV	BIAS	COV
Original								
No Imp. Correction	1	5.26%	0.887	8.26%	0.841	7.19%	0.959	8.80%
With Imp. Correctn	0.957	5.70%	0.837	8.22%	0.795	7.07%	0.915	9.42%
Scalar Correction	1 / 0.957		0.887 / 0.837		0.841/0.795		0.959/0.915	
No Imp. Correction	1	5.26%	1	8.26%	1	7.19%	1	5.62%
With Imp. Correctn	1	5.70%	1	8.19%	1	7.06%	1	5.87%
Linear Correction								
No Imp. Correction	1.035	5.35%	0.92	7.62%	0.87%	6.58%	0.992	8.77%
With Imp. Correctn	1.039	4.94%	0.90	4.28%	0.87%	3.30%	0.992	8.77%
	No imp: 0.957+0.004*beta				With imp: 0.861+0.024*beta			
Population:	14 tests		3 tests		3 test		20 tests	

Table 4.7: Formulae for γ^* for the most frequently encountered cases of stiffened webs, plates and flanges (continued) [129].

Kind of stiffening and loading	*Range of validity*	γ^*
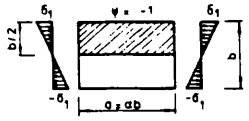		$\gamma^* = 1{\cdot}3$
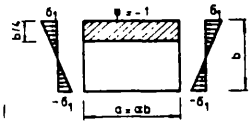	$\alpha \le 0{\cdot}5$	$\gamma^* = 2{\cdot}4 + 18{\cdot}4\delta$
	$\alpha > 0{\cdot}5$	$\gamma^* = (12 + 92\delta)(\alpha - 0{\cdot}3)$ with the maximum value $\gamma^* = 16 + 200\delta$
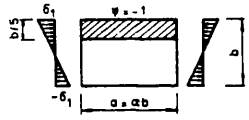	$0{\cdot}5 \le \alpha \le 1{\cdot}5$	$\gamma = 3{\cdot}87 + 5{\cdot}1\alpha + (8{\cdot}82 + 77{\cdot}6\delta)\alpha^2$
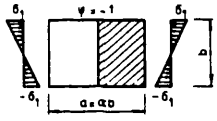	$0{\cdot}6 \le \alpha \le 0{\cdot}935$	$\gamma^* = 6{\cdot}2 - 12{\cdot}7\alpha + 6{\cdot}5\alpha^2$
	$\alpha > 0{\cdot}935$	practically ineffective
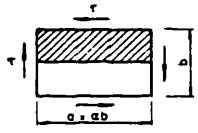	$0{\cdot}5 \le \alpha \le 2{\cdot}0$	$\gamma^* = 5{\cdot}4\alpha^2(2\alpha + 2{\cdot}5\alpha^2 - \alpha^3 - 1)$
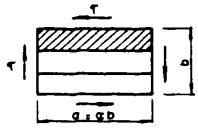	$0{\cdot}3 \le \alpha \le 1{\cdot}0$	$\gamma^* = 12{\cdot}1\alpha^2(4{\cdot}4\alpha - 1)$
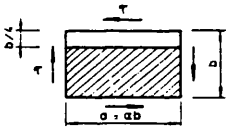	$0{\cdot}5 \le \alpha \le 2{\cdot}0$	$\gamma^* = 7{\cdot}2\alpha^2(1 - 3{\cdot}3\alpha + 3{\cdot}9\alpha^2 - 1{\cdot}1\alpha^3)$
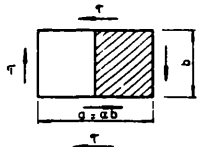	$0{\cdot}5 \le \alpha \le 2{\cdot}0$	$\gamma^* = \frac{5{\cdot}4}{\alpha}\left(\frac{2}{\alpha} + \frac{2{\cdot}5}{\alpha^2} - \frac{1}{\alpha^3} - 1\right)$
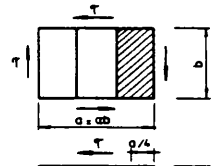	$1{\cdot}0 \le \alpha \le 3{\cdot}3$	$\gamma^* = \frac{12{\cdot}1}{\alpha}\left(\frac{4{\cdot}4}{\alpha} - 1\right)$
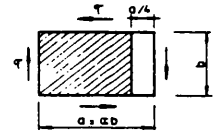	$0{\cdot}5 \le \alpha \le 2{\cdot}0$	$\gamma^* = \frac{7{\cdot}2}{\alpha}\left(1 - \frac{3{\cdot}3}{\alpha} - \frac{3{\cdot}9}{\alpha^2} - \frac{1{\cdot}1}{\alpha^3}\right)$
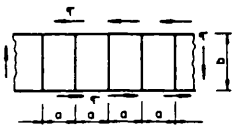	$0{\cdot}2 \le \alpha \le 1{\cdot}0$	$\gamma^* = \frac{28}{\alpha^2} - 20$

Table 4.7: Formulae for γ^* for the most frequently encountered cases of stiffened webs, plates and flanges (final) [129].

Kind of stiffening and loading	*Range of validity*	γ^*
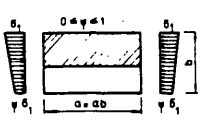	$\alpha < \sqrt{(8(1+2\delta)-1)}$	$\gamma^* = (0{\cdot}53+0{\cdot}47\psi)\left\{\frac{\alpha^2}{2}[16(1+2\delta)-2]-\frac{\alpha^4}{2}+\frac{1+2\delta}{2}\right\}$
	$\alpha > \sqrt{(8(1+2\delta)-1)}$	$\gamma^* = (0{\cdot}53+0{\cdot}47\psi)\left\{\frac{1}{2}[8(1+2\delta)-1]^2+\frac{1+2\delta}{2}\right\}$
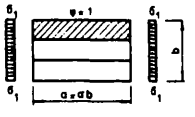	$\alpha < \sqrt{(18(1+3\delta)-1)}$	$\gamma^* = \frac{\alpha^2}{3}[36(1+3\delta)-2]-\frac{\alpha^4}{3}+\frac{1+3\delta}{3}$
	$\alpha > \sqrt{(18(1+3\delta)-1)}$	$\gamma^* = \frac{1}{3}[18(1+3\delta)-1]^2+\frac{1+3\delta}{3}$
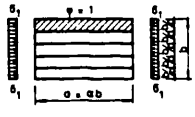	$\alpha < n\sqrt{(2(1+n\delta))}$	$\gamma^* = \frac{1}{n}[4n^2(1+n\delta)\alpha^2-\alpha^4]$
	$\alpha > n\sqrt{(2(1+n\delta))}$	$\gamma^* = 4n^3(1+n\delta)^2$
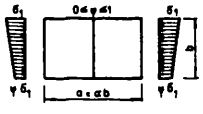	$0{\cdot}4 \le \alpha \le 1{\cdot}4$	$\gamma^* = \dfrac{4\left(\frac{4}{\alpha^2}-\frac{\alpha}{4}\right)}{\pi^2\alpha\left(1-\frac{\pi^2\alpha^4}{12a-48}\right)}$
	$\alpha > 1{\cdot}4$	practically ineffective
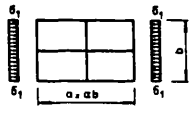	$0{\cdot}9 \le \alpha \le 1{\cdot}1$	$\gamma_l^* = \dfrac{(1+\alpha^2)^2[(1+2\delta_l)-1]}{2(1+p\alpha^3)}$
		where
		$p = \dfrac{\gamma_t}{\gamma_l} = \dfrac{I_t}{I_l}$
		subscript l is related to longitudinal stiffener subscript t to transverse stiffener

Table 4.8: Characteristics of the main ultimate strength models for steel plate girders [279].

ASPECTS OF METHODS	HERZOG Aarau	EVANS, PORTER & ROCKEY Cardiff	BERGFELT Gothenberg	STEINHARDT & VALTINAT Karlsruhe	OSTAPENKO et al Lehigh	KOMATSU Osaka	ROCKEY - SKALOUD Prague - Cardiff	HOGLUND Stockholm	FUJII Tokyo	DUBAS Zurich
1 Simplified method, easy for users	no	yes	yes	yes	no	no	no	yes	no	yes
2 Computer needed	no	charts	no	no	yes/no	yes	no/yes(1)	no	no	no
3 Account taken of longitudinal stiffeners	yes	yes	no	yes(2)	yes/no(3)	no	yes	no	no	no
4 Applicable to hybrid girders	yes	yes	yes	yes	yes	no	yes	yes	yes	yes
5 Applicable to unsymmetrical girders	yes	yes	yes	yes	yes	yes	no	no	yes	yes
6 Applicable to composite girders	no	nothing said	nothing said	yes	nothing said	no	no	no	nothing said	nothing said
7 Details for calculation of bending capacity	yes	yes	yes	yes	yes	no	yes	yes	yes	yes
8 Consideration of normal forces	no	no	yes	yes	no	no	yes	yes	no	yes
9 Details about σ_{cr} of compression flange	yes	mention -ed	no	mention -ed	yes	no	mention -ed	mention -ed	no	no
10 Pure shear	yes	yes	yes	yes	yes	yes	yes	yes	yes	yes
11 Normal stresses due to bending	yes	yes	yes	yes	yes	no	yes	yes	yes	yes
12 Combined shear and bending	yes	yes	yes	yes	yes	no	yes	yes	yes	yes

(1) for solving a cubic equation ;

(2) in the serviceability state ;

(3) computer method takes account of longitudinal stiffeners .

Table 4.9: **Comparison with experimental data of the main ultimate strength model predictions for steel plate girders [197, 279].**

METHOD	TRANSVERSE STIFFENERS ONLY			TRANSVERSE AND LONGITUDINAL STIFFENERS		
	no. of tests	mean	st. dev.	no. of tests	mean	st. dev.
HERZOG (Aarau)	42/164	0.99/1.04	0.2/0.19	48/73	1.01/1.05	0.21/0.16
EVANS, PORTER, ROCKEY (Cardiff)	44/164	1.02/0.98	0.06/0.06	66/73	1.0/1.0	0.07/0.07
BERGFELT (Gothenberg)	33	0.99	0.12	X	X	X
STEINHARDT & VALTINAT (Karlshruhe)	78	0.97	0.14	102	0.96	0.14
OSTAPENKO et al (Lehigh)	48	1.02	0.12	60	1.02	0.11
KOMATSU (Osaka)	36	1.07	0.17	X	X	X
ROCKEY &SKALOUD (Cardiff-Prague)	32	0.98	0.08	46	0.99	0.07
HOGLUND (Stockholm)	33	0.96	0.11	X	X	X
FUJII (Tokyo)	40	0.95	0.15	X	X	X
DUBAS (Zurich)	30	0.79	0.25	X	X	X
EUROCODE 3	164	1.08	0.16	73	1.09	0.13
EVANS (Cardiff-1988)	164	1.04	0.14	73	1.27	0.24

Table 4.10: Equivalent slenderness ratios for buckling of flat plates between stiffeners as suggested by the ALCAN design recommendations [217].

Slenderness Ratios for Buckling of Flat Plates Between Stiffeners

Stress	Panel form	Required Moment of Inertia of stiffener I_s [1]	For the plate of area, $a \times b$ λ
1. Compression	a) 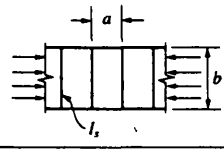	$0.03\left(\frac{b}{a}\right)^3 bt^3$ [2]	Edges pinned:– $\left[\frac{3.3}{1+\left(\frac{a}{b}\right)^2}\right]\frac{a}{t} \leq 1.63\frac{b}{t}$
	b) 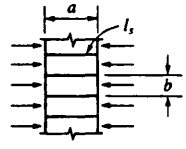	$A'\left(\frac{a}{\lambda}\right)^2$ λ = slenderness ratio for plate between stiffeners A' = area of stiffener + bt	All edges fixed:– $\left[\frac{2}{0.6+\left(\frac{a}{b}\right)^2}\right]\frac{a}{t} \leq 1.24\frac{b}{t}$
2. Bending	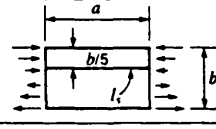	$2\left(\frac{at}{b}\right)^2(4A+bt)$ A = area of stiffener	Edges pinned:– $0.29\frac{b}{t}$
3. Shear	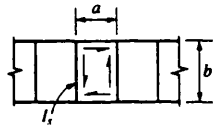	$\frac{Vb^2}{10E}$ V = maximum shear force at stiffener	Edges pinned:– $\frac{1.1}{\left[1+0.75\left(\frac{a}{b}\right)^2\right]^{1/2}}\frac{a}{t}$ [3] All edges fixed:– $\frac{0.85}{\left[1+0.63\left(\frac{a}{b}\right)^2\right]^{1/2}}\frac{a}{t}$ [3]

Slenderness Ratios for Flat Panels With Multiple Stiffeners and Corrugated Sheet

Stress	Panel Form	β [4] Stiffened flat sheet	β [4] Corrugated sheet	λ Stiffened flat sheet	λ Corrugated sheet
4. Compression	a) 	$0.55\left(\frac{t^3}{I}\right)^{1/4}$		$2.3\frac{\beta b}{t}$	
	b) 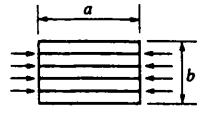	$1.8\left(\frac{I}{t^3}\right)^{1/4}$	$1.8\left(n\frac{r}{t}\right)^{1/2}$	1) $\frac{1}{\left[1+\left(\frac{a}{\beta b}\right)^4\right]^{1/2}}\frac{a}{r}$ 2) $0.7\frac{\beta b}{r}$	
5. Shear	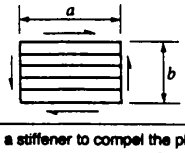	$1.8\left(\frac{I}{t^3}\right)^{1/4}$	$1.8\left(n\frac{r}{t}\right)^{1/2}$	1) $1.5\frac{a}{r\beta^{3/2}}$ [3] 2) $1.5\frac{b}{r\beta^{1/2}}$ [3]	1) $0.45\frac{a}{r}\left(\frac{\beta}{\eta}\right)^{1/2}$ [3] 2) $0.45\frac{b}{r}\left(\frac{\beta^3}{\eta}\right)^{1/2}$ [3]

(1) I_s is the inertia required of a stiffener to compel the plate to buckle between stiffeners.
(2) If longitudinal stiffeners are present the inertia, I_s, is increased by the ratio of the load carried by the longitudinally stiffened plate to that carried by the plate with transverse stiffeners only.
(3) The buckling stress is 0.6 of that given by this slenderness ratio.
(4) βb is the wave length of the buckle. For values of a less than βb, expression 1) gives λ. For greater values of a, expression 2) gives λ.

Nomenclature

- A = cross-sectional area of stiffener
- $A' = A + bt$
- a = dimension of panel in direction of stress
- b = dimension of panel at right angles to direction of stress
- F_s = shear buckling stress
- I = moment of inertia per unit width of stiffened sheet
- I_s = moment of inertia of a "rigid" stiffener
- r = radius of gyration of stiffened sheet
- t = thickness of web
- V = maximum shear force at a stiffener
- β = factor to give wave length of buckle, β_b
- η = ratio of developed to net width of corrugated sheet.

Table 4.11: **Bias and COV values for the strength modelling of perforated deep plate girders loaded in 'pure' shear. Bias is taken normally distributed (exp./theor.).**

Perforation	Pop.	Bias	COV(%)	Ref.
Webs having central circular holes				
(A) Accurate Method	19	1.209	8.31	[235]
(B) Approx. Method Rockey & Narayn appn	19	1.179	8.67	[228]
Webs with corner circular holes	8	1.094	7.12	[225]
Webs having central rectangular holes	11	1.14	8.27	[232]
Webs with eccentric holes				
(A) Accurate Method				
(a) Rectangular	3	1.293	1.5	[227]
(b) Circular	8	1.068	3.16	[227]
(c) All	11	1.129	9.7	[227]
(B) Approx. Method				
(a) Rectangular	3	1.186	7.75	[227]
(b) Circular	8	1.063	9.0	[227]
(c) All	11	1.019	13.1	[227]
Webs having central circular holes with reinforcement	22	1.067	11.5	[223]
Webs having central rectang. holes with reinforcement	8	1.17	3.7	[223]

Table 4.12: **Mean design curve for interframe shell collapse through 700 data points [261].**

$\frac{p_c}{p_{c5}}$	$\frac{p_{n1}}{p_{c5}}$
0.0	0.0
0.200	0.25
0.400	0.50
0.600	0.75
0.734	1.00
0.790	1.25
0.831	1.50
0.865	1.75
0.894	2.00
0.919	2.25
0.941	2.50
0.960	2.75
0.977	3.00
0.992	3.25
1.004	3.50
1.017	3.75
1.028	4.00
1.038	4.25
1.047	4.50
1.055	4.75
1.063	5.00
1.070	5.25
1.077	5.50
1.084	5.75
1.091	6.00
1.098	6.25
1.105	6.50
1.112	6.75
1.119	7.00

Table 4.13: **Bias and COV values for strength modelling of ring stiffened cylinders and dome ends.**

Model	Bias	COV	Comments
A. RING STIFFENED CYLINDERS			
A1. External Pressure Only			
Interframe Shell Collapse			
BS5500 (mean)	1.048	12.99	over all slenderness range [163]
Cho/Frieze	1.001	6.80	[257]
Odland/Faulkner	0.973	7.90	[99, 244] (paragraph 4.2.8)
General Instability			
p_n	1.25	15.2	76 machined cylinders [163]
p_n	0.95	12.6	72 numerical results [163]
p_n	1.303	5.5	24 experiments [163]
Overall Collapse-Frame Yielding			
BS5500 (σ_{tf})	2.48	62.0	35 fabricated models [163]
σ_{ff}	1.10	10.0	in [163] using the MoD C_n approach and summing the first 6 deformation components
Overall Collapse-Shell Yielding			
σ_{yp}	1.0	13.0	Morandi [163]
Tripping			
Faulkner	1.0	15.0	No exp. or num. data [163]
Morandi	1.0	15.0	No exp. or num. data [163]
B. DOME ENDS			
BS5500	1.017	15.53	complete range of $\bar{p}_c/p_{ys}$ [163]
Faulkner	1.0	14.0	60 torispherical tests only [274]
	1.0	15-16	tori-/hemi-spherical tests [274]

Table 4.14: **Bias and COV values for strength modelling of orthogonally stiffened cylinders.**

C. ORTHOGONALLY STIFFENED CYLINDERS			
C1. Axial Compression Only			
Interframe Column Buckling			
RCC	1.02	13.3	52 steel & al. offshore tests [276]
Glasgow	1.01	13.2	Recalibration of RCC work [276]
DnV	1.01	25.1	52 steel & al. offshore tests [276]
API-2U (orthpic)	0.87	24.0	52 steel & al. offshore tests [276]
API-2U (discrete)	0.99	18.4	52 steel & al. offshore tests [276]
ECCS	1.27	27.7	52 steel & al. offshore tests [276]
C2. External Pressure Only			
(a) Radial Pressure			
RCC	0.97	10.3	11 steel tests [276]
Glasgow	1.14	13.4	Recalibration of RCC work [276]
DnV	1.40	39.0	11 steel tests [276]
API-2U (orthpic)	0.87	46.2	11 steel tests [276]
API-2U (discrete)	1.21	14.5	11 steel tests [276]
(b) Hydrostatic Pressure			
RCC	1.012	13.0	10 tests [99, 244]
DnV	1.377	40.2	10 tests [208, 244]
API-2U	1.029	21.0	10 tests [244]
C3. Combination of External Pressure and Axial Load			
Interframe Column Buckling			
RCC	1.09	24.8	Parabolic intn-35 steel tests [276]
Glasgow	1.09	24.8	Recalibration of RCC work [276]
DnV	1.68	25.3	Circular intn-35 steel tests [276]
ECCS	1.387	37.98	Linear intn-21 tests [244]
API-2U(Discrete)	1.13	16.3	35 steel tests [276]

Figures

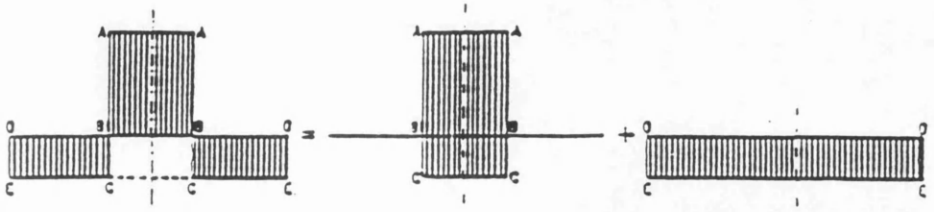

Figure 4.1: The Tendon Force concept [1].

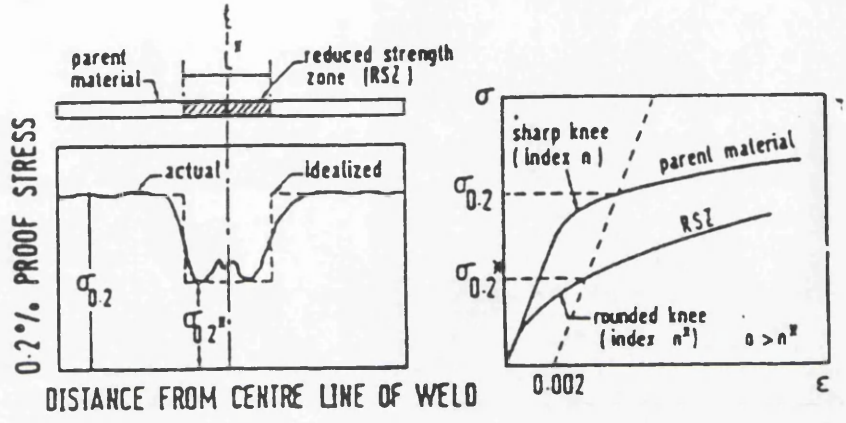

Figure 4.2: 'Parent-softened-material' model by Hill et al [17].

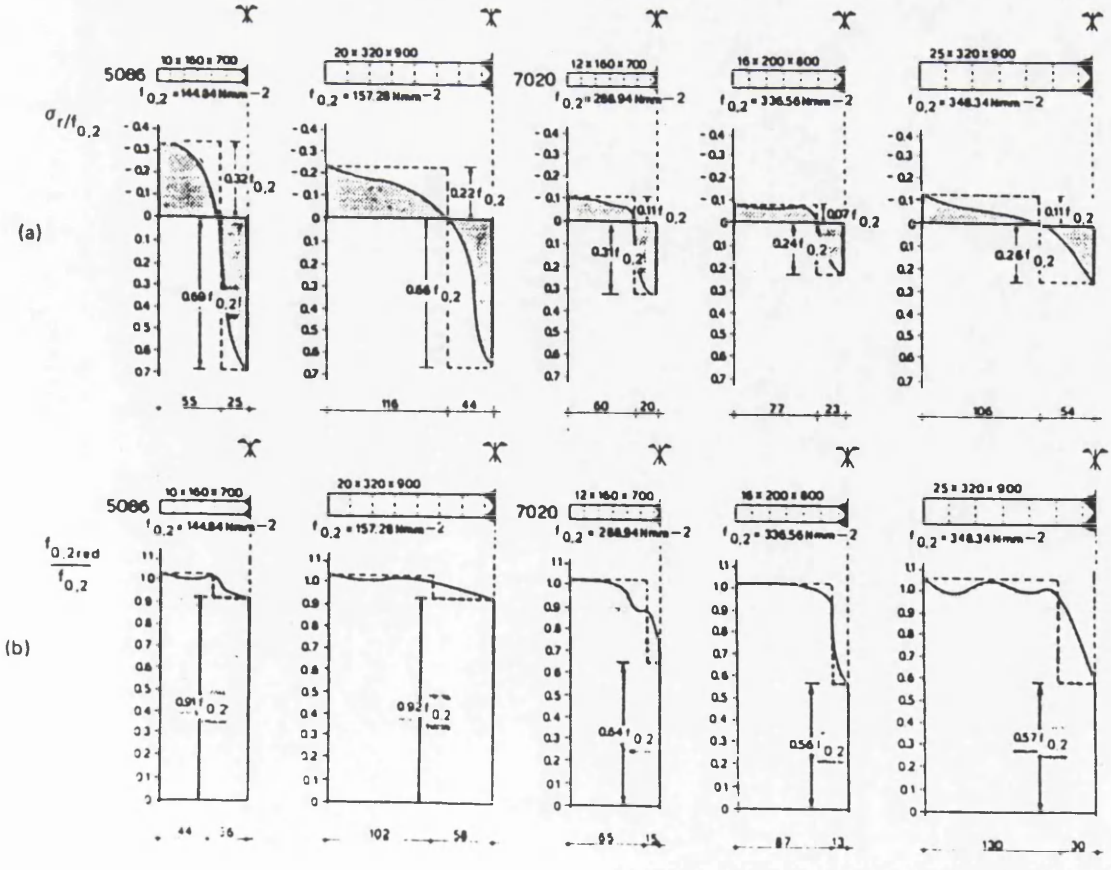

Figure 4.3: ECCS models applicable to butt-welded joints for (a) residual stress and (b) HAZ strength reduction [1].

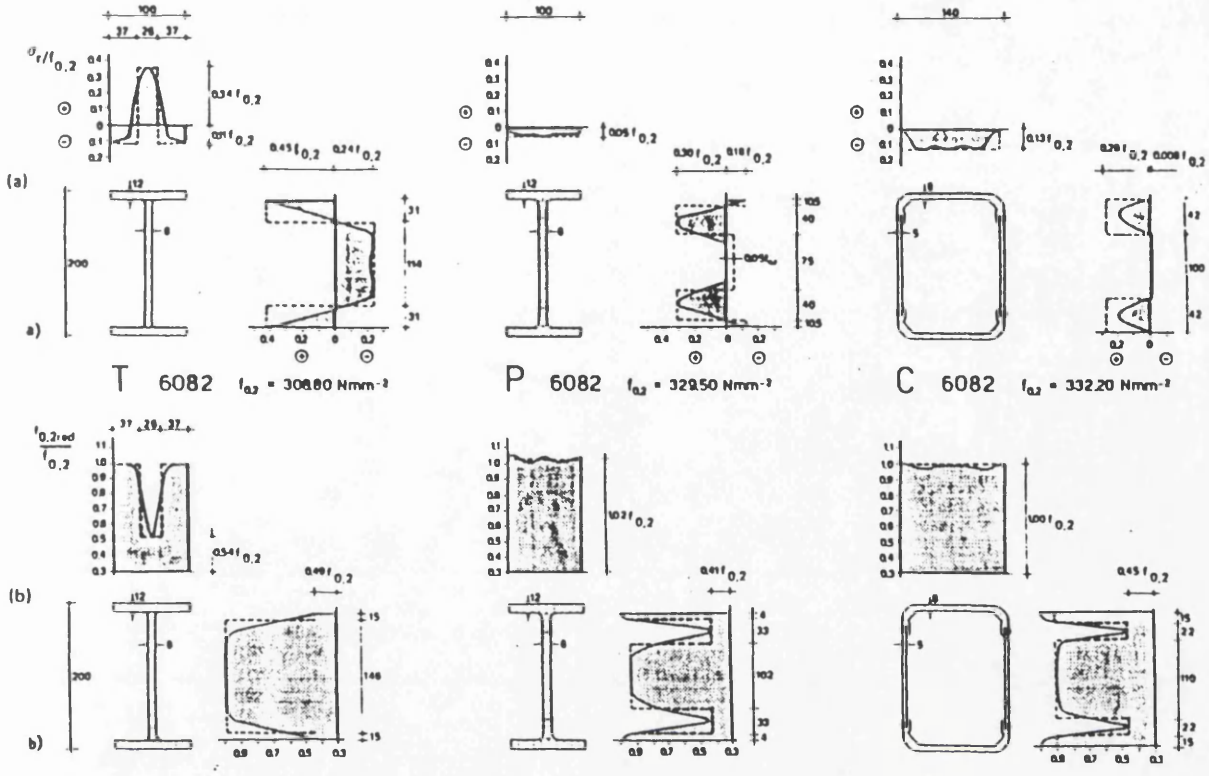

Figure 4.4: **ECCS models applicable to built-up welded sections for (a) residual stress and (b) HAZ strength reduction [1].**

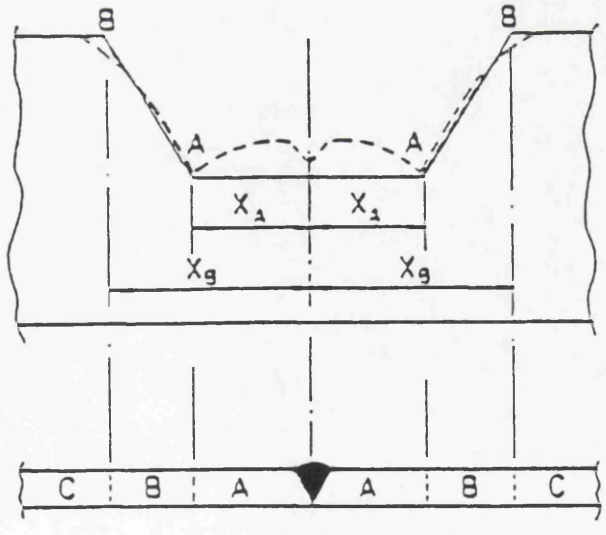

Figure 4.5: **Kelsey's original model assuming a three-part distribution of strength in the welded section [17].**

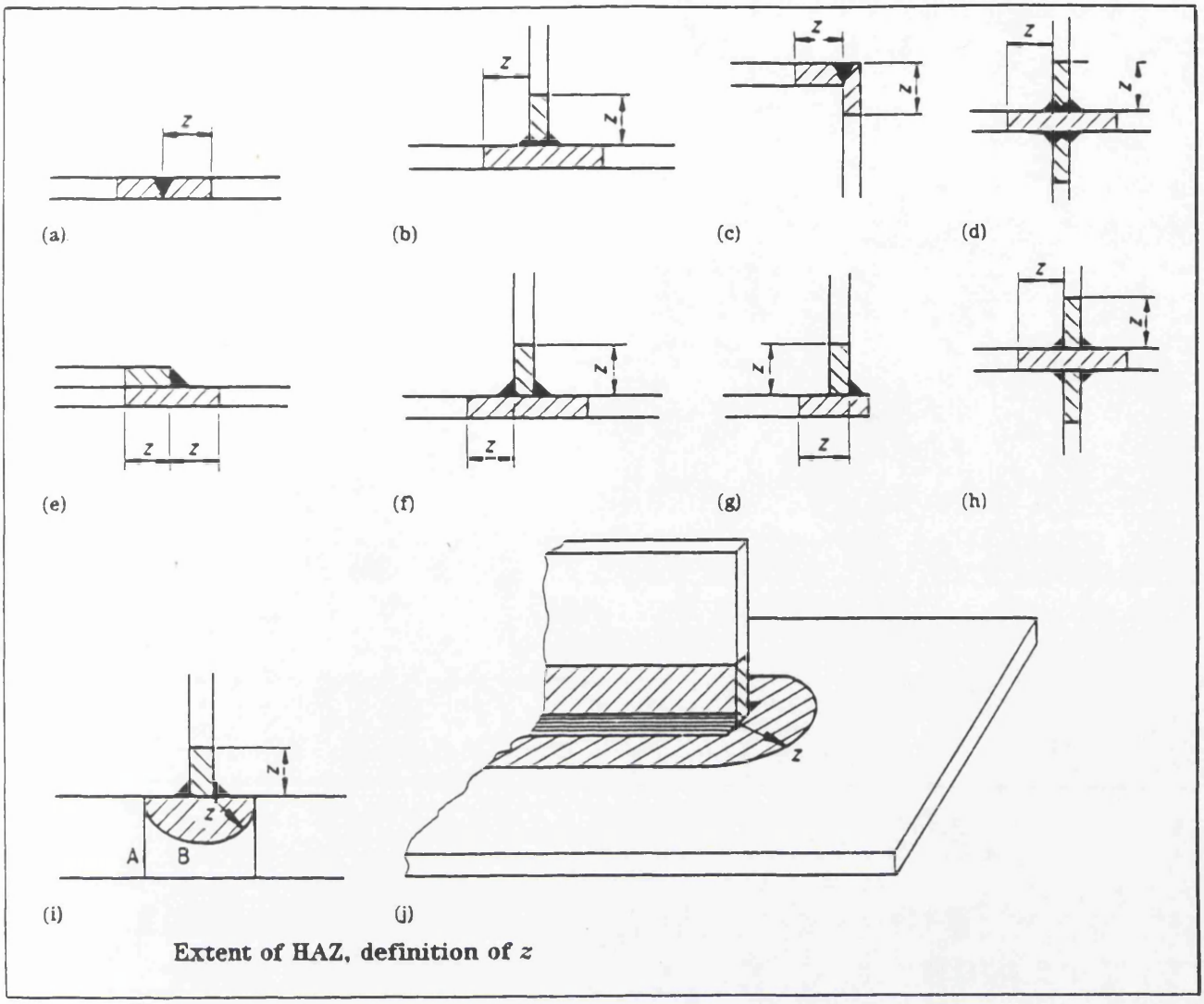

Figure 4.6: **Extent of HAZ softening as proposed in BS 8118 [19].**

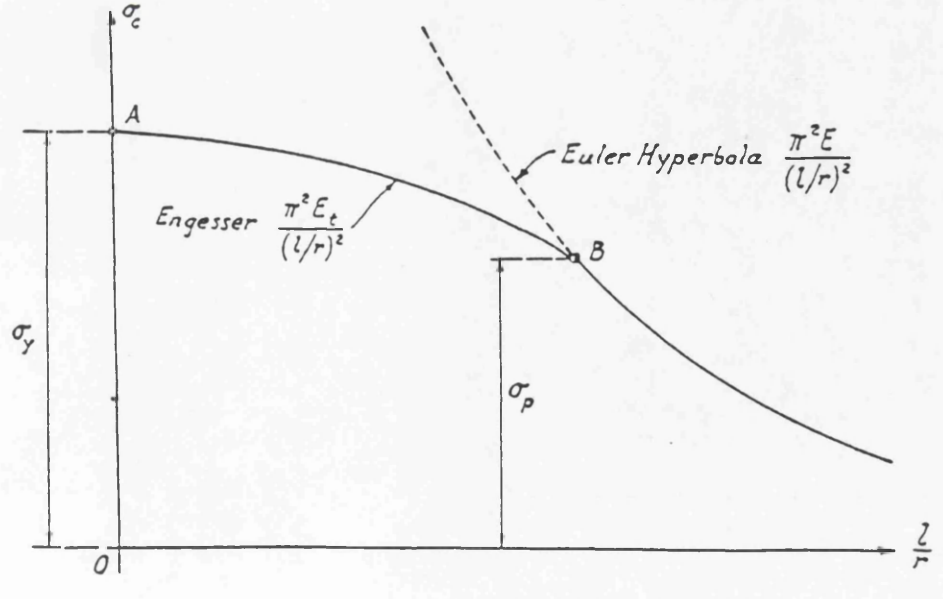

Figure 4.7: **Graphical representation of the tangent modulus reduction in the inelastic buckling of columns [29].**

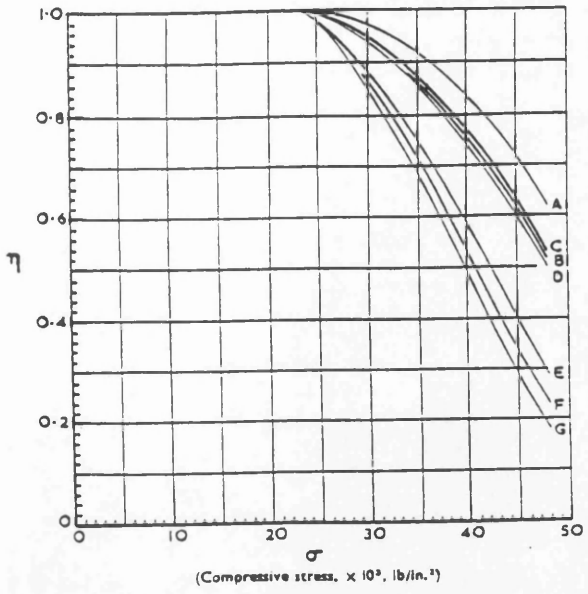

Figure 4.8: **Theoretical variation of Stowell's coefficient η for various types of plate buckling in compression [126].**

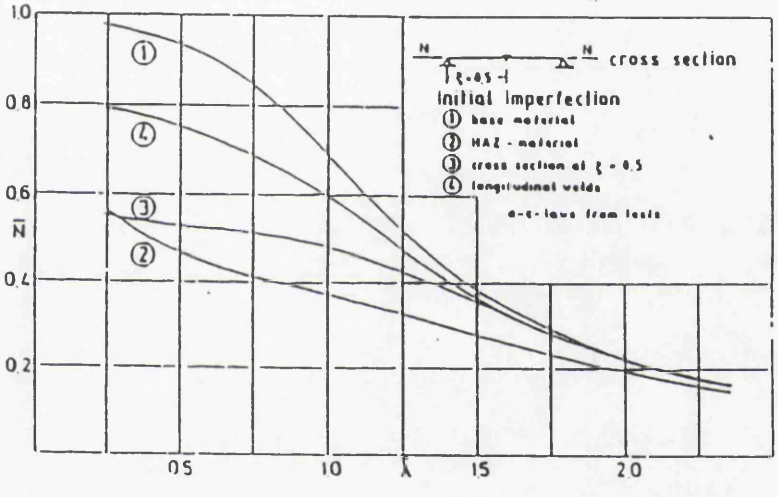

Figure 4.9: **Effect of welding and weld orientation on the buckling strength of aluminium struts [53].**

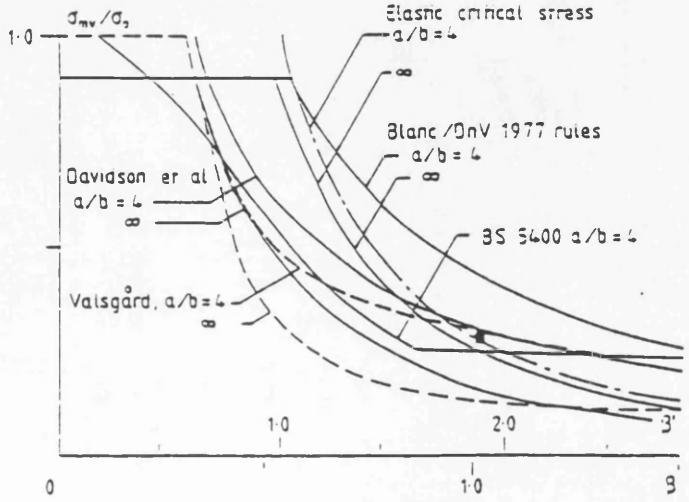

Figure 4.10: **Comparison of steel plate ultimate transverse strengths as recommended by a number of design formulations [65].**

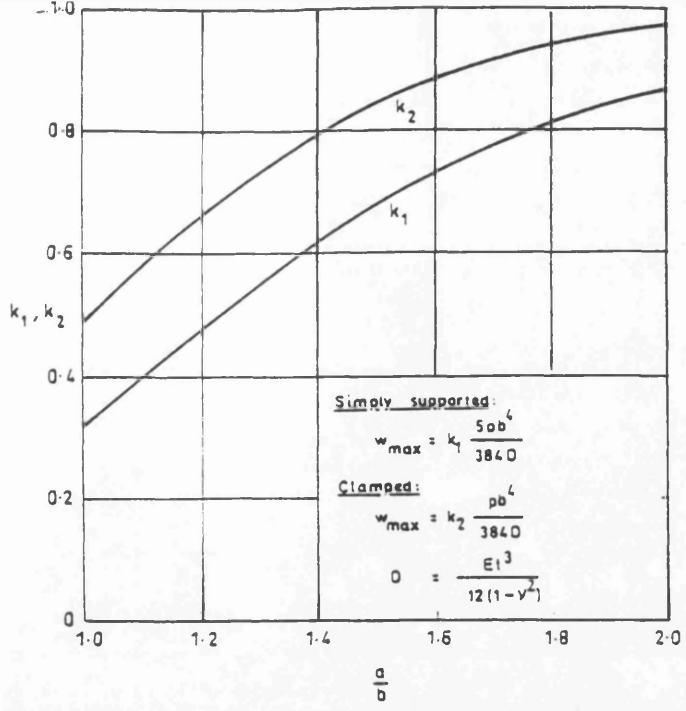

Figure 4.11: **Aspect ratio correction coefficient for elastic small deflection theory maximum deflection expressions [78].**

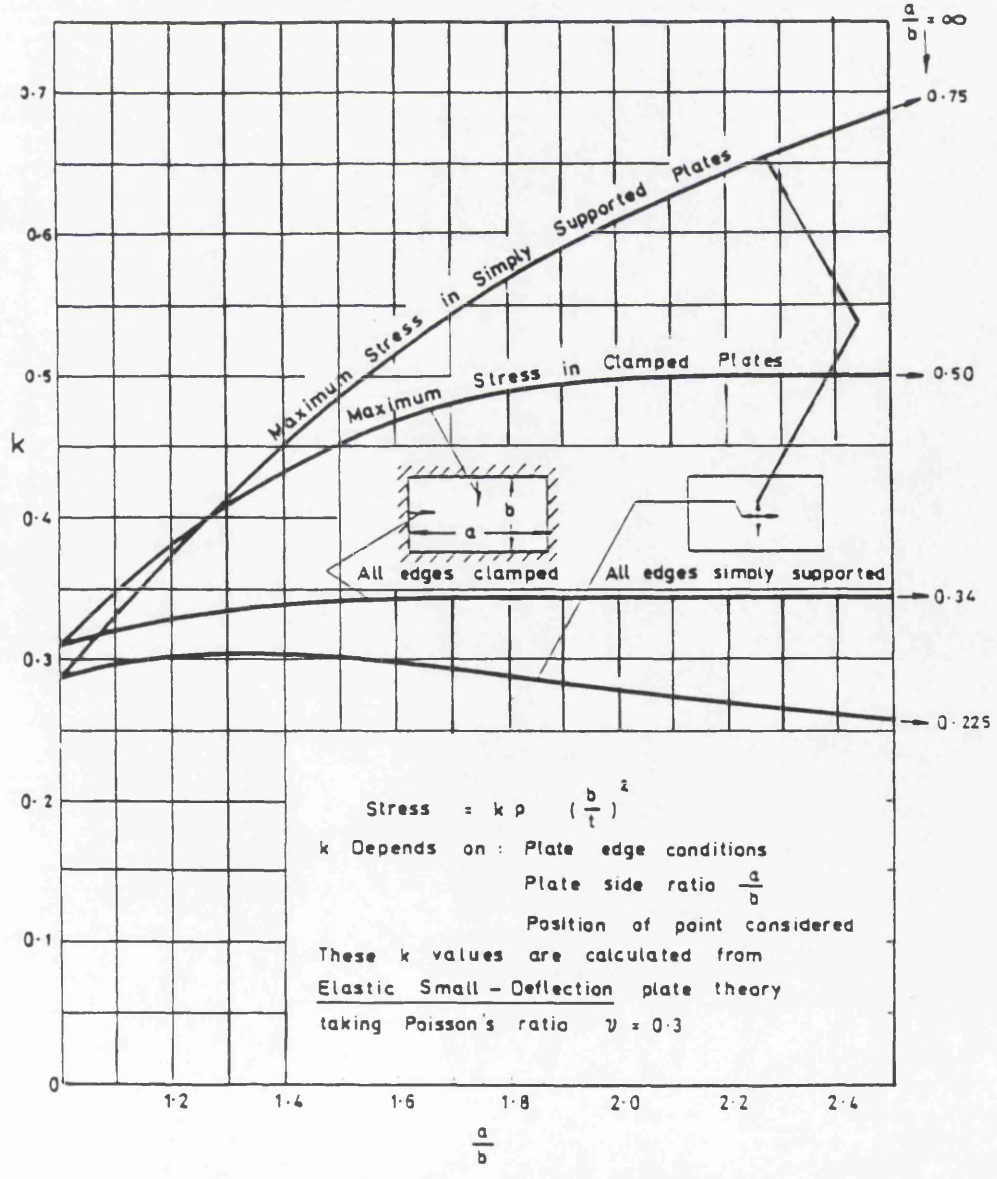

Figure 4.12: **Aspect ratio correction coefficient for elastic small deflection theory maximum stress expressions [78].**

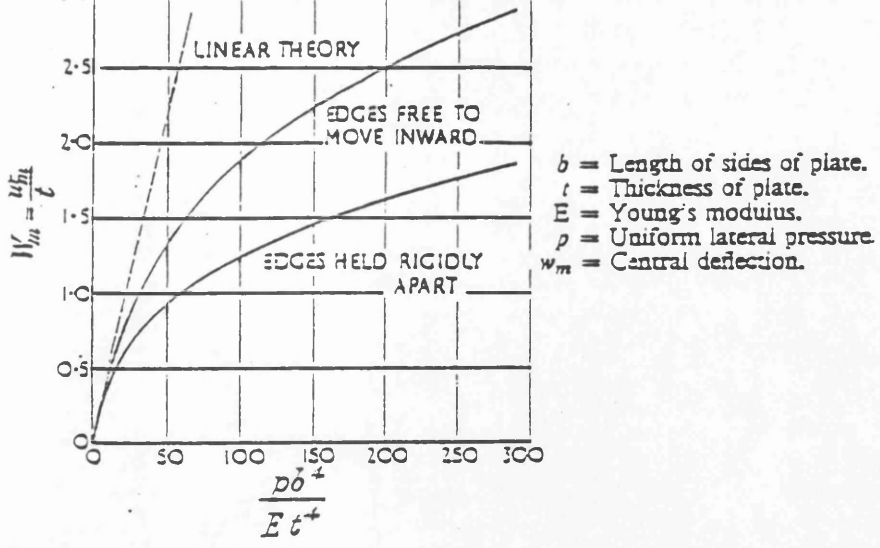

Figure 4.13: In-plane boundary condition effect on plate stiffness [79].

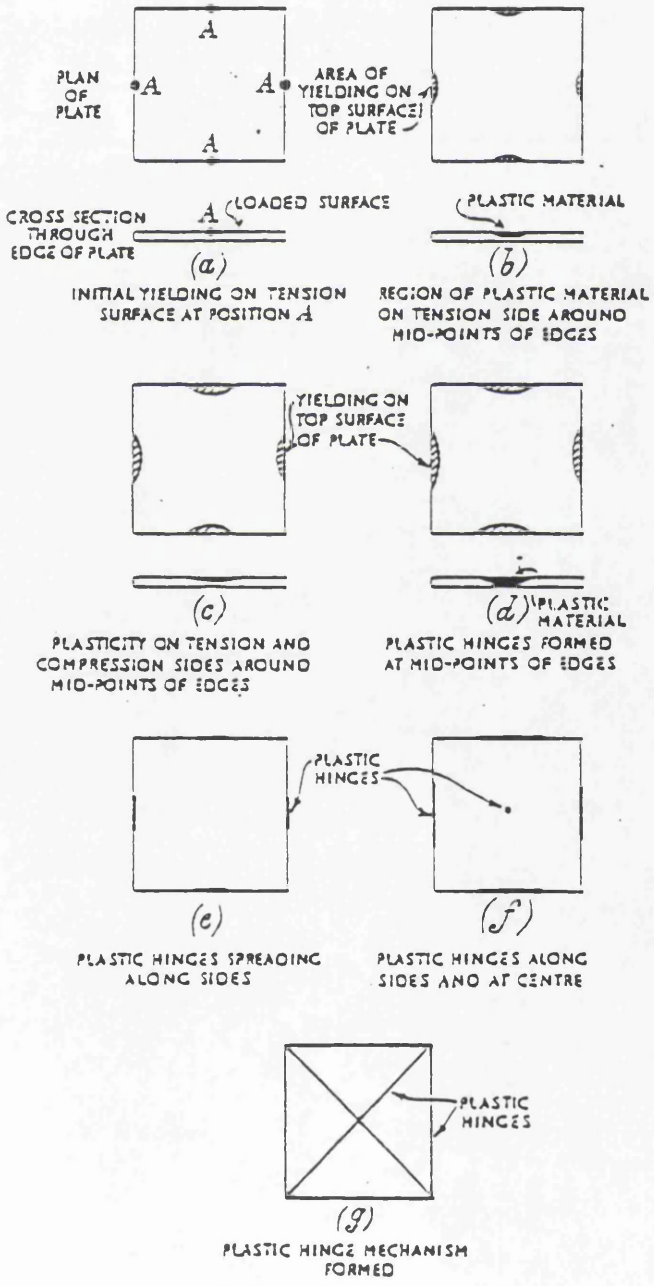

Figure 4.14: Spread of plasticity through a uniformly loaded plate with clamped edges [79].

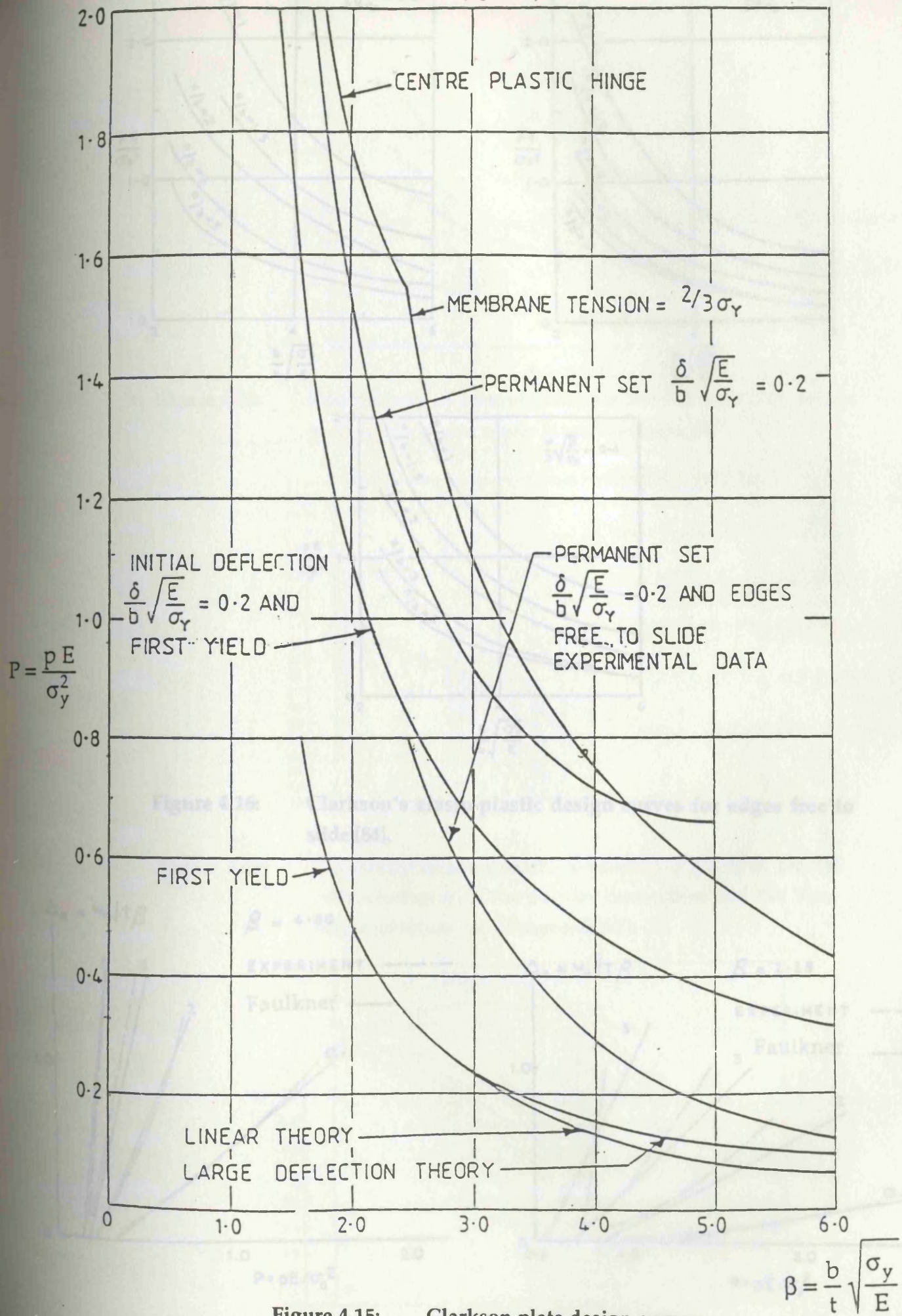

Figure 4.15: **Clarkson plate design curves.**

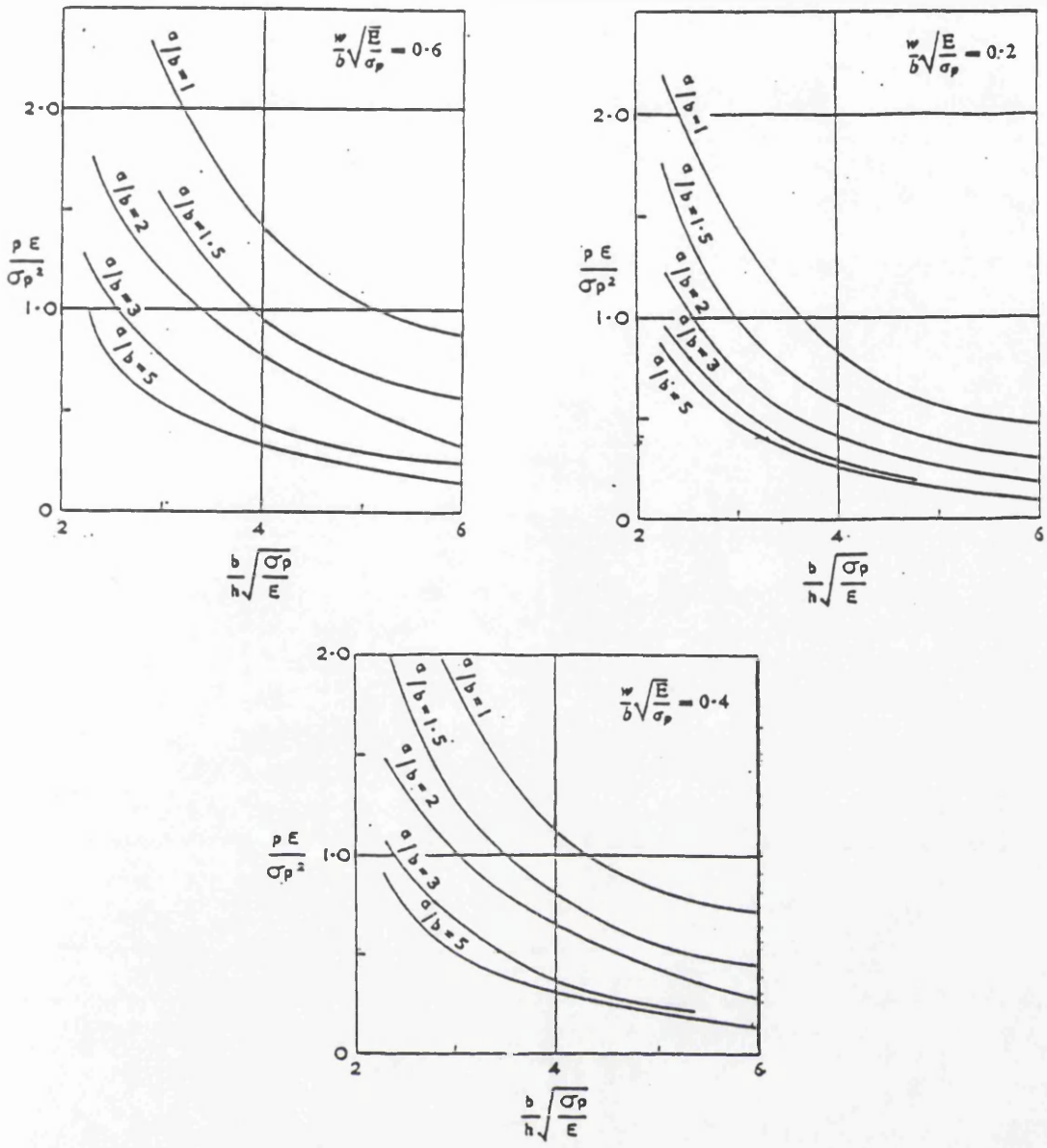

Figure 4.16: **Clarkson's elasto-plastic design curves for edges free to slide [84].**

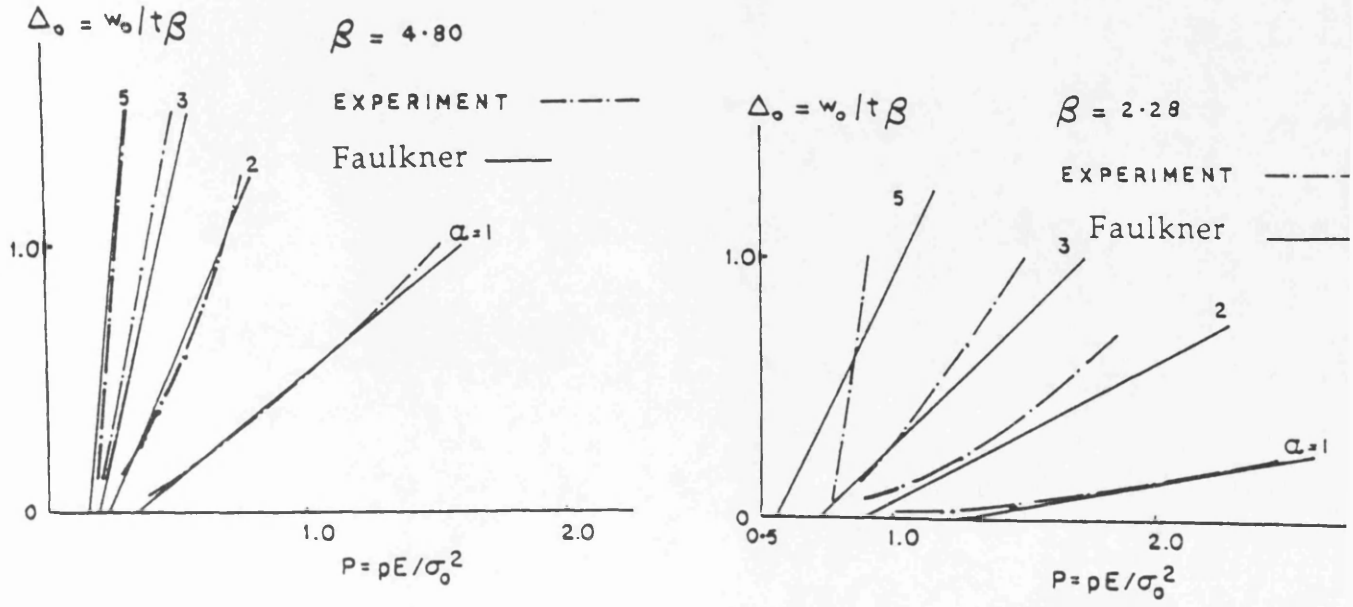

Figure 4.17: **Agreement of Faulkner's elasto-plastic expression with Clarkson's experimental data [42].**

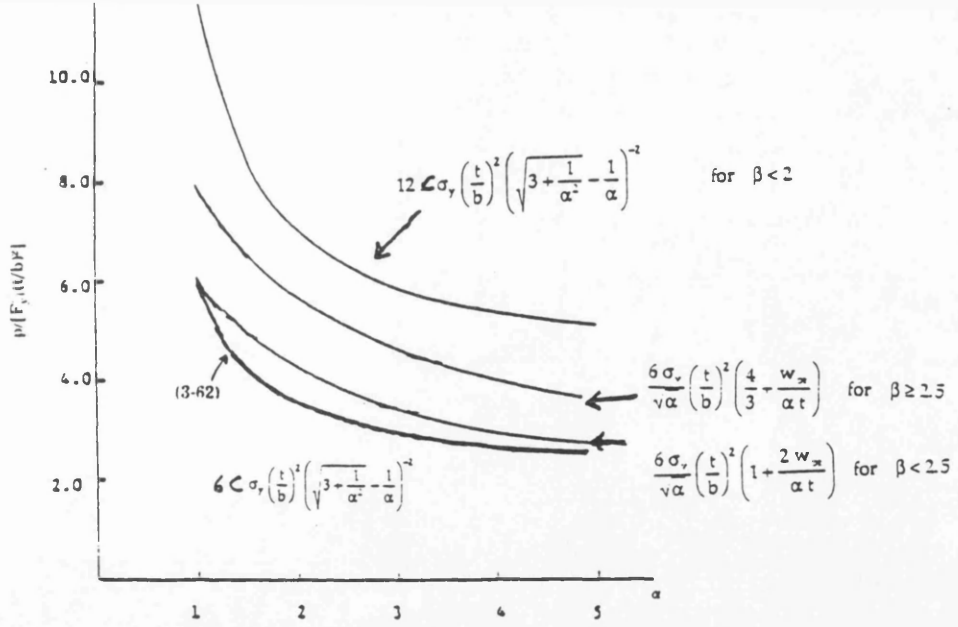

Figure 4.18: Comparison of formulations for the ultimate strength of rectangular plates under lateral pressure [95].

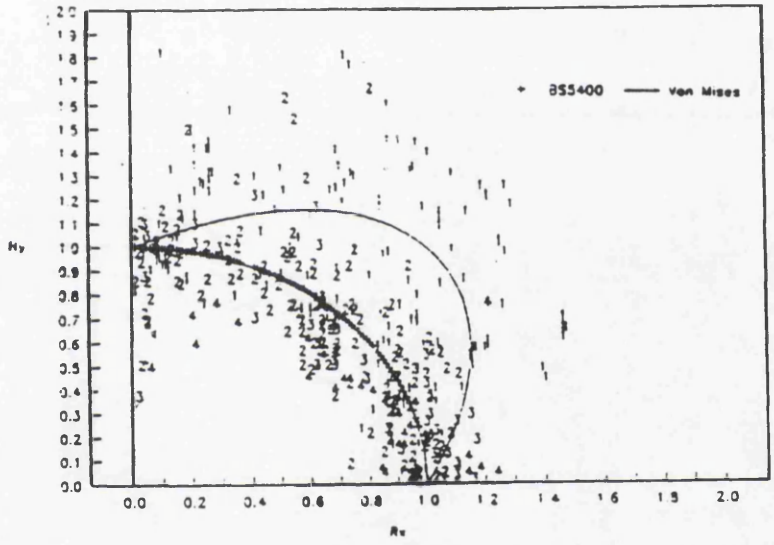

Figure 4.19: Experimental and numerical results for plates in biaxial compression with the circular interaction and the Von Mises criterion superimposed [67].

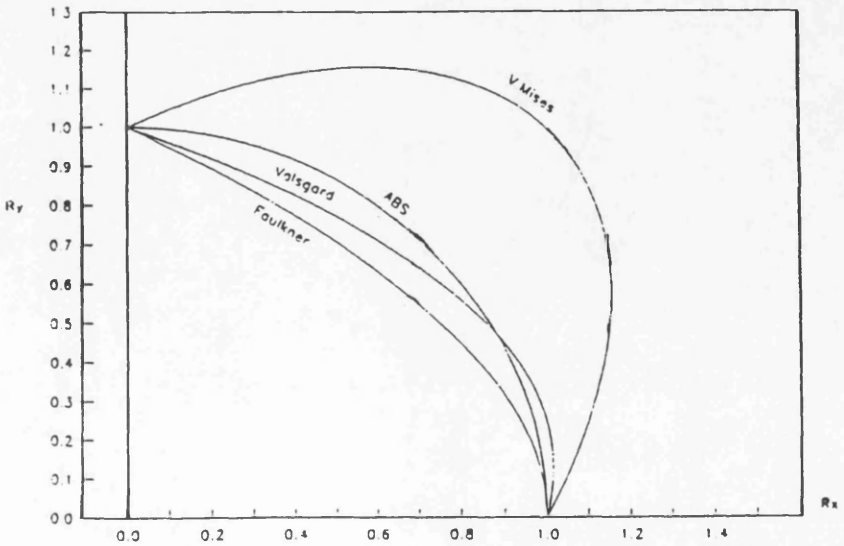

Figure 4.20: Interaction curve comparison for biaxial compression [67].

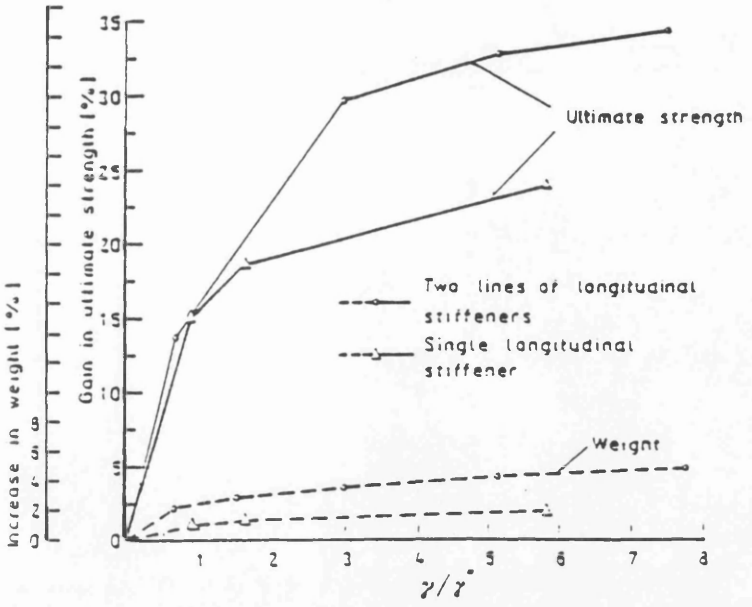

Figure 4.21: **Gain in ultimate strength and corresponding percentage increase in weight in terms of stiffener rigidity [129].**

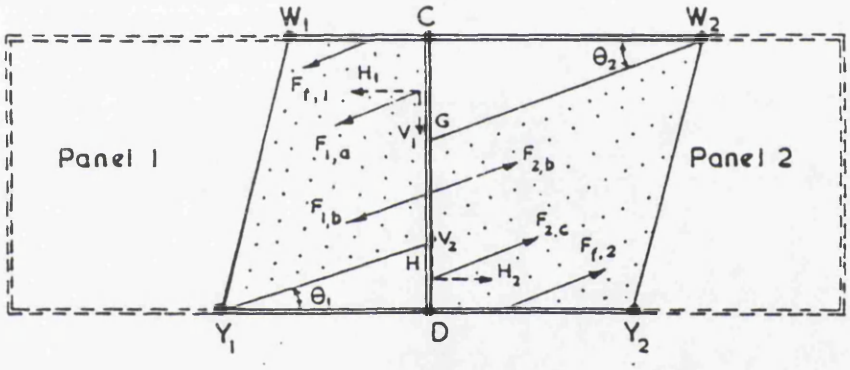

Figure 4.22: **Tension field loading on the vertical stiffener of a deep plate girder [200].**

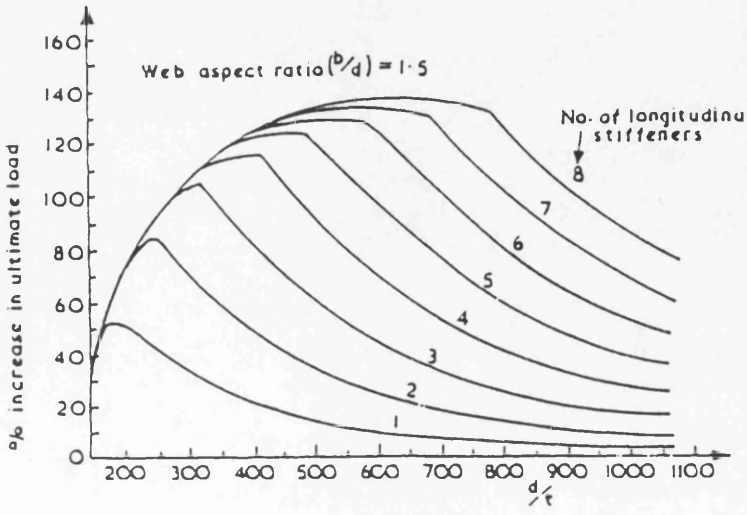

Figure 4.23: **Ardali's percentage increase in strength of shear webs with the number of longitudinal stiffeners [200].**

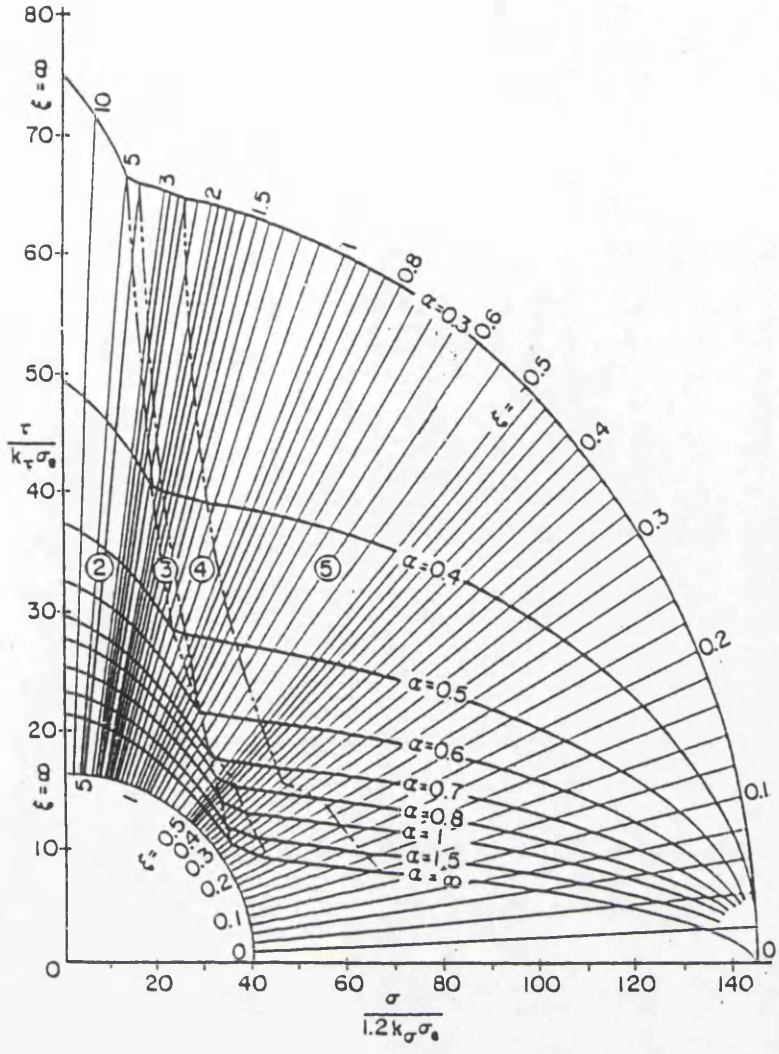

Figure 4.24: **Massonnet's chart for the optimum positioning of a longitudinal stiffener on a web plate, under the action of different shear to bending stress ratios ($\xi = \tau/\sigma$) [138].**

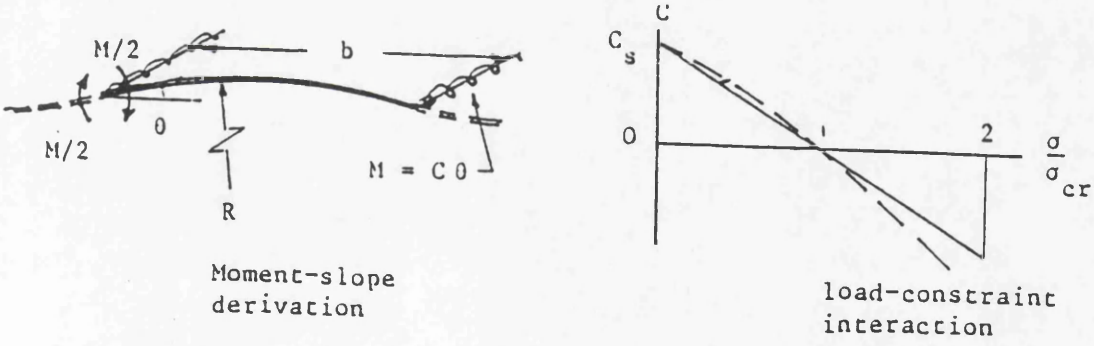

$$\frac{M}{2} = \frac{D}{R} \quad \text{and} \quad b = 2R\theta$$

$$\text{Hence } M = (4D/b)\theta = C_s\,\theta \text{ by definition}$$

$$\text{Hence } C_s = 4D/b = Et^3/2.73\,b$$

Figure 4.25: **Estimation of the rotational restraint C_s of the plate on stiffener tripping by Faulkner [154].**

	LOADING CONDITION IN THE PLATE			
1	Compression stresses linearly varying $0 \leq \psi \leq 1$	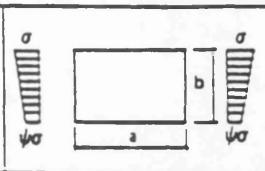	$\alpha \geq 1$	$k_\sigma = \frac{8.4}{1.1 + \psi}$
			$\alpha < 1$	$k_\sigma = \left(\alpha + \frac{1}{\alpha}\right)^2 \frac{2.1}{1.1 + \psi}$
2	Compression and tension stresses: Compression greater than tension $-1 \leq \psi \leq 0$	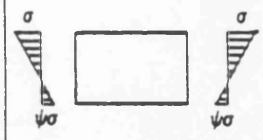		$k_\sigma = (1 + \psi)k_{\sigma,1} - \psi k_{\sigma,3} + 10\,\psi(1+\psi)$ with: $k_{\sigma,1}$ from case 1 for $\psi = 0$ $k_{\sigma,3}$ from case 3
3	Maximum values of compression and tension are equal $\psi = -1$		$\alpha \geq \frac{2}{3}$	$k_\sigma = 23.9$
4	Tension greater than compression $\psi < -1$		$\alpha < \frac{2}{3}$	$k_\sigma = 15.87 + 8.6\alpha^2 + \frac{1.87}{\alpha^2}$
5	Shear stress uniformly distributed	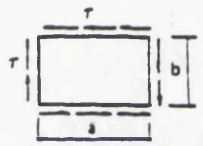	$\alpha \geq 1$	$k_\tau = 5.34 + \frac{4.00}{\alpha^2}$
			$\alpha < 1$	$k_\tau = 4.00 + \frac{5.34}{\alpha^2}$

Buckling coefficients k_σ		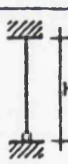	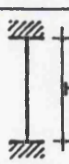	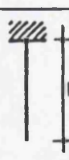	
Boundary conditions					
Loading conditions	$\alpha \geq 1.0$	$\alpha \geq 0.8$	$\alpha \geq 0.7$	$\alpha \geq 1.6$	$\alpha \geq 1.5$
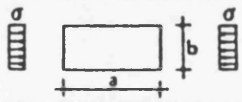	4.00	5.40	6.97	1.28	0.43
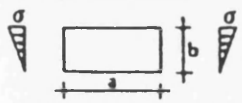	7.81	12.16	13.56	6.26	1.71
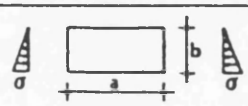	7.81	9.89	13.56	1.64	0.57

Figure 4.26: **Critical buckling coefficients for flat web plates under various in-plane, edge loading conditions [1].**

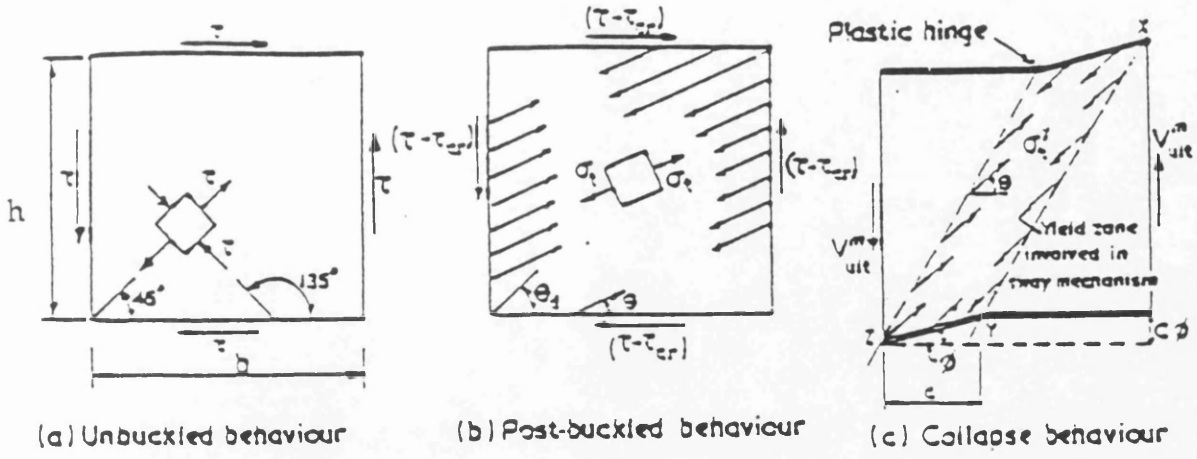

Figure 4.27: Three stages to failure of a girder web panel in shear [200].

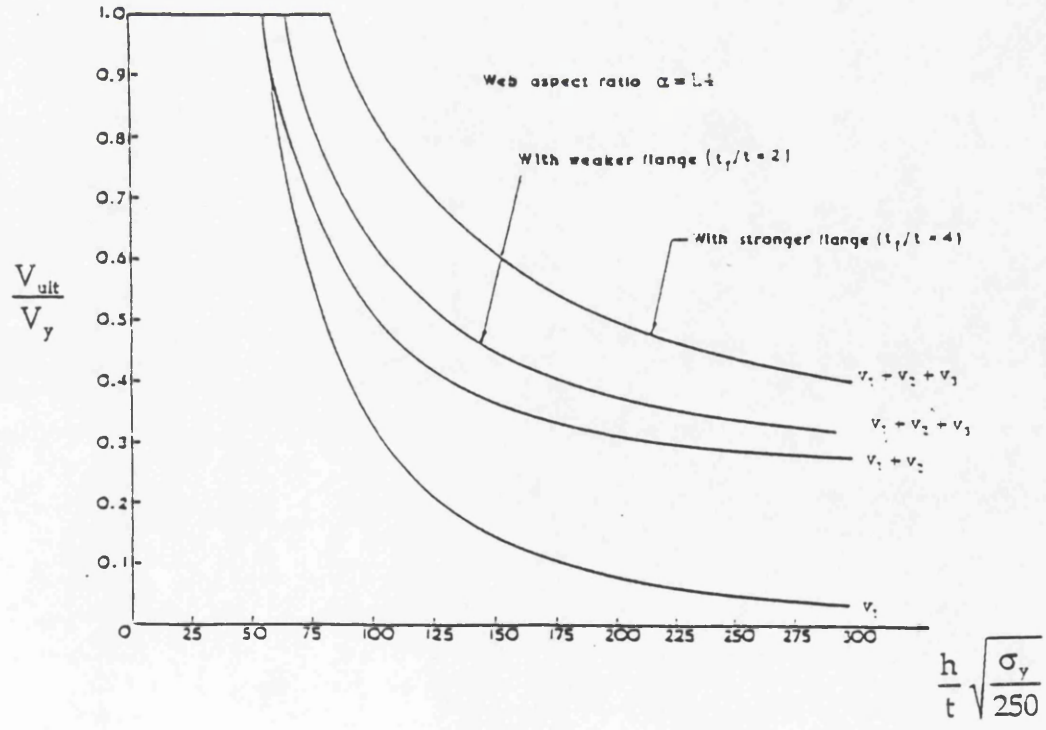

Figure 4.28: The contribution of the three strength terms to the total ultimate strength of a stiffened girder panel in shear [127].

Investigator	Mechanism	Web Buckling Edge Support	Unequal Flanges	Longitudinal Stiffener	Shear and Moment
Basler	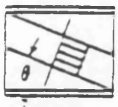	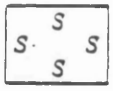	Immaterial	Yes, Cooper	Yes
Takeuchi	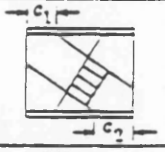	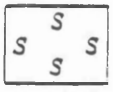	Yes	No	No
Fujii	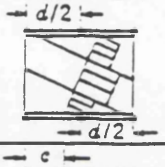	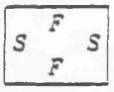	No	Yes	Yes
Komatsu	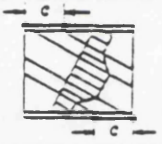	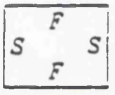	No	Yes, at mid-depth	No
Chern and Ostapenko		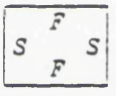	Yes	Yes	Yes
Rockey	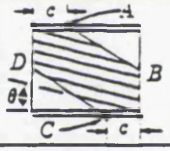	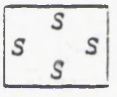	No	Yes	No
Höglund	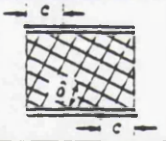	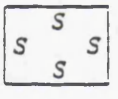	No	No	Yes
Herzog	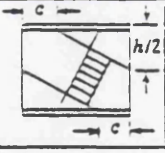	Web buckling component neglected	Yes, in evaluating c	Yes	Yes
Sharp and Clark		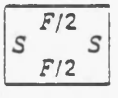	No	No	No
Steinhardt and Schröter		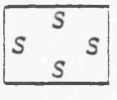		No	No

Figure 4.29: **Summary of ultimate strength models for deep plate girders in shear [280].**

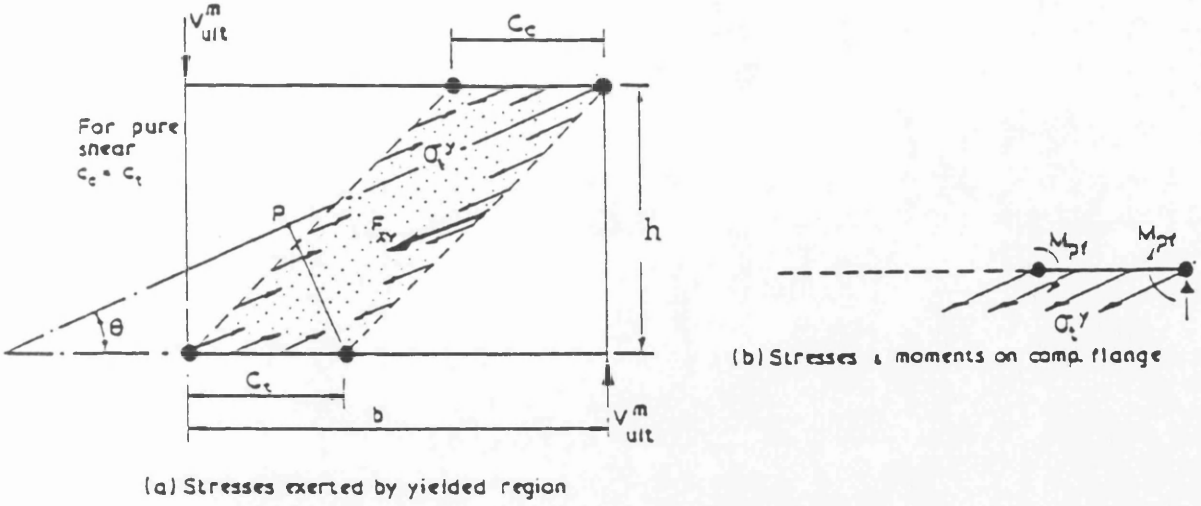

Figure 4.30: **Analytical modelling of the behaviour of a girder panel in shear based on the Cardiff assumptions [185].**

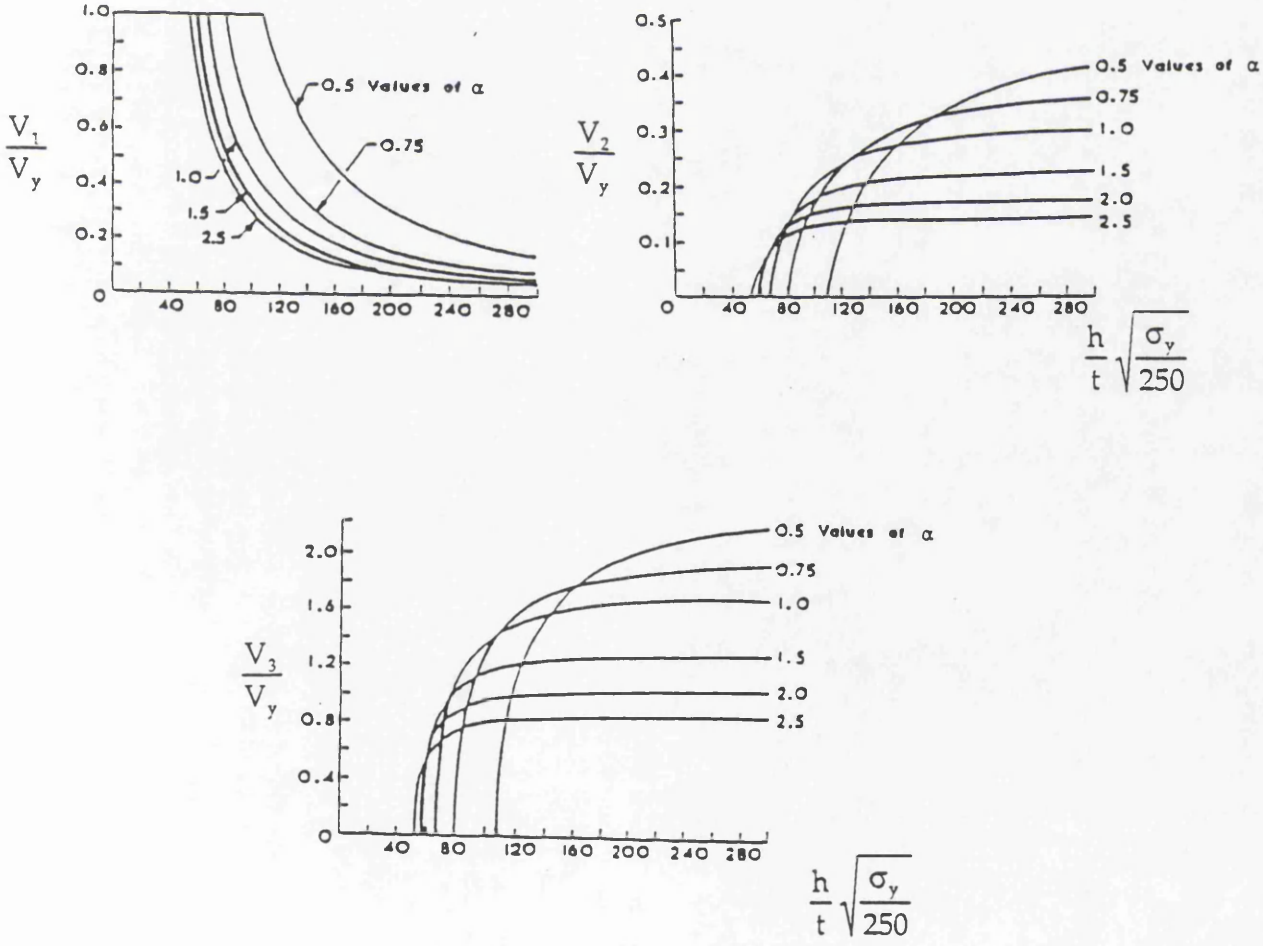

Figure 4.31: **Graphical representation of the effect on the individual strength components of the aspect ratio and slenderness of the web plate [127].**

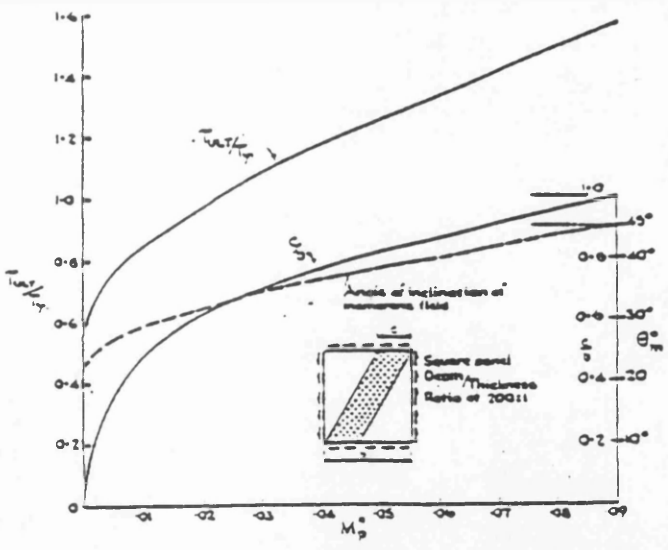

Figure 4.32: Relations between ultimate shear strength, optimum angle of tension band inclination, and the positions of the plastic hinges on the flanges, with flange rigidity M_p^* [198].

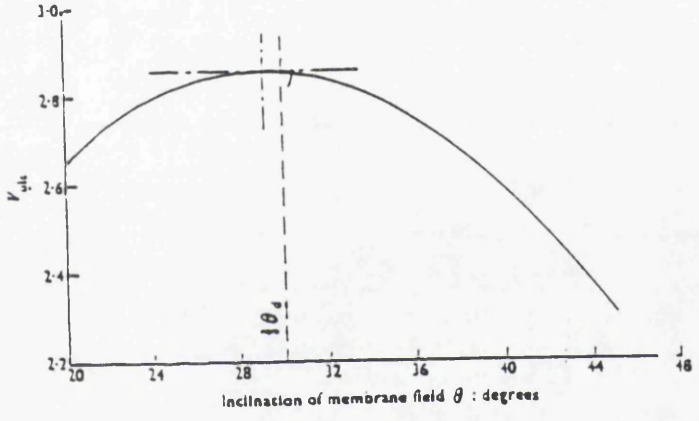

Figure 4.33: Variation of the ultimate strength of a deep plate girder with the inclination of the membrane field according to the Cardiff model [185].

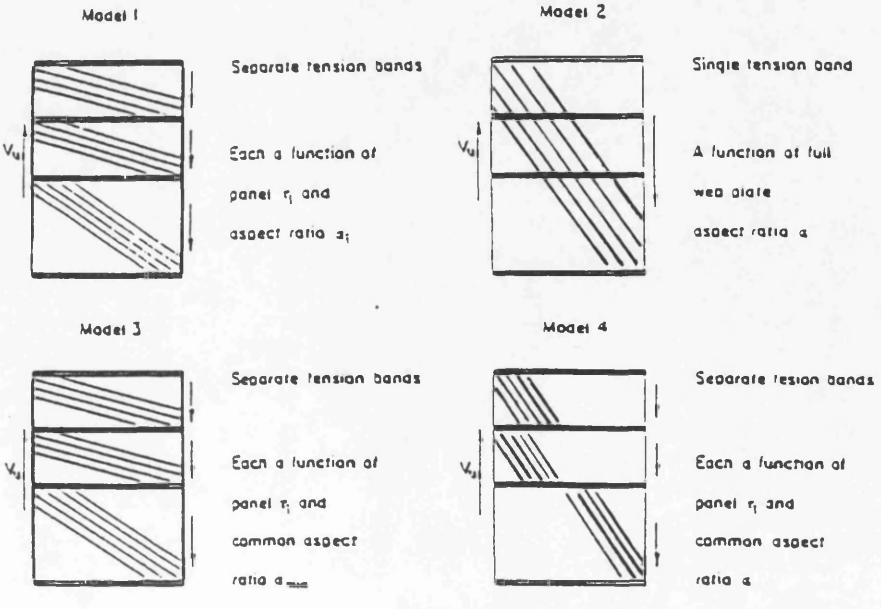

Figure 4.34: Tension field models for longitudinally stiffened webs [150].

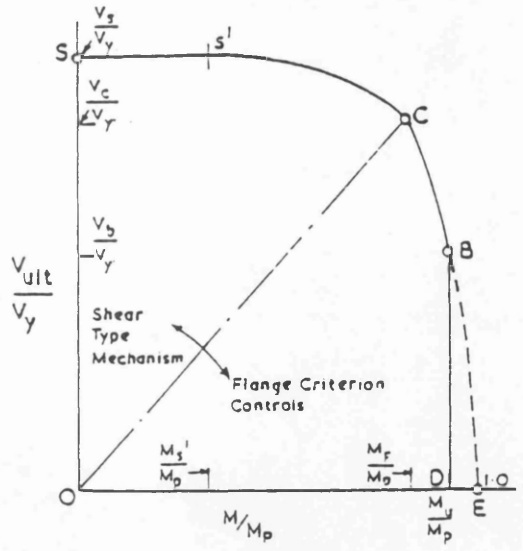

Figure 4.35: Interaction diagram between shear and bending effects as proposed by the Cardiff approach [200].

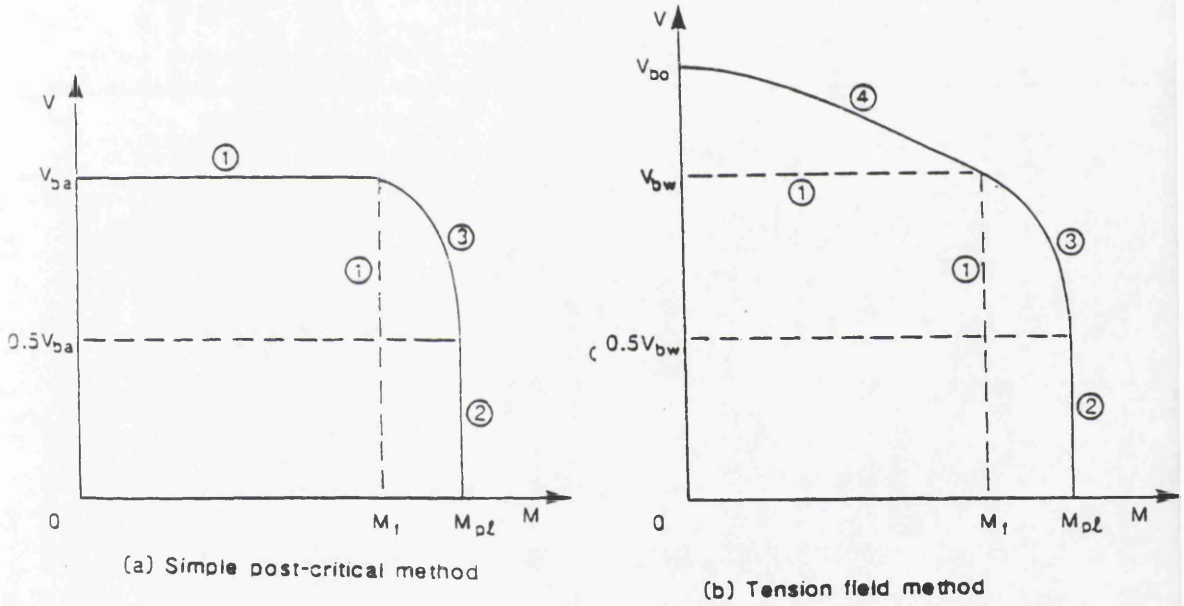

Figure 4.36: Interaction diagram between shear and bending effects as proposed by Eurocode 3 [170].

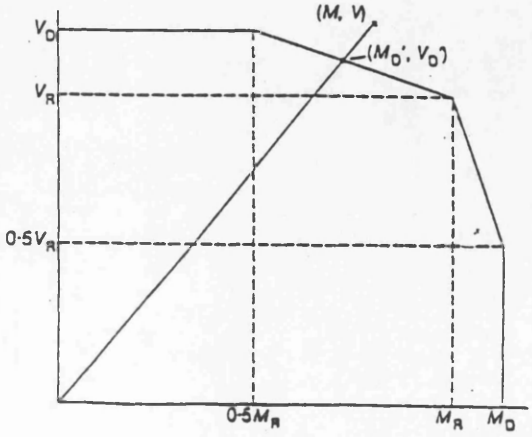

Figure 4.37: Interaction diagram between shear and bending effects as proposed in BS 5400 [96].

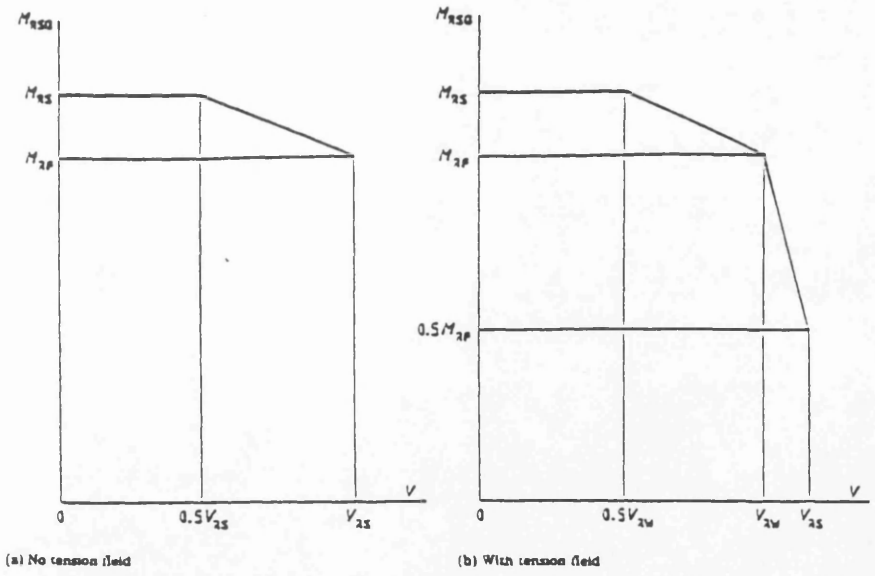

Figure 4.38: Interaction diagram between shear and bending effects as proposed in BS 8118 [194].

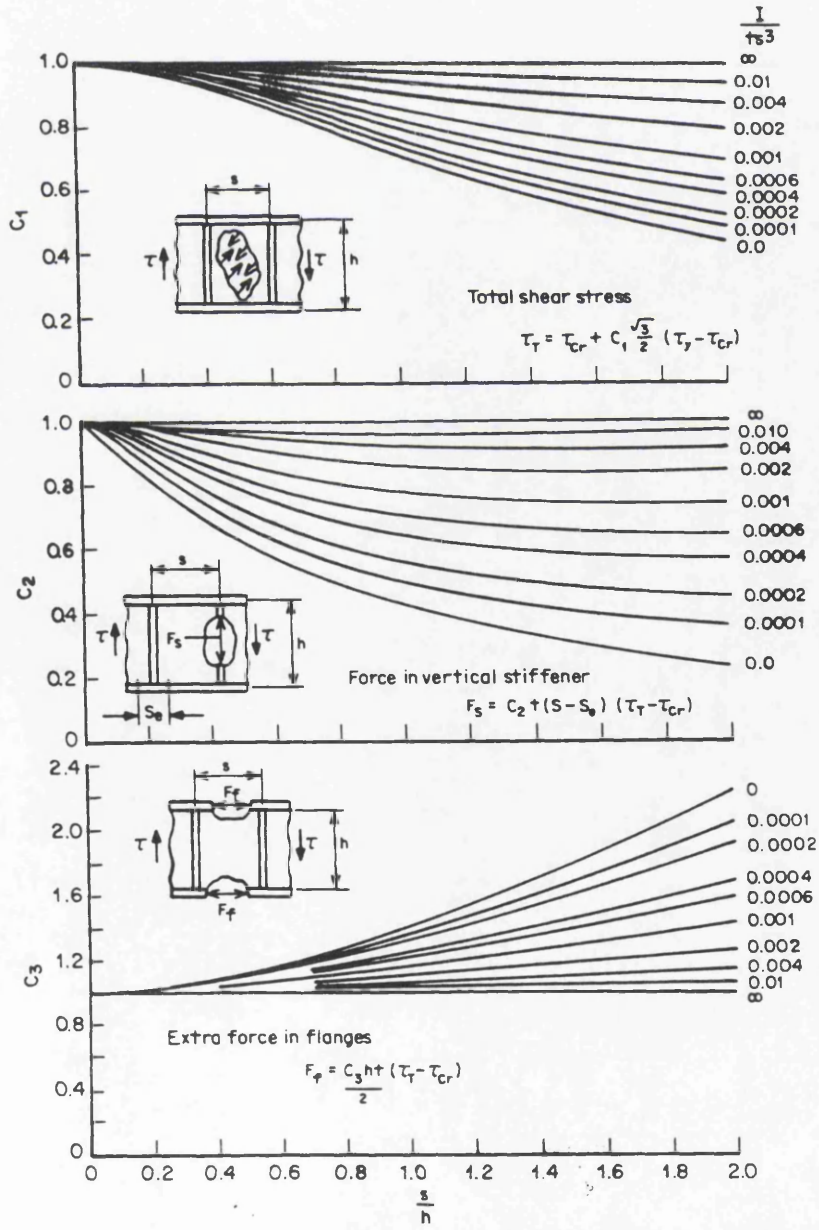

Figure 4.39: Stress coefficients applicable to the design of aluminium girders in the Aluminium Association proposals. I is the

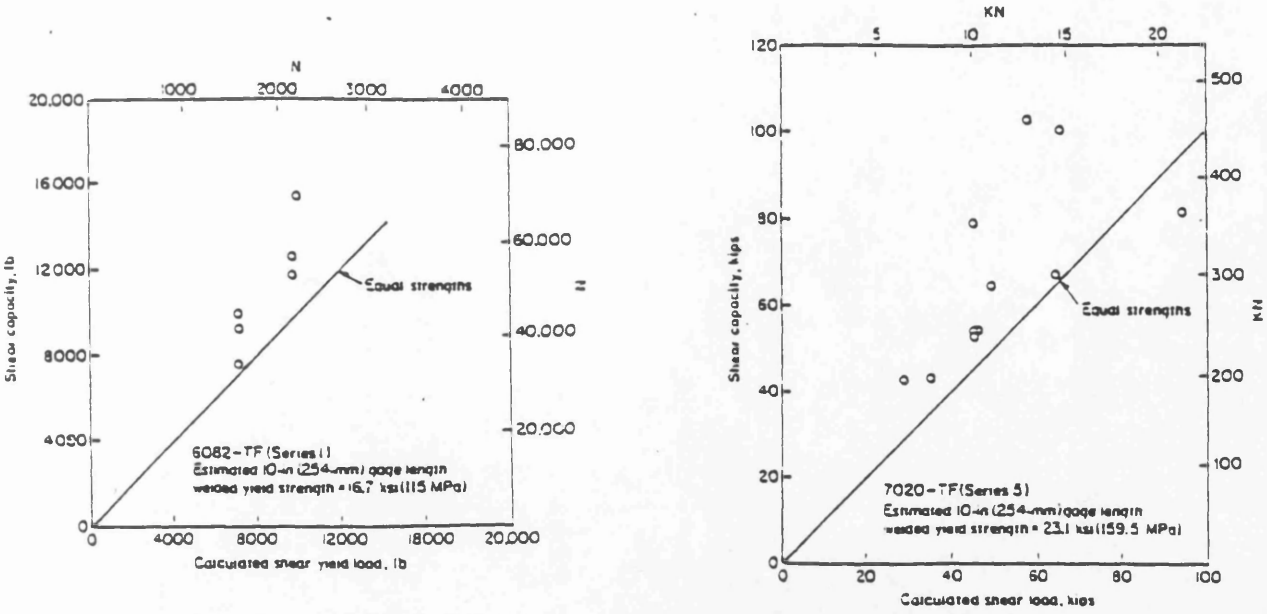

Figure 4.40: **Comparison of the Aluminium Association predictions with welded aluminium girder test results [219].**

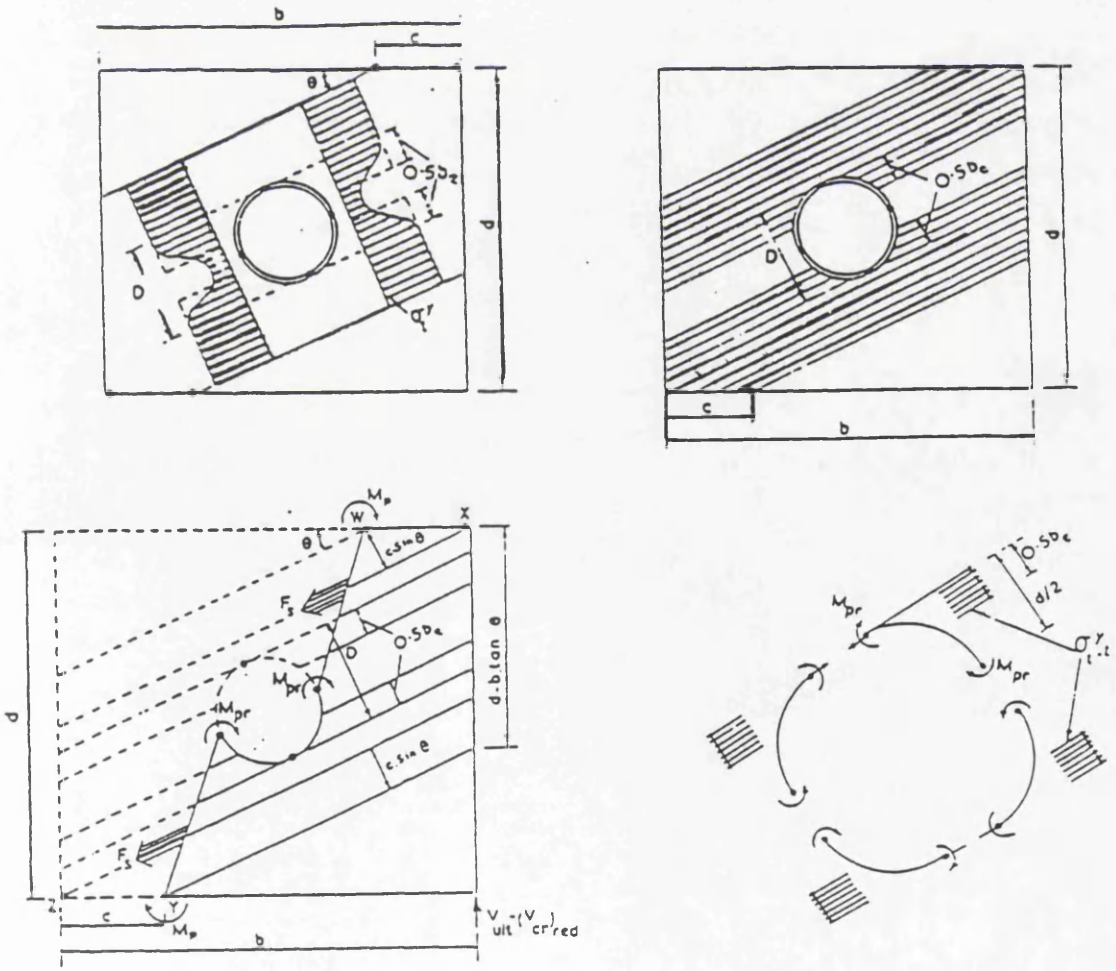

Figure 4.41: **Effective width approach and analysis of the shear ultimate strength of a web plate with centrally located, reinforced cut-out. [223, 226].**

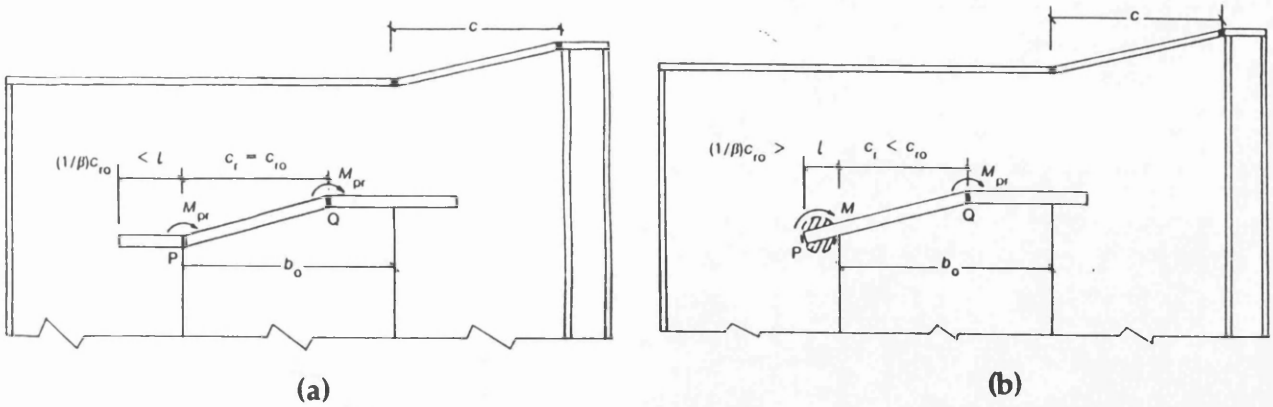

Figure 4.42: **Ultimate strength modelling for a web plate with a rectangular cutout bearing an (a) adequate (b) inadequate reinforcement [223].**

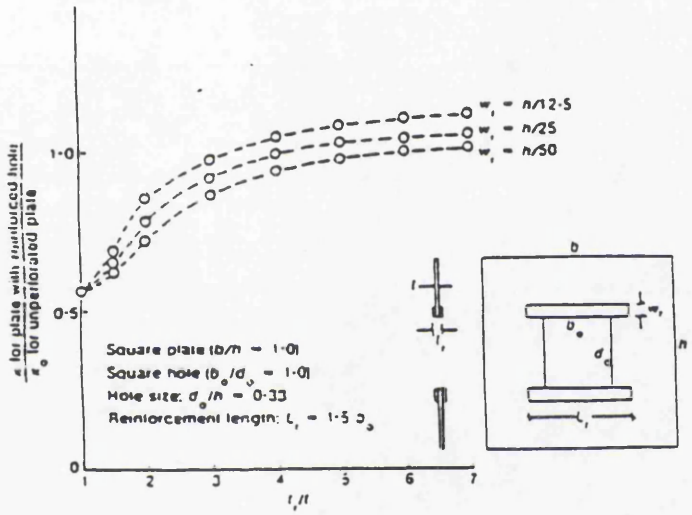

Figure 4.43: **Variation with the thickness and width of the reinforcement, of the critical buckling coefficient for a reinforced rectangular opening [223].**

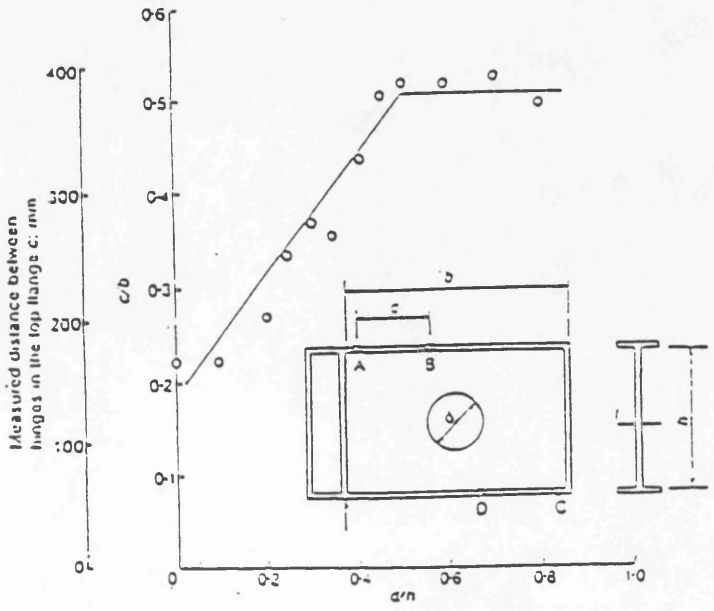

Figure 4.44: **Variation of the flange hinge position with the diameter of a centrally located, circular cutout [228].**

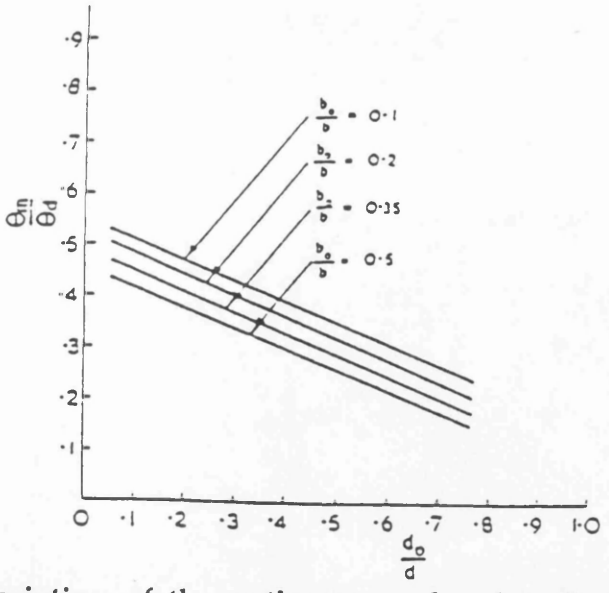

Figure 4.45: **Variation of the optimum angle of inclination of the tension field with the depth of a rectangular cutout [226].**

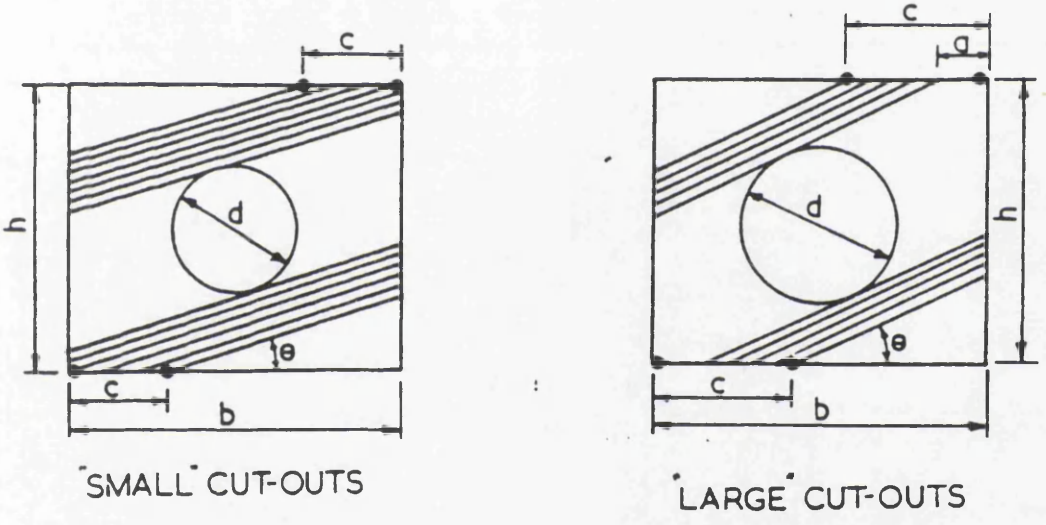

Figure 4.46: **Effect of the cutout size on the plastic hinge positioning on the flanges [235].**

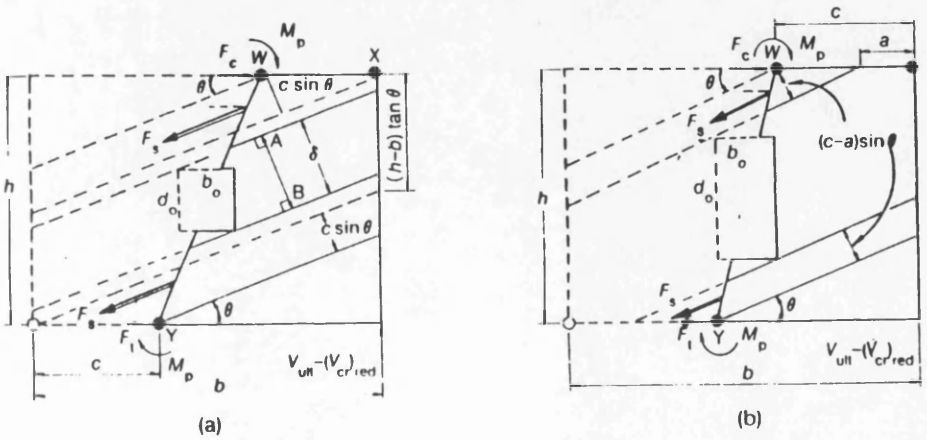

Figure 4.47: **Analytical model for the shear ultimate strength of a web panel containing a centrally located rectangular cutout [232].**

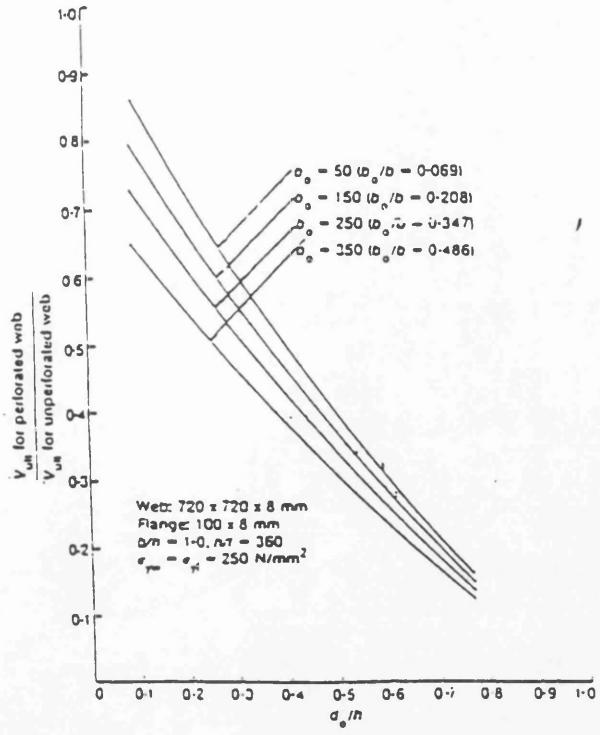

Figure 4.48: **Ultimate strength reduction with the increase in the depth of centrally located, unreinforced, rectangular cutouts on a girder web plate [232].**

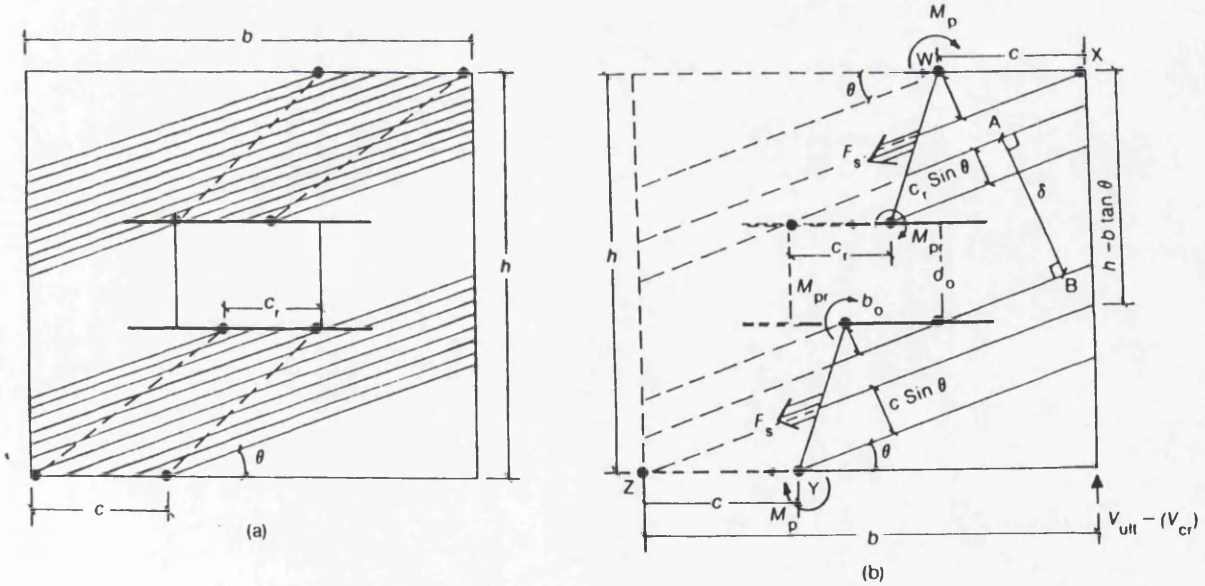

Figure 4.49: **Analytical model for the shear ultimate strength of a web panel containing a centrally located, rectangular, reinforced cutout [223].**

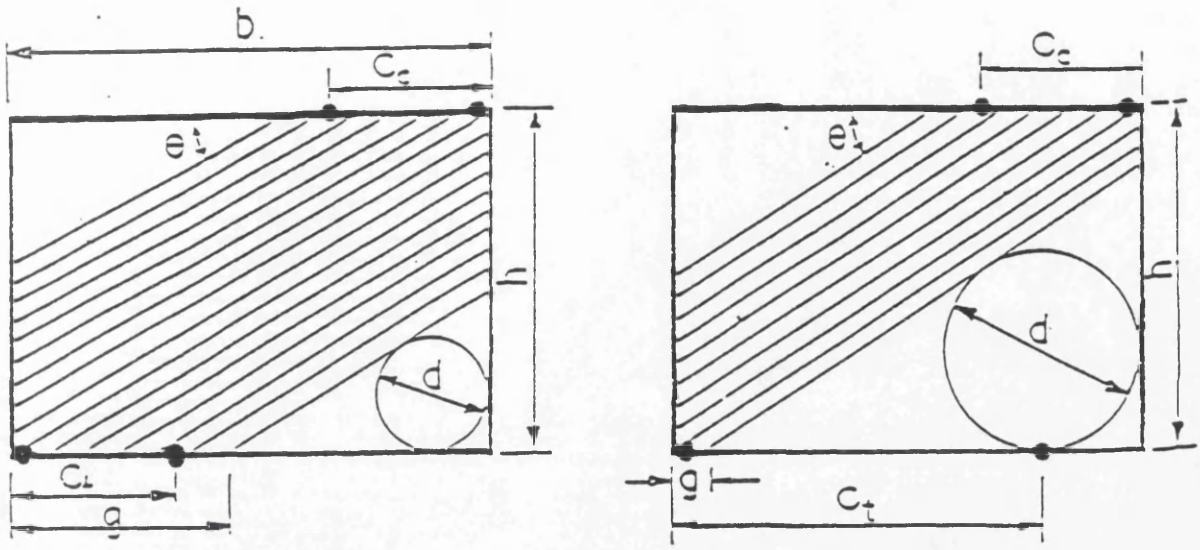

Figure 4.50: Effect of the size of a corner located web perforation on the tension field width and the position of flange plastic hinges [225].

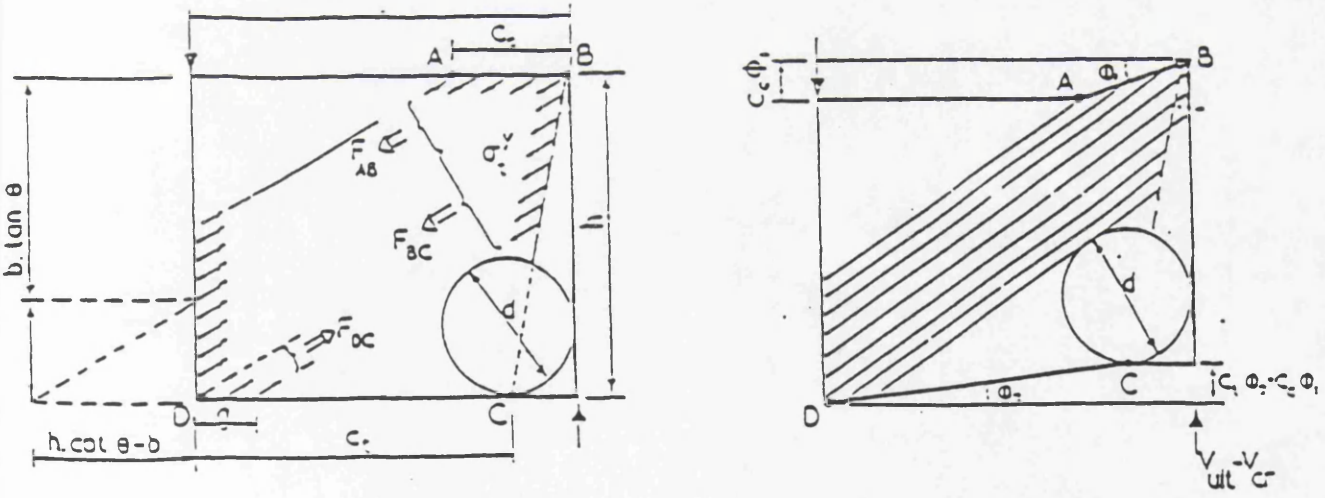

Figure 4.51: Analytical model for the shear ultimate strength of a web panel containing a corner located, circular, unreinforced cutout [225].

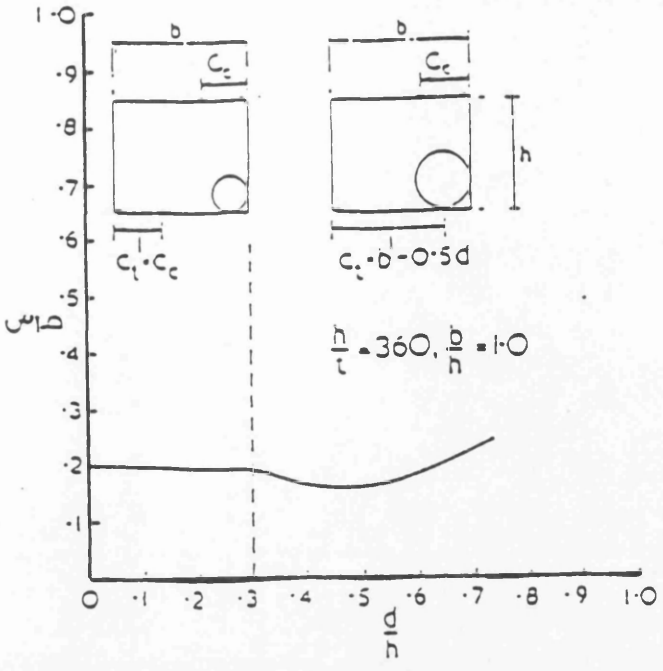

Figure 4.52: **Variation of the flange plastic hinge distances with the diameter of a corner located circular cutout [225].**

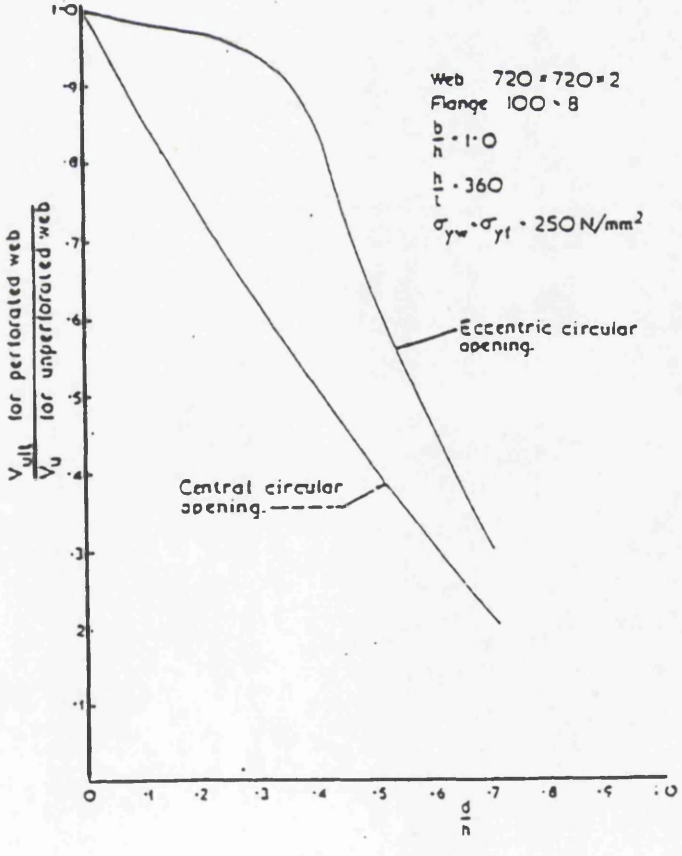

Figure 4.53: **Comparison of the induced reduction in ultimate strength if a circular cutout is placed from an eccentric position on the compression diagonal to a central position on the web plate [225].**

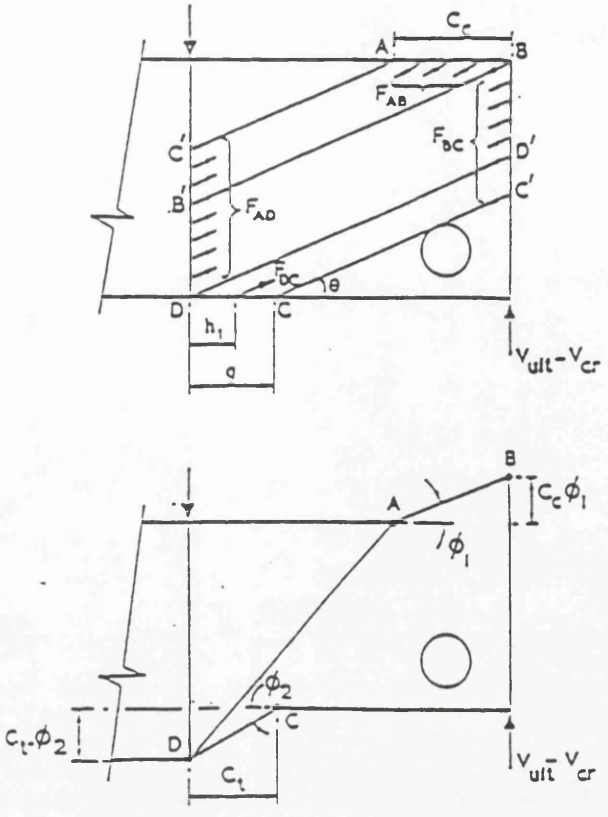

Figure 4.54: **Analytical model for the shear ultimate strength of a web panel containing an eccentrically located, circular, unreinforced cutout [227].**

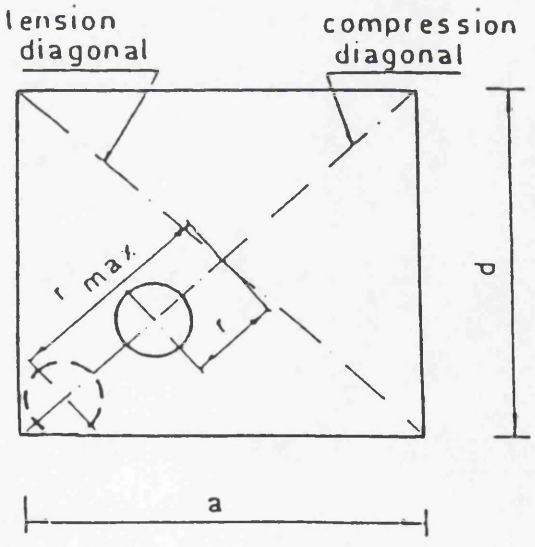

Figure 4.55: **Notation as used in the simplified model accounting for the ultimate strength of eccentrically located cutouts [145].**

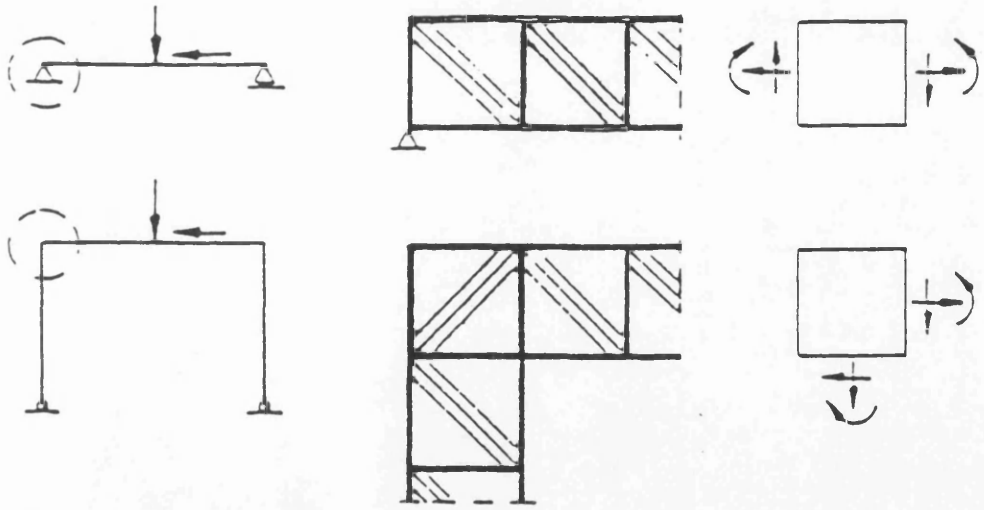

Figure 4.56: Inclination of tension bands and internal forces for knee joints of deep plate girders [242].

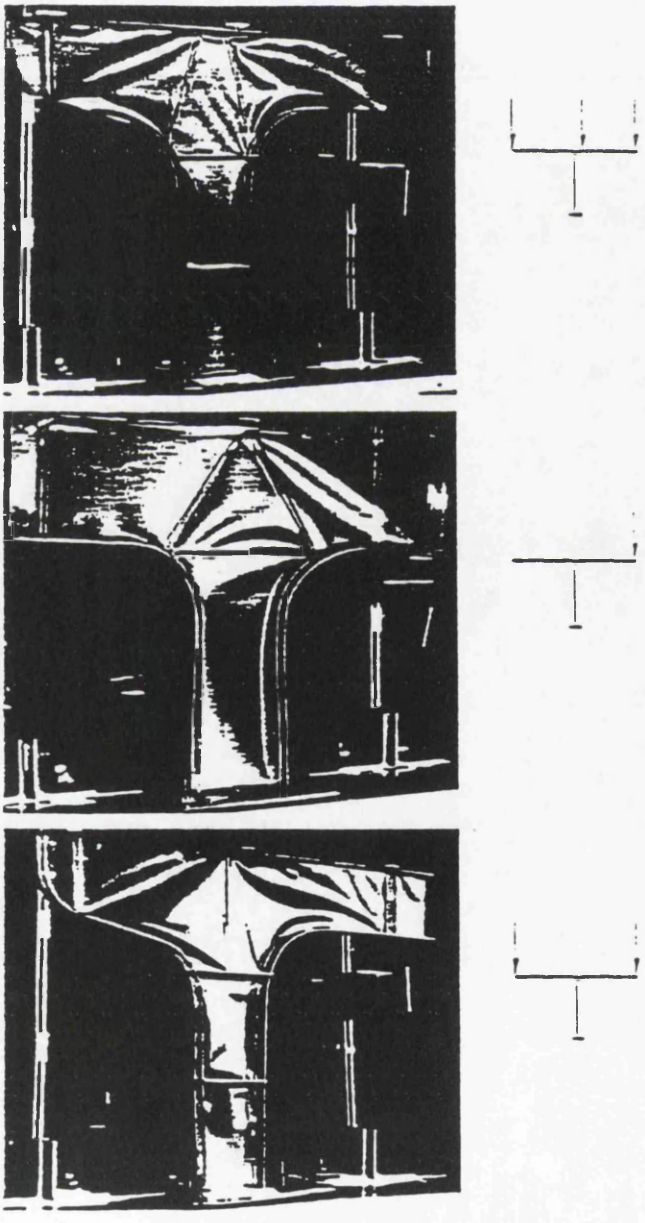

Figure 4.57: Bodarski's experimental investigations [239].

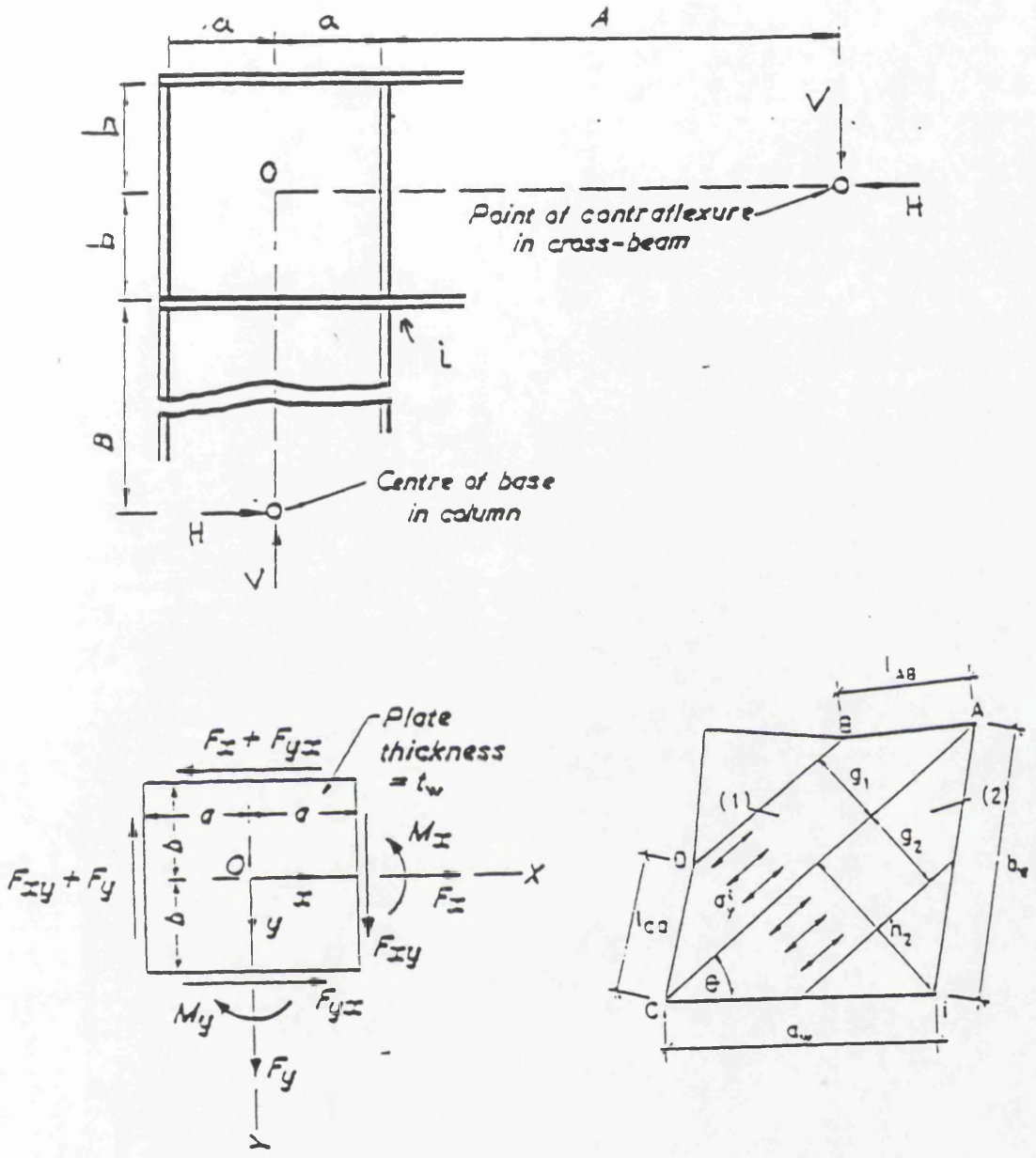

Figure 4.58: **Force, moment distribution on a flat rectangular corner plate and tension field geometry as assumed by Scheer [239].**

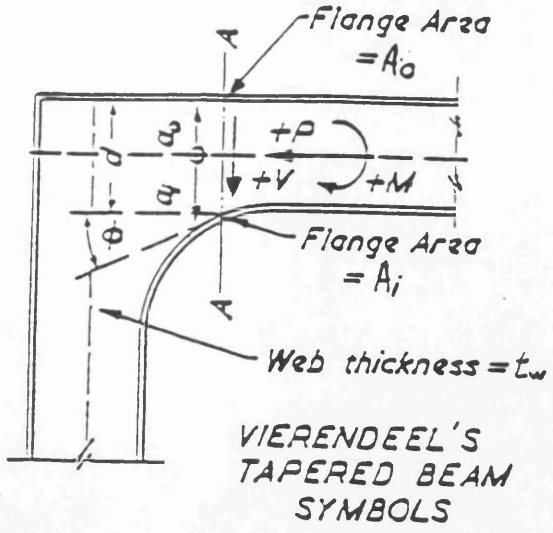

Figure 4.59: Vierendeel's Method [242].

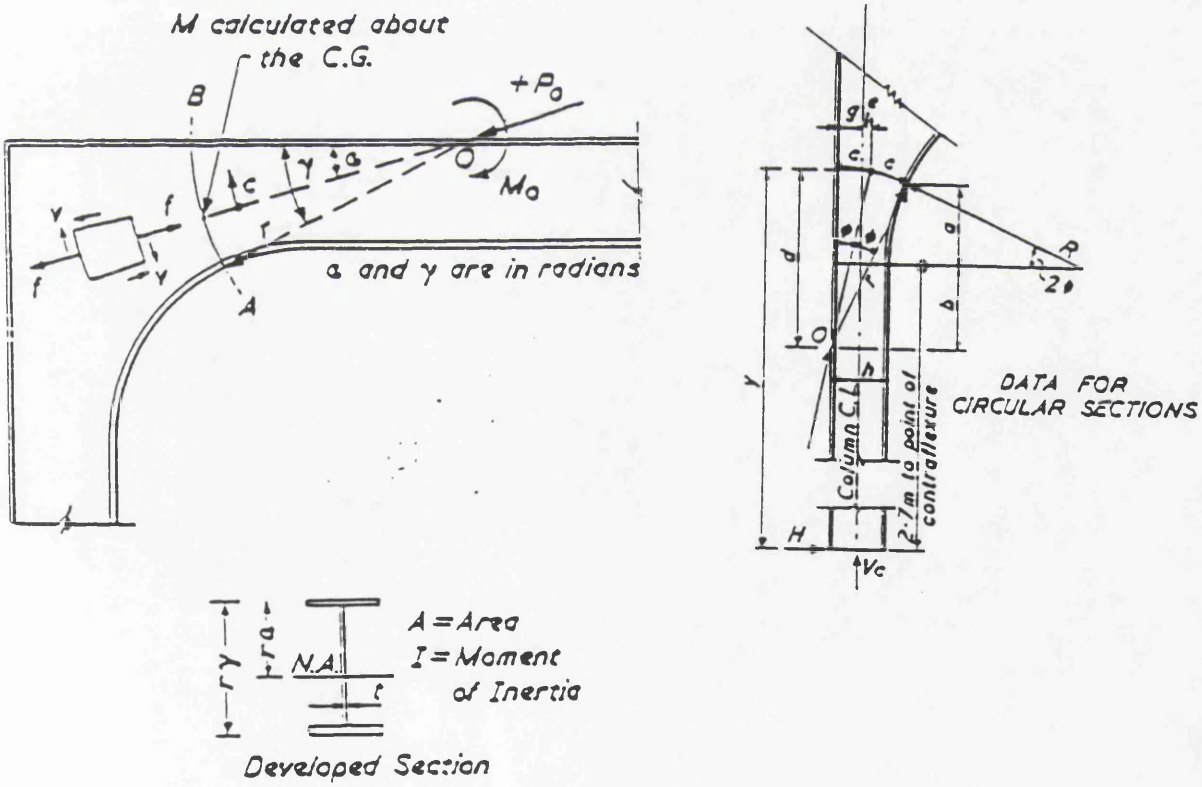

Figure 4.60: Olander's Method [242].

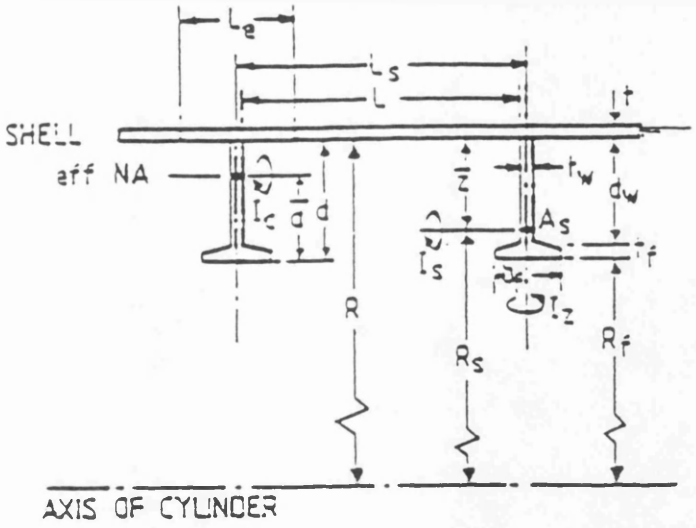

Figure 4.61: Notation of the geometry of ring framed cylinders [256].

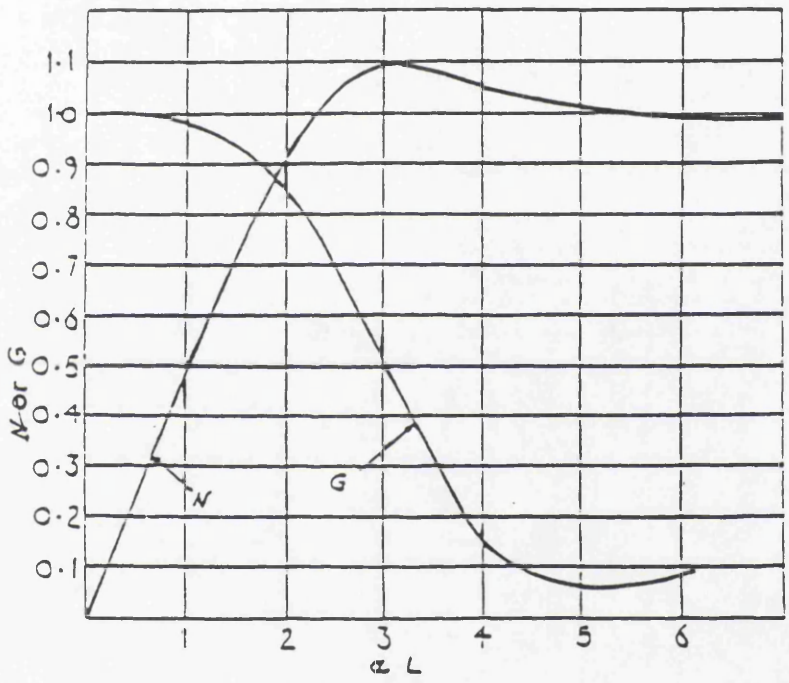

Figure 4.62: Transcendental functions for G and N.

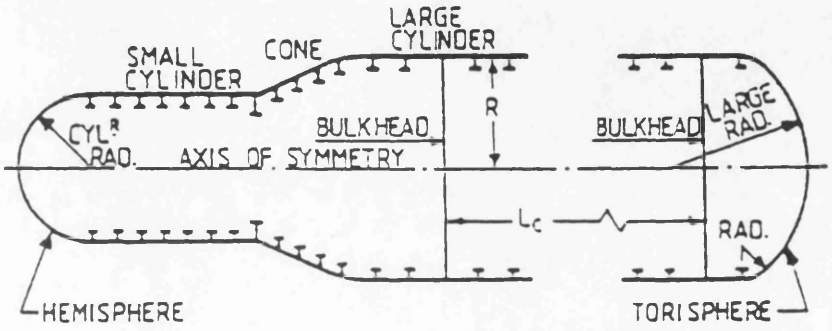

Figure 4.63: Variety of geometrical shapes in underwater hulls [256].

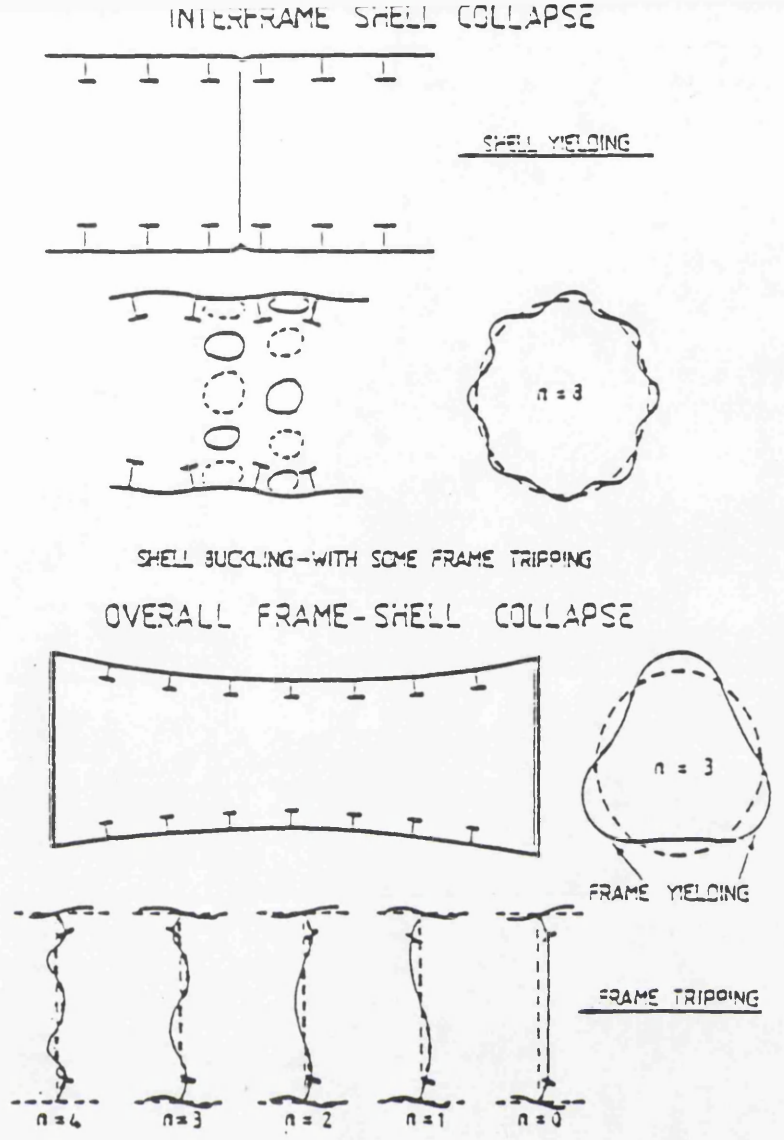

Figure 4.64: **Collapse modes of ring stiffened cylinders under external pressure [162].**

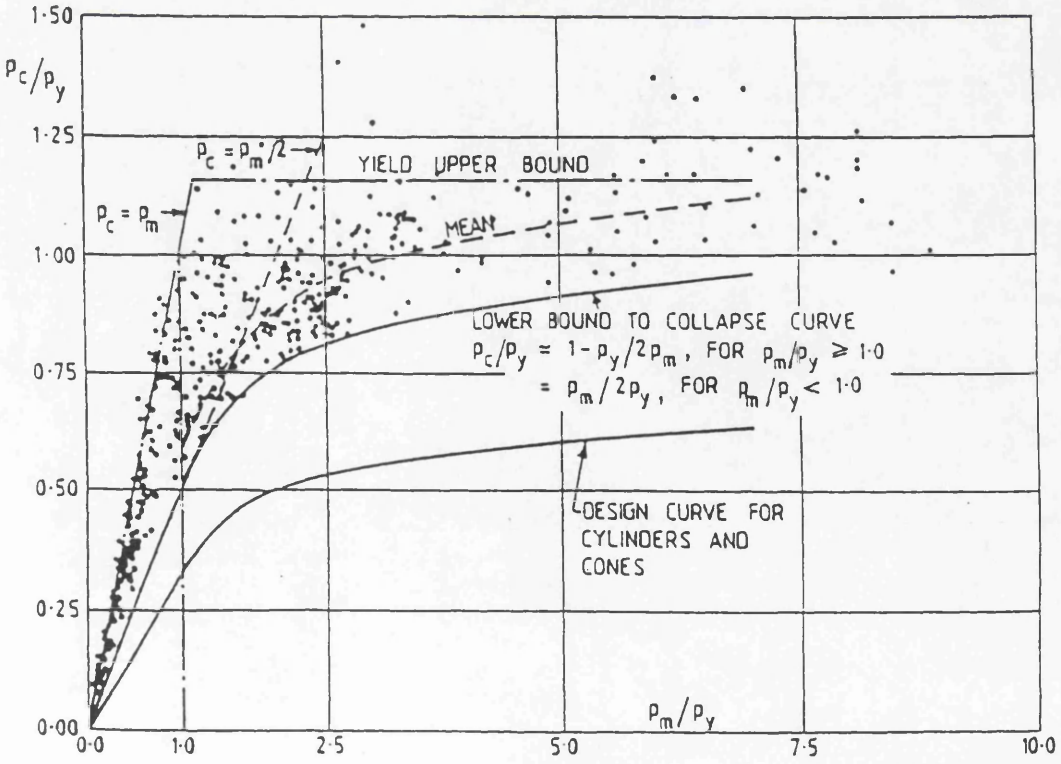

Figure 4.65: **Interframe shell collapse data and BS5500 guidelines [256].**

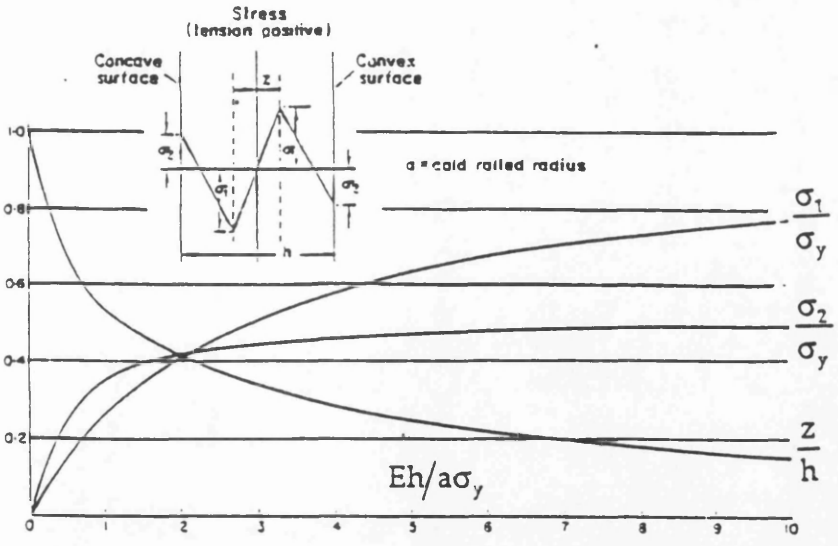

Figure 4.66: Cold-rolling residual stresses in shells [246].

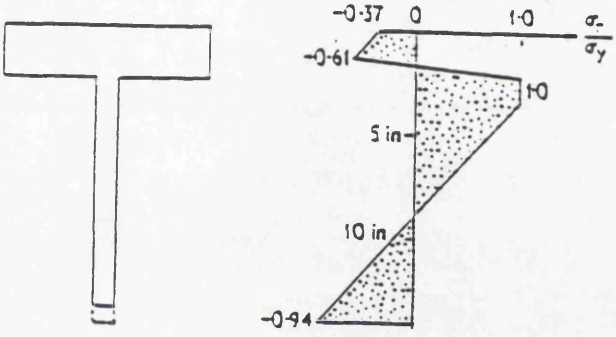

Figure 4.67: Cold bending and hot-rolling residual stresses in frames [7].

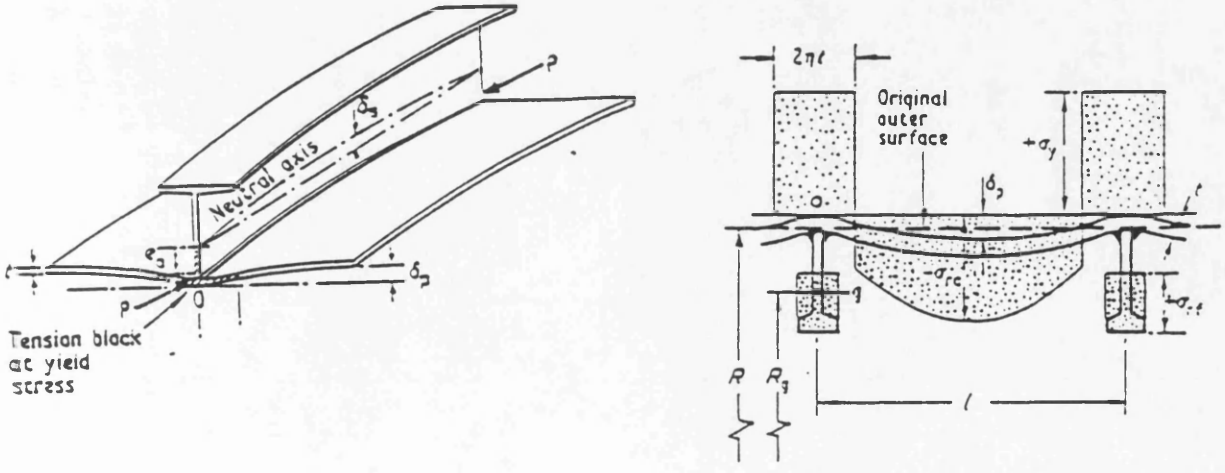

Figure 4.68: Weld shrinkage actions and their stress effects [7].

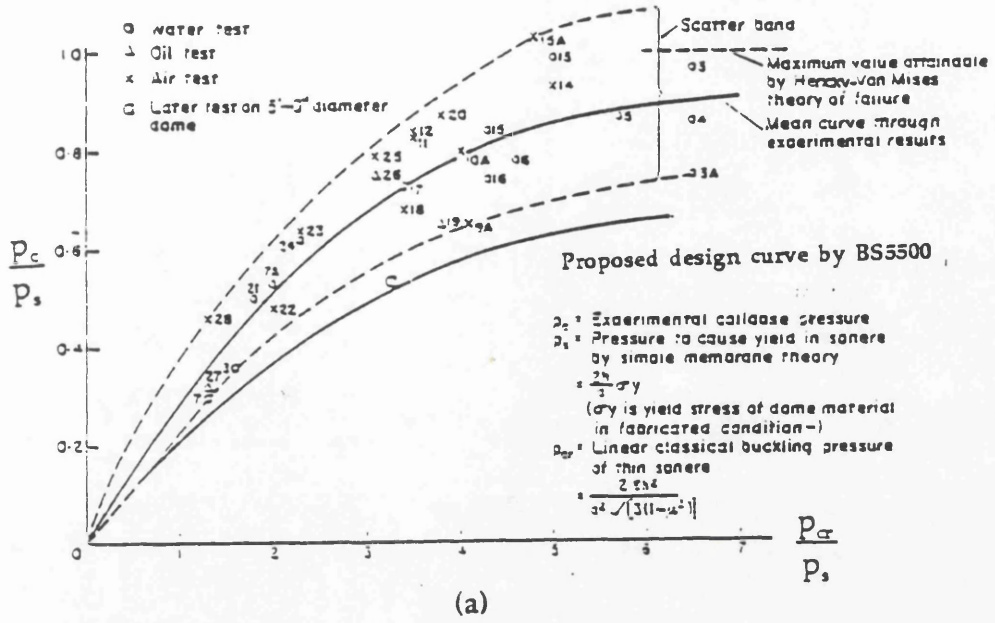

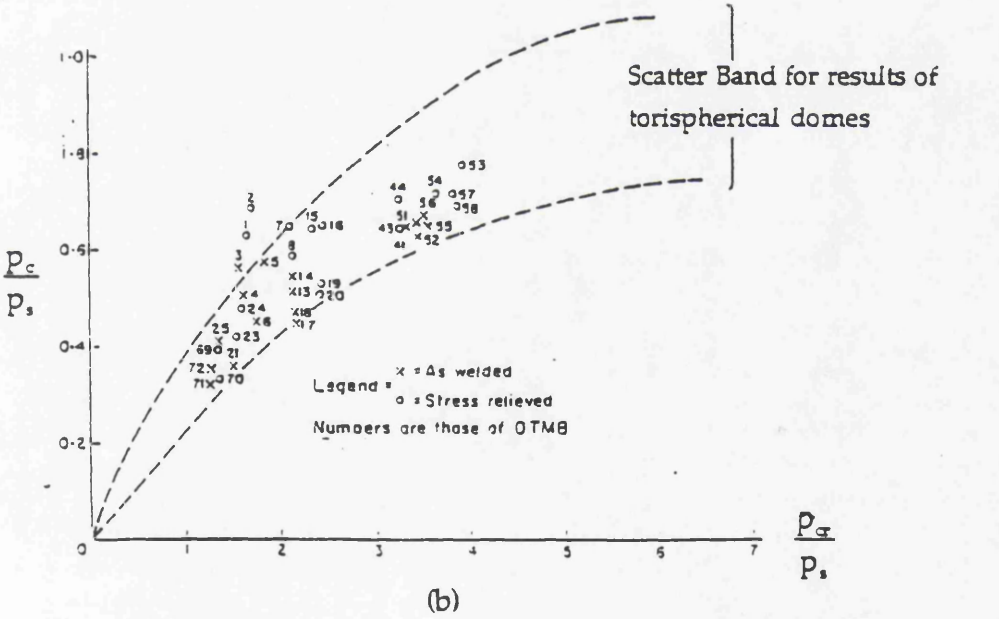

Figure 4.69: **Results of collapse tests on (a) torispherical, (b) hemispherical domes [272].**

CHAPTER 5

5.0 Reliability-Based Multiple Criteria Optimisation of a Fast SWATH Ship

5.1 Introduction

The increasing interest in recent years in fast multi-hull vessels such as catamarans, SWATH and surface effect ships, coupled with the critical weight arising from their relatively small waterplane area and much greater speed requirements, has lead to the need for a more rational approach to their structural design. Improvements in design can be expressed by the availability of reliable and accurate analysis tools, as well as in decision-making techniques both providing the potential of validating new concepts and generating competitive designs. An earlier presentation [1] outlined the main aspects of such a rational procedure by applying it to a simple 2-D FE model of a SWATH structure, the strength criteria based on DNV Classification Note 30.1 and limited to plate failure modes under in-plane compression. In a more recent paper [2],the design formulations were extended to ultimate strength considerations and the optimisation was carried out at component level. The number of components analysed was, however, limited to the cross-deck and cylindrical hulls and the analysis for the cross-deck was eventually of a deterministic nature due to unforeseen problems in the development of the computer code. The same load actions were used, as in the previous application [3].

This chapter brings together, under a global reliability-based optimisation procedure, all the main structural elements of a section of a SWATH ship, namely the cross-deck web frame structure, flat stiffened panels in the wet deck, haunch, the waterplane struts and finally the submerged cylindrical hulls (Fig. 5.1). Ultimate strength limit state modelling is used throughout. Hence, cross-deck design is based on the tension field approach to the design of deep web plate girders under shear, bending and combined loads and inclusive of the effects of lightening holes on strength. Flat stiffened panel behaviour is checked against stiffener tripping, interframe collapse and excessive stressing of the plating under lateral pressure loads. The submerged hulls are checked only against bay instability. Statistically, these failure modes are treated independently and adequate properties for the corresponding modelling uncertainty factors are based on comparisons with experimental information collected from the open literature. The safety

check for the individual failure modes is carried out using AFOSM reliability methods. For the system reliability, Ditlevsen bounds are used.

Design optimisation is achieved by filtering efficient (non-dominated) solutions obtained via sequential random generation of designs in the feasible design region. Final selection is performed by a goal programming approach which accounts for the designer's preferences. It was the structural weight, cost and minimum safety (reliability index) that were considered as design attributes. Aluminium alloy material, as well as realistic fabrication constraints, are incorporated in the analysis. The global design model was run on a RISC workstation connected to a Meiko supercomputing surface for parallel processing. The results are discussed and compared with actual design values of a SWATH in operation, and design alternatives with minimised weight and cost are presented. It is shown that cost, weight and safety can be included in the design process straight from the design concept level, as opposed to the current minimum weight design approaches.

5.2 The Optimisation Routine

The requirement in any design optimisation process is that, the final optimised design should satisfy a large and often conflicting number of limit state criteria, for a number of structural configurations being acted upon a variety of load combinations. The variety of types and conflicts in the requirements in such a process forms a fertile ground for the use of multiple criteria decision making techniques [4].

5.2.1 The Analysis versus the Design Approach

Each design option is identified as a point in the NV-dimensional design space X (Fig. 5.2), and its co-ordinates (design point) represent an individual set of the design variables under consideration. NV is the number of design variables (paras. 5.3, 5.5). Every design option can also be considered as a point in the NA-dimensional attribute space Y, NA being this time the number of design attributes (para. 5.6.3). Linear constraints (para. 5.6.1) limit the design space X to a subspace (of X) consisting only of feasible designs fit for analysis. Subsequent mapping of the design space X on to the attribute Y space (i.e. the *evaluation process*) corresponds to the calculation of the attribute function values for every individual set of design variables representing feasible designs. The reverse process is known as *design*.

The main difficulty that arises in establishing the design variables during the *design process*, given a set of design attributes, is the frequent requirement to solve non-linear equations which require the application of sophisticated convergence checks and/or linearisation methods. It would obviously be a lot simpler to choose randomly a large number of sets of design variables, establish the values of the design attribute functions, and hence choose the set of variables that satisfies most closely the designer's requirements. The only difficulty presented by this approach is that a very large number of designs will have to be chosen and tried individually on the functional criteria (e.g. ultimate strength formulations, attribute functions, etc.) before a final choice is made. The development of computer hardware, and availability of parallel processing with increased computational speed, make the substitution of the design process by a large number of evaluation processes worthwhile, in addition to permitting the use of more complex, and potentially more accurate, strength analysis functions. An additional advantage of such an 'analysis' approach is that the design procedure only requires a comparison of competing designs and therefore relative and not absolute values of design attributes are sufficient.

5.2.2 The Design Methodology

The design method used herein for structural design of the example SWATH ship (para. 5.3) consists of four main stages:

1. a stage for the *specification* of design variables (para. 5.3) and definition of the design goals (minimisation, maximisation)
2. a *synthesis stage*, generating designs in the feasible region of the design space. It is important that a sufficiently large set of designs is generated so that a reasonable number of them filters through to the next stage.
3. an *analysis stage* containing:
   (a) the definition of the design loads and consequent structural response estimation via FE modelling (para. 5.4)
   (b) a safety check against a library of serviceability and limit state failure modes (design criteria - para. 5.6.2)
   (c) the reliability analysis (para. 5.7)
   (d) the estimation of the attribute function values (para. 5.6.3).
4. *a selection stage* at which the choice among the non-dominated preferred solutions is made by means of some ranking technique.

Non-dominated solutions are those that correspond to designs which are better than any other feasible design in at least one objective, while the *preferred solution* is that selected from the non-dominated designs when the designer's preferences are introduced in the process. This is possible via the use of multiple criteria decision making techniques such as lexicographic ordering, value or utility function construction or goal seeking [5]. *Filtering of non-dominated designs* among feasible ones is performed with the simple 'more is better' dominance structure (Pareto dominance), a very efficient dominance algorithm according to Zanic et al [5]. These non-dominated solutions are then used for the generation of further non-dominated designs in a more concentrated region of the design space (adaptive random generation of further nondominated designs) which is then fed into a goal programming routine reflecting the designer's preferences with respect to the set of attributes.

These designer preferences are identified by the program as *inter-* and *intra-attribute preferences* and are treated separately. *Inter-attribute preference* refers to the relative importance of different attributes and is expressed in the form of weight factors [5]. The scale of comparison ranges from the case of 'equal importance of both attributes' to the case of 'absolute preference of one attribute over the other' (scale 1-9). *Intra-attribute preference* refers to preference within one attribute and is imposed on the process once a set of feasible designs has 'filtered' through the safety checks. A grading function is then defined for this set to express the designer's preference with respect to the attribute value. A more detailed description is provided in [6]. The analysis of the attribute space in search of the optimal solution is further facilitated by the graphic capabilities available by the program. This capability renders the process highly subjective as it encourages the specification of differing goals in the analysis, the modification and ranking of the designer's preferences thus allowing the designer's experience to filter through into the design process. The graphic capabilities provide the designer with some insight into the multi-dimensional design and/or the attribute space enabling:

- the inspection of the positions of maxima/minima of the attributes and the identification of any inherent penalties for departing from the optimum solution

- a better understanding of the design and attribute spaces (e,g. trends, ranges, 'good' points, multiple peaks, etc.)
- the identification of those design variables that lead to favourable attribute values and to reduction in the design space size.

More of the functional capabilities of the optimisation computer code/routine can be obtained from [1, 5]. The remaining part of this chapter will describe very briefly the characteristics of the computer program written by the author to provide the library of ultimate strength and serviceability constraints, as well as the stages in the process and the underlying assumptions as to the decisions taken in the reliability based optimisation of a specific SWATH structure.

It is perhaps worth mentioning that the whole procedure, due to the speed required and the complexity of calculation (over 25000 statements of optimisation code and 20000 statements of analytical modelling), was located on the transputer based 'computing surface' with 25 processors in parallel work at Glasgow University. The modular nature of the optimisation routine, and the interaction between the calculation modules, are described briefly in [1]. The development of the optimisation software used, and its adjustment into a parallel processing environment, was carried out at Zagreb University during 1990-92 by Professor Vedran Zanic and his collaborators, and was made available for this work during a research collaboration between Glasgow and Zagreb during the period 1992-93 under funding from the Joint Research Centre of the Commission of the European Union.

5.3 Application of the Optimisation Process to the Design Particulars of the Example Ship

FBM Marine's MV PATRIA, with particulars as shown in Table 5.1, was used as the design example case for application of the optimisation method. The structure is made of two aluminium alloys, the 6082 and 5083. The extruded sections (bulkhead plating, deck plating, side plating, haunch and strut) were constructed of the 6082-T6 heat-treated alloy, while the remainder of the structure (shell plating, constructed sections and deep frames) was made of the work-hardened 5083-H116 alloy which, being work hardened, also suffers from HAZ softening effects (para. 4.1.2, Chapter 4). The material characteristics considered are therefore as follows:

	Parent Proof Stress (N/mm^2)			Factor for HAZ Strength Reduction
	Tension	Comp.	Shear	
6082-T6	255	255	155	0.5
5083-H116	215	180	130	0.45

The main structural elements of the vessel are the cross-deck web frame structure, flat stiffened panels in the wet deck and haunch, waterplane struts and the submerged hulls (Table 5.2 and Figs. 5.1, 5.10). The frame spacing was 1250 mm throughout. The upper and wet decks are made from 4 mm aluminium extrusions which incorporate T-section longitudinals spaced 333 mm apart. Between frames and bulkheads are two transverse stiffeners of aluminium bulb sections 76 mm deep, extending in the cross-deck box to just outboard of the haunch where they discontinue. The cross-deck deep plate girders are constructed of 4 mm plating, with vertical stiffeners (40x5 flat bars) positioned 1000 mm apart, the subpanels thus identified carrying 400 mm diameter perforations. Furthermore, the haunches and struts are constructed of 6 mm extruded planking also carrying T-section longitudinals spaced 333 mm apart. Framing in the haunch and struts consists of extruded T-sections (200x6/75x10) over their complete lengths. The lower hulls are constructed of 6 mm shell, stiffened with fabricated T sections (200x5/75x10) and aluminium bulb sections 76 mm deep as longitudinals stiffeners.

For analysis, each of the structural elements is allocated its own set of design variables introduced as input and which may be categorised as follows:

(a) *Material properties* which consist of Young's modulus, material yield stress, type of material (steel or aluminium), type of alloy if the material is aluminium, Poisson's ratio, and density. Different materials (alloys or even type of material) can be allocated to each of the five structural elements, although the structural components of each of these elements must be of the same material. The term 'yield stress' implies either the yield stress of the material in the cases where steel is considered, or 0.2% proof stress in the case where an aluminium alloy is used instead. The

magnitude and extent of HAZ reduction effects for aluminium alloys are taken as recommended in BS 8118 (para. 4.1.2).

(b) *Stiffener specifications* in the longitudinal and transverse direction which consist of the type of profile (e.g. flat bar, bulb flat, angle, Tees), the dimensions of the web and flanges, the depth of the stiffener and the area of the bulb flange (if the stiffener is a bulb-flat). Each structural component may have a different type of stiffener in the transverse direction from that in the longitudinal direction (e.g flat bars intersecting Tees, etc.) and such a case is accommodated by the program.

(c) *Global dimensions* identifying the main structural components. These are the depth and width of the stiffened plating of the strut (1650 mm/1250 mm) and haunch (1900 mm/1250 mm), diameter of the underwater hulls (1800 mm), depth of cross-deck web (1000 mm), frame spacing (1250 mm), length of the cross-deck (14000 mm) and the length of the assumed corner joint (3000 mm). Similarity in structural arrangements and dimensions exists and is assumed (during optimisation) between the wet and main decks and the inner and outer parts of the haunch and the struts.

(d) *Secondary dimensions and variables* of those elements of the main structural components against which the safety checks will be carried out. This category consists of the number of stiffeners (and hence stiffener spacing) in both the global longitudinal and transverse directions, which identify both the stiffener lengths and the aspect ratios of flat plating on the:

- decks (2 longitudinals on the flanges over the distance identified by the vertical stiffeners of the girder web and 2 transverse stiffeners over the frame spacing distance)
- haunch (5 longitudinals and no vertical framing between any two adjacent frames)
- strut (4 longitudinals and no vertical framing between any two adjacent frames).

The number of vertical (6) and longitudinal stiffeners (0) on the web of the cross-deck may also be placed in this category. The optimisation routine and its random generator provide real numbers with decimal places as input values to the design variable, which is non-realistic when the design

variables represent the number of stiffeners! Hence, these numbers were rounded down to the nearest integer, an action that considerably delayed the execution of the process.

The indication of the presence on the web plates of the cross-deck of any perforations and their diameter/effective diameter (400 mm), as well as the number of frames between watertight bulkheads, is important additional input. The thicknesses of the plating on the individual decks (4 mm), struts (6 mm) haunch (6 mm), cylindrical shells (6 mm) and of the cross-deck web (4 mm), also require identification.

(e) *The number and identification of the normal and log-normal variables* assumed in the reliability analysis for each structural element (para. 5.7).

(f) *The load fields* acting at the edges of each of the main structural components. The maximum value of these stress fields is assumed for simplicity and conservatism to apply throughout the structural element and thus any diffusion of loads in the structure is neglected. Hence *for every structural element*, a set of the global longitudinal and transverse in-plane compressive loads, the shear loads, and the lateral pressure loads (identified by the response analysis of the structure (para. 5.4) and consequent FE analysis) is applied on each of the structural sub-elements for the safety checks. Uniform pressure load distribution was assumed on all flat plating coming into contact with the seaway and in-phase action of the maximum side force, and pressure loads was considered unlikely [1, 2] and thus neglected. The same pressure load value (0.055 N/mm^2) was used for the wet decks, hydrostatic pressure for cylindrical hull design, haunch and struts. The magnitudes of the loads are identified separately from the FE estimation, depending on their source (i.e. on whether the loads are due to pure compression or bending) and then superimposed for application on the structural elements. Although buckling analysis is carried out in the structure, no tensile checks are undertaken, therefore any global tension loads are neglected. The mean and COV values of the assumed loads are provided in paragraph 5.7.

(g) *Miscellaneous input* which mainly consists of controlling flag points introducing the designer's preferences on the procedures finally used, giving a choice on the serviceability criterion for plates under lateral

pressure (elastic, elastoplastic or fully plastic design). The designer can also prescribe a different design procedure (against lateral pressure load) for the plates on the main, against those on the wet decks, the strut and the haunch, but in the current application elastoplastic design was adopted for all plating, irrespective of global position. Additional input in this group is

- the dimensions of the haunch framing had to be introduced from the input file as these were not included in the optimisation procedure (and hence not randomly selected by the code)

- the dimensions of the transverse (in the global direction) bulb-flat stiffeners on the main and wet decks are also not optimised and their dimensions are also introduced from the input data file

- the designer's preferences on the extent of the residual stress in the plating, η, and on the preferred proportional limit to the material yield stress ratio, p_r. Separate values of p_r are allowed for by the program in accounting for inelastic effects for interframe collapse and tripping failure of the stiffeners. The current application has opted for a p_r value of 0.5 while η was taken equal to 3

- the coefficients controlling the stiffener spacing of flat plate elements and the relative depths of intersecting stiffeners, C_1 and C_2 respectively (para. 5.6.1). These are separately set for the decks, the haunch and the struts

- the designer's preferences when checking against stiffener tripping failure. The choice is available between Faulkner's approach (with rotational restraint at the web toe but no web deformation) or to neglect any rotational restraint at the web toe, or to use Adamchack's approach (limited rotational restraint neglecting any destabilisation of the stiffener by the plate but inclusive of web deformations). The current example uses Faulkner's procedure.

Of all the aforementioned variables, the ones finally optimised are shown in Table 5.3 including their mean and COV values. Further details on the distribution and COV values for the non-optimised design variables may be obtained from paragraph 5.7.

5.4 Load Estimation and Structural Response

The wave induced loads and motion responses were calculated by Pu [3, 7] using MARCHS [9, 10], a 3-dimensional oscillating source potential theory program coupled with a cross-flow approach to account for viscous damping effects (para. 2.1.3.3, Chapter 2). The inertial and hydrodynamic forces (weight, inertia and drag forces (Morison), the dynamic pressure forces (Froude-Krylov) and the diffraction forces) were calculated at mid-depth of the longitudinal plane through the centreline (Fig. 5.3) of the ship.

For the spectral analysis of motion response, loads, as well as pressure distribution on the submerged part of the hull, Pu opted for a short term extreme value prediction approach on grounds of simplicity. Methods for long term load predictions are presented in Chapter 2. In the spectral analysis, the Pierson-Moskowitz spectrum was adopted describing North Atlantic sea conditions with a design wave height of 3 m for a 6-hour sea assumed. The wind speed assumed for this specific wave height was 24 knots for use in the spectrum. The variation of wind speed with assumed wave height may be obtained from [11].

The motion responses of the ship were calculated at five headings (0°, 45°, 90°, 135° and 180°) for zero ship speed [3]. Table 5.4 presents the results for the *side force* and *induced bending moment* on the cross structure (as obtained by Pu [7]) for the 'most probable extreme value' (α=1), the 'extreme values with 1% probability of exceedence during one sea state' (α=0.01), and the design extreme value, assuming the structure encounters the same sea state 10 times in its lifetime (α=0.001). For the determination of the extreme loads Ochi's relevant formulations (para. 2.2.1.2, Chapter 2) were used.

According to Pu [7] (Table 5.4) the level of side force in beam seas (2,180 kN) was found to be the largest and in good agreement with FBM Marine's design value of 2,030 kN (Fig. 5.4). Similar agreement was observed for the theoretical value of maximum transverse bending moment (7,980 kNm) applied on the transverse frame (at the centreline transverse position) with the result of the 2-D FE analysis (8,130 kNm) later obtained. In turn, the yaw splitting moment in bow quartering seas (Table 5.4) was found [7] to be 6.9 times greater than that corresponding to beam seas. This large difference, when compared to the difference (reverse) between the magnitude of the side force in beam seas (2.76 times greater than), and that for the bow

quartering sea, supports the view that the load combination in bow quartering seas could be as important, or even more important, from any load combination in beam seas. However, in this study the beam sea load effects were only considered.

The pressure distribution on the circumference of the submerged hulls and wetted part of the struts, due to the wave induced side force, is a necessary load input for use in both 3-D and 2-D FE analyses. To obtain this distribution it was assumed [7] that a regular wave acts in the transverse direction, whose frequency and amplitude will result in the same extreme load as that estimated from short-term statistics. The resulting equivalent regular wave had a period of 5.236 and 1.25 m amplitude [7] and the resulting pressure distribution at a number of points on a section at the centre of gravity of the structure (6.8 metres aft of amidship) is shown in Figure 5.5. Such 'sectional' pressure distributions were also obtained at an additional 10 positions along the length of the hull, thus permitting the estimation of the longitudinal distribution of the hydrodynamic force, another necessary input to any global FE analysis. It is worth noting that the longitudinal distribution was found by Pu to be of a sinusoidal nature (Fig. 5.6) with the maximum value occurring at amidships of 56 kN/m. This value is approximately 1.5 times greater than the average value of 36 kN/m that would be obtained from Sikora's method [12] (uniform side load distribution with 10% increase, when applied locally) thus highlighting the sensitivity of such an assumption on the global underwater ship geometry.

The estimation of *inertial forces* requires the calculation of the vertical and roll accelerations. Pu carried out his investigations at three sections along the example ship placed at the centre of gravity and the fore and aft perpendiculars. It was shown that the largest *vertical acceleration* occurred at the aft perpendicular in following seas (0.38g) in contrast to the vertical acceleration due to beam sea response found to occur at the fore perpendicular (0.24g). The *roll accelerations* were found to be approximately equal to 0.1g and not varying significantly between the beam seas and other headings.

The buoyancy value used in the structural analysis was calculated at a mean draught of 2.7 metres and was taken equal to 169 tonnes. In addition, the design slamming pressure load was calculated according to the ABS Rules [13] and was found [1] to be 37.7 psi (=0.26 N/mm^2).

In determining the *response of the structure,* the level of shear lag resulting in the cross-deck, haunch and strut elements had to be established. The classical types of analysis are inadequate and one should resort to a costly and time consuming 3-D FE analysis to obtain the average field stresses which would act as the load input to the ultimate strength checks on the individual main structural components.

This analysis for the particular example ship was carried out by Pu and is fully reported in [3, 14]. The investigation also aimed at establishing the relative accuracy of stress estimations obtained by 3-D, 2-D and 1-D FE analyses to see if one of the latter two could substitute as a viable and accurate alternative to the inefficient 3-D analysis.

The 3-D mesh considered a transverse section of the hull of 5000 mm in length (approximately 1/7 of the length overall) (Fig. 5.7) consisting of 4 deep web frames spaced at 1250 mm apart and a central bulkhead. The total side force of 2.03 MN, calculated using the loading program [7, 10], was proportioned and applied uniformly and longitudinally on the lower hull at mid-draught. This analysis concluded that the transverse bending stress distributions *at a frame across the upper and wet decks* were found approximately uniform inboard of the haunch (Fig. 5.8a and 5.8b), while the peak in the upper deck stress occurs at the junction of cross-structure and inner haunch, and is attributed to the stiffness loss occurring on the deck due to the intermediate transverse stiffeners ending there. The stress then decreases, moving outboard towards the side shell. A similar pattern was observed for the deck stresses (in the global transverse direction) at the bulkhead positions with slightly higher stress magnitude occurring relative to that obtained at the frame positions. The resulting stress loads at the individual elements of the structure are presented in Table 5.8.

From the distributions of transverse stresses *along the top deck* the level of shear lag between the transverse frames and the transverse bulkhead was established. Shear lag was found to be less dominant (close to unity) inboard of the haunch (along the cross-deck), while just outboard of the haunch the effective breadth was found to be 0.9 of the overall breadth, reducing to 0.2 of the overall breadth next to the side shell. Similar stress distributions were obtained for the haunch/strut intersection [14]. The appreciable shear lag and effective breadth at the outer haunch and inner strut sides are

demonstrated by Figures 5.9a and 5.9b respectively. Averaging of shear lag for individual sections was carried out by the following approximate formulation derived by Pu [14]:

$$\sigma_{max}\, b_e = \int_{-b/2}^{b/2} \sigma_{nom}\, dz \;\Rightarrow\; b_e = b\left[1-\left(1-\frac{1}{7b}\right)^3\right] \le b$$

where b_e is the effective breadth, b is the full breadth, l is the frame length considered, σ_{max} and σ_{nom} are the maximum and average transverse bending stress respectively in the plate element, and dz is the incremental *width* of the section considered to act with the individual values of σ_{nom} at the integration process. The effective breadth ratios at the decks, haunch and strut areas were thus estimated to be 1.0, 0.6 and 0.45 respectively and were then used to create an equivalent 2-D model (Fig. 5.7). Pu's empirical formula was found to be accurate at areas of low stress variations (e.g. haunch (15% higher) and strut (3% lower)), but not in areas of high stress variations (e.g. cross-deck outboard of the inner intersection with the haunch) where the difference can be 28% on the conservative side. Pu thus demonstrated that 2-D and 1-D (beam and bar model) FE analyses can only be justified in preference to the more elaborate 3-D analysis in the area of low stress variations, where it is found to be quite good.

5.5 The Optimised Design Variables

Detailed material volume distributions for a frame section of the example ship are presented in Tables 5.5 and 5.6. An approximate estimate of the distribution of structural material volume among the main components of the section (Table 5.5) shows that nearly 50% of the volume is in the cross-deck and associated wet and deck plating and just over 20% of it is provided in the underwater cylindrical sections. The cross-deck web plating volume is relatively small because of the lightening holes which remove 14.2% of the excess material. The remaining 30% is evenly distributed between the haunch and the strut.

Furthermore, Table 5.6 presents a material volume breakdown in terms of plating and longitudinal/transverse stiffening. Not surprisingly, the plating is found to be 81% of the overall volume, with the stiffening volume nearly evenly distributed between the longitudinal and transverse directions. The cylinder shell is the largest contributor, mainly because of its larger

thickness and large surface area (relative, for example, to the deck plating). Scope for optimisation also exists for the cylindrical and haunch frames, while in the longitudinal direction the number and dimensions of the longitudinal extruded stiffeners could also benefit from particular re-designing.

As a result, it was decided to attempt the optimisation of all the plate elements independently, the longitudinal stiffening (assumed to consist of extrusions of fixed dimensions throughout), the strut structure, haunch plating and cylindrical shell. The haunch and ring frames were left unaltered despite their considerable contribution to volume. It is worth noting that the 'example' structure was already an 'optimised' design in the sense that the plating thickness (the second largest contributor to plate weight) was already down to its minimum acceptable value permitted from welding distortion considerations.

In a previous study [2], the depth of the cross-deck web was allowed to vary and was mainly responsible for the considerable weight and cost reductions that were noted (17.5 and 30% respectively). However, this present work neglects this aspect, perhaps arbitrarily, on the grounds that the web depth was fixed from operational requirements (e.g. minimum required tank volume). Such an assumption turned out to be very restrictive, especially in obtaining any significant weight reduction (Table 5.7).

Furthermore, restricting the number of free variables was deemed necessary, as it was the first time the program was tested to such an extent in the Glasgow environment, and considerable problems arose with available memory space. The number of design variables that the optimisation routine can handle is user defined and greatly dependent on the processing facilities available. Hence, the decision was taken to optimise a total of 15 variables defined below and in Table 5.7 and Fig. 5.10:

1. *the plate thicknesses*, i.e. those of the haunch, t_h, strut, t_s, the web plate of the cross-deck structure, t_t, the shell thickness of the underwater hulls, t_c and the thicknesses of the main and wet decks, t_d. Symmetry of construction was assumed for the main and wet decks.
2. *the frame spacing*, L_s, in the structure
3. *the frame dimensions*, i.e. those of the strut, $d_{w1}, t_{w1}, b_{f1}, t_{f1}$

4. *the cross-deck stiffening,* by permitting variation of the number of vertical stiffeners in the cross-deck web which would then define the stiffener spacing L_2,
5. *the main and wet deck stiffening,* by varying the number of longitudinal stiffeners (in the global longitudinal direction), and the number of transverse stiffeners (in the global transverse direction). In this way the plate aspect ratio of the wet and main deck plate elements as well as, the longitudinal stiffener spacing, L_1, are defined
6. *the dimensions of the main longitudinal stiffening,* by optimising the web thickness, t_{w2}, web depth, d_{w2}, and flange breadth b_{f2}. The flange thickness was not introduced as a free variable in an attempt to keep the number of optimisation variables to a minimum. Values for this parameter were determined from the corresponding flange breadth values by using local buckling criteria. The longitudinal stiffening was assumed to possess the same dimensions throughout the structure, thus taking advantage of the use of one type of extrusion globally.

The dimensional limits within which the free variables were allowed to vary during the optimisation process are shown in Table 5.3. The choices of these limits had to conform with what is generally available from the construction methods, extrusion manufacturing processes, etc. and can therefore benefit greatly from the designer's experience. A balance had to be struck between restricting some of these dimensions (e.g. flange dimensions, thicknesses etc.) to small values (and small variability range), and the need to obtain a sufficiently large number of efficient designs to provide a more dense non-dominated design space from which to select the optimum. It is also obvious that the larger the limit ranges, the longer the computational time. The limits finally presented in Table 5.3 were developed from larger ranges and reduced, bearing in mind all of the aforementioned points.

Additional linear checks and restrictions that were imposed on the free variables are described in greater detail in paragraph 5.6.1.

5.6 The Design Criteria

The design criteria form the basis against which the efficiency of each individual design is tried. They were divided into three groups:

1. linear constraints on the design variables restricting the design space
2. the analytical ultimate strength formulations
3. design criteria used to evaluate the performance of a given design and are expressed in the form design attribute functions.

The linear constraints distinguish between feasible and unfeasible design selections and are determined via a number of linear programming problems with maximisation and minimisation routines for each design variable. Non-linear programming constraints cannot be tackled by the optimisation procedure and had to be introduced as a separate check outside the optimisation program environment. In turn, the analytical strength checks are presented in the form of a library of serviceability and limit state failure modes, all described in paragraph 5.6.2. The design objectives are to achieve an acceptable design with the least weight and/or cost. Acceptability implies that safety should be within limited bounds set by the designer, or as required in design codes. No minimum limits on weight and cost have been imposed for obvious reasons!

5.6.1 Linear Constraints on Design Variables

The linear constraints on design variables restricting the design space are expressed in the form of linear programming problems for each design variable with all unfeasible points being immediately discarded. These are constraints on:

- the ranges of values the free variables are allowed to take during the optimisation process (Table 5.3)
- stiffener scantlings and spacing accounting for local buckling criteria.

The ability to change the limits of the range within which the free model variables are allowed to vary renders the procedure particularly adaptable to any special advantages and indeed limitations in construction faced by an individual shipyard (e.g. availability of standard sections, extrusions, crane lifting capacity, the dimensions of the structural elements that can be handled, and building strategies etc.).

The minimum acceptable plating thickness was set to 4 mm, a limit beyond which considerable and often aesthetically unacceptable welding distortions are generally expected to form. Additional restrictions have been

incorporated controlling the maximum and minimum values which the stiffener dimensions can attain. The maximum and minimum limits on dimensions were established from Alcan's aluminium profile catalogue, thus ensuring availability of the dimensions of the sections finally prescribed. The extrudability of aluminium is not, in general, expected to affect and discourage the use of more 'specialised' dimensions, but the cost of purpose-made dies would perhaps eventually be the prohibitive factor.

Bearing in mind the structure in question is made of aluminium, and constructed with a large number of extruded sections, it was decided to keep the longitudinal stiffener spacing and size (extruded planking) fixed throughout the structure (wet/deck, haunch, strut). This would generally reduce the material and construction costs by 'standardising' the construction, although such reductions are not reflected in the cost formulations finally used. The restrictions imposed on stiffener spacing of flat plate elements are:

$$0 \leq \frac{\text{spacing} - \text{flange breadth}}{\text{spacing}} \leq C_1$$

as well as on the relative depths of intersecting stiffeners, which are restricted by:

$$d_h \geq C_2 \times d_l$$

where d_h, d_l are the depths of the highest and the lowest stiffener at the intersection. The option exists for the use of different values of C_1 and C_2 depending on the structural element and the stiffener type (longitudinal or transverse) considered, and was introduced by the author to increase the flexibility of the program by making it adjustable to individual construction and welding practices. In the current investigation, and order to avoid limiting the design options by any local buckling or minor constructional criteria, the values of C_1 and C_2 are taken as 0.1 and 1.0 respectively.

The local buckling criteria applied on the stiffener flanges and webs ensure a safety factor of 3 against yield, as proposed in paragraph 4.3.5, Chapter 4:

For the web plate (dimensions d_w, t_w) $\quad d_w/t_w \leq 1.1\sqrt{E/\sigma_y}$

For the flange plate (dimensions $b_f, (w_f = 0.5b_f), t_f$) $\quad w_f/t_f \leq 0.36\sqrt{E/\sigma_y}$

For bulb-flats, only local buckling of the web plate is checked. Local buckling and relative stiffener depth criteria are introduced directly through the input datafile, as they can be formulated using a linear expression. However, this is not possible for stiffener spacing criteria due to the non-linearity of the expressions involved which had to be introduced in the main library of ultimate strength models. The non-linearity arises due to the decision to optimise (vary) the number of vertical stiffeners on the cross-deck as well as the number of longitudinals, instead of the stiffener spacing. This choice, however, ensures that an integer number of stiffeners in both cases would be selected. It is perhaps worth mentioning that all of these checks are applied to all the stiffeners, both in the global longitudinal and transverse global directions, and to all the structural elements that contain them, namely, the wet and main decks, struts, and haunch regions.

5.6.2 The Limit State Checks

The failure modes considered for each of the five structural elements analysed are presented in Table 5.2. Flat stiffened plating under in plane loading is checked against plate buckling, plate induced stiffener collapse and tripping failure of the stiffeners. These checks are available to both 'long' and 'wide' plates. For flat plates under lateral pressure loads a serviceability check is also available. The cross-deck is designed as deep-plate girder with flanges consisting of the main and wet deck plating. The breadths of these is taken as the full frame spacing of 1,250 mm and the thickness as an average value accounting for the presence of the stiffening and given by:

$$t = t_f + \frac{A_s}{b_s}$$

where t_f is the thickness of the main and wet decks, A_s, b_s, are the cross sectional area and spacing respectively of the transversely orientated stiffeners (in the global transverse direction). The longitudinal stiffeners are not included in the calculation as they do not contribute to the flange bending rigidity. The cylindrical hulls are designed against interframe shell

collapse only, while the intersection of the cross-deck and the haunch (referred to as knee-joint or corner joint herein) is checked against its ultimate bending moment capacity.

The advantages of aluminium in this type of construction, i.e. small structural weight and minimal corrosion compared to steel, are offset by a smaller Young's modulus and the complications arising from the more rounded material stress-strain curve and the HAZ softening occurring mainly in the heat-treated alloys. Hence, in the library of constraints due to be described, modelling of the HAZ is based on the recommendations of BS 8118 (para. 4.1.2) and the 0.2% proof stress value is used in place of yield stress in the formulations. This assumption is conservative, as it neglects the beneficial strain hardening effects characterising the behaviour of the aluminium alloys. The ultimate strength models, and any special considerations in modelling to account for the use of aluminium alloys, are briefly described next.

The Design of Flat Stiffened Plates: Stiffened flat plates are encountered on the main and wet decks, side shell, haunch and struts and are expected to experience *combined in-plane loads and lateral pressures.* Grillage behaviour under compressive-combined loading has not been investigated. Therefore, the local panel behaviour is taken as indicative of the overall grillage behaviour under various loading conditions. Safety was examined for plating in all these areas using models derived from first principles. The failure modes tackled are (Table 5.2):

- plate buckling between stiffeners
- plate induced interframe collapse of the stiffeners
- tripping failure of the stiffeners.

An additional check based on the elasto-plastic design approach was introduced as a serviceability criterion restricting the maximum deflection of the plate elements under lateral pressure loads to 1/75 of the plate width.

Plate buckling between stiffeners has been categorised as 'long' and 'wide' plate buckling, depending on the orientation of the plate to the primary compressive load, and the level of critical buckling strengths in the two directions. For 'long' plates Faulkner's effective width (para. 4.2.5.1) was used to describe the ultimate strength of the plate elements. Allowance for

uniform biaxial compression, shear and lateral loads is also incorporated in the model. The ultimate strength capacity is given by:

$$\frac{\sigma_u}{\sigma_y} = \frac{b_{em}}{b} = \begin{cases} \left(\frac{2}{\beta} - \frac{1}{\beta^2}\right) R_r R_m \\ R_m \end{cases}$$

where R_r is a plate strength reduction factor accounting for the detrimental effect of residual stresses and is a function of the level of locked-in residual stresses, the material yield stress and a slenderness dependent equation for the structural tangent modulus. R_m accounts for biaxial loading effects which are assumed to interact parabolically. For the case of *combined pressure and compression* a linear interaction between the compressive strength of a wide plate and lateral loading is conservatively assumed.

'Wide' plating is treated in a similar manner, using an effective width approach and the final ultimate strength expression is based on the French Bureau Veritas/Faulkner solution for a pinned plate:

$$\sigma_{ym} = \sigma_y \left[\frac{0.9}{\beta^2} + \frac{1.9}{\alpha\beta}\left(1 - \frac{0.9}{\beta^2}\right)\right] \qquad \text{for } \beta \geq 1 \text{ and } \alpha\beta \geq 1.9$$

Outside the stated limits the plate slenderness is sufficiently small to justify the assumption of a stocky plate and the change of failure mode from buckling to material yielding. No residual stress effects are then accounted for and the edge stress is always expected to reach yield stress levels.

Plate induced interframe collapse was tackled using Faulkner's reduced effective width approach to account for the continuous stiffness loss of the plating as load increases in the post-buckling regime. This effective width of plating is hence assumed to act with the stiffener as a column. The critical buckling load of the column is then given by :

$$\frac{\sigma_{cr}}{\sigma_y} = \begin{cases} 1/\lambda_{ce}^2 & \text{for } \lambda_{ce}^2 \geq 1/p_r \\ 1 - p_r(1-p_r)\lambda_{ce}^2 & \text{for } \lambda_{ce}^2 \leq 1/p_r \end{cases}$$

where λ_{ce} is the non-dimensional column slenderness and p_r is the structural proportional limit stress ratio. The reduction factor R_m is

imposed on b_e' as well when biaxial stressing is present. In the presence of lateral pressure loading a linear interaction is assumed between critical compressive buckling and lateral load. In this instance, the effective column length considered in the analysis will depend on the level of lateral pressure loads, and this has been empirically set by Faulkner in [15, 16]. A Johnson parabola inelastic correction, to the critical buckling load of the column arrangement, is introduced prior to its use in the linear interaction expression. Furthermore, in the presence of lateral pressure the load on the longitudinals was found by Faulkner in 1956 to be slightly less than the total load (Pxaxb) on the plate, because of the shear transfer to the short edges which may be represented by $P(b/\sqrt{2})^2$. This assumption was found to provide a good approximation and hence, for equilibrium, the equivalent longitudinal uniformly distributed load, $p_{l,u}$, is given by:

$$p_{l,u}\, a = P\left[a\, b - \frac{b^2}{2}\right] \quad \Leftrightarrow \quad p_{l,u} = P\, b\left[1 - (b/2\, a)\right]$$

where P is the lateral pressure load on the plate element while b and a are the width and length of the plate respectively.

In the absence of a thorough review of any closed form expressions describing the ultimate strength of *aluminium* stiffened plating, the approach already described for steel was used. Residual stress considerations remained unchanged (η=3.0 taken for both steel and aluminium), the 0.2% proof stress and the associated material properties were used in place of the 'steel' characteristics. HAZ softening was introduced as a reduction in the reduced effective plating width assumed to act with the stiffener in column collapse. The calculation of the extent and strength of the heat affected zone is based on BS 8118 recommendations. However, as the formulation seems to be independent of the overall plating breadth (or stiffener spacing) the actual extent of the HAZ is taken as a proportion of the reduced effective width as follows:

$$b_e' = b_e' - (\text{Area HAZ} / b\, t)\, b_e'$$

Proportioning of the HAZ with b_e' protects against unacceptably small values of the reduced effective width in addition to relating the HAZ and its effect to the plate geometry. The arbitrariness of this assumption was recognised and a more thorough investigation was carried out resulting in

the formulations of paragraphs 4.2.5.2-4.2.5.4, Chapter 4.

The check against *stiffener tripping* failure was carried out, based on Faulkner's model, accounting for the more realistic case of interaction between the buckling modes of the plate and the tripping modes of the stiffener. The possible destabilisation of the stiffener by the premature buckling of the plate was therefore an issue and was considered by Faulkner to follow a linear variation of the rotational restraint, C, with the axial load (for $\sigma/\sigma_{cr} \leq 2$). Hence the strength expression used is (para. 4.3.4):

$$\sigma_T = \frac{G J + \dfrac{m_T^2 \pi^2 E\left(I_z \bar{z}^2 + \Gamma\right)}{l^2} + \dfrac{C_s l^2}{m_T^2 \pi^2}}{I_o + \left(k C_s l^2 / \left(m_T^2 \pi^2 \sigma_{cr}\right)\right)} \qquad \text{and} \qquad C = C_s\left(1 - \frac{\sigma}{\sigma_{cr}}\right)$$

The average limiting tripping stress was then taken to be

$$\sigma_u = \sigma_T\left(\frac{A_s + b_e t}{A_s + b t}\right)$$

where b_e is the effective width of the plating as determined by an ultimate strength approach to the plates' post-buckling behaviour. The designer can then opt to account for the effect of end-moments, or lateral pressure loads, or their combination on the tripping strength, as recommended by Adamchack (paras. 4.3.4.2, 4.3.4.3). In the case of the particular example, slamming loads and in-plane compression loads were not found to be in phase, so the two loading cases were treated independently. For inelastic tripping the structural tangent modulus approach E_t is used, requiring that $\sigma_{Ti} = \sqrt{E_t/E}\,\sigma_{Te}$. E_t is defined by the Ostenfeld-Bleich parabolae.

To design the plates under *lateral pressure loading* the following choices are available (para. 4.2.7):

1. design the plating elastically to first yield with an appropriate thickness correction to account for aspect ratio effects. Curve-fitting expressions describing the variation of k_1 and k_2 (the correction factors for deflection and stress respectively to account for aspect ratio effects) with the aspect ratio were included in the program

2. design the plating elasto-plastically, based on w_{pt}, the maximum allowable permanent set deflection with edges free-to-slide using Faulkner's closed-form expressions derived from Clarkson's tests

3. design the plating assuming fully plastic collapse with the edges of the plating clamped and held apart. Three hinge collapse or roof-top collapse with or without accounting for membrane stresses are prescribed depending on whether the plating is 'long' or 'short', slender or stocky.

In the application described herein, elasto-plastic plate design was adopted primarily due to the more realistic boundary conditions implied. Hence, for plates with $1 \le \alpha \le 5$ and $2 \le \beta \le 6$, the allowable pressure, p, is expressed in terms of an allowable permanent set, w_{pt}, set, in the current application by default, equal to b/75:

$$p = \begin{cases} \dfrac{6\sigma_y}{\sqrt{\alpha}}\left(\dfrac{t}{b}\right)^2\left(1+\dfrac{2w_{pt}}{\alpha t}\right) & \text{for } \beta < 2.5 \\ \dfrac{6\sigma_y}{\sqrt{\alpha}}\left(\dfrac{t}{b}\right)^2\left(\dfrac{4}{3}+\dfrac{w_{pt}}{\alpha t}\right) & \text{for } \beta \ge 2.5 \end{cases}$$

Further research into the subject showed that the values presented in Appendix 4.2 may also be used instead of b/75. In the current computer code the designer is only given the option by the program to choose another value for w_{pt} but always in relation to the plate breadth. Furthermore, for $1 \le \alpha \le 5$ and $\beta < 2$ the elastoplastic approach is overruled in favour of the fully plastic design approach. This approach is based on the 'roof-top' collapse bending mechanism and having been developed for stocky plates, does not account for membrane effects:

$$p = 12\, C_{bc}\, \sigma_y \left(\frac{t}{b}\right)^2 \left(\sqrt{3+\frac{1}{\alpha^2}} - \frac{1}{\alpha}\right)^{-2}$$

Paragraph 4.2.7 and Appendix 4.3 provide more information on the remaining theoretical models available in the program. Designing elastically was considered too conservative, while a fully plastic approach was deemed to be too optimistic and uncharacteristic of the boundary conditions actually present in stiffened plating subjected to in-plane loading.

The Design of the Cross-Deck Girder: Of the variety of models for the ultimate strength of deep plate girders under shear and combined in-plane loading, the 1978 Cardiff model [17] was used for reasons presented in Chapter 4, paragraph 4.4.2.2. This has been adapted to account for the effects of in-plane compression in addition to in-plane shear and bending stresses in the web plate. Despite the expected variation of the bending, shear and direct in-plane stresses along the length of the cross-deck, these have been assumed to coexist and apply to all the web plate subpanels (identified by the vertical stiffeners) in the same way, with their maximum values being in phase - a conservative assumption.

Therefore, the ultimate strength in shear of a girder consists of the sum of the critical buckling stress, the capacity of the diagonal tension field, and the contribution of the flange hinges. The direct compression and bending stresses are both assumed to be taken by the flanges, while the shear loads are absorbed by the web only. Hence, the ultimate strength in shear of a plate girder is given by (para. 4.4.2.2):

$$V_{ult} = V_1 + V_2 + V_3 = V_{cr} + 0.5\,\sigma_t^y\, t \sin(2\theta)\,(h - b\tan\theta) + \sigma_t^y\, t\,(c_c + c_t)\sin\theta$$

The effect of coexistent direct and bending stresses on the critical buckling of the web plate is neglected, as these two loads are assumed to be taken up only by the flanges. Inelastic shear buckling occurs when the critical buckling stress exceeds $0.8\tau_y$ ($<3\tau_y$) and the inelastic critical buckling stress is then given by:

$$\tau_{cr,mod} = \tau_y\left(1 - 0.625\left(\sqrt{\tau_y / \tau_{cr}} - 0.8\right)\right)$$

The maximum value for the ultimate shear strength is obtained by trial and error of the values of θ, the inclination of the tension band to the horizontal, and not by the approximate formulation of 2/3 of the angle of inclination of the web diagonal. The expressions accounting for unequal flanges, or flanges of different materials, are used throughout the design process.

The beneficial effect of the longitudinal stiffeners on the web strength is incorporated by substituting the critical buckling stress for the web plate by the critical buckling strength of the weakest subpanel, as identified by the position of the longitudinal stiffeners (Cardiff, para. 4.4.2.2).

Furthermore, the effect of web perforations is accounted for by means of the conservative approach of Narayanan et al [18] (para. 4.5.2) which assumes that the reduction in ultimate strength of the plate girders is proportional to the increase in diameter of the cut-out. Hence, the ultimate strength capacity is obtained by linear interpolation between V_u, the unperforated ultimate strength, and the Vierendeel load V_v:

$$V_{ult} = V_v + (V_u - V_v)\left(1 - \frac{d}{h}\right) \qquad \text{where} \qquad V_v = \frac{2}{0.5\,b}\left(M_{pc} + M_{pt}\right)$$

Possible reinforcement of perforations is neglected. The diameter (or equivalent diameter) of the perforation is restricted to 2/3 of the web depth.

The co-existence of shear, direct compressive, and bending loads, is tackled via the Cardiff interaction diagram (para. 4.4.2.2 and Fig. 5.11). The original approach does not allow for any direct stresses, but their effects are included by superposition to the bending stress effects on the flange strength. The two main failure modes are identified by Region S-C on the curve (failure with a shear type mechanism) and region C-B on the curve (failure with a bending mechanism). Points S, C and C, B are connected by parabolae as experimentally shown by Porter et al. Inward collapse of the compression flange is assumed to occur at an applied bending moment M_u, obtained from Cooper's expression (para. 4.4.2.2):

$$\frac{M_u}{M_y} = 1 - 0.0005\frac{A_w}{A_f}\left(\frac{d}{t} - 5.7\sqrt{\frac{E}{\sigma_{yf}}}\right) \quad \text{for} \quad M_u < M_{fl,plastic}$$

This formula is also applicable to the case at which longitudinal stiffeners are present. The shear capacity at the point of failure mode changeover from a shear to a bending mechanism, V_C (point C), together with V_B, the minimum level of shear load beyond which failure occurs as 'pure bending', are calculated from empirical formulations (para. 4.4.2.2).

For reasons mentioned in paragraph 4.4.2.1 and because of its implementation in BS 8118, the conservative approach proposed by Burt and Evans [19] (para. 4.4.4.1) was used to calculate the ultimate strength of aluminium deep plate girders. It assumes that the complete web area suffers

a reduction in strength due to welding. Hence the reduction in ultimate strength will be to the reduction of the contribution of its post-buckling components, V_2, V_3 (para. 4.4.2.2):

$$V_{ult} = V_1 + w(V_2 + V_3)$$

The critical buckling strength contribution to ultimate strength remains unaffected. w ($=k_z$) is the percentage of material strength reduction given in paragraph 4.1.2. As nothing specific is available for the loading case where bending loads are predominant, it was assumed that Cooper's formula remains valid. The programmed approach for longitudinally stiffened aluminium plate girders is the same as that used for steel deep plate girders, in the absence of any specific guidance on the matter.

The Design of the Corner Joint Plate: Knee joints are generally designed based on their critical buckling load. Higher loading conditions are catered for, either by the introduction of haunches or by the insertion of 'doubler' plate patches to increase the web thickness. development of a post-buckling approach to design would lead to an even higher strength to weight efficient structure.

The ultimate strength model put forward by Scheer et al [20, 21] and recommended in Chapter 4 (para. 4.6) for the design of steel deep plate knee joints, presents a number of limitations if it is to be applied to the corner joint plate, and partial transverse bulkhead design of SWATH and multi-hull vessels. These limitations are:

1. it has only been tested for square steel panels but rectangular proportions are generally the norm
2. the model has not been compared against aluminium tests where strength reductions occur in the heat affected zones of the heat-treated alloys
3. no allowance is made for the presence of any horizontal and/or vertical stiffening on the web plate
4. the model does not allow for the presence of any perforations in the plating which would affect the extent and hence effectiveness of the tension field contribution.

These are the difficulties faced in applying the results of the German

research to the design of the 'corner' plate at the haunch/cross-deck intersection (Fig. 5.12). In the example ship:

- two vertical stiffeners exist, separating the knee plate into three subpanels
- each subpanel contains a circular perforation at mid-depth
- the plate is made of aluminium alloy
- the overall aspect ratio of the plate is 3.

Although no theoretically and experimentally justified answers to these effects are currently available, the approaches recommended in the Cardiff model [17, 18] can be used as a first approximation. In the presence of horizontal stiffeners, the Cardiff model recommends [17] the use of the critical buckling strength of the weakest subpanel as the only change in the ultimate strength formulation necessary. This approach was also used for the corner joint plate, for which τ_{cr} was taken as that of one of the subpanels (as they were all of the same dimensions). Furthermore, to account for HAZ effects, Evans et al's approach for deep plate girders [19] was also used. Hence, the ultimate moment carrying capacity of a knee joint about point i (Fig. 5.12) is given by:

$$M_u = M_{cr} + w\left(M_1 + M_2\right)$$

Information on the notation may be obtained from paragraph 4.6.2. Values for the percentage of material strength reduction, w, due to HAZ effects are available in paragraph 4.1.2 and Table 4.1. To account for the effect of web perforations the simplified method used for the design of deep plate girders (see earlier) was extended to the case of corner joints on the basis that corner joint design employs the principles of tension field strength modelling. To consider the effects of the perforation on the critical buckling moment M_{cr} solely would clearly be unconservative, as the assumed plate has high aspect ratio and hence the critical buckling moment contribution to the maximum moment capacity is not expected to be great. It may instead be assumed that the reduction in moment capacity of the joint plate will vary linearly with the perforation diameter. It would thereby fail between the moment capacity of the intact section in which only the four flanges are effective and in which no web is present, M_{hinge}, and the case where there are no perforations and the web is fully efficient, M_u:

$$M_{ult} = M_{hinge} + \left(M_u - M_{hinge}\right)\left(1 - \frac{\text{diameter of perforation}}{2b}\right)$$

where $M_{hinge} = M_A + M_B + M_C + M_D$, 2b is the web plate depth, while the plastic moment capacities of the plate flanges are M_A, M_B, M_C, M_D (para. 4.6.5). No experimental verification of this model exists in the literature and it should therefore be treated as provisional.

The Design of the Stiffening System of the Cross-Deck web plate (flat bars) has purposely been omitted from the variable selection procedure of the optimisation routine as well as any statistical treatment describing its strength. This was due to the memory limit imposed by the available computing facilities having a knock-on effect on the number of variables that could be tackled at any given instant by the program.

Flat-bar stiffening for both longitudinal and transverse stiffeners was chosen (normal practice for deep plate girders) and a parametric variation of the geometric variables enabled the selection of suitable designs for evaluation. The case of flanged stiffeners has also been accommodated in the program, with the additional check of local buckling criteria presented in paragraph 4.3.5. In addition, the longitudinal stiffeners must be able to support, up to the ultimate limit state, the load shedding due to plate buckling in the web subpanels, as well as being able to maintain nodal lines in the buckled web.

The material for these stiffeners was restricted to that of the web (σ_{yw}). Selection of the final dimensions was on the basis of minimum weight after satisfying rigidity and strength criteria. The weight criterion consisted of the estimation of an average thickness for the whole structural component consisting of the thickness of the web plate, and equivalent thicknesses for the longitudinal and vertical stiffeners:

$$t_{eq} \leq t_w + \left[\frac{A_{s,l}}{\left(N_l + 1/h_w\right)}\right] + \left[\frac{A_{s,t}}{b_w}\right]$$

where $A_{s,l}$, $A_{s,t}$ are the cross-sectional areas of the longitudinal and vertical stiffeners respectively. The dimensions of the longitudinal stiffeners are assumed to be fixed over the depth of the girder web plate. N_l is the number of longitudinal stiffeners over the complete depth of the girder web plate

while h_w, b_w are the depth and breadth of the girder web plate identified by the two vertical stiffeners on its edges. The criterion is based only on minimum equivalent thickness, as the length and the cost of the stiffeners will be fixed by global structural dimensioning, which remains unaffected by the optimisation procedure.

The rigidity of *vertical and longitudinal stiffeners* was checked against the criteria proposed by Maquoi and presented in paragraph 4.3.1.2 and Table 4.7. In cases where the number of stiffeners does not match those in the Table, then those immediately more conservative available in the Table would be considered by the program.

From a fabrication point of view, the range of dimensions that the transverse stiffeners could attain were restricted to:

$$4 \le t_{s,t} \le 20 \times \max\{t_{f,t}, t_{f,b}, t_w\}$$

$$0.001 \le d_{s,t} / \min\{b_{f,t}, b_{f,t}\} \le 0.5$$

where $t_{s,t}$, $t_{f,t}$, $t_{f,b}$, t_w are the web thicknesses of the vertical stiffener, the top and bottom flange of the girder and the web of the girder respectively. Similarly, $d_{s,t}$ is the depth of the web of the vertical stiffener and $b_{f,t}, b_{f,t}$ are the top and bottom flange widths of the assumed girder respectively.

In addition, the depth of the longitudinal stiffeners was restricted to 0.67 of the value chosen for the vertical stiffeners (i.e. depth of vertical stiffeners greater by a factor of 1.5) being intersected [6] while the limits of variability of thickness were kept the same as that used for the vertical stiffeners.

The program can only accommodate longitudinal stiffeners on the web plate of the cross-deck when spaced equi-distantly from each other. It is the required number of these stiffeners (maximum of 15 permitted) at the web that is introduced via the input file and then automatically their spacing is adjusted by the program and their exact position from the top flange (main deck) for each of the stiffeners is calculated and stored in a suitable array.

It is worth remembering that positioning any longitudinal stiffeners in the tensile zone of the neutral axis is not efficient if the bending load is not alternating. In multi-hulled vessels, however, bending loads on the cross-

structure are alternating and hence structural symmetry about the neutral axis should be sought after. For the same reason, perforations should be placed at the geometrical centroid of the web subpanels as these are identified by the vertical web stiffeners.

Complications arise when web perforations are required to co-exist with longitudinal stiffeners on the girder. In this case, the program checks the input (diameter of the cutout, number of stiffeners, position of stiffeners) and, if deemed necessary, overrules it. The reason for such a check is to protect the case where the input (randomly selected) sets one or more stiffeners to cross the cutout - an unrealistic situation. Hence, if the diameter (or equivalent diameter) of the perforation is greater than 2/3 of the web depth, the diameter is overruled and restricted to this value while the number of longitudinal stiffeners (if required) will then be restricted to 2. Their positions are then fixed at 0.1 of the web depth from the compression and tension flanges. No clearance considerations are required for welding at the stiffener toes as the stiffeners will generally be flat-bars. On the other hand, if the perforation diameter is less than 2/3 web depth then, in the presence of longitudinal stiffeners, the following actions are taken:

(a) if the diameter is less than $0.2\,d_w$, four stiffeners are placed at distances $0.123\,d_w$, $0.275\,d_w$, $0.725\,d_w$, and $0.877\,d_w$ from the top (main deck) flange or

(b) if the diameter is greater than $0.2\ d_w$ then 2 stiffeners are placed at $0.2\,d_w$ and $0.8\,d_w$ from the top (main deck) flange.

The stiffeners will then be placed at optimum positions on the web plate as these are accepted to be for bending loads (Table 4.7). In addition, these requirements on stiffener positioning indirectly ensure a limit on the minimum acceptable distance of a longitudinal stiffener from the edge of the perforation, when the latter is unstiffened. No such direct limit has been set in the program, but recent catamaran designs use a 20 mm distance imposed by classification requirements. If no perforation is present, and the required number of longitudinal stiffeners is either 2 or 4, then the input is overruled so that the stiffeners are placed at the optimum positions on the web plate, as these are accepted to be for bending loads.

The column strength check of the vertical stiffener and associated effective plating ($= t_w \sqrt{E/\sigma_{yw}}$) accounts for the eccentricity of the load with respect to

the stiffener neutral axis. The load action is that of the ultimate load capacity in shear of the web panel reduced by 80% of the critical buckling strength of this plate element, as recommended by Maquoi [22]. The critical buckling strength was also reduced by 20% to account for the detrimental effect of the initial imperfections [22]. A Perry-Robertson beam-column approach was chosen as best describing the stiffener behaviour:

$$\sigma_{max} = \frac{V}{A_s + b_e t_w} + \left[\frac{V(e_1 + e_2)}{Z(1 - V/V_{cr})} \right] \leq 1.6\,\sigma_{s,y}$$

where V and V_{cr} are the shear load (as identified above) and the critical buckling load of the assumed column. Z is the elastic section modulus of the section consisting of the stiffener and associated effective plating while $\sigma_{s,y}$ is the yield stress of the stiffener material which is taken equal to the girder web material for both the vertical and longitudinal stiffeners. In addition, e_1, e_2 are the eccentricity of the load to the neutral axis of the stiffener (stiffener and effective plating) neutral axis and the assumed initial deformation of the stiffener respectively. The initial deformation of 1/1000 of the stiffener length was assumed while the full stiffener length was conservatively taken as the buckling length (an effective length of 70% of the full length was assumed as safe and weight efficient option by Maquoi). A similar strength check was also used for the design of the longitudinal stiffeners. The loads actions considered, were those of the direct bending loads acting on the compression flange (a conservative but greatly simplifying assumption) while any lateral pressure loads were neglected. An initial out-of-straightness of length/500, for inclusion in the strength calculation was used as recommended by Maquoi and matching initial imperfections for both steel and aluminium columns. No tripping check is carried out for either the vertical or longitudinal stiffeners.

The Design of the Submerged Hulls: The primary loading on the cylindrical submerged hulls is either from water pressure or grounding and docking loads. In this particular application grounding was neglected on the grounds of not being a design load (accidental load). Furthermore, the docking arrangement is such that it induces a small bending moment in the structure and hence is also neglected. Although there will be a small contribution from the stresses due to longitudinal seaway bending, to simplify the analysis, this has not been considered here, although an

accurate ultimate strength model can handle the combined loading for orthogonally stiffened cylindrical structures (Appendix 4.6). Therefore, the only loading that is considered is the hydrostatic pressure at the operating mean draught, including the dynamic amplification (Table 5.8). The dynamic amplification effects were introduced by multiplying the hydrostatic pressure at 2.7m draught ($0.027N/mm^2$) by a factor of 2 (which appears to be a conservative practice of the offshore industry) resulting in a design pressure load of $0.055N/mm^2$.

The modes of failure for a ring-stiffened cylinder predominantly subjected to external pressure are well established [23] in submarine design, namely interframe shell collapse, general instability, frame tripping, shell yielding, frame yielding and their considerations in design procedures are described in section 4.7. Earlier optimisation investigations by Morandi [2], showed that interframe collapse dictated the final solution (safety index of 4 for interframe collapse versus safety indices in excess of 6.4 for frame yielding, general instability plate yielding and frame tripping). This conclusion coupled with the general need to keep the design checks to a minimum, led to the omission of all the aforementioned failure modes but interframe shell collapse which was accounted for via the a *mean* curve through experimental data (para. 4.7.1.1 and Table 4.12). In the absence of any considerable axial loads, ring framing between transverse bulkheads represents the least weight stiffening solution, and the potential of introducing any stringers in the optimisation solutions was neglected.

5.6.3 Design Attributes

Design attribute functions used are those of structural weight, cost, and an approximate system reliability measure expressed by Ditlevsen bounds. The component safety level (safety index) achieved for each of the failure modes was also calculated and used as lower acceptable bounds to safety values. These attributes are transformed to goals by asking for the maximisation of the safety index β, and the minimisation of the weight and cost.

The *mass*,W, of the structure is obtained by the summation of the individual masses obtained for each of the main structural elements. The structural volume is calculated first and converted to mass by multiplication with the material density.

In turn, the construction cost, C, is assumed proportional to structural mass and weld length and is therefore expressed in terms of equivalent cost [24, 25] given by,

$$C = C_m (W + k\, m\, J_L)$$

where W is the structural weight, C_m is the material cost assumed at £2,000/tonne, k is a factor expressing the relationship between the material costs and manhour cost while m expresses the average number of manhours per welding joint length, J_L. Both k and m are normalised by the material cost. The values assumed for these coefficients are [26]:

	k (tonnes/manhour)	m (manhours/m)
For Steel	0.05	1.0
For Aluminium	0.0072	2.0

The second term of the right hand side in the expression above, representing the labour costs of the construction, could be extended following more detailed research to include overhead costs (e.g. plate cutting and forming, the number and size of structural components relative to the number of workers handling them etc.), variations in the labour rate from yard to yard, the efficiency of the individual labour groups within a yard and relative to other yards. The size and capacity of the handling equipment such as cranes will also affect the labour cost as it could determine, among others, whether construction would be carried out undercover and away from the effects of the environment, or the efficiency and quality of construction would be adversely affected by bad weather. The effect on cost of corrective actions that are almost certainly linked with inefficient working practices, would also have to be accounted for. Furthermore, the material cost is a function of the grade (steel) and alloy (aluminium) and is always prone to specially negotiated prices. Such aspects have been studied by Winkle et al and were applied to the optimisation of stiffened grillages [24] and stiffened cylindrical structures [25].

The derivation of the values for coefficient k above was based on the assumption that it would require 2 workers to complete a job, each on a

salary of £15,000 a year. Furthermore, each is assumed to work 45 weeks for 37 hours every week, a total of 1,665 hours per year. Hence the construction cost per manhour results to

$$\frac{2 \times 15{,}000\,(£/\text{year})}{(45\text{wks}/\text{year}) \times (37\text{manhrs}/\text{wk})} = 18\,(£/\text{manhr})$$

The material cost for steel was assumed to be £360/tonne while for aluminium at £2500/tonne. Hence the normalised values of manhour cost with respect to the material cost (coefficient k) resulted as given in the Table above. In the example currently considered, it was assumed that 1 manhour is required per metre (1000 mm) of length for steel (although this varies between 0.8 to 1 manhour) and twice that time for aluminium material construction.

The simplicity of the cost expression reflects mainly the difficulty in obtaining accurate costing algorithms from the industry, which considering the current level of industrial competition is perhaps not so surprising. The minimal information available to the author has permitted the adjustment of these coefficients to aluminium applications, which considering the comparative nature of this study are more than sufficient. In estimating the joint lengths for the cross-deck structure, the perimeter of any cutouts in the web has been included as additional length as some cost incurs during the perforation procedure. The weight is of course reduced accordingly. In addition, single pass welds were assumed in the costing formulations. It is important to note, that similarities in the construction procedures and practices permitted the use of a costing model for steel to be applied to aluminium. The introduction of any special considerations such as the additional inert gas costs require additional attention and the industry can provide useful experience along these lines. Bearing in mind we are dealing with an aluminium structure which has been constructed with a large number of extruded sections (e.g. longitudinal stiffening), it has been decided to keep the longitudinal stiffener spacing fixed throughout the structure (wet/deck, haunch, strut). This would generally reduce the material and construction costs by 'standardising' the structure, although such reductions are not reflected in the cost formulations.

A more complicated cost function can also be used, but such a formulation is considered as too elaborate for the purpose of simple comparison between

alternative designs. If however, detail cost information is necessary for a particular design, then use can easily be made of costing algorithms reflecting the overhead and construction costs of individual constructors.

The structural component *reliability* and that of the complete structure are expressed in terms of the safety index, β, and Ditlevsen bounds respectively. The component safety indices and upper Ditlevsen bounds were first estimated for the original structure and used as lower limits for the corresponding values of the optimised designs. The exact determination of the probability of failure of a series (or parallel) system is not possible and hence a numerical calculation is necessary. As such an analysis is outside the scope of this work, Ditlevsen bounds were used to express the upper and lower limits (bounds) that the system reliability would obtain. According to Thoft-Christensen and Baker [27] the practical value of such bounds depends on how narrow they are. The upper limit would correspond to the case of uncorrelated system elements while the lower limit assumes full correlation. The system of structural components was taken as linear (system failure occurs with first component failure) with uncorrelated main structural components. In implementing the reliability approach to safety, all the deterministic safety checks for the individual failure modes were transformed to safety margin expressions by introducing the model uncertainty in the strength part of the equation. The model uncertainty factors used for the modes of failure considered are shown in Table 5.2.

In addition, the minimum target reliabilities used on the specific application were taken as the reliabilities for the individual structural components of the original example ship. An 'application independent' derivation of acceptable levels of failure probabilities on which the calibration of new designs could be based would be more appropriate. Such values can be obtained from similar existing ship designs currently in operation, as well as from an analysis of the safety levels implied by already existing and widely used design codes.

5.7 Reliability Aspects

The reliability analysis computer code uses the Advanced First Order Second Moment method and was originally developed by Das et al [29] for use in an interactive way. By this it is meant that the user of the program could alter the initial β values as well as the tolerance value for the

residuals, to insure that the code actually converges to the right safety index value. These corrective actions (initial 'manual' trials for the current application found that they were considerable and essential) cannot be undertaken in an 'automated' procedure such as that used for the current example and appropriate alterations, therefore, had to be introduced into the code by the author. Hence, in order to check the convergence of the program two initial values for β (3 and 10) were tried (for every design, every failure mode and every main structural element-very time consuming). If after 30 iterations (for every value of initial β) the reliability analysis did not converge to a value, then the initial β was increased by 2 (if the starting value was 3) or decreased by 2 (if the starting value was 10) and the process repeated. If however convergence was possible from one side (say the side of initial value of 1), then convergence from the other side (the side of initial value of 10) would also be checked. If that converged too so that a difference of less or equal to 0.1 is recorded between the two values of β, then the average of the two values is chosen as the final safety index. If the difference in safety indices was greater than 0.1, then the tolerance value for the residuals (initially taken to be equal to 0.01 - sufficiently large to speed up the convergence process but sufficiently small to avoid recalculation) was reduced by 10% and the reliability analysis would start all over again. If no convergence is obtained even after 20 such iterations then the design is rejected altogether.

Of all the design variables presented in paragraph 5.3, the ones finally optimised are shown in Table 5.3, inclusive of their mean and COV values but the number of stiffeners (assumed as design variable) are considered as deterministic for obvious reasons. The remaining design variables although not optimised, are included in the reliability analysis. In more detail, the following variables were considered for each of the main structural elements:

For stiffened flat plate design (decks, struts and haunches),

- 13 variables were assumed normally distributed. These variables were the thickness, length and width of the plate, the dimensions of the stiffener in the direction of loading (web depth and thickness, flange breadth - thicknesses obtained from local buckling criteria although it was recognised that such an approach would lead to thin flanges), the

load actions (direct, bending, shear and pressure loads), Young's modulus, frame spacing and the modelling uncertainty.

- the yield stress of the material was the only variable assumed to be lognormally distributed.

For cross-deck design,

- the normally distributed variables were the depth and thickness of the web, the thickness of the main and wet deck plating, the frame spacing, the diameter of the web cutout, the overall length of the cross-deck, the dimensions of the transverse stiffeners of both the main and wet decks, the load actions on the girder (bending stresses on the top and bottom flanges, shear stress in the web and direct compressive stress), Young's modulus and the uncertainty in modelling,

- while 3 variables, the yield stresses of the two flanges/main decks and the yield stress of the girder web plate, were assumed log-normally distributed.

For the corner joint design,

- the additional variable (to those used for the cross-deck) were the load actions on the haunch section ('column') of the corner joint (shear force, direct compressive stress, bending stresses on the top and bottom flanges), the length of the cross-deck part of the corner joint, the breadth and thickness of flanges (left and right belonging to the 'column' part of the joint), spacing of the stiffeners, cross sectional areas of the transverse stiffeners on the flanges of the joint, while,

- the variables lognormally distributed were the yield stresses of the side flanges and the main/wet decks and the yield stress of the girder web plate.

For the cylindrical structure,

- the shell diameter and thickness, frame dimensions, ring frame spacing and out-of-circularity were assumed normally distributed,

- the material yield stress and the load were assumed to be log-normal.

Generally, the variables corresponding to geometrical dimensions (e.g. length, depth, diameters, sectional areas etc.) are allocated a normal distribution and COV value of 2.5%. Similarly the yield stresses, for both steel and aluminium, were assumed log-normally distributed with a COV of 8%, while Young's modulus was assumed to demonstrate a normal distribution with a COV of 2% [30]. Usually live loads (e.g. machinery) and constant loads are assumed normal and seaway loads as log-normal. For simplicity, normal distributions have been assumed herein for all the loads and COV values of 15% allocated to them. All variables were assumed statistically uncorrelated.

Furthermore, Table 5.2 presents, for each main structural element, the modelling uncertainties associated with every failure mode under consideration. For plates under lateral pressure, no detailed comparison of the theoretical predictions with experimental data has been carried out. However, since in general failure modes involving tension are more predictable and more easily modelled than buckling failure modes, a low COV can be accepted. Hence, for the purpose of lateral strength of plates a COV value of 10% can only be considered as being conservative. For the cross-deck behaviour, the modelling uncertainties assumed were based on the review of approximately 250 experimental data carried out in Germany [20] during the development of the Eurocode 3 recommendations. The choice of the Cardiff model is justified because of the smaller COV obtained. The values assumed did correspond to the case of steel plate girders. It is notable, that no data exist on aluminium longitudinally stiffened plate girders, while for the vertically stiffened case the COV was later found to be as given in paragraph 4.4.4, Chapter 4. The lower hulls were checked against interframe shell collapse for which Morandi, based on a wealth of experimental information (700 data points), proposed mean of 1.026 mean and a COV of 7.6%. Guedes Soares [31] presented a review and comparison with 74 experimental data, of the strength predictions of three models describing the ultimate strength of stiffened plates in compression. It was then concluded (and later by Gordo et al [32]) that Faulkner's model provides mean strength predictions and found it to be both simple and sufficiently accurate for optimisation purposes. Pu later reviewed the modelling uncertainties for the design of stiffened steel flat plating [33] (paras. 4.2.4, 4.2.5, Chapter 4) but confirmed Guedes Soares' initial conclusions. Furthermore, comparison with a very limited number of experimental results (10 in number [21]) for steel knee joints suggest an

overestimation of strength of approximately 10% by the model used. Due to the lack of appropriate experimental values of relevant aluminium structures, the same modelling uncertainties as for the steel cases were chosen. This, of course, is based on the assumption that the same model can be applied to the specific structural arrangement of the example ship.

5.8 Discussion

It is believed that this chapter has succeeded in demonstrating that it is possible to combine a reliability-based multiple criteria optimisation procedure with ultimate strength modelling of local structural behaviour in order to address simultaneously weight, cost and safety issues even from the concept design stage. The use of a larger number of variables and/or of another example ship would have demonstrated this point more emphatically, at the expense of increased computational effort, which is anyway considerable due to the substitution of multi-objective, non-linear optimisation by the simpler multi-attribute checking and selection process.

The procedure which was applied to the design of the five main structural components of an example SWATH ship, allows the designer's preferences and requirements to be interactively applied at the input stage as linear constraints, while adjustment of the level of importance of the design attributes during the final design selection process is possible. Therefore, the potential of the described design tool is proportional to the designer's expertise so it is there to complement his experience rather than to replace it. This obvious flexibility of the procedure is underlined by the modular nature of the program allowing the optimisation process to concentrate to individual structural elements at the discretion of the designer as well as on global optimisation of the complete structure.

The main problem encountered in running the application, was that of time and computational effort required by the optimisation routine. This problem was aggravated by the addition of the library of ultimate strength constraints as the number of reliability iterations for each set of design variables, each structural component and its individual failure modes checked can potentially be enormous. Streamlining and further development of the program are essential to address the problem of speed

although the modularity of the program provides, potentially, great flexibility by permitting the introduction/upgrading of other/new ultimate strength and cost models as this research and technology develop. Even the limits on target reliabilities for both the individual structural elements as well as for the complete system can also be easily altered at will via the input datafile.

The limits on the minimum values of target reliabilities used on the specific application were those implied by the individual structural components of the original design. A more general and 'application independent' levels of safety for calibration of the optimised structures need however to be prescribed. Such target levels of safety indices can only be obtained either from analysis of a large number of similar existing ship designs and/or from an analysis of the safety levels implied by already existing and widely used and respected design marine codes. At the local structure level, the experience of other disciplines (e.g. civil engineering) could assist in setting the target of safety for the individual structural components. Extension of the method to other geometries (e.g. catamarans) would be very useful.

In turn, the cost functions obviously require both refinement and the co-operation of the marine industry. Such a refinement should consider the extra cost of the welding techniques, welding consumables and special welding environment required in aluminium construction in addition to the effect of the welded thicknesses on the number of welding passes required. The cost benefits obtained by the use of extrusions should not be neglected but this has to be balanced against the complexity and quantity of the extruded sections which would almost invariably render the standardisation of the costing procedure more difficult. Reduced handling costs and other aspects closely linked with the light weight of aluminium (e.g. transportation aspects) should also affect the costing function.

The ultimate strength modelling requires further attention. Although the models are sufficiently well calibrated for steel applications, their application to aluminium structures is in need of further research and comparison with experimental/numerical data to account more thoroughly for the HAZ softening, the residual stress effects and the more rounded shape of the stress-strain material curve in aluminium structures.

Table 5.7 presents the original design values in comparison with those identified by the optimisation process. It is obvious that the optimised solution provides disappointingly small improvements in weight, cost and system reliability. These improvements were made possible only due to the redesigning of the haunch and strut frame and the reduction in thickness of the strut and haunch plate elements. Furthermore, the small improvement in total cost is more associated with the reduction of weight (and hence material cost) rather than a reduction in the construction expenses. Perhaps, such a small improvement in weight is not so surprising, if one considers the fact that the plate thicknesses for the main and wet deck plating, which are the greatest contributors to the weight, were down to their minimum acceptable values of 4 mm in the first place.

It is worth noting that even this small weight gain was obtained at the expense of safety. The restrictions on minimum target reliabilities for the individual components had to be relaxed (Table 5.7), but the optimised values are not either too different or too small. This last point encourages the acceptance of these values. Only a minor drop on the required upper Ditlevsen bound level resulted which was more than acceptable. After all this criterion is approximate in its own right. It is obvious from Table 5.7, that the strength of the knee joint dictates the final solution, while the design of the cross-deck is dominated by shear collapse. Stiffened plate failure on the other hand is dominated by interframe collapse for the decks and tripping for the haunch and strut.

Despite these rather disappointing results, the optimisation of an already optimised design can still be a small consolation prize in its own right. Irrespective of the quantitative value of the final solution, qualitatively the procedure is sound as it 'homed-in' close to the original design after all.

References

1) Zanic, V., Das, P.K., Pu, Y., Faulkner, D., 'Multiple Synthesis Techniques Applied to Reliability-Based Design of a SWATH Ship Structure', Proc., 5th Intl. Symp. Integrity of Offshore Structures, 17-18 June 1993, Glasgow, EMAS Scientific Publishers, 1993.

2) Das, P.K., Tolikas, C., Morandi, A.C., Zanic, V., Warren, N.F., 'Multiple Criteria Synthesis Technique Applied to the Reliability Based Structural Design of Hull Components of a Fast SWATH Ship', Proc., Second International Conference on Fast Sea Transportation (FAST' 93), 12-15 December 1993, Yokohama, The Society of Naval Architects of Japan, 1993.

3) Faulkner, D., Das, P.K., Djatmiko, E.B., 'Some Aspects of Structural Design of Fast Multi-Hull Ships', loc. cit. 1, 1993.

4) Yu, P.O., 'Multiple Criteria Decision Making', Plenum Press, New York, 1985.

5) Zanic, V., Grubisic, I., Trincas, G., 'Multi-Attribute Decision Making System Based on Random Generation of Non-Dominated Solutions: An Application to Fishing Vessel Design', Proc. 5th Intl. Symp. Practical Design of Ships and Mobile Offshore Units (PRADS 92), J. Caldwell, Ward (Eds.), Vol. 2, Newcastle Upon Tyne, Elsevier Applied Science, 1992.

6) Das, P.K., Zanic, V., Faulkner, D., 'Reliability-Based Design Procedure of Stiffened Cylinders Using Multiple Criteria Optimisation Techniques', Proc., Offshore Technology Conference (OTC), Houston, Texas, 1993.

7) Pu, Y., 'On Prediction of Primary Loads on SWATH Ships', Dept. Report No. NAOE-93-21, Department of Naval Architecture and Ocean Engineering, University of Glasgow, Glasgow, May 1993.

8) Chan, H-S, 'A Three Dimensional Technique for Predicting First- and Second-Order Hydrodynamic Forces on a Marine Vehicle Advancing in Waves', PhD Thesis, University of Glasgow, 1990.

9) Chan, H-S , 'Prediction of Motion and Wave Loads of Twin-Hull Ships', Jnl. Marine Structures, Vol. 6, 1993.

10) Chan, H.S., Djatmiko, E.B., Miller, A.F., Caldwell, L.B., 'Structural Loading Aspects in the Design of SWATH Ships', loc. cit. 5, 1992.

11) Carter, D. J. T., Challenor, P. G., Ewing, J. A., Pitt, E. G., Srokoszi, M. A., Tucker, M. J., 'Estimating Wave Ultimate Parameters for Engineering Applications', Offshore Technology Report, OTH86 228, Department of Energy, HMSO, 1986.

12) Sikora, J.P., Disenbacher, A.L., 'SWATH Structure: Navy Research and Development Applications', Jnl. Marine Technology, SNAME, Vol. 27, No. 4, 1990.

13) American Bureau of Shipping, 'Preliminary Guide for Building and Classing SWATH Vessels', Draft, ABS, New York, 1990.
14) Das, P.K., Pu, Y., 'Finite Element Based Structural Analysis of SWATH', Dept. Report No. NAOE-93-20, Department of Naval Architecture and Ocean Engineering, University of Glasgow, Glasgow, May 1993.
15) Faulkner, D., 'Compression Strength and Chance', Defence Fellowship Thesis for the U.K. Ministry of Defence, Massachussets Institute of Technology, 1971.
16) Faulkner, D., Adamchak, J.C., Snyder, G.J., Vetter, M.F., 'Synthesis of Welded Grillages to Withstand Compression and Normal Loads', Computer and Structures, Vol. 3, 1973.
17) Rockey, K.C., Evans, H.R., Porter, D.M., 'A Design Method Predicting the Collapse Behaviour of Plate Girders', Proc. ICE, Vol. 65, Part 2, March 1978.
18) Narayanan, R. and Rockey, K.C., 'Ultimate Load Capacity of Plate Girders with Webs Containing Circular Cutouts', Proc. Instn Civil Engineers, Vol. 71, Part 2, 1981.
19) Evans, H.R., Burt, C.A., 'Ultimate Load Determination for Welded Aluminium Plate Girders', Proc. Intl. Conf. Steel and Aluminium Structures, R. Narayanan (Ed.), Vol. 2, 8-10 July 1987, Cardiff, Elsevier Applied Science, London, 1987.
20) Scheer, J., Pasternak, H., 'Zum Nachweis von Vollwandtragern mit Dunnen Stegen und Quersowie Auch Langssteigen in Regelwerkedn', Bauingenieur, Vol. 64, 1989.
21) Scheer, J., Pasternak, H., Schween, T., 'Zum Tragverhalten Ausgesteifter Rahmenecken mit Schlanken Stegen, Stahlbau, Vol. 60, 1991.
22) Maquoi, R., 'Plate Girders', Chapter 2.6, in Constructional Steel Design: An International Guide, P.J. Dowling, J.E. Harding, R. Bjorhovde (Eds.), Elsevier Applied Science, London, 1992.
23) British Standards Institution, 'British Standard Code of Practice BS 5500: Specification for Unfired Fusion Welded Pressure Vessels', BSI, London, 1991.
24) Winkle, I.E., Baird, D., 'Towards More Effective Structural Design Through Synthesis and Optimisation of Relative Fabrication Costs', Trans. RINA, Vol. 127, 1985.
25) Frieze, P.A., Winkle, I.E., Das, P.K., Baird, D., 'Optimisation of Stiffened Cylinders in Offshore Construction', Trans. RINA, Vol. 128, 1986.

26) Morandi, A.C., Zanic, V., Das, P.K., Faulkner, D., 'An Investigation on the Application of Alternative Materials to Externally Pressurised Vessels, Proc. Conf. Structural Materials in Marine Environments, 11-12 May 1994, The Institute of Materials, London, 1994.

27) Thoft-Christensen, P., Baker, M.J., 'Structural Reliability Theory and Its Applictions', Springer-Verlag, Berlin, 1982.

28) Thoft-Christensen, P., Murotsu, Y., 'Appliction of Structural Systems Reliability Theory', Springer-Verlag, Berlin, 1986.

29) Das, P.K., 'A Program Note on Structural Reliability Assessment of Stiffened Panels of Ship Hull Girder and Results of a Tanker Example Problem', Report, No. 94302, British Maritime Technology, May 1986.

30) International Ship and Offshore Structures Congress, 'Report of Committee III.3: Material and Fabrication Factors', Proc. 12th ISSC, N.E. Jeffrey, A.M. Kendrick (Eds.), 12-16 September 1994, St. John's, Newfoundland, Canada, 1994.

31) Guedes Soares, C., Soreide, T.H., 'Behaviour and Design of Stiffened Plates under Predominantly Compressive Loads', Intl Shipbuilding Progress, Vol. 30, 1983.

32) Gordo, J.M., Guedes Soares, C., 'Approximate Load Shortening Curves for Stiffened Plates under Uniaxial Compression', loc. cit. 1, 1993.

33) Pu, Y., Das, P.K., 'Ultimate Strength and Reliability Analysis of Stiffened Plates', Report No. NAOE-94-37, Dept. of Naval Architecture and Ocean Engineering, University of Glasgow, Dec. 1994.

Tables

Table 5.1: The particulars of the example SWATH ship.

Displacement	169 tonnes
Mean draught, T	2.7 m
Lower hull length	31.05 m
Length overall	36.5 m
Lower hull diameter, H_D	1.8 m
Strut width, T_s	1.0 m
Submerged strut height, D_s	1.1 m
Box width, B	13.0 m
Hull separation (to centre)	10.0 m
Water plane coefficient, C_{wp}	0.95
Strut height, S_H	1.65 m
Box depth, D_B	1.0 m
Section depth, D	5.9 m

Table 5.2: Main structural components, failure modes and associated modelling uncertainties.

Strl. Component	Failure Mode	Uncertainty Mean/COV
Cross-Deck	Shear mechanism	0.98/6.0
	Shear/bending mech.	1.0/7.0
	Bending/shear mech.	
	Bending failure	0.992/4.5
Flat plating		
(a) Long	Strength under lateral pressure	1.0/10.0-8.0
	Plate buckling strength	0.98/11.0-5.0
	Tripping strength of stiffener	1/15.0-12.0
	Plate induced column collapse	1.041/12.0-15.0
(b) Wide	Strength under lateral pressure	1.0/10.0-8.0
	Plate buckling strength	0.98/11.0-5.0
	Tripping strength of stiffener	1/15.0-12.0
	Plate induced column collapse	1/15.0-12.0
Knee-joint	Ultimate bending moment capacity	0.908/11.5
Cylindrical Hulls	Interframe collapse	1.026/7.6

Numbers in bold correspond to values for the case the material is aluminium. Where no such values are quoted those of steel are used .

Table 5.3: Optimised variables, assumptions on their statistical behaviour, and range of variation.

Structural Component	Design Variables	Mean	COV	Range
Cross-Deck, Decks & Knee-Joint†	-Web plate thickness	4	2.5	4-8
	-Thickness of top/wet deck plating	4	2.5	4-8
Framing†	-Frame spacing	1250	2.5	900-1700
Haunch†	-Plate thickness	6	2.5	4-8
Strut†	-Plate thickness	6	2.5	4-8
	-Web depth of frame	200	2.5	100-410
	-Web thickness of frame	6	2.5	4-8
	-Flange breadth of frame	75	2.5	30-120
	-Flange thickness of frame	10	2.5	6-12
Hulls†	-Cylinder shell thickness	6	2.5	4-8
Stiffening*†	-No. of vertical stiffeners in cross deck web	6	-	3-7
	-No. of longitudinals on the 'flanges of the cross deck	2	-	1-7
	-No. of transverse (in global transverse direction) stiffeners on the 'flanges'of the x-deck	2	-	1-7
	-Web depth of longitudinals	43	2.5	30-120
	-Web thickness of longitudinals	4	2.5	4-8
	-Flange breadth of longitudinals	50	2.5	35-160
Loads	-Direct in-plane stress		15	
	-Bending Stress		15	
	-Shear Stress		15	
	-Lateral pressure		15	
Material properties	-Yield Stress (Log-normal)	217.5	8	
	-Young's Modulus (Normal)	71,000	2	

*Longitudinal stiffening has been assumed to be the same for the complete structure.
This assumption models best the use of extruded sections.
† Optimised design variables. The remaining are simply treated statistically.
All dimensions in mm and N/mm2.

Table 5.4: **Maximum side force and bending moments applied on the example ship for a number of wave headings and probability of occurrences of the extreme values [3].**

Dirctn.	Force/Bend. Mmt.	α=1	α=0.01	α=0.001
0°	Side Force (kN)	62	78	84
	Bending Mmt (kNm)	360	440	480
	Yaw Splitting Mmt (kNm)	700	870	950
45°	Side Force (kN)	600	750	810
	Bending Mmt (kNm)	2100	2700	2970
	Yaw Splitting Mmt (kNm)	5200	6460	7010
90°	Side Force (kN)	1610	2010	2180
	Bending Mmt (kNm)	5910	7360	7980
	Yaw Splitting Mmt (kNm)	782	971	1050
135°	Side Force (kN)	585	729	791
	Bending Mmt (kNm)	1980	2460	2670
	Yaw Splitting Mmt (kNm)	5380	6680	7240
180°	Side Force (kN)	103	128	139
	Bending Mmt (kNm)	569	708	768
	Yaw Splitting Mmt (kNm)	520	647	701

Table 5.5: **Material volume distribution as a percentage of the total structural weight of half frame section of the example ship.**

Structural Component	Volume ($x10^{-6}$ mm^3)	Percentage of the total (%)
Top-Deck	43.550	18.63
Wet-Deck	43.550	18.63
Cross-Deck	25.026	10.72
Total (Deck)	112.126	47.98
Haunch	38.475	16.46
Strut	33.405	14.29
Cylindrical Hulls	49.725	21.27
Total (SECTION)	233.74	100

Table 5.6: **Material volume distribution for the plating, longitudinal and transverse stiffeners as a percentage of the total structural weight of half frame section of the example ship.**

Structural Component	Volume ($x10^{-6}$ mm^3)	Percentage of the total (%)
Plating		
Top-Deck	35.00	14.97
Wet-Deck	35.00	14.97
Cross-Deck	24.03	10.28
Haunch	28.50	12.19
Strut	24.75	10.59
Cylindrical Hulls	42.40	18.14
Total (Plating)	189.68	81.15
Longitudinal Stiffening		
Top-Deck	8.55	3.65
Wet-Deck	8.55	3.65
Haunch	3.575	1.53
Strut	3.220	1.38
Cylindrical Hulls	negligible	-
Total (Long. Stiffening)	23.895	10.22
Transverse Stiffening		
Top-Deck	negligible	-
Wet-Deck	negligible	-
Cross-Deck (vertical)	1.00	0.43
Haunch	6.40	2.74
Strut	5.435	2.32
Cylindrical Hulls	7.325	3.13
Total (Transv. Stiff.)	20.16	8.63
Total (Stiffening)	44.06	18.85
Total (SECTION)	233.74	100.0

Table 5.7: **Original versus final (optimised) design variables and comparison of safety.**

Structural Component	Design Variables	Original (mm)	Optimised (mm)	Min. β Orig.	Min. β Opt.
Cross-Deck				5.89	5.68
Decks				3.21	3.22
Knee-Joint	t_t	4	4	2.14	2.15
	t_d	4	4		
Frame spacing	L_s	1250	1245		
Haunch	t_h	6	5.5	3.82	3.74
Strut	t_s	6	5.5	4.90	5.18
	d_{w1}	200	180		
	t_{w1}	6	6		
	b_{f1}	75	70		
	t_{f1}	10	9		
Cylindrical Hulls	t_c	6	6	4.23	4.26
	L_2	1000	1000		
	L_1	333.33	333.33		
	d_{w2}	43	40		
	t_{w2}	4	4		
	b_{f2}	50	45		
Weight		11.09 t	10.83 t		
Cost		£72,800	£72,400		
Ditlevsen Upper Bound		0.0168	0.0164		

Table 5.8: **Load actions for each gross element based on F.E. calculations.**

Structural Component	Load Type	Value (N/mm^2)
Cross-Deck		
(a) Cross-deck Girder	Bending moment stress	43.5
	Direct in-plane stress	6.0
	Shear stress	10.0
	Lateral Pressure	0.055
(b) Deck plating	Bending moment stress	43.5
	Direct in-plane stress	6.0
	Shear stress	10.0
	Lateral Pressure	0.055
Haunch	Bending moment stress	24.0
	Direct in-plane stress	0.0
	Shear stress	10.0
Strut	Bending moment stress	15.0
	Direct in-plane stress	0.0
	Shear stress	10.0
Knee-joint	Bending moment stress	43.5
	Direct in-plane stress	6.0
	Shear stress	10.0
Cylindrical Hulls	External pressure	0.055

Figures

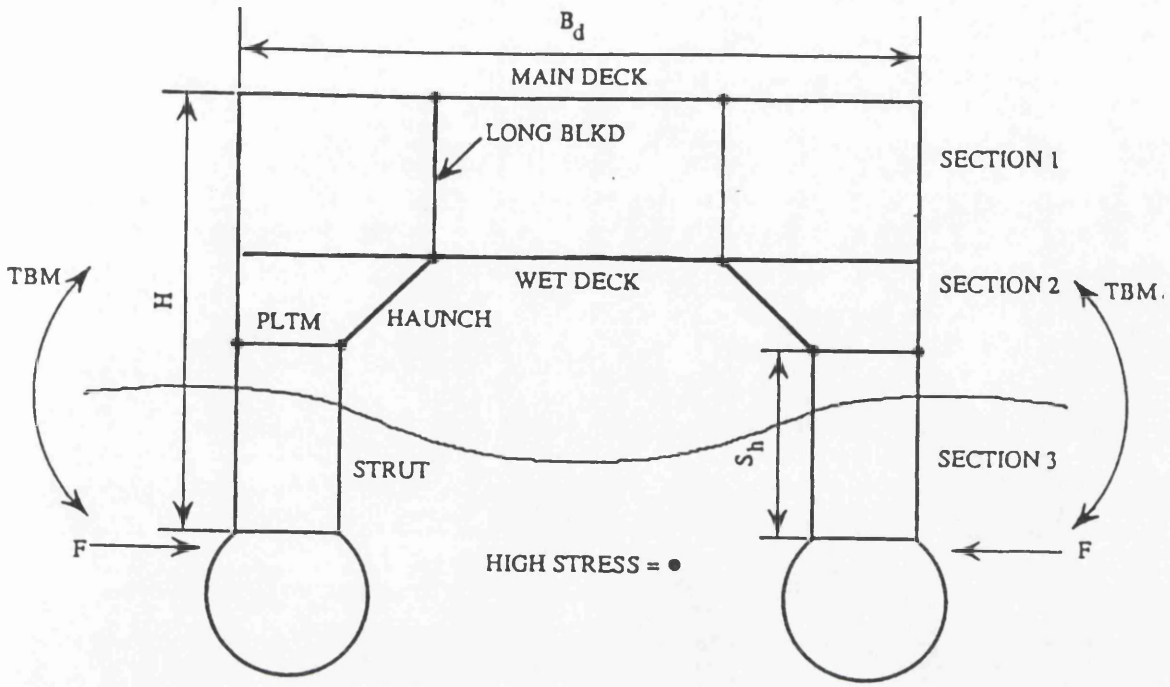

Figure 5.1: The main structural elements of a SWATH ship section.

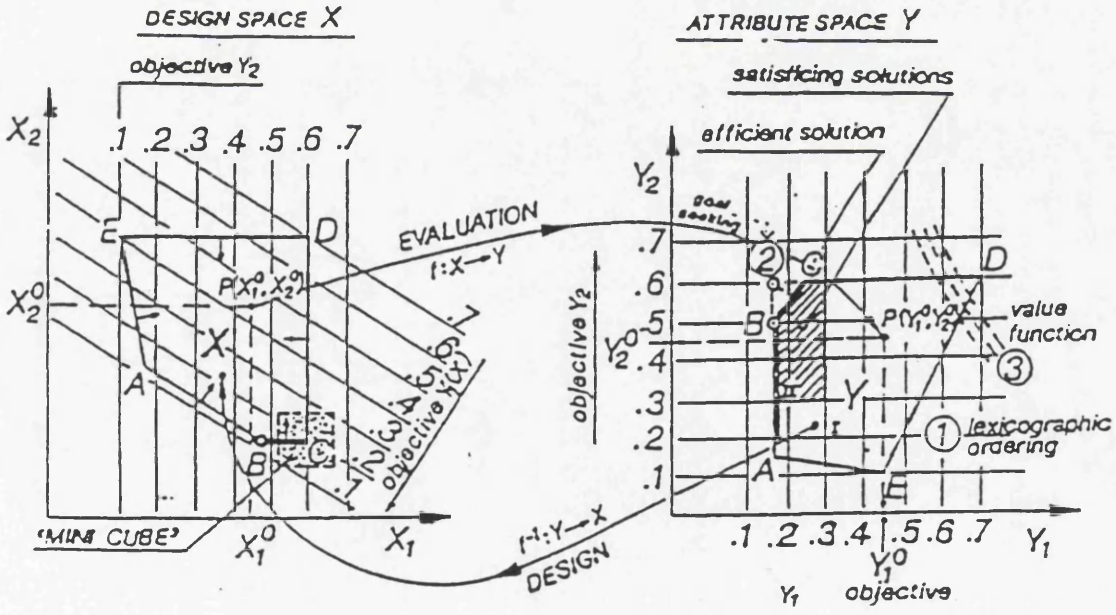

Figure 5.2: The transformation of design space into attribute space in a structural synthesis exercise [5].

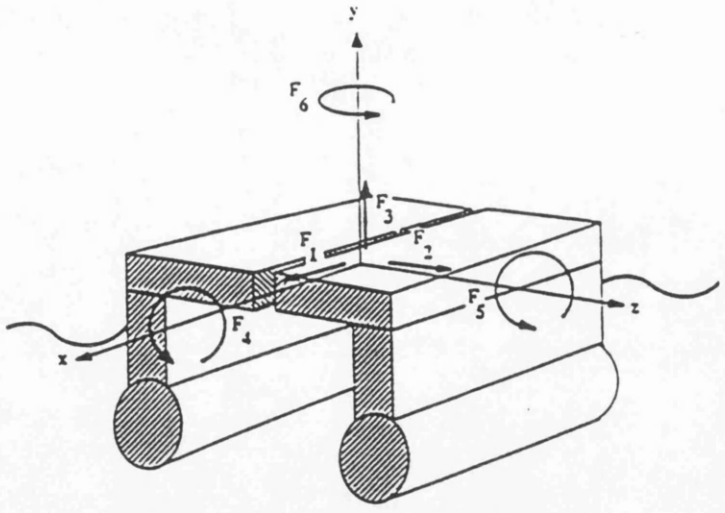

Figure 5.3: Inertial and hydrodynamic forces calculated on the longitudinal plane through the centreline of the ship [12].

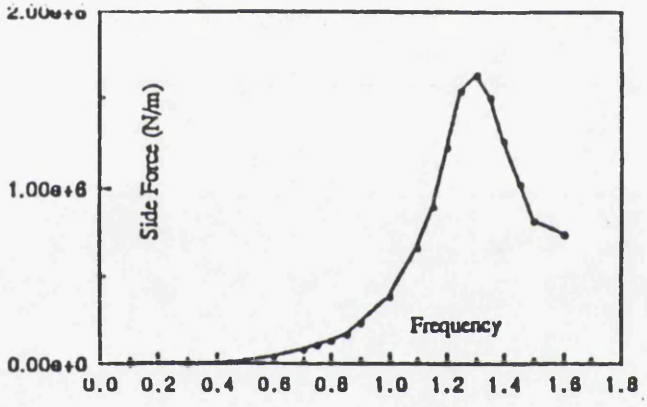

Figure 5.4: RAO of side force at beam sea and zero forward speed [1].

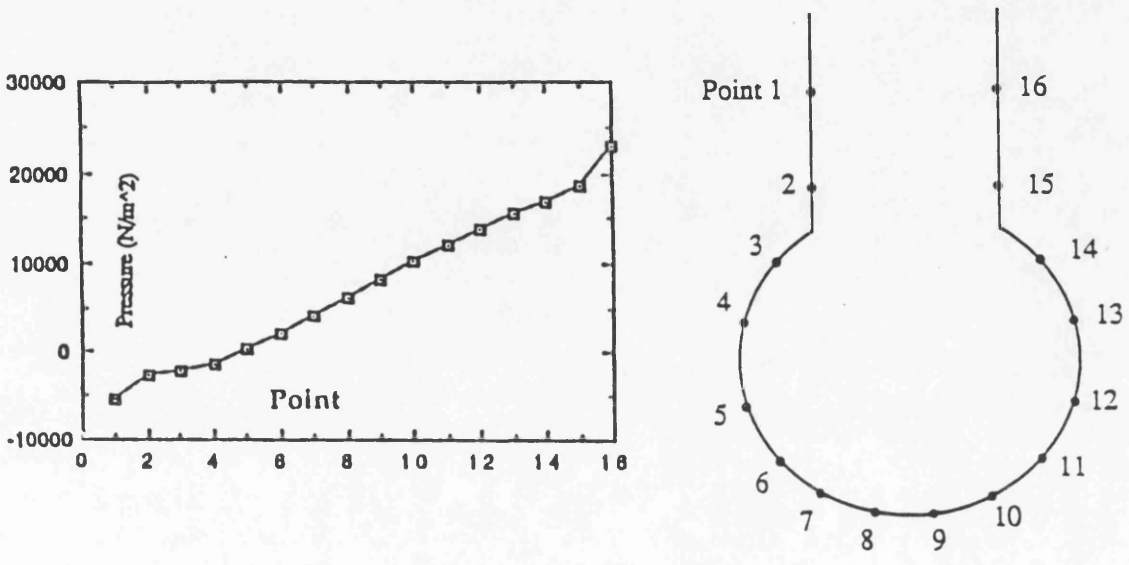

Figure 5.5: Instantaneous pressure distribution at the lower strut and hull section [1, 16].

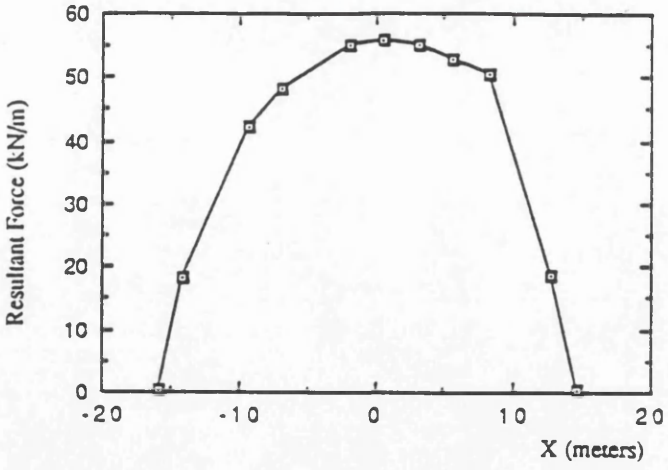

Figure 5.6: Longitudinal distribution of hydrodynamic pressure on the underwater hulls of the example ship [16].

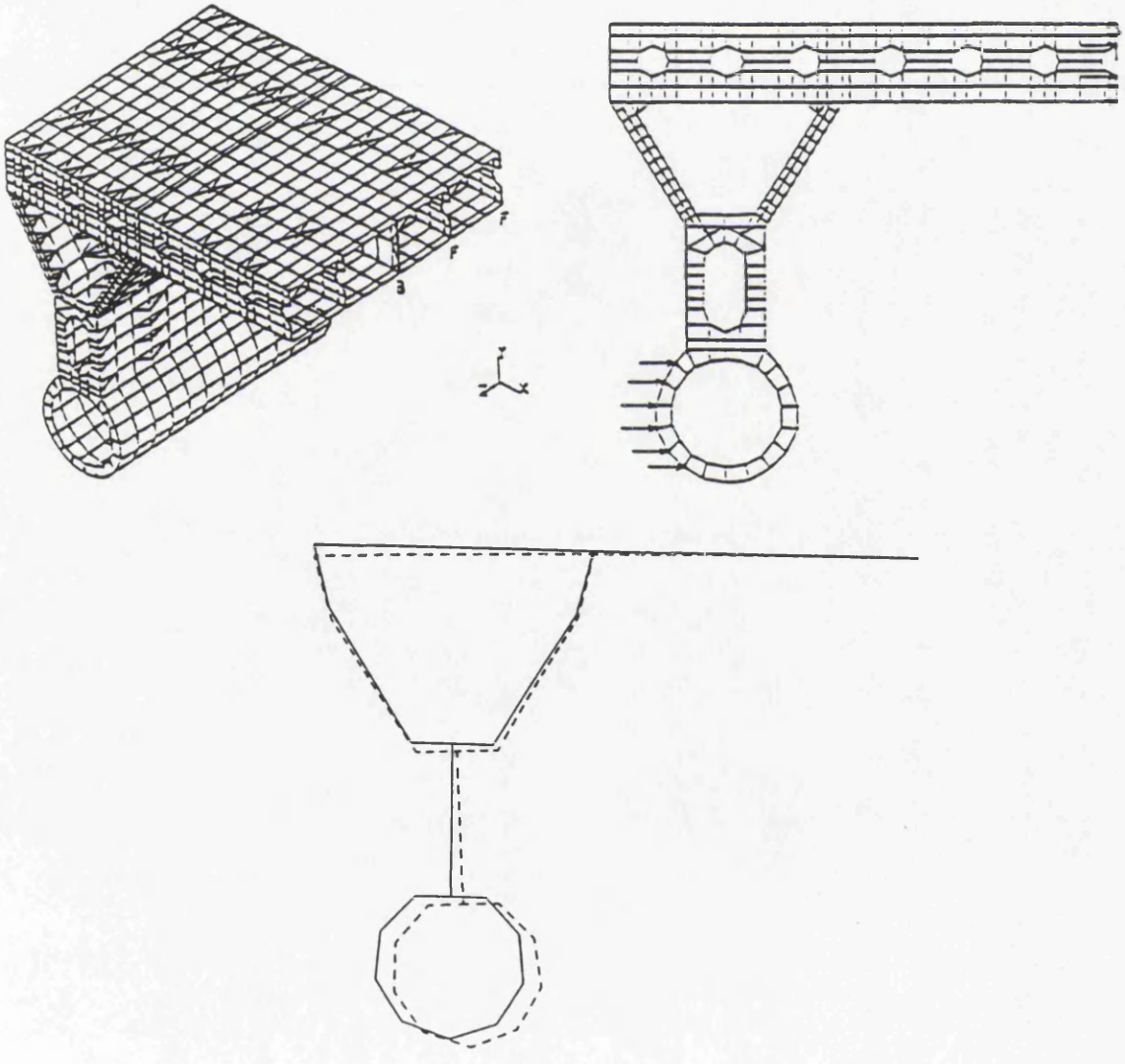

Figure 5.7: 3-D, 2-D and 1-D FE representation of the example ship [2, 16].

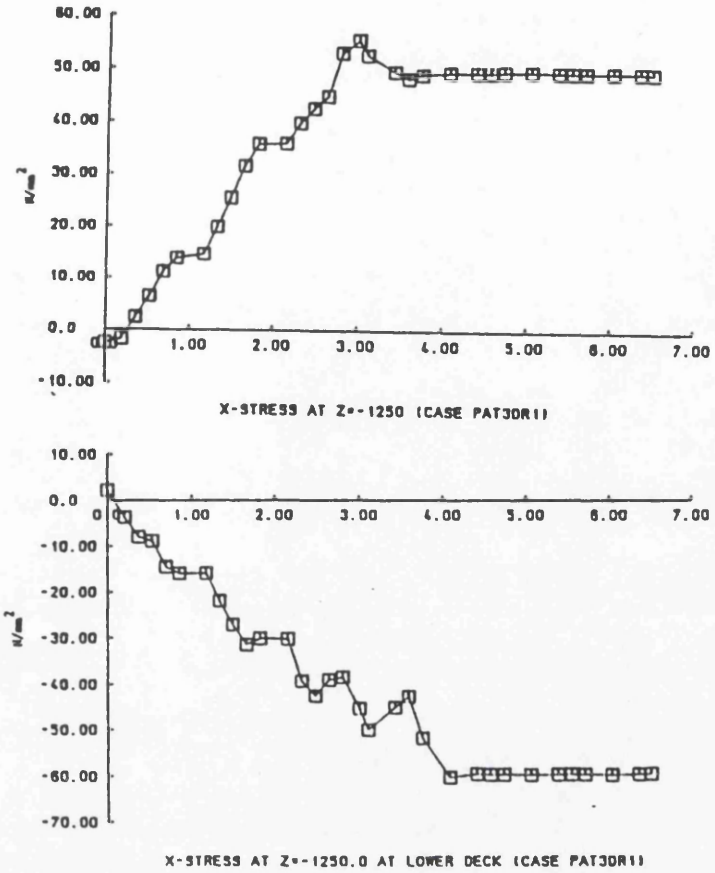

Figure 5.8: Transverse stress distribution across (a) the upper and (b) the lower deck at a frame position [3, 16].

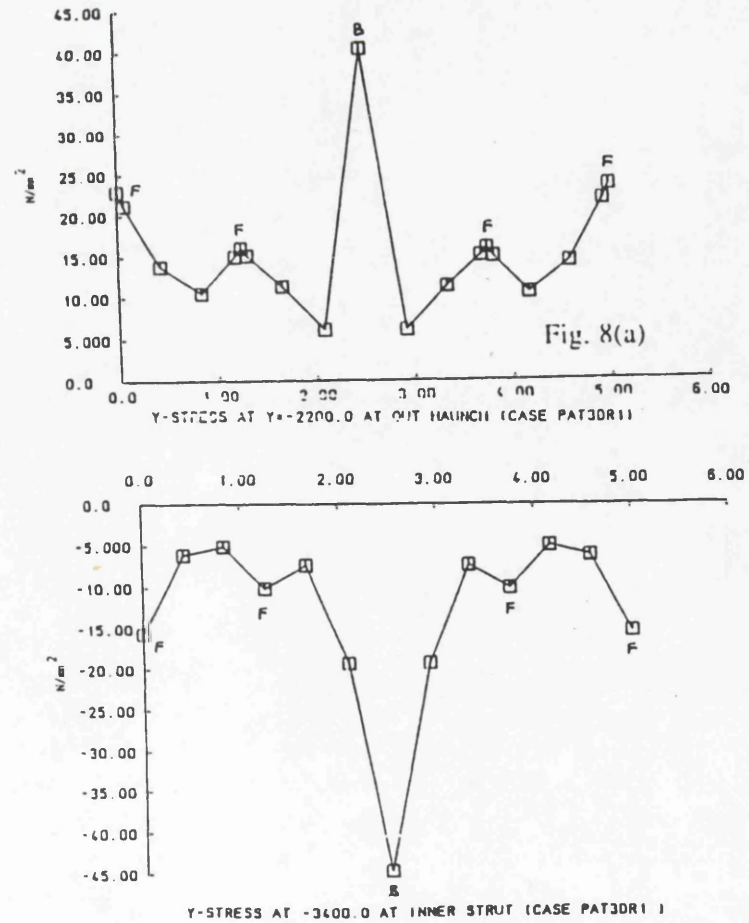

Figure 5.9: Stress distribution along (a) the outer haunch and (b) the inner strut side plating [3, 16].

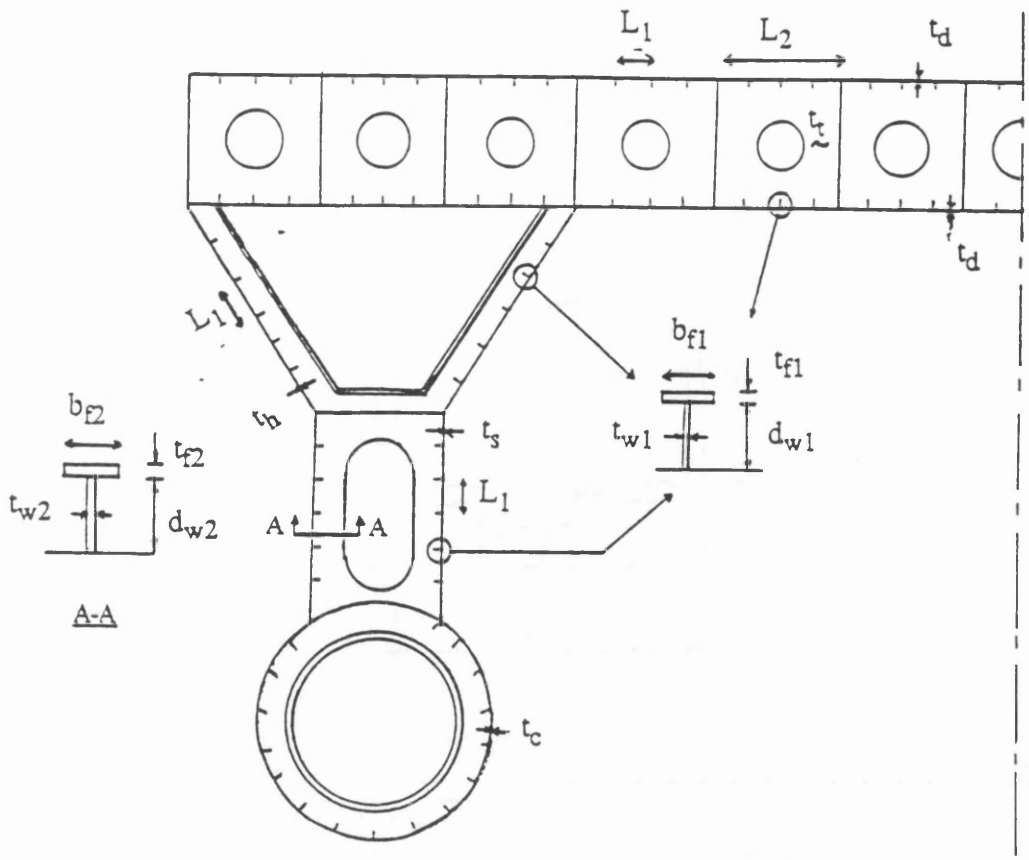

Figure 5.10: The optimised variables of the example ship.

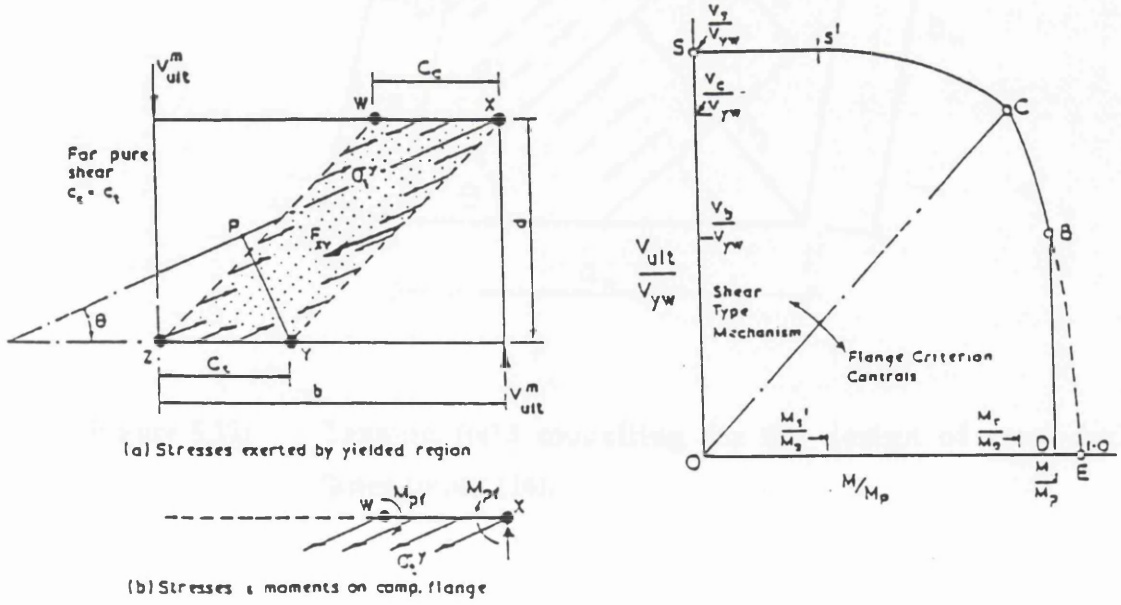

Figure 5.11: Tension field modelling and interaction curve for the design of the cross-deck girder web as proposed by Cardiff [20].

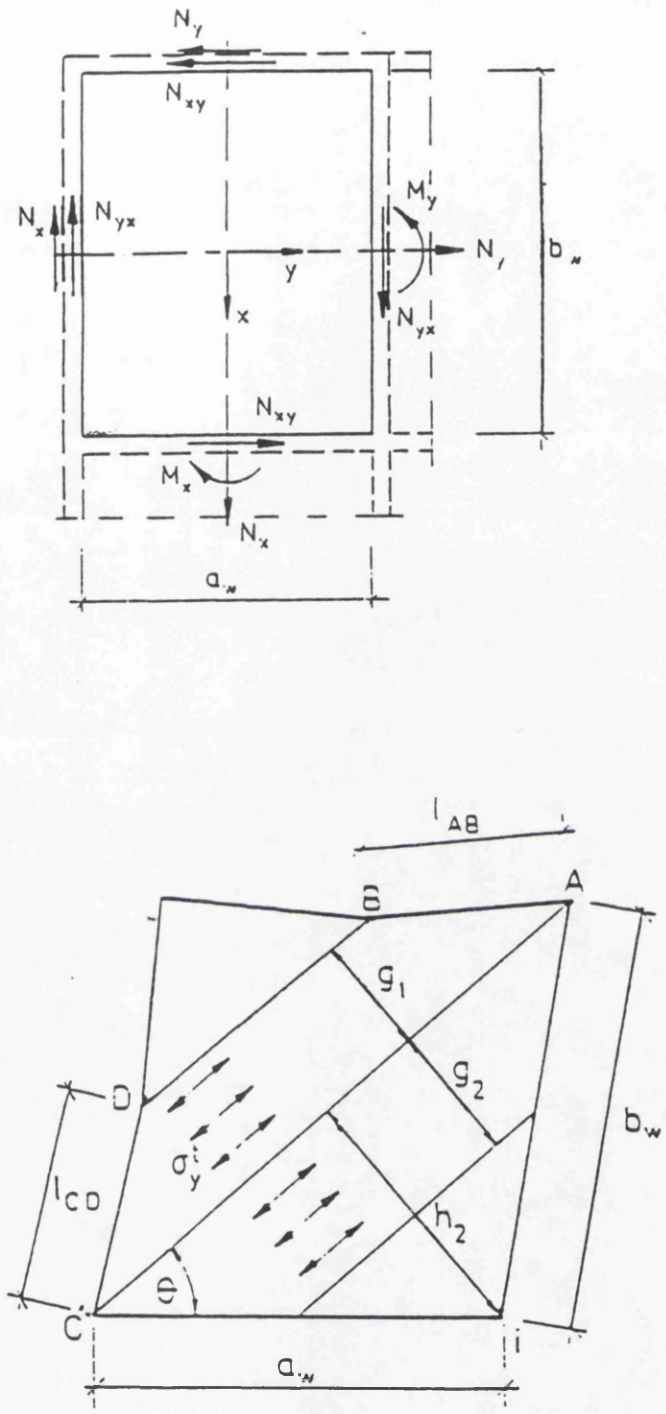

Figure 5.12: Tension field modelling for the design of cross-deck 'knee-joints' [24].

CHAPTER 6

6.0 Conclusions

The aim of this thesis has been to review the aspects pertinent to the structural design and provide the background work and guidance for the development of a future code for fast marine vehicles and SWATH ship in particular. Recognising the importance of material selection and the increasing use of aluminium as a main structural material for main structural components, attention has been paid to both steel and aluminium applications.

It has therefore been inevitable that a large number of topics had to be covered in order to provide the reader with the overall picture of the structural design problems expected in this novel form of transportation. As a result, no claim for completeness is made herein, but instead proper balance had to be struck between large variety and detail. The bias towards an 'in width' study of the topic was felt as providing the best means of identifying the degree of interrelation and interaction of the various aspects of structural design, and has therefore been actively pursued herein.

The SWATH ship was chosen as an example for two main reasons. Firstly to conclude the lengthy and considerable involvement of the Department of Naval Architecture and Ocean Engineering, University of Glasgow, into the load and response prediction of these vessels, by extending the research effort into the development of a rational structural design procedure appropriate for SWATHs and indeed any other fast marine vehicle. The second reason has been the SWATH ship's high weight fraction, which is the highest amongst all the buoyancy supported vessels. Hence, it forms an excellent candidate for benefiting from any optimisation of its structural scantlings. The advantages and disadvantages of this specific concept, all stem from its small waterplane area and have been adequately described in Chapter 1. It is unfortunate, that the end of the Cold War has identified the end, together with so many other things, of the interest in the SWATH concept as a stable platform for use in heavy weather which after all is its main advantage. Despite the construction of the biggest SWATH ship, the 3,500 tonne Radisson Diamond three years ago to serve as a cruise liner, the concept does not seem to enjoy the popularity that catamarans and indeed SES ships do. After all, in terms of transport efficiency, these two vessels have been shown to achieve the highest values, despite their high initial

cost and the difficulties in the development of lifting systems for larger size SES craft. Catamarans are generally viewed as having the greater potential for size increase, and hence, their development is actively pursued in both Europe and the Far East. In addition, as the payload capacity decreases with increasing speed the current trend is towards small, passenger carrying, fast craft but for fast cargo vessels with increased payload demand and intended for longer routes, new, large displacement solutions are being considered in the Japan and Korea. Considering that the more weight sensitive and hence complex design concepts are closely associated with high speed and impose payload limitations, catamarans are likely to dominate the high displacement range (6,000 - 12, 000 tonnes). For displacements up to 6,000 tonnes SES ships remain an attractive option as they have been tried for payloads of 1,000 tonnes. For smaller sizes of vessels, where payload capabilities are not usually a requirement, advanced technological concepts like hovercraft, foil-catamarans, SESs and perhaps WIG craft will be of much better value for the passenger transportation market.

It is of course worth remembering that the success and final establishment of fast marine transportation as a popular and easily accessible means of travelling, will depend on three key players, the passengers, the operators, and the governments.

The passengers are those to whom the new service is aimed at, and it is their approval that will dictate future developments. They present the largest factor of unpredictability in the final choice of transportation, as personal preferences are varied and difficult to predict. The success of the particular service will depend on the level of travel comfort provided which is particularly prone to personal preferences, experience and expectations. Slower, overnight ferry services might still prove attractive, if larger passenger areas, better on board-entertainment and the potential to 'take the car' are available. The fare in a faster service is currently approximately 50% greater, and indeed remains characteristically uncompetitive with respect to the other modes of transportation, both in terms of fare level against speed of travel and fare level against distance travelled. Although, market research has shown that current ferry passengers would be prepared to pay extra for the service, the acceptable level of fares will be dependent on the travel duration, frequency of travel, facilities and space available on board and at the port terminals as well as the ease by which this mode will link to other land/air transport modes.

The operator in turn is bound by technical, financial and governmental policy limitations. Financially he has to overcome the understandably higher risk involved with this type of investment, arising mainly due to the lack of information feed-back from the relatively limited number of vessels currently in service. The higher capital cost that might arise due to specialised materials, construction techniques, duplication of machinery and propulsion systems etc., will certainly have the owner thinking twice before committing himself to the fast ferrying option. However, this has to be carefully balanced against savings in operational costs arising from the smaller number of crew, and hence larger (and more frequently) available fare earning space. Proper management is essential.

Governmental policies are not so clear cut in Europe as they are in the Far East. Although both geographical locations are faced with extreme overburdening of their land and air transportation systems, it is only in Japan that a modal shift to fast marine transportation is encouraged by the national government. Developments in Europe relative to the Common Market and the introduction of free trade and competition across European borders does not permit discriminatory policies in favour of marine transportation, whether this is 'fast' or 'slow'. The additional difficulty exists, that the technological and operational challenges involved in the new concepts cannot be tackled by individual companies alone. Their solution would require a long-term strategy based on partnerships, rather than short-term collaboration that would result in bitter competition in one or two years time. Government fiscal policies characterised by co-operation rather that protectionism, coupled with a sound transportation policy aimed at the years ahead will greatly encourage inter-firm collaboration. It should also guarantee a local market for the new technology thus encouraging collaboration between shipbuilding firms on strategic issues, allowing competition only where necessary.

In general fast marine transportation remains an expensive and costly service and its success will have to be based on routes where the vessels will not be expected to compete with conventional transport systems. Island or inter-island sea routes thus become particularly attractive. In fact, it is seems that fast sea transportation will face competition in the longer routes (150/200 nautical miles) where the overnight ferry provides the opportunity to transform the crossing to an overnight mini-cruise. The shorter routes

(50/150 nautical miles) are expected to be dominated by fast marine concepts. Such routes are numerous in northern and especially southern Europe, a popular holiday destination.

Apart from the socio-economic benefits, the introduction of fast marine transportation requires radical changes in the design thinking and operation of these vessels. In design thinking, the mood has to move away from a 'rule-based' approach to a more rational procedure. The novelty of the concepts, renders the answer to the question of safety, its definition and means of quantifying it, even more urgent and essential. Hence, the need exists for a probability-based evaluation of the structural integrity, simultaneously providing a framework for sensitivity analyses and the more explicit consideration and evaluation of uncertainties associated with the design variables. Such an approach would also permit the determination of efficient and more economical inspection and repair strategies. This is particularly useful for novel designs for which the ability to compare alternative designs is essential and currently very limited. Of the existing reliability methods, AFOSM combines both simplicity of application and sufficient accuracy and was therefore preferred for use in this work. The background and guidance on the means of deriving partial safety factors and good strength modelling have been described in sufficient detail in Chapter 1. Structural redundancy and a 'system' approach to structural integrity analysis, both requiring the examination of all possible load paths and modes of incremental collapse were not considered. The main stages in this rational design procedure and its advantages have been adequately presented in Chapter 1, and have been used in this work as the framework for the review and recommendations that have been tackled and presented.

In terms of material selection, the expected move towards designs of larger displacements coupled with the weight sensitivity of the structure, requires the application of advanced lightweight materials. The attractiveness of steel, in terms of ease of fabrication, maintainability fatigue and fire resistance, makes it a prime candidate for very large designs (>10,000 tonne, 46 knots, 120 m in length) where the question of structural stiffness rather than weight sensitivity controls the material selection. Structures in high strength steels however, are prone to higher and earlier fatigue damage and therefore particular attention and alterations to the design of local structural

details is necessary. For intermediate displacement designs (75 m in length, >1,000 tonnes), where weight sensitivity is even more important, lightweight materials are preferred. Considering that both material and construction cost of titanium is prohibitive to its widespread application, aluminium and FRP provide handy alternatives. Structural design with FRP is not so straightforward (in contradiction to its construction advantages) and its inability to provide adequate stiffness in conjunction with its low fire resistance, restrict its use to secondary structural elements and indeed small vessels. In terms of cost, none of the composites is found to be competitive with steel or aluminium in stiffness sensitive applications and only glass-based composites can compete but only in strength-critical areas. The construction costs associated with these materials are similar to aluminium construction for sandwich structures but increase considerably for single-skin construction.

Aluminium provides a mean route in achieving sufficient stiffness and light weight in construction and is quite attractive due to its low density, corrosion resistance and light weight. The advantages and disadvantages have been presented in Chapter 1, but the characteristics that will dominate the response and behaviour of an aluminium structure is the susceptibility of the 6000 series and some 5000 series alloys to HAZ softening as well as the relatively small modulus of elasticity which renders the structure particularly prone to buckling, vibration and large displacements.

Considerable *cost benefits* are possible in using steel in a homogeneous construction or aluminium/FRP/steel in a hybrid construction while the largest *weight benefits* are observed by using aluminium throughout the structure, or, in the case of hybrid construction, by using a FRP hull/alloy box/alloy superstructure construction arrangement, at least for medium sized SWATH ships. It is worth remembering that the cost advantages of preferring a specific material should be based on an overall construction cost and maintainance analysis, and not on the relative material purchasing costs.

The problem of estimation of both primary and secondary loads on SWATH ships was tackled in Chapter 2. Of the primary loads, the side load at zero speed in beam seas is the most dominant and seems to act as the main load input to any structural design procedure. This however, does not mean that the remaining loads (longitudinal, torsional, fatigue) should be neglected

and appropriate empirical expressions have been presented. These were the result of the most extensive experimental studies carried out in the USA and are highly recommended for preliminary design evaluations. The international effort in theoretical prediction of the load and response of SWATH ships has also been briefly described but sufficiently referenced. Earlier approaches were based on two-dimensional strip theory whose main drawback was that load predictions can only be made in the direction in which the section is chosen in. Current developments move along the 3-D panel theory, which offers the advantage that it allows the inclusion of wave load effects in all directions thus facilitating consideration of the pitch and yaw motion effects which would otherwise be neglected. Hence, 3-D approaches accounting for forward speed effects (translating-pulsating sources) are widely used nowadays (e.g. in the US and the Royal Navy) in the detailed design of SWATH ships.

The description of the seaway can either be short- or long-term. The spectral representation is only applicable for short term wave records whose surface is assumed to be a stationary, Gaussian process. The prediction, on the other hand, of the characteristics of long-term extreme values deals with the occurrence of extreme events which cannot be described by a normal distribution because, in a long-term description of the sea, the significant wave height and zero up-crossing period will vary, and are by no means stationary processes. Hence, the definition of a long term distribution for extreme value environmental statistics over the lifetime of the vessel is required. Two methods are available for estimation of the maximum lifetime wave load action as well as the lifetime fatigue loading on the structure; the design sea load method and the lifetime weighted sea method. The latter is preferred by the US Navy for application to both monohulls and SWATH ships, while the former is a more simplified approach preferred by the Royal Navy. The US Navy approach is the more accurate in the sense that it accounts in greater detail of the environmental considerations for all operational modes over the vessel's lifetime and is justified for locations in the structure where failure will automatically imply structural collapse, although this is quite rare. The Royal Navy approach requires the simplified description of the long-term stress range history over the vessel's lifetime in the form of a Weibull distribution and is more acceptable for structural areas where fatigue crack will merely lead to load shedding to other structural components (Chapter 2).

Of the secondary loads dominating the structural weight of the wet decks and side plating, it is in slamming loads that the work described herein has concentrated. The historical development of the topic has been presented followed by a description of large scale tests into the phenomenon, undertaken in the Department. All researchers are in agreement on the presence of the air cushioning effect, in the case of flat bottom impact, resulting in a significant reduction in the peak impact pressure. Furthermore, the pressure developed during flat impact is not evenly distributed over the flat surface. On the evaluation of the effect of structure/model weight variation it is generally agreed that the heavier structure/model (with the same geometrical size) will result in larger magnitude and shorter duration impact pressures. Furthermore, the pressure is directly proportional to the square of the drop velocity. At very high mass loading the peak impact pressure tends to fall below the line of proportionality, and may bring about a linear relationship between maximum pressure and drop velocity. In contrast to the flat bottom impact, the pressure behaviour of wedge shaped bodies is characterised by the larger peak pressure which occurs at a short distance away from the keel rather than along the keel. Experimental evidence shows the largest impact pressure away from the keel would be experienced on wedge shape bodies with a deadrise angle of about 3-4°. The expectation of larger impact pressure occurring at lower deadrise angles than 3° is not satisfied due to the fact that at such angles the cushioning effect of the entrapped air still exists, although not as intense as in the case of flat bottom impact. There are some areas that have not been sufficiently incorporated in the slamming investigations by drop test models, like the effects of structural flexibility, disturbed (irregular) water surface, and forward speed. In addition, verification of drop test data should be made against the information from seakeeping tests. The inclusion of the structural flexibility and irregularity of the seaway may well lead to a shift from the current static load to more realistic dynamic load criteria.

The experimental work described herein, has since been extended to smaller scale tests by Zhu and Faulkner, in the attempt to identify the possibility of obtaining reliable slamming data from small scale drop tests and deriving load predictions formulations for direct use in design. The possible effects of scaling laws need to be addressed before design guidelines are proposed.

Design considerations against fatigue were tackled in Chapter 3 concentrating more towards aluminium applications. The specific aspects affecting the fatigue strength of welded joints, irrespective of material type have been reviewed. Geometrical misalignment is detrimental to the fatigue life of welds as it amplifies any nominally applied stress range, but its effects should only be considered in the presence of axial loads on the joint. The sole presence of repeated bending stress loads in the structure will not justify the use of any of the load amplification factors presented in paragraph 3.2.1. Furthermore, the fatigue strength of a joint decreases with an increase in the attachment length (in the direction of loading), plate thickness and the width of the stressed member. Proper thickness correction factors are recommended and should be introduced to account for the fact that the test data on which the S-N curves were based have been derived for a particular thickness, which is not necessarily that encountered in an actual design problem. The use of high tensile strength materials, will certainly increase the static and elasto-plastic buckling strength of the individual structural components and joints. Unfortunately, it also usually increases the applied stress range level in the structure and reduces its fatigue life. Careful and more complex design of the sensitive joints will have to be undertaken in order to counterbalance this problem.

Corrosion is (together with temperature, see later), one of the environmental factors that will affect the fatigue life of welded joints. In steel joints, corrosion effects are quite notable, having been known to reduce the fatigue strength of offshore structure joints by a factor as high as 50%. The simultaneous depression of the endurance limit is so large it is perhaps best ignored. In aluminium however, weathering corrosion is not a problem as oxidisation of the material's surface ceases naturally. When aluminium welds in saltwater environments are considered however, experimental investigations reviewed in Chapter 3 have concluded that at R=0.5 at least 30% strength reductions (at 10^5 and10^6 cycles) have been observed for both 5083 and 6063 alloys. In the 5083 alloys the reduction seems to be the greatest (app. 40%), being worst for fillet welds (48%). The 6063 alloys present similar levels of strength reduction (app. 30%) for both butt and fillet welds. Limited experimental data have shown that at least for the 7000 series alloys shot-peening has been found to benefit the corrosion strength of aluminium welded details by increasing it at least by a factor of 4. Galvanic corrosion should be avoided in aluminium by separating dissimilar metallic materials either by painting or use of a a proper sealant.

Stress corrosion is also important for magnesium (Mg) alloys (5000 series alloys) with increased levels of cold forming or annealing at temperatures greater than 60°C, only if the Mg contents are greater than 2.7% (5083, 5086 and 5456). Alloys containing less than 3% magnesium, have no exfoliation and stress corrosion problems. In the annealed state, the Mg alloys may be considered as non-sensitive to stress corrosion up to Mg levels of 7%.

Furthermore, the fatigue strength of steel joints decreases with increasing temperature while at low temperatures steel becomes particularly prone to brittle fracture, especially those in the high strength end of the range. Aluminium on the other hand maintains its fatigue strength down to temperatures as low as -196°C but elevated temperatures (300°C and 400°C) were found to reduce the fatigue strength values by factors up to 50% for both smooth and notched specimens. The design codes generally limit their application to specific temperature ranges.

Of the alloy types available and widely used in structural engineering, the 7000 series have been found to exhibit 44% higher fatigue strength than the 5000/ 6000 series alloys over the complete cycle range. It is worth noting that considerable differences are observed between the 5000 and 6000 series in the low cycle-high stress range, the high-cycle range showing no difference. Current aluminium fatigue design codes make no distinction between different alloy types.

The need for more rational, reliability based limit state checks is also expected to shift the design against fatigue away from the currently applicable lower bound strength solutions and to reliability-based derivation of safety factors on load and strength. Therefore, the method of deriving such factors to a pre-specified level of safety for the fatigue strength check has been described in some detail in Chapter 3. The safety margin can be expressed through empirical S-N curves, or through the more theoretical fracture mechanics approach and these have been appropriately described. Due consideration has been paid to the uncertainties inherent in Miner's damage rule, and the levels of uncertainties for their variables are recommended based on extensive work carried out mainly for the offshore industry. The method for deriving partial safety factors for spectrum loading has also been described but not applied herein. A rather extensive description of the background and recommendations of the current

aluminium fatigue codes was also presented which has demonstrated that both the reliability-based ERAAS and the BS 8118 recommendations reflect the state-of-the-art in aluminium fatigue design mainly due to the fact that they have benefited from a thorough review of available experimental data and the undertaking of extra tests mainly in Europe in the last 15 years. A historical review of these developments and tests has been presented and available comparisons of the various aluminium design codes as presented in the literature have also been reviewed (para. 3.6.5). Comparison is in general not so easy as the design S-N curves, as well as the categories of details in classes, is different in the various codes due to the different sets of experimental data used for each case. The lack of a standardised detail categories between the two codes generally hinders the comparison by forcing the use of equivalent details.

The last part of Chapter 3 dwelled on aspects of weldability of aluminium, and weld repair methods. Hot tearing and solidification cracking are the main causes of low weldability in aluminium alloys. Tearing sensitivity is at a maximum for an alloy content between 1% and 3% (e.g. 2000 and 5000 series) with copper being the alloying element with the largest negative influence on MIG/TIG weldability. On the other hand, liquifaction in the HAZ can give cracking in alloys (e.g. 6082) which are not considered susceptible to tearing. As hot tearing is primarily controlled by grain boundary liquifaction, a high solidification temperature should have a negative influence on the weldability, the value of which has been found to reduce when the solidification interval is increased. Generally copper and elements like lead and bismuth, which are added to improve machining characteristics, have the largest deteriorating effect on the MIG/TIG weldability. Gas weldability is also adversely influenced by lead and bismuth in addition to silicon, manganese and magnesium alloying elements.

The identification of the best ultimate limit state strength models and serviceability requirements for all structural components and failure modes was carried out in Chapter 4. Closed form solutions describing their behaviour under prescribed stress fields and stress field interactions were reviewed and recommended while their accuracy is presented in terms of the bias and standard deviation relative to experimental and/or numerical data. In accounting for welded aluminium in structural design, one should consider the level of residual stresses locked-in the structure, the reduction of the material strength due to HAZ softening and the considerable strain

hardening observed in aluminium's stress-strain curves. HAZ softening is more significant in the 6000 and 7000 series alloys and in the 5000 series alloys only when these are at a work-hardened temper. It is the extent and strength of this reduction that investigators and codes have attempted to model as accurately as possible, and the recommendations by Dwight and Robertson in Cambridge (para. 4.1.2) correspond to the state-of-the-art and have been employed in the latest BS 8118 structural code. Furthermore, the effect of residual stresses in lowering the resistance of aluminium compression bars was found experimentally to be approximately 40% lower than the effect on steel bars, mainly due to the increased heat conductivity of the former material. The beneficial effect of strain hardening, is normally neglected, a conservative but simplifying assumption.

If attention is drawn to the stability of the structural components of the SWATH ship, the first observation would be that the cross-deck deep web plate girder is loaded under shear, direct and bending in plane loads. Therefore a review and comparison of the available ultimate strength design methods was presented. The tension field approach has been found to dominate the design thinking, the main differences in the models arising in the assumed boundary conditions for the web, the inclination and width of the tension band and the tensile stress distribution within this band. The Cardiff model is to be preferred for reasons presented in paragraph 4.4, and has been used in the application example described in Chapter 5. Although, models exist which tackle the interaction between shear and bending loads on deep-plate girders, none accounts for the additional presence of in-plane, direct compressive loads as applicable to the SWATH example. These have been introduced as a superposition to the bending stresses acting on the flanges, a theoretically sound solution. The beneficial effect of the presence of horizontal stiffeners in the 'girder' web are also properly accounted for in the final proposed expressions. Four failure modes are possible (para. 4.4.2.4) ranging from 'pure shear' loading to pure bending, depending on the relative magnitudes of in-plane shear and direct/bending loads acting on web panel. Patch loading, however, has not been addressed. The conservative extension of the theory to aluminium girders already exists as the model has been introduced in the BS 8118 code of practice. In accounting for the HAZ softening effects, the complete web area (and not just the HAZ) is assumed to possess reduced material strength thus affecting the contributions of the tension field and the flange plastic hinges to the overall ultimate strength.

The ultimate strength of perforated girders has also been investigated (para. 4.5). Although cutting a hole in the web plate reduces its shear buckling resistance and ultimate strength considerably, the reduction in *bending strength* is small because the flanges carry most of the bending moment. The positioning of an opening at the centre of the web results in the biggest reduction of the width of the post-buckling tension band thus reducing the ultimate shear capacity of the girder. Therefore, where possible, the cutout should be placed eccentrically to the centre and on the compression diagonal. The extreme case of positioning the perforation in a web corner (and away from the anchoring corners of the tension band) offers the advantages of an increased critical buckling shear stress and an increased tension band width and thus an increased ultimate shear strength relative to the values obtained for the centrally located cutout cases. In the cases where alternating loads exist, the openings can only be placed centrally on the web. Detailed models, based on the Cardiff model exist for the cases of single, circular and rectangular perforations positioned centrally, eccentrically and on the corner of the web panel and relative to the tension field band. No models are available for perforated aluminium plate girders, and hence the approach used by Cardiff for the unperforated cases has been extended for use in the example of Chapter 5. No experimental/numerical support to this proposal exists as yet. For design, a conservative approach by Narayanan et al which assumes that the reduction in ultimate strength of the plate girders is proportional to the increase in diameter (or equivalent diameter) of the cut-out while the ultimate strength capacity is obtained by linear interpolation between the unperforated ultimate strength and the Vierendeel load, is recommended and has been used in Chapter 5. The effect of the reinforcements may also be included via accounting for the formation of 4 extra plastic hinges on the reinforcement itself and the resulting extension of the tensile band relative to the unreinforced case. Suitable reinforcements could be designed to restore the strength of the girder to that of an unperforated web and the subject is sufficiently referenced in paragraph 4.5.5.

Stiffened flat plating is used in a SWATH structure on the main and wet decks, the haunch, side shell, and strut arrangements. In tackling the buckling question of stiffened/unstiffened plate elements use of an 'equivalent' column approach is usually made. Boundary conditions can be considered in detail but pinned assumptions are more widely acceptable as

simplifying and conservative. Modelling their strength can be carried out either via a 'Perry-Robertson' beam-column approach which concentrates more on the effects of initial imperfections and does not directly account for the effects of residual stresses or via a 'column' approach which concentrates in the effects of residual stresses but does not account implicitly for the effects of initial imperfections. Although, most aluminium design codes follow the beam-column representation of strength by appropriately calibrating Perry's constant to experimental data, it is the detailed consideration of residual stress effects and the potential to extend this method to account for HAZ strength reductions that makes the column approach most attractive. It is therefore recommended through Faulkner's effective width model and has been adopted in a new model proposed for the design of unstiffened aluminium flat plates. The accuracy of this model has been proven for steel plated structures (paras. 4.2.4, 4.2.5) , and its ability to predict the strength of 'long', unstiffened, welded and unwelded aluminium plates has been tried in 4.2.5.3 against a limited number of experimental data. For unwelded, plates, the agreement of Faulkner's model with experimental data is excellent. For welded plates, the additional effect to residual stresses of HAZ softening had to be accounted for. Therefore, the reduction in strength in the heat affected zones was appropriately balanced over the complete section of the plate through an 'equivalent strength' value. This strength was obtained from plate stiffness considerations of the heat affected and non-heat affected zones.

In accounting for the *residual stress reduction* effects and inelastic behaviour, it must be remembered that the main difference between the mild steel and aluminium alloy stress-strain curves is that the former demonstrate clearly an elastic to plastic behaviour transition point. The proportional limit can thus simply be defined. In aluminium however, material non-linearities characterise the curve throughout the stress-strain range and hence the application of residual stresses in the model becomes more complex. Using Faulkner's steel assumptions which are equally applicable to aluminium structures, in addition to the Ramberg-Osgood representation of the material stress strain curve the value of the 'inelastic' collapse stress may be obtained and hence the reduction in the ultimate strength of a long plate determined. Comparison of the model with limited experimental data has yielded very encouraging results, but more tests and comparisons are required before a final statement can be given with respect to its accuracy. This is mostly needed for the 'transversely welded' plate case.

It is interesting to note that, in accounting for the effects of the weld orientation relative to the compressive load and its position on the plate, the extensive numerical and experimental research into the behaviour of aluminium welded columns has been reviewed and its main recommendations adopted in the plate model.

The extension of the 'long, unstiffened aluminium plate' model to the stiffened case is straightforward as demonstrated in paragraph 4.2.5.4. The way the model has been developed, permits the possibility of different alloy materials being considered for plate and stiffener, the need to account for construction aspects arising from the use of extruded sections and the effect that the position along the length of the stiffener of a possible transverse weld will have on the overall column strength. Hence, separate account is made for the case of non-welded stiffeners or extrusions and for stiffeners welded at their toes. The approach has not been tested against experimental data and is presented herein as a rational extension to the unstiffened aluminium plate approach presented in paragraph 4.2.5.3. Appropriate experimental data are very limited and thus a more thorough investigation and evaluation is recommended as further work.

Interaction expressions accounting for the effects of co-existence of in-plane load (any combination of axial, biaxial compression, in-plane shear) and lateral loads, are generally derived based on numerical and experimental data, as a result of a simple curve fitting exercise. The most extensive review of available data has been carried out by Guedes Soares and Gordo and the recommendations proposed herein are a direct result of their work. As a general comment, it may be said that for biaxial loading a generalised von Mises expression is used by the various codes, ranging from circular to parabolic and to expressions permitting tensile and compressive loads to act in-plane. The most 'mechanically correct' interaction expression is the one that accounts for both the aspect ratio as well as slenderness effects on the plate behaviour. In the presence of lateral pressure load, it is a linear interaction expression between the pressure load and a form of 'equivalent' uniaxial in-plane compressive load. Uniaxial (or 'equivalent' uniaxial) compression and shear are normally obtained from a circular interaction expression.

Numerical and experimental investigations into the possibility of applying interaction expressions derived for steel plates for aluminium plate components, have concluded that this is possible except in the cases of stocky plates loaded transversely and plates with small imperfections, for these cases the maximum reduction in strength observed was not greater than 5%. In addition, aluminium plates were found to be less imperfection sensitive than their steel equivalents and their load-deflection curves in the post-buckling range are flatter than steel thus enabling plate grillages to sustain greater loads.

Stiffeners throughout the structure should be designed against a rigidity and a strength criterion (para. 4.3). For the rigidity criterion, Maquoi's proposals for the minimum rigidity (γ) that longitudinal or transverse stiffeners should possess in order to guarantee rigid nodes of attachment to the plate under a variety of load conditions, should be used. Amplification factors are also introduced on the optimum rigidity values depending on the type of stiffeners, the type of the stiffener cross-section and the thickness ratio of the plate. Furthermore, the vertical stiffeners which define the main web subpanels at the cross deck girder should be designed so as to withstand the compressive components of the tension field formed on the web plate in the post-buckled regime in addition to to the destabilising bending moments introduced by the out-of-straightness of the longitudinal stiffeners (paras. 4.3.2 and 4.3.3). Similarly, any horizontal stiffeners present are also designed to withstand possible direct compressive loads, this time externally applied. Guidance is provided for the proper load estimation for both stiffener types, while for the longitudinal stiffeners means are available for determining their number and position on the plate, as these two factors are expected to affect the structural weight and behaviour (para. 4.3.3.1). In designing against tripping, it must be borne in mind that this failure may be avoided by appropriate proportioning of the stiffener dimensions, by using symmetrical stiffener cross-sections or by the introduction of tripping brackets. The benefits of the latter measure are questionable especially as it is on the assumption of pinned boundary conditions at the stiffener toe that their use becomes worthwhile. For the majority of structures, tripping failure is independent of the unsupported length as the plating provides a stabilising (or destabilising) rotational restraint to the stiffener. To account for the plate contribution to strength, Faulkner's closed form expression which explicitly introduces the degree of restraint the plate offers to the rotation of the stiffener about its toe, is recommended. It does not however,

consider the effect of web deformations occurring at positively restrained conditions at the toe, and is hence found to be conservative. Morandi's inclusion of this aspect, has resulted in an expression, which although accurate with respect to numerical data, is quite complicated for direct use in design. Finally, the serviceability requirements proposed for the stiffeners, apart from the rigidity requirements mentioned earlier, are those which refer to the relative dimensions of the flange and web of the stiffeners. A yiled stress safety factor of 3 against critical, elastic buckling is recommended (para. 4.3.5) to avoid local buckling of these stiffener components.

The stability of ring and stringer stiffened shells against external pressure loads is also addressed (para. 4.7). To obtain a weight efficient cylindrical structure when it is externally pressurised it is worth remembering that, the shell thickness and hence weight decreases with decreasing frame spacing, that the high strength material is advantageous only when high external pressures are expected, that the ring frame cross sectional area increases with increasing frame spacing and finally that the structural weight is not proportional to the level of external pressure loading. Of the two main modes of failure, interframe shell collapse forms the basis for design while overall collapse, which is frame induced, is avoided by large safety factors. The former can occur in the form of elastic shell buckling for the more slender geometries and appears in the form of a number of circumferential waves with one-half wave between frames or in the form of interframe yielding (axisymmetric plastic deformation), a characteristic of stocky shells. On the other hand, in overall collapse, frame failure can occur either by frame yielding, shell yielding, or frame tripping (interacting with shell buckling). General instability is sensitive to shape imperfections and its prediction is therefore less certain. Hence, it is designed out by dimensioning the ring frames against o-o-c bending stresses and by providing them with adequate rigidity against tripping. In design the BS 5500 proposals should be used on the basis of conservatism and wider acceptance, while for tripping, Faulkner's closed form expression accounting for the interaction of shell and frame is to be preferred especially considering the undue conservatism of the BS 5500 requirement. Generally, in the design of cylindrical externally pressurised structures of a given radius, the stiffener spacing is governed by interframe shell collapse, the stiffener size is governed by general instability and volume requirements in the cylinder, while the proportions of the frames are governed by tripping

and local buckling considerations. To design any conical transition joints, Niordson's proposals (para. 4.7.2) are recommended as being sufficiently tried and require the use of the same strength formulations and criteria as for cylindrical elements under external pressure, but with appropriate modifications to account for the taper angle. For the design of dome ends under external pressure loads (para. 4.7.3), Faulkner's proposed Merchant-Rankine interaction between elastic and inelastic sphere collapse pressures offers a mean curve through experimental data and is recommended.

For the design of orthogonally stiffened cylindrical structures under axial and pressure loads, the failure modes that should be considered are the buckling of shell element between the stiffeners (serviceability), bay instability, the tripping of stringers and/or ring frames, and finally general instability. General instability is designed out by the choice of conservative dimensions for the ring frames and based on the same procedures as for the ring framed cylinders. Hence, the design of orthogonally stiffened cylinders proceeds as a stringer stiffened only, over the bay length between frames and for the former three failure modes. For this purpose, the 1991 RCC revised proposals demonstrate the best agreement with steel experimental data and have therefore been recommended.

In applying the steel models for cylindrical sections under external pressure, to aluminium constructions, Kendrick's procedure is recommended. The equivalence comes by replacing σ_y with the 0.2% proof stress, $\sigma_{0.2}$, and by replacing Young's modulus E, by the secant modulus, E_s, defined at the 0.2% proof stress by $\sigma_{0.2} / \varepsilon_{0.2}$. The comparison of this proposal against the aluminium shell data has not been carried out, but its general effect would be to increase the shell slenderness, resulting in reduced compression strength. The check of this expression and the possible extension of the aluminium flat plate model (para. 4.2.5.3) to shells could offer the basis of future theoretical and experimental investigations.

An attempt has also been made to view the web plate in the plane of the cross-deck/haunch intersection as a 'knee-joint', like those encountered in civil engineering practice. The main difference is that in this specific case the web is deep and slender and therefore cannot be designed based on the plastic approaches used for the standard beam-to-column frame connections. Research work carried out in Germany on steel knee-joints of deep girders and columns (para. 4.6) has been reviewed and extended to the

current application, rather arbitrarily and without the support of experimental data (Chapter 5). Possible extension to aluminium construction of the model has also been attempted. The changes to the original model suggested herein, have a sound theoretical basis and were based on approaches used for the design of deep plate girders. They still however, remain mere suggestions until appropriate experimental data become available.

It is believed that Chapter 5 has succeeded in demonstrating that it is possible to combine an AFOSM reliability-based multiple criteria optimisation procedure with ultimate strength modelling of local structural behaviour in order to address simultaneously weight, cost and safety issues even from the concept design stage. The use of a larger number of variables and/or of another example ship would have demonstrated the effectiveness of the method more emphatically, at the expense of increased computational effort. The design optimisation was achieved by obtaining efficient solutions via random generation of designs in the feasible design region. Final selection was performed by a goal programming approach based on the criteria of structural weight, cost and minimum safety (reliability index). Aluminium alloy material, as well as realistic fabrication constraints, are incorporated in the analysis.

The structural design variables optimised were the plate thicknesses, frame spacing, the frame dimensions in the strut, the cross-deck stiffening, the main and wet deck stiffening, and finally the dimensions of the main longitudinal stiffening throughout the structure. The choices of the limits within which these variables were allowed to vary, had to conform with what is generally available from the construction methods, extrusion manufacturing processes, etc. and would benefit greatly from the designer's experience. Only one transverse slice of the vessel was chosen and optimised as representative of the vessel's geometry.

The design criteria were introduced in the form of linear constraints on the design variables in the design space, analytical ultimate strength formulations and design attribute functions.The linear constraints imposed accounted for constructional aspects, the possibility of the use of extrusions, restrictions on the minimum stiffener spacing, the relative depths of intersecting stiffeners, thus making the process adjustable to individual construction and welding practices. The ultimate limit state checks

considered were described in Chapter 5. It is worth noting at this point, that the modularity of the computer code coupled with an efficient optimisation algorithm, can accommodate hybrid material construction cases in the search for the best solution in terms of safety, cost or weight solution. Such an investigation will be very useful and can initially be restricted to the allocation of different materials to different structural components, and then extended to the use of alternative material stiffeners and plating within the same structural component. The effectiveness of the connection joints will have to be guaranteed for the options finally considered.

In the design attribute functions, a simplified cost expression was used which reflects mainly the difficulty in obtaining accurate costing algorithms from the industry but considering the comparative nature of this study they were more than sufficient. The cost model can be extended to include overheads (e.g. plate cutting and forming, the number and size of structural components relative to the number of workers handling them etc.), variations in the labour rate from yard to yard, the efficiency of the individual labour groups within a yard and relative to other yards. The size and capacity of the handling equipment such as cranes will also affect the labour cost as it could determine, among others, whether construction would be carried out undercover and away from the effects of the environment, or the efficiency and quality of construction would be adversely affected by bad weather. The effect on cost of corrective actions that are almost certainly linked with inefficient working practices, would also have to be accounted for. Furthermore, the material cost is a function of the grade (steel) and alloy (aluminium) and is always prone to specially negotiated prices. The introduction of any special considerations such as the higher inert gas cost, welding consumable cost and the number of welding passes required, require additional attention and the industry can provide useful experience along these lines. The cost algorithm should finally reflect the beneficial effects of standardisation introduced by extrusions in every aspect of the construction process. This has to be balanced against the complexity and quantity of the extruded sections which are likely to render the standardisation of the costing procedure more difficult.

The procedure described in Chapter 5 also allows the designer's preferences and requirements to be interactively applied and therefore its potential is proportional to his expertise, complementing his experience rather than

replacing it. This obvious flexibility of the procedure is underlined by the modular nature of the program allowing the optimisation process to concentrate on individual structural elements at the discretion of the designer as well as on global optimisation of the complete structure.

Unfortunately, the main problem encountered in running the application, was that of time and computational effort required by the optimisation routine. Streamlining and further development of the program are essential to address the problem of speed, although its modularity provides, potentially, great flexibility by permitting the introduction/upgrading of other/new ultimate strength and cost models as research and technology develop.

The limits on the minimum values of target reliabilities used in the specific application were those implied by the individual structural components of the original design. A more general and 'application independent' levels of safety for calibration of the optimised structures need however to be prescribed. Such target levels of safety indices can only be obtained either from analysis of a large number of similar existing ship designs and/or from an analysis of the safety levels implied by already existing and widely used and respected design marine codes. At the local structure level, the experience of other disciplines (e.g. civil engineering) could assist in setting the target of safety for the individual structural components. Extension of the method to other geometries (e.g. catamarans) would be very useful.

The optimised solution has provided disappointingly small improvements in weight, cost and system reliability for the chosen design, for reasons explained in Chapter 5. Nevertheless, the optimisation of an already good design can still be important in its own right.

Appendix 6.1 provides a condensed version of the more important Design Recommendations drawn from the main chapters under the headings:

- Preliminary Considerations
- Load Estimation Recommendations
- Fatigue Strength Modelling Recommendations
- Ultimate Strength Modelling Reccomendations

References to the appropriate sections in the main text are provided.

APPENDICES

APPENDIX 1.1: The Types of Advanced Marine Vehicles

There are three ways of supporting a ship and its cargo on the water. The traditional solution has been static buoyancy lift although hydrodynamic lift, as obtained by hydrofoils, has been in use for many years in fast passenger vessels. Powered static lift is only now becoming more attractive through the SES concept but has been in limited use in air cushion vehicles for quite sometime too. The current trend is more towards hybrid solutions combining two or all three of the lift forces, the most popular being the surface effect ships.

The most common types of fast marine vehicles are the *displacement types* either in their *monohull or twin/multi-hull* versions. The monohull design has evolved from round bilge to chine type with a deep-V hull and is quite attractive because of its low building costs and limited technological risks. Their high wave making resistance however, renders them uneconomic at high speeds. Multi-hull vessels on the other hand, have the advantage of greater deck space and improved stability characteristics arising from the distribution of the buoyancy away from the centreline. Of these, catamarans are most popular despite their operational limitations at rough weather. Improvements in the seakeeping capability of twin-hull vessels, and indeed any displacement vessel, is only available via the SWATH concept whose high resonant frequencies are not in phase with the swell frequencies in a developing seaway. The disadvantage of this concept is that very high speeds are attainable at the expense of considerable power consumption and hence their speed is usually restricted to a maximum of approximately 35 knots.

Planing hulls and hydrofoils with fully submerged or surface piercing foils belong to the category of vessels whose operation is based on hydrodynamic lift. Planing hulls are usually the norm for small, fast pleasure craft but their operation is very sensitive to sea conditions. Hydrofoils are limited in size, but provide reduced wave making resistance mainly due to the foil being the only part of the hull in contact with the water. The surface piercing hydrofoils, have good seakeeping and speed characteristics and are intrinsically stable, but are limited by the foil interference with the water surface. On the other hand, submerged foil hydrofoils present good seakeeping characteristics but require a sophisticated foil control system as

they are intrinsically unstable. Although specific designs are on offer in Japan, Korea and the USA, hydrofoils offer the least scope for size and payload increase and hence their further development is not actively pursued worldwide. A more recent development in Korea and Japan, is that of foil-assisted catamarans, the amount of hydrofoil lift varying between 20-80% of the total depending on the design. Flaps on the foils provide roll, heave and pitch control. The main advantage of this concept is that it permits the development of efficient designs depending on the speed and craft sizes [1]. For a given speed, as the craft size increases the proportion of lift available by the foils diminishes, until the concept reduces to a catamaran with ride control foils. Hence, an efficient design can be developed over a wide range of vessel sizes. A very good historical review of the developments and applications of hydrofoil technology and its hybrid applications worldwide is provided in [2-4].

Ships with *dynamic or powered lift* are more weight critical than those supported by buoyancy as an increase in the main dimensions will not necessarily compensate for a weight/payload increase. This occurs because the structural weight is proportional to the third power of length while the lift of a foil or planning surface or an air cushion is proportional to the square of length. In any case, powered air static lift vehicles are of two types, hovercrafts and surface effect ships (SES). In the former case the air-bubble containing 'skirt' extends over the perimeter of the craft and the propulsive efficiency is considerably reduced because the propulsion is not of marine type but 'air based'. SESs present an hybrid form between a catamaran and a hovercraft by containing the air-bubble between the two side hulls and two (fore and aft) 'skirts'. This bubble normally supports 80% of the weight of the vessel. The popularity of surface effects ships may be traced back to their limited resistance to high speeds (wetted area and wavemaking resistance) as available in hovercraft, and the efficient marine propulsion (waterjets) as available in catamarans.

Another rather distict concept, which be loosely placed in the 'dynamic lift' category is the Wing-in-Ground-Effect concept (WIG). These craft own their lift and high speed on a hybrid design between hovercraft and aeroplane which uses the aerofoil lifting effect when operating close to the sea or land surface. It is a technology not well developed worldwide except in Russia [5-7] were it has seen great growth in the form of large cargo-transportation amphibious craft. China is also actively involved in the concept. The main

argument is whether this technology is categorised as marine vehicles or aircraft, with the knock-on problem of classification and operation restrictions. The debate on this matter is on-going between the Russians who prefer to see the technology as fast *marine* craft rather than accept the *hydroplane* viewpoint of the western world.

References

1) Faulkner, D., Blyth, A.G., Marchant, A., Morrison, B.F.M., Mulligan R.D., Phillips, S.J., 'High Speed Marine Transport', One-Day Seminar on OSTEMS visit to Japan and S. Korea, RINA, London, 30 June 1994.
2) Meyer, J.R., 'Hybrid Hydrofoil Technology', Proc., 1st Intl. Conf. Fast Sea Transportation (FAST'91), K.O. Holden, O. Faltinsen, T. Moan, June 1991, Trondheim, Tapir Publishers, Norway, 1991.
3) Meyer, J.R., Wilkins, J.R.Jr., 'Hydrofoil Development and Applications', Proc., Intersociety High Performance Marine Vehicle Conference (HPMV'92), Arlington, Virginia, American Society of Naval Engineers, 24-27 June 1992.
4) Meyer, J.R., 'Hybrid Hydrofoil Technology Applications', Proc., Intersociety High Performance Marine Vehicle Conference (HPMV'92), Arlington, Virginia, American Society of Naval Engineers, 24-27 June 1992.
5) Rozhdestvensky, K.V., Synitsin, D.N., 'State-of-the-Art and Perspectives of Development of Ekranoplans in Russia', Plenary Session, Proc., 2nd Intl. Conf. Fast Sea Transportation (FAST'93), 12-15 December 1993, Yokohama, The Society of Naval Architects of Japan, 1993.
6) Bogdanov, A. I., Synitsin, D.N., 'New IMO High Speed Craft Code and the Problems of Ekranoplans Certification', loc. cit. 5, 1993.
7) Hooker, S.F., Terry, M.R., 'Hydroaviation', Proc., Intersociety High Performance Marine Vehicle Conference (HPMV'92), Arlington, Virginia, American Society of Naval Engineers, 24-27 June 1992.

APPENDIX 1.2: The Major Research Programmes in Fast Marine Transportation Concepts

Current research effort into fast marine transportation seems to be advancing along two rather distinct routes [loc. cit. 1]. European yards restrict their research and development to monohull designs [1, 2, 3] with only some research institutions currently actively involved in the design and development of *small,* passenger vehicles in the form of catamarans, SES and SWATH ships. Although conceptual designs are available in Europe for larger, high payload cargo catamarans up to 1,000 t payload, no major construction has been carried out, except perhaps the sole example of the Stena HSS Catamaran and the SWATH cruise liner 'Radisson Diamond' [4]. On the other hand, Japanese and Korean shipyards are concentrating on large multihull vessels and particularly hybrid designs. As pointed out in the conclusions of a recent fact-finding visit of a team of experts [5] to Japan and South Korea, the shipyards actively involved in the design and construction of advanced marine vehicles are specialising at most in three concepts each.

Japanese research and development efforts concentrate on the catamaran concept and some variations like foil-assisted (e.g. Hitachi Zosen), super-slender twin-hull (e.g. IHI), SWATH (e.g Mitsui, also specialising in hovercrafts) and hydrofoils (e.g Mitsubishi, Kawasaki under liscence from Boeing, USA). Air-cushion vehicle designs are also available (e.g. Mitsui) but further developments are not actively pursued. In parallel to these developments, in an attempt to extend the technology and advantages of high speed marine travel to the transportation of payloads of considerable magnitude, the Japanese ministry of transport has launched, in collaboration with 7 major Japanese shipyards the Techno-Superliner (TSL) project [6, 7, 8]. Two distinct concepts are investigated by the project, both required to carry 1,000 metric tonnes over 5000 nautical miles at a speed of 50 knots. The first concept (TSL-A) is an 127 metre surface effect ship considered by Mitsubishi and Mitsui. A 70m prototype able to carry a payload of 200 tonne at a speed of 40 knots has already been built with sea trials completed in late 1994. The second concept (TSL-B) is a hybrid of a foil/submerged hull concept developed by Kawasaki Heavy Industries, Hitachi Zosen, Ishikawajima-Harima Heavy Industries, NKK Corporation and Sumitomo Heavy Industries. Although a 17m long prototype has been

constructed and sea trials have been completed, further development of this concept is unlikeley as its primary aim was to develop the associated technologies for use in the (TSL-A) project [5]. The results of sea trials on both concepts are expected to be reported in September 1995 at the Fast'95 conference in Germany [9].

The Korean activities in turn, include a range of foil catamarans up to 12,000 tonnes and 50 knots (e.g, Hyundai), ultra-slender catamaran (e.g. Daewoo), surface effect ships (e.g. Daewoo, Samsung, Semo, Hanjin), SWATH ships (e.g. Hyundai), hovercraft (e.g. Hanjin) and monohulls (e.g. Halla). Generally, twin-hull designs are the most favoured in both Korea and Japan. Faulkner et al in [5] provide a summary Table of the concepts developed in both Korea and Japan. Non-hybrid twin hull craft (i.e. planing, wavepiercing, SWATH, catamarans) constitute approximately 30% of all concepts being built or investigated in the Far East. Inclusion of hybrid craft would increase this percentage to 75%. The SWATH concept is not actively pursued by the Far Eastern yards. More detailed and technical information on the developments may be obtained from [loc. cit. 1].

In Europe, the four year Norwegian High Speed Marine Vehicle Research Programme was launched in 1988 under the initiative of MARINTEK and the NTH and under the auspices of the Norwegian Council of Research [10]. Its main aim was to integrate in a 'global' research effort all aspects affecting the design, construction and operation of fast marine vehicles, through the improvement of old and/or development of new design practices. It has suceeded in increasing both the number of employees working in the norwegian fast craft marine industry and the total industrial turnover by factors 2 and 3 respectively. In the technological field, the project concentrated in the development and prototype construction of foil catamarans and SESs [11, 12], mainly for passenger transportation. Sizes up to 40m length, transporting 350-400 passengers at speeds of 45-50 knots, have been considered. Particular effort has been paid in motion control system design and development, noise reduction, while the application of advanced composites and lightweight materials coupled with a fresh look at strength design formulations have been encouraged. Work is currently underway on the design of large, fast cargo ships of 90-100m length with payload of 500-800 tonnes and a range of 500-700 nautical miles. Different concepts (catamarans, SWATHs, SESs, monohulls) are studied for different types of cargo transportation in european waters. The work on small

marine craft is also used as a 'scaled' down prototype basis for larger scale designs. The norwegians seem to be the only nation which have extended their research into the development of general safety and economic guidelines. Studies have been undertaken in the attempt to reduce operational costs and improve passenger safety. Considerable effort has been invested in the improvement of machinery reliability while the development of operating and emergency procedures and procedures for evaluation of the competence and training level of the crew are currently considered. Furthermore, standards have been derived for the arrangement of bridge equipment [13], working conditions, navigation equipment, fire safety as well as limitations on the effects of collision loads and operational practices. Current research, (to be completed in 1996) has extended in more detail into aspects of structural design, mainly though in the accurate prediction of dynamic loading and response [14-17] and the reliability of machinery systems [18].

The German Research Program for fast and unconventional ships commenced in 1990 and concentrates on three main concepts, the conventional planing and semi-planing catamarans (SUS-A), SWATH ships (SUS-B) and SESs (SUS-C). Research into catamarans has proceeded in hydrodynamic investigations (hull resistance and ship performance in calm water and waves) of a series of catamarans with four length to beam ratios (7.5-13.5), three dead rise angles and different frame characteristics. Symmetrical, semisymmetrical and asymmetrical forms are examined and hard chine and round bilge catamarans compared. A variety of propulsors have also been investigated. Conceptual designs have been prepared for river-, passenger-, container- and car/passenger-catamaransof lengths between 20 m and 70 m and speeds up to 30 knots. The maximum displacement investigated is that of 1,000 t (cargo-catamaran). The research effort in SWATH ships (SUS-B) also aimed in creating hydrodynamic and conceptual design information for different types of SWATH ships for a variety of operational roles (e.g. passenger and cargo transportation, ferries and research vessels). The research effort has concentrated on seakeeping, resistance and propulsion, maneuvrability and stress analysis and the creation of systematic hull forms for design. Studies into slamming is also scheduled but no results have as yet been published. A major aspect of this work has been the development of numerical tools for the calculation of resistance in waves, slamming, and response to waves. Such tools have been developed for resistance estimation but not tested against test data as

well as for the motion prediction and load estimation of the systematic series using strip theory for twin-hulls. Load predictions were however tested against experimental data and were found to be satisfactory only when cross-flow forces were included. Speed effects do not seem to have been considered yet and further research is underway along these lines. Research efforts in aspects of structural design and lightweight construction, seakeeping and maneuvering have not, however, commenced. Details of the status and results of these programs up until the end of 1993 are presented in [19-23].

As described by Faulkner in [24] UK activities in the field of fast marine transportation are not as organised and frequent as in the other European countries described above. Universities have been and are involved in individual projects referring to stability, motion control, manoeuvering, hydrodynamics, structural design and material aspects, but very few of them are interrelated. The U.K. industry is also actively involved in the design and construction of small vessels but the degree of co-operation and 'nationalistic' approach observed in Far Eastern European countries and Norway is missing. More details may be obtained from [24].
An update on the worldwide research and developments is expected in [9].

References

1) Arena, G., De Martini, L., 'Operational and Cost Analysis of Fincantieri's Fast Ferries', Proc., 2nd Intl. Conf. Fast Sea Transportation (FAST'93), 12-15 December 1993, Yokohama, The Society of Naval Architects of Japan, 1993.
2) Arena, G., Farinetti, V., 'Introducing Eurofast', loc. cit. 1, 1993.
3) Moret, J.A., Perez de Lucas, A., Tejedor, J.L., 'Fast Ferry Mestral, A Reliable Answer in Fast Ferry Design', loc. cit. 1, 1993.
4) Anonymous, 'A Technical Analysis of the Stena HSS', Ship and Boat International, May 1995.
5) Faulkner, D., Blyth, A.G., Marchant, A., Morrison, B.F.M., Mulligan R.D., Phillips, S.J., 'High Speed Marine Transport', One-Day Seminar on OSTEMS visit to Japan & S. Korea, RINA, London, 30 June 1994.
6) Ozawa, H., Morishita, S., Aoyagi, A., Kato, K., Tanaka, O., Fukushima, M., 'The Second Stage of the TSL-A Program', loc. cit. 1, 1993.
7) Kusaka, Y., Wada, Y., Takashina, J., Ishikawa, S., Matsui, R., Matsuda, K., 'Research on Hydrodynamic Performance of TSL-A', loc. cit.1, 1993.

8) Sueoka, H., Sakai, F., Kuramoto, Y., Fukuoka, T., Nishimura, K., 'Integrated Structural Design and Strength Evaluation System for 'TECHNO-SUPERLINER-A', loc. cit. 1, 1993.
9) Proceedings 3d International Conference on Fast SeaTransportation (FAST'95), Travemunde, Germany, 25-27 September 1995.
10) Holden, K.O., 'The Norwegian High Speed Marine Vehicle Research Programme', loc. cit. 1, 1993.
11) Minsaas, K.J., 'Design and Development of Hydrofoil Catamarans in Norway', loc. cit. 1, 1993.
12) Steen, S., Ulstein, T., Faltinsen, O.M., 'Seakeeping and Comfort of Large SES', loc. cit. 1, 1993.
13) Solberg, T., Aare, O., 'Operational Procedures and Standards for the Operating Compartment', loc. cit. 1, 1993.
14) Svensen, T.E., Valsgard, S., 'Design Philosophy and Design Procedures for Large High Speed Craft', loc. cit. 1, 1993.
15) Tonnessen, R., Vada, T., Nestergard, A., 'A Comparison of an Extended Strip Theory with a Three-Dimensional Theory for Computation of Response and Loads, loc. cit. 1, 1993.
16) Kvalsvold, J., Faltinsen, O.M., 'Hydroelastic Modelling of Slamming Against the Wetdeck of a Catamaran', loc. cit. 1, 1993.
17) Wu, M-K., Hermundstad, O.A., Moan, T., 'Hydroelastic Analysis of Ship Hulls at High Forward Speed', loc. cit. 1, 1993.
18) Moksnes, P.O., 'Diesel Engine Behaviour Subject to Transient Loading in High Speed Vessels', loc. cit. 1, 1993.
19) Kraus, A., Naujeck, A., 'SUS-A, The State of the Art of the German Research Program for Fast Catamarans', loc. cit. 1, 1993.
20) Muller-Graf, B., 'SUS-A, The Scope of the VWS Hard Chine Catamaran Hull Series 89', loc. cit. 1, 1993.
21) Nitz, A., Muxfeldt, H., 'SUS B, First Results of the German Research Project for SWATH Ships-Conceptual Design of a 90m SWATH', loc. cit. 1, 1993.
22) Bertram, V., 'SUS B, A Computational Fluid Dynamics Method for SWATH Ships', loc. cit. 1, 1993.
23) Blume, P., Soding, H., 'SUS B, Numerical Simulation and Validation for SWATH Ships in Waves', loc. cit. 1, 1993.
24) Faulkner, D., 'High Speed Marine Transport: Statements of Some UK Activities', Report NAOE-94-18, Department of Naval Architecture and Ocean Engineering, University of Glasgow, Glasgow, 1994.

APPENDIX 1.3: The Steps in the Evaluation of Partial Safety Factors

1. Determining the limits of applicability of the code to be calibrated, in terms of materials and structural components

2. Identifying the level of safety required from each of the structural components in question (usually obtained by a reliability analysis of already existing designs and/or code checks)

3. Determining the failure functions for the individual structural components and for every load case under consideration

4. Identifying the modelling uncertainties and the randomness of the design variables involved

5. Decision on suitable safety format of the check expression, i.e. the number of PSFs in the expression, their position in the expression, and the variables with which each of the PSFs will be directly linked

6. Decision on whether the inputs to the check equations as values for the random variables will be mean or characteristic (nominal) values. This decision will greatly depend upon the efficiency and accuracy of the quality control procedures used by the material manufacturer as well as by the constructor. It is these limits that will influence the final acceptable tolerance levels (for both material and geometrical properties)enforced by the code draughter and will determine whether mean or characteristic values should be used in the code expressions. Generally, variables with small sensitivity coefficients α_i (low dependency of strength on its value) should be represented by their mean values (e.g. most dimensions) and variables with large sensitivity coefficients (e.g. most loads and material strengths) by their characteristic values (generally 5% and 95% fractiles)

7. Variation of the values of the PSFs and estimation of the reliability index for each set of chosen PSFs. These have to lie within a preset range and as close as possible to the required level of target reliability for the structural component, or to the global reliability index in the case where a uniform safety level is required throughout the structure.

APPENDIX 3.1: Experimental Investigations into the Fatigue Strength of Aluminium Weldments

The development of the more recent aluminium fatigue design codes (e.g. BS 8118, ERAAS) has demanded (a) the re-evaluation of old fatigue data usually carried out in small scale and (b) the generation of new data, more 'application specific' and in large scale. The following experimental research projects aimed to satisfy both of these goals for *aluminium joints*:

(1) the ALDABA project [1] which commenced in 1980

(2) the ECCS activity resulting in the 1991 recommendations (COST 506 Program) [2, 3, 4]

(3) the EUREKA project [5] undertaken by Denmark, France, Germany, Italy, Portugal, Holland and Spain concerned the investigation of the behaviour of welded, bolted and bonded aluminium alloy joints

(4) the ALFABET project, joining existing databanks in Germany and the USA and expecting to provide a system of information sources on design procedure and reliability estimates for aluminium structures [1].

The latter three projects aimed at enriching the existing databanks with more realistic and representative full-scale fatigue test data. In addition, aluminium fatigue data compilations exist at the Welding Institute, Cambridge by Guerney and Maddox (sources of data referenced in [6]), in Europe by Haibach and Atzori [7] and in the USA by Oliver and Ritter [8].

The ALDABA (CAFDEE) Databank: Aluminium fatigue test data in the form of a databank were first initiated by Munse, followed by Saunders in the early 1970s when the Welding Research Council (WRC) databank was formed at the Iowa State University. In parallel (in late 1960s), Kosteas developed relevant statistical regression analysis software at the University of Karlsruhe by Steinhardt and Kosteas. The Committee on Aluminium Fatigue Data Exchange and Evaluation (CAFDEE) was founded in 1980 based on the co-operation of these two institutions. Its aim was, and is, to collect and analyse aluminium fatigue data obtained worldwide, thus

forming the **Aluminium Data Bank**, as well as assisting in and planning additional experimental tests and code developments. Many countries are represented on the Committee both at the academic and industrial levels. A summary of the CAFDEE study is presented in [9]. In 1982 the Bank contained the results of over 1100 test programs with approximately 12,000 individual test results [10] and in 1992 approximately 15,000 data points [1]. The CAFDEE data bank also contains data on fatigue crack growth, bolted joints fatigue and adhesively bonded joint fatigue. Since 1985 there is a simultaneous installation and operation of ALDABA in the University of Munich and Iowa State University. The development of the ECCS European Recommendations on fatigue design of aluminium structures [3] was based on this databank (with additions of further large scale test data).

The ECCS Large Scale Model Activity: Considering the previous work of the ECCS TC2 and the interests of several national bodies, as well as the difficulties in evaluating and analysing previously derived small scale data and data stored in ALDABA, the European Aluminium Association (EAA) put forward in June 1988 the COST 506 Program of the Commission of the European Communities to provide the first comprehensive outline for the fatigue behaviour of structural components (especially beams) in aluminium [2, 4].

To enhance this data and to overcome the limitations introduced by small scale test data, fatigue tests on large welded beams [11, 12] were carried out at the Technical University of Munich between 1982 and 1991, yielding approximately 1000 experimental data. Two different full scale beam projects were performed, Project A (1982-1986) and Project B (1987-1991) [12]. Three different alloys were tested-7020, 5083 and 6005. These tests contributed significantly to the structural detail classification of the ERAAS Rules.

Further fatigue tests were performed by Alusuisse on full and half depth stiffeners, welded on extruded 6000 series beams and on various web attachments [13, 14] between 1988-1990 (20,000 data points) in support of the development of the ECCS recommendations. Evaluation of both the TUM and these results (a total of 414 test points) is presented in [13, 15]. These tests, together with work by Fisher and Menzemer [16], increased the TUM data points to 2500.

Ondra and Kosteas in [11] report the existence of experimental results by Maddox and Webber (1987) of small specimens with induced high residual stresses (sources of data referenced in [6]), which they compare with the TUM data. No specific reference is however provided.

The EUREKA Project, EU 269 [5], commenced in 1989 and completed by 1992 was undertaken by Denmark, France, Germany, Italy, Portugal, Holland and Spain. It focused on the behaviour of welded, bolted and bonded joints made of 5000, 6000 and 7000 series aluminium alloys. It consisted of three phases, concentrating on the evaluation of already existing data, additional experimental testing of structural details with associated fracture mechanics evaluations and proposal of fatigue life estimation methods for design code application, respectively. The results and conclusions are presented by Soetens et al in [5].

The ALFABET Project: The **A**luminium **F**atigue **B**ehaviour and **E**valuation **T**ask Project (ALFABET), currently underway between the Munich and Iowa Universities, aims at providing a complete computer aided system for fatigue design of aluminium structures. This is envisaged to be carried out by linking ALDABA (and additional fatigue data updating it) as one information source to further information sources and decision making tools (e.g. literature, books, manuals, expert knowledge) and then to design recommendations based on reliability estimates. All these will be accessed and connected via computers and computer terminals. The project is developed in three phases [1]:

Phase I: Development and enrichment of the data bank

Phase II: Formation of links between data description and data analysis (detail classification, description and evaluation, graphics, design parameters, manufacturing options, quality criteria, welding technology information)

Phase III: Integration of Phases I and II into a system by providing interface and feedback information to the user. It concerns the integration of criteria and manufacturing parameters as well as assessment procedures for components and structures.

A detailed description and the layout of the menu driven computer program permitting interaction and analysis with the database, as well as the information technology aspects supporting it, are presented in more

detail in [1]. Information on the user-friendliness and interactive capabilities and program flowchart are provided.

References

1) Saunders, W.W., Ondra, R., Kosteas, D., 'State of the Art of the ALFABET Project', Proc. 5th Int. Conf. on Aluminium Weldments, D. Kosteas, R. Ondra, F. Ostremann, (eds.), Munich, 27-29 April 1992, Aluminium Verlag GmbH, Dusseldorf, 1992.
2) Kosteas, D., Uhry, A., 'Fatigue Behaviour of Welded Aluminium Structures - European Full Scale Tests. Part 1 (Kosteas): Analysis, Results and Proposals, Part 2 (Uhry): Statistical Analysis, Part 3 (Kosteas): Data Base', Commission of the European Communities-Cost 506 Program-European Aluminium Association, Munich/ Voreppe, March/April 1989.
3) European Convention for Constructional Steelwork, 'European Recommendations for Aluminium Alloy Structures-Fatigue Design', Committee TC2-TG4, 1991.
4) Hirt, M.A., Kimberley, G.J., Smith, I.F.C., 'Fatigue Behaviour of Aluminium Beams with Welded Attachments', loc. cit. 1, 1992.
5) Soetens, F., van Straalen, J.J., Dijkstra, O.D., 'Experimental and Theoretical Study on the Fatigue Behaviour of Aluminium Structures', loc. cit. 1, 1992.
6) Maddox, S.J., 'Fatigue Design of Welded Aluminium Alloy Structures', Proc. 2nd Int. Conf. on Aluminium Weldments, D. Kosteas, (ed.), Munich, 24-26 May 1982, Aluminium Verlag GmbH, Dusseldorf, 1982.
7) Haibach, E., Atzori, B., 'A Statistical Re-analysis of Fatigue Test Results on Welded Joints in AlMg5', Laboratorium fur Betriebefestigkeit, Rept. No. FB-116, Darmstadt, 1974.
8) Olivier, R., Ritter, W., 'Catalogue of S-N Curves of Welded Joints in Steel, Parts 1-5', Deutscher Verband fur Scweisstechnik, Dusseldorf, Germany, 1979-1982.
9) Kosteas, D., Saunders, W.W., 'Evaluation of Fatigue Strength for Common Welded Joints in Aluminium Alloys', Proc. 3d Int. Conf. on Aluminium Weldments, D. Kosteas, (ed.), Munich, 15-17 April 1985, Aluminium Verlag GmbH, Dusseldorf, 1985.

10) Kelsey, R.A., Nielsen, H., 'Aims and Scope of CAFDEE', loc. cit. 6, 1982.
11) Ondra, R., Kosteas, D., 'Fatigue Behaviour of Welded Aluminium Beams', loc. cit. 1, 1992.
12) Kosteas, D., 'Aluminium Beam Test Programme: Assessing the Results' Proc. Int. Conf. on Fatigue of Welded Constructions, S.J. Maddox (ed.), Brighton, England, 7-9 April 1987, The Welding Institute, Abington, 1988.
13) Ondra, R., Kosteas, D., 'Evaluation of Welded Attachments Under Combined Fatigue Loads', Proc. Int. Conf. on Steel and Aluminium Structures, ICSAS'91, S.L. Lee and N.E. Shanmugam, (eds.), Singapore, 22-24 May 1985, Elsevier Applied Science, London, 1985.
14) Jaccard, R., 'Unpublished Internal Reports and Materials Provided by Alusuisse, Zurich, Switzerland, for the EAA-ECCS Fatigue Workshops in Munich and Zurich 1990', 1990.
15) Kosteas, D., 'European Recommendations for Fatigue Design of Aluminium Structures', loc. cit. 1, 1992.
16) Menzemer, C.C., Fisher, J.W., 'Fatigue Behaviour of Welded Aluminium Structures', loc. cit. 1, 1992.

APPENDIX 4.1: HAZ Effect Modelling by Robertson and Dwight

In 1985 work at Cambridge University by Robertson and Dwight [1, 2] tackled the question of HAZ effect representation in the most comprehensive way to date. Their work concentrated in providing accurate estimates of the extent and the strength of the HAZ softening using Kelsey's [3] earlier description (Fig. 4.5) assuming a three-part distribution of strength in the welded section. It was shown that the *extent* of the HAZ is affected by:

- the metal temperature at the beginning of welding
- the built-up of temperature in multi-pass welds
- neighbouring parallel welds; if these are laid simultaneously the extent of their combined HAZ increases
- the positioning of the weld too near to a free edge. The HAZ softening increases as in this case the heat dispersal is by far less efficient. In this case the effect was found to depend on the ratio between the distance of the weld to the free edge and the extent of the HAZ calculated disregarding the free edge effect.

It is important to remember that the following description of the model is only valid in the absence of any 'free-edge' effects. This is the case when the 'free-edge' is located further than 3r from the weld. Fiurthermore, it relates to MIG welding process. TIG welding tends to produce additional softening due to the possibility of the torch dwelling in the spot.

For design purposes the assumed step change from welded to parent material strength values is taken to occur at a distance from the weld (or the root of the weld) given by:

$r = (x_A + x_B)/2$	For thin plates (<10mm)
$r = \sqrt{0.5\,(x_A^2 + x_B^2)}$	For thick plates (>25mm)

Roberston's investigations have resulted in the following models in three thickness ranges; thermal control is assumed throughout but correction factors are introduced when this fails and elevated temperatures exist:

1. For thin plates (up to 10mm app.) the extent of the HAZ measured from the centre-line or root of a weld was found to be proportional to A_w/N and inversely proportional to the mean thickness of the heat flow paths. Rosenthal's 2D heat flow model [4] was used in the modelling resulting in the following recommendations:

• *For Bead and Butt Welds-SINGLE PASS*

$$x_A = k_A (A_w/2) \qquad \text{and} \qquad x_B = k_B (A_w/2)$$

where A_w and d are the weld deposit area and plate thickness respectively and

	k_A	k_B
For 6000 series alloys	3.0	6.6
For 7000 series alloys	5.8	8.0

• *For Bead and Butt Welds-MULTIPLE PASS*

The same expressions should be used provided that A_w is taken as the deposit area of the largest pass. It is unlikely that multiple passes will be required in thin plating.

• *For Fillet Welds*

For single fillet corner weld r is obtained via the above equations and measured as shown in Figure A4.1.1. For T-fillet joints, r is measured from both welds (Fig. A4.1.1b) and the net area is the HAZ assumed. r is now taken as 2/3 of the value for bead and butt welds to allow for the presence of three heat-paths (against two for the butts). For the cruciform joint r is measured as for the fillet joints and is taken as either 2/3 or 1/2 of the bead and butt weld values depending on whether there are three or four heat-paths available during welding.

• *The effect of initial temperature*

The effect of initial temperature (insufficient thermal control) is accounted for, by multiplying the r value determined above by a factor F given by:

$$F = (T_p - 20)/(T_p - T_o)$$

where T_p is the peak temperature and T_o is the initial temperature (both in °C). Hence:

Alloy series	Increase in F (from/to)	Temp. increase (from/to)
7000	1 to 3.0	40°C to 150°C
6000	1 to 2.2	50°C to 150°C

T_p values are given by:

	6000 series	7000 series
Edge of zone A	520 °C	275 °C
Edge of zone B	240 °C	205 °C

2. For thick plates (exceeding 25mm app.) the extent of the HAZ is measured radially and was found to be proportional to $\sqrt{A_w/N}$ where A_w is the total section area of the weld deposit per pass and N is the number of heat flow paths adjacent to the weld. Rosenthal's 3D heat flow model [4] was employed in the theoretical modelling. For a thick plate zones A, B, C are separated by semi-circular arcs of radii x_A and x_B given by:

- *For All Welds-SINGLE PASS*

$$x_A = k_A \sqrt{A_w} \qquad \text{and} \qquad x_B = k_B \sqrt{A_w}$$

where A_w and d are the weld deposit area and plate thickness respectively band

	k_A	k_B
For 6000 series alloys	1.7	2.6
For 7000 series alloys	2.4	2.8

• *For All Welds-MULTIPLE PASS*

For multi-pass welds it is assumed that each pass has a 'zone of influence' of radius r (Fig. A4.1.2) where r is as given above for a surface run. The total HAZ is defined by all the overlapping arcs. Its boundary may be approximated by drawing tangents at a perpendicular distance r from the preparation (as shown in the figure) and the area thereby enclosed is the assumed HAZ used in design.

• *The effect of initial temperature*

The effect of initial temperature is accounted for, by multiplying the r value determined above by a factor F given by:

$$F = \sqrt{(T_p - 20)/(T_p - T_o)}$$

where T_p is the peak temperature and T_o is the initial temperature (both in degrees centigrade) . T_p values are as given earlier. Hence:

Alloy series	Increase in F (from/to)	Temp. increase (from/to)
7000	1 to 1.7	40°C to 150°C
6000	1 to 1.4	50°C to 150°C

3. For intermediate thickness plates (in the range 10-25mm app.) separate estimates based on the 'thin' and 'thick' models should be carried out and the smaller of the HAZ areas found should be chosen. To avoid discrepancies arising by employing the thick model to relatively thin plates (e.g. 17mm) the following r values should be used for the calculation of the 'thick' plate estimate:

For 6000 series alloys	r	greater of 180/d	or	14mm
For 7000 series alloys	r	greater of 270/d	or	17mm

The estimation of the **severity of softening** is based on a simplified

approach in terms of the factor s (the ratio of HAZ strength to parent strength). This approach assumes that the reduction in strength is a function of the alloy alone neglecting the possible variations due to the size of the weld and the thermal history. It is therefore pessimistic when applied to welds which are small in relation to the thickness of the plate. Hence the estimation of s was based on the most adverse conditions likely to occur in practice. Therefore Robertson and Dwight recommend:

For 6000 series alloys	s = 0.5
For 7000 series alloys	s = 0.75

Special attention should be drawn to transversely loaded welds. In this case it is necessary to base the design of the joint on the strength at the critical position A (Fig. 4.5) or the strength of the weld metal itself. For 6000 series plates it was estimated [2] that with a 5000 series filler point A is critical while for a 4000 series filler the weld metal and point A are of comparable strength. For 7000 series plates with their 5000 series standard filler the critical position is the weld metal position which is usually weaker than position A although under certain circumstances the reverse may be the case [2]. Hence to cover both possibilities, Robertson suggests the use of a reduced strength equal to 60% of the parent material strength (if the metal temperature at the start of the weld cannot be guaranteed to be below 40°C. Temperature built-up between weld passes was accounted for by a factor α although for thin material temperature built up is not the norm. α is assumed to vary as follows:

Alloy series	α increase (from/to)	Temp. increase (from/to)
7000	1 to 3.0	40°C to 150°C
6000	1 to 2.2	50°C to 150°C

References

1) Robertson, I., 'Strength Loss in Welded Aluminium Structures', Ph.D. Dissertation, Cambridge University, 1985.

References

1) Robertson, I., 'Strength Loss in Welded Aluminium Structures', Ph.D. Dissertation, Cambridge University, 1985.
2) Robertson, I., Dwight, J.B., 'HAZ Softening in Welded Aluminium', Proc. 3d Int. Conf. on Aluminium Weldments, Munich, 15-17 April 1985.
3) Kelsey, R.A., 'Effect of Heat Input on Welds in Aluminium Alloy 7039', Welding Journal Research Supplement, 1971.
4) Rosenthal, D., 'The Theory of Moving Sources of Heat and its Application to Metal Treatments', Trans. ASME, Vol. 68, 1946.

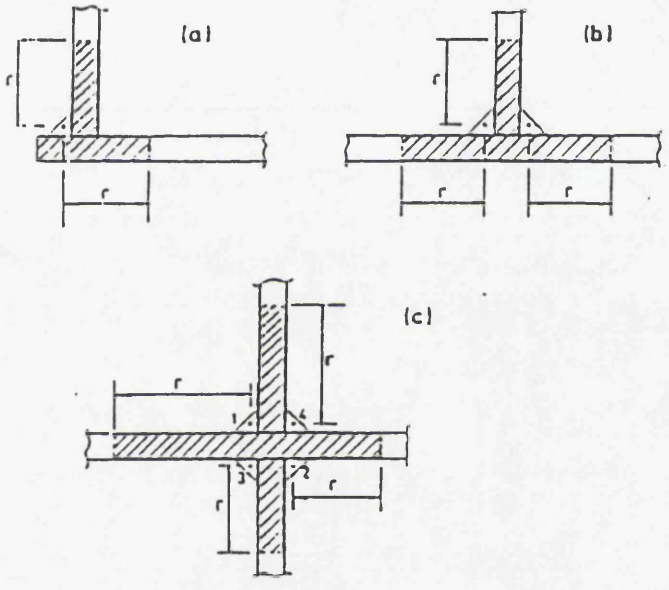

Figure A4.1.1: Extent of the HAZ as recommended by Robertson [17].

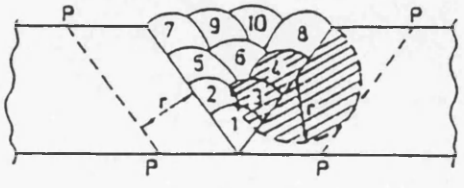

Figure A4.1.2: Robertson's recommended method for estimating the HAZ extent for a multi-pass weld [17].

APPENDIX 4.2: Initial and Final Permanent Set Values

In 1974, Faulkner presented the results of measurements of values of central plate deflections on British frigates [1, 2], recommending the following expression for their representation:

$$w_o/t = \begin{cases} 0.12\beta^2 (t_w/t) & \text{for } \beta \le 3 \\ 0.15\beta^2 (t_w/t) & \text{for } \beta > 3 \end{cases} \qquad \text{for} \quad t_w > t$$

t_w,t are the web and plate thicknesses respectively. A normal distribution of deflection amplitudes was observed with COV in the range between 0.3 and 0.6. High COV values corresponded to heavily welded (and hence thicker) plating [2]. It must be noted that the measurements were on single-pass welds. Multi-pass welds result in larger deformations.

Antoniou in 1980 [3] presented the following expression for the value of assumed initial permanent set in the analysis of plate behaviour for lateral as well as in plane loads:

$$w_o/t = 0.073\,\beta^{1.65} \left(\frac{t_w}{t}\right)^{0.42} \qquad \text{for} \qquad \beta \le 2.5$$

This formula was based on a regression analysis of over 2000 values of w_o/t measured on newly built steel merchant ships over a period of 10 years. For steel plates, Antoniou was more specific in proposing the following expressions for maximum initial deflection assumed:

$$\frac{w_{pt}}{t} = \begin{cases} 0.014\dfrac{b}{t} - 0.32 & \text{for } t \ge 14\,\text{mm} \\ 0.018\dfrac{b}{t} - 0.55 & \text{for } t < 14\,\text{mm} \end{cases}$$

The main difference of Faulkner's recommendation from that of Antoniou was the linear relationship of the magnitude of the initial deflection with the web to plate thickness ratio t_w/t. Antoniou opted for an exponential relationship.

More recently, Jastrzebski and Kmiechik suggested another relation following measurements in merchant ships [4]:

$$w_{pi}/t = 0.0094\,(b/t) - 0.205$$

These investigations have led to the general adoption of equations centred around $w_{pi}/t = 0.1\,\beta^2$. Masabuchi has presented more complex formulations in 1970 [5].

There is insufficient information for the weld induced distortions on stiffeners. According to Faulkner in [6], stiffener (initial or permanent set) deflections of the order of $w_{stiffener}/l \approx 0.001$ have been measured. This relationship, being also typical of civil engineering structures, is finally recommended. l is the stiffener length.

Because of the variety of serviceability requirements no universal value of acceptable permanent set, w_{pt}, can be set. For naval vessels and every weight critical structure, a relatively large value of $w_{pt}/b = 1/50$ is accepted. For cargo ships the ratio may drop down to 1/100 [7]. This out-of-flatness may be about 1/75 of the plate width in aircraft carrier deck structures. Concentrated loads will generally alter these values as they are assumed to act with any coexistent uniformly distributed pressure loads.
Faulkner in [8] presents the following limits on permissible maximum deflection, based on U.K. naval experience:

- For bottom plating and strength deck $w_{pt}/t = 0.25\,\beta$
- For decks, bulkheads and remaining structure $w_{pt}/t = 0.5\,\beta$

API Bulletin-2V [9] in turn, recommend the use of $w_{pt}/t = 0.2\,\beta$. In the presence of coexisting in-plane compressive loads, the allowable maximum permanent set must be restricted, to protect against reductions in plate buckling strengths.

References

1) Faulkner, D., 'Compression Strength of Welded Grillages', Chapter 21 in Ship Structural Design Concepts, H.R. Evans (Ed.), Cornell Maritime Press, 1975.
2) Faulkner, D., 'Effects of Residual Stresses on the Ductile Strength of

Plane Welded Grillages and of Ring Stiffened Cylinders', Jnl. Strain Analysis, Vol. 12, No. 2, 1977.

3) Antoniou, A.C., 'On the Maximum Deflection of Plating in Newly Built Ships', Jnl. Ship Research, Vol. 24, No. 1, March 1980.
4) Guedes Soares, C., 'A Code Requirement for the Compressive Strength of Plate Elements', Jnl. Marine Structures, Vol. 1, 1988.
5) Masabuchi, K., 'Control of Distortion and Shrinkage on Welding', Welding Research Council, Bull. No. 149, 1970.
6) Faulkner, D., 'Effects of Residual Stresses on the Ductile Strength of Plane Welded Grillages and of Ring Stiffened Cylinders', Jnl. Strain Analysis, Vol. 12, No. 2, 1977.
7) Hughes, O.F., 'Plate Bending', Chapter 9 in Ship Structural Design; A Rationally Based Computer-Aided Optimisation Approach, SNAME, New Jersey, 1988.
8) Faulkner, D., 'Strength of Welded Grillages Under Combined Loads', Chapter 22 in Ship Structural Design Concepts, H.R. Evans (Ed.), Cornell Maritime Press, 1975.
9) American Petroleum Institute, 'Bulletin on Design of Flat Plate Structures', API Bulletin 2V, First Edition, May 1987.

APPENDIX 4.3: The Design of Flat Plating Under Lateral Pressure

Elastic Small Deflection Design (Not recommended)

For long plates the maximum elastic deflection is given by:

$$w_{max} = \begin{cases} 5\,k_1\,C & \text{for simply supported edges} \\ k_1\,C & \text{for clamped edges} \end{cases} \quad \text{where} \quad C = \frac{p\,b^4\left(1-\upsilon^2\right)}{32\,E\,t^3}$$

and the maximum stress in the plate is given by (Figs.4.11, 4.12):

$$\sigma_{max} \le k_2\,p\left(\frac{b}{t}\right)^2$$

where

$$k_1 = \begin{cases} -0.0269\,\alpha^4 + 0.3409\,\alpha^3 - 1.599\,\alpha^2 + 3.296\,\alpha - 1.517 & \text{for } 1 \le \alpha \le 2.4 \quad \text{(s.suppd)} \\ 1 & \text{for } \alpha > 2.4 \\ 0.0052\,\alpha^3 - 0.5275\,\alpha^2 + 1.781\,\alpha - 0.98224 & \text{for } 1 \le \alpha \le 2.6 \quad \text{(clamped)} \\ 1 & \text{for } \alpha > 2.6 \end{cases}$$

and for the maximum stress, the correction factor becomes:

$$k_2 = \begin{cases} -0.018\,\alpha^4 + 0.1736\,\alpha^3 - 0.599\,\alpha^2 + 0.8389\,\alpha - 0.1054 & \text{for } 1 \le \alpha \le 3 \quad \text{(s-suppd)} \\ 0.25 & \text{for } \alpha > 3 \\ -0.0162\,\alpha^4 + 0.188\,\alpha^3 - 0.813\,\alpha^2 + 1.552\,\alpha - 0.603 & \text{for } 1 \le \alpha \le 1.6 \quad \text{(clamped)} \\ 0.34 & \text{for } \alpha > 1.6 \end{cases}$$

Elasto-Plastic Design

Boundary Conditions: Edges Free to Slide,

- For $1 \le \alpha \le 5$ and $2 \le \beta \le 6$, the allowable pressure, p, is expressed in terms of an allowable permanent set, w_{pt}

$$p = \begin{cases} \dfrac{6\,\sigma_y}{\sqrt{\alpha}}\left(\dfrac{t}{b}\right)^2\left(1 + \dfrac{2\,w_{pt}}{\alpha\,t}\right) & \text{for } \beta < 2.5 \\ \dfrac{6\,\sigma_y}{\sqrt{\alpha}}\left(\dfrac{t}{b}\right)^2\left(\dfrac{4}{3} + \dfrac{w_{pt}}{\alpha\,t}\right) & \text{for } \beta \ge 2.5 \end{cases}$$

- For $1 \le \alpha \le 5$ and $\beta < 2$, the elastoplastic approach is overruled and the fully plastic design approach of Wood is used. It is based the 'roof-top' collapse bending mechanism, not accounting for membrane effects:

$$p = 12\, C_{bc}\, \sigma_y \left(\frac{t}{b}\right)^2 \left(\sqrt{3 + \frac{1}{\alpha^2}} - \frac{1}{\alpha}\right)^{-2}$$

Fully Plastic Design
Boundary Conditions: Clamped apart

The criteria are either three hinge collapse or roof-top collapse with or without accounting for membrane stresses depending on whether the plating is 'long' or 'short', slender or stocky. Specifically,

- For 'long' plates ($\alpha \ge 2.5$) failure occurs by three-hinge collapse:

$$p_{3h} = \frac{4\, \sigma_y}{\sqrt{1 - \upsilon + \upsilon^2}} \left(\frac{t}{b}\right)^2$$

- For 'short' plates ($\alpha < 2.5$) - Roof Top Collapse Mechanism

$$p = \begin{cases} 12\, C_{bc}\, \sigma_y \left(\frac{t}{b}\right)^2 \left(\sqrt{3 + \frac{1}{\alpha^2}} - \frac{1}{\alpha}\right)^{-2} & \text{for } \beta < 2 \\ 8\, C_{bc}\, \sigma_y \left(\frac{t}{b}\right)^2 \left(\frac{w_{pt}}{t}\right) \left(1 - \frac{32}{\pi^3} \operatorname{sech}\left(\frac{\pi \alpha}{2}\right)\right)^{-1} & \text{for } \beta \ge 2 \end{cases}$$

C_{bc} is equal to 1 for clamped plates and equal to 0.5 for simply supported plates.

APPENDIX 4.4: Morandi's Model for the Stiffener and Ring-Frame Design Against ElasticTripping

As a result of the inaccuracies occurring in tripping stress predictions due to the neglect of the web deformation effects, Morandi [1, 2] adapted Adamchack's previous theoretical approach for flat stiffened panels [3] accounting for web deformations, to the case of ring frames. Morandi's expression does not tackle tripping failures in the inelastic range for which the approach recommended by Faulkner is used (Chapter 4):

For T-Stiffeners $\sigma_T = \dfrac{b - \sqrt{b^2 - 4\,a\,c}}{2\,a}$ where

$$a = (A1)^2\left(c_5\,c_3 - c_4^2\right) + \frac{c_2\,c_6}{(A2)}$$

$$b = c_2 c_6 + c_1 c_7 + \left[GJ + E\Gamma_2 (A1)^2\right]\left[c_3 (A1)^2 + \left(\frac{c_2}{(A2)}\right)^2\right] +$$

$$E\Gamma_1 (A1)^2\left[\frac{c_5}{d_c^2}(A1)^2 + \frac{c_2}{9\,(A2)}\right] + \frac{4 c_1 c_2 d_c^2}{9\,(A2)}(A1)^2$$

$$c = \frac{4}{9} c_1\,c_2\,d_c^2\,(A1)^{-2} + \left[G\,J + E\,\Gamma_2\,(A1)^2\right]\left[c_1 + c_2 + E\,I_z\,(A1)^4\right] + E\,\Gamma_1\,(A1)^2\left[c_1 + \frac{c_2}{9}\right]$$

$$c_1 = \frac{E\,t_w^3}{4\,d_c^2} \qquad c_2 = \frac{9\,C_{on}}{4\,d_c^2} \qquad c_3 = A_s - \frac{18}{35} t_w d_c \qquad c_4 = \frac{3}{35} t_w d_c^2 \qquad c_5 = I_s - \frac{11}{35} t_w d_c^3$$

$$c_6 = I_s - \frac{A_s\,d_c^2}{9} - \frac{3}{7} t_w d_c^3 \qquad c_7 = I_s + b_f t_f d_c^2$$

Stiffened Panels under compressive loads should be checked against elastic tripping failure based on the expression that follows:

$$A1 = \frac{m\,\pi}{l} \qquad A2 = \sigma_{cr,plate} \qquad C_{on} = 1 - \frac{\sigma_e}{\sigma_{cr,el}} \quad \text{for} \quad \sigma_e \le 2\,\sigma_{cr,el}$$

Ring Framed Cylinders under compressive loads should be checked against elastic tripping failure based on the expression that follows.

$$A1 = \frac{n}{R} \qquad A2 = \xi\,p_m \qquad C_{on} = 1 - \frac{p}{p_{mn}} \quad \text{for} \quad p \le 2\,p_{mn}$$

For Flat Bar Stiffeners $\sigma_T = \dfrac{b - \sqrt{b^2 - 4\,a\,c}}{2\,a}$ where

$$a = a_1^2 + \left(\frac{75}{4}\right) a_1\, a_3$$

$$b = 225\left(1-\upsilon^2\right) a_1\, a_2 + 2\,a_1^3 + 90\left(1-\upsilon\right) a_1^2 + 525\, a_1 + \frac{75}{4} a_3 \left[84 + \frac{42}{5} a_1 \left(3 - 5\upsilon\right) + a_1^2\right]$$

$$c = a_1^4 + 90(1-\upsilon)a_1^3 + \left[1029 - 21(2+5\upsilon)^2\right]a_1^2 + 3150(1-\upsilon)a_1 + 225\left(1-\upsilon^2\right)a_2\left[84 + \frac{42}{5}a_1(3-5\upsilon) + a_1^2\right]$$

$$a_1 = \left((A1)\, d_w\right)^2 \qquad a_2 = \frac{C_{on}\, d_w}{E\, t_w^3} \qquad a_3 = \frac{C_{on}}{(A2)\, d_w\, t_w}$$

where A1, A2 and C_{on} are as given earlier.

References

1) Morandi, A.C., 'Computer Aided Reliability Based Design of Ring-Stiffened Cylindrical Shells Under External Pressure', Ph.D. Thesis, University of Glasgow, September 1994.
2) Morandi, A.C., Das, P.K., Faulkner, D.F., 'An Outline of the Application of Reliability Based Techniques to Structural Design and Assessment of Submarines and Other Externally Pressurised Cylindrical Structures', Jnl. Marine Structures, Vol. 7, 1994.
3) Adamchak, J.C., 'Design Equations for Tripping of Stiffeners Under Inplane and Lateral Loads', DTNSRDC Report No. 79/064, Maryland, October 1979.

APPENDIX 4.5: Flowchart of Scheer et al's Procedure for Estimating the Ultimate Strength of Knee Joint Plating [1]

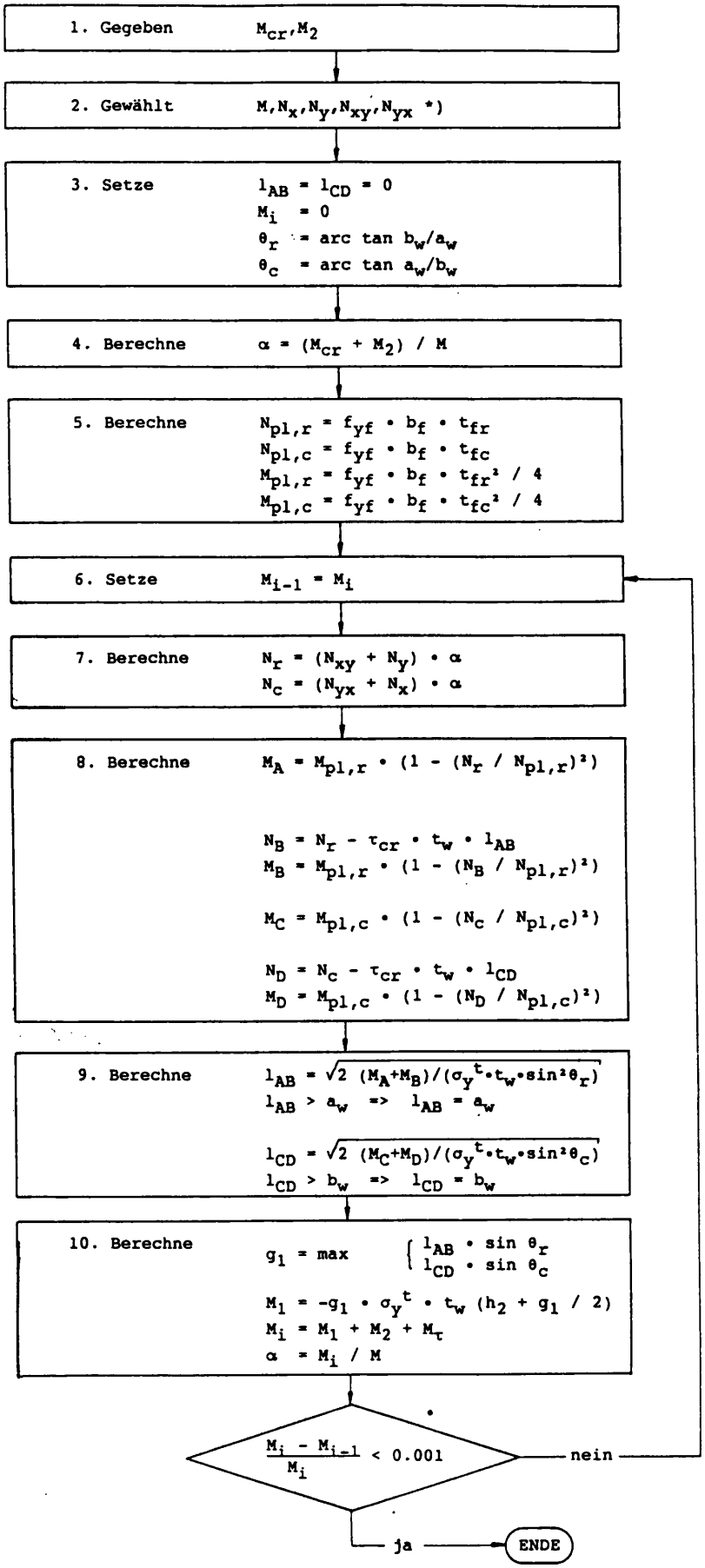

References

1) Scheer, J., Pasternak, H., Schween, T., 'Zum Tragverhalten Ausgesteifter Rahmenecken mit Schlanken Stegen', Stahlbau, Vol. 60, 1991.

APPENDIX 4.6: Proposed Strength Models for Ring/Stringer Stiffened Cylindrical Shells After the 1991 Re-evaluation of the RCC Formulations [1]

A.1 Axial Compression

It is basically the RCC formulation with a revised value for the bias for the shell knockdown factor.

(i) Elastic buckling stress for perfect curved panel of mean radius R, arc length s:

$$\sigma_{cr} = 0.904E\left(\frac{t}{s}\right)^2\left(4+\frac{3Z_s^2}{\pi^4}\right) \text{ for } Z_s \le 11.4$$

$$= 0.605E\left(\frac{t}{R}\right) \text{ for } Z_s > 11.4\,;\; Z_s = \frac{s^2}{Rt}\sqrt{1-v^2}$$

(ii) Knockdown factor (lower bound):

$$\varrho_n = 1 - 0.019Z_s^{1.25} + 0.0024Z_s\left(1-\frac{R}{300t}\right) \text{ for } Z_s \le 11.4$$

$$\varrho_n = 0.27 + \frac{1.5}{Z_s} + \frac{27}{Z_s^2} + 0.008\sqrt{Z_s}\left(1-\frac{R}{300t}\right) \text{ for } 11.4 < Z_s \le 70$$

(iii) Bias for mean knockdown factor:

$$B = 1.25 \quad \text{for } \lambda_n = \sqrt{\sigma_y/(\varrho_n\sigma_{cr})} > 1$$

$$= 1 + 0.25\,\lambda_n \quad \text{for } \lambda_n \le 1$$

$\varrho = B\varrho_n$ mean knockdown factor

(iv) Elastic buckling stress for imperfect shell:

$\sigma_{icr} = \varrho\sigma_{cr} = B\varrho_n\sigma_{cr}$

$\lambda = \sqrt{\sigma_y/\sigma_{icr}}$ reduced slenderness parameter

(v) Assume for weld tension block parameter in shell:

η = 4.5 for continuous structural fillet welds
= 3.0 for light fillet welds
= 0 for stress-relieved structure

(vi) Residual stress reduction factor:

$$R_r = 1 - \left\{ \frac{2\eta}{(s/t - 2\eta)} \frac{\lambda^4}{(1+0.25\lambda^4)^2} \frac{\lambda^2}{(1.05\lambda - 0.28)} \right\}, \text{ for } \lambda > 0.53$$

$$= 1 \quad , \text{ for } \lambda \le 0.53$$

(vii) Shell reduced effective width (minimum) and shell effective width (minimum):

$$\frac{s'_{em}}{s} = (0.53/\lambda)R_r \text{ , for } \lambda > 0.53, = 1 \text{ for } \lambda \le 0.53$$

$$\frac{s_{em}}{s} = \left(\frac{1.05}{\lambda} - \frac{0.28}{\lambda^2}\right)R_r \text{ for } \lambda \ge 0.53, = 1 \text{ for } \lambda \ge 0.53$$

(viii) Elastic critical stress for column-shell combination:

$$\sigma_e = \frac{\pi^2 E I'_e}{L^2(A_s + s_{em}t)} + Q_s \frac{0.605E(t/R)}{1 + A_s/s_{em}t} \quad \text{where:}$$

$$I'_e = I_s + \left(\frac{A_s(z_s + t/2)^2}{1 + A_s/s'_{em}t}\right) + \frac{s'_{em}t^3}{12}$$

$$I'_e = I_s + \left(\frac{A_s(z_s + t/2)^2}{1 + A_s/s'_{em}t}\right) + \frac{s_{em}t^3}{12}$$

$\psi = \sigma_e / \sigma_y$, $Q_s = 0.75$ assumed knockdown factor

(ix) Inelastic buckling stress using Ostenfeld-Bleich structural tangent modulus approach:

$$\sigma_{ic} = \{1 - p_s(1 - p_s)/\psi\}\sigma_y, \text{ for } \psi \ge p_s$$

$$= \psi\sigma_y \text{ for } \psi < p_s \text{ , where } p_s = \sigma_{ps}/\sigma_y$$

p_s = 0.5 in general ; 0.75 for stress-relieved structures

(x) Revised shell reduced slenderness parameter and effective width of shell:

$$\lambda_e = \sqrt{\frac{\sigma_{ic}}{\sigma_{icr}}} = \lambda\sqrt{\frac{\sigma_{ic}}{\sigma_y}}$$

$$\frac{s_e}{s} = \left(\frac{1.05}{\lambda_e} - \frac{0.28}{\lambda_e^2}\right)R_r \text{ for } \lambda_e \ge 0.53, = 1 \text{ for } \lambda_e < 0.53$$

(xi) Average ultimate collapse stress:

$$\sigma_u = \sigma_{ic}\left[\frac{A_s + s_e t}{A_s + st}\right]$$

Using the above formulations, the mean and cov of the modelling parameter for the 52 (steel + aluminium) data set are: $\bar{X}_m$ = 1.01 and v_{X_m} = 13.3%.

A.2 Radial Pressure

The preferred provisional strength formulation for radial pressure is that of API Bul 2U discrete, but with some changes in the effective pressure correction factor.

(i) Local buckling pressure for ring-stiffened cylinder of mean radius R, thickness t, unsupported length L:

$$p_{eL} = \frac{1.27}{A^{1.18} + 0.5}E(t/R)^2 \text{ , for } M_x > 1.5 \text{ and } A < 2.5$$

$$= \frac{0.92}{A}E(t/R)^2 \text{ , for } 2.5 < A < 0.208\ R/t$$

$$= 0.836C_p^{-1.061}E(t/R)^3 \text{ , for } 0.208 < C_p < 2.85$$

$$= 0.275E(t/R)^3 \text{ , for } C_p > 2.85$$

where: $A = M_x - 1.17, M_x = L/\sqrt{R/t}, C_p = At/R$

(ii) Plastic collapse pressure of stringer stiffener-shell combination:

$$p_s = \frac{16}{sL^2}A_s[z_s]\sigma_y$$

(iii) Effective pressure correction factor:

$$K_p = 0.25 + 0.85g/500 \text{ , for } g \le 500$$

$$= 0.98 + 0.12g/500 \text{ , for } 500 < g < 2500$$

where $g = M_x M_\theta L t A_s / I_s$, $M_\theta = s^2/Rt$

(iv) Bay inelastic failure pressure and stress:

$$p_{cb} = (p_{eL} + p_s)K_p$$

$$\sigma_{ecb} = p_{cb}(R/t + 0.5)K_{eL}$$

where $K_{eL} = 1$, for $M_x \ge 3.42$

$$= 1 - \varepsilon\psi \text{ , for } M_x < 3.42$$

$$\varepsilon = (A/L_e t + 1)^{-1} ; A = A_r(R/R_r)^2$$

R_r = radius to centroid of ring stiffener

$L_e = 1.56\sqrt{Rt} + t_w \le L$

$\psi = 1.0$, for $M_x \le 1.26$

$= 1.58 - 0.46M_x$, for $1.26 < M_x < 3.42$

$= 0$, for $M_x \ge 3.42$

Using these formulations the statistical results for the 11 models are: $\bar{X}_m = 1.14$ and $v_{X_m} = 13.4\%$.. The model will be improved by incporating the best features of the RCC model.

A.3 Combined Axial Compression and Radial Pressure

With terms as defined in the text, the failure interaction equation is:

$$\left(\frac{R_x}{\phi_x}\right)^2 + R_x R_\theta \left[\frac{2\sqrt{(1-\phi_x^2)(1-\phi_\theta^2)}}{\phi_x\phi_\theta} - 1\right] + \left(\frac{R_\theta}{\phi_\theta}\right)^2 = 1$$

Using this the statistical results for the 35 models using the above recommended axial and radial strength models are $\bar{X}_m = 1.10$ and $v_{X_m} = 21.1\%$.

References

1) Das, P.K., Faulkner, D., Zimmer, R.A., 'Selection of Robust Strength Models for Efficient Design of Ring and Stringer Stiffened Cylinders Under Combined Loads', Proc. OMAE '92, Calgary, June 1992.

APPENDIX 4.7: Shear Centres and Warping Constants [1]

Section	Distance to shear centre, C e	Warping constant H
1.* 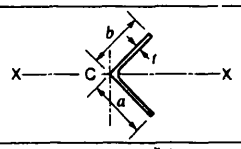		$\frac{t^3(b^3 + a^3)}{36}$
2.* 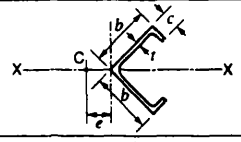	$\frac{bc^2(3b - 2c)}{1.4[2b^3 - (b - c)^3]}$	$\frac{2}{3}b^2c^3t - I_x e^2$
3. 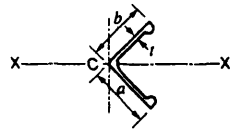		$I_s(b^2 + a^2) + \frac{t^3(b^3 + a^3)}{36}$ I_s = inertia of bulb about median line of leg
4.* 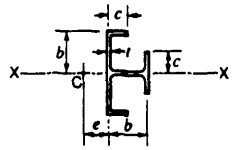	$\frac{bc^2t}{I_x}\left(b - \frac{2}{3}c\right)$	$\frac{4}{3}b^2c^3t - I_x e^2$
5. 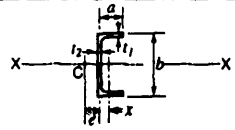	$\bar{x}\left(\frac{b}{2r_x}\right)^2$	$\frac{a^3b^2t_1}{6} - I_x e^2$
6.* 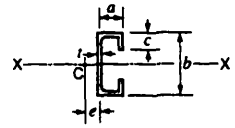	$\frac{ab^2ct}{I_x}\left[\frac{1}{2} + \frac{a}{4c} - \frac{2}{3}\left(\frac{c}{b}\right)^2\right]$	$\frac{a^2t}{6}(4c^3 + 3b^2c + 6bc^2 + ab^2) - I_x e^2$
7. 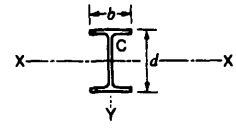		$\frac{I_y d^2}{4}$
8. 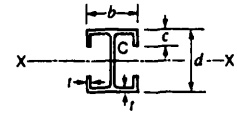		$\left(\frac{I_y d^2}{4}\right) + c^2b^2t\left(\frac{d}{2} + \frac{c}{3}\right)$
9.* 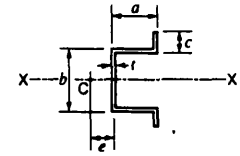	$\frac{ab^2ct}{I_x}\left[\frac{1}{2} + \frac{a}{4c} - \frac{2}{3}\left(\frac{c}{b}\right)^2\right]$	$\frac{a^2t}{6}(4c^3 + 3b^2c - 6bc^2 + ab^2) - I_x e^2$
10.* 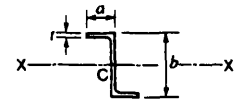		$\frac{a^3b^2t}{12}\left(\frac{a + 2b}{2a + b}\right)$

*Uniform thickness, t
N.B. dimensions a, b, c, d, e, $\bar{x}$, are measured along and to median lines.

References

1) Marsh, C., Strength of Aluminium', Alcan Canada Products Limited, Fifth Edition, Canada, 1983.

APPENDIX 6.1: Design Recommendations

This Appendix provides a condensed version of the more important Design Recommendations drawn from the main chapters under the following headings:

- Preliminary Considerations
- Load Estimation Recommendations
- Fatigue Strength Modelling Recommendations
- Ultimate Strength Modelling Reccomendations

References to the appropriate sections in the main text are provided.

For Fatigue design the models are lower bound at about 2 standard deviation levels below the mean of the test data. For ultimate strength the models are aimed at being close to the mean values, and with two or three exceptions this is achieved.

PRELIMINARY CONSIDERATIONS

The widespread use of Fast Marine Vehicles is a question of *supply* and *demand*. **Demand** depends on passenger, operator and government requirements, and the available fast ship designs should address these considerations (sections. 1.1-1.2) in a balanced manner if they are to succeed. **Supply** of the appropriate technology and designs will have to address technical as well as strategic challenges and depends on:

- *industrial aspects* (partnerships and long-term collaboration, para. 1.4)

- *operational aspects* (training, 'aircraft' technology and operation, human error minimisation, para. 1.4) and addressed by the new IMO HSC rules

- *Research and Development* (as identified by observed failures in AMVs, page 41) in the following areas

(a) machinery reliability (Machinery failures more than doubled between 1985-89 vs. 1980-1984)
(b) load prediction tools
(c) permissive instead of prescriptive regulations
(d) ultimate strength-based structural design codes possessing reliability based partial safety factors thus encouraging first principle design. The reasons for such a choice are described in para. 1.5, but they mainly reflect the weight criticality of AMVs and the uncertainties in load estimation, operational profiles, the design variable values and the accuracy of strength prediction models

- The assumed *target reliability* used for partial safety factor calibration should be based on
  - existing designs, or
  - the values implied by current design codes, or
  - taken as $\beta=4$ for novel designs
- The *format* of the *safety check* expression should be kept as simple as possible and close to the form

$$\gamma_Q \gamma_f Q \leq \phi_R R$$

BUT choices must be made relative to the number of PSFs and the positions of the PSFs in the design equations (paras. 1.5.4.3, 1.5.4.4)

- The *variability* of the design variables in *strength modelling* may be assumed as:

Item	Distribution type	COV %	Bias ζ_i %
Yield Stress	LN	6-9	10 to 15
Young's Modulus	LN	1-3	-2 to 2
Plate Thickness	N	1-4	-2 to 2
Cross Section of Scantlings	N	2-4	-2 to 2
Welding Stresses	LN**	10-15	
Plate Distortions	N*	30-50	
Stiffener Distortions	N*	10-15	

N=Normal Distribution, LN=Log-Normal Distribution
(*) the same type of distribution as for cross sectional dimensions assumed
(**) the same type of distribution as for yield stress assumed

(e) new materials and hybrid construction but current trends are
- GRP for $\Delta < 50$ tonne and V<44 knots
- aluminium for all displacements and V>30 knots
- steel for $\Delta > 120$ tonne and V>20-30 kn and increasingly replacing aluminium at higher speeds and displacements
- high strength steel for designs above 1000 tonnes and 46 knots

• In the structural design and analysis of SWATH ships the designer should consider the (para. 1.8.3)

(a) *shear lag* which affects the buckling efficiency of the plating
(b) *high stress concentrations* on the transverse bulkheads at four locations
(c) *shear stresses* present in the cross-deck girder and transverse bulkheads
(d) a first shot at the *stress distribution and magnitude* in the deck, side plating and at the *stress concentration* points can be obtained via *Sikora and Disenbacher's* parametric expressions (para. 1.8.3). They are conservative for smaller vessels so for greater accuracy FE analysis is recommended
(e) the available means for stress and stress concentration reduction are presented in para. 1.8.3 from which the radius of curvature at the haunch intersection with the cross deck is the best for stress concentration reduction while the partial transverse bulkheads is the most weight efficient approach.

LOAD ESTIMATION RECOMMENDATIONS

Three means of estimating the *primary loads* on SWATH ships are:

(a) Empirical formulations (at the concept design stage)
(b) Theoretical estimations based on spectral determination of the sea conditions and structural response
(c) Experimental Investigations.s

(A) EMPIRICAL FORMULATIONS should be preferred at the design concept stage. The design load expressions recommended for the individual primary load components are

- **Longitudinal loads** - Sikora's empirical algorithm (para. 2.1.1.1)
- **Vertical shear loads** - Empirical US Navy algorithm (par. 2.1.1.2)
- **Side force**
  - Most significant primary loads, are *maximum* at beam seas and zero speed, *half* in bow and stern quartering seas, and *zero* in head and following seas
  - Sikora and Disenbacher empirical relationship (para. 2.1.3.1) recommended--Conservative for vessels smaller than 3000 tonnes--Used by both US and RN (with changes as described in para. 2.1.3.1--factor 1.584 higher than US) Navies and the ABS SWATH code
  - If ship's main dimensions unknown $0.95\,\Delta$-$1.0\,\Delta$ should be used as first shot
  - *Point of application* for design purposes at 0.5-0.6 draft
  - *Longitudinal distribution* may be assumed uniform (para. 2.1.1.3) but dependent on geometry (para. 5.4)
  - For a given wave height, maximum at wave lengths 3-4 times the underwater beam
  - Maximum side load to *decreases* as a fraction of Δ as Δ increases above 400 tonnes
- **Torsional loads**
  - Sikora et al's expressions (para. 2.1.1.5) are recommended-applicable for seas between 15° and 45° off beam

    $T = 0.13\,F_{max}\,L_s$ for the cross deck

    $T = 0.29\,F_{max}\,L_s$ for the struts
  - For the yaw torsional moment Sikora and Disenbacher's expression proposed (para. 2.1.1.5)
- **Load Combinations** - Kennel's expressions are recommended (para. 2.1.3.2)
- **Slamming loads**
  - this is the most important secondary load, which governs the local structural design of the wet deck, haunch, strut and it is amplified by ship speed
  - *Maximum* within 20% of L_{OA} from the bow,

dropping linearly from there onwards to a distance of 40% of L_{OA} from the bow where the pressure level is at 50% of that at the bow

- Design pressure measured at model scale must be scaled to full scale values and adjusted for different panel sizes for use in design (par. 2.1.2)
- Simple formulation by *Allen and Jones* (para. 2.5.1) is recommended. It is the most widely acceptable and is used by ABS SWATH Code draft. It allows pressure value predictions for a number of advanced marine craft and requires no advance knowledge of vehicle motion

(B) THEORETICAL ESTIMATIONS (para. 2.1.3.3) of motions and hydrodynamic loads may be carried out in two ways:

(a) *Two-Dimensional Strip Theory-* Should be avoided as it only permits predictions in the direction in which the section is chosen and is hence *less accurate*

(b) *3-Dimensional Sink-Source Theory* --Should be *preferred* as it allows the inclusion of wave load effects in all directions thus facilitating consideration of the pitch and yaw motion effects which would otherwise be neglected- Price et al incorporated the effect of **hydro-elasticity** on structural responses, Chan accounted for **forward speed effects** (translating-pulsating sources)-Additional European computer code developments are available by the National Technical University of Athens (NTUA) and NTH Norway.

(C) The SPECTRAL DESCRIPTION of the sea state and motion/structural response can either be carried out based either on short- or long-term statistics

(a) *Short Term Statistics*

- short term wave records used to define the irregularity of the seaway and describe normal seaway conditions (para. 2.2.1)
- description is in the *frequency domain* either in terms of *significant wave height, zero crossing period* or preferably in terms of extremes, i.e. *Extreme Wave Heights and the Most Probable Extreme Wave Heights* (para. 2.2.1.2)

- the wave height and period follow a Rayleigh distribution for a *narrow banded spectrum,* developed seas, BUT
- *Correct* for *wide-bandedness* (ε>0.6) the significant wave height (para. 2.2.1.1) and Extreme Wave Heights (para. 2.2.1.2)
- Of the available theoretical *spectra* (para. 2.2.2.)
  - P-M spectrum *most widely used* (for fully developed seas)
  - Bretschneider spectrum is mostly used in the Gulf of Mexico
  - JONSWAP spectrum (γ=3.3) used in the North Sea for storms
  - Ochi spectrum accounts for the presence of swell
- Necessary *Corrections* of energy spectra (if not already included in the spectrum itself) for (para. 2.23) are for
  - Short-Crested Waves (except for the JONSWAP spectrum)
  - Frequency of encounter (forward speed and direction)

(b) *Long-Term Statistics*

- are based on a long-term distribution of the short term seaway statistics and should be used for the prediction of long term extreme values accounting for the occurrence of rare events (para. 2.3)
- predict the largest value of the wave height or response for a given probability of this largest value being exceeded
- *Two Methods* to calculate the long-term probability density function for extreme motion/response values
  - **Design Sea Load Method** (para. 2.3.1)
    NOT for fatigue damage estimation as it neglects all the load conditions linked to every significant wave height other than that specific combination of heading, frequency and speed that results in the highest response level
  - **Lifetime Weighted Sea Method** (para. 2.3.2)
    Total lifetime response of the ship the sum of a series of short-term responses appropriately weighted to account for the relative amount of exposure of the ship to the various levels of sea severity---More accurate but computationally intensive and is mostly used for fatigue life estimations
  - The probability density function of peak values of response for the ship's lifetime is usually chosen from Log-normal, Weibull, Gumbel and the Fisher Tippett II distributions. *Log-Normal and Weibull distributions are used widely and are recommended.*

- Two *Load Prediction methods* are available for *Fatigue Design:*

(a) The **Lifetime Weighted Sea Method** (paras. 2.3.2, 2.4)- Should be preferred for detailed fatigue design and for critical joints whose failure will not lead to load shedding but to the rare case of structural failure. It is used by the US Navy (para. 2.4.2)

(b) The **Simplified Method** (para. 2.4)- Is preferred at the concept design stage and for joints whose failure will only lead to load shedding
  - proposed by Munse et al it considers a two-parameter *Weibull* distribution for the long-term stress-range distribution ignoring any sequence effects
  - the shape parameter ξ of the Weibull distribution is a function of the type of structure, its dynamic characteristics and the location of its operation (para. 2.4)
  - used by the Royal Navy ($\xi = 1$ -exponential distribution, $D = \Delta = 1$, design stress value corresponds to a probability of exceedence α of 0.01 in the ship's life (para. 2.4.3)
  - It is also used by most marine design codes and recommended by Moan, Faulkner, and Nordenstrom (DNV) it is also proposed herein

(c) The ***corrections applied on the stress-range loading*** should be for
  - *Wide bandedness*--Wirshing and Light's method based on the rainflow cycle counting method (para. 2.4.1) should be used
  - *Two segment fatigue strength curves*--Wirshing and Chen's (para. 2.4.1) method should be used

(D) EXPERIMENTAL INVESTIGATIONS (para. 2.1.3.4) are essential in calibrating theoretical predictions but are currently only restricted to novel designs for which the computer codes have not in general been properly tested.

FATIGUE STRENGTH MODELLING RECOMMENDATIONS FOR THE MAIN STRUCTURAL COMPONENTS

In analysing a joint for its **fatigue strength** one should make allowances for the following:

(a) *Weld Orientation* usually accounted by the joint classification system
- transverse welds lowest fatigue strength (para. 3.2)

(b) *Weld Size*-Larger Length, thickness, width of welded element, all lower the mean fatigue strength

- **Thickness correction essential** (page 185) as code S-N data available for specific thicknesses
- **Length and Thickness correction** - Part of the classification system

(c) *Weld Type-* butt-failure at the *weld toe*

- fillet-H=t guarantees failure at the *weld toe* (para. 3.2) - good *root penetration* important, *partial* root penetration welds help reduce the leg length and hence the amount of weld material deposited (page 183)

(d) **Misalignment correction** (angular or linear misalignment or thickness differences) should only considered in the presence of *axial stresses*- the stress magnification factor is dependent on level of eccentricity and/or thickness difference (para. 3.2.1).

(e) *Discontinuity effects*- Included in the fatigue data, no correction essential

(f) *Material Strength/Alloy Type*

- High material strength encourages high stress ranges to be exercised on the joints thus deteriorating fatigue life
- **unwelded** - beneficial only on *crack initiation* stage (page 186)
- **welded** - Has no effect in crack propagation stages which depend on E instead (page 186)
- *Alum.* - 7000 sers 40% *higher strength* than 5000/6000 (pg 189)
  - 5000 vs. 6000 series unaffected at high cycle range but large differences observed at low cycle range (pg 189)
- *Indications* of high strength material enhancing the effect of weld improvement techniques (para. 3.8.1)

(g) *Corrosion* negates the effect of any endurance limit

- *Steel* - Reduction in strength by a factor of 2
- *Alum* - **UNWELDED**
  (a) Weathering Corrosion - is Self Arresting
  (b) Galvanic Corrosion-occuring between dissimilar metals and hence protection is required (page 187)
  (c) Stress Corrosion - Occurring in 5000 series ONLY
  Insensitive if annealed and < 7% Mg (page 187)
  OR cold formed and annealed at >60° &<3% Mg

WELDED (page 188) Strength reductions

For 5083 alloy - BUTT 40%, FILLET 50%, (R=0.5)
For 6063 alloy - BUTT 53%, FILLET 22% (R=0.5)

- Shot peening improves the fatigue and corrosion fatigue life of aluminium transverse butts of 7000 series 3- to 6-fold (para. 3.2.1)

(h) *Temperature Effects on Fatigue Strength*

- *Steel* - reduction with high temperature (limit of code applicability 375° C), brittle with low temperature
- *Aluminium* - High temperature leads to 50% REDUCTION
- Low temperature leads to 15-60% INCREASE
- Limit of code applicability 100° C

(i) *Effect of E*

- 'Steel data may be used for aluminium joints by direct division by 3, a generally applied policy
- This is not always true as ratios vary between 2-2.5, 3 being most applicable to longitudinal non-load carrying fillet welds (para. 3.3.5)

(j) *Co-existence of Normal and Shear Stresses*

- The equivalent principal stress expression by ERAAS should be used (para. 3.3) in this case
- In terms of weld orientation a weld should be considered as 'longitudinal' if the welding line is within 30° of the principal stress direction

(k) *The Effect of Mean Stresses* - Should be accounted for via the Goodman plot (page 190)

- **Fatigue Strength Criteria**

- Empirical S-N curves used in the medium to high cycle range
- Theoretical crack propagation, expressed in two ways (para. 3.5.1):
  (a) limiting the stress intensity factor, K, to the fracture toughness K_C
  (b) restricting the crack size to below a preset critical size, a_{crit}, set from serviceability considerations
- Theoretical, *strain* dependent expression should be used in low cycle fatigue, e.g. Coffin-Manson Law accounting for plasticity at the crack tip (para. 3.3.3)

- **Fatigue Damage Summation Rules**

- Miner's Rule - Widely used and thus recommended but *accurate only* for *narrow banded* spectra and *large* block lengths, and *sensitive to load sequencing* (para. 3.3.4.1). Damage predictions vary between 0.47-1.0
- Guerney's Rule - Addresses Miner's discrepancies but not widely used (para. 3.3.4.1)
- Miner's rule leads to satisfactory predictions for R=0 BUT Guerney's rule is more accurate at higher mean stresses

- **Uncertainties in Miner's Fatigue Damage Model** (para. 3.4.2.3) to be used in a reliability analysis of the fatigue strength are:

Item	Distribution	Bias	COV
Primary Load, B	Log-Norm	0.7	50%
Strength, K	Log-Norm	S-N data	70%
Test data, N	Log-Norm		36-48% for steel 27% for Alumnm
Fatigue Damage Δ	Log-Norm	1.0	65%

- **The Fatigue Strength Design Codes Recommended are**

- BS 5400, Offshore, DEn Based on Welding Institute Data, for STEEL
- BS 8118 The most *conservative aluminium code* -Proposed by the ISSC'94 and recommended herein (para. 3.6.5)
- ERAAS Mean strength predictions relative to other codes (para. 3.6.5)

- **Effects of Post-Weld Repair Techniques**

Post Weld Repair methods (para. 3.8.1) interfere with the mechanisms of crack initiation and propagation. These are:

(a) *Weld Toe Dressing*- **mechanical** (hammer peening, shot peening, disc grinding or, machining) - para. 3.8.1
- **TIG/plasma dressing**--AVOIDED (inefficient)

(b) *Residual Stress*
- **cold working** (hammer /shot peening)
- **prior-overloading** (Risk of deformation)
- **spot heating** (costly, avoid for aluminium)

(c) **Hammer Peening** provides **the best** results from all methods

(d) *Indications* exist that high strength material enhances the effect of weld improvement techniques (para. 3.8.1)

(e) For **Aluminium** the fatigue strength depends on (para. 3.8.1)

- *Filler Wire* - reduced porosity filler wire improves the fatigue life of reinforced welds but not of unreinforced ones. Overwelding reduces the fatigue strength by 10%
- *Pore Size* - not number of pores. Pores of 30% weld volume reduce the fatigue strength by 20%
- *Welding Method* - Gas welding leads to strength reductions of 50% in butts, and 67% in fillets
  - Electron Beam welding is found to provide inconsistent observations
- *Repair Method* - Shot-peening provides 50% strength improvement on fillets, and 100% on butts)
  - TIG dressing leads to improvements in fatigue lives in the ratios between 1.9-3.3 for butt welds, and 2.8-7.2 for fillets
  - Peening before preloading leads to 40% strength increase
  - Preloading before peening leads to 60% strength increase for butts, and 30% for fillets
- *Comment* - A strength improvement factor of **1.4** may be used for all properly applied repair techniques in all types of aluminium joints

• **Weldability:** It is important to check the weldability (para. 3.8.3) of alloys chosen if good fatigue life is to be obtained. Weldability *reduces* with an increase in- Solidification Interval Temperature. **Low Weldability** is due to

(a) **Hot Tearing** in grain boundaries (Max. for alloy content 1%-3%)

(b) **Solidification** HAZ **Cracking**

Guidance on the weldability of the various aluminium alloys is available in the ALUSELECT database and BS 8118, texts which are highly recommended (para. 3.8.3).

ULTIMATE STRENGTH MODELLING RECOMMENDATIONS FOR THE MAIN STRUCTURAL COMPONENTS

The *'Transfer of Technology'* from *'steel'* to *'Aluminium'* requires proper account to be taken of:

(a) Rounded material stress -strain curve (strain hardening)
(b) Residual stress effects
(c) HAZ material strength reduction in certain aluminium alloys

- *5000 & 6000 series alloys are mostly used in marine applications*

1. 5000 series easier to roll, better corrosive resistance than 6000 series, moredifficult to extrude and hence mostly used for plating
2. 6000 higher strength, easier to extrude, less corrosive resistance than 5000 series, so used as stiffener and for extruded sections
3. 6000 series heat-treated and hence more affected by welding than 5000 series that remain unaffected unless they are in their work-hardened temper

- **Strain Hardening**

The strain hardening advantages of the aluminium alloy is generally neglected in the modelling of the buckling phenomena, but its consideration is beneficial in the strength of beams and beam columns, for the cases where plasticity and plastic hinge formation are considered to be the failure criteria. For such cases it is difficult to identify a failure point as such, and hence failure may be assumed to occur at strains of 5-10 $\varepsilon_{0.2}$ or 5-10 $\theta_{0.2}$ for axial tension and bending respectively.

- **Residual Stresses**

The thermal diffusion factor in aluminium is 10 times higher than that of steel and hence (para. 4.1.1.1)

(a) Extrusions - Neglect residual stresses
Hot-rolled steel profiles - Residual stresses = 0.3-0.5 yield
(b) Welded sections - *Steel*-tensile resid. strss. at yield level
- *Aluminium*-tensile resid. strss. at 0.6 of Y
(c) The Cambridge residual stress model is preferred in modelling over the ECCS as the British model allows extrapolation to all types of joints (para. 4.1.1.2)

- **HAZ Softening Considerations**

HAZ material strength reduction is more significant in the 6000 and 7000 series alloys and in the 5000 series alloys only when these are at a work-hardened temper

Modelling requires the determination of the *extent and magnitude of HAZ softening*. The *BS 8118 proposals* are the most detailed and hence are recommended for use herein (para. 4.1.2.2)

- Extent - is dependent on thickness, proximity of other welds/ free edges, weld deposit area
- Reduction - is dependent on alloy and its treatment

General Comments on the Design of Steel and Aluminium Flat Plates

(a) Flat stiffened plates are treated as 'columns', the effects of residual stresses and initial imperfections accounted for by either the tangent modulus approach or the Perry-Robertson approach

- *Perry-Robertson* - accounts explicitly for imperfection effects but not residual stresses Used mainly in Europe and is conservative for reasons mentioned in pg 266.
- *Tangent Modulus* - widely used in the USA and Canada. It accounts explicitly for residual stress effects and implicitely for average imperfections and is preferable (para 4.2.2)

(b) *Inelastic behaviour* best treated by the *Tangent Modulus approach* (para. 4.2.2). Effect of larger initial imperfections however must be accounted for by the use of correction factors based on experimental data

- The recommended design models with their associated uncertainties for the main structural components of SWATH ships are presented in the Tables below for both aluminium and steel applications

Model	Material	Bias	COV(%)	Ref. Paragraph
Ultimate Strength of 'Long' Plates in Compression				
G. Soares	Steel	1.031	10	4.2.4
Tolikas	5083	0.99	6	4.2.5.3
	6082	1.0	5	4.2.5.3
		or use steel model with $\sigma_{0.2}$ and E_s replacing σ_y and E		
Ultimate Strength of 'Long' Stiffened Plates in Compression				
Faulkner	Steel	1.041	11.7	4.2.5
	Alum	use steel model with $\sigma_{0.2}$ and E_s replacing σ_y and E **or** Tolikas model (para. 4.2.5.4)		
Ultimate Strength of 'Wide' Plates in Compression				
Soares/Faulkner	Steel	0.99	13	4.2.6
	Alum	use steel model with $\sigma_{0.2}$ and E_s replacing σ_y and E		
Plates Under Lateral Pressure				
	Steel/Alum	1.0	5	Appendix 4.3

Steel - **Elasto-Plastic Design (Appendix 4.3)**

For $1 \le \alpha \le 5$ and $2 \le \beta \le 6$, the allowable pressure, p, is expressed in terms of an allowable permanent set, w_{pt}

For $1 \le \alpha \le 5$ and $\beta < 2$ fully plastic design approach of Wood is used ('roof-top' collapse bending mechanism, without membrane effects)

- **OR Fully Plastic Design (Appendix 4.3)**

For 'long' plates ($\alpha \ge 2.5$) three-hinge collapse assumed

For 'short' plates ($\alpha < 2.5$) - Roof Top Collapse Mechanism with or without accounting for membrane stresses depending on the value of the plate slenderness β

Alum - Use 'STEEL' models--strain hardening neglected. Conservative to use reduced material strength for material suffering from HAZ softening and models based on bending strength of plates (e.g. formation of plastic hinges) (para. 4.2.7.5)

Model	Material	Bias	COV(%)	Ref. Paragraph
Ultimate Strength of Plates in Biaxial Compression				
Odland/Faulkner	Steel	0.99	13.1	4.2.8
	Alum	use steel model with $\sigma_{0.2}$ and E_s replacing σ_y and E (par. 4.2.11)		
Ultimate Strength of Plates in Biaxial Compression & Lateral Pressure				
Soares/Gordo	Steel	0.99	11	4.2.9
	Alum	use steel model with $\sigma_{0.2}$ and E_s replacing σ_y and E (par. 4.2.11)		
Ultimate Strength of Plates in Biaxial Compression & Shear				
Soares/Gordo	Steel	1.07	6.0	4.2.10
	Alum	use steel model with $\sigma_{0.2}$ and E_s replacing σ_y and E (par. 4.2.11)		
Stiffener Design				
Tripping Check				
Faulkner's plate/ stiffener intctn	Steel	1.0	15	4.3.4.1, 4.3.4.4
	Alum.	use steel model with $\sigma_{0.2}$ and E_s		
Strength Check	- Treated as stiffened plates in compression (paras. 4.2.5 & 4.2.5.4) with an effective width of plating			
	- Vertical and longitudinal stiffeners of deep plate girders treated via a Perry-Robertson expression. Loads estimated as for BS 8118 in paras. 4.3.2.1 and 4.3.3.2 and strength as in paras. 4.3.2.2 and 4.3.3.3.			
Stiffness Check	- Maquoi's Criteria based on Orthotropic Plate Theory (para. 4.3.1.2) are recommended			
Local Buckling Criteria (para. 4.3.5)				
Steel	- Assume safety factor of 3 on yield against critical buckling of stiffener components			
Alum	- use steel criteria with $\sigma_{0.2}$, and E_s			

Model	Material	Bias	COV(%)	Ref. Paragraph
Ultimate Strength of Unperforated Deep Plate Girders (Cross-Deck)				
1. Shear Dominated Failure				
Cardiff	**Steel**-Vert. stiff.	0.98	6.0	4.4.2.2
	Steel-Long. stiff	1.0	7.0	4.4.2.2
BS 8118	**Alum.**-Vert. stiff.	1.74	11.6	4.4.2.2
	Alum.-Long. stiff.	1.51	6.4	4.4.2.2
2. Bending Dominated Failure				
Cooper	**Steel**-Vert. & Long. Stiff.	1.008	4.5	4.4.2.4
BS 8118	**Alum.**	1.0	5.0 (assumed) as criterion is first yield of flanges	

Cardiff model is recommended accounting for the effect of longitudinal stiffeners as recommended by the Cardiff approach (para. 4.4.2.3) and *without* considering the effect of the tension field component on the flange rigidity

The effect of *bending and direct* in-plane loads should be accounted for as recommended in para. 4.4.2.4

Ultimate Strength of Perforated Deep Plate Girders (Cross-Deck Structure)

- Note the restrictions on the perforation dimensions relative to those of the web panel (paras. 4.5.2 & 4.5.3)
- Nothing has been published for *Aluminium Perforated* girders or for the loading case of *co-existent* shear, *bending and direct stresses*- Assumptions as proposed by Cardiff model for the unperforated deep plate girder cases is hence recommended for this case (para. 4.5.6)
- The *design of reinforcements* for any web plate perforations should be carried out as referenced in para. 4.5.5
- *Least ultimate strength of perforated girder* when the perforation is located at the centre of the web panel, *maximum* when at the compression diagonal corner, BUT for *alternating shear loads* perforations should be placed only at the center

1. Unreinforced, circular, centrally positioned perforations				
Narynn/Rockey (simplified)	**Steel**	1.18	9.0	4.5.2
	Alum	nothing published, as in para. 4.5.6		

2. Reinforced, circular, centrally positioned perforations

Naryn/Der Avan.	**Steel**	1.07	11.5	4.5.1 & 4.5.2
	Alum	nothing published, as in para. 4.5.6		

3. Unreinforced, rectangular, centrally positioned perforations

Naryn/Der Avan.	**Steel**	1.14	8.3	4.5.1 & 4.5.2
	Alum	nothing published, as in para. 4.5.6		
or	**Steel & Alum**	Transform rectangular opening to its 'equivalent diameter' circular perforation (para. 4.5.4) and use simplified expression		

4. Reinforced, rectangular, centrally positioned perforations

Naryn/Der Avan.	**Steel**	1.17	4.0	4.5.1 & 4.5.2
	Alum	nothing published, as in para. 4.5.6		

5. Unreinforced, eccentrically positioned perforations (circular & rectangular)

Naryn et al	**Steel**	1.20	13.0	4.5.4
	Alum	nothing published, as in para. 4.5.6		

Ultimate Strength of Deep Plate Knee Joints (Haunch-Strut Intersection)

Braunsweig	**Steel**	0.91	11.5	4.6-4.6.3
	Alum	nothing published, as in para. 4.6.6		

- The model has not been extended to account for the presence of
  - *longitudinal/vertical stiffeners* on the web plate
  - *web perforations*

  These can be *arbitrarily* accounted as shown in paras. 4.6.4 and 4.6.5.
- The design of knee-joints with *Tapered or Curved Flanges* should be carried out based on either Vierendeel's tapered Beam Formulae or Olander's Formulations (para. 4.6.7)

The Design of Stiffened Cylindrical Structures Under Pressure Loads

1. Ring Stiffened Cylinders Under External Pressure only

1.1 Interframe Shell Collapse

BS 5500	**Steel**	1.05	13.0	4.7.1.1
(mean curve)	**Alum**	use steel model with $\sigma_{0.2}$ and E_s replacing σ_y and E		

Chosen on the basis of minor conservatism and wider acceptance and not on the best modelling uncertainty values.

1.2 General Instability

Bryant 2-term expression	**Steel**	0.95	13.0	4.7.1.2
	Alum	use steel model with $\sigma_{0.2}$ and E_s replacing σ_y and E		

1.3 Overall Collapse-Frame Yielding

Perry-Robertson*	**Steel**	1.1	10.0	4.7.1.3
	Alum	use steel model with $\sigma_{0.2}$ and E_s replacing σ_y and E		

(*) Note that these uncertainties have been obtained by assuming

$$C_n = \frac{a + b\,n}{n^2 - 1}$$

based on RN submarine data and where the out-of-circularity varies with the number of circumferential waves (page 389). The BS 5500 assumption of o-o-c of 0.005R is found in Table 4.13 to be overly conservative and unrealistic for modes above n=2.

2. Dome End Design

Faulkner	**Steel**	1.0	15.0	4.7.3
	Alum	use steel model with $\sigma_{0.2}$ and E_s replacing σ_y and E		

3. Design of Conical Transitions

The conical transition joints should be designed according to *Niordson's* proposals (para. 4.7.2). The use of the same strength formulations and criteria as for cylindrical elements under external pressure is required but with appropriate modifications to account for the taper angle. The uncertainties to be assumed should be those appropriate to the individual strength models used for cylindrical sections. For *Aluminium* applications use the steel models with $\sigma_{0.2}$ and E_s replacing σ_y and E.

4. Orthogonally Stiffened Cylinders

4.1 Under Axial Compression only

Glasgow-(RCC recalibration)	**Steel**	1.01	13.2	Appendix 4.6
	Alum	use steel model with $\sigma_{0.2}$ and E_s replacing σ_y and E		

4.2 Under External Pressure only

Glasgow-(RCC recalibration)	**Steel Alum**	1.14	13.4	Appendix 4.6 use steel model with $\sigma_{0.2}$ and E_s replacing σ_y and E

4.3 Combination of External Pressure and Axial Load

Glasgow-(RCC recalibration)	**Steel Alum**	1.09	25.0	Appendix 4.6 use steel model with $\sigma_{0.2}$ and E_s replacing σ_y and E